DISSERTATION

REACTIVITY AND SELECTIVITY IN THE POLYMERIZATION OF MULTIFUNCTIONAL ACRYLIC MONOMERS BY CHIRAL ZIRCONOCENIUM CATALYSTS

Submitted by

Fernando Vidal Peña

Department of Chemistry

In partial fulfillment of the requirements

For the Degree of Doctor of Philosophy

Colorado State University

Fort Collins, Colorado

Summer 2017

Doctoral Committee:

Advisor: Eugene Y.-X. Chen

Richard G. Finke
Steven Strauss
Ellen Fisher
David Wang

ABSTRACT

REACTIVITY AND SELECTIVITY IN THE POLYMERIZATION OF MULTIFUNCTIONAL ACRYLIC MONOMERS BY CHIRAL ZIRCONOCENIUM CATALYSTS

Described in this dissertation are the results of investigating the reactivity and selectivity in the polymerization of multifunctional acrylic monomers by chiral cationic zirconocenium catalysts. The unprecedented precision polymer synthesis method developed in this work—the polymerization of polar divinyl monomers that is not only living but also simultaneously chemoselective and stereoselective—has enabled the synthesis of well-defined highly stereoregular functionalized polymers bearing reactive C=C bonds on every chiral repeat unit. Thus, under ambient conditions, chiral *ansa*-ziroconocenium catalysts of the appropriate symmetry (C_2- vs C_S-ligated) have afforded highly isotactic and highly syndiotactic double-bond-carrying polymers, respectively, with controlled molecular weights and narrow dispersities. The enantiomorphic-site controlled, conjugate-addition coordination polymerization mechanism is responsible for the observed high degree of control over the polymerization characteristics, chemoselectivity and stereochemistry. Soft-material applications of such stereoregular and reactive ene-bearing polymers have also explored, including chemical post-functionalization to functional materials, photocuring to elastic films, and molecular recognition to robust crystalline supramolecular stereocomplexes and helical C_{60} inclusion complexes.

A class of important biorenewable monomers containing one methacrylic C=C and two ester groups, namely itaconic esters and anhydride, have been examined, for the first time, for their

polymerizability towards both neutral and cationic bridged *ansa*-zirconocenes and nonbridged zirconocenes. This investigation has yielded a fundamental understanding of the reactivity of the zirconocene complexes towards such monomers, specifically the fundamental chain initiation and propagation steps, structures of resting metallocyclic chelates, as well as kinetic and thermodynamic intermediates.

DEDICATION

To Carmen Marqués Gil and Elena Pezzi Martínez,

those tenderhearted giants upon whose shoulders I stood for the first time

and whose life lessons will walk with me forever.

A Carmen Marqués Gil y Elena Pezzi Martínez,

aquellas cariñosas gigantes sobre cuyos hombros me alcé por primera vez

y cuyas lecciones vitales caminarán conmigo por siempre.

TABLE OF CONTENTS

CHAPTER 1

Introduction

The dissertation presented hereinafter was conceived in a "journals-format" style, in agreement with the Graduate School guidelines at Colorado State University, and it contains four manuscripts. Three of the manuscripts have already been published in peer-reviewed chemistry journals, including two full-paper articles in the *Journal of the American Chemical Society* and one invited account article in *Synlett*, while the fourth manuscript has been completely prepared and submitted to *Organometallics*. The purpose of this dissertation work is to utilize the readily available chiral *ansa*-zirconocenes as catalysts to polymerize challenging multifunctional polar vinyl monomers, since their successful chemoselective and stereoselective polymerization would produce densely functionalized and stereoregular materials with interesting mechanical and physical properties. However, significant challenges exist in such cases as polymerization incompatibilities may arise either from the inability of the chiral catalyst to distinguish between two polymerizable groups or the presence of a competing functional group in the monomer chemical structure. The former case is exemplified by the employment of divinyl polar monomers, where the catalysts must select between the methacrylic (conjugated) C=C and the non-conjugated C=C for obtaining lineal and soluble polymers with controlled molecular weights and narrow molecular weight distributions (Figure 1.1). The later case is explored by the investigation of biorenewable dialkyl itaconates and itaconic anhydride, which contain two ester groups capable of coordinating to the active cationic Zr metal center and potentially competing for such coordination during the polymerization propagation "catalytic" cycle.

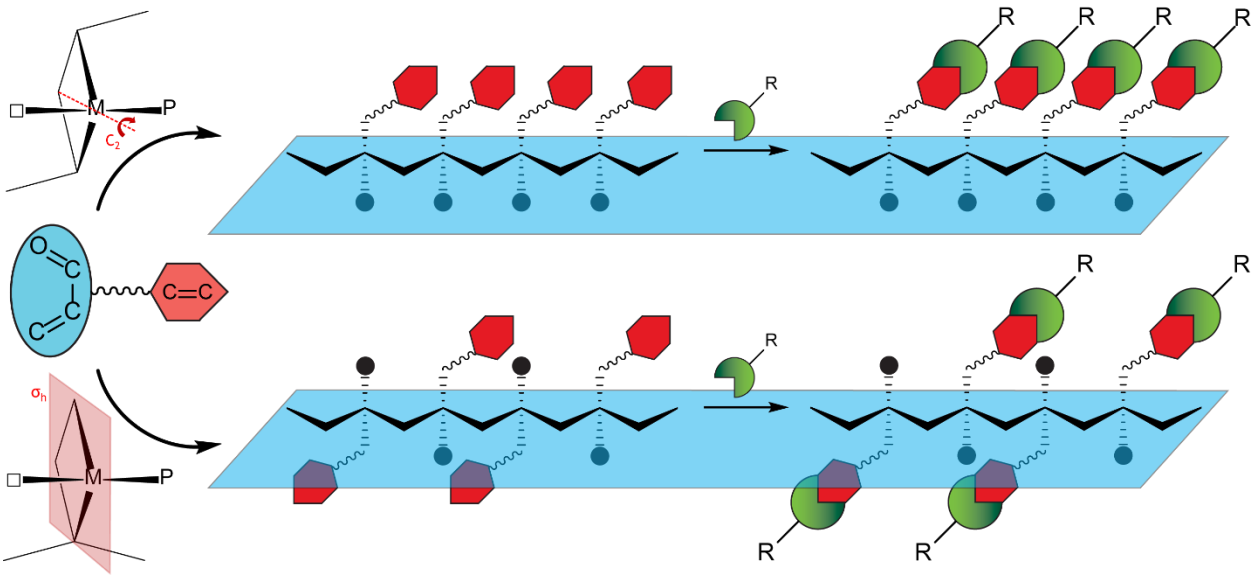

Figure 1.1. Chemo- and stereoselective polymerization of multifunctional polar vinyl monomers leads to stereoregular functional materials that can be subsequently post-functionalized.

The results of these fundamental investigations are discussed in detail in the following chapters:

2) Chemoselective, Stereospecific, and Living Polymerization of Polar Divinyl Monomers by Chiral Zirconocenium Catalysts
3) Robust Crosslinked Stereocomplexes and C_{60} Inclusion Complexes of Vinyl-Functionalized Stereoregular Polymers Derived from Chemo/Stereoselective Coordination Polymerization
4) Reactivity of Bridged and Nonbridged Zirconocenes towards Biorenewable Itaconic Esters and Anhydride
5) Precision Polymer Synthesis via Chemoselective, Stereoselective, and Living/Controlled Polymerization of Polar Divinyl Monomers

Chapter 2 reports the first successful polymerization of polar divinyl monomers that is simultaneously chemoselective, isospecific, *and* living at ambient temperature by using a cationic C_2-ligated *ansa*-zirconocenium ester enolate catalyst. The utilization of vinyl methacrylates and

acrylamides containing ester OR groups with different sterics and orientations (sp^2 vs sp^3 hybridized carbons) led to polymers with increased stereoregularity, from iso-enriched atactic, to highly isotactic, to perfectly isotactic polymers. Mechanistic studies, both synthetic and kinetic, were conducted to elucidate the origin of the observed perfect chemoselectivity and the high degree of control over the polymerization characteristics. The exploration of these new materials for post-functionalization was performed by both thiol-ene "click" derivatization to the corresponding thiolated polymers as well as thin-film casting and photocuring.

The chemoselective, syndiospecific, and controlled polymerization of polar divinyl monomers by a cationic C_S-ligated *ansa*-zirconocenium ester enolate catalyst is described in Chapter 3. Syndiotactic polymers with high to quantitative tacticity were obtained with the vinyl methacrylates and acrylamides, and mechanistic studies, including both experimental and theoretical, were presented to account for the observed high levels of stereocontrol. Apart from the extensive studies in the polymer post-functionalization, these stereoregular vinyl-functionalized polymers were also utilized in molecular recognition to obtain crystalline stereocomplexes and C_{60} inclusion complexes. The crosslinking of the pendant C=C bonds in those supramolecular structures afforded robust crosslinked materials with high trapping efficiency of the guest (macro)molecules.

In Chapter 4, an extensive investigation of the reactivity of two classes of zirconocenes (bridged and non-bridged) towards dialkyl ester itaconates and itaconic anhydride is described. Important similarities, but also notable differences, were found between these two classes of metallocene complexes in the first monomer insertion event and in the subsequent polymerization behavior towards other acrylic monomers. These results further highlight the *ansa*-effects in the metallocene polymerization chemistry and the importance of the formation and ring-opening of

the 8-membered chelating intermediates involved in the metallocene-mediated conjugate-addition polymerization.

Chapter 5 consists of a concise review and critical account in the field of the chemoselective polymerization of multifunctional polymers, with both metal-based and organocatalyzed polymerization methods. The post-functionalization of the corresponding polymeric materials is also described and compared.

All the experimental details, methods, materials characterizations, supporting figures, and additional tables corresponding to each of the individual chapters are consecutively included in Appendixes at the end of this dissertation. This arrangement keeps the consistency with the already published work and also provides a more readable organization of the research contents within the main chapters.

CHAPTER 2

Chemoselective, Stereospecific, and Living Polymerization of Polar Divinyl Monomers by Chiral Zirconocenium Catalysts[*]

2.1. Summary

This contribution reports the first chemoselective, stereospecific, and living polymerization of polar divinyl monomers, enabled by chiral *ansa*-zirconocenium catalysts through an enantiomorphic-site controlled coordination-addition polymerization mechanism. Silyl-bridged-*ansa*-zirconocenium ester enolate *rac*-(SBBI)Zr^{+}(THF)[OC(O^{i}Pr)=CMe_2][$MeB(C_6F_5)_3$]$^{-}$ [**2**, SBBI = (dimethyl)silyl-bis(benz[*e*]-η^5-indenyl)], has been synthesized and structurally characterized, but it exhibits low to negligible activity and stereospecificity in the polymerization of polar divinyl monomers including vinyl methacrylate (VMA), allyl methacrylate (AMA), 4-vinylbenzyl methacrylate (VBMA), and *N*,*N*-diallyl acrylamide (DAA). In contrast, ethylene-bridged-*ansa*-zirconocenium ester enolate *rac*-(EBI)Zr^{+}(THF)[OC(O^{i}Pr)=CMe_2] [$MeB(C_6F_5)_3$]$^{-}$ [**1**, EBI = ethylene-bis(η^5-indenyl)] is highly active and stereospecific in the polymerization of such monomers including AMA, VBMA and DAA. The polymerization by **1** is perfectly chemoselective for all four polar divinyl monomers, proceeding exclusively through conjugate addition across the methacrylic C=C bond while leaving the pendant C=C bonds intact. The polymerization of DAA is most stereospecific and controlled, producing essentially stereo-perfect isotactic PDAA with [*mmmm*] > 99%, M_n matching the theoretical value (thus a quantitative

[*] This dissertation chapter contains the manuscript of a full paper published in the *Journal of the American Chemical Society* [Vidal, F.; Gowda, R. R.; Chen, E. Y.-X. *J. Am. Chem. Soc.* **2015**, *137*, 9469-9480]. This work was supported by the National Science Foundation (NSF-1300267). We thank Boulder Scientific Co. for the research gift of $B(C_6F_5)_3$. R. R. Gowda carried out the synthesis and structural characterization of chiral metallocene complex **2**.

initiation efficiency), and a narrow molecular weight distribution ($Đ$ = 1.06–1.16). The stereospecificity is slightly lower for the AMA polymerization, but still leading to highly isotactic PAMA with 95–97% [*mm*]. The polymerization of VBMA is further less stereospecific, affording PVBMA with 90–94% [*mm*], while the polymerization VMA is least stereospecific. Several lines of evidence from both homo- and block-copolymerization results have demonstrated living characteristics of the AMA polymerization by **1**. Mechanistic studies of this polymerization have yielded a monometallic coordination-addition polymerization mechanism involving the eight-membered chelating intermediate. Post-functionalization of isotactic polymers bearing the pendant vinyl group on every repeating unit via the thiol-ene "click" reaction achieves a full conversion of all the pendant double bonds to the corresponding thioether bonds. Photocuring of such isotactic polymers is also successful, producing an elastic material readily characterizable by dynamic mechanical analysis.

2.2. Introduction

Since the discovery of Ziegler-Natta polymerization, metal-mediated coordination polymerization has evolved into arguably the most powerful technique for controlling the polymerization stereochemistry.[1] In the polymerization of vinyl monomers, the metal-mediated coordination polymerization can be categorized into coordination-insertion and coordination-addition polymerizations. The coordination-insertion polymerization is typically catalytic in both fundamental monomer enchainment and polymer chain production, and is applied to nonpolar olefins as well as copolymerization of nonpolar and polar olefins.[2] In comparison, the coordination-addition polymerization concerns conjugated polar olefins such as acrylics and is commonly living or quasi-living, thus non-catalytic in polymer chain production,[3] although the

catalytic coordination-addition polymerization of acrylics has recently been established by zirconocenium-hydridoborate ion pairs via a hydride-shuttling chain transfer mechanism.[4]

Polymers bearing active vinyl groups attached to the main chain can be readily post-functionalized through the retaining vinyl groups to a variety of useful functional materials.[5] However, polymerization of divinyl monomers with complete chemoselectivity by safeguarding one of the reactive vinyl groups while selectively polymerizing the other has been a challenging task. Vinyl methacrylates, such as allyl methacrylate (AMA) that exhibits a large reactivity difference (r_1/r_2 = 30) between the conjugated (r_1 = 1.8) and non-conjugated (r_2 = 0.06) vinyl groups, appear to be good candidates for achieving complete chemoselective polymerization, but its radical polymerization[6] still cannot maintain the chemoselectivity throughout the entire reaction process, especially in the later stage of the polymerization when additions to the pendant non-conjugated double bonds also occur, resulting in gelation due to formation of cross-linked network structures.[7] The radical polymerization of vinyl methacrylate (VMA, r_1 = 18, r_2 = 0.011) in the presence of a suitable aluminum Lewis acid achieved the chemoselectivity up to 85% monomer conversion to produce a soluble polymer,[8] and anionic polymerization of VMA showed high chemoselectivity.[9] For polar divinyl monomers with a similar reactivity for both vinyl groups such as 4-vinylbenzyl methacrylate (VBMA; r_1 = 1.04 for the methacrylic C=C bond and r_2 = 0.85 for the styrenic C=C bond), their radical polymerizations can lead to gelation even at the early stage of the reaction.[10] Group transfer polymerization of VBMA yielded PVBMA with a broad molecular weight distribution ($Đ$) of 8.2, due to polymerization of some styrenic double bonds as well.[11] Anionic polymerization of VBMA by resonance-stabilized initiators such as 1,1-diphenylhexyl lithium and trityl potassium was controlled and selective towards polymerizing the polar double bonds at –78 °C, but such desired characteristics were lost when the reaction was

carried out at higher temperatures (−20 °C or above).[12] Most recently, the complete chemoselective polymerization of AMA, VBMA and VMA has been achieved at room temperature (RT) utilizing the Lewis pair (LP) cooperativity in the LP polymerization[13] by *N*-heterocyclic carbene (NHC) and *N*-heterocyclic carbene olefin (NHO) based LPs consisting of NHC/$B(C_6F_5)_3$[14] and NHC or NHO/$Al(C_6F_5)_3$,[10] producing uncross-linked, soluble functional polymers with $Đ$ <1.6.

Ideally, polymerization of such polar divinyl monomers should be not only chemoselective, but also stereospecific and living, thus offering an opportunity to synthesize advanced functional polymeric materials with both well-controlled chain structures and stereochemistry, two essential features affecting the physical and mechanical properties of the polymers. To meet this challenge, we hypothesized that chiral *ansa*-zirconocenium ester enolate complexes, which are known to polymerize alkyl methacrylates[15,16] and acrylamides[17] in a stereospecific and living fashion, should be chemoselective, stereospecific, and living in polymerization of polar divinyl monomers, due to their catalyst site-controlled coordination-addition mechanism that should involve exclusive conjugate addition across the methacrylic double bond that is most activated via coordination of the conjugated carbonyl to the cationic Zr center, thus leaving the pendant C=C bonds intact (Figure 2.1). Such well-defined polymers could be post-functionalized via the thiol-ene "click" reaction[18] and/or photocuring to advanced functional materials.

2.3. Results and Discussion

Synthesis and Structure of *rac*-(SBBI)Zr^+(THF)[$OC(O^iPr)=CMe_2$][$MeB(C_6F_5)_3$]$^-$ (2). Chiral ethylene-bridged-bis(indenyl)-*ansa*-zirconocenium ester enolate *rac*-(EBI)Zr(THF)-[$OC(O^iPr)=CMe_2$]$^+$ [$MeB(C_6F_5)_3$]$^-$ [**1**, EBI = ethylene-bis(η^5-indenyl)][15] has been a workhorse catalyst for stereospecific and living coordination-addition polymerization of polar conjugated

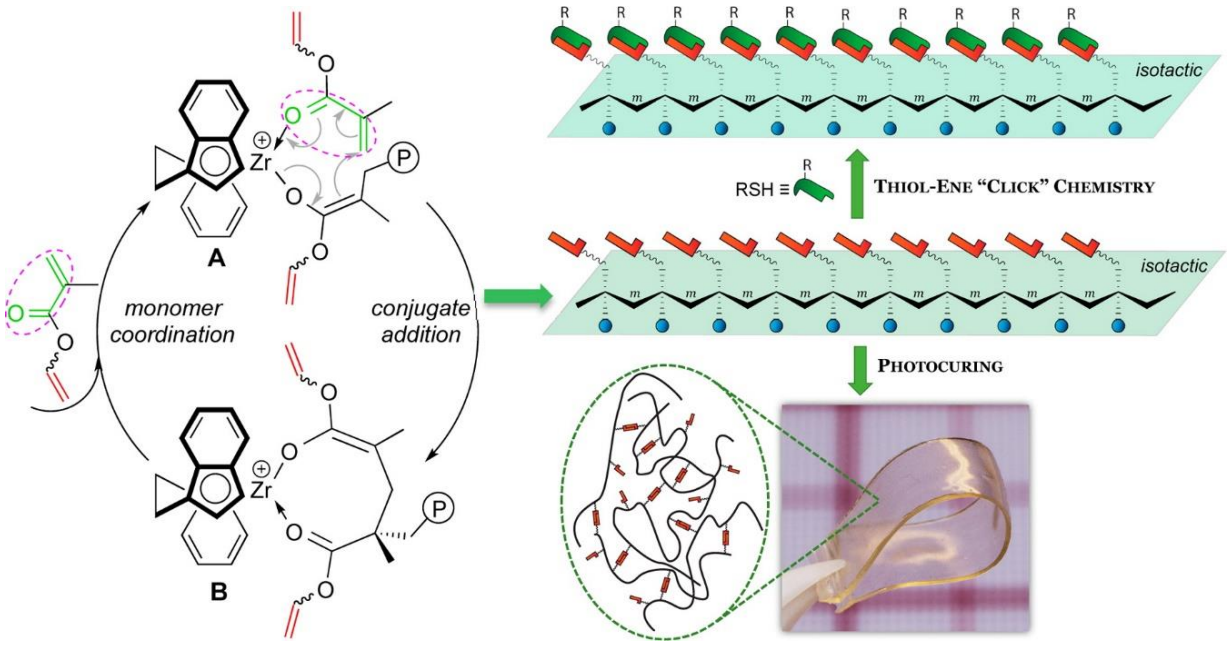

Figure 2.1. Schematic representation of the *hypothesis* for isotactic acrylic polymers carrying pendant vinyl groups to be synthesized by stereospecific coordination-addition polymerization of polar divinyl monomers with chiral zirconocenium catalysts and subsequently post-functionalized via the thiol-ene "click" reaction and photocuring to advanced functional materials.

alkenes or *α*,*β*-unsaturated esters and amides (acrylic monomers), which enabled the synthesis of highly isotactic poly(methacrylate)s,[15,16] poly(acrylamide)s,[17] poly(*β*-methyl-*α*-methylene-*γ*-butyrolactone),[19] as well as optically active helical poly(*N*,*N*-diarylacrylamide)s.[20] In the case of the coordination-insertion polymerization of propylene, it has been shown that catalysts based on silyl-bridged-bis(substituted indenyl)-*ansa*-zircononcenes are superior to those ethylene-bridged analogues in both activity and stereospecificity.[21] Interestingly, for coordination-addition polymerization of methyl methacrylate (MMA), an opposite trend was observed, with the ethylene-bridged-bis(indenyl)-based catalyst producing PMMA having a higher isotacticity (96% *mm*) than that (90% *mm*) produced by the silyl-bridged-bis(indenyl)-based catalyst.[22] Hence, we were interested in examining if substituents on the indenyl rings could render a chiral silyl-bridged-*ansa*-zircononcenium ester enolate catalyst to exhibit superior catalytic performance to the

ethylene-bridged catalyst **1** in the coordination-addition polymerization of polar divinyl monomers.

Using the general procedure previously established for the synthesis of **1**,[15,16,23] Scheme 2.1 outlines the synthetic route to the new chiral, silyl-bridged-*ansa*-zirconocene ester enolate *rac*-(SBBI)Zr^{+}(THF) [$OC(O^{i}Pr)=CMe_2$][$MeB(C_6F_5)_3$]$^{-}$ [**2**, SBBI = (dimethyl)silyl-bis(benz[*e*]-η^5-indenyl)]. Starting from the neutral ligand bis[3,3'-(3-*H*-benz[*e*]indenyl)]dimethylsilane,[21a] the corresponding C_2-chiral zirconocene amide complex, *rac*-(SBBI)$Zr(NMe_2)_2$, was prepared as orange crystals in 68% yield, using the modified procedure for the stereoselective amine-elimination approach to the ethylene-bis(indenyl) derivative, *rac*-(EBI)$Zr(NMe_2)_2$.[24] Next, alkylation of the amide complex with excess $AlMe_3$ led to the corresponding dimethyl complex *rac*-(SBBI)$ZrMe_2$. Treatment of the dimethyl derivative with Me_3SiOTf afforded the methyl triflate complex *rac*-(SBBI)ZrMe(OTf) as orange crystals, which was subsequently reacted with $Me_2C=C(O^{i}Pr)OLi$ to form the methyl ester enolate precatalyst, *rac*-(SBBI)ZrMe[$OC(O^{i}Pr)=CMe_2$] (pre-**2**) in 86% yield (Figure. S2.6). In the final step, the cationic ester enolate **2** was cleanly and quantitatively generated by *in situ* mixing of pre-**2** with $(C_6F_5)_3B\cdot THF$ in CD_2Cl_2 at RT (Figure. S2.7), following the procedure established for generation of cation **1**.[15,16] After methide abstraction by the borane, the methyl group downfield-shifted drastically in ^{1}H NMR from δ –0.78 ppm (C_7D_8) when attached to Zr in pre-**2** to δ 0.48 ppm (CD_2Cl_2) now attached to B of the anion [$MeB(C_6F_5)_3$]$^{-}$ in **2**; this chemical shift is identical to that observed in cation **1**[15] and nearly identical to that reported for the unassociated, free [$MeB(C_6F_5)_3$]$^{-}$ anion (δ 0.51 ppm in CD_2Cl_2).[25] The non-coordinating nature of the anion [$MeB(C_6F_5)_3$]$^{-}$ in **2** is also established by the ^{19}F NMR spectrum in which a small chemical shift difference of < 3 ppm

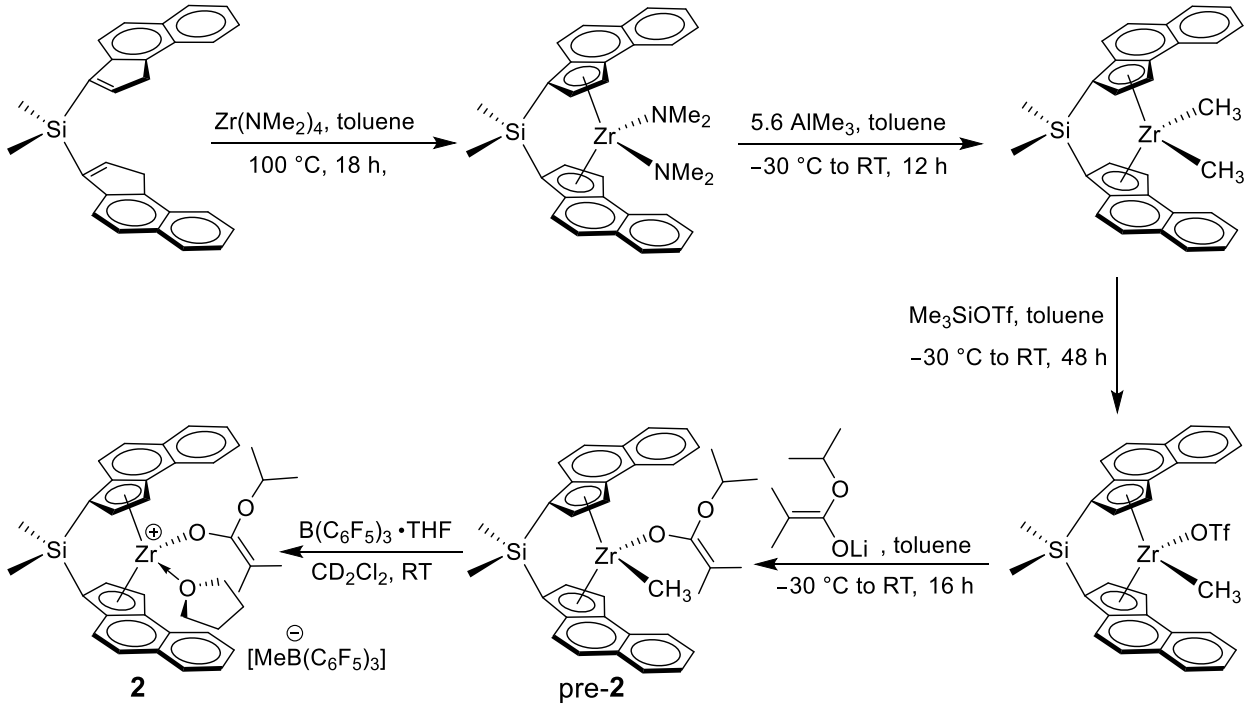

Scheme 2.1. Synthetic route to *rac*-(SBBI)Zr^{+}(THF)[OC(O^{i}Pr)=CMe_2][$MeB(C_6F_5)_3$]$^{-}$ (**2**).

between the *para*- and *meta*-fluorines is diagnostic of the non-coordinating [$MeB(C_6F_5)_3$]$^{-}$ anion[25,26] [Δ(*m*,*p*-F) = 2.6 ppm in **2**].

Single crystal X-ray diffraction analysis confirmed the molecular structure of **2** as depicted in Scheme 2.1, featuring the unassociated ion pair consisting of the THF-stabilized zirconocene ester enolate cation and the methyl borate anion (Figure 2.2). The coordinated THF is datively bonded to Zr with a Zr(1)–O(1) distance of 2.202(16) Å, whereas the ester enolate ligand is covalently bonded to Zr with a Zr(1)–O(2) distance of 1.943(15) Å. The C(50)=C(51) double bond in the ester enolate moiety is characterized by a bond distance of 1.332(3) Å and sums of the angles 359.9º and 360.0º around C(50) and C(51), respectively, for sp^2-hybridized C(50) and C(51) with a trigonal-planar geometry. The average B–C(aryl) distance (1.661 Å) is identical to that observed in the non-coordinating [$MeB(C_6F_5)_3$]$^{-}$ anion,[25] but the B–C(methyl) distance [1.641(4) Å] is

slightly shorter than that [1.663(5) Å] reported for the $[MeB(C_6F_5)_3]^-$ anion that is still coordinated to the cationic Zr center.[27]

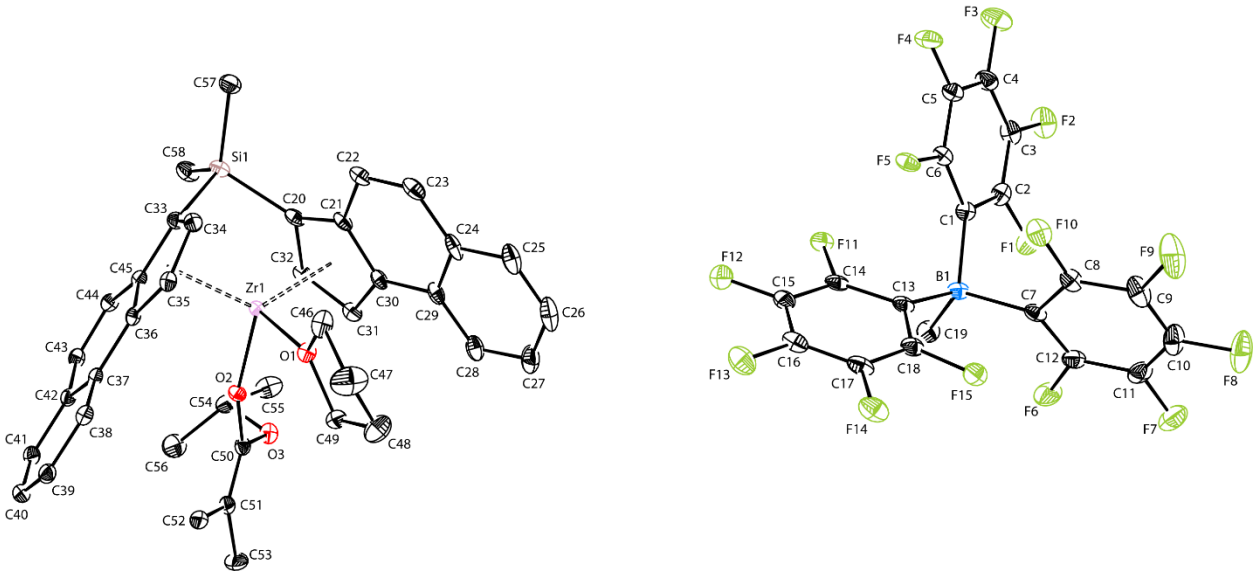

Figure 2.2. X-ray crystal structure of *rac*-(SBBI)Zr^+(THF)[OC(O^{i}Pr)=CMe_2][$MeB(C_6F_5)_3$]$^-$ (**2**) with thermal ellipsoids drawn at the 40% probability. Selected bond lengths (Å) and angles (°): Zr(1)–O(1) 2.202(16), Zr(1)–O(2) 1.943(15), Zr(1)–Cp(1) 2.537(av.), Zr(1)–Cp(2) 2.552(av.), C(50)–C(51) 1.332(3), B(1)–C(1) 1.675(4), B(1)–C(7) 1.650(4), B(1)–C(13) 1.659(4), B(1)–C(19) 1.641(4); O(2)–Zr(1)–O(1) 92.69(6), C(1)–B(1)–C(7) 103.4(2), C(1)–B(1)–C(13) 113.1(2), C(7)–B(1)–C(13) 113.1(2).

Polymerization Characteristics of Polar divinyl Monomers by Chiral Zirconocene Catalysts. Previous reports from our group have shown that the polymerization of acrylic monomers such as alkyl methacrylates and *N*,*N*-dialkyl or diaryl acrylamides by cationic, C_2-ligated chiral *ansa*-zirconocene complexes such as **1** is isospecific and living, which proceeds through a monometallic, catalyst-site-controlled coordination-addition polymerization mechanism via eight-membered-ring ester or amide enolate intermediates.[15,16,17,19,20] In this work, we utilized such isospecific catalysts to polymerize acrylic monomers carrying a pendant C=C double bond, including VMA, AMA, VBMA, and *N*,*N*-diallyl acrylamide (DAA), aiming to achieve the chemoselective, stereospecific, and living polymerization of such monomers (Figure 2.3).

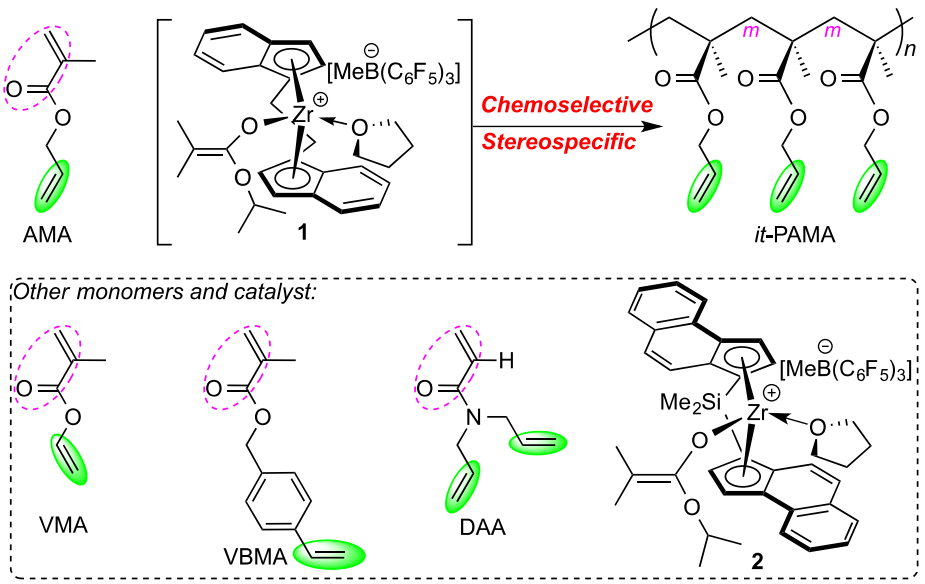

Figure 2.3. Chemoselective and stereospecific polymerization of polar divinyl monomers and structures of monomers, catalysts, and polymers (only one example shown).

Selected results for the polymerization of the four representative polar divinyl monomers by catalyst **1**, which is generated by *in-situ* mixing of *rac*-(EBI)ZrMe[OC(O^{i}Pr)=CMe$_2$] (pre-**1**) and $(C_6F_5)_3B{\cdot}THF$ in CH_2Cl_2 or toluene at RT,[15,16] are summarized in Table 2.1. First, control experiments were performed by mixing each monomer (200 equiv.) with the pre-**1** and the activator $(C_6F_5)_3B{\cdot}THF$ individually in CH_2Cl_2, followed by stirring each mixture at RT for 24 h. No monomer conversion or gel formation was detected from those control runs, indicating that neither the neutral precatalyst nor the activator itself can promote the polymerization. Second, initial polymerization scanning revealed that the cationic **2** exhibited low stereospecificity even for the parent monomer MMA and low to negligible activity for polymerization of the current polar divinyl monomers (Table S2.1). Hence, the subsequent polymerization studies focused exclusively on catalyst **1**.

Table 2.1. Selected results of polymerization of polar divinyl monomers by catalyst **1**[a]

run no.	M	[M]/[**1**]	solvent	time (min)	conv.[b] (%)	M_n[c] (kg/mol)	$Đ$[c] (M_w/M_n)	[*mm*][d] (%)	[*mr*][d] (%)	[*rr*][d] (%)	T_g[e] (°C)
1	VMA	100	DCM	5	99	20.6	1.18	50.9	29.6	19.5	44.5
2	VMA	200	DCM	10	99	35.7	1.18	51.4	28.8	19.8	44.2
3	VMA	400	DCM	15	97	64.0	1.29	52.8	28.0	19.2	49.0
4	AMA	48	Tol	5	97	8.50	1.19	95.6	2.9	1.5	−13.0
5	AMA	97	Tol	7	95	15.5	1.18	95.5	3.0	1.5	−5.7
6	AMA	193	Tol	15	93	33.2	1.19	95.8	2.8	1.4	−2.7
7	AMA	300	Tol	45	97	43.8	1.18	97.0	2.0	1.0	−0.3
8	AMA	400	Tol	90	96	59.8	1.25	96.3	2.5	1.2	0.0
9	VBMA	100	DCM	15	75	15.3	1.18	90.0	6.4	3.6	44.5
10	VBMA	100	DCM	30	95	31.3	2.94	90.0	6.9	3.1	48.2
11	VBMA	100	Tol	30	99	27.1	3.03	93.6	4.3	2.1	57.0
12	VBMA	200	Tol	60	75	30.0	1.42	92.8	4.8	2.4	61.0
13	DAA	101	DCM	30	99	18.3	1.06	> 99	–	–	–
14	DAA	202	DCM	120	97	30.2	1.16	> 99	–	–	–

[a] Conditions: solvent (DCM = CH_2Cl_2 or Tol = toluene) = 5 mL; ambient temperature (~23 °C). n.d. = not determined. [b] Monomer (M) conversion measured by ^{1}H NMR. [c] Number-average molecular weight (M_n) and polydispersity ($Đ$) determined by gel-permeation chromatography (GPC) relative to poly(methyl methacrylate) standards. [d] Tacticity measured by ^{1}H or ^{13}C NMR in $CDCl_3$. [e] Glass-transition temperature (T_g) measured by differential scanning calorimetry (DSC).

Next, we examined the polymerization of VMA in [VMA]/[**1**] ratios ranging 100–400 or with 1.0–0.25 mol% catalyst loadings (runs 1–3, Table 2.1). These reactions were homogeneous in CH_2Cl_2 and proceeded to high conversions (>99%) without signs of gel formation. The polymerizations were rapid, achieving quantitative or near quantitative conversion in short times (5–15 min). The number-average molecular weight (M_n) of the resulting PVMA increased from 20.6 kg/mol to 35.7 kg/mol to 64.0 kg/mol with an increase in the [VMA]/[**1**] ratio from 100 to 200 to 400, respectively, while the molecular weight distribution remained relatively narrow ($Đ$ = 1.18–1.29, Figure 2.4), showing some characteristics of a living polymerization. The PVMA materials produced by **1** are completely soluble in common organic solvents such as $CHCl_3$, toluene and DMF, showing no signs of crosslinking. The materials exhibited a glass-transition temperature (T_g) between 44 and 49 °C and showed an onset decomposition temperature (T_d) of

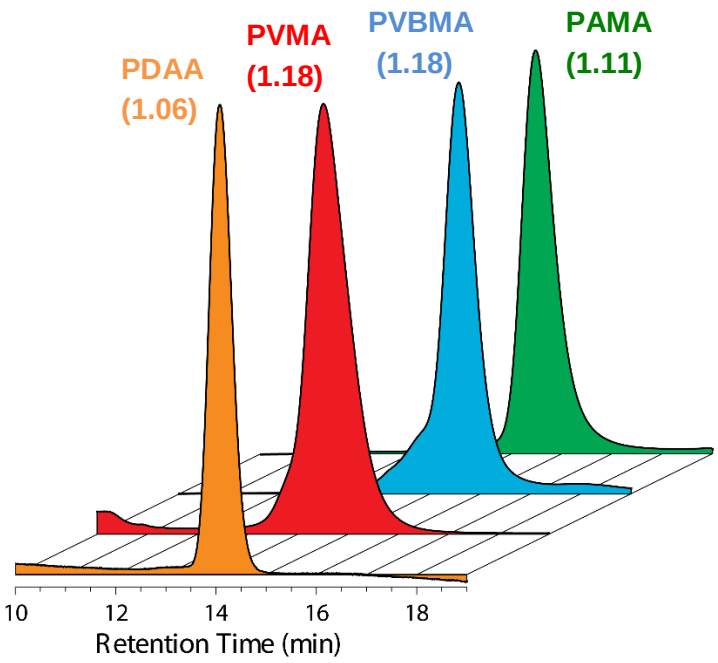

Figure 2.4. Representative GPC traces of the polymers produced and associated *Đ* values.

279 °C and a two-step decomposition window accompanied by two maximum rate decomposition temperatures (T_{max}) of 324 °C and 411 °C (Figure S2.2). Significantly, ^{1}H NMR spectrum of the isolated PVMA revealed complete disappearance of the methacrylic =CH_2 proton signals at δ 6.23 and 5.68 ppm and complete retention of the pendant vinyl group –CH=CH_2 proton signals centered at δ 4.88, 4.60 and 7.14 ppm (Figure S2.13), indicating that the polymerization proceeded exclusively through conjugate addition across the methacrylic double bond. However, the PVMA produced is only an isotactic-biased material, with [*mm*] = 51–53%. In comparison, polymerization of alkyl methacrylates such as *n*-butyl methacrylate by catalyst **1** produces highly isotactic polymer with [*mm*] up to 99%.[15] In short, the coordination-addition polymerization of VMA by catalyst **1** is controlled and chemoselective, but it lacks high stereospecificity thus producing only iso-biased PVMA.

In sharp contrast, the polymerization of AMA by catalyst **1** is not only controlled and completely chemoselective but also highly stereospecific. Thus, varying the [AMA]/[**1**] ratio from

48 to 400 (runs 4–8, Table 2.1), the polymerization in toluene achieved high conversions and produced the corresponding PAMA with gradually increased M_n from 8.5 kg/mol to 59.8 kg/mol while the $Đ$ remained narrow (from 1.11 to 1.25, Figure 2.4). The initiation efficiency [I^* = M_n(calcd)/M_n(exptl), where M_n(calcd) = MW(M) × [M]/[**1**] × conv (%) + MW of chain-end groups] of this polymerization was relatively high (71–84%). The isolated PAMA is soluble in common organic solvents and exhibited a T_g ranging from –13 °C to 0 °C which gradually increased as M_n increased (runs 4–8, Table 2.1). This polymer is rather stable if stored at RT in the dark, but crosslinking occurred within 24 h of exposure to ambient laboratory light conditions, after which addition of $CHCl_3$ to the sample revealed the formation of insoluble cross-linked fractions. Hence, the samples of this polymer were stored in brown bottles at −20 °C to preserve the integrity of the polymer for further functionalization studies (*vide infra*). Polymerizations carried out in CH_2Cl_2 yielded PAMA materials with similar characteristics to those produced in toluene, but the activity was lower.

The chemoselectivity of the AMA polymerization by **1** is perfect, as evidenced by the complete retention of the vinyl groups (δ 5.91, 5.31 and 5.20 ppm in ^{1}H NMR, Figure 2.5). Significantly, the AMA polymerization is also highly stereospecific, producing *it*-PAMA with a high isotacticity of [*mm*] = 95–97% (Figure 2.5) and 2[*rr*]/[*mr*] = 1, indicative of the enantiomorphic-site controlled mechanism. Furthermore, the ^{13}C NMR spectrum of the polymer provided corroborated evidence for the formation of the highly isotactic *it*-PAMA (Figure. 2.6). It is intriguing that the placement of the sp^3-hybridized (bulkier) CH_2 group between the ester oxygen atom and the sp^2-hybridized (less bulky) vinyl moiety in the case of AMA had such a profound effect on the polymerization stereospecificity (relative to VMA without the CH_2 group), highlighting the importance of the sterics and orientation of the ester OR group of the methacrylate

monomer in the transition state structure that determines the stereospecificity of the metallocene-catalyzed polymerization.[28]

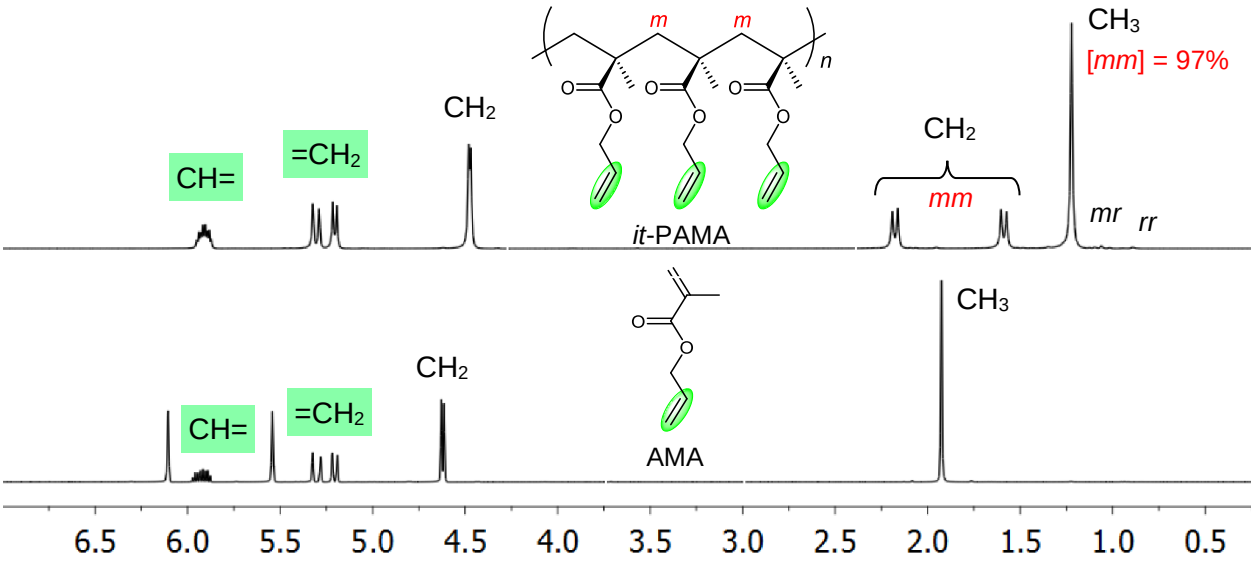

Figure 2.5. Overlay of ^{1}H NMR ($CDCl_3$, 25 °C) spectra of the monomer AMA and polymer *it*-PAMA.

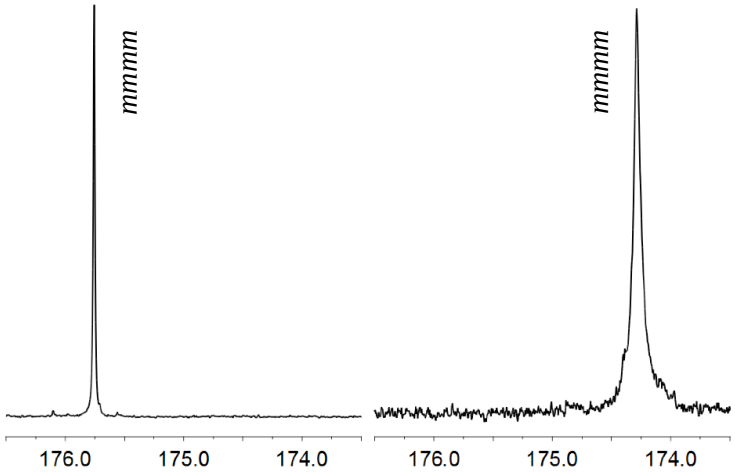

Figure 2.6. ^{13}C NMR spectra ($CDCl_3$, 50 °C) showing the C=O pentad (*mmmm*) region of the highly isotactic PAMA (left) and highly isotactic PDAA (right).

Chemoselective polymerization of VBMA is especially challenging for free radical or anionic polymerization, due to similar reactivity ratios between the methacrylic C=C bond (r_1 = 1.04) and styrenic C=C bond (r_2 = 0.84).[29] However, the metallocene-catalyzed coordination-addition polymerization readily promotes the chemoselective polymerization of VBMA. For example, the VBMA polymerization in a [VBMA]/[**1**] ratio of 100 in CH_2Cl_2 (runs 9–10) and toluene (run 11, Table 2.1) achieved high (95%) to almost quantitative (99%) conversion while maintaining a homogenous solution with no gelation or precipitation to yield completely soluble polymers. Subsequent analysis of the isolated material by ^{1}H NMR showed that the methacrylate vinyl protons (δ 5.57 and 6.14 ppm) completely disappeared while the vinylbenzyl moiety (δ 5.18, 5.65 and 6.61 ppm) was left intact (Figure S2.16). Note that the integration for the signals corresponding to the vinylbenzyl group matched with those of the main-chain aliphatic backbone, implying the vinylbenzyl moiety was retained in every repeating unit. Although the PVBMA obtained at 75% conversion had a narrow polydispersity $Đ$ = 1.18 (Figure 2.4) and a quantitative I* of 100% (run 9), the PVBMA produced at near quantitative conversions of 95% or 99% started to show much higher $Đ$ values of ~3, indicating possible polymerization of the styrenic moiety by the cationic catalyst after the complete or nearly complete conversion of the methacrylic C=C bond. In addition, thermal crosslinking of the isolated PVBMA can be observed even in the solid state when stored at RT. Indeed, analysis of PVBMA by differential scanning calorimetry (DSC) showed a thermal crosslinking exothermic peak with an onset temperature and a peak maximum of 119 °C and 164 °C, respectively. Importantly, the resulting PVBMA is isotactic, with [*mm*] = 90.0%–93.6%. A test of the polymer stereoerrors gave 2[*rr*]/[*mr*] = 1, confirming the same enantiomorphic-site controlled mechanism as that described for AMA polymerization.

The chemoselectivity and stereospecificity of catalyst **1** toward polymerization of polar divinyl monomers is further demonstrated by investigation into the polymerization characteristics of the acrylamide monomer DAA. Specifically, the polymerization with a [DAA]/[**1**] ratio of 101 in CH_2Cl_2 achieved 99% conversion in 30 min (run 13), producing the corresponding soluble PDAA with M_n = 18.3 and $Đ$ = 1.06 (Figure 2.4). The run at a higher [DAA]/[**1**] ratio of 202 in CH_2Cl_2 proceeded in a similar controlled fashion, affording PDAA with M_n = 30.2 and $Đ$ = 1.16 as well as a quantitative I* value of 99% (run 14). Although the activity of the DAA polymerization is the slowest of the series, quantitative or near quantitative DAA conversion can be achieved in all the tested ratios without any sign of polymer crosslinking or degradation in solution. PDAA showed a high T_d of 445 °C and a single decomposition window with a high T_{max} of 469 °C (Figure S2.5). Importantly, the quantitative chemoselectivity and stereospecificity of this polymerization were confirmed by the analysis of the ^{1}H (Figure S2.12) and ^{13}C NMR (Figure 2.6) spectra of the isolated material.

Livingness, Kinetics and Mechanism of Polymerization. Three lines of key evidence, summarized below using the AMA polymerization by **1** as an example, clearly showed living characteristics of this polymerization. First, the M_n of PAMA increased linearly (R^2 = 0.996) with an increase in the [AMA]/[**1**] ratio from 50 to 400 (Figure 2.7), while the $Đ$ remained narrow (from 1.11 to 1.25). Second, a plot of the polymer M_n vs. monomer conversion at a fixed $[AMA]_0/[\mathbf{1}]_0$ ratio 300 also gave a straight line (R^2 = 0.995), which was coupled with the small $Đ$ values (Figure 2.8). Third, block copolymerizations by **1** allowed the synthesis of the well-defined block copolymers PMMA-*b*-PAMA and PMMA-*b*-PDAA with unimodal, narrow MW distributions ($Đ$ = 1.14–1.28). The block copolymerizations were started by polymerization of MMA (200 equiv., 100% conversion in 30 min), followed by AMA (200 equiv., 97% conversion, 60 min) or DAA

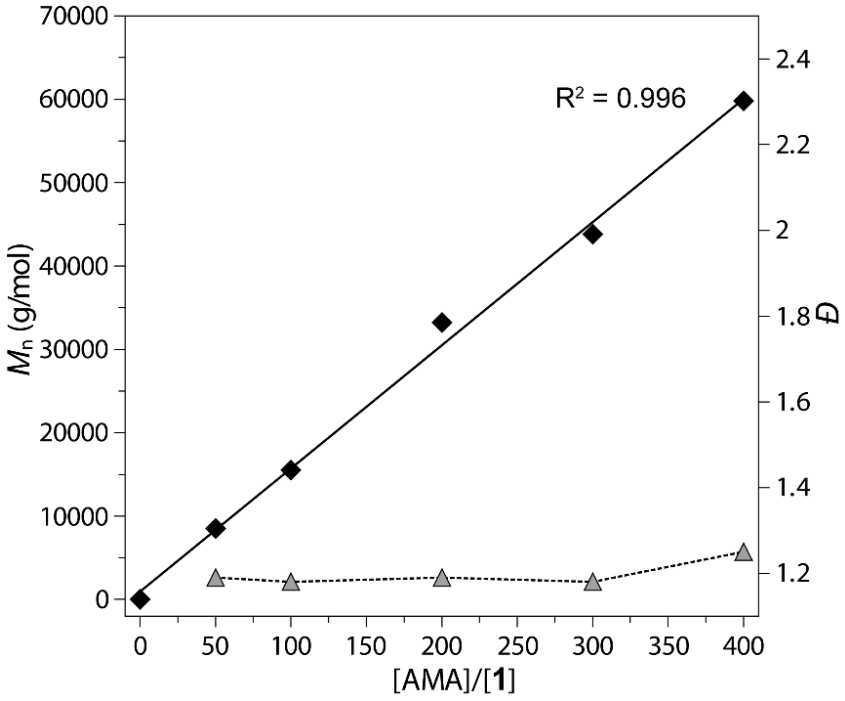

Figure 2.7. Plot of M_n and $Đ$ of *it*-PAMA produced by **1** vs. $[AMA]_0/[\mathbf{1}]_0$ ratio (toluene, 23 °C).

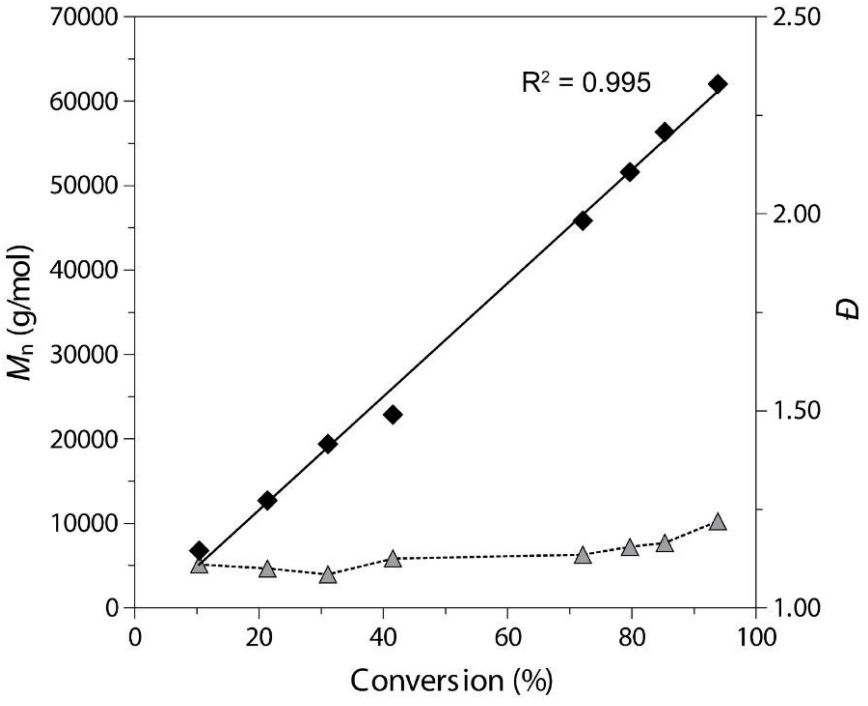

Figure 2.8. Plot of M_n and $Đ$ of *it*-PAMA produced by **1** vs. monomer conversion with a $[AMA]_0/[\mathbf{1}]_0$ ratio of 300 (toluene, 23 °C).

(200 equiv., 99% conversion, 120 min) polymerization, producing in both cases well-defined block copolymers PMMA-*b*-PAMA ($Đ$ = 1.28) and PMMA-*b*-PDAA ($Đ$ = 1.14). The measured M_n's of the resulting PMMA-*b*-PAMA and PMMA-*b*-PDAA were 65.6 kg/mol and 69.8 kg/mol, respectively, corresponding to an I^* value of ~70% for both cases. As a quantitative or near quantitative conversion was achieved for both monomers in the block copolymerization, the molar composition of the block copolymers measured by ^{1}H NMR was the same as the molar feed ratio (1:1). Also as expected, two T_g's were observed for PMMA-*b*-PAMA, characteristic of each of the component segments: $T_g(1)$ = 56.6 °C for the *it*-PMMA block, $T_g(2)$ = 6.5 °C for the *it*-PAMA block. Both block copolymers are also highly isotactic, similar to their respective isotactic homopolymers. It is worth noting here that reversing the addition sequence of both block copolymerizations resulted in formation of either a block-/homopolymer mixture or only a homopolymer, due to a change of the basicity and the coordination strength to the metal center of the incoming monomer relative to the last coordinated monomer unit in the chelating catalyst resting state (e.g., **B** in Figure 2.1), which determines whether the second monomer can ring-open the chelate to be polymerized or not, characteristic of the metallocene-mediated coordination-addition block copolymerization (i.e., monomers can only be copolymerized in order of increasing coordination strength).[3a,17]

Next, we examined the kinetics of AMA polymerization by catalyst **1**, revealing the polymerization is first-order with respect to monomer concentration [AMA] for all the $[AMA]_0/[\mathbf{1}]_0$ ratios investigated (48 to 322, Figure 2.9). A double logarithm plot (Figure 2.10) of the apparent rate constants (k_{app}), obtained from the slopes of the best-fit lines to the plots of $\ln([AMA]_0/[AMA]_t)$ vs. time, as a function of $\ln[\mathbf{1}]_0$, was fit to a straight line (R^2 = 0.995) with a slope of 1.1. Thus, the kinetic order with respect to [**1**], given by the slope of ~ 1, reveals that the

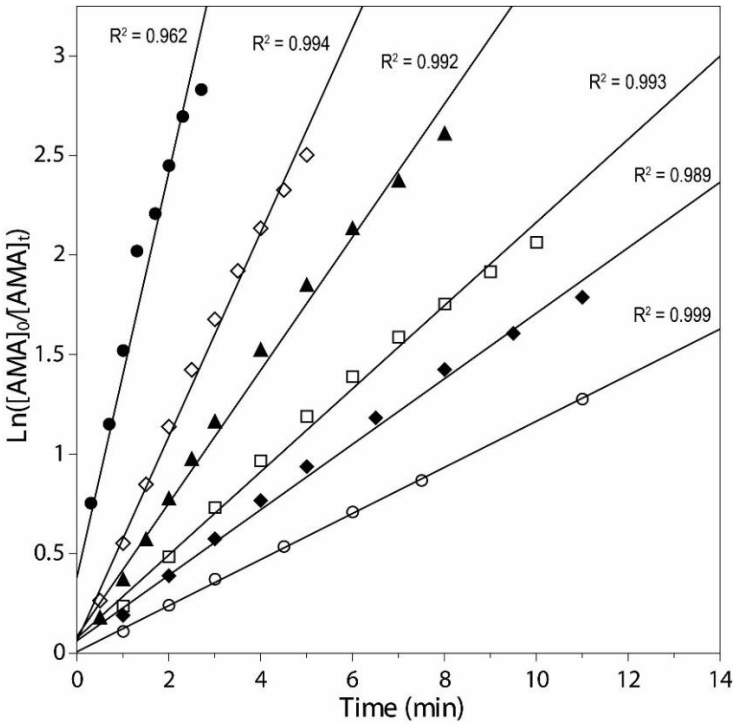

Figure 2.9. Semilogarithmic plots of ln{$[AMA]_0/[AMA]_t$} vs. time for the polymerization of AMA by **1** in toluene at 23 °C. Conditions: $[AMA]_0$ = 0.697 M; $[\mathbf{1}]_0$ = 14.44 mM (●), 7.22 mM (◊), 5.41 mM (▲), 3.61 mM (□), 2.89 mM (♦), 2.16 mM (○).

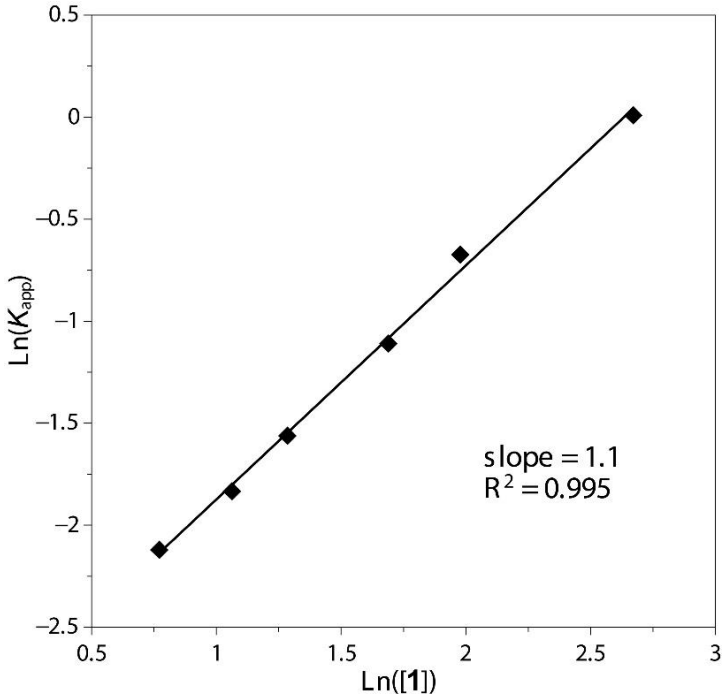

Figure 2.10. Plot of ln(k_{app}) vs. ln[**1**] for the AMA polymerization by **1** in toluene at 23 °C.

propagation is also first order in catalyst concentration. These results indicate that the resting state in the proposed monometallic propagation "catalysis" cycle (Scheme 2.2) is the cyclic ester enolate **B**, which was structurally modeled by the isolated cationic cyclic ester enolate complex **3** (*vide infra*), and that associative displacement of the coordinated ester group by incoming monomer to regenerate the active species **A** is the rate-determining step (i.e., **B** → **A**, Scheme 2.2). These key features of the mechanism are the same as those already shown for the coordination-addition polymerization of alkyl methacrylates.[15,16]

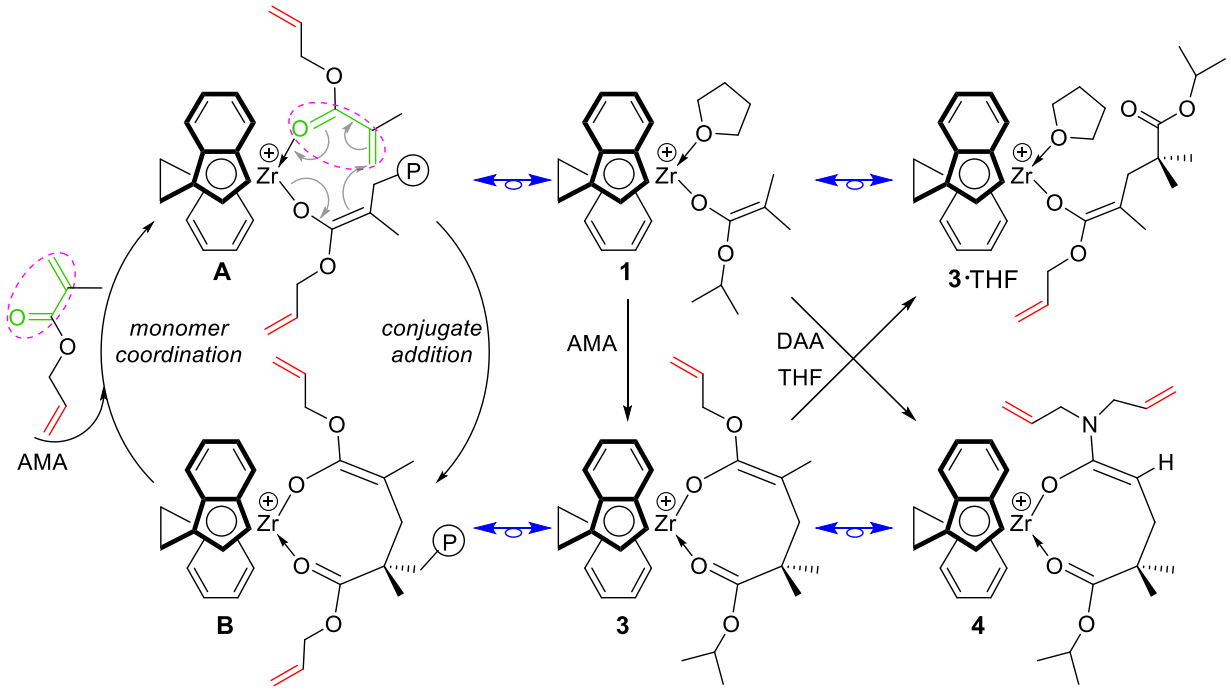

Scheme 2.2. Proposed mechanism (propagation catalysis cycle) for the chemoselective and stereospecific polymerization of AMA by *rac*-**1** as well as structures of **1**, **3**, **3**·THF, and **4** as synthetic structural models for active species **A** and resting state chelate **B**.

The above-proposed mechanism suggests the possibility to isolate the first-monomer-addition product **3** serving as the structural model of the resting intermediate **B**, since the monomer addition is fast relative to the monomer coordination in the propagation "catalysis" cycle depicted in Scheme 2.2. Accordingly, we carried out the stoichiometric reaction between the cationic ester enolate **1** (itself also a structural model for the active species **A**) and one equivalent of AMA in

CD_2Cl_2 at RT. Monitoring the reaction by ^{1}H NMR revealed rapid consumption of AMA upon its addition, but the signals corresponding to Zr species suggested coexistence of two separate species, **3** and **3**·THF (Figure S2.8). Signals characteristic of **3** are a septet at δ 4.36 ppm for –OC*H*Me$_2$ of the coordinated isopropyl ester group [–C(O^{i}Pr)=O], a sharp singlet at δ 1.64 ppm for =C*Me*, and two doublets at δ 1.43 and 1.32 ppm for –OCH*Me*$_2$. The chemoselective Michael addition of AMA is confirmed by the observation of the fully intact allyl group in **3** with its characteristic signals at δ 5.87, 5.29, 5.23, and 3.83 ppm. However, the color of the mixture changed from bright red to orange upon standing at RT for several hours, indicating the spontaneous evolution of the reaction. Indeed, the ^{1}H NMR spectrum confirmed the formation of **3**·THF as the major product, which corresponds to the cleavage (opening) of the eight-membered chelate in **3** by the free THF present in the solution, as evidenced by the observations of: (a) the markedly downfield shifting of –OC*H*Me$_2$ from δ 4.36 in **3** to 4.96 ppm in **3**·THF for the non-coordinated isopropyl ester group; (b) the upfield shifting of signals corresponding to the coordinated THF molecule in **3**·THF (δ 3.66 and 3.52 ppm for α-CH_2, δ 1.87 ppm for β-CH_2, vs. signals at δ 3.88 and 1.96 ppm for the free THF); and (c) the appearance of only one doublet for –OCH*Me*$_2$ of the non-coordinated isopropyl ester group, which was also upfield shifted from the coordinated analogue to δ 1.25 ppm.

Being isostructural to complex **1** and active species **A**, complex **3**·THF was isolated in the preparative scale as a bright yellow powder. The coordinated THF molecule was not removed even after extensive drying *in vacuo* for 8 h at RT or heating at 80 °C for 1 h in C_6D_5Br, indicating the strong coordination of THF to the cationic Zr center; the bound THF was not displaced by the added AMA, explaining the inability of this species to polymerize AMA. The polymerization of AMA by **1** was completely shut down when carried out in THF. On the other hand, the discrete complex **3** can be generated by *in situ* mixing of AMA·B(C_6F_5)$_3$ and *rac*-

(EBI)ZrMe[OC(O^{i}Pr)=CMe$_2$] in the absence of THF. A kinetic competence check was performed by addition of 10 equivalents of AMA to the *in situ* generated **3**, which was accompanied by instantaneous formation of *it*-PAMA, thereby confirming the role of **3** as the resting propagating intermediate in the polymerization of AMA by catalyst **1**.

Isolation of the chelating amide enolate intermediate **4** derived from the stoichiometric reaction of **1** and DAA went more smoothly, thanks to its thermal stability and the inability of THF to ring-open the chelate, thus cleanly generating the spectroscopically and analytically pure product **4**. Multi-nuclear (Figure 2.11, Figure S2.9) and multi-dimensional (Figures S2.10 and S2.11) NMR spectra are consistent with the proposed structure, analogous to the previously isolated eight-membered chelate from the reaction of **1** and *N*,*N*-dimethylacrylamide.[17] Notably, the ^{1}H NMR signal for –OC*H*Me$_2$ (δ 3.72 ppm, sept) attached to the enolate ligand in **1** is downfield shifted to δ 4.65 ppm for –OC*H*Me$_2$ now attached to an ester group in **4**, which is consistent with the ^{13}C NMR chemical shift differences for the *C*(O) carbon: 154.1 ppm for the enolate in **2** [O*C*-(O^{i}Pr)=] and δ 185.0 ppm for the ester in **4** [*C*(O^{i}Pr)=O]. More importantly, the chemoselective Michael addition of the monomer through the conjugated double bond is confirmed by the presence of the intact –N(CH$_2$CH=CH$_2$)$_2$ moiety in **4**, as evidenced by (a) ^{1}H NMR: δ 5.79 and 5.55 ppm (NCH$_2$C*H*=CH$_2$); δ 5.31, 5.24, and 5.11 ppm (NCH$_2$CH=C*H*$_2$); δ 3.91, 3.81, 3.64, and 3.32 ppm (NC*H*$_2$CH=CH$_2$)], and (b) ^{13}C NMR: δ 132.3 and 131.5 ppm (NCH$_2$*C*H=CH$_2$); δ 119.7 and 119.0 ppm (NCH$_2$CH=*C*H$_2$); δ 48.85 and 48.66 ppm (N*C*H$_2$CH=CH$_2$). The rotation of the allyl amide group around the OC–N bond on the ^{1}H NMR time scale at 25 °C explains the broadening of its signals, but the peaks are markedly sharper 0 °C. Another advantage of recording the ^{1}H NMR at 0 °C is the assignment of the C*H* signal on the 8-membered ring chelating ligand, which was not detectable at 25 °C due to the overlapping with the broad signals in the olefinic

region. At 0 °C the C*H* signal appeared at a much higher field than expected (1.23 ppm), as it was clearly shown by the correlation with the vicinal CH_2 protons in the 2D COSY (Figure S2.10). Moreover, the 2D HSQC NMR (Figure S2.11) supports the identification of the corresponding carbon signal in the ^{13}C NMR spectrum, which is also highly upfielded (37.69 ppm, Figure S2.9). These spectroscopic results suggest that, at lower temperatures, the C*H* moiety in complex **4** could be shielded by the *N*-allyl group (restricted rotation at 0 °C) or complex **4** could be stabilized by a resonance structure where the CH enolate carbon has a more negative charge distribution (i.e., π-allyl type structure). Nevertheless, a kinetic competence check on the isolated chelate **4** revealed that it polymerized 200 equivalents of DAA rapidly to produce PDAA with a narrow MW distribution of $Đ = 1.17$ and a high isotacticity of [*mm*] > 99%, similar to the polymerization started directly with catalyst **1**, thereby confirming the role of the amide enolate **4** as the resting propagating intermediate in the polymerization of DAA by catalyst **1**.

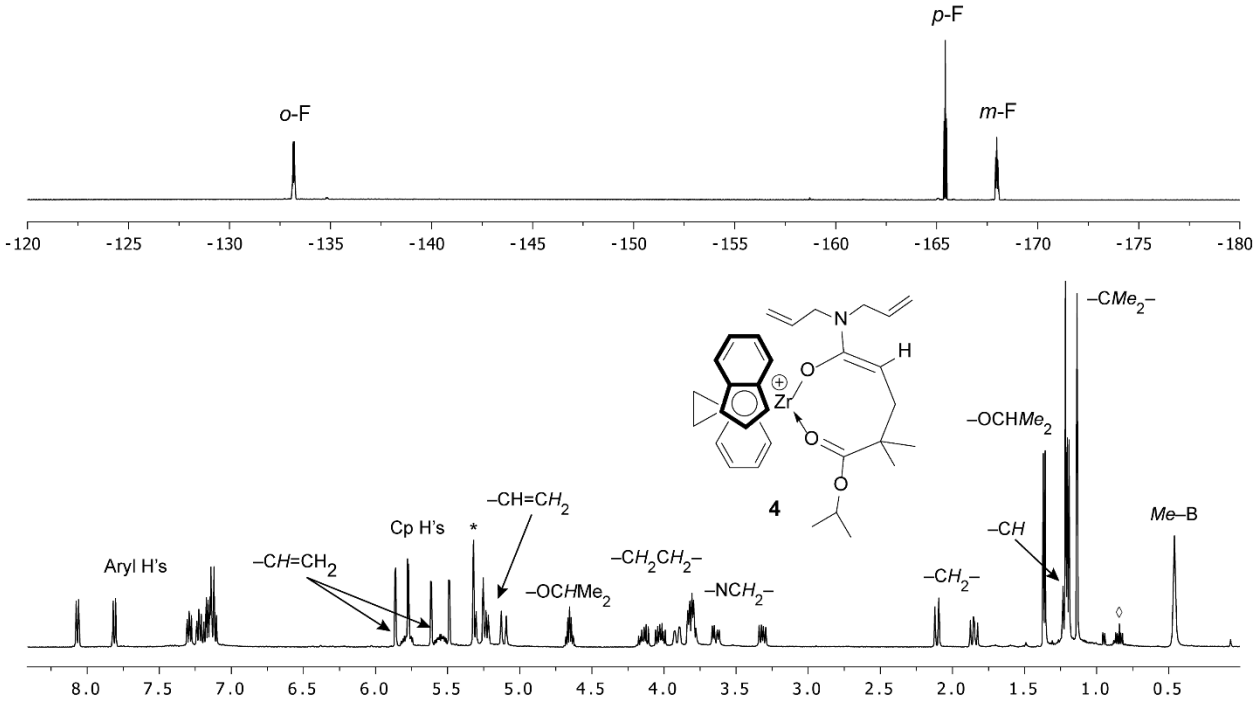

Figure 2.11. ^{1}H (bottom) and ^{19}F NMR (top) spectra (CD_2Cl_2, 0 °C) of the isolated **4**. Residual NMR and hexanes solvent peaks are labeled as * and ◊, respectively.

Post-Functionalization to Functional Materials. Post-functionalization of isotactic polymers bearing the pendant vinyl (–CH=CH_2) functional group on every repeating unit was performed through two approaches: the thiol-ene "click" reaction and photo-curing. The former approach has been widely used and proven to be highly effective for functionalization of ene-bearing polymers.[18] We first examined functionalization of *it*-PAMA (M_n = 59.8 kg/mol, $Đ$ = 1.25) and *it*-PDAA (M_n = 18.3 kg/mol, $Đ$ = 1.06) with two model thiols, 4-*tert*-butylbenzylmercaptan (RSH1) and 1-adamantanethiol (RSH2), using the click reaction with 2,2-dimethoxy-2-phenylacetophenone (DMPA) as the photoradical initiator under photochemical conditions (RT, UV lamp centered at 350 nm) in chloroform (Scheme 2.3). The efficiency of this reaction was monitored and confirmed by ^{1}H NMR (Figure 2.12), showing a full conversion of all the pendant double bonds in 2 h; this is evidenced by complete disappearance of the ^{1}H NMR signals corresponding to the olefinic protons in *it*-PAMA (δ 5.91, 5.31, and 5.20 ppm) and *it*-PDAA (δ 5.69 and 5.09 ppm) and appearance of new signals due to the formation of the C–SR bond, observed at δ 2.46 (*it*-PAMA-SR1), 2.57 (*it*-PAMA-SR2), 3.24 (*it*-PDAA-SR1), and 3.60–2.29 ppm (*it*-PDAA-SR2, overlapping with other peaks) for the thioether RSCH_2– protons. The stereochemistry of the resulting thiolated polymers was found to be identical to the parent polymers, with high isotacticity of >95% for *it*-PAMA-SR and >99% for *it*-PDAA-SR in all the cases. However, the thiolated PAMA-SR polymers, which are still soluble in common organic solvents, exhibited much higher MW and $Đ$ values (M_n = 190 kg/mol, $Đ$ = 9.42 for *it*-PAMA-SR1; M_n = 106 kg/mol, $Đ$ = 5.12 for *it*-PAMA-SR2), indicative of some degree of light crosslinking due to the non-selective radical initiation in the presence of the high concentration of reactive C=C pendant groups. On the other hand, *it*-PDAA underwent a much more controlled thiol-ene "click" functionalization, as the MW of the resulting thiolated polymer compares well with the calculated

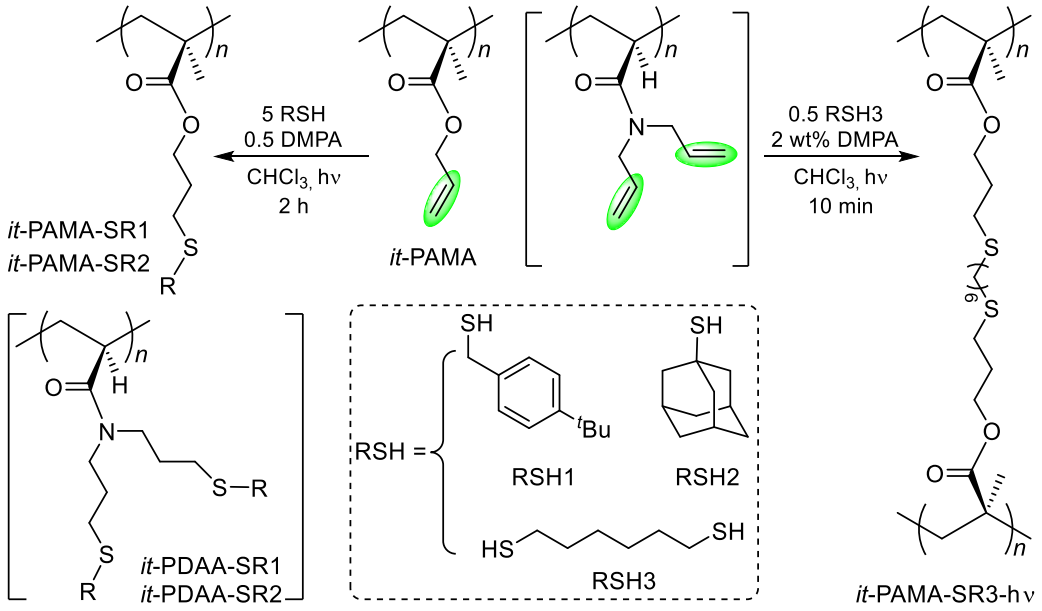

Scheme 2.3. Post-functionalization of *it*-PAMA and *it*-PDAA via the thiol-ene click chemistry.

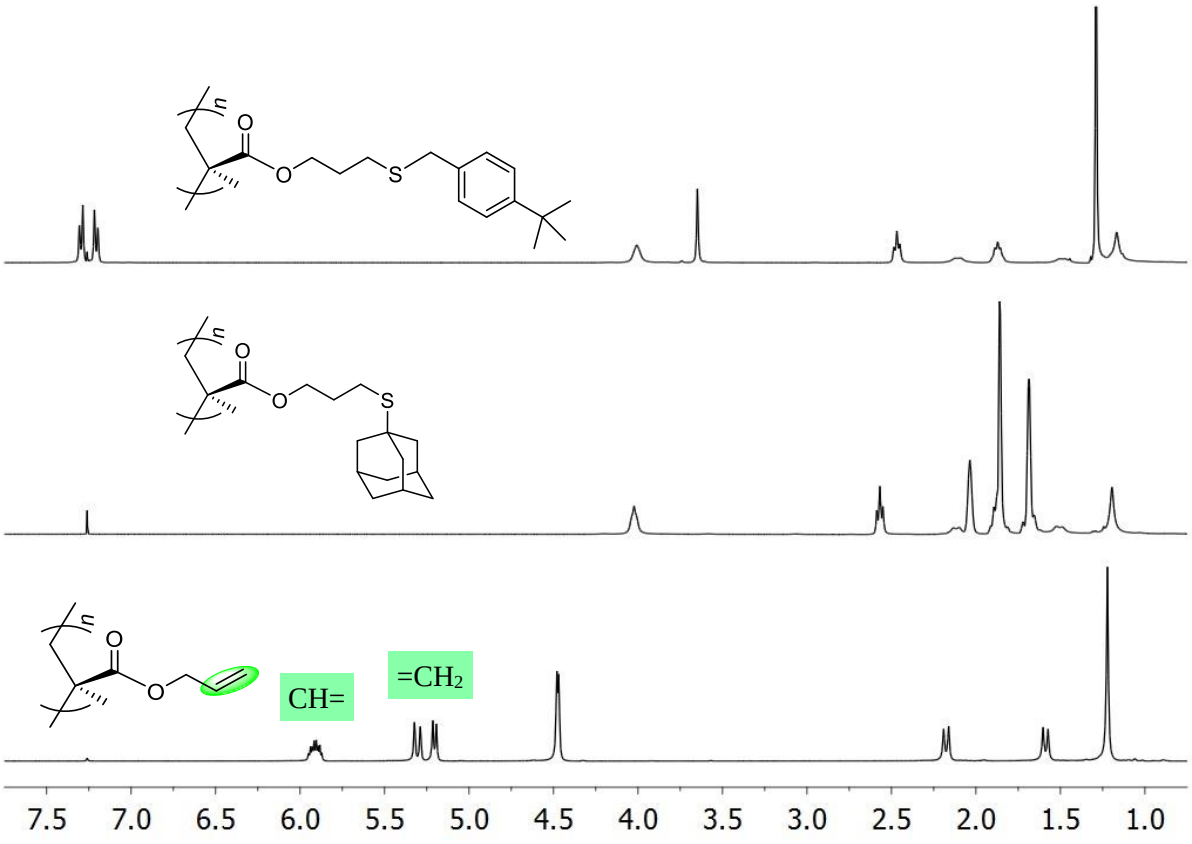

Figure 2.12. Overlay of ^{1}H NMR ($CDCl_3$, 23 °C) spectra of *it*-PAMA, *it*-PAMA-SR1, and *it*-PAMA-SR2.

value for both thiolate derivatives although the *Đ* values became larger after the thiol-ene reaction: M_n = 36.4 kg/mol (vs. the calculated M_n of 36.3 kg/mol) and *Đ* = 2.68 for *it*-PDAA-SR1; M_n = 36.2 kg/mol (vs. the calculated M_n of 35.1 kg/mol), *Đ* = 2.54 for *it*-PDAA-SR2. Worth noting here is that, when the functionalization was performed using the radical thermoinitiation (i.e., azobis(isobutyronitrile) as the initiator in 1,2-dichlorobenzene, at 70 °C for 24 h), the conversion of all pendant C=C bonds was complete, but the resulting polymer showed a much higher degree of crosslinking with formation of insoluble fractions.

To examine effects of the pendant group functionalization on the polymer thermal properties, the thiol-functionalized polymers were further characterized by thermal gravimetric analysis (TGA) and DSC, along with their parent polymers. The thiolated *it*-PAMA materials with both 4-*tert*-butylbenzylmercaptan (T_g = 22.1 °C) and 1-adamantanethiol (T_g = 85.5 °C) exhibited a much higher T_g than the parent *it*-PAMA (T_g = 0 °C); the decomposition onset temperature was also substantially enhanced from a T_d of 235 °C of the parent *it*-PAMA to a T_d of 306 and 347 °C of *it*-PAMA-SR1 and *it*-PAMA-SR2, respectively (Figure S2.4). While the parent *it*-PDAA showed no T_g on its DCS trace, the thiolated analogues *it*-PDAA-SR1 and *it*-PDAA-SR2 revealed a T_g of 42.9 and 146.1 °C, respectively, but a noticeable decrease in T_d from 445 °C of the parent *it*-PDAA to 317 and 405 °C of the thiolated derivatives was observed (Figure S2.5). It is apparent from the above results that the thiolated isotactic polymers bearing the adamantane group exhibit a much higher T_g and T_d than the polymers carrying the 4-*tert*-butylbenzyl group.

To investigate the photo-curing approach, we subjected *it*-PAMA to controlled crosslinking conditions under UV (350 nm) photoradical initiation with DMPA in chloroform inside a Luzchem photoreactor for 10 min. This approach produced an elastic, translucent but colorless thin film (*it*-PAMA-*hv*). The FT-IR spectrum of the film showed the same features as

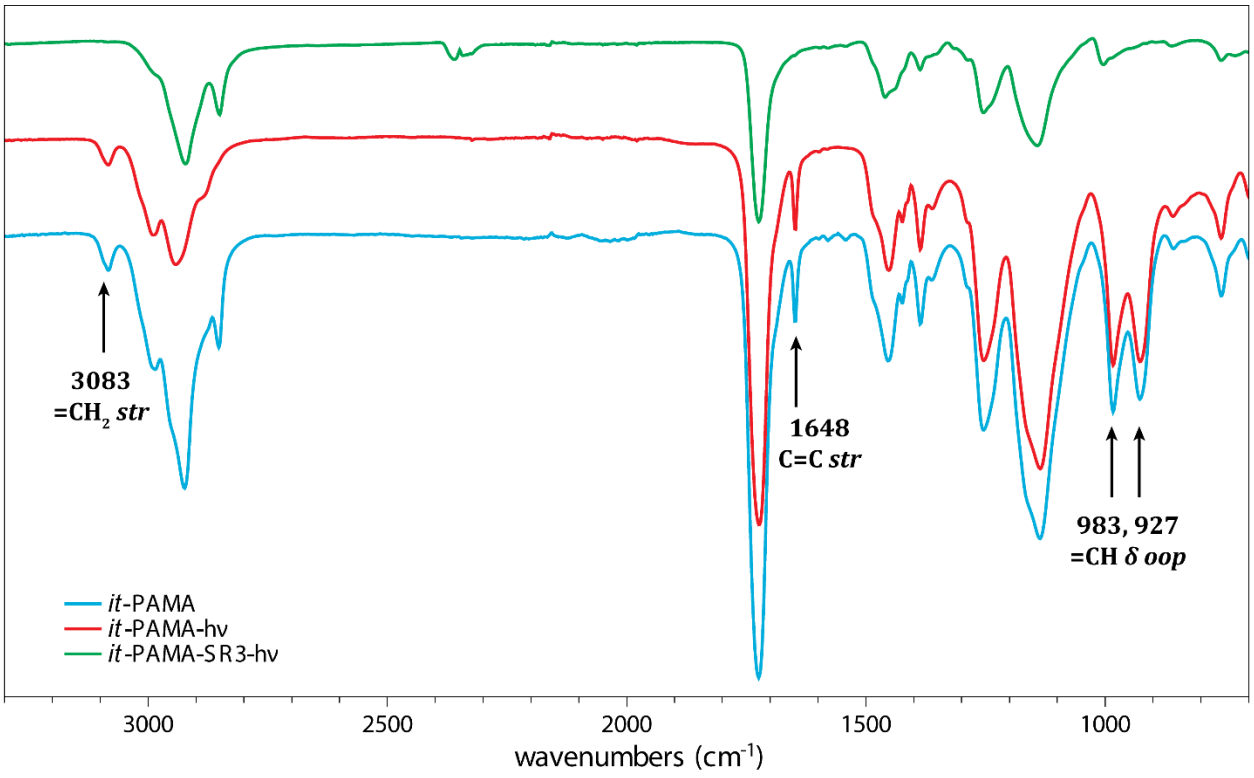

Figure 2.13. Overlay of IR spectra of *it*-PAMA, *it*-PAMA-*hv*, and *it*-PAMA-SR3-*hv*.

those of the uncrosslinked polymer; of particular interest here are the absorption bands corresponding to the pendant C=C bonds in the cross-linked film [3083 (=CH_2 *str*.); 1648 (C=C *str*.); 983 and 927 (=CH δ *oop*) cm^{-1}], indicating that a significant proportion of olefinic groups did not participate in the photocuring process that yielded the film (Figure 2.13). The thermal mechanical property of this material was characterized by dynamic mechanical analysis (DMA), and the resulting curves of storage modulus (E'), loss modulus (E'') and tan δ (E''/E') vs. temperature are shown in Figure 2.14. This analysis gave values of E' = 2.674 GPa and E'' = 71.91 MPa at −100 °C, or E' = 292.6 MPa and E'' = 199.0 MPa at 25 °C. The T_g of this photo-cured *it*-PAMA-*hv* obtained from the peak maxima on the tan δ curve is 36.5 °C, which is about 30 °C higher than that of the parent *it*-PAMA. The T_g, if taken as the peak value on the E'' curve, is lower (17.9 °C). When the photocuring of *it*-PAMA was carried out in the presence of 0.5 equivalents of a bifunctional thiol (1,6-hexanedithiol, RSH3), a brittle material (*it*-PAMA-SR3-*hv*, Scheme

2.3) was obtained instead, which was not suitable for DMA analysis in the tension film mode for a comparative study. Interestingly, the analysis of *it*-PAMA-SR3-*hv* by FT-IR revealed no absorption bands attributable to the olefinic groups (Figure 2.13), indicating a complete consumption of the pendant C=C bonds. Hence, a combination of photocuring with the thiol-ene "click" reaction in the presence of a photoradical initiator and a dithiol can completely cure the *it*-PAMA carrying the pendant C=C bonds.

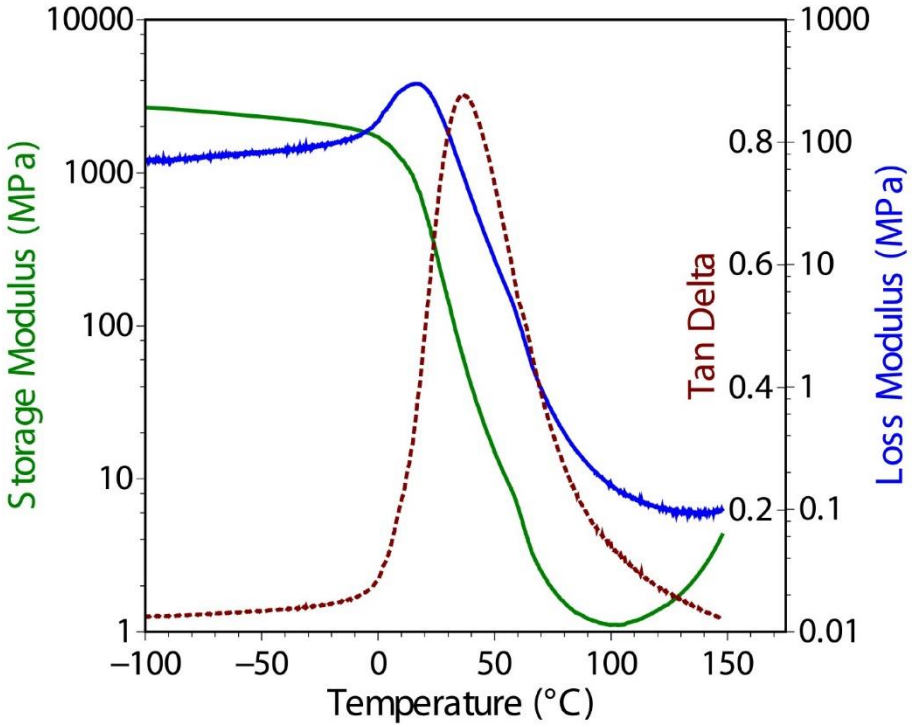

Figure 2.14. Thermal mechanical spectrum of *it*-PAMA-*hv* obtained by DMA analysis.

2.4. Conclusions

In summary, this work has developed the first *chemoselective*, *stereospecific*, and *living* polymerization of polar divinyl monomers using a chiral *ansa*-zirconocenium ester enolate catalyst. The perfect chemoselectivity is originated from the fact that the polymerization proceeds exclusively through conjugate addition across the methacrylic double bond, which is most

activated via coordination of the conjugated carbonyl to the cationic Zr center, while leaving the pendant C=C bonds intact. The stereospecificity is due to an enantiomorphic-site controlled, coordination-addition polymerization mechanism enabled by the chiral *ansa*-zirconocenium ester enolate catalyst, whereas the living nature of the polymerization is brought about by the fast chain initiation through the ester enolate ligand and the lack of problematic chain transfer or termination events, thanks to the chelating resting intermediate involved in the propagation "catalysis" cycle. Key conclusions drawn from our study of the four sub-areas of the subject are summarized as follows:

Catalyst Structure. Although only two chiral C_2-ligated *ansa*-zirconocenium ester enolate catalysts have been investigated in this study, the two catalysts have yielded drastically different results. While the newly synthesized and structurally characterized silyl-bridged-*ansa*-zirconocenium ester enolate **2** exhibits low to negligible activity and stereospecificity in the polymerization of the current polar divinyl monomers, the ethylene-bridged-*ansa*-zirconocenium ester enolate **1** is highly active and stereospecific in the polymerization of such monomers. These results showed remarkable sensitivity of the polymerization activity and stereospecificity to a subtle catalyst structure change.

Monomer Structure. The polymerization by catalyst **1** is completely chemoselective for all four representative polar divinyl monomers investigated in this study. The resulting polymers exhibit controlled MW and low *Đ* values, with the polymerization of DAA showing the highest degree of control over the polymer M_n (nearly identical to the theoretical value) and *Đ* values (1.06–1.16). The DAA polymerization is also most stereospecific, producing essentially stereo-perfect isotactic PDAA with [*mmmm*] > 99%, followed by AMA polymerization, which still led to highly isotactic PAMA with 95–97% [*mm*]. The polymerization of VBMA is further less

stereospecific, while the polymerization VMA is least selective. The drastically different stereochemical control over VMA and AMA, where the only structural difference between the two monomers is an additional CH_2 group inserted into the ester oxygen atom and the vinyl carbon in AMA, suggests that the subtle steric difference affects the orientation of the ester OR group and thus its steric interactions with the ligand framework of the catalyst in the transition state determining the stereochemistry of the addition.

Kinetics and Mechanism. We obtained three lines of key evidence from both homo- and block-copolymerization experiments to demonstrate living characteristics of the AMA polymerization by **1**. The results of the AMA polymerization kinetics are consistent with the proposed monometallic coordination-addition polymerization mechanism. Synthetic efforts have generated or isolated the first monomer-addition products, **3**, **3**·THF and **4**, serving as suitable structural models for active species **A** and resting state chelate **B** (Scheme 2.2) as well as for performing kinetic competence checks, thus providing additional support for the proposed mechanism.

Post-functionalization. We employed the thiol-ene "click" reaction and photo-curing approaches to post-functionalize isotactic polymers (*it*-PAMA and *it*-PDAA) bearing the pendant vinyl group on every repeating unit. For the thiol-ene reaction, a full conversion of all the pendant double bonds to the corresponding thioether bonds has been achieved for both isotactic polymers, whereas the reaction with *it*-PDAA is more controlled for the MW of the resulting thiolated polymer. The photo-curing approach in the presence of a photoradical initiator produced an elastic material readily characterizable by DMA. Performing the photocuring of *it*-PAMA in the presence of 1,6-hexanedithiol produced completely cured *it*-PAMA with all pendant C=C bonds consumed or crosslinked.

REFERENCES

(1) Selected reviews: (a) *Stereoselective Polymerization with Single-Site Catalysts*, Baugh, L. S.; Canich, J. A. M., Eds.; CRC Press/Taylor & Francis Group: Boca Raton, FL, **2008**. (b) Resconi, L.; Chadwick, J. C.; Cavallo, L. in *Comprehensive Organometallic Chemistry III;* Bochmann, M. Vol. Ed.; Mingos, M. P.; Crabtree, R. H. Chief Eds.; Elsevier: Oxford, **2007**; Vol. 4, pp 1005−1166. (c) Coates, G. W. *Chem. Rev.* **2000**, *100*, 1223−1252. (d) Brintzinger, H. H.; Fischer, D.; Mülhaupt, R.; Rieger, B.; Waymouth, R. M. *Angew. Chem., Int. Ed.* **1995**, *34*, 1143−1170.

(2) Selected recent examples and reviews: (a) Jian, Z.; Baier, M. C.; Mecking, S. *J. Am. Chem. Soc*. **2015**, *137*, 2836–2839. (b) Ota, Y.; Ito, S.; Kuroda, J.; Okumura, Y.; Nozaki, K. *J. Am. Chem. Soc*. **2014**, *136*, 11898–11901. (c) Nakamura, A.; Anselment, T. M. J.; Claverie, J. P.; Goodall, B.; Jordan, R. F.; Mecking, S.; Rieger, B.; Sen, A.; van Leeuwen, P. W. N. M.; Nozaki, K. *Acc. Chem. Res.* **2013**, *46*, 1438–1449. (d) Delferro, M.; Marks, T. J. *Chem. Rev.* **2011**, *111*, **2450–2485**. (e) Nakamura, A.; Ito, S.; Nozaki, K. *Chem. Rev.* **2009**, *109*, 5215–5244. (f) Berkefeld, A.; Mecking, S. *Angew. Chem., Int. Ed.* **2008**, *47*, 2538–2542. (g) Luo, S.; Vela, J.; Lief, G. R.; Jordan, R. F. *J. Am. Chem. Soc.* **2007**, *129*, 8946–8947. (h) Domski, G. J.; Rose, J. M.; Coates, G. W.; Bolig, A. D.; Brookhart, M. *Prog. Polym. Sci.* **2007**, ***32***, 30−92. (i) Jensen, T. R.; Yoon, S. C.; Dash, A. K.; Luo, L.; Marks, T. J. *J. Am. Chem. Soc.* **2003**, *125*, 14482−14494. (j) Gibson, V. C.; Spitzmesser, S. K. *Chem. Rev.* **2003**, ***103***, 283–315. (k) Coates, G. W.; Hustad, P. D.; Reinartz, S. *Angew. Chem. Int. Ed. Engl.* **2002**, ***41***, 2236–2257. (l) Ittel, S. D.; Johnson, L. K.; Brookhart, M. *Chem. Rev.* **2000**, *100*, 1169–1204.

(3) Selected examples and reviews: (a) Zhang, N.; Salzinger, S.; Soller, B. S.; Rieger, B. *J. Am. Chem. Soc.* **2013**, *135*, 8810−8813. (b) Chen, E. Y.-X. *Chem. Rev.* **2009**, *109*, 5157–5214. (c) Lian, B.; Spanio, T. P.; Okuda, J. *Organometallics* **2007**, *26*, 6653−6660. (d) Lian, B.; Thomas, C. M.; Navarro, C.; Carpentier, J.-F. *Organometallics* **2007**, *26*, 187−195. (e) Stojcevic, G.; Kim, H.; Taylor, N. J.; Marder, T. B.; Collins, S. *Angew. Chem. Int. Ed.* **2004**, *43*, 5523−5526. (f) Strauch, J. W.; Fauré, J.-L.; Bredeau, S.; Wang, C.; Kehr, G.; Fröhlich, R.; Luftmann, H.; Erker, G. *J. Am. Chem. Soc.* **2004**, *126*, 2089–2104. (g) Frauenrath, H.; Keul, H.; Höcker, H. *Macromolecules* **2001**, *34*, 14–19. (h) Bandermann, F.; Ferenz, M.; Sustmann, R.; Sicking, W. *Macromol. Symp.* **2001**, *174*, 247–253. (i) Yasuda, H. *Prog. Polym. Sci.* **2000**, ***25***, 573−626. (j) Cameron, P. A.; Gibson, V.; Graham, A. J. *Macromolecules* **2000**, *33*, 4329–4335. (k) Li, Y.; Ward, D. G.; Reddy, S. S.; Collins, S. *Macromolecules* **1997**, *30*, 1875–1883. (l) Deng, H.; Shiono, T.; Soga, K. *Macromolecules* **1995**, *28*, 3067-3073 (m) Collins, S.; Ward, S. G. *J. Am. Chem. Soc.* **1992**, *114*, 5460–5462. (n) Yasuda, H.; Yamamoto, H.; Yokota, K.; Miyake, S.; Nakamura, A. *J. Am. Chem. Soc.* **1992**, *114*, 4908−4909.

(4) (a) He, J.; Zhang, Y.; Chen, E. Y.-X. *Macromol. Symp.* **2015**, *349*, 104–114. (b) Zhang, Y.; Caporaso, L.; Cavallo, L.; Chen, E. Y.-X. *J. Am. Chem. Soc*. **2011**, *133*, 1572–1588.

(5) (a) Gao, H.; Matyjaszewski, K. *Prog. Polym. Sci.* **2009**, *34*, 317−350. (b) Li, Z.; Day, M.; Ding, J.; Faid, K. *Macromolecules* **2005**, *38*, 2620−2625. (c) Percec, V.; Auman, B. C. *Macromol. Chem. Phys.* **1984**, *185*, 2319−2336.

(6) (a) Ma, J.; Cheng, C.; Sun, G. R.; Wooley, K. L. *Macromolecules* **2008**, *41*, 9080−9089. (b) París, R. J.; Fuente, L. D. *J. Polym. Sci., Part A: Polym. Chem.* **2005**, *43*, 6247−6261. (c) París, R. J.; Fuente, L. D. *J. Polym. Sci., Part A: Polym. Chem.* **2005**, *43*, 2395−2406. (d)

Nagelsdiek, R.; Mennicken, M.; Maier, B.; Keul, H.; Hartwig, H. *Macromolecules* **2004**, *37*, 8923−8932.

(7) Vardareli, T. K.; Keskin, S.; Usanmaz, A. *J. Macromol. Sci., Part A: Pure Appl. Chem.* **2008**, *45*, 302−311.

(8) Sugiyama, F.; Satoh, K.; Kamigaito, M. *Macromolecules* **2008**, *41*, 3042−3048.

(9) (a) Lu, Z.; Lee, S. Y.; Goh, S. H. *Polymer* **1997**, *38*, 5893−5895. (b) Fukuda, W.; Nakao, M.; Okumura, K.; Kakiuchi, H. *J. Polym. Sci. Part A: Polym. Chem.* **1972**, *10*, 237−250.

(10) Jia, Y.-B.; Ren, W.-M.; Liu, S.-J.; Xu, T.; Wang, Y.-B.; Lu, X.-B. *ACS Macro Lett.* **2014**, *3*, 896–899.

(11) Pugh, C.; Percec, V. *Polym. Bull.* **1985**, *14*, 109−116.

(12) Mohan, Y. M.; Raghunadh, V.; Sivaram, S.; Baskaran, D. *Macromolecules* **2012**, *45*, 3387−3393.

(13) Chen, E. Y.-X. *Top. Curr. Chem.* **2013**, *334*, 239–260.

(14) Chen, J.; Chen, E. Y.-X. *Isr. J. Chem.* **2015**, *55*, 216–225.

(15) Bolig, A. D.; Chen, E. Y.-X. *J. Am. Chem. Soc.* **2004**, *126*, 4897−4906.

(16) Rodriguez-Delgado, A.; Chen, E. Y.-X *Macromolecules* **2005**, *38*, 2587−2594.

(17) (a) Mariott, W. R.; Chen, E. Y.-X. *Macromolecules* **2005**, *38*, 6822−6832. (b) Mariott, W. R.; Chen, E. Y.-X. *Macromolecules* **2004**, *37*, 4741−4743.

(18) For selected reviews, see: (a) Barner-Kowollik, C.; Du Prez, F. E.; Espeel, P.; Hawker, C. J.; Junkers, T.; Schlaad, H.; Van Camp, W. *Angew. Chem. Int. Ed.* **2011**, *50*, 60–62. (b) Hoyle, C. E.; Bowman, C. N. *Angew. Chem. Int. Ed.* **2010**, *49*, 1540−1573. (c) Iha, R. K.; Wooley, K. L.; Nyström, A. M.; Burke, D. J.; Kade, M. J.; Hawker, C. J. *Chem. Rev.* **2009**, *109*, 5620–

5686. (d) Binder, W. H.; Sachsenhofer, R. *Macromol. Rapid Commun.* **2008**, *29*, 952–981. (e) Binder, W. H.; Sachsenhofer, R. *Macromol. Rapid Commun.* **2007**, *28*, 15–54.

(19) Chen, X.; Caporaso, L.; Cavallo, L.; Chen, E. Y.-X. *J. Am. Chem. Soc*. **2012**, *134*, 7278–7281.

(20) (a) Miyake, G. M.; Chen, E. Y.-X. *Macromolecules* **2008**, *41*, 3405−3416. (b) Miyake, G. M.; Mariott, W. R.; Chen, E. Y.-X. *J. Am. Chem. Soc.* **2007**, *129*, 6724−6725.

(21) (a) Stehling, U.; Diebold, J.; Kirsten, R.; Röll, W.; Brintzinger, H.-H.; Jüngling, S.; Mülhaupt, R.; Langhauser, F. *Organometallics* **1994**, *13*, 964–970. (b) Spaleck, W.; Küber, F.; Winter, A.; Rohrmann, J.; Bachmann, B.; Antberg, M.; Dolle, V.; Paulus, E. F. *Organometallics* **1994**, *13*, 954–963.

(22) Bolig, A. D.; Chen, E. Y.-X. *J. Am. Chem. Soc*. **2002**, *124*, 5612–5613.

(23) Mariott, W. R.; Rodriguez-Delgado, A.; Chen, E. Y.-X. *Macromolecules* **2006**, *39*, 1318−1327.

(24) Diamond, G. M.; Jordan, R. F.; Petersen, J. L. *J. Am. Chem. Soc.* **1996**, *118*, 8024–8033.

(25) Klosin, J.; Roof, G. R.; Chen, E. Y.-X.; Abboud, K. A. *Organometallics* **2000**, *19*, 4684–4686.

(26) Horton, A. D.; de With, J.; van der Linden, A. J.; van de Weg, H. *Organometallics* **1996**, *15*, 2672–2674.

(27) Yang, X.; Stern, C. L.; Marks, T. J. *J. Am. Chem. Soc.* **1991**, *113*, 3623–3625.

(28) (a) Caporaso, L.; Cavallo, L. *Macromolecules* **2008**, *41*, 3439–3445. (b) Caporaso, L.; Gracia-Budrìa, J.; Cavallo, L. *J. Am. Chem. Soc.* **2006**, *128*, 16649−16654.

(29) Greenley, R. Z. In *Polymer Handbook,* 3rd ed.; Immergut, E. H., Brandup, J., Eds.; Wiley: New York, **1989**; pp 267−274.

CHAPTER 3

Robust Crosslinked Stereocomplexes and C_{60} Inclusion Complexes of Vinyl-Functionalized Stereoregular Polymers Derived from Chemo/Stereoselective Coordination Polymerization[*]

3.1. Summary

The successful synthesis of highly syndiotactic polar vinyl polymers bearing the reactive pendant vinyl group on each repeat unit, which is enabled by perfectly chemoselective and highly syndiospecific coordination polymerization of divinyl polar monomers developed through this work, has allowed the construction of robust crosslinked supramolecular stereocomplexes and C_{60} inclusion complexes. The metal-mediated coordination polymerization of three representative polar divinyl monomers, including vinyl methacrylate (VMA), allyl methacrylate (AMA), and *N*,*N*-diallyl acrylamide (DAA) by C_s-ligated zirconocenium ester enolate catalysts under ambient conditions exhibits complete chemoselectivity and high stereoselectivity, thus producing the corresponding vinyl-functionalized polymers with high (92% *rr*) to quantitative (>99% *rr*) syndiotacticity. A combined experimental (synthetic, kinetic, and mechanistic) and theoretical (DFT) investigation has yielded a unimetallic, enantiomorphic-site controlled propagation mechanism. Post-functionalization of the obtained syndiotactic vinyl-functionalized polymers via the thiol-ene click and photocuring reactions readily produced the corresponding thiolated polymers and flexible crosslinked thin film materials, respectively. Complexation of such

[*] This dissertation chapter contains the manuscript of a full paper published in the *Journal of the American Chemical Society* [Vidal, F.; Falivene, L.; Caporaso, L.; Cavallo, L.; Chen, E. Y.-X. *J. Am. Chem. Soc.* **2016**, *138*, 9533-9547]. This work was supported by the US National Science Foundation (NSF-1300267) for the study carried out at Colorado State University. L. Cavallo thanks the HPC team of Enea (www.enea.it) for using the ENEA-GRID and the HPC facilities CRESCO (www.cresco.enea.it) in Portici, Italy. We thank Boulder Scientific Co. for the research gifts of $B(C_6F_5)_3$ and $[Ph_3C][B(C_6F_5)_4]$. L. Falivene, L. Caporaso, and L. Cavallo performed the computational portion of this work.

syndiotactic vinyl-functionalized polymers with isotactic poly(methyl methacrylate) and fullerene C_{60} generates supramolecular crystalline helical stereocomplexes and inclusion complexes, respectively. Crosslinking of such complexes afforded robust crosslinked stereocomplexes that are solvent resistant and also exhibit considerably enhanced thermal and mechanical properties as compared to the uncrosslinked stereocompexes.

3.2. Introduction

Owing to its unique feature that each enchaining monomer must be coordinated to the catalyst site, which can be rationally designed by tuning the electronic, steric, and symmetry properties of the ancillary ligand, metal-mediated coordination polymerization has evolved into arguably the most powerful technique for precisely controlling the polymerization stereochemistry.[1] In the case of vinyl monomers—a class of the technologically most important monomers, the metal-mediated coordination polymerization can be categorized into coordination-insertion polymerization, typically for catalytic polymerization of nonpolar olefins as well as copolymerization of nonpolar and polar olefins,[2] and coordination-addition polymerizations, commonly for living or quasi-living and stereospecific polymerization of conjugated polar olefins such as acrylic monomers.[3,4]

Specifically focusing on polar divinyl monomers, rendering their chemoselective polymerization is important for the synthesis of vinyl-functionalized polymers, which can be post-functionalized—through the retaining vinyl groups attached to the main chain—into a variety of useful functional materials.[5] However, polymerization of such monomers with complete chemoselectivity by safeguarding one of the reactive vinyl groups while selectively polymerizing the other has been a challenging task for the radical polymerization (especially during the later

stage),[6] group-transfer polymerization,[7] or anionic polymerization carried out at −20 °C or above.[8] In the cases where complete chemoselectivity has been achieved utilizing the Lewis pair cooperativity in the Lewis pair polymerization,[9] the resulting uncross-linked, soluble functional polymers exhibited a broad molecular weight distribution (*Đ*) and low tacticity,[10] due to non-living and non-stereoselective features of this polymerization. In this context, coordination-addition polymerization of divinyl polar monomers is advantageous due to its high degree of control over polymerization characteristic, even at ambient temperature. For instance, the polymerization of allyl methacrylate (AMA) by half-metallocene yttrium catalysts was shown to be both living and chemoselective.[11]Furthermore, a chiral C_2-ligated *ansa*-zirconocenium ester enolate complex, [*rac*-$C_2H_4(\eta^5$-indenyl$)_2$Zr(THF)]$^+$ [OC(O^{i}Pr)=CMe$_2$][MeB(C_6F_5)$_3$]$^-$ (**1**),[12] which is known to mediate stereospecific and living polymerization of simple alkyl methacrylates such as methyl methacrylate (MMA)[12,13] and acrylamides,[14] is not only completely chemoselective and living, but also highly isospecific, in the polymerization of polar divinyl monomers at ambient temperature.[15] The origin of the perfect chemoselectivity and high isoselectivity arises from the catalyst site-controlled coordination-addition mechanism that dictates exclusive conjugate additions across the methacrylic double bond that is activated via coordination of the conjugated carbonyl to the cationic, chiral Zr center, thus leaving the pendant C=C bond intact.

Stereocomplexation between a pair of diastereomeric polymer chains of isotactic (*it*) and syndiotactic (*st*) poly(methylate methacrylate) (PMMA) in a typical 1/2 *it*-PMMA/*st*-PMMA ratio, when annealed in the solid state or crystallized in suitable solvents, generates a crystalline stereocomplex, *sc*-PMMA, representing a rare example of helical supramolecular structures based on a vinyl polymer.[16] Polar donor solvents such as acetone, THF, DMSO and DMF are known to promote such stereocomplexation and thus referred as complexing solvents, while chlorinated

solvents such as chloroform and dichloromethane decomplex the *sc*-PMMA polymer pair and are accordingly non-complexing or de-complexing solvents. Although the structure of *sc*-PMMA has received several revisions since the first report of the *sc*-PMMA structure model,[17] its formation can be readily identified or characterized by gelation or precipitation of the crystalline complex in a complexing solvent, a high endothermic melting-transition temperature (T_m up to 210 °C) by differential scanning calorimetry (DSC), and a characteristic diffraction peak ($2\theta \sim 4.35$ °) by powder X-ray diffraction (pXRD).[18,19] Worth noting here is that the formation of *sc*-PMMA was reported to be restricted to *it*-PMMA, but the ester group of the *st*-counterpart can be modified to extend to other *st*-poly(methacrylate)s.[19] In addition, the formation of *sc*-PMMA is not limited to the blending of the preformed *it*- and *st*-PMMA diastereomeric polymer pair, as *in situ* stereocomplexing polymerization of MMA using a pair of diastereospecific coordination polymerization catalysts has led to rapid, high-yield, ambient-temperature production of *sc*-PMMA with a high T_m of up to 217 °C.[20] Furthermore, supramolecular *sc*-PMMA/silicate nanocomposites[21] were fabricated by mixing dilute THF solutions of *in situ* polymerized *it*-/*st*-PMMA/silicates,[22] and crystalline hybrid polymer stereocomplexes between POSS (polyhedral oligomeric silsesquioxane) end-capped *it*- and *st*-PMMA-POSS chains were also synthesized.[23] Lastly, owing to its large helical cavity (~ 1 nm), syndiotactic *st*-PMMA, while does not crystallize by itself, co-crystallizes with specific organic solvents such as benzene [24] and encapsulates guest nanocages such as fullerenes C_{60} and C_{70}[25] and MA-POSS [23] to form unique crystalline helical inclusion complexes.

In light of the above overviewed unique ability of highly syndiotactic *st*-PMMA to form helical supramolecular structures of stereo- and inclusion complexes, we hypothesized that highly syndiotactic vinyl-functionalized poly(methacrylate)s, synthesizable from the proposed

chemoselective and syndiospecific coordination polymerization of divinyl monomers, should form stereocomplexes with *it*-PMMA and inclusion complexes with C_{60} which, after crosslinking, should lead to robust, solvent and thermally resistant crosslinked stereocomplexes (Figure 3.1) and inclusion complexes. Such robust supramolecular stereocomplexes should solve the problem of decomplexation of the current stereocomplex and inclusion complex structures in non-complexing solvents and also enhance thermal and mechanical properties of the material. Accordingly, this report presents a full account of our work towards this central objective by first achieving chemoselective and syndiospecific polymerization of divinyl polar monomers to synthesize highly syndiotactic vinyl-functionalized polymers, next post-functionalizing and photocrosslinking such polymers into functional materials, and finally complexing such polymers to robust supramolecular stereo- and inclusion complexes followed by crosslinking.

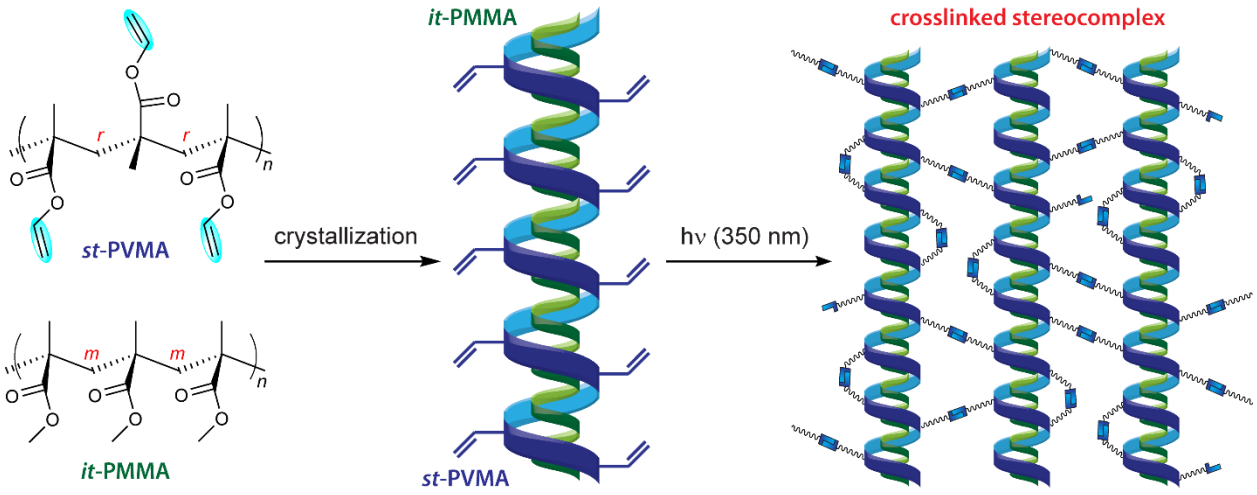

Figure 3.1. Schematic representation of the *hypothesis* for stereocomplexation between syndiotactic acrylic polymers carrying pendant vinyl groups and *it*-PMMA and subsequent photocuring to robust crosslinked supramolecular structures.

3.3. Results and Discussion

Chemoselective and Syndiospecific Polymerization of Polar Divinyl Monomers. The first task of this study was to synthesize highly syndiotactic acrylic polymers carrying pendant vinyl groups via the development of chemoselective and syndiospecific polymerization. Previous reports from our group have shown neutral C_s-ligated zirconocene ester enolate complexes (pre-catalysts) such as [Ph_2C(Cp)(2,7-^{t}Bu$_2$-Flu)]Zr[OC(O^{i}Pr)=CMe_2]$_2$ (**2**, Cp = η^5-cyclopentadienyl; Flu = η^n-fluorenyl), [Ph_2C(Cp)(Flu)]Zr[OC(O^{i}Pr)=CMe_2]$_2$ (**3**), and [Ph_2C(Cp)(Flu)]ZrMe-[OC(O^{i}Pr)=CMe_2] (**4**) can be readily activated with either [Ph_3C][$B(C_6F_5)_4$] (via hydride abstraction, followed by Michael addition), $B(C_6F_5)_3$ or THF·$B(C_6F_5)_3$ (via methide abstraction), to generate the corresponding cationic complexes (catalysts) **2**$^+$[$B(C_6F_5)_4$]$^-$, **3**$^+$[$B(C_6F_5)_4$]$^-$, **4**$^+$[$MeB(C_6F_5)_3$]$^-$, and **4**$^+$(THF)[$MeB(C_6F_5)_3$]$^-$ (**5**, Scheme 3.1), respectively.[26] Such cationic complexes have been shown to promote rapid and syndiospecific polymerization of MMA at ambient temperature to produce highly syndiotactic *st*-PMMA with syndiotacticity up to 94% *rr*, proceeding through a monometallic, catalyst-site-controlled coordination-addition polymerization mechanism via eight-membered-ring ester enolate intermediates.[26] Accordingly, **2**$^+$[$B(C_6F_5)_4$]$^-$, **3**$^+$[$B(C_6F_5)_4$]$^-$, **4**$^+$[$MeB(C_6F_5)_3$]$^-$ (generated by in-reactor activation), and **5** (generated by pre-activation) were employed for the current investigation into the polymerization of the three representative polar divinyl monomers, AMA, vinyl methacrylate (VMA), and *N*,*N*-diallyl acrylamide (DAA), aiming to achieve chemoselective and syndiospecific polymerization of such monomers and thus produce the corresponding highly syndiotactic polar vinyl polymers carrying a pendant C=C bond in every repeat unit (Scheme 3.1).

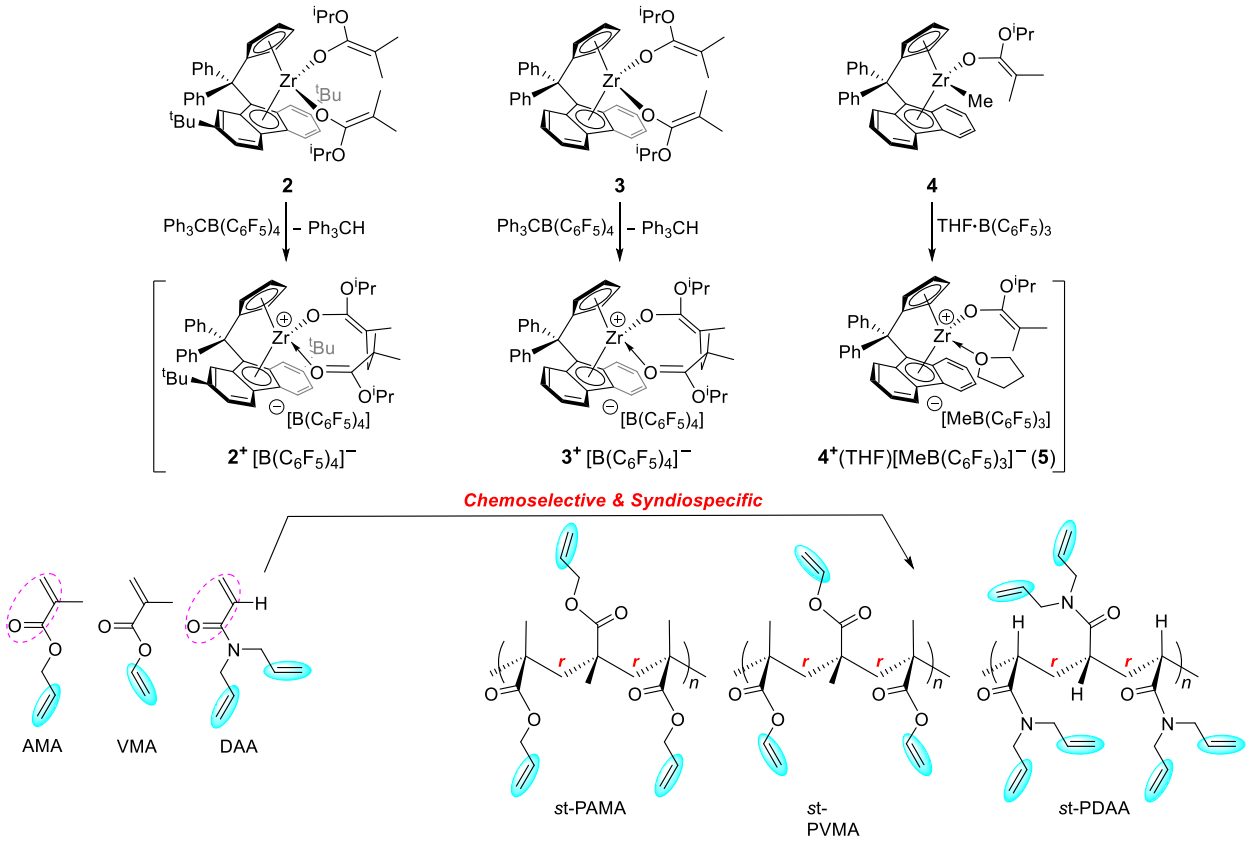

Scheme 3.1. Chemoselective and syndiospecific polymerization of polar divinyl monomers as well as structures of monomers, catalysts, and polymers involved in this study.

Selected results for the polymerization of the three representative polar divinyl monomers by pre-catalysts **2**–**4** are summarized in Table 3.1. At the outset, control runs showed that neither the neutral pre-catalyst nor the activator itself exhibited any activity toward such monomers. In contrast, cationic complexes **2**$^+$[B(C$_6$F$_5$)$_4$]$^-$, **3**$^+$[B(C$_6$F$_5$)$_4$]$^-$, and **4**$^+$[MeB(C$_6$F$_5$)$_3$]$^-$, derived from activation with [Ph$_3$C][B(C$_6$F$_5$)$_4$] (for bis-enolate precatalysts **2** and **3**) or B(C$_6$F$_5$)$_3$ (for mono-enolate precatalyst **4**), are highly active, quantitatively chemoselective, and also syndiospecific for polymerizations of such polar divinyl monomers at ambient temperature. Starting with the AMA polymerization in CH_2Cl_2 at 25 °C, **3**$^+$[B(C$_6$F$_5$)$_4$]$^-$ (0.5 mol% loading) afforded *st*-PAMA with a high syndiotacticity of [*rr*] = 92.4% and perfect chemoselectivity (Figure S3.2), but achieved a maximum monomer conversion of only 55% in 1 h (run 2). Cationic complex **4**$^+$[MeB(C$_6$F$_5$)$_3$]$^-$

Table 3.1. Polymerization of polar divinyl monomers (M) by precatalysts **2**–**4** [a]

run no.	M	Pre-cat.	Activator	Temp (°C)	Time (min)	conv. [b] (%)	M_n [c] (kg/mol)	$Đ$ [c] (M_w/M_n)	[*rr*][d] (%)	[*mr*][d] (%)	[*mm*][d] (%)
1	AMA	**2**	$[Ph_3C][B]$	25	180	92.7	55.3	1.33	87.9	10.6	1.5
2	AMA	**3**	$[Ph_3C][B]$	25	60	55.1	35.0	1.56	92.4	6.0	1.6
3	AMA	**4**	[B]	25	60	53.0	24.5	1.32	90.7	7.4	1.9
4	VMA	**2**	$[Ph_3C][B]$	25	60	96.2	42.9	1.40	87.0	10.5	2.5
5	VMA	**3**	$[Ph_3C][B]$	25	30	98.3	42.5	1.38	92.4	7.0	0.6
6	VMA	**4**	[B]	25	30	98.5	41.2	1.36	93.0	6.4	0.6
7	VMA	**4**	[B]·THF	25	10	100	42.5	1.36	93.5	6.1	0.4
8	VMA	**3**	$[Ph_3C][B]$	0	30	100	86.7	1.21	95.7	2.9	1.4
9	VMA	**4**	[B]·THF	0	30	97.0	98.3	1.17	94.8	3.5	1.7
10	DAA	**3**	$[Ph_3C][B]$	25	10	89.0	47.5	1.34	>99	–	–
11	DAA	**4**	[B]·THF	25	10	94.5	42.9	1.29	>99	–	–

[a] Conditions: activator $[Ph_3C][B] = [Ph_3C][B(C_6F_5)_4]$, $[B] = B(C_6F_5)_3$; solvent (3.0 mL) CH_2Cl_2 for runs 1–9, toluene for runs 10 and 11; [M]/[cat] = 200; *pre-activation* method (pre-mixing of pre-catalyst with activator, followed by addition of monomer), except for runs #3 and #6 where the *in-reactor activation* method was used (pre-mixing of monomer with activator, followed by addition of pre-catalyst). [b] Monomer (M) conversion measured by ^{1}H NMR. [c] Number-average molecular weight (M_n) and dispersity ($Đ$) determined by gel-permeation chromatography (GPC) relative to PMMA standards. [d] Tacticity measured by ^{1}H or ^{13}C NMR in $CDCl_3$.

performed similarly (run 3 vs. 2). Interestingly, $\mathbf{2}^+[B(C_6F_5)_4]^-$, the more electron-rich and sterically encumbered catalyst with two substituted *tert*-butyl groups on the Flu ring, achieved a much higher monomer conversion of 92.7% and thus a higher molecular weight polymer (M_n = 55.3 kg/mol, $Đ$ = 1.33), but it produced *st*-PAMA with a lower syndiotacticity of [*rr*] = 87.9% (run 1). The isolated *st*-PAMA (M_n = 35.0 kg/mol, [*rr*] = 92%, run 2) is soluble in common organic solvents and exhibited a glass transition temperature (T_g) at 54 °C, as measured by DSC, which is considerably higher than the counterpart *it*-PAMA (–13 °C to 0 °C, in the order of increasing M_n).[15] A thermal crosslinking exothermic peak with an onset temperature and a peak maximum of 142 °C and >200 °C, respectively, was also observed on the DSC curve.

Moving to VMA polymerization, all three C_s-ligated catalysts are perfectly chemoselective and highly syndiospecific. Again, the two catalysts without the *tert*-butyl substitution, $\mathbf{3}^+[B(C_6F_5)_4]^-$ and $\mathbf{4}^+[MeB(C_6F_5)_3]^-$, exhibited similar polymerization characteristics (run 5 vs. 6),

including high activity (>98% conversion in 30 min), medium molecular weight (M_n = 41.2–42.5 kg/mol), medium dispersity ($Đ$ = 1.36–1.38), and high syndiotacticity ([*rr*] = 92.4% and 93.0%). The polymerization by cation **5** {= **4**(THF)$^+$[MeB(C_6F_5)$_3$]$^-$, generated from the reaction of **4** + THF·B(C_6F_5)$_3$, Scheme 3.1} was even more rapid, achieving 100% monomer conversion in only 10 min without signs of gel formation and also producing *st*-PVMA with a high syndiotacticity of [*rr*] = 93.5% (run 7). When the polymerization was carried out at 0 °C, the molecular weight of the resulting polymer was much higher and the dispersity became narrower, while still achieving quantitative or near quantitative conversion: M_n = 86.7 kg/mol, $Đ$ = 1.21, [*rr*] = 95.7% by **3**$^+$[B(C_6F_5)$_4$]$^-$ (run 8); M_n = 98.3 kg/mol, $Đ$ = 1.17, [*rr*] = 94.8% by **5** (run 9). The chemoselectivity of the VMA polymerization is also perfect, as revealed by complete disappearance of the methacrylic =CH_2 proton signals at δ 6.23 and 5.68 ppm and complete retention of the pendant vinyl group –CH=CH_2 proton signals centered at δ 7.14, 4.91, and 4.63 ppm (Figure 3.2), indicating that the polymerization proceeded exclusively through conjugate addition across the methacrylic double bond. Significantly, analysis of the triad stereoerrors of the resulting *st*-PVMA gave 2[*mm*]/[*mr*] ~ 1 (0.97 for both runs 8 and 9), indicative of an enantiomorphic-site controlled mechanism. Furthermore, the ^{13}C NMR spectrum of the polymer in the C=O pentad (*rrrr*) region provided collaborative evidence for the formation of the highly syndiotactic *st*-PVMA (Figure 3.3). DSC analysis of the highly syndiotactic *st*-PVMA showed a T_g of ~100 °C, which is considerably higher than *at*-PVMA (44–49 °C),[15] as well as a thermal crosslinking exothermic peak with an onset temperature and a peak maximum of 153 °C and 184 °C, respectively. We also examined the degree of the polymerization control over molecular weight by varying the [VMA]/[**5**] ratio from 100 to 900 (0.11 mol% catalyst loading) in CH_2Cl_2 at ambient temperature, all of which runs proceeded to high conversions without signs of gel formation. The M_n value of

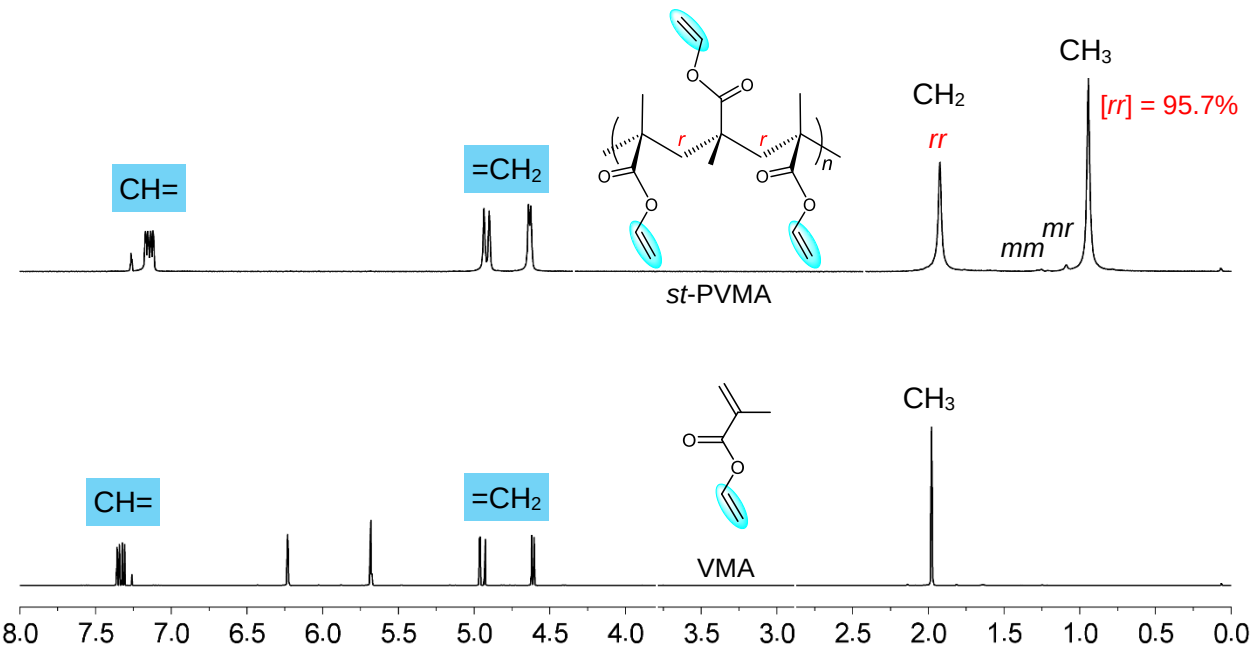

Figure 3.2. Overlay of ^{1}H NMR ($CDCl_3$, 25 °C) spectra of VMA and *st*-PVMA.

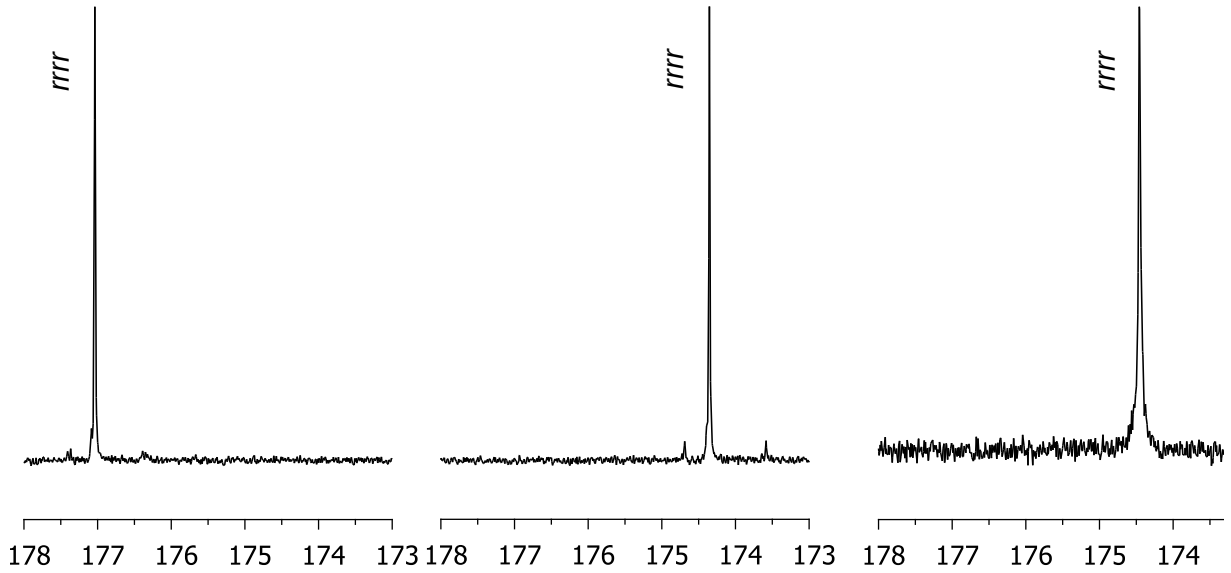

Figure 3.3. ^{13}C NMR spectra ($CDCl_3$, 50 °C) showing the C=O pentad (*rrrr*) region of *st*-AMA (left, run 2), *st*-PVMA (center, run 8) and *st*-PDAA (right, run 10).

the resulting *st*-PVMA increased linearly (R^2 = 0.992) from 29.6 kg/mol (*Đ* = 1.28) to 164 kg/mol (*Đ* = 1.48, Figure 3.4) as the [VMA]/[**5**] ratio was increased from 100 to 900, showing the ability of this polymerization system to control the resulting polymer molecular weight while maintaining the relatively low dispersity.

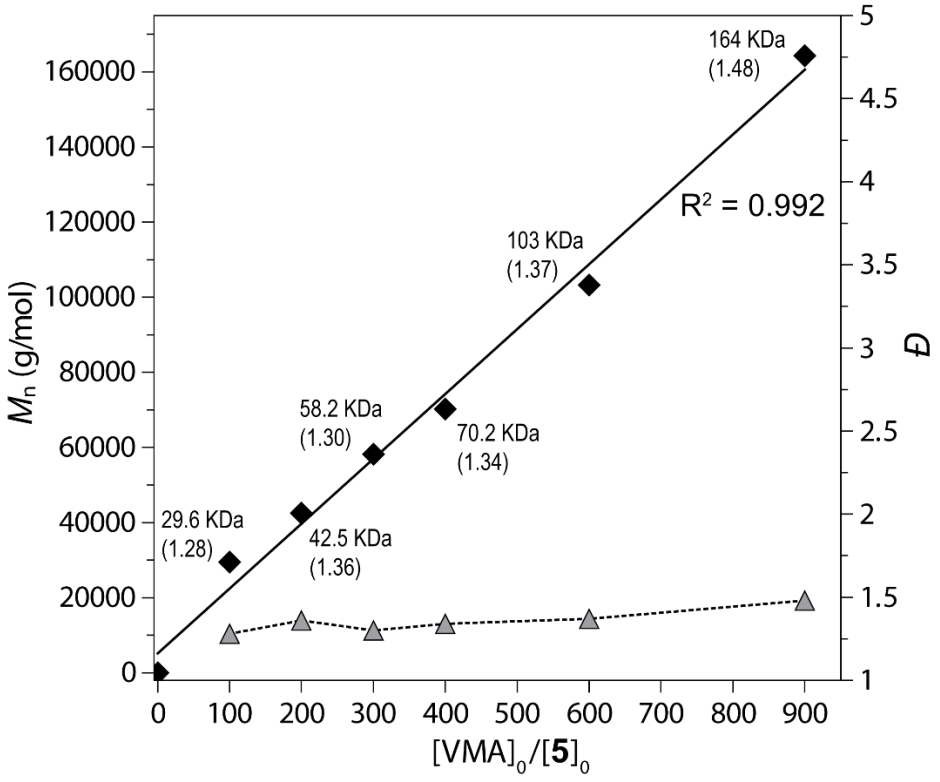

Figure 3.4. Plots of M_n (kg/mol or kDa) and *Đ* (shown in parenthesis) of *st*-PVMA produced by **5** vs. $[VMA]_0/[\mathbf{5}]_0$ ratio (CH_2Cl_2, 23 °C).

The chemoselectivity and stereospecificity of $\mathbf{3}^+[B(C_6F_5)_4]^-$ and **5** toward the polymerization of DAA were also carefully examined. Remarkably, this polymerization not only was rapid, achieving 89.0% (run 10) and 94.5% (run 11) conversions in 10 min, it also exhibited both *quantitative chemoselectivity* (Figure S3.3) *and syndiospecificity* ([*rr*] > 99%, Figure 3.3). DSC analysis of the highly syndiotactic *st*-PDAA showed a T_g of 35.8 °C as well as a thermal crosslinking exothermic peak with an onset temperature and a peak maximum of 216 °C and 290 °C, respectively. Worth noting also is that *st*-PDAA is soluble in common solvents of a wide

polarity range, including MeOH, DMF, THF, acetone, $CHCl_3$, Et_2O, and toluene, whereas *it*-PDAA is found soluble only in limited solvents such as $CHCl_3$ and CH_2Cl_2. In comparison, the initiator efficiency (I^*), calculated as $I^* = M_n(\text{calcd})/M_n(\text{exptl})$, where $M_n(\text{calcd}) = \text{MW(M)} \times [M]_0/[Zr]_0 \times \text{conversion \%} + \text{MW of chain-end groups}$, was in the range of 43–55 % for AMA polymerization at RT, 51–54 % for VMA polymerization at RT, and 57–67 % for DAA polymerization at RT.

Mechanism of Polymerization. Next, we examined the kinetics of VMA polymerization by catalyst **5**, revealing the polymerization is first-order with respect to monomer concentration [VMA] for all the six $[VMA]_0/[\mathbf{5}]_0$ ratios investigated (150 to 500, Figure 3.5). A double logarithm plot (Figure 3.6) of the apparent rate constants (k_{app}), obtained from the slopes of the best-fit lines to the plots of $\ln([VMA]_0/[VMA]_t)$ vs. time, as a function of $\ln([\mathbf{5}]_0)$, was fit to a straight line ($R^2 = 0.986$) with a slope of 1.1. Thus, the kinetic order with respect to [**5**], given by the slope of ~ 1, reveals that the propagation is also first order in catalyst concentration. These results indicate that the resting state in the proposed monometallic propagation "catalytic" cycle (Scheme 3.2) is the cyclic ester enolate **B**, which was structurally modeled by the isolated cationic cyclic ester enolate complex **6** (*vide infra*), and that associative displacement of the coordinated ester group by incoming monomer to regenerate the active species **A** (structurally modeled by complex **5**) is the rate-determining step (i.e., **B** → **A**, Scheme 3.2). These key features of the mechanism are the same as those already established for the coordination-addition polymerization of alkyl methacrylates.[3b,15 ,26]

To provide further evidence to support the mechanism outlined in Scheme 3.2, cation **5** was reacted with 1 equiv of VMA to cleanly generate the corresponding single-monomer-addition product, the eight-membered metallacycle [27] resting intermediate {[Ph_2C(Cp)(Flu)]Zr-

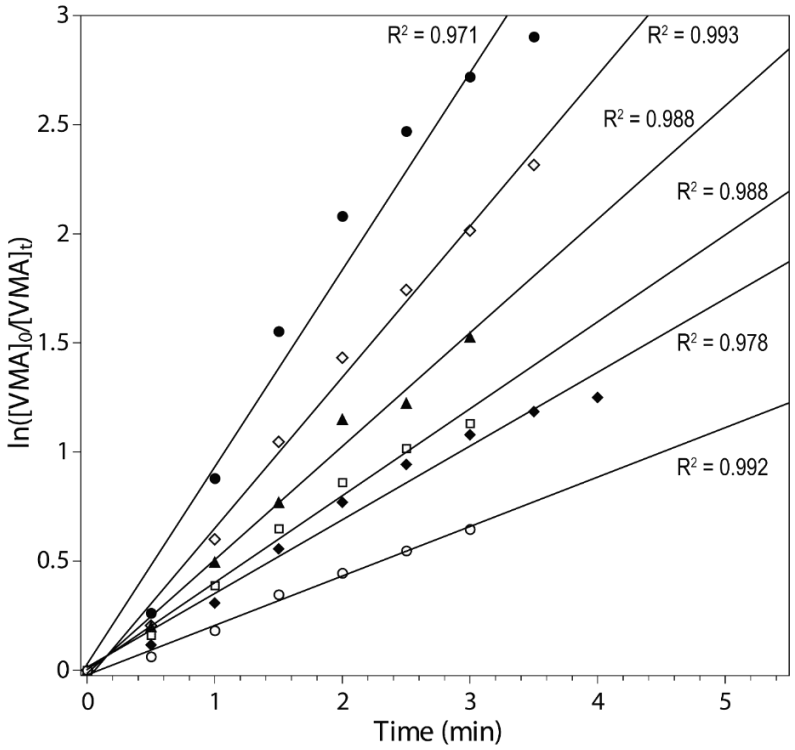

Figure 3.5. Semilogarithmic plots of ln{[VMA]$_0$/[VMA]$_t$} vs. time for the polymerization of VMA by **5** in CH_2Cl_2 at 23 °C. Conditions: [VMA]$_0$ = 0.832 M; [**5**]$_0$ = 5.55 mM (●), 4.16 mM (◊), 3.33 mM (▲), 2.77 mM (□), 2.07 mM (♦), 1.66 mM(○).

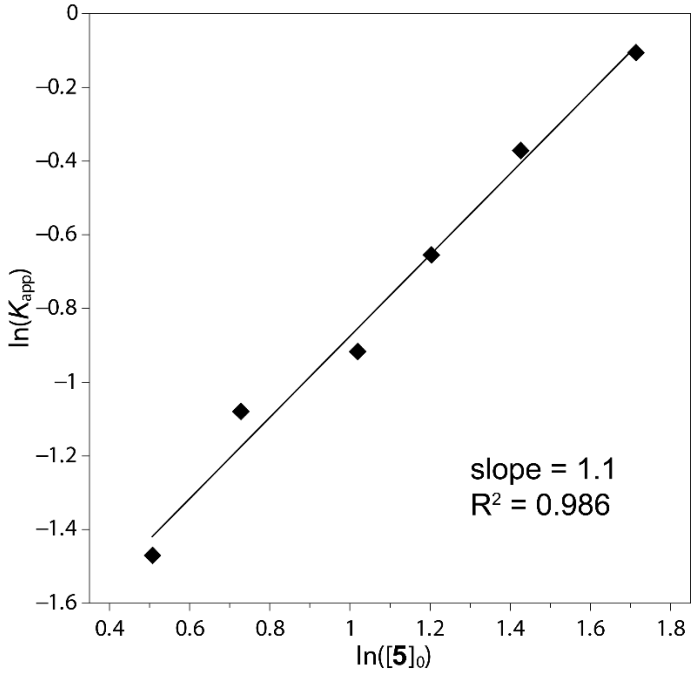

Figure 3.6. Plot of ln(k_{app}) vs. ln([**5**]$_0$) for the VMA polymerization by **5** in CH_2Cl_2 at 23 °C.

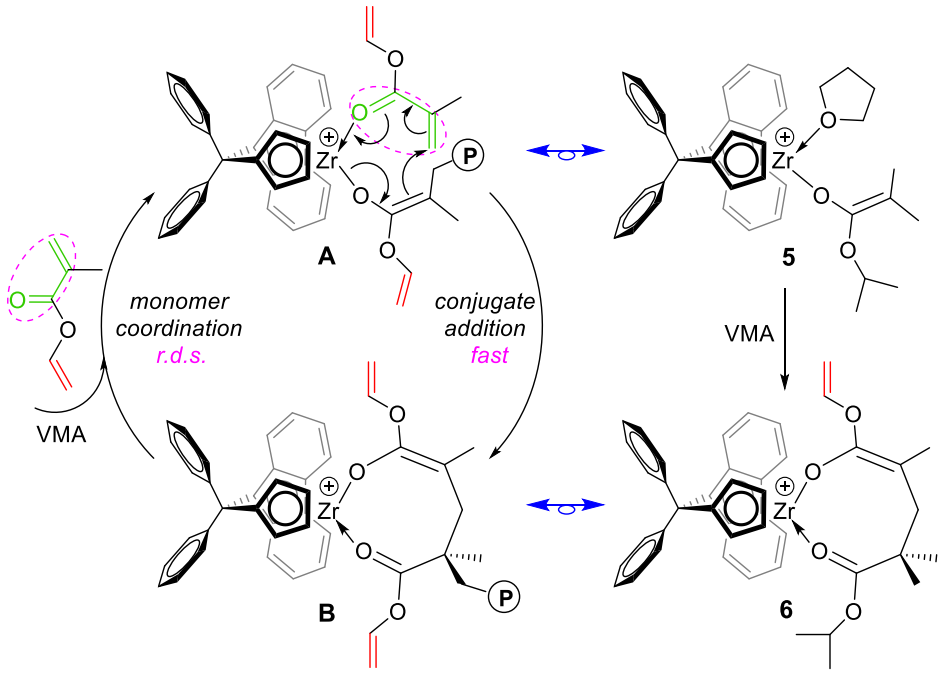

Scheme 3.2. Proposed mechanism (propagation "catalytic" cycle) for the chemoselective and syndiospecific polymerization of VMA as well as the structures of **5** and **6** as synthetic structural models for active species **A** and resting state chelate **B**, respectively.

$[OC(OCH{=}CH_2){=}CMeCH_2C(Me_2)C(O^iPr){=}O]\}^+[MeB(C_6F_5)_3]^-$ (**6**) (Figure 3.7). This intermediate can also be generated and isolated in >91% yield via the 1:1 ratio reaction of the pre-catalyst **4** with the borane-monomer adduct $VMA{\cdot}B(C_6F_5)_3$ (see the Apendix B for procedures and characterizations). Likewise, the metallacycle corresponding to the first AMA addition intermediate $\{[Ph_2C(Cp)(Flu)]Zr[OC(OCH_2CH{=}CH_2){=}CMeCH_2C(Me_2)C(O^iPr){=}O]\}^+$ $[MeB(C_6F_5)_3]^-$ (**7**) was generated in the similar fashion (see the Appendix B and Figure S3.4). The successful generation and isolation of the first-monomer-addition product **6**, serving as the structural model of the resting intermediate **B**, implies that the monomer addition is fast relative to the monomer coordination in the propagation "catalytic" cycle depicted in Scheme 3.2 (otherwise, only polymers or oligomers, plus the unreacted **5** or **4**, would be formed). Importantly, addition of excess of VMA to a solution of **6** brought about rapid polymerization of VMA into *st*-PVMA, thereby confirming cation **6** as the resting intermediate of the catalytic cycle by this kinetic

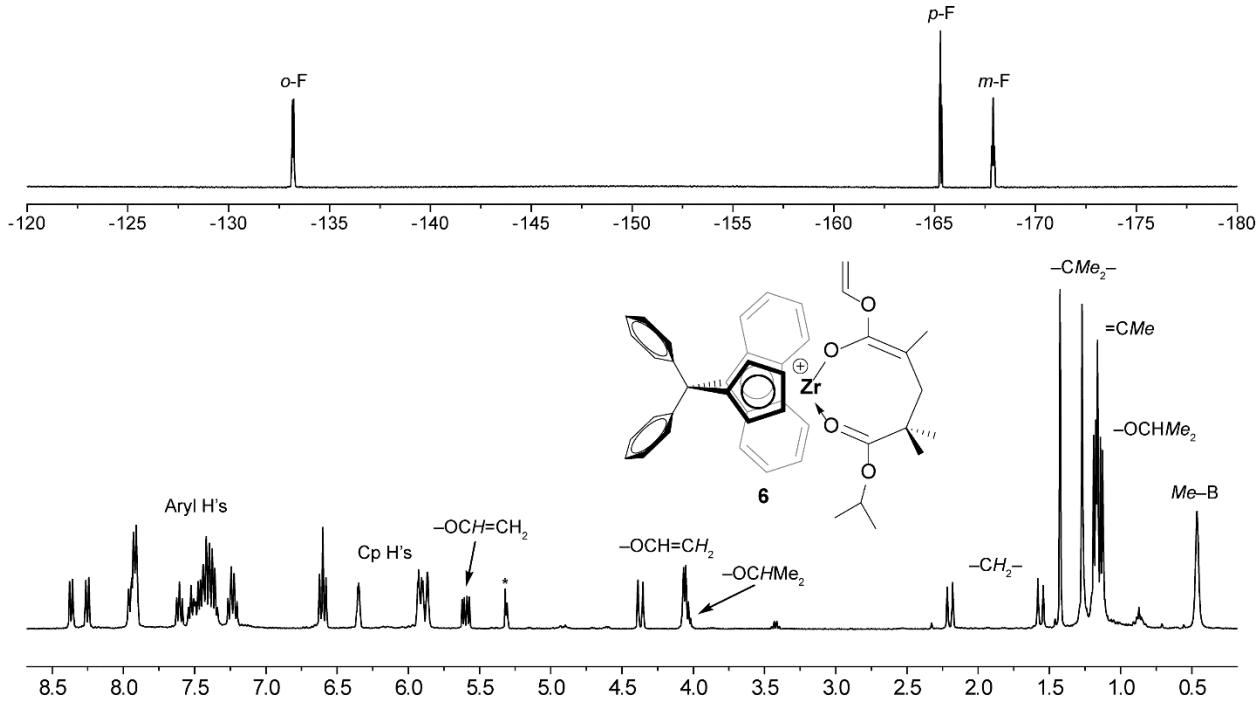

Figure 3.7. ^{19}F NMR (top) and ^{1}H (bottom) spectra (CD_2Cl_2, 25 °C, residual NMR labeled as *) of the isolated cationic complex **6**. Anion $[MeB(C_6F_5)_3]^-$ omitted for clarity.

competence check. Overall, all the experimental evidence to date is consistent with the polymerization mechanism depicted in Scheme 3.2.

Mechanism of Stereoselection. Next, we investigated the mechanism of stereoselection by a computation study via DFT calculations. This needed study was prompted by an interesting observation that, while the polymerizations of AMA and VMA by the C_2-ligated catalyst **1** were drastically different, leading to formation of highly isotactic PAMA with [*mm*] = 95–97% and isotactic-biased PVMA with [*mm*] = 51–53%, respectively,[15] both polymerizations of AMA and VMA by C_s-ligated catalysts afforded highly syndiotactic polymers, with even higher syndiotacticity of [*rr*] = 94–96% achieved for the VMA polymerization (*vide supra*). Thus, it is intriguing that the placement of the sp^3-hybridized CH_2 group between the ester oxygen atom and the sp^2-hybridized vinyl moiety in the case of AMA substantially enhanced the isospecificity of the polymerization but had no effect on (or even slightly reduced) the syndiospecificity of the

polymerization, relative to VMA without the CH_2 group, highlighting the importance of the sterics and orientation of the ester OR group of the methacrylate monomer in the transition state (TS) structure that determines the stereospecificity of the metallocene-catalyzed polymerization.[26a,28] Accordingly, DFT calculations were performed to provide a rationalization of the above experimentally observed high isospecificity in AMA polymerization and the low isospecificity in VMA polymerization by C_2-ligated catalyst **1** (EBI-Zr) system, as well as the high syndiospecificity in both AMA and VMA polymerizations with C_s-ligated catalyst **5** [Ph_2C(Cp)(Flu)Zr] system.

We calculated all the TSs for AMA and VMA additions involving the *re* and *si* prochiral faces of the growing chain by considering geometries where the pendant group of the monomer and of the chain are located on opposite sides (*trans*) or on the same side (*cis*) of the metallocene equatorial belt. In addition, for the C_2-symmetric EBI-Zr system, the g^+ and g^- conformations of the metallocene bridge have been considered.[28] In all the geometries a ^{t}Bu group was used to model the remaining of the growing chain. For the sake of simplicity, we anticipate that with the (*S*,*S*)-EBI-Zr based system all competitive geometries show a g^+ conformation of the metallocene bridge. The favored TS involves the *si* face of the chain and shows a *trans* geometry whereas the *cis* geometry is favored for the competitive *re*-face addition, with both monomers. Finally, with the (*S*)-Ph_2C(Cp)Flu-Zr system a *trans* geometry is favored in both TSs.[26a,28]

The geometries and the corresponding free energy ΔG_{Stereo} (kcal/mol, DCM) of the competitive TSs are reported in Figure 3.8 for **1** and in Figure 3.9 for **5** with both monomers. Focusing on AMA addition, with **1** the TS involving the *si*-face of the growing chain is favored by a ΔG_{Stereo} of 5.6 kcal/mol (Figure 3.8a vs. 3.8b). Competition is with addition of the *re*-face, which is disfavored by steric repulsion between the 6-membered ring of the indenyl ligand and the

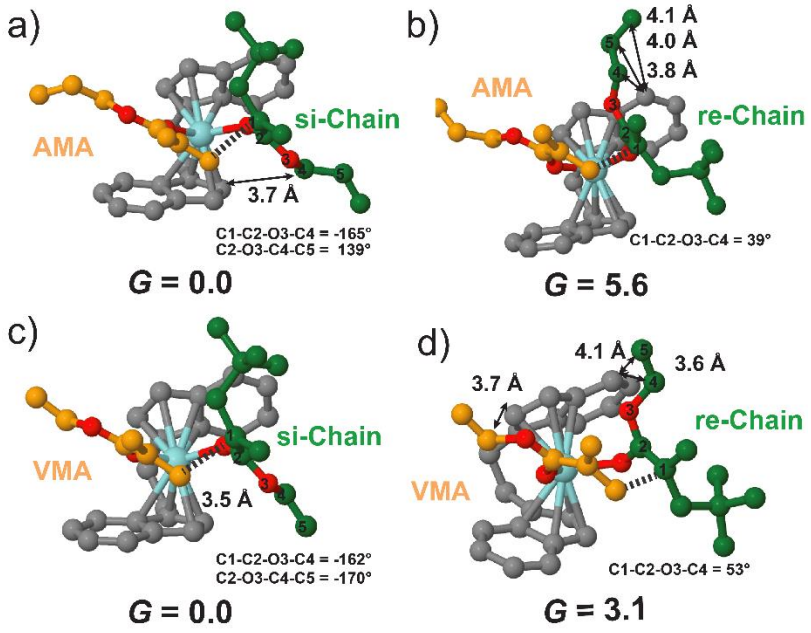

Figure 3.8. Transition state geometries for the competitive addition at the *si* and *re* face of the growing chain for AMA (**a** and **b**) and VMA (**c** and **d**), respectively, with (*S*,*S*)-EBI-Zr system (**1**). The free energies (kcal/mol, DCM) are relative to the TS involving the *si* face of the growing chain (**a** and **c**). The dashed line indicates the emerging C–C bonds.

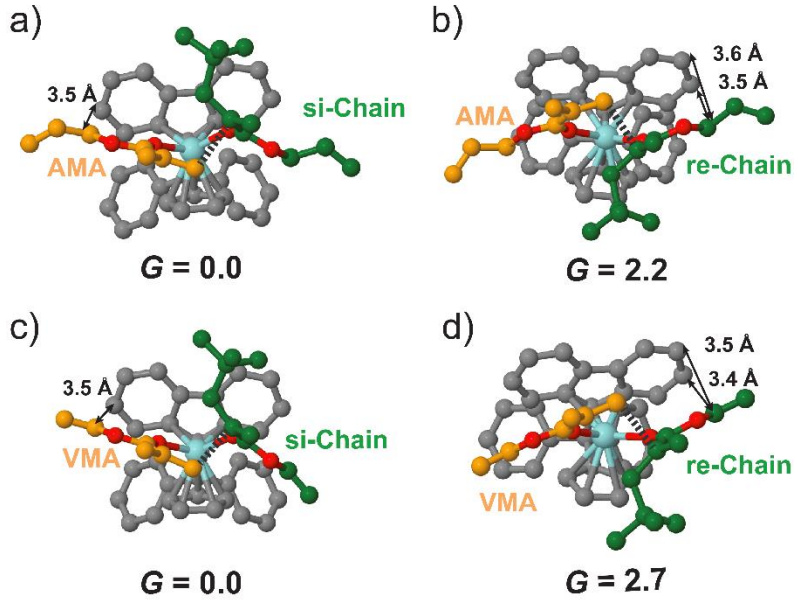

Figure 3.9. Transition state geometries of the competitive addition at the *si* and *re* face of the growing chain for AMA (**a** and **b**) and VMA (**c** and **d**), respectively, with (*S*)-Ph_2C(Cp)Flu-Zr system (**5**). The free energies (kcal/mol, DCM) are relative to the TS involving the *si* face of the growing chain (**a** and **c**). The dashed line indicates the emerging C–C bonds.

-OR group of the growing chain. To alleviate this steric clash the pendant –OR group of the chain rotates away from the indenyl ligand resulting in a gauche conformation of the C1-C2-O3-C4 dihedral angle (Figure 3.8b). Differently, in the favored *si*-face addition TS the C1-C2-O3-C4 dihedral angle is much closer to the ideal *trans* value (Figure 3.8a). The high ΔG_{Stereo} of 5.6 kcal/mol is in qualitative agreement with the high isotacticity of the obtained PAMA.

The competitive TSs geometries associated with VMA addition are compared in Figures 3.8c and 3.8d. In this case, addition of the *si*-face is favored by a ΔG_{Stereo} of 3.1 kcal/mol over addition of the *re*-face. As for AMA, the TS for addition of the *re*-face is disfavored by steric interaction between the pendant group of the chain and the indenyl ligand, resulting in a less stable conformation assumed by the growing chain, with a C1-C2-O3-C4 dihedral angle of 53° (Figure 3.8d). Although still rather large in absolute value, the ΔG_{Stereo} of 3.1 kcal/mol calculated for VMA is 2.5 kcal/mol lower than the ΔG_{Stereo} calculated for the AMA, in qualitative agreement with the observed much lower isotacticity of the produced PVMA. The lower stability of the favored *si*-face TS for VMA is responsible for the observed lower selectivity in the polymerization of VMA relative to AMA: the different nature of the ester carbon in the chain, sp^2 for VMA *vs* sp^3 for AMA, induces a different steric interaction between the chain and the metallocene skeleton, mainly in the favored *si*-face TSs (Figure 3.8a vs. 3.8c). In fact, despite the fact that the *si*-chain is located in the open part of the catalyst, being away from from the 6-membered ring of the indenyl ligand, in the case of VMA the rigid –O-CH=CH_2 group is forced to be close to the 5-membered ring of the ligand (see short distances reported in Figure 3.8c). Conversely, in the case of AMA, the sp^3 ester carbon of the –O-CH_2-CH=CH_2 moiety allows the chain to rotate away from the 5-membered ring of the ligand, minimizing unfavorable interaction between the –OR group of the growing chain

and the metallocene skeleton (compare the value of 139° for the C2-O3-C4-C5 dihedral angle in the case of AMA vs. the value of -170° in the case of VMA in Figures 3.8a and 3.8c, respectively).

Moving to C_S-ligated catalyst **5**, with both monomers, the favored TS involves the *si*-face of the chain, which is located in an open part of the space away from the fluorenyl moiety of the ligand (Figures 3.9a and 3.9c). Steric interaction between the monomer and the metallocene skeleton can be observed for both AMA and VMA. The competitive *re*-face TSs are disfavored by steric interaction between the chain and the ligand (see the short distance in Figures 3.9b and 3.9d). The rather similar ΔG_{Stereo} of 2.7 kcal/mol and 2.2 kcal/mol, calculated for VMA and AMA, respectively, are in good agreement with the experimentally observed similar syndiotacticity of PVMA and PAMA (although the syndiotacticity of PVMA is somewhat higher than that of PAMA, *vide supra*).

Post-Functionalization and Photocrosslinking to Functional Materials. Post-functionalization of syndiotactic polymers bearing the pendant vinyl (–CH=CH_2) functional group on every repeating unit was performed through two approaches: the thiol-ene "click" reaction and photocuring. The former approach has been widely used and proven to be highly effective for functionalization of ene-bearing polymers.[29] We first examined functionalization of *st*-PVMA (M_n = 40.9 kg/mol, $Đ$ = 1.19) and *st*-PDAA (M_n = 373 kg/mol, $Đ$ = 1.43) with two model thiols, 4-*tert*-butylbenzylmercaptan (RSH1) and 1-adamantanethiol (RSH2), using the click reaction with 2,2-dimethoxy-2-phenylacetophenone (DMPA) as the photoradical initiator under photochemical conditions (RT, UV lamp centered at λ = 350 nm) in chloroform (Scheme 3.3). The pendant vinyl groups were completely converted into new –CH_2CH_2-SR groups, as confirmed by ^{1}H NMR spectra (Figure 3.10 & Figure S3.5), which also showed that the tacticity of the resulting thiolated polymers was the same as the parent polymers in all the cases. GPC analysis of the thiolated

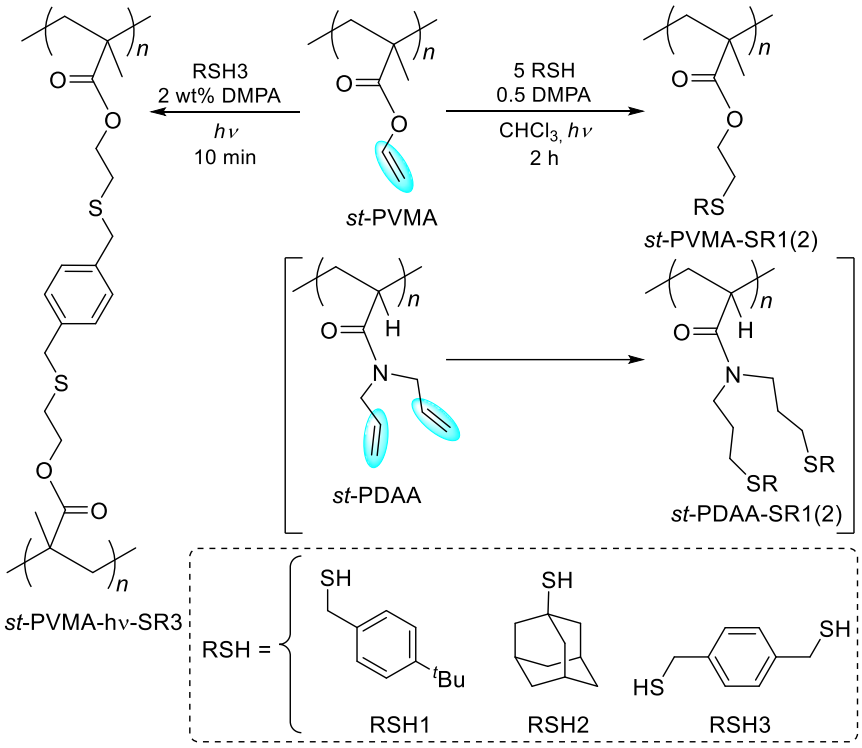

Scheme 3.3. Post-functionalization of *st*-PVMA and *st*-PDAA via the thiol-ene "click" chemistry.

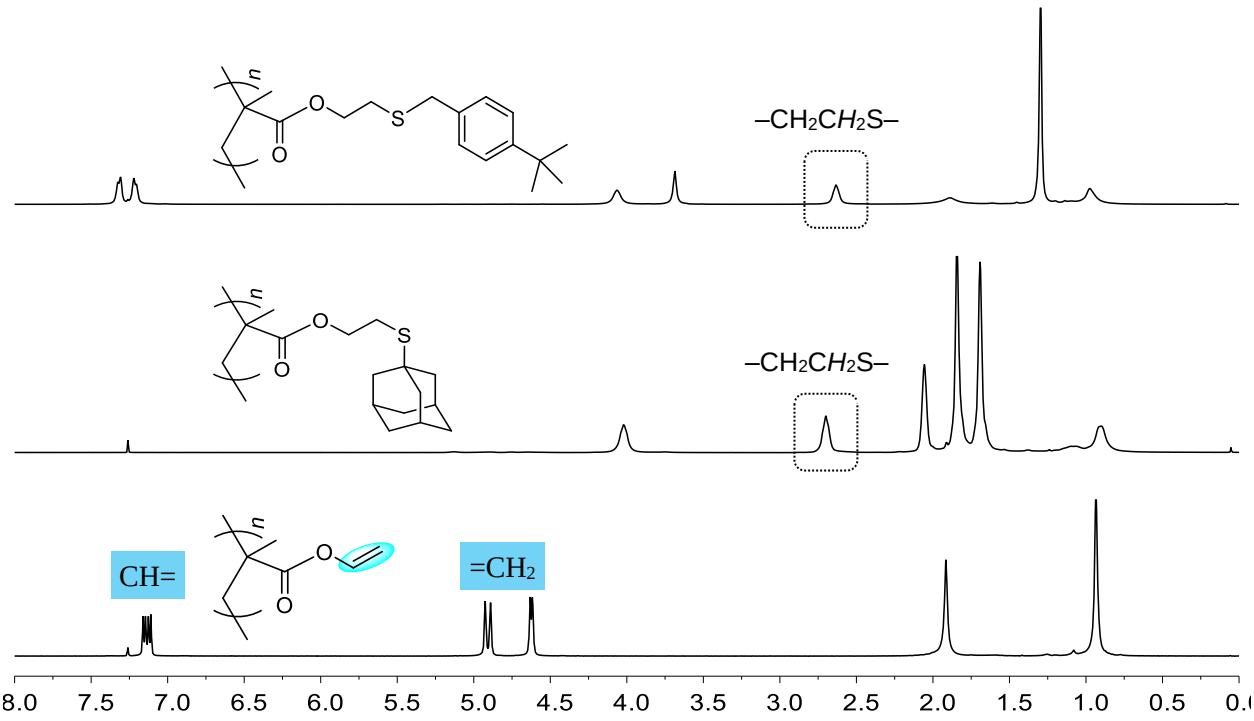

Figure 3.10. Overlay of ^{1}H NMR ($CDCl_3$, 25 °C) spectra of *st*-PVMA (bottom), *st*-PVMA-SR1 (top), and *st*-PVMA-SR2 (middle).

polymers, which are all soluble in chloroform, showed an increase in the M_n and $Đ$ values (Figure S3.6), indicative of some degree of light crosslinking due to the non-selective radical initiation in the presence of the high concentration of reactive C=C pendant groups. The thermal properties of the functionalized polymers were also significantly affected by the inclusion of the –SR groups. For instance, the first-step onset decomposition temperature (T_d) of *st*-PVMA (234 °C) measured by thermal gravimetric analysis (TGA) was enhanced by 62 °C to T_d = 296 °C of both *st*-PVMA-SR1 and *st*-PVMA-SR2 (Figure S3.7), attributed to the transformation of the –OCH=CH_2 group into the –OCH_2CH_2SR moiety, which was accompanied by a change in the T_g from 102 °C of *st*-PVMA to 39 °C and 118 °C of *st*-PVMA-SR1 and *st*-PVMA-SR2, respectively (Figure S3.8, top). In sharp contrast, *st*-PDAA exhibited a lower T_g (Figure S3.8, bottom), but high thermal stability than its thiolated polymers *st*-PDAA-SR1 and *st*-PDAA-SR2 (Figure S3.9).

Owing to the presence of the pendant vinyl groups, *st*-PVMA can also be readily photocured into flexible thin films for examining their thermo-mechanical properties. Thus, a solvent casted *st*-PVMA film was subjected to controlled crosslinking conditions under UV (350 nm) photoradical initiation with DMPA inside a Luzchem photoreactor for 10 min, producing a flexible, translucent, colorless thin film (*st*-PVMA-*hv*, Figure 3.11). A crosslinker, 1,4-benzenedimethanethiol (RSH3), was also added in varied amounts (2.5, 5, and 10 mol%) to prepare films with increased crosslinking and brittleness as the amount of RSH3 increases. Dynamic mechanical analysis (DMA) showed an increase in T_g from the parent *st*-PVMA film (105 °C) to the photocured *st*-PVMA-*hv* film (111 °C) after 10 min of UV irradiation, which was accompanied by an increase in both storage modulus (E') and loss modulus (E'') in both glassy (values reported at 25 °C) and rubbery (values reported at 150 °C) states, Figure 3.12 and Table 3.2 (entry 2 vs. 1). A further increase in T_g (measured by the peak maxima of the tan δ (E''/E')

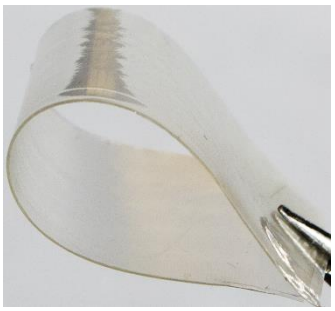

Figure 3.11. Photograph of solvent casted and photocured *st*-PVMA-*hv* film (0.06 mm thick).

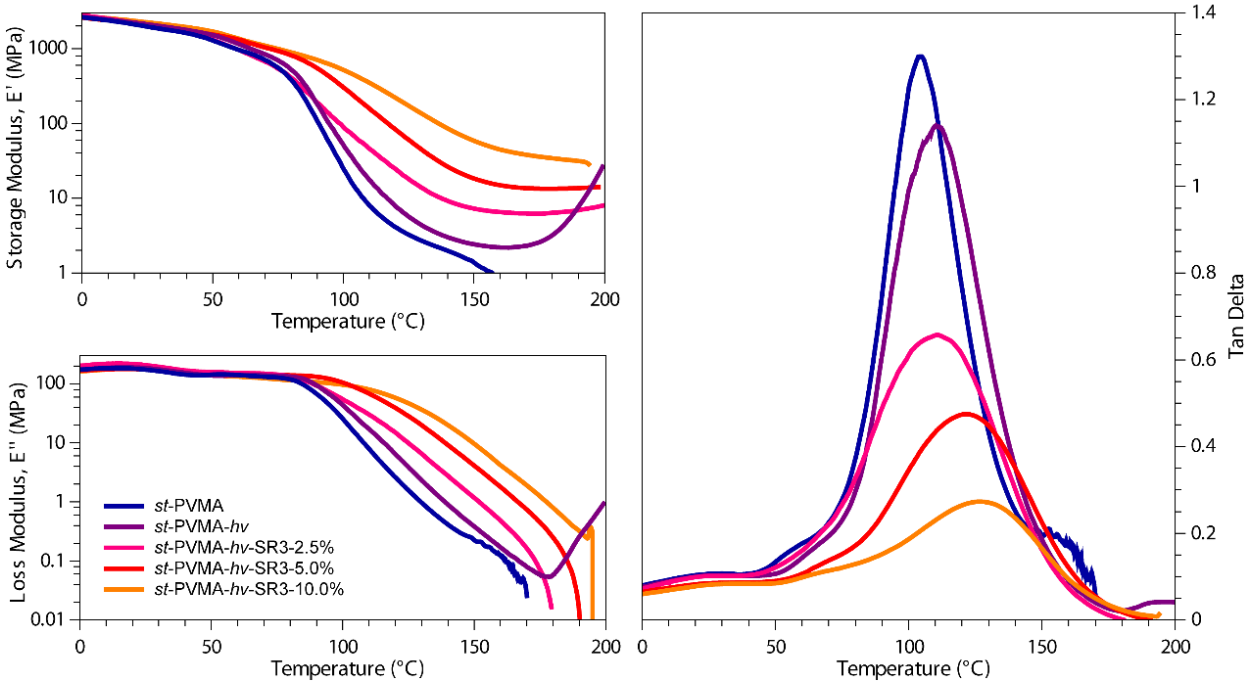

Figure 3.12. Storage modulus (*E*', top left), loss modulus (*E*'', bottom left), and tan δ (*E''*/*E'*, right) of *st*-PVMA (blue), photocured *st*-PVMA-*hv* (purple), *st*-PVMA-*hv*-SR3-2.5% (pink), *st*-PVMA-*hv*-SR3-5% (red), and *st*-PVMA-*hv*-SR3-10% (orange) determined by DMA analysis (3 °C min^{-1} temperature ramp rate).

curve in the DMA analysis) to 112, 121, and 128 °C was observed when the amount of the added crosslinker RSH3 was increased from 2.5 to 5.0 to 10 mol%, respectively (Table 3.2). This observed increasing T_g trend is a result of an increase in the degree of crosslinking, as characterized by the gradual increase in both *E*' and *E*'' values in the rubbery state (values reported at 150 °C, from entries 3 to 5, Table 3.2). On the other hand, TGA traces of all the thin films derived from *st*-PVMA were rather similar, displaying similar decomposition profiles (Figure S3.10). Likewise,

Table 3.2. Selected thermo-mechanical properties of parent and photo-cured polymers characterized by DMA.

entry no.	Polymer	T_g (°C)	E', 25 °C (GPa)	E'', 25 °C (MPa)	E', 150 °C (MPa)	E'', 150 °C (MPa)
1	*st*-PVMA	105	1.64	171	1.16	0.22
2	*st*-PVMA-*hv*	111	1.75	190	1.96	0.34
3	*st*-PVMA-*hv*-SR3-2.5%	112	1.73	178	6.00	0.95
4	*st*-PVMA-*hv*-SR3-5%	121	2.06	175	18.3	4.11
5	*st*-PVMA-*hv*-SR3-10%	128	1.32	107	34.5	5.67
6	*st*-PDAA-*hv*	56.1	1.04	90.7	49.8	5.47

a thin film of *st*-PDAA was also solvent casted and subsequently photocured in the presence of 2 wt% of DMPA. The resulting material, *st*-PDAA-*hv*, exhibited a T_g of 56.1 °C as measured by DMA (Figure S3.11).

Stereocomplexation and Photocuring to Robust Crosslinked Stereocomplexes. Stereocomplexes of diastereomeric polymer chains were formed effectively by mixing 10 mg/mL acetone solutions of *it*-PMMA with *st*-PVMA (designated *sc*-PMMA-PVMA, Figure 3.1) or *it*-PMMA with *st*-PAMA (designated *sc*-PMMA-PAMA) at 40 °C in 1:1 and 1:2 *it*-/*st*-polymer ratios, which were left to slowly crystallize at room temperature to obtain colorless, transparent thin films. The formation of such stereocomplexes is readily evident by observing a characteristic T_m peak from the DSC curves (Figure 3.13 and Figure S3.12) and a characteristic diffraction peak at $2\theta = 4.56$ ° ($d = 1.94$ nm) from the pXRD patterns (Figure 3.14a).[18] Interestingly, the T_m of the stereocomplexes was not significantly affected by the molar ratio of the diasteromeric polymer pair tested (1:1 vs. 1:2), but it is sensitive to the molecular weight of the *it*-PMMA component (Table 3.3). For instance, *sc*-PMMA-PVMA showed a T_m of 165 °C and 164 °C (in 1:1 and 1:2 ratios, respectively) with *it*-PMMA of M_n = 26.4 kg/mol ($Đ$ = 1.06, [*mm*] = 92.2), while the same stereocomplex displayed a much higher T_m of 188 °C and 186 °C (in 1:1 and 1:2 ratios, respectively) with *it*-PMMA of much higher molecular weight (M_n = 136 kg/mol, $Đ$ = 1.19, [*mm*]

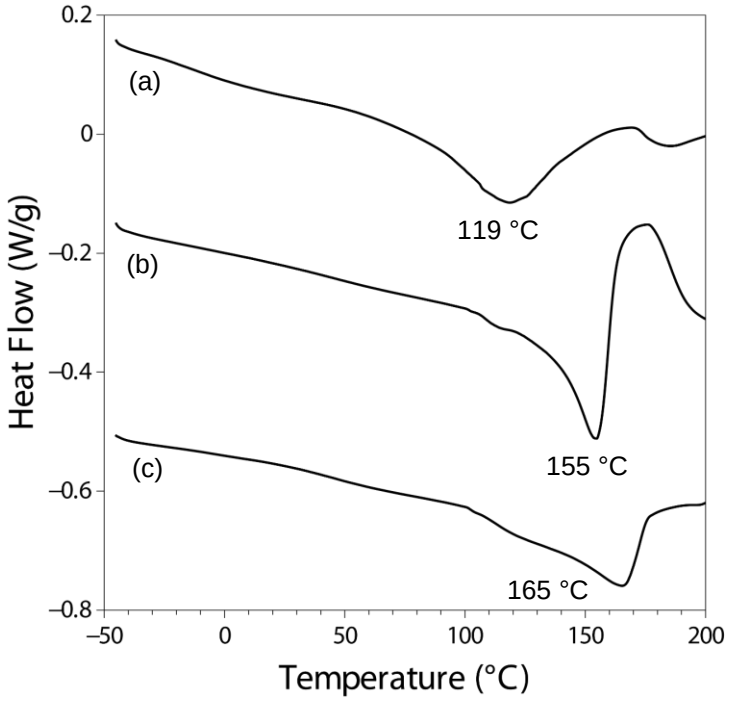

Figure 3.13. Representative DSC (10 °C min^{-1}) curves: (a) *sc*-PAMA-PMMA (Table 3.3, entry 1); (b) *sc*-PMMA-PAMA (Table 3.3, entry 3); and (c) *sc*-PMMA-PVMA (Table 3.3, entry 11) obtained by crystallization from acetone solutions.

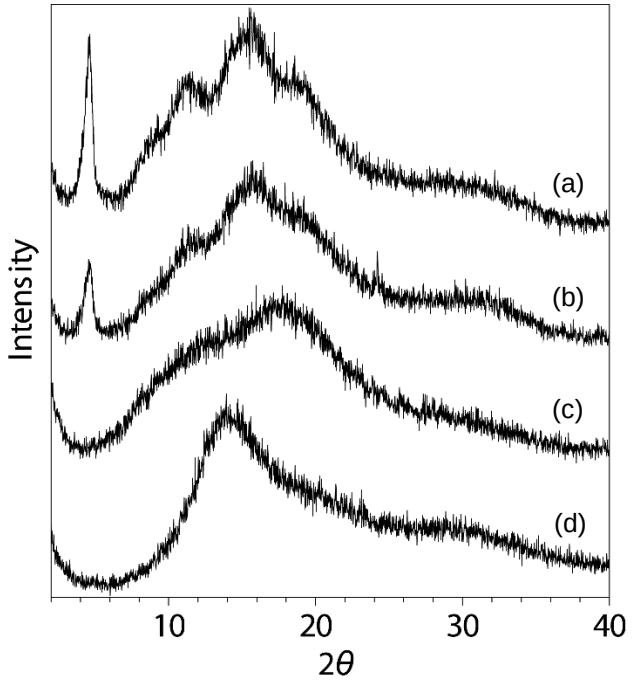

Figure 3.14. pXRD patterns of *sc*-PMMA-PVMA (a) and photocrosslinked *sc*-PMMA-PVMA-*hν* (b). Constituent diastereomeric polymers *st*-PVMA (c) and *it*-PMMA (d) included as a comparison.

Table 3.3. Stereocomplexation and photocrosslinking results [a]

entry no.	syndiotactic polymer	isotactic polymer	molar ratio (*st*/*it*)	T_m [b] (°C)	crosslinked vinyl polym.[c] (%)	trapped PMMA[c] (%)	PMMA trapping eff.[c] (%)
1	*st*-PMMA	*it*-PAMA	1:1	119	91.4	15.6	29
2	*st*-PAMA	–	–	–	97.2	–	–
3		low MW *it*-PMMA	1:1	155	77.7	12.5	23.0
4		low MW *it*-PMMA	2:1	157	85.8	20.0	29.9
5		high MW *it*-PMMA	1:1	165	85.5	51.8	73.4
6		high MW *it*-PMMA	2:1	168	84.7	50.5	67.2
7		(*it*-PMMA)$_{0.83}$-*b*-(*it*-PAMA)$_{0.17}$	1:1	168	63.7	49.1	86.7
8		(*it*-PMMA)$_{0.67}$-*b*-(*at*-PVMA)$_{0.33}$	1:1	170	79.0	63.0	89.6
9		(*it*-PMMA)$_{0.88}$-*ran*-(*it*-PAMA)$_{0.12}$	1:1	–	94.4	86.9	95.5
10	*st*-PVMA	–	–	–	58.3	–	–
11		low MW *it*-PMMA	1:1	165	56.5	56.2	99.6
12		low MW *it*-PMMA	2:1	164	56.2	13.5	31.4
13		high MW *it*-PMMA	1:1	188	62.7	50.5	88.6
14		high MW *it*-PMMA	2:1	186	54.1	39.0	78.7
15		(*it*-PMMA)$_{0.83}$-*b*-(*it*-PAMA)$_{0.17}$	1:1	181	66.4	58.5	93.9
16		(*it*-PMMA)$_{0.67}$-*b*-(*at*-PVMA)$_{0.33}$	1:1	182	71.1	59.8	92.6

[a] Polymer data: *st*-PAMA, M_n = 39.9 kDa, $Đ$ = 1.45, [*rr*] = 91.8; *it*-PAMA, M_n = 32.4 kDa, $Đ$ = 1.10, [*mm*] = 96.5; *st*-PVMA, M_n = 52.1 kDa, $Đ$ = 1.31, [*rr*] = 91.7; *st*-PMMA, M_n = 36.3 kDa, $Đ$ = 1.29, [*rr*] = 93.7; low MW *it*- PMMA, M_n = 26.4 kDa, $Đ$ = 1.06, [*mm*] = 92.2; high MW *it*-PMMA, M_n = 136.1 kDa, $Đ$ = 1.19, [*mm*] = 96.4; (*it*-PMMA)$_{0.83}$-*b*-(*it*-PAMA)$_{0.17}$, M_n = 89.6 kDa, $Đ$ = 1.37, [*mm*] = 93.1%; (*it*-PMMA)$_{0.67}$-*b*-(*at*-PVMA)$_{0.33}$, M_n = 76.8 kDa, $Đ$ = 1.49, [*mm*] = 79.8%, (*it*-PMMA)$_{0.88}$-*ran*-(*at*-PAMA)$_{0.12}$, M_n = 156 kDa, $Đ$ = 1.83, [*mm*] = 95.9%. [b] T_m measured by DSC. [c] See Appendix B.1 for the quantification method.

= 96.4). As expected, *it*-PAMA did not form a stereocomplex with either *st*-PAMA or *st*-PVMA in different ratios (1:1 and 1:2) and solvents (acetone and toluene) but, surprisingly, *it*-PAMA produced a weak stereocomplex with *st*-PMMA in both 1:1 and 1:2 ratios from their blends in acetone solutions, as revealed by broad T_m transitions of 119 °C (Figure 3.13a) and 120 °C, respectively. To further examine the effects of the ester group in the isotactic polymer chain on the formation of stereocomplexes, we also attempted the stereocomplexation between isotactic poly(*n*-butyl methacrylate) ([*mm*] = 96.9%, M_n ~ 28 kg/mol) and *st*-PVMA or *st*-PAMA in acetone (complexing solvent) in 1:1 and 1:2 *it*/*st* molar ratios. However, the resulting materials showed

only two T_g's corresponding to the constituent polymers, indicating that the stereocomplexation was hindered by the size of the *n*-butyl ester group of the isotactic polymer chain.

Control experiments by mixing *it*-PMMA with *st*-PVMA or *st*-PAMA in CH_2Cl_2 in a 1:1 *it*/*st* ratio led to amorphous polymer blends, which exhibited only the glass transitions corresponding to the constituent polymers of the blends, plus typical crosslinking exotherms of the vinyl-containing polymers appeared at temperatures higher than 150 °C. These results indicate that, just like *sc*-PMMA-PMMA, CH_2Cl_2 is also a non-complexing solvent for stereocomplexes *sc*-PMMA-PVMA and *sc*-PMMA-PAMA, the formation of which requires the use of complexating solvents such as acetone or toluene.

Under UV (350 nm) irradiation in the presence of photoradical initiator DMPA, the stereocomplex *sc*-PMMA-PVMA was successfully photocured into crosslinked, insoluble stereocomplex *sc*-PMMA-PVMA-*hv* (*c.f.*, Figure 3.1). The photocured stereocomplex exhibited a broad melting transition centered at ~150 °C (Figure S3.13), and a characteristic diffraction peak at 2θ = 4.56 °C (d = 1.94 nm) (Figure 3.14 b), thus confirming the stereocomplex structure is retained after crosslinking. Thin films of *sc*-PMMA-PVMA and photocrosslinked *sc*-PMMA-PVMA-*hv* were prepared and subsequently analyzed by DMA (Figure 3.15). While *it*-PMMA and *st*-PVMA showed a single sharp glass transition T_g at 45.2 °C and 105 °C, respectively, measured by the maxima of the tan δ curve, the stereocomplex sample *sc*-PMMA-PVMA showed two weak transitions at higher temperatures of 62.2 °C and 135 °C. The photocrosslinked samples *sc*-PMMA-PVMA-*hv* exhibited a similar behavior with a shift of the transitions to even higher temperatures of 67.2 °C and 158 °C, attributable to the crosslinking of the polymer networks. Noteworthy also is that the stereocomplex exhibited considerably higher storage modulus than its constituent *it*-PMMA and *st*-PVMA at high temperatures and that the crosslinked stereocomplex

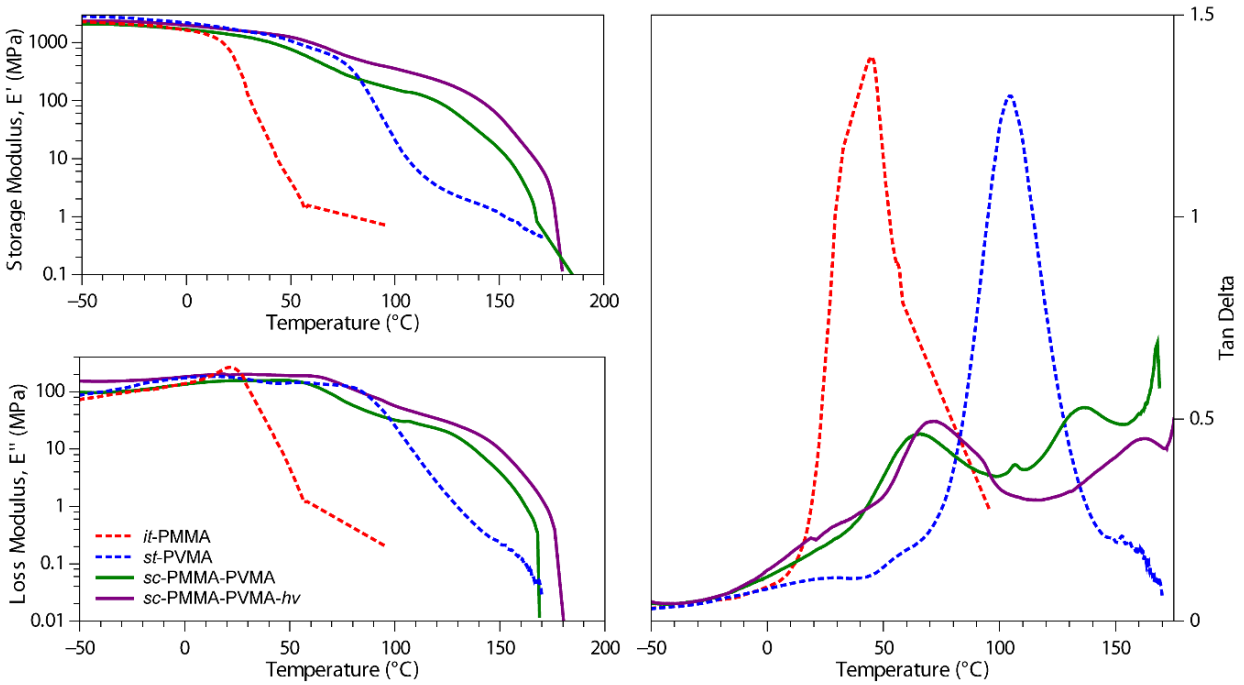

Figure 3.15. Storage modulus (E', top left), loss modulus (E'', bottom left), and tan δ (E''/E', right) of *it*-PMMA (red), *st*-PVMA (blue), *sc*-PMMA-PVMA (green), and *sc*-PMMA-PVMA-*hv* (purple) determined by DMA analysis (3 °C min^{-1} temperature ramp rate).

had the highest modulus. For instance, at 95 °C, E' was measured to be 0.713, 43.8, 175, and 392 MPa for *it*-PMMA, *st*-PVMA, *sc*-PMMA-PVMA, and *sc*-PMMA-PVMA-*hv*, respectively. Overall, these thermo-mechanical and X-ray diffraction analysis results demonstrate that stereocomplex formation significantly increases storage and loss moduli over the constituent *it*- and *st*-polymers at temperatures > 100 °C and that the photocured stereocomplex retains the stereocomplex structure but with considerably enhanced thermal and mechanical properties of the material.

Besides the above demonstrated enhanced thermal and mechanical properties of the crosslinked stereocomplex, we anticipate another novel feature of the crosslinked stereocomplex: it should be solvent resistant and thus cannot be decomplexed in a non-complexing (or decomplexing) solvent such as chloroform, in contrast to the conventional *it*-PMMA/*st*-PMMA stereocomplex. To this end, we examined if the *it*-PMMA helical chains can be trapped inside the

stereocomplex crosslinked via the outer helical layer of the vinyl-containing *st*-polymer. At the outset, a control experiment that consisted of a sample of *sc*-PMMA (a mixture of *it*-PMMA and *st*-PMMA in 1:1 ratio) containing 2 wt% of DMPA and subjected to UV irradiation (λ = 350 nm) for 2 h showed that the resulting stereocomplex was still completely soluble in chloroform and no PMMA was trapped due to no crosslinked chains. Using thermal crosslinking to trap the *it*-PMMA chains by annealing stereocomplex samples of *sc*-PMMA-PVMA and *sc*-PMMA-PAMA over 200 °C, at which temperature thermal crosslinking occurs, was unsuccessful; while the *st*-polymer was successfully crosslinked at this temperature, the *it*-PMMA chains were released from the melt. Next, *sc*-PMMA-PVMA and *sc*-PMMA-PAMA were photocrosslinked with 2 wt% of DMPA under UV irradiation (λ = 350 nm) for 2 h at room temperature. The crosslinked material was extracted with chloroform (a decomplexing solvent) for 24 h at 40 °C to promote the possible release of the complexed, but untrapped, *it*-PMMA. The amount of the crosslinked *st*-polymer as well as the trapped *it*-PMMA was quantified by ^{1}H NMR analysis (see Appendix B.1). The *it*-PMMA trapping efficiency was calculated as the percentage of the experimental *it*-PMMA content (wt%) found *vs* the theoretical *it*-PMMA content in the crosslinked stereocomplex if all the initial *it*-PMMA was effectively trapped. Table 3.3 summarized our study of *it*-PMMA trapping efficiency as a function of (a) *it*-PMMA molecular weight; (b) molar ratio of *it*-PMMA to *st*-PVMA (or *st*-PAMA); and (c) use of block and random copolymers incorporating the photo-crosslinkable units.

The results summarized in Table 3.3 showed that a control sample of *st*-PAMA afforded a much higher degree of crosslinking (97.2%) compared to *st*-PVMA (58.3%) when photocured under the same conditions. Similarly, stereocomplexes containing both *it*-PAMA and *st*-PAMA samples were more effectively photocrosslinked (from 63.7% to 91.4% degree of crosslinking)

than those containing *st*-PVMA (which achieved only 54.1% to 71.1%). Note that the self-crosslinking ability of *st*-PVMA in a sample crystallized from a CH_2Cl_2 solution (Table S3.1) was higher (82.4%), indicating that crystallization conditions impact the self-crosslinking ability of *st*-PVMA in the solid state. Under both conditions (acetone and CH_2Cl_2) tested, *st*-PAMA showed considerably better self-crosslinking ability (>95%) than *st*-PVMA, indicating that a longer, more flexible allyl ester group can be more efficiently crosslinked than the shorter and more rigid vinyl group in the VMA repeat unit. Stereocomplexes of *sc*-PMMA-PAMA with high MW *it*-PMMA (M_n = 136.1 kg/mol, $Đ$ = 1.19) achieved a higher PMMA trapping effiency (up to 73.4%, entry 5) than those stereocomplexes (up to 29.9, entry 4) with low MW *it*-PMMA (M_n = 26.4 kg/mol, $Đ$ = 1.06). No correlation was observed between the PMMA trapping efficiency and the molar ratio of the diastereomeric polymer pair. To possibly further enhance the PMMA trapping efficiency, we employed a new strategy of using block copolymers of *it*-PMMA with PAMA and PVMA to form stereocomplexes with *st*-PAMA and *st*-PVMA. Indeed, the PMMA trapping efficiency was enhanced to 86.7 and 89.6% (entries 7 and 8), indicating that a portion of the crosslinkable block is also photocured. The highest PMMA trapping efficiency of 95.5% (entry 9) was obtained from a blend of *st*-PAMA with a random copolymer, (*it*-PMMA)$_{0.88}$-*ran*-(*it*-PAMA)$_{0.12}$, but the stereocomplexation was hindered by the random placement of AMA units in the *it*-PMMA chain. In comparison, the PMMA trapping efficiency was generally higher (up to quantitative) for the stereocomplexes formed with *st*-PVMA (entries 11–16) than those with *st*-PAMA (entries 3–9). Again, higher PMMA trapping efficiencies were observed when block-copolymers containing crosslinkable AMA or VMA units were employed as the isotactic component to form the stereocomplex (> 92.6%, entries 15 and 16).

Additional control studies used the non-stereocomplexed control samples prepared by mixing *it*-PMMA with *st*-PVMA or *st*-PAMA in a non-complexing solvent (CH_2Cl_2), which were photocured under identical conditions to those reported for Table 3.3. The samples were further analyzed to quantify the capacity of the crosslinked *st*-vinyl polymers to trap *it*-PMMA and the results were summarized in Table S3.1. The results showed that the *it*-PMMA trapping efficiency was almost negligible (0.6 to 2.6%), indicating that the photocrosslinked polymer blends are not capable of trapping the *it*-PMMA chains. These control experiments highlight the importance of the polymer supramolecular structure to efficiently trap the *it*-PMMA chains, achievable only when the stereocomplexes are formed. For instance, while the *sc*-PMMA-PVMA formed in acetone had a PMMA trapping efficiency of 99.6% (entry 11, Table 3.3), the same mixture made in CH_2Cl_2 only showed a PMMA trapping efficiency of 2.6% (entry 4, Table S3.1).

We also investigated the possible complexation of *st*-PVMA and *st*-PAMA with fullerene C_{60} to form an inclusion complex, *ic*-PVMA-C_{60} or *ic*-PAMA-C_{60}. The material formed between *st*-PVMA and C_{60} exhibited a broad melting transition peak at temperature > 150 °C, which was overlapped with much intense exothermic peaks (due to thermally induced crosslinking), thus offering no clear evidence for the inclusion complex formation. However, we obtained conclusive evidence that *st*-PAMA readily forms inclusion complexes *ic*-PAMA-C_{60} (Figure 3.16) with C_{60} in different ratio combinations (Table 3.4). The formation of such inclusion complex was evidenced by the appearance of a sharp melting transition from 200 to 211 °C (Figure 3.17), observed from the DSC analysis of the resulting product after crystallization. The DSC thermograms of commercial fullerene C_{60}, *st*-PAMA, a non-inclusion mixture of *st*-PAMA/C_{60} (obtained from the annealing of the blend at 80 °C for 20 h), and *ic*-PAMA-C_{60} are shown in Figure 3.18 for comparison. The first-order transition in the DSC thermogram of C_{60} corresponds to the

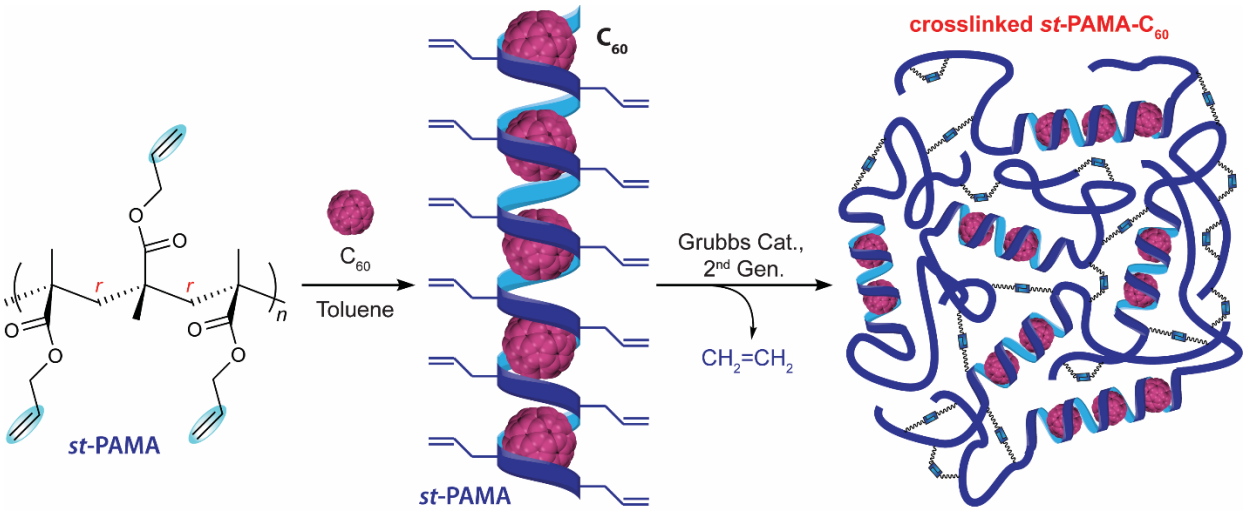

Figure 3.16. Schematic representation of inclusion complex formation of *ic*-PAMA-C_{60} and its crosslinking *via* olefin metathesis.

Table 3.4. Results of complexation between *st*-PAMA and C_{60} and subsequent crosslinking by olefin metathesis [a]

entry no.	*st*-PAMA concentration (mg mL^{-1})	C_{60} solution (mg mL^{-1})	solvent	T_g [b] (°C)	T_m [b] (°C)	yield after crosslinking (%) [c]	encapsulated C_{60} content (wt%) [d]
1	5.0	1.0	Tol	47.9	200	n.d.	n.d.
2	5.0	2.0	Tol	53.1	206	n.d.	n.d.
3	10.0	1.0	Tol	53.6	207	>99	3.39
4	10.0	2.0	Tol	52.8	205	>99	4.77
5	10.0	10.0	Tol-DCB	56.3	207	>99	9.18
6	20.0	1.0	Tol	52.6	–	n.d.	n.d.
7	20.0	2.0	Tol	55.1	211	n.d.	n.d.
8	20.0	10.0	Tol-DCB	57.3	207	n.d.	n.d.

[a] Conditions: 2.0 mL solvent (Tol = toluene or Tol-DCB = toluene/1,2-dichlorobenzene mixture in 50:50 vol%), except for entries 1 and 2 (5.0 mL); Grubb's catalyst 2nd Gen. (2 mol%); *st*-PAMA (M_n = 39.9 kDa, $Đ$ = 1.45, [*rr*] = 91.8); n.d. = not determined. [b] T_g and T_m before crosslinking measured by DSC. [c] Determined by gravimetric measurements. [d] Calculated by TGA.

well-known phase transition between a simple cubic (sc) lattice (below the T_{tr} = −14.8 °C) and a face-centered cubic lattice (fcc).[30] The *st*-PAMA shows a T_g of 49.9 °C, plus broad thermal crosslinking exothermic peak at temperature > 150 °C, whereas the non-inclusion complex mixture of *st*-PAMA/C_{60} shows both mentioned features of the individual components. In sharp contrast,

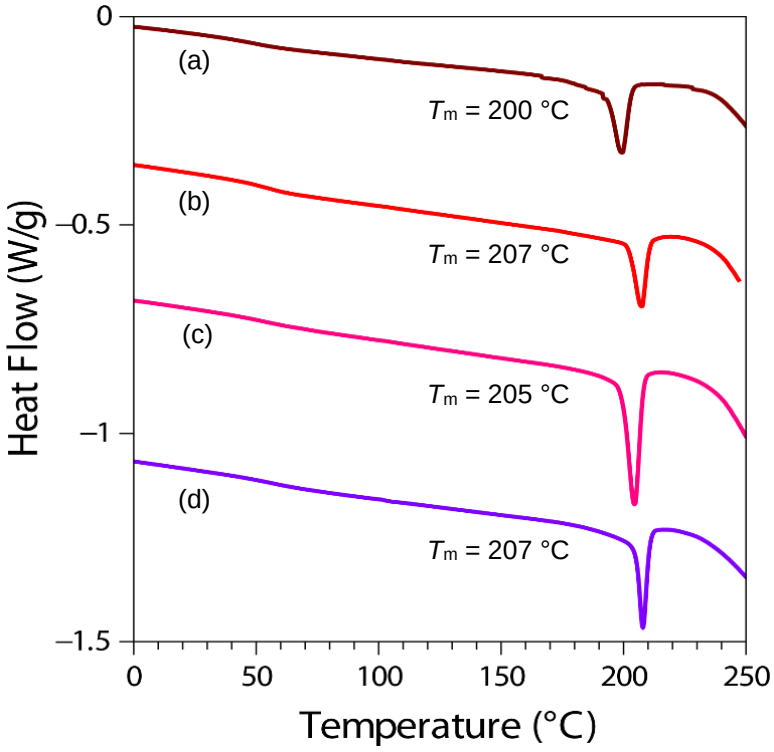

Figure 3.17. DSC thermograms (10 °C min^{-1}) of *ic*-PAMA-C_{60} produced from toluene solutions of *st*-PAMA and C_{60}: Table 3.4, entry 1 (a), entry 3 (b), entry 4 (c), and entry 8 (d).

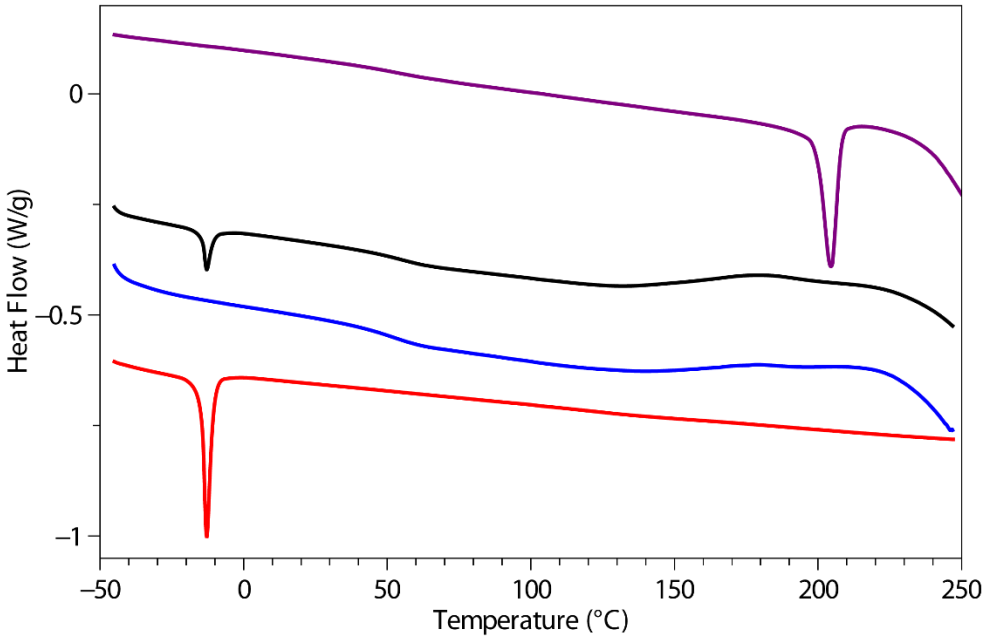

Figure 3.18. DSC (10 °C min^{-1}) thermograms of: commercial fullerene C_{60} powder (red); *st*-PAMA (blue); annealed blend of *st*-PAMA/C_{60} at 80 °C for 20 h (black); and *ic*-PAMA-C_{60} from Table 3.4, entry 4 (purple).

the *ic*-PAMA-C_{60} obtained by crystallization from toluene exhibits a novel feature: a markedly sharp melting transition at T_m = 205 °C, indicative of the inclusion complex formation.

Three approaches were explored to produce crosslinked *ic*-PAMA-C_{60}. First, photochemically induced radical crosslinking with DMPA as the initiator under UV irradiation (λ = 350 nm) in solution or solid state did not produce the crosslinked product, as the crystallized material was again completely soluble in toluene. Second, thermally induced radical crosslinking with BPO (benzoyl peroxide) as the initiator also failed to afford the target crosslinked *ic*-PAMA-C_{60}. Third, recognizing C_{60} as an excellent radical trap,[31] we turned out attention to non-radical crosslinking methods. To this end, successful crosslinking of *ic*-PAMA-C_{60} was achieved using 2 mol% of the Grubbs catalyst (2^{nd} Gen.) [32] in toluene at room temperature for 2 h (Figure 3.16; entries 3–5, Table 3.4). However, the DSC thermogram of the material obtained from the solution-phase metathesis crosslinking of *ic*-PAMA-C_{60} exhibited no melting transition peak but a T_g of 106 °C, which is about 50 °C higher than the parent *st*-PAMA. This result indicates most, if not all, the helical inclusion complex structure was disrupted by this solution crosslinking reaction to form a mostly amorphous crosslinked structure (Figure 3.16).

Once successfully crosslinked, the C_{60} encapsulated inside the network of crosslinked *st*-PAMA-C_{60} cannot be reversibly recovered by dissolution of the inclusion complex as it is no longer soluble in toluene. A control reaction was performed to assess the Ru catalyst residue in the crosslinked complex by performing a crosslinking reaction of *st*-PAMA under the same conditions but without C_{60}. The content of C_{60} in the crosslinked complex was calculated through TGA analysis (Figure 3.19) by subtracting the residue in the trace at 500 °C of *st*-PAMA-C_{60}, minus the control experiment (3.49 wt%). These results indicated an uptake of C_{60} up to 9.18 wt% in the crosslinked *st*-PAMA-C_{60} when a 10.0 mg/mL solution of C_{60} in the feed was employed.

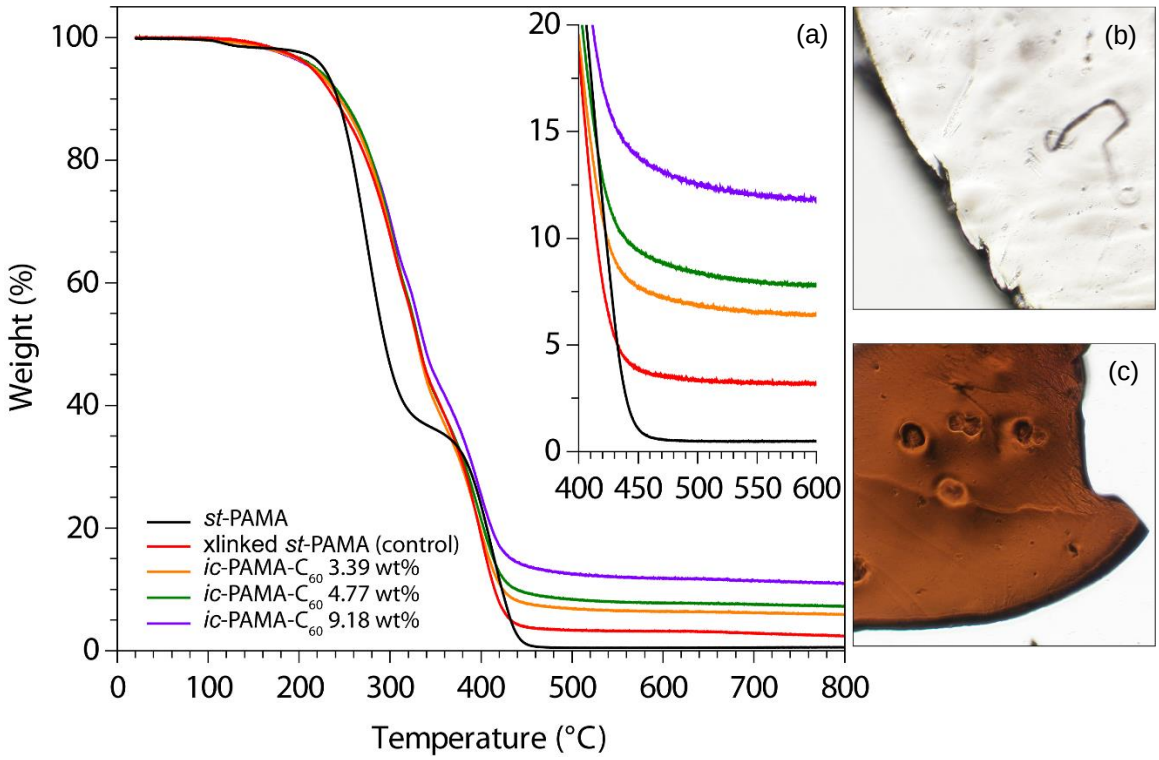

Figure 3.19. (a) TGA (10 °C min^{-1}) traces of *st*-PAMA (black), crosslinked *st*-PAMA control (red), crosslinked *ic*-PAMA-C_{60} 3.43 wt% (orange), crosslinked *ic*-PAMA-C_{60} 4.77 wt% (green), and crosslinked *ic*-PAMA-C_{60} 9.18 wt% (purple); (b) microphotograph of *st*-PAMA film sample, and (c) microphotograph of crosslinked *ic*-PAMA-C_{60} 4.77 wt% film.

3.4. Conclusions

The perfectly chemoselective and highly syndiospecific coordination polymerization of divinyl polar monomers developed through this work has enabled the synthesis of highly syndiotactic polar vinyl polymers bearing the pendant reactive C=C bond on each repeat unit. Polymerization of three representative polar divinyl monomers (AMA, VMA, and DAA) by the C_s-ligated zirconocenium ester enolate catalysts under ambient conditions all achieved complete chemoselectivity and high stereoselectivity, producing the corresponding vinyl-functionalized polymers with syndiotacticity following this trend: *st*-PDAA (> 99% *rr*) > *st*-PVMA (96% *rr*) > *st*-PAMA (92% *rr*). Careful examination of the VMA polymerization by catalyst **5**, including synthetic, kinetic and mechanistic studies, showed that the polymerization follows a unimetallic,

enantiomorphic-site controlled mechanism through the cationic cyclic metallacycle resting intermediate and exhibits the ability to control the resulting polymer M_n and $Đ$ values. DFT calculations on free energy ΔG_{Stereo} of the transition state geometries for the competitive (correct and incorrect enantiofacial) additions in the polymerization of AMA and VMA provided a theoretical basis for the observed large difference in isotacticity of the polymers produced by C_2-ligated catalyst **1**, but the rather similar syndiotacticity of the polymers produced by C_5-ligated catalyst **5**.

The pendant vinyl groups of the obtained syndiotactic polymers can be completely converted into the corresponding thiolated polymers of the same tacticity, via the thiol-end click reaction with different thiols. Such polymers can also be readily photocured into flexible, crosslinked thin films for examining their thermo-mechanical properties, which revealed an expected increase in T_g, E', and E'' values as the degree of crosslinking increases.

Vinyl-functionalized syndiotactic polymers, *st*-PVMA and *st*-PAMA, can readily form crystalline stereocomplexes with *it*-PMMA in a 2:1 or 1:1 molar ratio, but *st*-PVMA appears to form a stronger stereocomplex, as evidenced by the observed higher T_m, presumably due to the higher syndiotacticity of the constituent *st*-PVMA. Interestingly, *it*-PAMA also formed a weak stereocomplex with *st*-PMMA, and isotactic block copolymers *it*-PMMA-*b*-*it*-PAMA and *it*-PMMA-*b*-*it*-PVMA, but not their random copolymers, readily form crystalline stereocomplexes with either *st*-PAMA or *st*-PVMA; both findings extended the *it*-polymer capable of stereocomplexation beyond *it*-PMMA. The *it*-/*st*- stereocomplex, *sc*-PMMA-PVMA, can be readily photocured into a crosslinked, insoluble stereocomplex that exhibits high *it*-PMMA trapping efficiencies. Thermo-mechanical and X-ray diffraction analysis results showed that stereocomplex formation significantly increases storage and loss moduli over the constituent *it*-

and *st*-polymers at temperatures > 100 °C and that the photocured stereocomplex retains the stereocomplex structure but with considerably enhanced thermal and mechanical properties of the material.

st-PAMA readily forms inclusion complexes, *ic*-PAMA-C_{60}, with C_{60} in different ratio combinations. Crosslinking of *ic*-PAMA-C_{60} was achieved successfully *via* olefin metathesis using the Grubbs catalyst (2^{nd} Gen.), while the photocuring in the presence of the photoinitiator was unsuccessful, attributable to C_{60} being an excellent radical trap. The encapsulated C_{60} in the resulting crosslinked *st*-PAMA-C_{60} can no longer be released by dissolution of the inclusion complex, in contrast to the uncrosslinked inclusion complex.

REFERENCES

(1) Selected reviews: (a) *Stereoselective Polymerization with Single-Site Catalysts*, Baugh, L. S.; Canich, J. A. M., Eds.; CRC Press/Taylor & Francis Group: Boca Raton, FL, **2008**. (b) Resconi, L.; Chadwick, J. C.; Cavallo, L. in *Comprehensive Organometallic Chemistry III;* Bochmann, M. Vol. Ed.; Mingos, M. P.; Crabtree, R. H. Chief Eds.; Elsevier: Oxford, **2007**; Vol. 4, pp 1005−1166. (c) Coates, G. W. *Chem. Rev.* **2000**, *100*, 1223−1252. (d) Brintzinger, H. H.; Fischer, D.; Mülhaupt, R.; Rieger, B.; Waymouth, R. M. *Angew. Chem., Int. Ed.* **1995**, *34*, 1143−1170.

(2) Selected recent examples and reviews: (a) Jian, Z.; Baier, M. C.; Mecking, S. *J. Am. Chem. Soc.* **2015**, *137*, 2836–2839. (b) Ota, Y.; Ito, S.; Kuroda, J.; Okumura, Y.; Nozaki, K. *J. Am. Chem. Soc.* **2014**, *136*, 11898–11901. (c) Nakamura, A.; Anselment, T. M. J.; Claverie, J. P.; Goodall, B.; Jordan, R. F.; Mecking, S.; Rieger, B.; Sen, A.; van Leeuwen, P. W. N. M.; Nozaki, K. *Acc. Chem. Res.* **2013**, *46*, 1438–1449. (d) Delferro, M.; Marks, T. J. *Chem. Rev.* **2011**, *111*, **2450–2485**. (e) Nakamura, A.; Ito, S.; Nozaki, K. *Chem. Rev.* **2009**, *109*, 5215–5244. (f) Berkefeld, A.; Mecking, S. *Angew. Chem., Int. Ed.* **2008**, *47*, 2538–2542. (g) Luo, S.; Vela, J.; Lief, G. R.; Jordan, R. F. *J. Am. Chem. Soc.* **2007**, *129*, 8946–8947. (h) Domski, G. J.; Rose, J. M.; Coates, G. W.; Bolig, A. D.; Brookhart, M. *Prog. Polym. Sci.* **2007**, *32*, 30−92. (i) Jensen, T. R.; Yoon, S. C.; Dash, A. K.; Luo, L.; Marks, T. J. *J. Am. Chem. Soc.* **2003**, *125*, 14482−14494. (j) Gibson, V. C.; Spitzmesser, S. K. *Chem. Rev.* **2003**, *103*, 283–315. (k) Coates, G. W.; Hustad, P. D.; Reinartz, S. *Angew. Chem. Int. Ed. Engl.* **2002**, *41*, 2236–2257. (l) Ittel, S. D.; Johnson, L. K.; Brookhart, M. *Chem. Rev.* **2000**, *100*, 1169–1204.

(3) Selected reviews: (a) Soller, B. S.; Salzinger, S.; Rieger, B. *Chem. Rev.* **2016**, *116*, 1993–2022. (b) Chen, E. Y.-X. *Chem. Rev.* **2009**, *109*, 5157–5214. (c) Yasuda, H. *Prog. Polym. Sci.* **2000**, *25*, 573−626.

(4) Selected examples: (a) Zhang, N.; Salzinger, S.; Soller, B. S.; Rieger, B. *J. Am. Chem. Soc.* **2013**, *135*, 8810−8813. (b) Chen, X.; Caporaso, L.; Cavallo, L.; Chen, E. Y.-X. *J. Am. Chem. Soc*. **2012**, *134*, 7278–7281. (c) Miyake, G. M.; Mariott, W. R.; Chen, E. Y.-X. *J. Am. Chem. Soc.* **2007**, *129*, 6724−6725. (d) Lian, B.; Spanio, T. P.; Okuda, J. *Organometallics* **2007**, *26*, 6653−6660. (e) Lian, B.; Thomas, C. M.; Navarro, C.; Carpentier, J.-F. *Organometallics* **2007**, *26*, 187−195. (f) Stojcevic, G.; Kim, H.; Taylor, N. J.; Marder, T. B.; Collins, S. *Angew. Chem. Int. Ed.* **2004**, *43*, 5523–5526. (g) Strauch, J. W.; Fauré, J.-L.; Bredeau, S.; Wang, C.; Kehr, G.; Fröhlich, R.; Luftmann, H.; Erker, G. *J. Am. Chem. Soc.* **2004**, *126*, 2089–2104. (h) Frauenrath, H.; Keul, H.; Höcker, H. *Macromolecules* **2001**, *34*, 14–19. (i) Bandermann, F.; Ferenz, M.; Sustmann, R.; Sicking, W. *Macromol. Symp.* **2001**, *174*, 247–253. (j) Cameron, P. A.; Gibson, V.; Graham, A. J. *Macromolecules* **2000**, *33*, 4329–4335. (k) Li, Y.; Ward, D. G.; Reddy, S. S.; Collins, S. *Macromolecules* **1997**, *30*, 1875–1883. (l) Deng, H.; Shiono, T.; Soga, K. *Macromolecules* **1995**, *28*, 3067–3073. (m) Collins, S.; Ward, S. G. *J. Am. Chem. Soc.* **1992**, *114*, 5460–5462. (n) Yasuda, H.; Yamamoto, H.; Yokota, K.; Miyake, S.; Nakamura, A. *J. Am. Chem. Soc.* **1992**, *114*, 4908−4909.

(5) (a) Gao, H.; Matyjaszewski, K. *Prog. Polym. Sci.* **2009**, *34*, 317−350. (b) Li, Z.; Day, M.; Ding, J.; Faid, K. *Macromolecules* **2005**, *38*, 2620−2625. (c) Percec, V.; Auman, B. C. *Macromol. Chem. Phys.* **1984**, *185*, 2319−2336.

(6) Selected examples: (a) Sugiyama, F.; Satoh, K.; Kamigaito, M. *Macromolecules* **2008**, *41*, 3042−3048. (b) Ma, J.; Cheng, C.; Sun, G. R.; Wooley, K. L. *Macromolecules* **2008**, *41*,

9080−9089. (c) Vardareli, T. K.; Keskin, S.; Usanmaz, A. *J. Macromol. Sci., Part A: Pure Appl. Chem.* **2008**, *45*, 302−311. (d) París, R. J.; Fuente, L. D. *J. Polym. Sci., Part A: Polym. Chem.* **2005**, *43*, 6247−6261. (e) París, R. J.; Fuente, L. D. *J. Polym. Sci., Part A: Polym. Chem.* **2005**, *43*, 2395−2406. (f) Nagelsdiek, R.; Mennicken, M.; Maier, B.; Keul, H.; Hartwig, H. *Macromolecules* **2004**, *37*, 8923−8932.

(7) Pugh, C.; Percec, V. *Polym. Bull.* **1985**, *14*, 109−116.

(8) Selected examples: (a) Mohan, Y. M.; Raghunadh, V.; Sivaram, S.; Baskaran, D. *Macromolecules* **2012**, *45*, 3387−3393. (b) Lu, Z.; Lee, S. Y.; Goh, S. H. *Polymer* **1997**, *38*, 5893−5895. (c) Fukuda, W.; Nakao, M.; Okumura, K.; Kakiuchi, H. *J. Polym. Sci. Part A: Polym. Chem.* **1972**, *10*, 237−250.

(9) Chen, E. Y.-X. *Top. Curr. Chem.* **2013**, *334*, 239–260.

(10) (a) Chen, J.; Chen, E. Y.-X. *Isr. J. Chem.* **2015**, *55*, 216–225. (b) Jia, Y.-B.; Ren, W.-M.; Liu, S.-J.; Xu, T.; Wang, Y.-B.; Lu, X.-B. *ACS Macro Lett.* **2014**, *3*, 896–899.

(11) Xu, T.; Liu, J.; Lu, X.-B. *Macromolecules* **2015**, *48*, 7428–7434.

(12) Bolig, A. D.; Chen, E. Y.-X. *J. Am. Chem. Soc.* **2004**, *126*, 4897−4906.

(13) Rodriguez-Delgado, A.; Chen, E. Y.-X. *Macromolecules* **2005**, *38*, 2587−2594.

(14) (a) Mariott, W. R.; Chen, E. Y.-X. *Macromolecules* **2005**, *38*, 6822−6832. (b) Mariott, W. R.; Chen, E. Y.-X. *Macromolecules* **2004**, *37*, 4741−4743.

(15) Vidal, F.; Gowda, R. R.; Chen, E. Y.-X. *J. Am. Chem. Soc.* **2015**, *137*, 9469−9480.

(16) Selected examples of *sc*-PMMA: (a) Ren, J. M.; Satoh, K.; Goh, T. K.; Blencowe, A.; Nagai, K; Ishitake, K.; Christofferson, A. J.; Yiapanis, G.; Yarovsky, I.; Kamigaito, M.; Qiao, G. G. *Angew. Chem. Int. Ed.* **2014**, *53*, 459–464. (b) Goh, T. K.; Tan, J. F.; Guntari, S. N.; Satoh, K.; Blencowe, A.; Kamigaito, M.; Qiao, G. G. *Angew. Chem. Int. Ed.* **2009**, *48*, 8707–8711.

(c) Kawauchi, T.; Kumaki, J.; Yashima, E. *J. Am. Chem. Soc.* **2006**, *128*, 10560–10567. (d) Kawauchi, T.; Kumaki, J.; Okoshi, K.; Yashima, E. *Macromolecules* **2005**, *38*, 9155–9160. (e) Serizawa, T.; Hamada, K.-I.; Akashi, M. *Nature* **2004**, *429*, 52–55. (f) Slager, J.; Domb, A. J. *Adv. Drug Delivery Rev.* **2003**, *55*, 549–583. (g) Serizawa, T.; Hamada, K.; Kitayama, T.; Fujimoto, N.; Hatada, K.; Akashi, M. *J. Am. Chem. Soc.* **2000**, *122*, 1891–1899. (h) Hatada, K.; Kitayama, T.; Ute, K.; Nishiura, T. *Macromol. Symp.* **1998**, *132*, 221–230. (i) te Nijenhuis, K. *Adv. Polym. Sci.* **1997**, *130*, 67–81; 244–246. (j) Spevacek, J.; Schneider, B. *Adv. Colloid Interface Sci.* **1987**, *27*, 81–150. (k) Watanabe, W. H.; Ryan, C. F.; Fleischer, Jr. D. C.; Garret, B. S. *J. Phys. Chem.* **1961**, *65*, 896–896. (l) Fox, T. G.; Garret, B. S.; Goode, W. E.; Gratch, S.; Rincaid, J. F.; Spell, A.; Stroupe, J. D. *J. Am. Chem. Soc.* **1958**, *80*, 1768–1769.

(17) (a) Christofferson, A. J.; Yiapanis, G.; Ren, J. M.; Qiao, G. G.; Satoh, K.; Kamigaito, M.; Yarovsky, I. *Chem. Sci.* **2015**, *6*, 1370–1378. (b) Kumaki, J.; Kawauchi, T.; Ute, K.; Kitayama, T.; Yashima, E. *J. Am. Chem. Soc.* **2008**, *130*, 6373–6380. (c) Kumaki, J.; Kawauchi, T.; Okoshi, K.; Kusanagi, H.; Yashima, E. *Angew. Chem. Int. Ed.* **2007**, *46*, 5348–5351. (d) Schomaker, E.; G. Challa, G. *Macromolecules* **1989**, *22*, 3337–3341. (e) Bosscher, G.; ten Brinke, G.; Eshuis, A.; Challa, G. *Macromolecules* **1982**, *15*, 1364–1368. (f) Kusanagi, H.; Tadokoro, H.; Chatani, Y. *Macromolecules* **1976**, *9*, 531–532. (g) Liquori, A. M.; Anzuino, G.; Coiro, V. M.; D'Alagni, M.; de Santis, P.; Savino, M. *Nature* **1965**, *206*, 358–362.

(18) (a) Asai, S.; Kawano, T.; Hirota, S.-I.; Tominaga, Y.; Sumita, M.; Mizumoto, T. *Polymer* **2007**, *48*, 5116–5124. (b) Schomaker, E.; Challa, G. *Macromolecules* **1988**, *21*, 2195–2203. (c) Bosscher, F.; ten Brinke, G.; Challa, G. *Macromolecules* **1982**, *15*, 1442–1444.

(19) (a) Hatada, K.; Kitayama, T.; Ute, K.; Fujimoto, N.; Miyatake, N. *Macromol. Symp.* **1994**, *84*, 113–126. (b) Kitayama, T.; Fujimoto, N.; Hatada, K. *Polym. Bull.* **1991**, *26*, 629–636.

(20) Escudé, N. C.; Ning, Y.; Chen, E. Y.-X. *Polym. Chem.* **2012**, *3*, 3247–3255.

(21) Mariott, W. R.; Escudé, N. C.; Chen, E. Y.-X. *J. Polym. Sci. Part A: Polym. Chem.* **2007**, *45*, 2581−2592.

(22) Mariott, W. R.; Chen, E. Y.-X. *J. Am. Chem. Soc.* **2003**, *125*, 15726–15727.

(23) Escudé, N. C.; Chen, E. Y.-X. *Chem. Mater.* **2009**, *21*, 5743–5753.

(24) (a) Kusuyama, H.; Miyamoto, N.; Chatani, Y.; Tadokoro, H. *Polymer* **1983**, *24*, 119–122. (b) Kusuyama, H.; Takase, M.; Higashihara, Y.; Tseng, H.-T.; Chatani, Y.; Tadokoro, H. *Polymer* **1982**, *23*, 1256–1258.

(25) (a) Kawauchi, T.; Kitaura, A.; Kawauchi, M.; Takeichi, T.; Kumaki, J.; Lida, H.; Yashima, E. *J. Am. Chem. Soc.* **2010**, *132*, 12191–12193. (b) Kawauchi, M.; Kawauchi, T.; Takeichi, T. *Macromolecules* **2009**, *42*, 6136–6140. (c) Kawauchi, T.; Kitaura, A.; Kumaki, J.; Kusanagi, H.; Yashima, E. *J. Am. Chem. Soc.* **2008**, *130*, 11889–11891. (d) Kawauchi, T.; Kumaki, J.; Kitaura, A.; Okoshi, K.; Kusanagi, H.; Kobayashi, K.; Sugai, T.; Shinohara, H.; Yashima, E. *Angew. Chem. Int. Ed.* **2008**, *47*, 515–519.

(26) (a) Zhang, Y.; Ning, Y.; Caporaso, L.; Cavallo, L.; Chen, E. Y.-X. *J. Am. Chem. Soc.* **2010**, *132*, 2695–2709. (b) Ning, Y.; Chen, E. Y.-X. *J. Am. Chem. Soc.* **2008**, *130*, 2463−2465.

(27) Zhang, Y.; Caporaso, L.; Cavallo, L.; Chen, E. Y.-X. *J. Am. Chem. Soc*. **2011**, *133*, 1572–1588.

(28) (a) Caporaso, L.; Cavallo, L. *Macromolecules* **2008**, *41*, 3439–3445. (b) Caporaso, L.; Gracia-Budrìa, J.; Cavallo, L. *J. Am. Chem. Soc.* **2006**, *128*, 16649−16654.

(29) For selected reviews, see: (a) Barner-Kowollik, C.; Du Prez, F. E.; Espeel, P.; Hawker, C. J.; Junkers, T.; Schlaad, H.; Van Camp, W. *Angew. Chem. Int. Ed.* **2011**, *50*, 60–62. (b) Hoyle, C. E.; Bowman, C. N. *Angew. Chem. Int. Ed.* **2010**, *49*, 1540−1573. (c) Iha, R. K.; Wooley, K. L.; Nyström, A. M.; Burke, D. J.; Kade, M. J.; Hawker, C. J. *Chem. Rev.* **2009**, *109*, 5620–5686. (d) Binder, W. H.; Sachsenhofer, R. *Macromol. Rapid Commun.* **2008**, *29*, 952–981. (e) Binder, W. H.; Sachsenhofer, R. *Macromol. Rapid Commun.* **2007**, *28*, 15–54.

(30) (a) Skokan, E. V.; Alioshina, V. E.; Spiridonov, F. M.; Arkhangelsky, I. V.; Davydov, V. Y.; Tamm, N. B.; Sidorov, L. N. *J. Phys. Chem.* **1995**, *99*, 16116–16118. (b) Saito, R.; Dresselhaus, G.; Dresselhaus, M. S. *Phys. Rev. B* **1994**, *49*, 2143–2147. (c) Fischer, J. E.; Luzzi, D. E.; Kniaź, K.; McGhie, A. R.; Ricketts-Foot, D. A.; Romanow, W. R.; Vaughan, G. B. M.; Heiney, P. A.; Li, D.; Smith, A. L.; Strongin, R. M.; Cichy, M. A.; Brard, L.; Smith, A. B. *Phys. Rev. B* **1993**, *47*, 14614–14617. (d) Heiney, P. A.; Fischer, J. E.; McGhie, A. R.; Romanow, W. J.; Denenstein, A. M.; McCauley Jr, J. P.; Smith, A. B.; Cox, D. E. *Phys. Rev. Lett.* **1991**, *66*, 2911–2914.

(31) Tzirakis, M. D.; Orfanopoulos, M. *Chem. Rev.* **2013**, *113*, 5262–5321.

(32) Scholl, M.; Ding, S.; Lee, C. W.; Grubbs, R. H. *Org. Let.* **1999**, *1*, 953–956.

CHAPTER 4

Reactivity of Bridged and Nonbridged Zirconocenes towards Biorenewable Itaconic Esters and Anhydride[*]

4.1. Summary

This work investigates the reactivity of neutral and cationic complexes of both bridged *ansa*-zirconocenes, *rac*-[$C_2H_4(Ind)_2$]ZrMe[OC(O^{i}Pr)=CMe$_2$] (**1**) and *rac*-[$C_2H_4(Ind)_2$]Zr$^+$(THF)[OC(O^{i}Pr)=CMe$_2$][MeB(C_6F_5)$_3$]$^-$ (**1**$^+$), and nonbridged zirconocenes, Cp*(^{n}PrCp)ZrMe[OC(O^{i}Pr)=CMe$_2$] (**14**) and Cp*(^{n}PrCp)Zr(THF)[OC(O^{i}Pr)=CMe$_2$]$^+$[MeB(C_6F_5)$_3$]$^-$ (**14**$^+$), towards biorenewable itaconic dialkyl esters (itaconates) and anhydride (IA). Behaving similarly, both cationic complex **1**$^+$ and **14**$^+$ react readily with itaconates to form cleanly single-monomer-addition products, 8-membered-ring metallocycles **2** and **16**, respectively, and neutral enolate complexes **1** and **14** insert one equivalent of IA to afford the single IA addition products **5** and **18**. Behaving differently, the 8-membered-ring chelates **2** derived from the bridged metallocene framework undergo slow isomerization at room temperature via ligand exchange between the coordinated and uncoordinated ester groups to form thermodynamically favored 7-membered-ring chelates **4**, while the 8-membered chelates **16** derived from the sterically more crowded unbridged metallocene framework are stable at room temperature and do not undergo such isomerization. The above cationic complexes exhibit no reactivity towards further additions of itaconates. Replacing itaconates with more basic monomers such as *N*,*N*-dimethylacrylamide

[*] This dissertation chapter contains the manuscript for a full paper submitted to the journal *Organometallics*.This work was supported by the US National Science Foundation (NSF-1300267). We thank Dr. Brian Newell for help in solving the crystal structure of **9**$^+$, and Boulder Scientific Co. for the research gifts of B(C_6F_5)$_3$ and Cp*(^{n}PrCp)ZrCl_2.

that can ring-open the resting chelating intermediate, however, brings about effective and controlled polymerization by the 8-membered Zr-itaconate metallocycles **2** and **16**, but not 7-membered **4**, producing either highly isotactic (>99% *mm*) polymers (by **2**) or polymers with narrow molecular weight distributions ($Đ$ <1.19, by **16**). These results further highlight the *ansa*-effects in the metallocene polymerization chemistry and the importance of the formation and ring-opening of the 8-membered chelating intermediates involved in the metallocene-mediated conjugate-addition polymerization.

4.2. Introduction

Biomass-derived itaconic acid has received increased attention in recent years as a more sustainable alternative to petroleum-based building blocks for obtaining new renewable polymeric materials, due to structural resemblance of its derivatives to other widely used acrylic monomers, such as methyl methacrylate (MMA).[1] Its large world-wide production by fermentation with fungus *Aspergillus terreus* is still by far the largest source of itaconic acid and its derivatives,[2] and has uplifted this dicarboxylic ene-bearing monomer as one of the most important chemical platforms derived from renewable resources.[3] Among other applications, dialkyl ester derivatives of itaconic acid, or itaconates such as dimethyl itaconate (DMIA) and diisopropyl itaconate (D^{i}PrIA), and cyclic itaconic anhydride (IA) have been explored as vinyl monomers by free radical polymerization with α,α'-azobisisobutyronitrile[4] and atom transfer radical polymerization.[5] More recently, efforts have been made to exploit the use of the diacid (or diester) units as the polymerizable handle in condensation polymerization to obtain unsaturated polyesters, and their applications have been expanded to drug-delivery, shape memory, and elastomeric materials.[6] However, to the best of our knowledge, such monomers have not been examined using the metal-

mediated coordination polymerization method, which has the potential to produce stereoregular itaconate polymers for enhanced physical and chemical properties.

Coordination-addition polymerization of conjugated acrylic monomers mediated by cationic chiral *ansa*-zirconocenium ester enolate catalysts has proven to be a powerful method for obtaining highly stereoregular polymers in a living/controlled manner.[7] For instance, highly isotactic poly(methyl methacrylate) (PMMA), with isotacticity [*mm*] triads up to 97%, has been readily produced at room temperature by C_2-ligated zirconocenium ester enolate complex *rac*-(EBI)Zr^{+}(THF)[OC(O^{i}Pr)=CMe_2][Me$B(C_6F_5)_3]^{-}$ (**1**$^{+}$, EBI = ethylene-bis-indenyl) very efficiently, with higher to near quantitative catalyst efficiency.[8,9] Highly syndiotactic PMMA, with syndiotacticity [*rr*] triads up to 94% has also been synthesized under ambient conditions, using C_S-ligated zirconocenium ester enolate complex {[Ph_2C(Cp)(2,7-$^{t}Bu_2$Flu)]Zr(THF)[OC(O^{i}Pr)=CMe_2]}$^{+}$[Me$B(C_6F_5)_3]^{-}$ (Flu = η^{n}-fluorenyl).[10] Other acrylic monomers, such as *N*,*N*-dimethylacrylamide (DMAA), biorenewable butyrolactones such as β-methyl-α-methylene-γ-butyrolactone, and divinyl monomers such as allyl methacrylate and 4-vinylbenzyl methacrylate were also efficiently polymerized to give highly stereoregular polymers.[11,12,13,14,15] Such polymerizations are typically living or quasi-living, allowing for precise control over the polymer chain structures. The origin of the chemo- and stereoselectivity observed in this precision polymerization of polar vinyl or polar divinyl monomers arises from the enantiomorphic-site-controlled, coordination-addition mechanism, in which the fundamental steps of the propagation sequence requires the Michael-addition of the nucleophilic ester enolate chain-end onto the conjugated C=C double bond of the coordinated incoming monomer to form an 8-membered-ring chelate (resting state).[16]

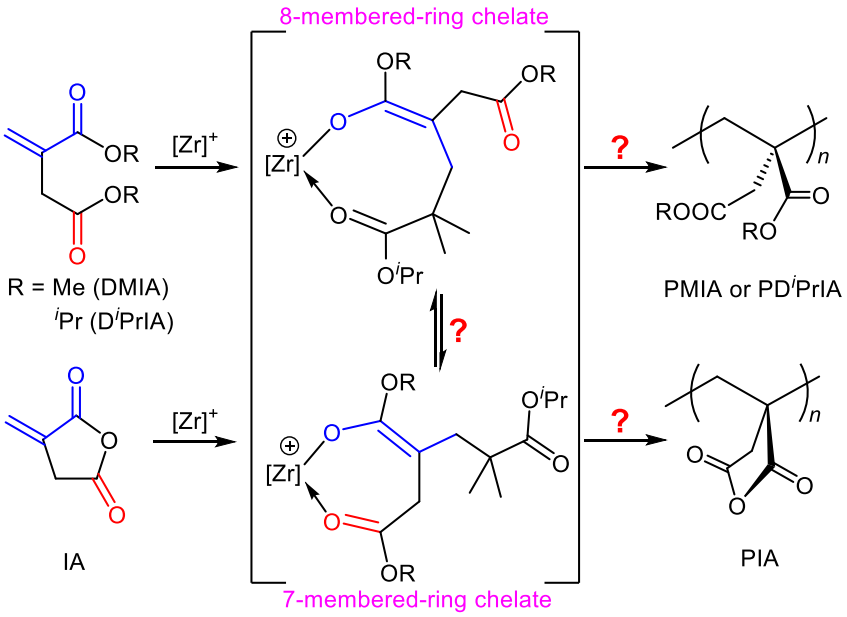

Scheme 4.1. A working hypothesis on the possible single-monomer-addition structures and their reactivity towards subsequent monomer additions, where $[Zr]^+$ represents bridged *rac*-(EBI)Zr(THF)[OC(O^{i}Pr)=CMe$_2$]$^+$[MeB(C$_6$F$_5$)$_3$]$^-$ (**1**$^+$) and unbridged Cp*(^{n}PrCp)Zr(THF)[OC(O^{i}Pr)=CMe$_2$]$^+$[MeB(C$_6$F$_5$)$_3$]$^-$ (**14**$^+$).

In our continued effort to better understand the implications of the resting intermediate in the chain initiation and propagation reactions, we envisioned that the extra ester group in the dialkyl ester itaconates and itaconic anhydride, as compared to the alkyl group (Me or H) in methacrylates and acrylamides, would present an extra chemical handle to further test the requisites of the chain-growth reaction. Upon addition of the first monomer, the resulting Zr-itaconate metallacycle could exhibits two possible isomers: 8-membered chelate vs. 7-membered chelated (Scheme 4.1). Two important fundamental questions immediately emerge: (1) What are the structure and reactivity of the resulting first-monomer addition product (8-membered metallacycle vs 7-membered one), and (2) What are the effects of the metallocene initiator/catalyst structure (bridged vs. unbridged) on the resulting addition product. To address these two fundamental questions, we employed two types of metallocenium catalysts in this study: a C_2-ligated *bridged ansa*-zirconocenium ester enolate, **1**$^+$, and a sterically encumbered *non-bridged*

metallocenium ester enolate, Cp*(^{n}PrCp)Zr(THF)[OC(O^{i}Pr)=CMe$_2$]$^+$[MeB(C$_6$F$_5$)$_3$]$^-$ (**14**$^+$). Overall, this study has successfully answered the above two fundamental questions and also uncovered not only similar monomer insertion and polymerization chemisty, but also some intriguing differences, between these two classes of metallocene complexes.

4.3. Results and Discussion

Reactivity of *C*$_2$-Ligated Bridged *ansa*-Zirconocenium Complexes with Dialkyl Itaconates. First, we focused our attention to the cationic chiral *ansa*-zirconocenium ester enolate *rac*-(EBI)Zr$^+$(THF)[OC(O^{i}Pr)=CMe$_2$][MeB(C$_6$F$_5$)$_3$]$^-$ (**1**$^+$), which is generated *in-situ* from the reaction of *rac*-(EBI)ZrMe[OC(O^{i}Pr)=CMe$_2$] (**1**) with (C$_6$F$_5$)$_3$B·THF and is a highly active and efficent metallocene catalyst for the polymerization of a wide variety of polar (meth)acrylic and acrylamide substrates, including the renewable and biomass-derived methylene butyrolactones and other challenging polar divinyl acrylic monomers, with high levels of stereoselectivity and control.[11,15] In sharp contrast, addition of an excess amount of itaconates DMIA, DiPrIA, or IA to **1**$^+$ at ambient or higher temperatures (up to 100 °C), resulted in no monomer conversion even after prolonged periods of time. Thus, we next examined the stoichiometric reactions between catalyst **1**$^+$ and the itaconate monomers to determine whether the origin for this lack of polymerization activity was due to catalyst decomposition or catalytic incompetency for chain initiation and/or propagation.

To this end, we designed a series of NMR-scale stoichiometric reactions to examine the reactivity of the isopropyl ester enolate ligand in **1**$^+$ to undergo the first nucleophilic Michael-addition over the conjugated C=C bond of the itaconate monomers, which is a key step for the analogous initiation in the polymerization of (meth)acrylates and acrylamides.[8,9,12,13,17,18,19,20]

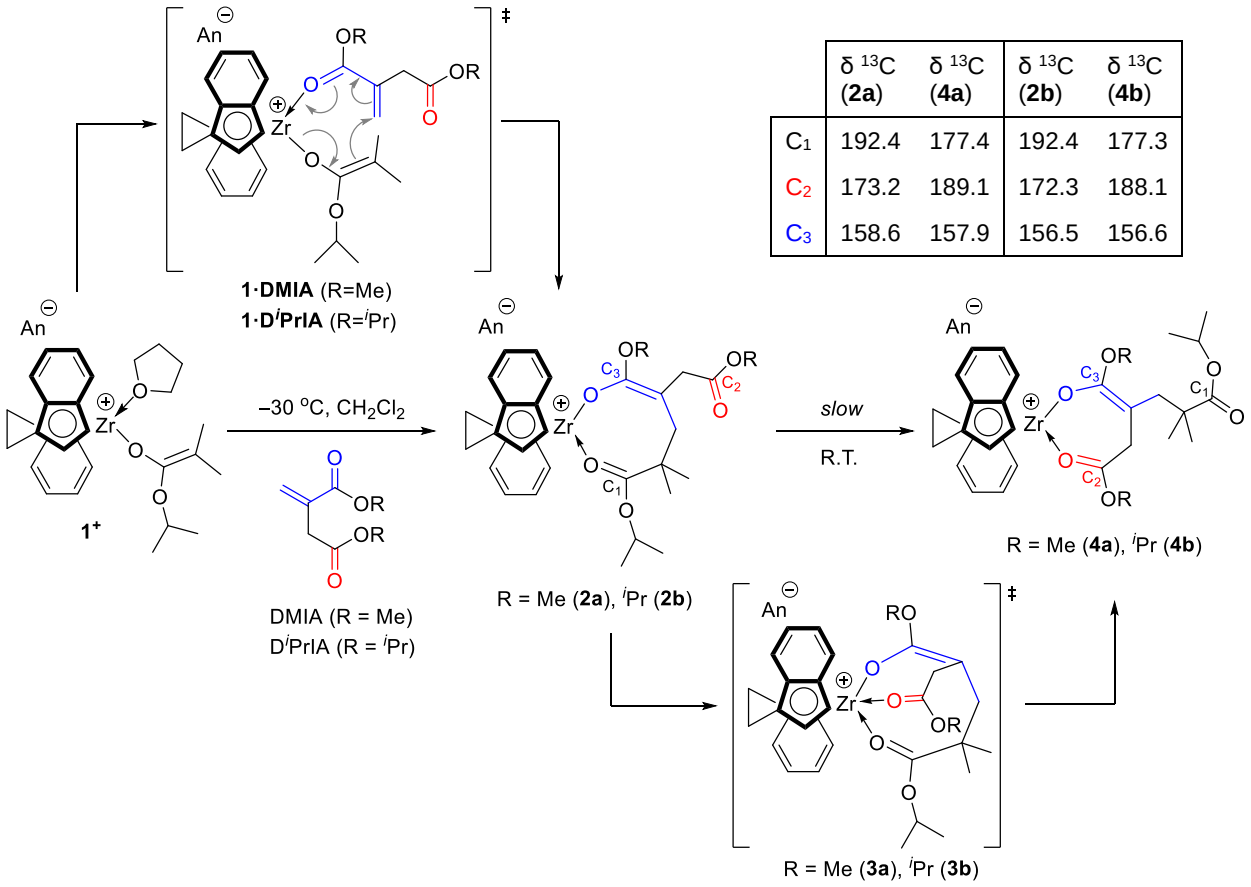

	δ ^{13}C (**2a**)	δ ^{13}C (**4a**)	δ ^{13}C (**2b**)	δ ^{13}C (**4b**)
C_1	192.4	177.4	192.4	177.3
C_2	173.2	189.1	172.3	188.1
C_3	158.6	157.9	156.5	156.6

Scheme 4.2. Proposed reactivity of C_2-ligated cationic *ansa*-zirconocenium complex **1**$^+$ with dialkyl itaconates and ^{13}C NMR chemical shifts (CD_2Cl_2, ppm) for the carbonyl carbons in kinetic products **2a** and **2b** as well as thermodynamic products **4a** and **4b**. An$^-$ = $[MeB(C_6F_5)_3]^-$.

Indeed, the reaction between one equivalent of DMIA or D^{i}PrIA and the preformed **1**$^+$ at −30 °C in CD_2Cl_2 showed instantaneous consumption of the monomers and clean formation of single-addition products **2a** and **2b**, respectively (Scheme 4.2), as bright red solutions. These structures are analogous to those obtained under otherwise identical conditions between **1**$^+$ and MMA (or other acrylamide and divinyl acrylic monomers) and resemble the resting intermediate in the MMA polymerization,[9,13,14,15,19] except that the newly formed metallocene complexes **2a** and **2b** contain an extra non-coordinated carbonyl group derived from the *β*-alkyl ester (the non-conjugated ester group) in the itaconates. Thus, detection of **2a** and **2b** indicated that the α-alkyl ester (the conjugated ester group) of the dialkyl itaconates can replace the datively bonded THF ligand in **1**$^+$

to form the catalyst-monomer complexes or adduct intermediates **1·DMIA** and **1·D^{i}PrIA**, which rapidly undergo Michael-addition via nucleophilic attack of the ester enolate ligand to form the 8-membered-ring chelates **2a** and **2b**. Interestingly, monitoring the reactions by ^{1}H NMR upon warming to ambient temperature and standing for 24 h revealed a slow, but clean, evolution to products **4a** and **4b** as orange and red solutions, respectively. We hypothesized that such kinetic to thermodynamic product transformation arose from a slow ligand exchange on going from the the coordinated isopropyl ester in **2a** (and **2b**) to the *β*-alkyl ester in **4a** (and **4b**), resulting in the shrinkage of the ring size from an 8- to 7-membered chelate structure. In addition, an associative mechanism involving a five-coordinated Zr center (**3a** and **3b**) was considered to be more favorable than the alternative dissociative mechanism, due to the high oxophilicity of the cationic Zr and the observed inability of the more sterically hindered Cp*(^{n}PrCp)Zr system to form the 7-membered-ring chelate analogue (*vide infra*). Furthermore, a hypothetical dissociation of the coordinated *β*-alkyl ester in the intermediates **3a** and **3b** would revert them back to the starting complexes **2a** and **2b** and is non-productive, but the successful and clean isolation of complexes **4a** and **4b** in the preparative scale and at room temperature (see Appendix C.1 for details) suggests that the dissociation of the isopropyl ester group derived from the mono ester enolate ligand in **1**$^{+}$ was more favorable and irreversible.

The stability of complexes **2a** and **2b** for over 24 h at −18 °C allowed their full spectroscopic characterization by ^{1}H and ^{13}C NMR at this temperature. Raising the temperature again above 0 °C or warmer allowed for the gradual evolution to thermodynamically more stable complexes **4a** and **4b**, indicative of a kinetic barrier for forming five-coordinated intermediate **3**. Thus, upon addition of stoichiometric amounts of dialkyl itaconates, dissociation of the coordinated THF molecule in **1**$^{+}$ was indicated by characteristic peaks at 3.66 and 1.80 ppm (for α

and β H's, respectively) in the ^{1}H NMR and at 67.94 and 25.71 ppm (for α and β C's, respectively) in the ^{13}C NMR. Formation of complexes **2a** and **2b** was also supported by other ^{1}H NMR resonances: (1) appearance of the methylene protons (2.29 and 1.72 ppm for **2a**, 2.23 and 1.71 ppm for **2b**) derived from the consumption of the vinylic protons of DMIA and D^{i}PrIA; (2) the marked chemical downfield shifting of the septet for –OC*H*Me$_2$ at 3.73 ppm of the isopropyl ester enolate in **1**$^{+}$, to 4.27 and 4.19 ppm of the –OC*H*Me$_2$ now attached to the ester group in **2a** and **2b**, respectively; (3) the alkyl ester groups in the DMIA and D^{i}PrIA showed a clear downfield shift in their ^{1}H NMR spectra as they went from free itaconates (singlets at 3.73 and 3.66 ppm for the two –OMe in DMIA, and doublets at 1.23 and 1.20 ppm for the two –OCHMe$_2$ in D^{i}PrIA) to the addition products **2a** (singlets at 3.64 and 3.09 ppm for the two –OMe) and **2b** (doublets at 1.37 and 1.23–1.19 ppm for the –OCH*Me*$_2$); and (4) the upfield shifting of the >CMe$_2$ (1.19 and 1.09 ppm for **2a**, 1.13 and 0.98 for **2b**). Importantly, the resonances appearing in the carbonyl region of the ^{13}C NMR clearly suggested the presence of two types of the carbonyl carbons in accordance with the open chelate structures proposed for **2a** and **2b**. Using compound **2a** as an example, apart from the ester enolate ligand [O*C*(OMe)=] at 158.6 ppm (C_3), two carbonyl signals were observed at 173.2 ppm (C_2), typical of a free non-coordinated alkyl ester, and at 192.4 ppm (C_1), which indicates a more deshielded alkyl ester as a consequence of its coordination to the cationic Zr center (Scheme 4.2). The ^{13}C–^{1}H HMBC spectra of **2a** recorded at −5 °C (Figure 4.1-(i)) showed a clear correlation between the signal at 192.4 ppm and the –OC*H*Me$_2$ of the isopropyl ester, therefore providing further evidence for the 8-membered-ring chelate ligand structure through the coordination of the carbonyl in the [*C*(O^{i}Pr)=O] moiety as depicted in Scheme 4.2. All other correlations in the 2D spectrum, as well as the analogous case observed for the otherwise similar complex **2b** (Figure S4.42-(i)), pointed to the same conclusion.

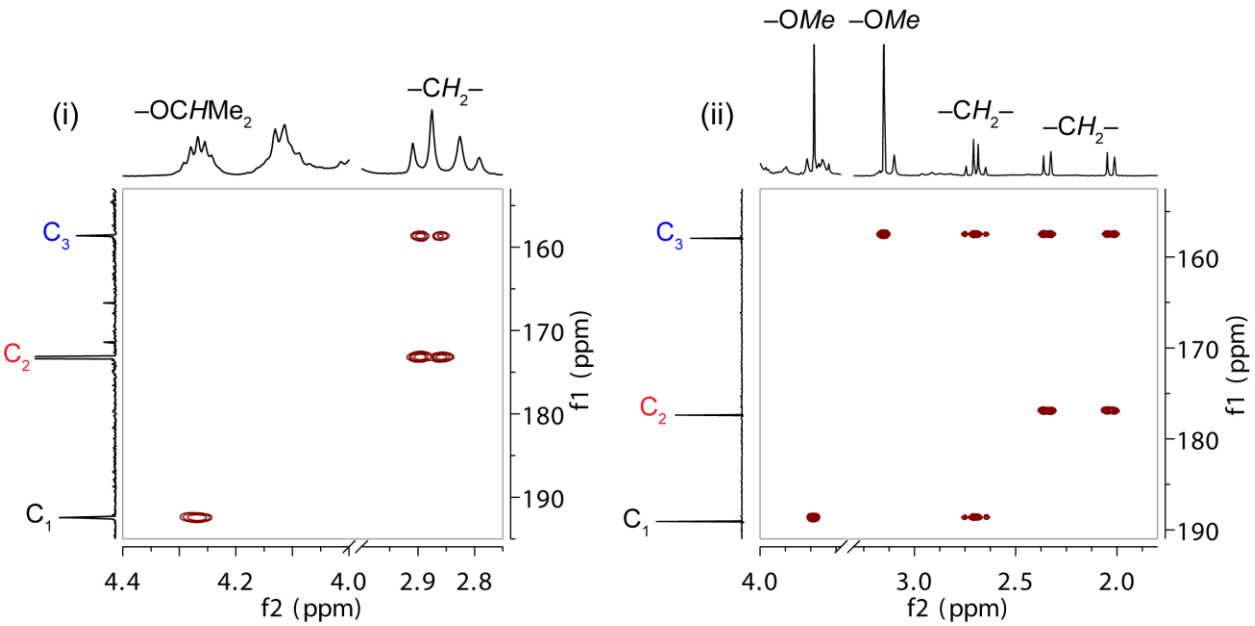

Figure 4.1. Selected portions of ^{13}C–^{1}H HMBC (CD_2Cl_2, −5 °C) 2D NMR spectra of complexes **2a** (i) and **4a** (ii) are shown for comparison.

Complexes **4a** and **4b** were also isolated in a preparative scale after stirring solutions of **2a** and **2b**, respectively, in CH_2Cl_2 at room temperature for 24 h. This intriguing structural evolution on going from an 8- to 7-membered-ring chelate structure is clearly illustrated in Figure 4.2, which shows the downfield shifting of the resonance at 4.27 ppm, corresponding to the coordinated –OC*H*Me$_2$ in **2a**, to 4.89 ppm, now the free –OC*H*Me$_2$ in **4a**. Likewise, the –OC*H*Me$_2$ resonance in **2b** was also found downfield shifted from 4.19 ppm (coordinated) to 4.93 ppm (free) in **4b**. Other important chemical shift differences that indicated such structural evolution are: (1) the shifting of the alkyl esters signals in **4a** (singlets at 3.73 and 3.15 ppm for the two –OMe) and **4b** (doublets at 1.43, 1.23 and 0.97 ppm for the –OCH*Me*$_2$); (2) the upfield shifting of the diastereotopic methylene protons of the pendant itaconate moiety in **2a** (doublets at 2.89 and 2.81 ppm) and **2b** (doublets at 2.89 and 2.79 ppm), now part of the 7-membered ring chelate ligand in **4a** (doublets at 2.73 and 2.67 ppm) and **4b** (doublets at 2.70 and 2.65 ppm); and (3) the slight shifting of the >CMe_2 (1.12 and 1.06 ppm for **4a**, 1.14 and 1.09 for **4b**), now part of the pendant alkyl chain.

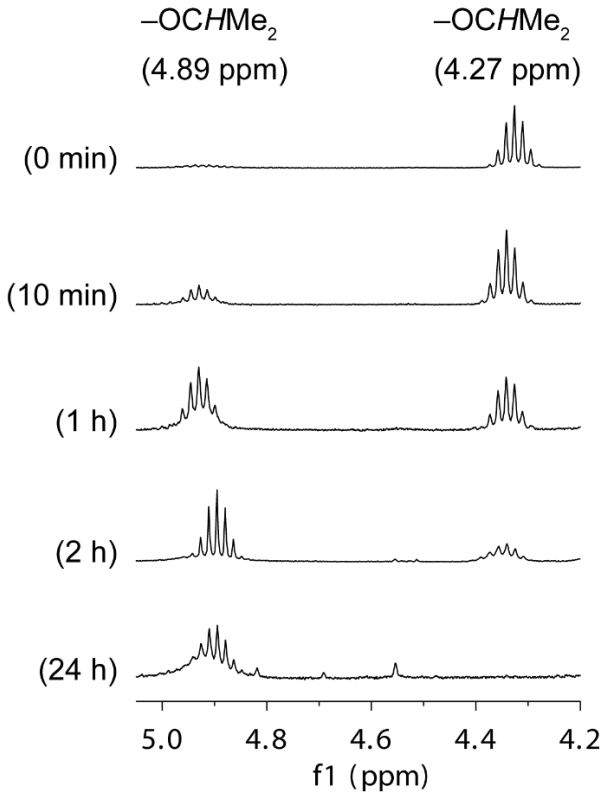

Figure 4.2. Time evolution of the –OC*H*Me_2 region of the ^{1}H NMR spectrum (CD_2Cl_2, 25 °C) of **2a** in CD_2Cl_2 at ambient temperature.

More importantly, the marked chemical shift differences in the carbonyl region of the ^{13}C NMR spectra, recorded at room temperature (Scheme 4.2), provided corroborative evidence for the proposed 7-membered ring structures **4a** and **4b**. Using compound **4a** as an example, the ester enolate ligand [O*C*(OMe)=] remained almost constant at 157.9 ppm (C_3), as its pivotal position didn't change from **2a** to **4a**; however, the resonance at 177.4 ppm (C_1), typical of a non-coordinated alkyl ester, now belongs to the free isopropyl ester [*C*(O^{i}Pr)=O], formerly coordinated to the Zr in **2a**; while the much deshielded resonance at 189.1 ppm (C_2) corresponds to the *β*-methyl ester [*C*(OMe)=O], now coordinated to the cationic Zr center. Similarly for **4b**, a signal at 156.6 ppm (C_3) is assigned for the coordinated ester enolate [O*C*(O^{i}Pr)=], a signal at 177.3 ppm (C_1) for the free isopropyl ester [*C*(O^{i}Pr)=O], formerly coordinated to Zr, and a signal at 188.1 ppm (C_2) for the coordinated *β*-isopropyl ester [*C*(O^{i}Pr)=O]. These assignments were supported

by the correlations observed in the ^{1}H-^{13}C HMBC experiments, as shown in Figure 4.1-(ii) and Figure S4.42-(ii).

Based on the stoichiometric reactions described above, coupled with control experiments in which extra equivalents of DMIA, D^{i}PrIA and MMA were added to preformed complexes **2a**, **2b**, **4a**, and **4b** showed no monomer conversion, we concluded that the lack of polymerization activity of $\mathbf{1}^{+}$ towards dialkyl itaconates was due to the inability of the first monomer-addition product to further enchain the incoming monomer molecules. Furthermore, we monitored the addition of 2 equivalents of MMA to complexes **2a** and **2b** by ^{1}H NMR and observed no apparent interaction, followed by the identical evolution previously observed into complexes **4a** and **4b**. These results indicate that the incoming monomer molecules are incapable of ring-opening the 8- or 7-membered ring chelate to enter the coordination site, thus precluding from subsequent Michael additions for chain growth.

Reactivity of *C*$_2$-Ligated Bridged *ansa*-Zirconocene Complexes with Itaconic Anhydride. Next, we investigated the reactivity of complex $\mathbf{1}^{+}$ with one equivalent of IA (Scheme 4.3). Upon mixing, the red solution of $\mathbf{1}^{+}$ turned yellow and an intractable mixture was observed by ^{1}H NMR; even at −80 °C no clean product was observed. Furthermore, the color change was followed by rapid decomposition, preventing any further product identification. We hypothesized that the formation of the direct addition product of $\mathbf{1}^{+}$ and IA, represented by unstable complex **6** (*vide infra*), was unfavorable due to the intrinsic ring strain that the internal sp^2 hybridized C=C in the cyclic enolate anhydride exerted over the 8-membered-ring chelate structure, resulted from the coordination of the isopropyl ester to the cationic Zr center. It is also possible that the THF molecule present in the reaction mixture partially displaced the chelate oxygen of the isopropyl ester to release the chelate ring strain. This high ring-strain phenomenon would also explain the

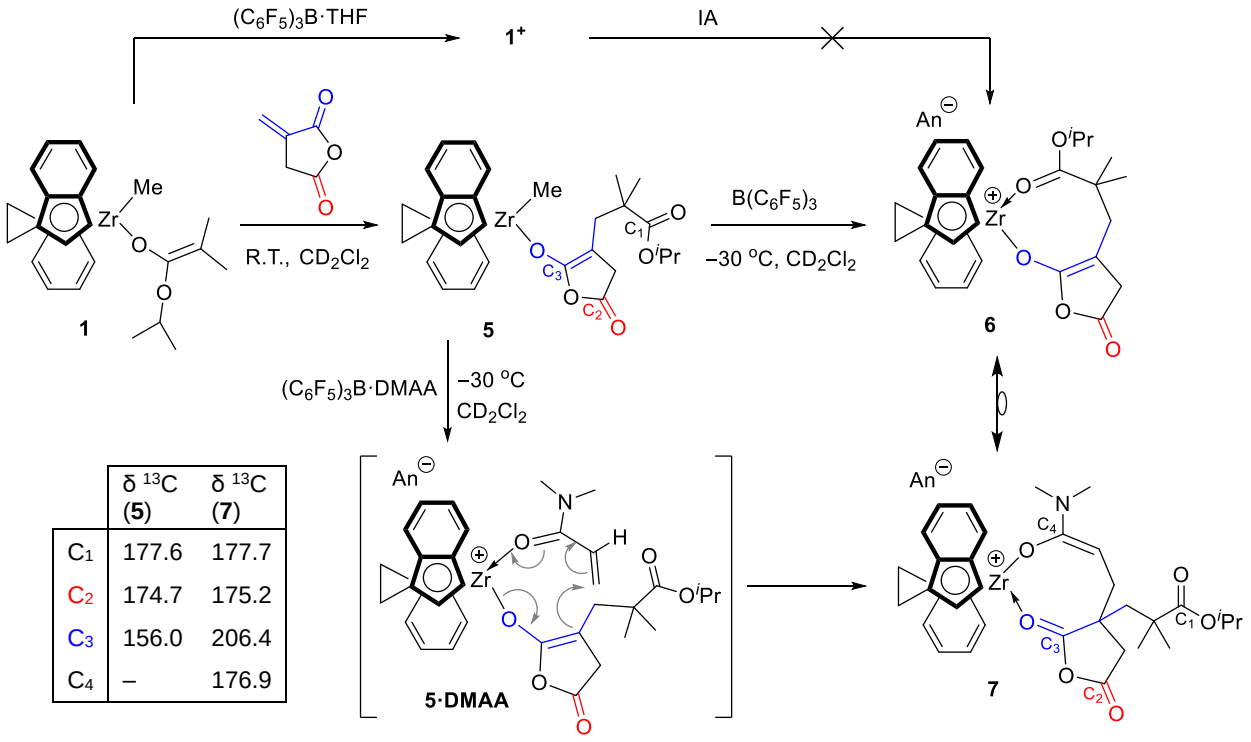

Scheme 4.3. Reactivity of neutral *ansa*-zirconocene complex **1** and cationic $\mathbf{1}^+$ with itaconic anhydride (IA) and ^{13}C NMR chemical shifts (CD_2Cl_2, ppm) for the carbonyl carbons in products **5** and **7**. An^- = $[MeB(C_6F_5)_3]^-$.

inability of complex $\mathbf{1}^+$ to polymerize IA, since an 8-membered-ring structure, containing a strained cyclic enolate anhydride, would be required for a monometallic coordination-addition polymerization analogous to the polymerization of other acrylic monomers. On the contrary, structurally comparable α-methylene-γ-butyrolactones (MBLs), which consist of a 5-membered ring lactone only lacking of one carbonyl oxygen, can be readily polymerized by cationic $\mathbf{1}^+$ by a monometallic site-controlled mechanism.[11] A unimetallic coordination-addition mechanism was also observed in the polymerization of MBLs by *ansa*-half-sandwich rare-earth-metal catalysts,[21] but a bimetallic mechanism was found by neutral samarocene(II) complex, $Cp^*_2Sm(THF)_2$.[22]

Interestingly, we found that neutral *ansa*-zirconocene methyl ester enolate, **1**, reacts with one molecule of IA to cleanly form single addition product **5** (Scheme 4.3). The reaction occurred rapidly at ambient temperature and in a polar non-coordinating solvent (CH_2Cl_2), in a fashion

analogous to that between **1** and MMA.[9] Not surprisingly, neutral complex **5** did not add more equivalents of IA and thus there was no chain propagation. Neutral complex **5** is stable in solubtion at room temperature for several days, presumably due to the unstrained cyclic enolate anhydride, enabled by the non-coordinated isopropyl ester group to the Zr which is already coordinatively saturated with a methyl ligand. Several attempts to grow single crystals suitable for X-Ray crystallography were unsuccessful, but key features in the ^{1}H and ^{13}C NMR spectra of the isolated product provided clear evidence to support the proposed structure of **5**: (1) the downfield shifting of the septet at 3.65 ppm for –OC*H*Me$_2$ of the isopropyl ester enolate in **1** to 4.89 ppm of the –OC*H*Me$_2$ now attached to the ester group in **5**; (2) the markedly upfield shifting of the methylene protons in the IA ring from 3.62 ppm of the free monomer to 2.95 ppm in **5**; (3) a new sharp singlet at 1.90 ppm for the methylene protons resulted from the vinyl addition; (4) the two inequivalent –OCH*Me*$_2$ in **1** (doublets at 1.01 and 0.94 ppm) now a single doublet at 1.19 ppm in **5**; and (5) the shifting of the >CMe$_2$ (from 1.40 and 1.17 ppm in **1** to 0.99 and 0.97 ppm in **5**) and the −Me ligand (from −0.96 ppm in **1** to −0.85 ppm in **5**). Collaboratively, the chemical resonances observed in the carbonyl region of the ^{13}C NMR spectrum, typical of free alkyl esters, was also consistent with an open structure in which both oxygen atoms of the akyl {177.6 ppm for [*C*(O^{i}Pr)=O], C$_1$} and anhydride ester groups {174.7 ppm for [CH$_2$*C*(O)=O], C$_2$} are not coordinated to the Zr center, as shown in the ^{13}C–^{1}H HMBC spectrum (Figure 4.3-(i)).

Subsequently, we examined the activation of complex **5** with one equivalent of B(C$_6$F$_5$)$_3$ in CD$_2$Cl$_2$ at −30 °C, aiming for the formation and stabilization of the corresponding cationic complex **6** through the coordination of the isopropyl ester group in the absence of an external donor such as THF. Indeed, complex **6** was observed by ^{1}H and ^{19}F NMR (Figure S4.11), but it rapidly decomposed at room temperature in less than 20 min, precluding from its isolation and further

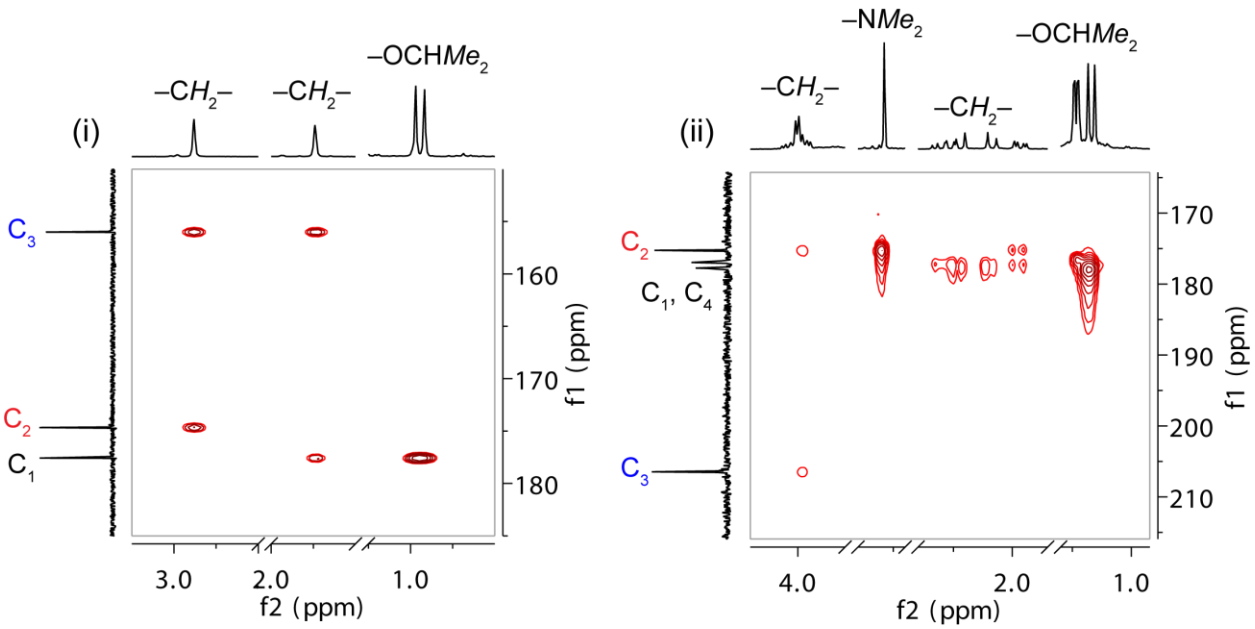

Figure 4.3. Selected portions of ^{13}C–^{1}H HMBC (CD_2Cl_2, 25 °C) 2D NMR spectra of complexes **5** (i) and **7** (ii).

characterization. Interestingly, the existence of two broad signals at 4.94 and 4.36 ppm for the –OC*H*Me$_2$, with an combined integral value of 1 H, together with broad singlets for the methylene protons in the cyclic anhydride (3.36 ppm) and the 8-membered-ring chelate (2.00 ppm), suggested a dynamic behavior on the ^{1}H NMR time scale at this temperature, presumbably due to the ring strain caused by the sp^2 hybridization in the cyclic enolate anhydride. Nevertheless, the clean methyl abstraction by B(C_6F_5)$_3$ was confirmed in the ^{1}H NMR spectrum of **6** by the disappearance of the methyl signal in **5** (−0.85 ppm) and the appearance of a characteristic broad peak at 0.49 ppm in **6** for the resulting uncoordinated anion [MeB(C_6F_5)$_3$]$^-$, also supported by the ^{19}F NMR by resonances at −133.03 (d, *o*-F), −165.09 (t, *p*-F), and −167.71 ppm (m, *m*-F). Other significant signals in the ^{1}H NMR to support structure **6** are: a sharp singlet for the ethylene bridge at 4.12 ppm; two doublets for the diasterotopic isopropyl groups at 1.37 and 1.33 ppm; and two singlet for the two >CMe$_2$ at 1.30 and 1.25 ppm.

The above experimental results led to a hypothesis that if the instability of complex **6** to form an 8-membered-ring chelate structure is originated from the ring strain of the enolate anhydride, then subsequent regeneration of the anhydride should be favorable as it releases the chelate strain. To this end, concomitant activation of neutral enolate anhydride **5** and addition of a monomer with stronger basicity, such as dimethyl acrylamide (DMAA), should undergo Michael-addition through an intermediate, **5·DMIAA**, in which the DMAA occupies the open coordination site and prevents a strained chelate analogous to **6**. Indeed, addition of $(C_6F_5)_3B$·DMAA adduct in stoichiometric amount to **5** cleanly formed the much less strained amide ester enolate **7** with regeneration of the cyclic anhydride. As we expected, complex **7** was more stable in solution at room temperature, thus allowing for its full 1D ^{1}H, ^{19}F, ^{13}C NMR and 2D ^{1}H–^{13}C HMBC NMR analysis before its degradation. Clean abstraction of the methyl group in **5** and formation of the anion, $[MeB(C_6F_5)_3]^-$, was once again observed by the ^{1}H (broad singlet at 0.51 ppm) and ^{19}F NMR spectra. Other notable features in the ^{1}H NMR spectra of **7** include: (1) the downfield shifting of the methylene protons of the cyclic anhydride from 2.95 ppm in **5** to 3.98 ppm in **7**; (2) two sharp singlets for the NMe_2 at 3.26 and 2.79 ppm; (3) a new doublet for the C=C*H* of the amide ester enolate at 2.52 ppm; (4) a set of diasterotopic methylene protons for $–CH_2–$ in the chelate ring and the non-coordinated alkyl chain between 2.29–1.96 ppm; and (5) a clear shift of the isopropyl ester groups (doublets at 1.24 and 1.23 ppm) and the $>CMe_2$ (1.18 and 1.15 ppm). Collaboratively, analysis of the ^{13}C NMR spectrum of **7** revealed a set of 4 carbonyl C's supporting the 8-membered ring chelate structure depicted in Scheme 4.3, which assignment was corroborated by the ^{1}H–^{13}C HMBC spectrum (Figure 4.3-(ii)): a coordinated amide ester enolate [O*C*(NMe_2)=] at 176.9 ppm (C_4), two non-coordinated alkyl esters at 177.7 ppm (C_1) of the isopropyl [*C*(O^iPr)=O] and at 175.2 ppm (C_2) of the cyclic anhydride [CH_2*C*(O)=O], and finally a very

deshielded carbonyl carbon of the coordinated cyclic anhydride at 206.4 ppm (C_3), thus confirming the transformation of the cyclic anhydride enolate in **5**.

Reactivity of Unbridged Zirconocene Complexes with Dialkyl Itaconates and Itaconic Anhydride. To examine the possible *ansa*-effects on the reactivity of zirconocene complexes with itaconates and IA, we next synthesized unbridged zirconocene enolate complexes and subsequently investigated their reactivity towards such substrates.

The successful synthetic routes to zirconocene diester enolate complexes can differ significantly depending on the metallocene framework around the metal. For instance, while unbridged Cp_2Zr or C_S-ligated *ansa*-zirconocene [(Ph_2C)(2,7-di-^{t}Bu-fluorenyl)Zr] diester enolates can be obtained directly from the simple reaction of the dichloride species with lithium alkylisobutyrates,[23,24] the diester enolates of the C_2-ligated bis(indenyl)-type *ansa*-zirconocene require the use better leaving groups, such as the triflate ligand, to provide clean product formation.[8] Similarly to the bis(Cp) system, we initially examined the dichloride complex of the unbridged but more sterically encumbered Cp*(^{n}PrCp)$ZrCl_2$ [Cp*(^{n}PrCp) = (η^5-pentamethylcyclopentadienyl)(η^5-*n*-propylcyclopentadienyl)] (**8**) (for steric protection of the Zr center and solubility reasons) with the aim to form the corresponding diester enolate complex. However, the reaction with Li[OC(O^{i}Pr)=CMe_2] produced exclusively the mono-substituted ester enolate complex Cp*(^{n}PrCp)ZrCl[OC(O^{i}Pr)=CMe_2] (**10**, Scheme 4.4), even when the reaction was performed at higher temperatures (toluene, 100 °C) or in excess of the lithium enolate. Both the integrals in the ^{1}H NMR spectrum of the isolated crystalline product and the pattern of the Cp protons indicate an unsymmetrically substituted Zr center, consistent with the proposed structure **10**. Further reaction of the monochloride complex **10** with alkylating reagents, such as MeMgCl or MeLi, failed to generate the monomethyl monoester enolate complex

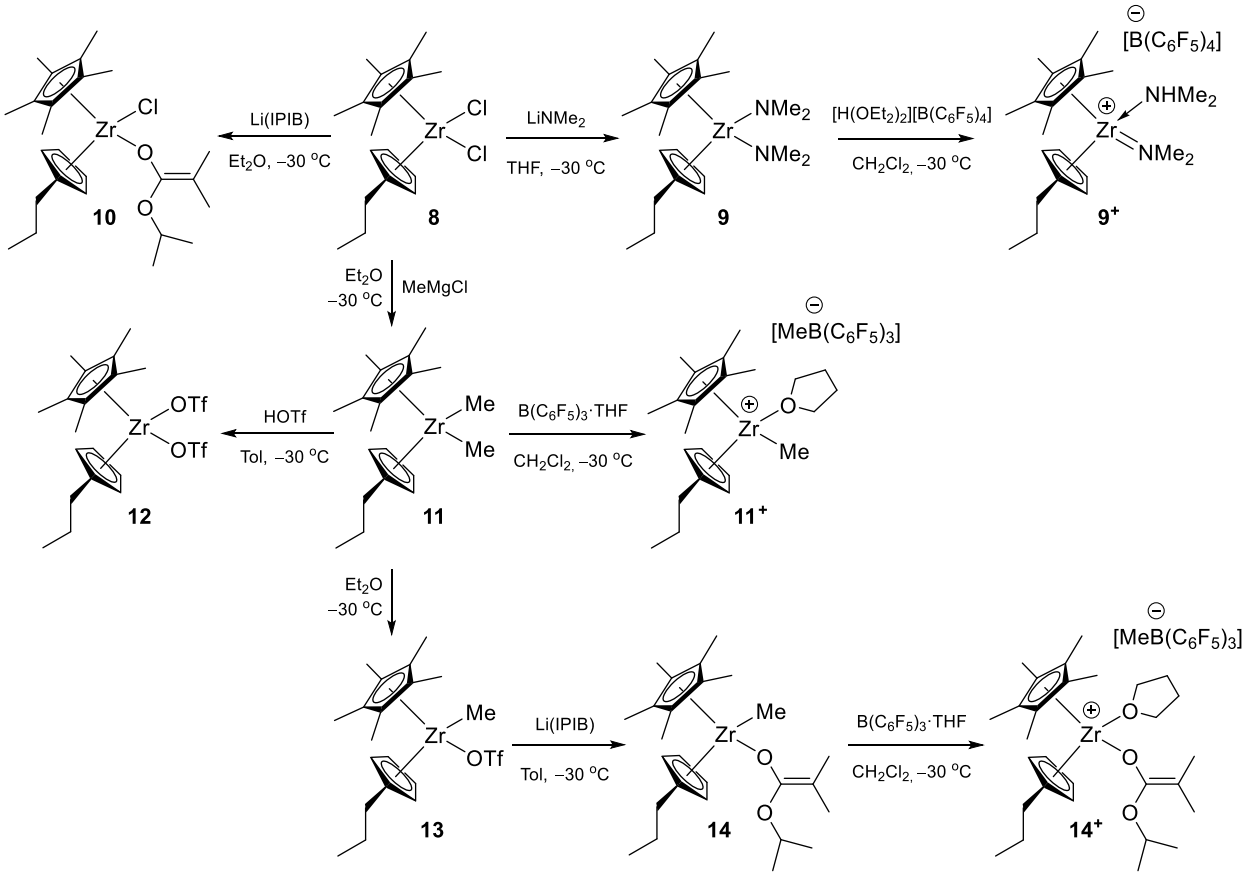

Scheme 4.4. Synthetic route to neutral and cationic complexes of Cp*(^{n}PrCp)Zr.

Cp*(^{n}PrCp)ZrMe[OC(O^{i}Pr)=CMe$_2$] (**14**). Alternatively, the dichloride complex **8** was treated with two equivalents of the less bulky LiNMe$_2$ to form the crystalline (bis)amido complex Cp*(^{n}PrCp)Zr(NMe$_2$)$_2$ (**9**, Scheme 4.4). Reaction of **9** with one equivalent of the Jutzi's salt, [H(OEt$_2$)$_2$][B(C$_6$F$_5$)$_4$], at −30 °C produced the cationic complex [Cp*(^{n}PrCp)Zr(HNMe$_2$)=NMe$_2$]$^+$ [B(C$_6$F$_5$)$_4$]$^-$ (**9**$^+$), stabilized by the released co-product dimethyl amine (Scheme 4.4). The structure was confirmed by ^{1}H, ^{13}C NMR and X-Ray crystal analysis (Figure 4.4, S4.16, and S4.17).

Scheme 4.4 outlines the alternative procedure for obtaining neutral mono-ester enolate zirconocene complex **14** and the generation of the corresponding cationic complex Cp*(^{n}PrCp)Zr(THF)[OC(O^{i}Pr)=CMe$_2$]$^+$[MeB(C$_6$F$_5$)$_3$]$^-$ (**14**$^+$), which was inspired by the efficient formation of neutral mono-ester enolate complexes of C_2 and C_S-ligated *ansa*-zirconocenes.[25]

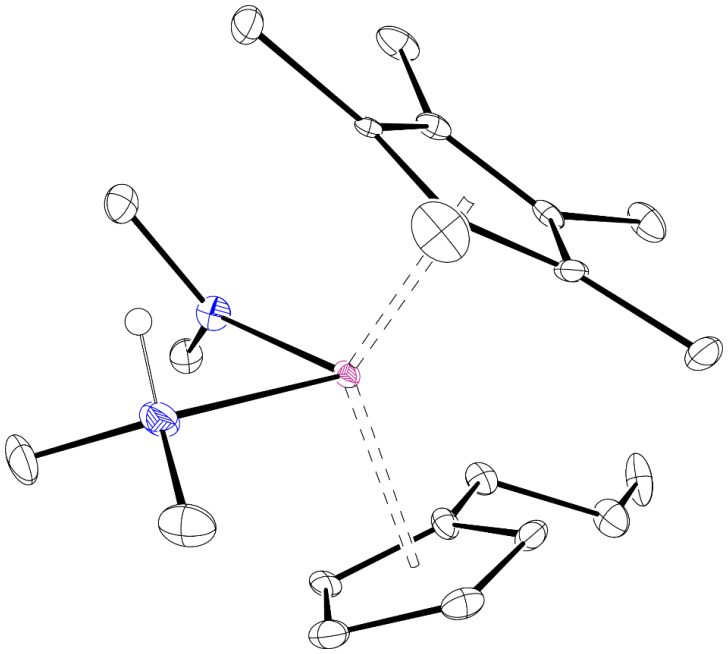

Figure 4.4. X-ray crystal structure of $[Cp^*(^nPrCp)Zr(HNMe_2)=NMe_2]^+[B(C_6F_5)_4]^-$ (**9**$^+$), with thermal elipsoids drawn at 30% probability (anion $[B(C_6F_5)_4]^-$ was omitted for clarity).

Thus, dichloride **8** was conveniently converted into the dimethyl derivative $Cp^*(^nPrCp)ZrMe_2$ (**11**) with MeMgCl and subsequently transformed into the methyl triflate $Cp^*(^nPrCp)Zr(OTf)Me$ (**13**) by means of Me_3SiOTf. Alternatively, treatment of dimethyl **11** with 2 equivalents of triflic acid quantitatively generated the (bis)triflate complex $Cp^*(^nPrCp)Zr(OTf)_2$ (**12**). Surprisingly, reaction of **12** with 2 equivalents of $Li[OC(O^iPr)=CMe_2]$ failed to form the diester enolate derivative, attributable to the sterics of the intended bis(enolate) complex, and mixtures of mono-substituted products were obtained instead. On the other hand, methyl triflate **13** reacted cleanly with one equivalent of $Li[OC(O^iPr)=CMe_2]$ to afford the methyl zirconocene ester enolate **14**. Characteristic ^1H signals in the NMR spectrum include the septet at 4.07 ppm for the methine proton in $-OCHMe_2$, the two doublets centered at 1.19 ppm for the two diasterotopic $-OCHMe_2$, and two singlets at 1.88 and 1.66 ppm for the two isopropylidene methyl groups.

Reaction of **14** with $(C_6F_5)_3B\cdot THF$ was instantaneous, leading to the corresponding cationic complex **14**$^+$ quantitatively at low or ambient temperature in CH_2Cl_2. The abstraction of

the methyl ligand was observed in the ^{1}H NMR (Figure S4.30) by a dramatic shift from a sharp singlet at 0.15 ppm in **14** to a broad signal at 0.49 ppm in **14**$^+$, typical of the uncoordinated counterion $[MeB(C_6F_5)_3]^-$; and the coordination of the THF molecule was clearly indicated by the chemical shifts at 4.16–4.02 and 2.17 ppm (for the α–C*H*$_2$ and β–C*H*$_2$, respectively), downfield shifted with respect to the free THF (3.66 and 1.80 ppm). Similarly to **14**, the dimethyl **11** was activated by $(C_6F_5)_3B\cdot$THF to form the cationic complex $[Cp^*(^n PrCp)Zr(THF)Me]^+[MeB(C_6F_5)_3]^-$ (**11**$^+$, Scheme 4.4). The ^{1}H NMR spectral differences between the neutral and the cationic species are similar to that of **14** and **14**$^+$, with the most notable being the shift of the resonance at −0.35 ppm of the two methyl groups in **11** to a broad signal at 0.48 ppm in **11**$^+$, and the two resonances of the Cp protons in the symmetrically substituted **11** (5.71 and 5.35 ppm) being split into four resonances in the now unsymmetrically substituted **11**$^+$ (6.25, 6.03, 5.90, and 5.79 ppm).

With the unbridged cationic zirconocenium complexes on hand, we subsequently examined their ability to polymerize DMIA, D^{i}PrIA, and IA, and found that cationic dimethylamido **9**$^+$, methyl **11**$^+$, and ester enolate **14**$^+$ produced no polymer products up to 24 h at room temperature (in CH_2Cl_2) or 100 °C (in C_6H_5Br). Only complex **9**$^+$ showed some catalytic activity in isomerization of DMIA and D^{i}PrIA (50 equiv) into the corresponding dimethyl and diisopropyl citraconates, respectively. A bimolecular polymerization pathway, known to be well controlled in the polymerization of MMA by two-component unbridged Cp_2Zr-type system,[23,24,26] was also employed by activating only half equivalent of **9**, **11**, and **14** with $[H(OEt_2)_2][B(C_6F_5)_4]$ or $(C_6F_5)_3B\cdot$THF to generate the correspond neutral/cationic complex mixtures, **9**/**9**$^+$, **11**/**11**$^+$, and **14**/**14**$^+$ in 1:1 ratios; they too produced no polymer products.

To seek insight into the lack of the polymerization activity of such cations, we investigated the stoichiometric reactions between the cations and the monomer. First, the reaction of **9**$^+$, **11**$^+$,

and **14**$^{+}$ with one equivalent of IA at −30 °C was followed by NMR, revealing in all cases instantaneous decomposition products. Attempts to detect any clean addition products at −80 °C were also unsuccessful. Second, we surveyed the reactivity of the dialkyl itaconates with cationic amido zirconocene **9**$^{+}$. NMR-scale reactions between **9**$^{+}$ and 1 equivalent of DMIA or D^{i}PrIA at −30 °C showed intractable mixtures of products, including partial formation of dialkyl citraconates. Third, we examined the stoichiometric reaction between **11**$^{+}$ and one equivalent of dialkyl itaconates at −30 °C. Key chemical shift differences in both the ^{1}H and ^{13}C NMR spectra (Figures S4.32 and S4.34) pointed to a ligand exchange between the coordinated THF and the dialkyl itaconates to form itaconate adducts **15a** and **15b** (Scheme 4.5), with no signs of methyl addition to the coordinated monomer.

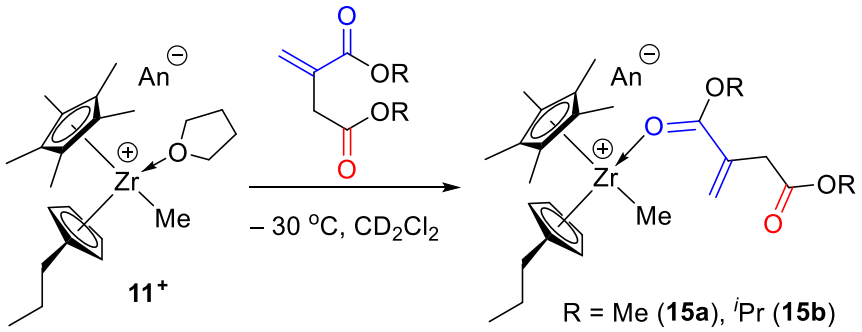

Scheme 4.5. Reactivity of cationic complex **11**$^{+}$ with dialkyl itaconates. An^{-} = [MeB(C$_6$F$_5$)$_3$]$^{-}$.

Next, we investigated the stoichiometric reactions between the *in-situ* generated mono ester enolate **14**$^{+}$ and one equivalent of the dialkyl itaconates. The reaction at −30 °C proceeded cleanly and produced 8-membered chealting complexes **16a** and **16b** (Scheme 4.6) as a result of the fast conjugated Michael-addition of the ester enolate ligand to the conjugated C=C double bond of the coordinated monomers DMIA and D^{i}PrIA, via the proposed catalyst-monomer complexes or intermediates **14·DMIA** and **14·D^{i}PrIA**, respectively. However, in sharp contrast to the reactivity observed with C_2 ligated *ansa*-zirconocene complexes **2a** and **2b** (*vide supra*), species **16a** and **16b** are stable in solution at room temperature and undergo no evolution via ligand exchange

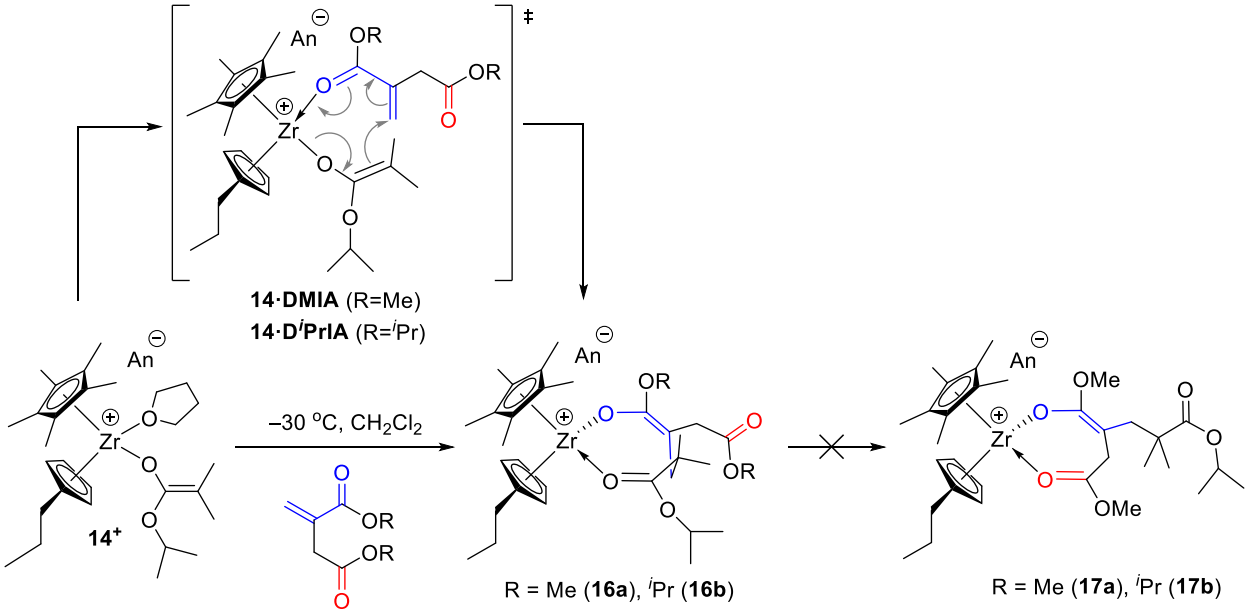

Scheme 4.6. Reactivity of cationic complex **14**$^{+}$ with dialkyl itaconates. An^{-} = [MeB(C_6F_5)$_3$]$^{-}$.

between the two available carbonyl oxygens (i.e., conversion from the 8-membered-ring to the 7-membered-ring chelate structures, **17a** and **17b**, Scheme 4.6), up to 24 h or under heating. We attributed the observation that the sterically crowded Zr center in **16a** and **16b** do not undergo such transformation to the smaller bitting angle and the higher steric hindrance of the Cp*(^{n}PrCp) ligand system, further supporting our former hypothesis that a stererically demanding five-coordinated intermediate is required on going from the 8-membered-ring chelate species to the 7-membered-ring ones.

The formation of the single monomer addition products was clearly indicated by the ^{1}H NMR spectra that showed complete and rapid consumption of the vinylic resonances of the conjugated C=C in the dialkyl itaconates, accompanied by formation of diasteromeric methylene signals at 2.64 and 1.84 ppm in **16a**, and at 2.64 and 1.90 ppm in **16b**. Moreover, the septet at 4.02 ppm for –OC*H*Me$_2$ of the coordinated isopropyl ester enolate group (^{13}C resonance at 154.9 ppm for [O*C*(O^{i}Pr)=]) in **14**$^{+}$ was markedly downfield shifted to 4.96 and 4.98 ppm (for **16a** and **16b**, respectively) for the –OC*H*Me$_2$ of the now coordinated isopropyl ester group (new ^{13}C resonances

at 193.8 and 193.7 ppm for [*C*(O^{i}Pr)=O] in **16a** and **16b**, respectively). The assignment of the carbonyl resonances in the ^{13}C NMR was supported by 2D ^{1}H–^{13}C HMBC experiments recorded at room temperature in CD_2Cl_2 (Figure 4.5). For instance, the resonances observed at 173.5 and 172.5 ppm, chemical shifts of which are typical of those of free alkyl ester carbonyl carbons, showed strong correlations with the diasterotopic protons of the vicinal methylene group at 3.10 and 2.93 ppm for **16a**, and 3.14 and 2.95 ppm for **16b**. These observations led to the conclusion that the non-coordinated carbonyl signals indeed corresponded to the *β*-alkyl ester carbonyl carbons originated from the dialkyl itaconates.

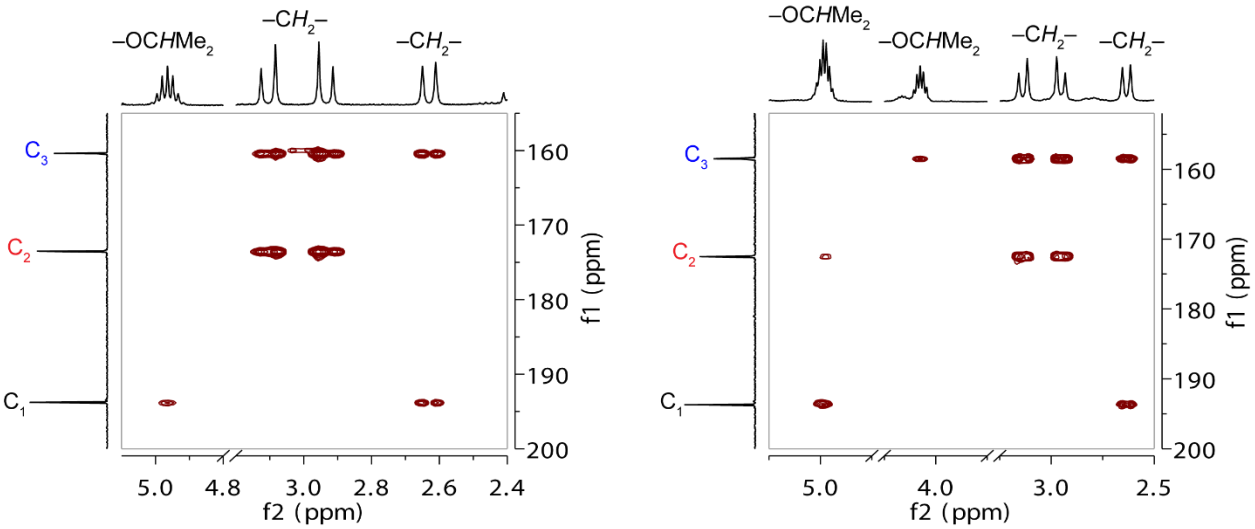

Figure 4.5. Selected portions of ^{13}C–^{1}H HMBC (CD_2Cl_2, 25 °C) 2D NMR spectra of complexes **16a** (left) and **16b** (right) shown for comparison.

Again, control experiments showed no further consumption of excess DMIA, DiPrIA, or MMA. Thus, the lack of polymerization activity of **14**$^{+}$ towards dialkyl itaconates can be attributable to the inability of the incoming monomer to enter the coordination sphere of the Zr center in the pre-formed 8-membered-ring chelate complexes **16a** and **16b**, and thus preventing from further chain growth.

As in the case of C_2-ligated *ansa*-zirconononocene complex **1**, unbrdiged neutral methyl ester enolate zirconocene **14** reacts with IA instantaneously to generate cleanly the corresponding single

monomer addition product **18** (Scheme 4.7). The generation of the cyclic enolate anhydride was evidenced by key resonances observed in the ^{1}H and ^{13}C NMR spectra, including: (1) the complete disappearance of the vinylic protons of IA and appearance of new methylene protons (sharp singlet at 2.11 ppm); (2) the marked downfield shifting of the septet for –OC*H*Me$_2$ at 4.07 ppm of the isopropyl ester enolate in **14** to 4.92 ppm of the –OC*H*Me$_2$ now attached to the ester group in **18**; (3) the upfield shifting of the >CMe$_2$ (1.07 and 1.05 ppm) and the methyl ligand (−0.06 ppm); and (4) only one doublet for the isopropyl group (1.21 ppm). In addition, the resonances corresponding to the carbonyl carbons in the ^{13}C NMR spectrum of isolated complex **18** at 177.7 ppm for the [*C*(O)=O] of the cyclic anhydride and at 174.9 ppm for the [*C*(O^{i}Pr)=O] of the isopropyl ester are typical of that of free non-coordinated carbonyl esters, indicative of the open chain structure as depicted in Scheme 4.7, in which the terminal isopropyl ester group is not coordinated to the metal center.

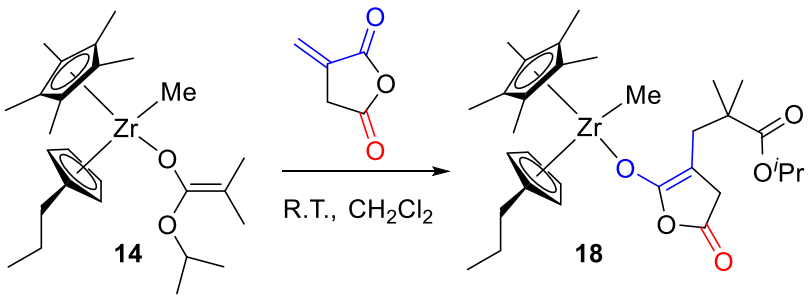

Scheme 4.7. Reactivity of neutral zirconocene complex **14** with itaconic anhydride.

Reactivity of Zr-Itaconate Chelates towards Acrylic Monomers. It has been well established that coordination-addition polymerization of polar vinyl monomers by cationic zirconocenium catalysts occurs through a labile 8-membered-ring chelate intermediate (resting state, exemplified by **B** in Scheme 4.8) formed upon Michael-addition of the growing ester enolate chain-end onto the conjugated C=C of the incoming monomer (active species, exemplified by **A** in Scheme 4.8).[8,9,10,13,14,15,17,18,22,27] Moreover, it has been determined that the ring-opening of the

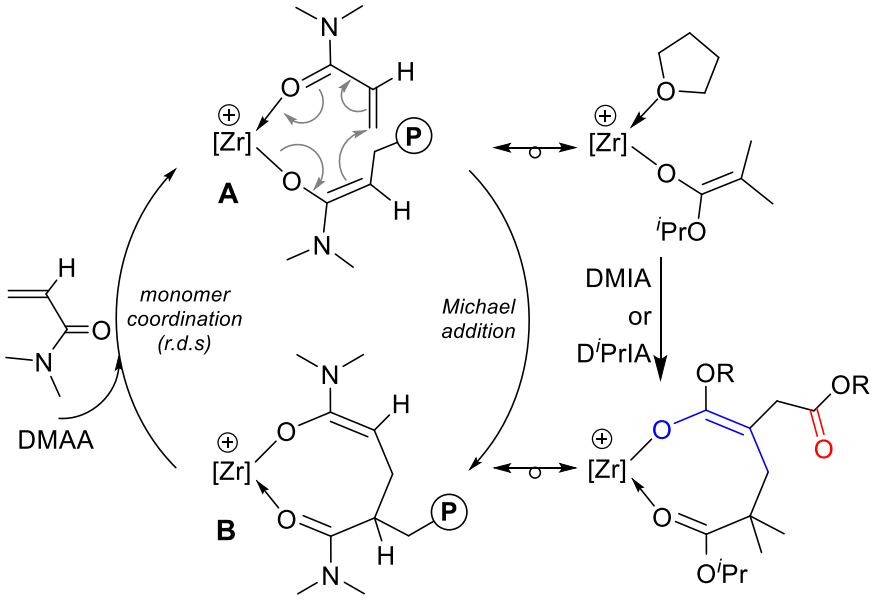

Scheme 4.8. Monometallic coordination-addition polymerization mechanism of DMAA by Zr-itaconate chelates **2a**(**b**) and **16a**(**b**). [Zr] = [*rac*-(EBI)]Zr, [Cp*(^{n}PrCp)]Zr, paired with [MeB(C_6F_5)$_3$]$^-$ as the counterion.

resting state to accommodate the coordination of the new incoming monomer is the rate determining step (r.d.s.) of the polymerization reaction. In this work, we have shown that DMIA, D^{i}PrIA, and MMA were not capable of ring-opening the 8- and 7-membered-ring chelate complexes formed after the first monomer addition took place and effectively prohibitting the polymerization reaction. Furthermore, our synthetic and mechanistic studies with two cationic mono ester enolate zirconocenium complexes, C_2-ligated *ansa*-metallocenium **1**$^+$ and the unbridged metallocenium **14**$^+$, suggested that the basicity of the conjugated carbonyl oxygen in the incoming monomer must be high enough so that displacement of the chelating carbonyl ester can occur; subsequent fast Michael-addition of the enolate polymer chain-end would propagate the polymerization reaction. Accordingly, we hypothesized that a highly basic acrylamide monomer, such as DMAA, should be capable of ring-opening Zr-itaconate 8- and 7-membered-ring chelates **2a**(**b**) and **16a**(**b**) and thus promote the DMAA polymerization.

Control experiments were first performed with newly synthesized unbridged cationic complexes dimethyl **11**$^+$ and mono ester enolate **14**$^+$ for the polymerizations of MMA and DMAA in order to assess their polymerization behavior (Table S4.1). Polymerization of MMA by catalysts **11**$^+$ and **14**$^+$ produced syndiotactic-enriched PMMA in a well-controlled fashion, achieving quantitative conversion in 24 h; the PMMA produced had unimodal and narrow molecular weight distribution with M_n = 13.8–17.5 kg/mol, $Đ$ = 1.20–1.21, and initiator efficiency I* = 86–109%. The similarity found between both catalytic systems indicated a similarly efficient initiation reaction promoted by the nucleophilic attack of the methyl ligand and the enolate (OC(O^{i}Pr)=CMe$_2$) in **11**$^+$ and **14**$^+$, respectively. On the other hand, the polymerization of DMAA by **11**$^+$ and **14**$^+$ was much faster, achieving quantitative conversions in 3 and 1 h, respectively. However, important differences in the iniation rate *vs* propagation rate were observed between catalysts **11**$^+$ (bimodal distribution) and catalyst **14**$^+$ (unimodal distribution with narrow $Đ$), indicating that the more coordinating and much more reactive DMAA was highly susceptible to differences in the nucleophilic character of the initiating ligand (methyl *vs* enolate).

Next, 8-membered-ring Zr-itaconate chelates **2a**(**b**) and **16a**(**b**) were employed for polymerizations of MMA and DMAA. While **2a**(**b**) exhibited no activity toward MMA polymerization, they initated rapid polymerization of DMAA (entries 1-2, Table 4.1), achieving full conversion in 30 min. The polymerization activity of **16a**(**b**) was noticeably lower, requiring 24 h to achieve quantitative monomer conversion, but the polymerization was well controlled, producing PDMAA with M_n close to the theoretical value and low $Đ$ values of 1.14 –1.19 (entries 3 and 4). It is worth noting here that neither MMA nor DMAA could be efficiently polymerized by 7-membered-ring chelates **4a** and **4b**, highlighting *the importance of the labile 8-membered-ring chelate as the reactive propagating intermediate*, as it can be ring-opened for further

Table 4.1. Results of DMAA polymerization by Zr-itaconate catalysts.[a]

run no.	Catalyst	Monomer	Time (h)	conv.[b] (%)	M_n[c] (kg/mol)	$Đ$[c]	I*[d] (%)	[*mm*][e] (%)	[*mr*][e] (%)	[*rr*][e] (%)
1	**2a**	DMAA	0.5	100	14.9[f]	n.d.	102	> 99	–	–
2	**2b**	DMAA	0.5	100	24.6[f]	n.d.	61	> 99	–	–
3	**16a**	DMAA	24	100	20.1	1.19	75	n.d.	n.d.	n.d.
4	**16b**	DMAA	24	100	20.0	1.14	76	n.d.	n.d.	n.d.

[a]Conditions: solvent (DCM) = 3 mL; ambient temperature (~23 °C); $[M]_0/[catalyst]_0$ = 150; n.d. = not determined. [b]Monomer (M) conversion measured by ^{1}H NMR. [c]Number-average molecular weight (M_n) and polydispersity ($Đ$) determined by gel-permeation chromatography (GPC) relative to PMMA standards. [d]Initiator efficiency (I*) = M_n(calcd)/M_n(exptl), where M_n(calcd) = MW(M) × $[M]_0/[catalyst]_0$ × conversion% + MW of chain-end groups. [e]Tacticity measured by ^{1}H NMR in $CDCl_3$. [f]Calculated by ^{1}H NMR.

monomer enchainment. In contrast, 7-membered-ring chelates, which are more thermodynamically stable isomers, cannot undergo ring-opening events, even with highly basic acrylamide monomers, therefore rendering them inactive for polymerization.

Further analysis of the ^{1}H NMR of the isolated highly isotactic PDMAA obtained by **2a** and **2b** allowed for identification of their polymer end-groups (Figure S4.44). The minor resonances at ~3.5 ppm (singlets, –O*Me*) and ~4.7 ppm (sept, –OC*H*Me$_2$), with integrals matching well with the expected polymer molecular weight, confirmed the presence of a dimethyl or diisopropyl ester at the polymer terminus derived from the original dimethyl or diisopropyl itaconate in **2a** and **2b**, respectively. Moreover, low molecular weight PDMAA sample prepared by **2a** and **2b** were analyzed by MALDI-TOF mass spectrometry (Figure 4.6). The plot of *m*/*z* values of the spectrum peaks vs the number of DMAA repeat units gave a straight line (Figure 4.7), with a slope corresponding to the mass of the monomer and the intercept to the sum of the masses of Na^+ (from the added NaI) and the expected end group, $C_{14}H_{24}O_6$ and $C_{18}H_{32}O_6$, which is equal to the sum of [OC(O^{i}Pr)=CMe$_2$] plus DMIA or D^{i}PrIA, respectively. Identical results were obtained with low molecular weight samples of PDMAA obtained by Zr-itaconate chelates **16a** and **16b**, also confirming the presence of the dialkyl itaconates as part of the chain end (Figures

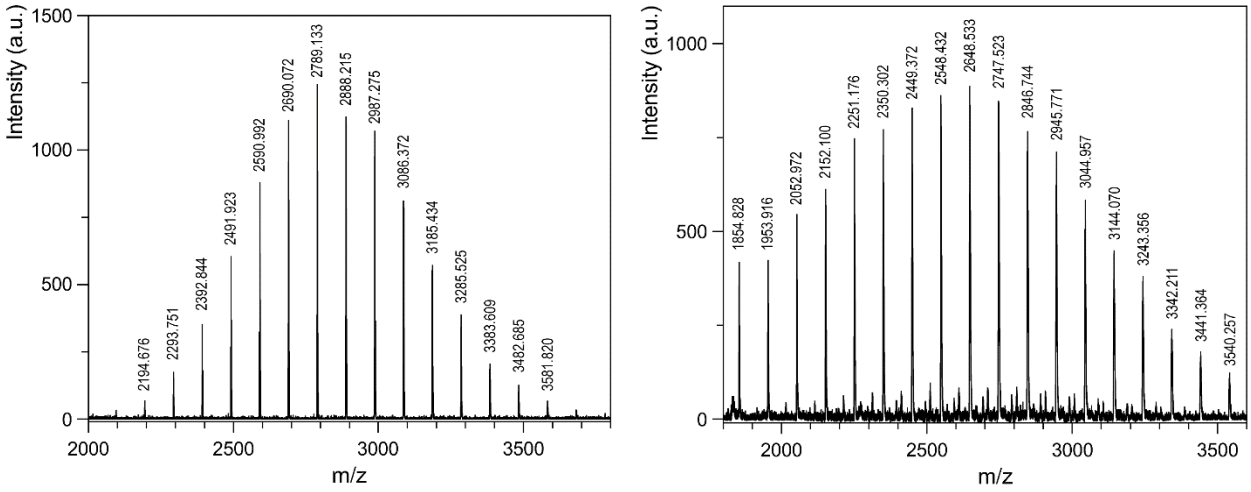

Figure 4.6. Portion of the MALDI-TOF mass spectrum of the low-molecular-weight PDMAA produced by **2a** (left) and **2b** (right) at 23 °C in CH_2Cl_2.

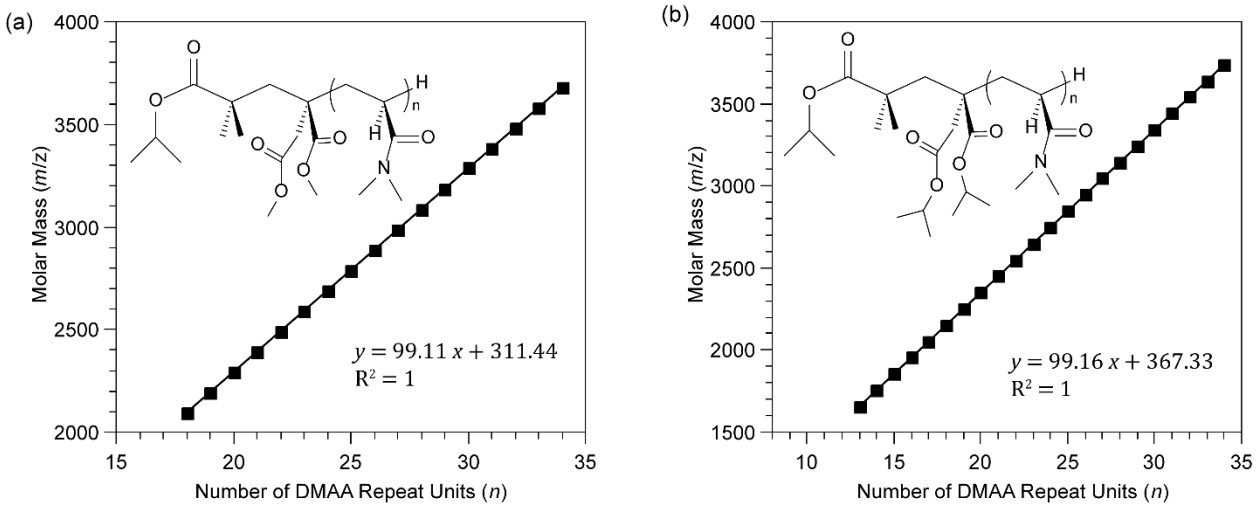

Figure 4.7. Plots of *m*/*z* values vs the number of DMAA repeat units (*n*) from the MALDI-TOF spectra in Figure 4.6 left (a) and Figure 4.6 right (b).

S4.45 to S4.48). These results led to a conclusion that the polymerization of DMAA initiated by the 8-membered-ring chelates **2a**(**b**) and **16a**(**b**) followed the same initiation/propagation mechanism established for cationic *ansa*-zirconocene ester enolate complex $\mathbf{1}^+$ (Scheme 4.8).[12,13]

4.4. Conclusions

In summary, we have investigated extensively the reactivity of neutral and cationic complexes of both bridged *ansa*-zirconocenes and unbridged zirconocenes towards biorenewal itaconic esters (itaconates) and anhydride (IA). In this study, bridged *ansa*-zirconocene complexes are represented by C_2-ligated, *rac*-(EBI)Zr-bassed *ansa*-zirconcene mono ester enolate complex **1** and its corresponding cationic *ansa*-zirconcenium ester enolate complex $\mathbf{1}^+$, while unbridged zirconocenes are exemplified by the newly synthesized Cp*(^{n}PrCp)Zr-based mono ester enolate **14** and its corresponding cationic ester enolate complex $\mathbf{14}^+$. The results of this investigation revealed similar monomer insertion and polymerization chemisty between these two classes of metallocene complexes, but some noteworthy differences as well.

Ansa-zirconcenium ester enolate $\mathbf{1}^+$ reacts with dialkyl itaconates such as DMIA and D^{i}PrIA to form cleanly single-monomer-addition products, 8-membered-ring metallocycles **2** with chelation through dative coordination of the ester group derived from the initiating ester enolate ligand to Zr. Interestingly, metallocycles **2**, as the kinetic products of this nucleophilic addition reaction, undergo slow ligand exchange between the coordinated (chelated) ester group with the non-coordinated β-alkyl ester group of the itaconates at room temperature to form thermodynamically favored 7-membered-ring chelates **4**, via the proposed 5-coordinated transition state structure **3**. While cationic $\mathbf{1}^+$ reacts with IA to afford an intractable product mixture, the neutral zirconocene **1** reacts cleanly with IA to afford the single IA addition product **5**. Behaving similarly, unbridged zirconocenium ester enolate $\mathbf{14}^+$ reacts with itaconates to afford the corresponding 8-membered-ring metallocycles **16**, and the neutral ester enolate **14** reacts with IA to the single IA addition product **18**. However, unlike labile 8-membered chelates **2** derived from the *ansa*-zirconocenium **1**, the 8-membered chelates **16** derived from the sterically more crowded

unbridged zirconocenium **14** are stable at room temperature and do not undergo the ligand exchange to form hypothesized 7-membered ring chelates **17**.

The above cationic complexes, either before the stoichiometric reaction with itaconates or after, exhibit no reactivity towards further additions of itaconates, therefore no chain propagation and growth. Based on the hypothesis that the origin of this lack of polymerization activity arises from the inability of the incoming monomer to ring-open the first monomer addition product, the 8-membered-ring chelate, more basic monomers such as DMAA were employed to test this hypothesis. Indeed, 8-membered metallocycles **2** (from the bridged zirconocene) and **16** (from the unbridged zirconocene), but not 7-membered **4**, effectively polymerize DMAA in a controlled manner, producing either highly isotactic PDMAA with *mm* >99%, by **2**, or PDMAA with narrow molecular weight distributions with $Đ$ =1.14 –1.19, by **16**.

REFERENCES

(1) (a) Llevot, A.; Dannecker, P.-K.; von Czapiewski, M.; Over, L. C.; Söyler, Z.; Meier, M. A. R. *Chem.-Eur. J.* **2016**, *22*, 11510-11521. (b) Yao, K.; Tang, C. *Macromolecules* **2013**, *46*, 1689-1712.

(2) (a) Hajian, H.; Wan Yusoff, W. M. *Curr. Res. J. Biol. Sci.* **2015**, *7*, 37-42. (b) Klement, T.; Büchs, J. *Bioresource Technology* **2013**, *135*, 422-431. (c) Willke, T.; Vorlop, K. D. *Appl Microbiol Biotechnol* **2001**, *56*, 289-295.

(3) (a) Bozell, J. J.; Petersen, G. R. *Green Chemistry* **2010**, *12*, 539-554. (b) Geilen, F. M. A.; Engendahl, B.; Harwardt, A.; Marquardt, W.; Klankermayer, J.; Leitner, W. *Angew. Chem.-Int. Edit.* **2010**, *49*, 5510-5514. (c) Medway, A. M.; Sperry, J. *Green Chemistry* **2014**, *16*, 2084-2101.

(4) (a) Yang, J.-Z.; Otsu, T. *Polym. Bull.* **1991**, *25*, 145-152. (b) Otsu, T.; Yamagishi, K.; Yoshioka, M. *Macromolecules* **1992**, *25*, 2713-2716. (c) Otsu, T.; Watanabe, H. *Eur. Polym. J.* **1993**, *29*, 167-174. (d) Otsu, T.; Yamagishi, K.; Matsumoto, A.; Yoshioka, M.; Watanabe, H. *Macromolecules* **1993**, *26*, 3026-3029.

(5) (a) Fernández-García, M.; Fernández-Sanz, M.; de la Fuente, J. L.; Madruga, E. L. *Macromol. Chem. Phys.* **2001**, *202*, 1213-1218. (b) Szablan, Z.; Toy, A. A.; Terrenoire, A.; Davis, T. P.; Stenzel, M. H.; Müller, A. H. E.; Barner-Kowollik, C. *J. Polym. Sci. Pol. Chem.* **2006**, *44*, 3692-3710.

(6) (a) Robert, T.; Friebel, S. *Green Chemistry* **2016**, *18*, 2922-2934. (b) Vilela, C.; Sousa, A. F.; Fonseca, A. C.; Serra, A. C.; Coelho, J. F. J.; Freire, C. S. R.; Silvestre, A. J. D. *Polym. Chem.* **2014**, *5*, 3119-3141.

(7) Chen, E. Y.-X. *Chem. Rev.* **2009**, *109*, 5157-5214.

(8) Bolig, A. D.; Chen, E. Y.-X. *J. Am. Chem. Soc.* **2004**, *126*, 4897-4906.

(9) Rodriguez-Delgado, A.; Chen, E. Y.-X. *Macromolecules* **2005**, *38*, 2587-2594.

(10) Zhang, Y.; Ning, Y.; Caporaso, L.; Cavallo, L.; Chen, E. Y.-X. *J. Am. Chem. Soc.* **2010**, *132*, 2695-2709.

(11) Chen, X.; Caporaso, L.; Cavallo, L.; Chen, E. Y.-X. *J. Am. Chem. Soc.* **2012**, *134*, 7278-7281.

(12) Mariott, W. R.; Chen, E. Y.-X. *Macromolecules* **2004**, *37*, 4741-4743.

(13) Mariott, W. R.; Chen, E. Y.-X. *Macromolecules* **2005**, *38*, 6822-6832.

(14) Vidal, F.; Falivene, L.; Caporaso, L.; Cavallo, L.; Chen, E. Y.-X. *J. Am. Chem. Soc.* **2016**, *138*, 9533-9547.

(15) Vidal, F.; Gowda, R. R.; Chen, E. Y.-X. *J. Am. Chem. Soc.* **2015**, *137*, 9469-9480.

(16) Vidal, F.; Chen, E. Y.-X. *Synlett* **2017**, *28*, 1028-1039.

(17) Miyake, G.; Caporaso, L.; Cavallo, L.; Chen, E. Y.-X. *Macromolecules* **2009**, *42*, 1462-1471.

(18) Miyake, G. M.; Chen, E. Y.-X. *Macromolecules* **2008**, *41*, 3405-3416.

(19) Ning, Y.; Chen, E. Y.-X. *Macromolecules* **2006**, *39*, 7204-7215.

(20) Ning, Y.; Chen, E. Y.-X. *J. Am. Chem. Soc.* **2008**, *130*, 2463-2465.

(21) Hu, Y.; Miyake, G. M.; Wang, B.; Cui, D.; Chen, E. Y.-X. *Chem.-Eur. J.* **2012**, *18*, 3345-3354.

(22) Miyake, G. M.; Newton, S. E.; Mariott, W. R.; Chen, E. Y.-X. *Dalton Trans.* **2010**, *39*, 6710-6718.

(23) Li, Y.; Ward, D. G.; Reddy, S. S.; Collins, S. *Macromolecules* **1997**, *30*, 1875-1883.

(24) Collins, S.; Ward, D. G.; Suddaby, K. H. *Macromolecules* **1994**, *27*, 7222-7224.

(25) Rodriguez-Delgado, A.; Mariott, W. R.; Chen, E. Y.-X. *J. Organomet. Chem.* **2006**, *691*, 3490-3497.

(26) Collins, S.; Ward, D. G. *J. Am. Chem. Soc.* **1992**, *114*, 5460-5462.

(27) (a) Mariott, W. R.; Rodriguez-Delgado, A.; Chen, E. Y.-X. *Macromolecules* **2006**, *39*, 1318-1327. (b) Ning, Y.; Caporaso, L.; Correa, A.; Gustafson, L. O.; Cavallo, L.; Chen, E. Y.-X. *Macromolecules* **2008**, *41*, 6910-6919. (c) Zhang, Y.; Caporaso, L.; Cavallo, L.; Chen, E. Y.-X. *J. Am. Chem. Soc.* **2011**, *133*, 1572-1588. (d) He, J.; Zhang, Y.; Chen, E. Y.-X. *Macromol. Symp.* **2015**, *349*, 104-114.

CHAPTER 5

Precision Polymer Synthesis via Chemoselective, Stereoselective, and Living/Controlled Polymerization of Polar Divinyl Monomers[*]

5.1. Summary

Post-polymerization modification of polymers carrying reactive side-chain groups has been a successful method to introduce target functionalities into polymer systems, based commonly on atactic amorphous polymers. Effective synthetic methods for obtaining stereoregular functional polymers from polymerization of polar divinyl monomers must achieve not only high chemoselectivity and livingness of the polymerization, but also high stereoregularity of the polymer main-chain backbone, preferably under ambient reaction conditions for a facile manipulation over the spatial orientation of such functional groups. In this Account article, we review some recent metal-mediated coordination polymerization systems that are simultaneously chemoselective, stereoselective, and living/controlled for obtaining highly stereoregular and densely functionalized polymers. In addition, we compare such results with those obtained by certain organocatalysts and describe the efforts to post-functionalize the olefin-carrying stereoregular polymers with the efficient thiol-ene "click" reaction.

5.2. Introduction

Soft polymeric materials have become indispensable in our modern society, since their intrinsic tunability and industrial scale production have allowed their applications in almost every

[*] This dissertation chapter contains the manuscript of an invited account paper published in *Synlett* [Vidal, F.; Chen, E. Y.-X. *Synlett* **2017**, *28*, 1028-1039].This work was supported by the US National Science Foundation (NSF-1300267).

technological advance. However, controlling the chemical structure of polymer backbones, chain-ends, and reactive pendant groups during or after the polymerization takes place is crucial for attaining desired thermomechanical properties or supramolecular assemblies for specialty applications, which remains as one of the challenges in polymer synthesis.[1,2,3,4,5] Polymerization techniques have traditionally exploited *orthogonal reactivity* of monomers or initiators bearing a polymerizable group separated from a functionalizable handle, which can be subsequently reacted in a quantitative manner for obtaining a wide array of polymer families and topologies, such as linear, star, block-, graft-, brush (co)polymers, as well as supramolecular assemblies, dendrimers, and crosslinked networks.[2,4,6] This strategy allows the inclusion of desired functionalities that otherwise would be incompatible with the polymerization method, while safeguarding the integrity of the polymer backbone. Many living polymerization techniques have been utilized for carrying orthogonally reactive side-groups at every repeat unit or at the chain terminus with excellent control over the polymer number-average molecular weight (M_n) and molecular weight distribution ($Đ$), including living radical polymerizations (such as atom transfer radical polymerization, ATRP, and reversible addition-fragmentation chain transfer polymerization, RAFT),[7,8,9,10] living anionic and cationic polymerizations,[11,12] ring opening polymerization (ROP),[8,13] and ring opening metathesis polymerization (ROMP).[14] However, reversible protection/deprotection reactions in stepwise post-functionalization processes might be required when functional groups are incompatible with such polymerization methods, making the overall material synthesis less efficient.[15] Moreover, the lack of control over the stereo-microstructures in the resulting atactic materials limits the number of polymer structures and properties that can be attained.

Alternatively, *chemoselective* polymerization[16] of monomers containing two polymerizable functionalities represents a more straightforward method for obtaining densely functionalized materials with reactive groups distributed at every repeat unit of the polymer backbone. Thus, direct post-modification of the functional polymers is possible without the need of cumbersome protecting/deprotecting reactions, which in turn decreases the number of synthetic and purification steps, and thus overall increases the efficiency and ease of the process. In this context, polar divinyl acrylic monomers that contain a conjugated acrylic moiety and an unconjugated double bond are desirable candidates for applying chemoselective polymerization methods, since their conjugated C=C double bond and the non-conjugated vinyl group inherently have reactivity differences that can be used advantageously. Under the basis of the Alfrey and Price (*Q* and *e* values) theory, divinyl monomers can be regarded as a copolymerization system of two independent and competing vinyl monomers.[9,10,17,18] For instance, vinyl methacrylate (VMA, Scheme 5.1) can be approximated to a pair of monomers consisted of methyl methacrylate (MMA) and vinyl acetate (VAc), and the reactivity ratios of both vinyl groups can be calculated accordingly (r_1 = 18.0 for the conjugated C=C, r_2 = 0.011 for the non-conjugated C=C, Table 5.1). Hence, their relative reactivity ratio differences (r_1/r_2 ~ 1700) are sufficiently disparate to promote chemoselective radical and anionic polymerization of the methacrylic C=C double bond under certain controlled conditions. However, the use of suitable aluminum Lewis acid additives, low temperatures, and inert conditions were required to maintain the chemoselectivity of the polymerization at high conversions and produce soluble polymers with relatively high M_n.[19]

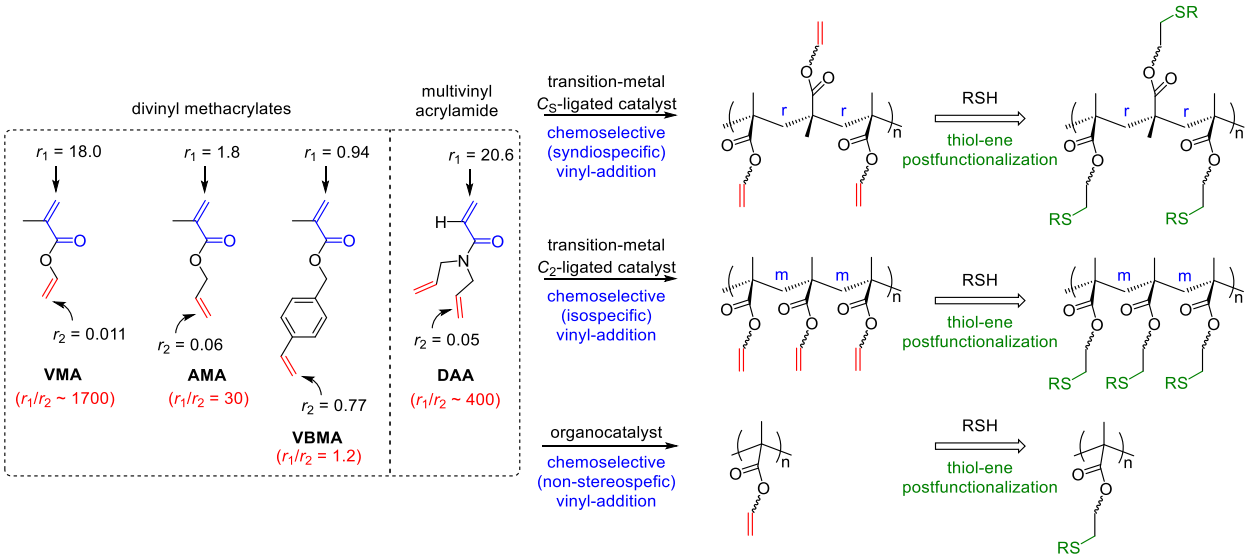

Scheme 5.1. Acrylic polar divinyl monomers and their reactivity ratios (calculated as shown in Table 5.1 footnote) and the structure of the stereoregular ene-bearing polymers obtained through chemoselective polymerization *via* vinyl addition of the conjugated methacrylic C=C double bond.

Table 5.1. Q and e values, and reactivity ratio differences ($\boldsymbol{r_1/r_2}$) estimated for selected polar divinyl monomers.[a]

divinyl monomer[b]	equivalent monomer pairs[b]	Q_1	e_1	Q_2	e_2	r_1/r_2
VMA	MMA / VAc	0.78	0.40	0.026	−0.88	~1700
AMA	MMA / AAc	0.78	0.40	0.24	−1.07	30
VBMA	MMA / MSt	0.78	0.40	1.10	−0.60	1.2
DAA	DEAA / ASA	0.48	−0.31	0.024	−0.41	~400

[a]Q and e values were obtained from the *Polymer Handbook*,[17] and the reactivity ratios were calculated using the Alfrey and Price equations: $r_1 = (Q_1/Q_2) \cdot \exp[-e_1(e_1 - e_2]$; $r_2 = (Q_2/Q_1) \cdot \exp[-e_2(e_2 - e_1]$. [b]Monomer abbreviations: VMA, vinyl methacrylate; AMA, allyl methacrylate; VBMA, 4-vinylbenzyl methacrylate; DAA, *N*,*N*-diallyl acrylamide; MMA, methyl methacrylate; DEAA, *N*,*N*-diethyl acrylamide; VAc, vinyl acetate; AAc, allyl acetate; MSt, *p*-methyl styrene; ASA, *N*-allylstearamide.

Allyl methacrylate (AMA) is another polar divinyl monomer targeted for chemoselective polymerization in which the vinyl group reactivity ratio differences are much smaller (r_1 = 1.8, r_2 = 0.06, r_1/r_2 = 30). Not surprisingly, the radical polymerization of AMA cannot maintain the chemoselectivity of the polymerization process, especially at the later stages of the polymerization when depletion of the conjugated C=C double bonds enforces the reactivity of the non-conjugated

vinyl groups during the propagation reaction, producing insoluble crosslinked gels.[9,20] An even more challenging monomer is 4-vinylbenzyl methacrylate (VBMA), because the reactivity ratios for the methacrylic C=C (r_1 = 0.94) and the styrenic vinyl group (r_2 = 0.77) are similar (r_1/r_2 = 1.2). In fact, VBMA turns almost immediately into a crosslinked gel upon indiscriminate radical polymerization of both vinyl groups.[21] Group transfer polymerization (GTP) of VBMA achieved linear PVBMA but with a broad *Đ* of 8.2,[22] and anionic polymerization required low temperature (−78 °C) to selectively polymerize the conjugated double bond, while the controlled characteristics of the polymerization were lost at temperatures above −20 °C.[23]

Ideally, chemoselective polymerization of polar divinyl monomers should be both living, for control over M_n and *Đ*, *and* stereospecific, for control over the polymer microstructures derived from the regular orientation of the side-chain functionalities. In this Account, we describe recent advances made in controlling the chemoselectivity of the polymerization of polar divinyl monomers with an emphasis on obtaining highly stereoregular polymeric materials. We also discuss some applications in the direct post-modification of the obtained olefin-bearing stereoregular methacrylic polymers into functionalized polymers by the thiol-ene "click" reaction.

5.3 Metal-Catalyzed Coordination-Addition Polymerization of Polar Divinyl Monomers

Since the inception of the coordination polymerization of methacrylic monomers such as MMA by single-site metallocene complexes in the early 1990's,[24,25] extensive research efforts have focused on both expanding the monomer scope and controlling the polymerization characteristics, especially with regard to relative rates of initiation vs propagation (for control over the polymer molecular weight and its distribution) and stereoregularity (for enhanced thermal and mechanical properties) at room temperature or above.[26] Significant advances were made over the

next couple decades to uncover the living and controlled production of highly isotactic ([*mm*] ≥ 95%) and highly syndiotactic ([*rr*] ≥ 95%) PMMA materials with the judicious use of bridged group IV *ansa*-metallocenium complexes, C_2-ligated {*rac*-(EBI)Zr(THF)[OC(O^{i}Pr)=CMe$_2$]}$^+$ [MeB(C$_6$F$_5$)$_3$]$^-$ (EBI = ethylene-bis-indenyl) (**1**) and C_S-ligated, {[Ph$_2$C(Cp)(2,7-^{t}Bu$_2$Flu)]Zr(THF)[OC(O^{i}Pr)=CMe$_2$]}$^+$ [MeB(C$_6$F$_5$)$_3$]$^-$ (Flu = η^n-fluorenyl) (**2**), respectively (Scheme 5.2).[27,28,29] This polymerization method was successfully expanded to other polar vinyl monomers such as (meth)acrylamides,[30,31] and biorenewable butyrolactones,[32] achieving also high levels of stereoselectivity. Finally, "catalytic" production of PMMA chains was attained with the discovery of a new internal hydride-shuttling chain-transfer mechanism promoted by a zirconocenium catalyst paired with a [HB(C$_6$F$_5$)$_3$]$^-$ anion, which involves a reversible hydride addition/abstraction sequence that releases vinylidene-terminated polymer chains.[33]

Regardless of the *ansa*-metallocene's symmetry (C_2 or C_S), the mechanism of the metal-catalyzed polymerization reaction via coordination-addition (Scheme 5.2) involves the nucleophilic attack of the growing ester enolate chain end onto the conjugated methacrylic C=C double bond of a coordinated new monomer (i.e., conjugate Michael-addition), forming an 8-membered-ring ester enolate chelate (resting states **B** and **D**). The rate-determining step of this "catalytic" propagation cycle is the ring-opening of the chelate by the incoming monomer to regenerate the active species (**A** and **C**). Both the kinetic studies and the isolation of cationic cyclic ester enolate complexes (exemplified by **1·MMA** and **2·MMA**), which serve as structural models of the resting state, have corroborated this proposed monometallic, catalyst-site controlled, polymerization mechanism in a number of occasions.[28,29,31,34]

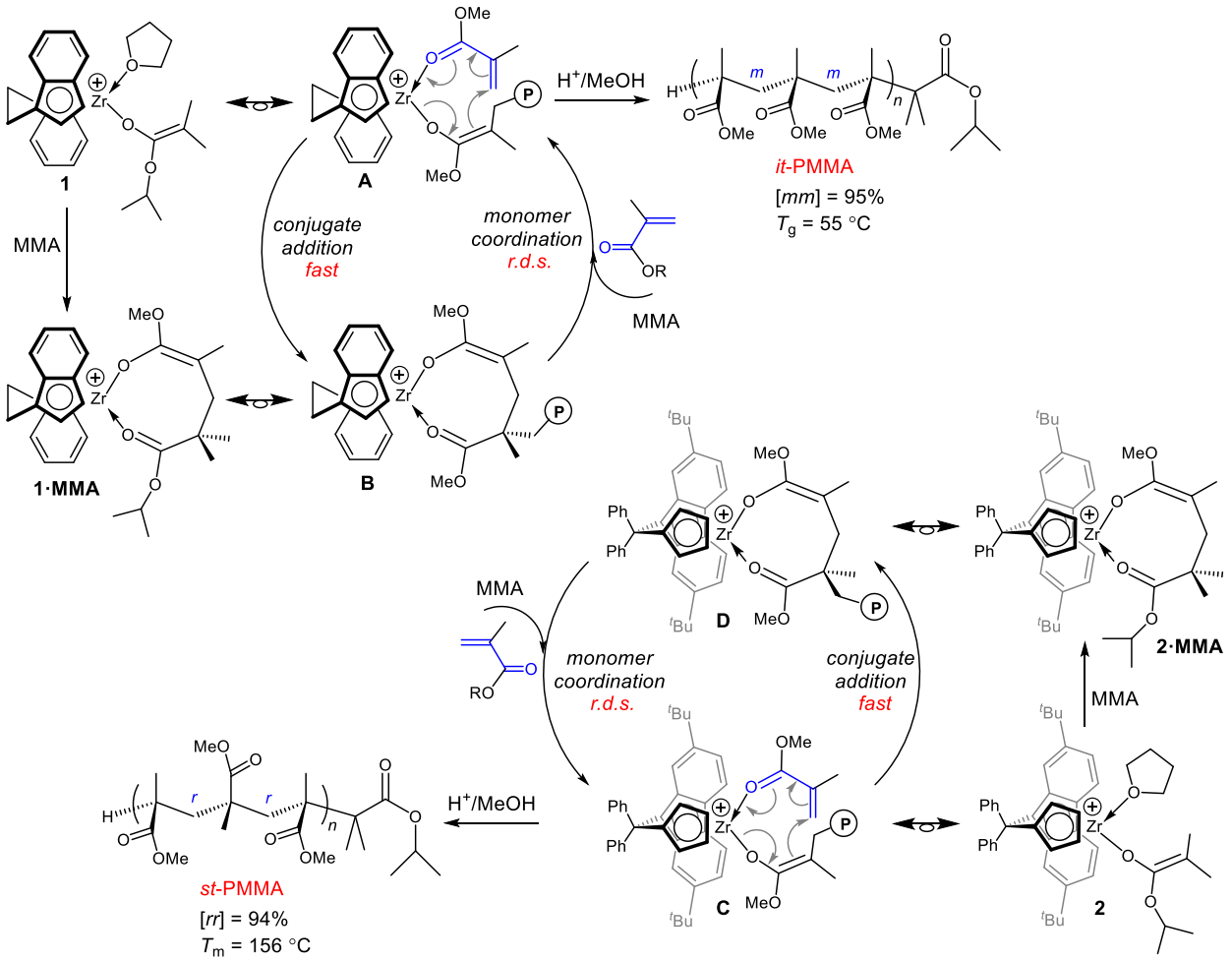

Scheme 5.2. Coordination-addition polymerization mechanism by C_2-ligated zirconocenium catalyst (**1**) that leads to highly isotactic PMMA (top left cycle), and by C_S-ligated zirconocenium catalyst (**2**) that leads to highly syndiotactic PMMA (bottom right cycle).

Recognizing the advantageous implications of the coordination-addition mechanism for the polymerization of polar divinyl monomers, we hypothesized that the oxophilicity of the cationic zirconocenium center would mandate exclusive vinyl addition through the methacrylic double bond, which is selectively activated by the coordination of the conjugated carbonyl group, and thus leaves the non-conjugated double bond intact. The results of this investigation were published in 2015 using the metal-catalyzed polymerization with the aforementioned C_2-ligated cationic complex **1**, achieving the simultaneous control over the chemo- and stereoselectivity of the polymerization, while also rendering the polymerization living at room temperature.[35]

Specifically, we found that polymerization of VMA by **1** was completely chemoselective and proceeded to complete consumption of the monomer homogenously without signs of gelation. The perfect retention of all the pendant vinyl groups was corroborated by the ^{1}H and ^{13}C NMR spectra of the isolated (and completely soluble) polymeric material. The polymerization achieved quantitative or near quantitative conversions (97–99%) rapidly (5–15 min) with relatively low catalyst loadings (1–0.25 mol %) in different [VMA]/[**1**] ratios, while keeping narrow molecular weight distributions ($Đ$ = 1.18–1.29). However, catalyst **1** was unable to promote high stereoselectivity for the polymerization of VMA, achieving only isotactic-biased *at*-PVMA ([*mm*] up to 53%).

On the other hand, high stereoseletivity was observed in the polymerization of AMA by **1** (Scheme 5.3). Highly isotactic *it*-PAMA ([*mm*] up to 97%) was produced with an enantiomorphic-site controlled mechanism, while the polymerization was simultaneously completely chemoselective, efficient (high conversions, 93–97%, in short times, 5–90 min) and well controlled (narrow $Đ$ = 1.18–1.25, and relatively high initiation efficiency, I* = 71–84%). The living characteristics of this polymerization was further confirmed with linear plots of M_n vs conversion and [AMA]/[**1**] ratios, as well as by obtaining well-defined block copolymers with unimodal, low $Đ$ values.

The monomer scope of the chemoselective and stereoselective polymerization by **1** was investigated with other methacrylic and acrylamide monomers. For example, the challenging chemoselective polymerization of VBMA to form highly isotactic *it*-PVBMA ([*mm*] up to 94%) was accomplished in high conversions (95–99%) with no gelation or precipitation. ^{1}H and ^{13}C NMR of the obtained material confirmed the complete consumption of the methacrylic C=C double bonds while retaining all the vinylbenzyl units. However, it was noticed that the narrow $Đ$

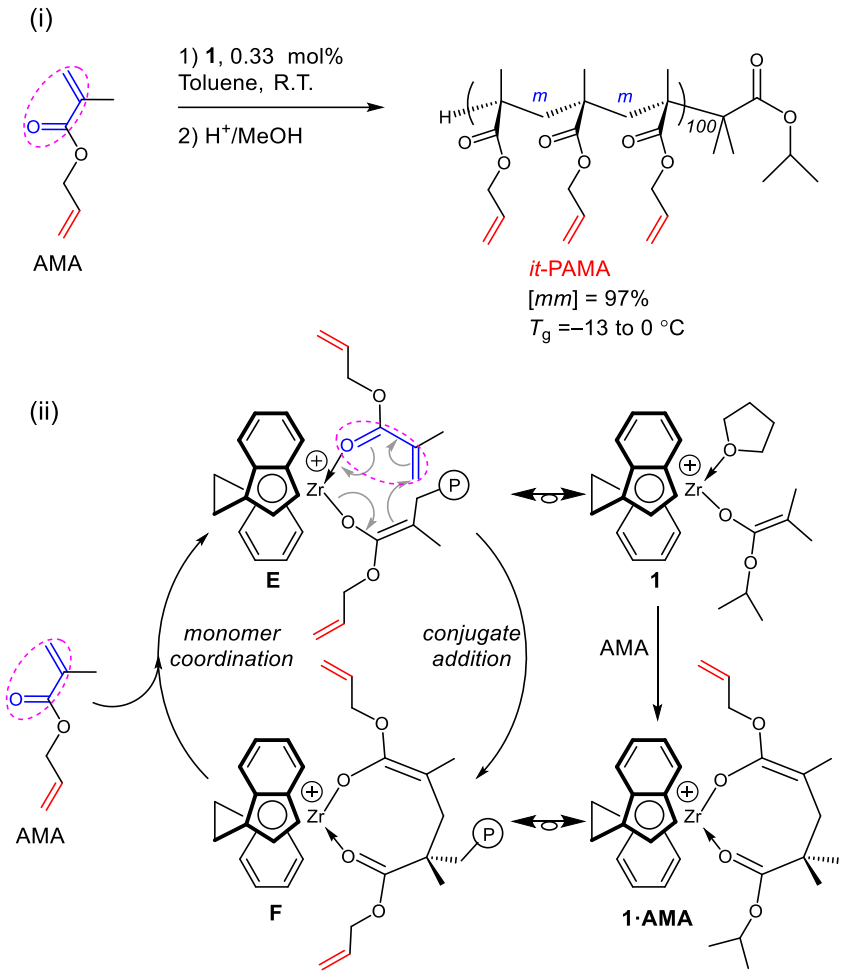

Scheme 5.3. Chemoselective and stereospecific polymerization of AMA by **1** to produce highly isotactic PAMA (**i**) and its coordination-addition polymerization mechanism (**ii**).

obtained at conversions of 75% (1.18–1.42) increased at near quantitative conversions to $Đ$ ~3, which indicated a possibly low degree of polymerization of the styrenic C=C when the methacrylic C=C was depleted. Finally, polymerization of *N*,*N*-diallyl acrylamide (DAA), a polar multivinyl monomer with estimated reactivity ratios of those in between VMA and AMA (Scheme 5.1 and Table 5.1), by **1** was the most efficient of all the monomers tested, achieving not only complete chemoselectivity, but also the highest level of isotacticity ([*mm*] > 99%), efficiency (quantitative I^* and conversions), and control ($Đ$ = 1.06–1.16).[35]

Kinetic and mechanistic studies, including the isolation of three structural models of the active species and the resting-state intermediates, have concluded that the coordination-addition polymerization reaction was indeed the origin of the perfect chemoselectivity, while the enantiomorphic-site control mechanism was responsible for the high levels of stereoselectivity observed (Scheme 5.3).[35] The sharp contrast in the stereoregularity between PVMA (mainly atactic, [*mm*] up to 53%) and PAMA (highly isotactic [*mm*] up to 97%) was observed, pointing to the important effects of monomer steric bulkiness and orientation, especially in terms of the hybridization of the α-carbon of the OR ester group, in the structures of the transition-states (TSs) determining the setereoselection.

The chemoselective coordination-addition polymerization of AMA by other transition metals was exemplified soon after by Xu and coworkers using neutral half-metallocene yttrium catalysts **3** and **4** (Figure 5.1).[36] Although this metal-catalyzed polymerization didn't achieve the same high level of stereoselectivity (*st*-PAMA with [*rr*] up to 73% was obtained), the polymerization was shown to be well-controlled (low $Đ$ = 1.06–1.08 and high I^* = 91–93%) and living at ambient temperature. Kinetic studies and MALDI-TOF analysis of end-groups indicated that the propagation reaction for AMA polymerization followed the same mono-metallic coordination-addition mechanism as the one observed for group IV cationic metallocenes in MMA polymerization, which is indeed responsible for the observed chemoselectivity.

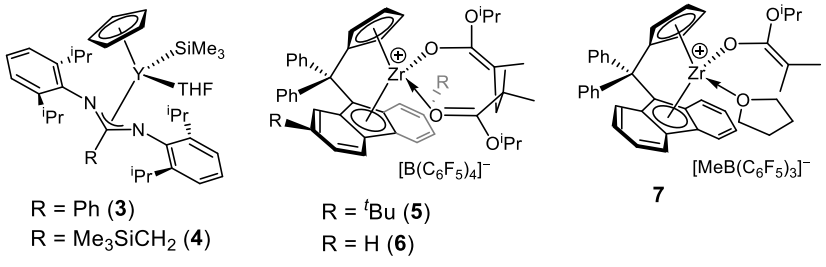

Figure 5.1. Neutral half metallocene yttrium catalysts (**3** and **4**) and C_S-ligated cationic zirconocenium catalysts (**5**, **6** and **7**) employed for the syndioselective polymerization of polar vinyl monomers.

Much higher levels of syndioselectivity, coupled with perfect chemoselectivity, were obtained by our group in 2016 by using cationic C_S-ligated zirconocenium catalysts **5**, **6**, and **7** (Scheme 5.4 and Figure 5.1).[37] Thus, complete chemoselective polymerization of VMA, AMA, and DAA was achieved for all the C_S-ligated zirconocenium catalysts tested, independent of the mode of activation (methyl or hydride abstraction) and the activation sequence (i.e., either the preactivation method by premixing of a precatalyst with an activator followed by addition of monomer, or in-reactor activation method by premixing of monomer with activator followed by addition of catalysts), highlighting the selectivity and robustness of the active species for this polymerization.

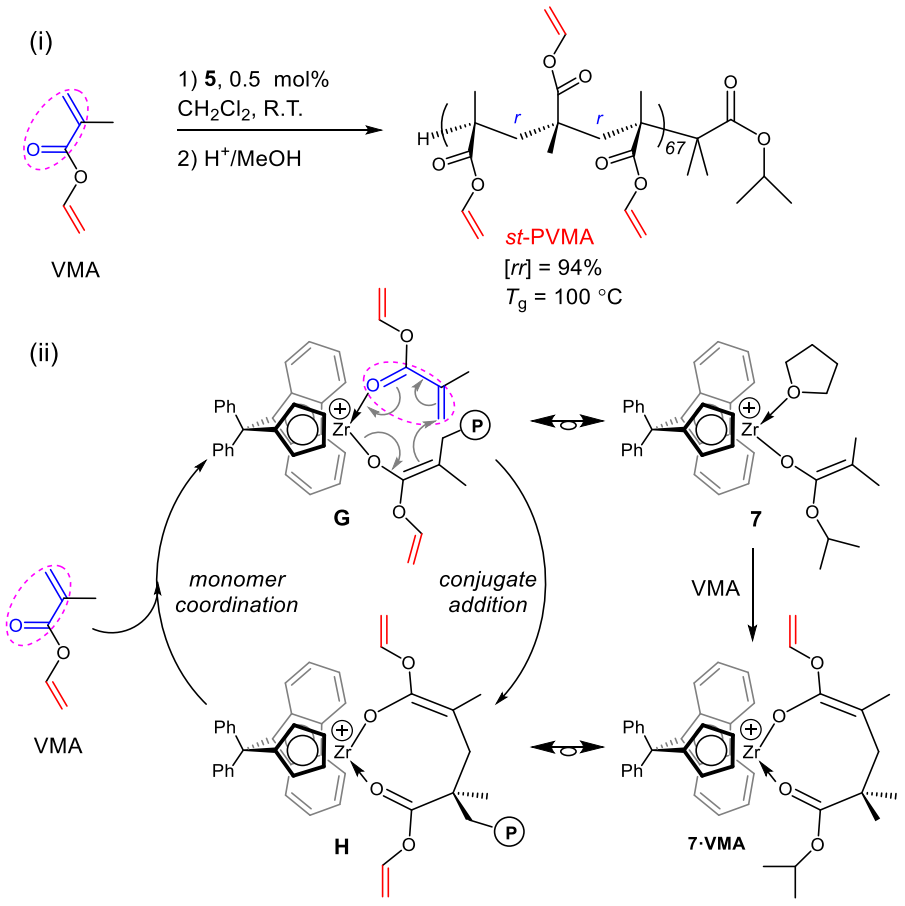

Scheme 5.4. Chemoselective and stereospecific polymerization of VMA by **7** to produce highly syndiotactic PVMA (**i**) and its coordination-addition polymerization mechanism (**ii**).

The sterically more demanding and more electron-rich catalyst **5** (Scheme 5.2), which possesses *tert*-butyl groups at the 2- and 7-postions of the fluorenyl ligand, showed the highest level of syndioselectivity in MMA polymerization ([*rr*] = 95%), but exhibited lower syndioselectivity in the polymerization of AMA and VMA, producing *st*-PAMA and *st*-PVMA with [*rr*] of 87.9% and 87.0%, respectively. On the other hand, this catalyst was rather reactive achieving high monomer conversions (92.7% and 96.2% for AMA and VMA, respectively) in short times, relatively high molecular weights (M_n = 55.3 kg/mol and 42.9 kg/mol for *st*-PAMA and *st*-PVMA, respectively) and medium *Đ* values (1.33 and 1.40 for *st*-PAMA and *st*-PVMA, respectively) at room temperature.

Catalysts **6** and **7** performed similarly for each of the monomers tested, and produced higher levels of syndioselectivity at room temperature for the polymerization of VMA, AMA, and DAA with %[*rr*] values up to 92.4, 93.5, and >99, respectively. Catalysts **6** and **7** were highly active in the polymerization of VMA, achieving near quantitative or quantitative conversions rapidly and producing polymers with M_n = 41.2–42.5 kg/mol and *Đ* = 1.36–1.38. The control of the polymerization characteristics was improved at 0 °C, with even lower *Đ* values (1.17–1.21) and higher [*rr*] values (94.8–95.7%), while still achieving near full monomer conversions. Polymerization characteristics of AMA by **6** and **7** were also satisfactory at room temperature, leading to syndiotactic polymers with high [*rr*] values (90.7–92.4%), predicted molecular weights (M_n = 24.5–35.0 kg/mol), and medium *Đ* values (1.32–1.56). Excellent performance of catalysts **6** and **7** was demonstrated in the polymerization of the acrylamide monomer DAA, achieving *simultaneously* both quantitative chemoselectivity *and* syndiospecificity ([*rr*] > 99%).[37]

A series of kinetic, synthetic, and mechanistic studies showed that the stereo- and chemoselectivity is originated from the mono-metallic, enantiomorphic-site-controlled mechanism

described above. The computational study compared the stereoselectivity differences observed in the polymerization of VMA and AMA by C_2-ligated catalyst **1** (low *vs* high isospecificity) and C_S-ligated catalyst **6** (high syndiospecificity in both cases).[37] We found a difference of 2.5 kcal/mol between the ΔG_{Stereo} of the TS for the addition of VMA and AMA by C_2-ligated catalyst **1**, consistent with the large differences in stereoselectivity observed with these two monomers. The higher ΔG_{Stereo} calculated for AMA was explained by the differences in the steric interactions between the monomer ester group and the metallocene skeleton, induced by the different nature of the sp^2 and sp^3 carbons of VMA and AMA respectively. On the other hand, we found a much smaller difference of 0.5 kcal/mol between the ΔG_{Stereo} of the TSs for the addition of VMA and AMA by C_S-ligated catalyst **6**, also consistent with the high levels of stereoselectivity observed in the polymerization of both VMA and AMA achieved by **6**.

Additionally, these highly syndiotactic ene-bearing methacrylate polymers were utilized in developing robust stereocomplexes with *it*-PMMA and inclusion complexes with fullerene C_{60} upon crystallization in complexing solvents.[37] The structure of the former was corroborated by the melting transitions in the differential scanning calorimetry (DSC) traces of the stereocomplexes (T_m = 155–170 and 164–188 °C, for stereocomplexes formed between *it*-PMMA and *st*-PAMA or *st*-PVMA, respectively), and a characteristic peak in the powder X-Ray diffraction patterns (2θ = 4.56°), while inclusion complexes with C_{60} presented sharp melting transitions (T_m = 200–207 °C) in their DSC traces. This novel strategy provided with crosslinking points across the helical structures, which were advantageously utilized to obtain robust crosslinked stereocomplexed materials with improved thermal and mechanical properties and high PMMA trapping efficiency (up to 100%). The crosslinked *st*-PAMA-C_{60} inclusion complex also showed a relatively high encapsulated C_{60} content.

5.4. Organocatalyzed Conjugated-Addition Polymerization of Polar Divinyl Monomers

Organocatalytic polymerization has been a subject of much recent interest due to its potential to substitute polymerization systems that traditionally required the use of otherwise more toxic and expensive transition metal-containing catalysts. Our groups developed Lewis pair polymerization (LPP) that utilizes main-group classical Lewis adducts (CLAs) or frustrated Lewis pairs (FLPs) between sterically encumbered Lewis bases (LBs) such as *N*-heterocyclic carbenes (NHCs) and phosphines and strong organo-Lewis acids (LAs) such as $Al(C_6F_5)_3$, for the highly active polymerization of polar vinyl monomers such as MMA and biorenewable γ–methyl-α-methylene-γ-butyrolactone ($_\gamma$MMBL) (Figure 5.2).[38,39] The generation of phosphonium or imidazolium zwitterionic species through the activation of the conjugated C=C by the LA to form enol-aluminate reactive species is key to achieve the high reactivity of this polymerization system,

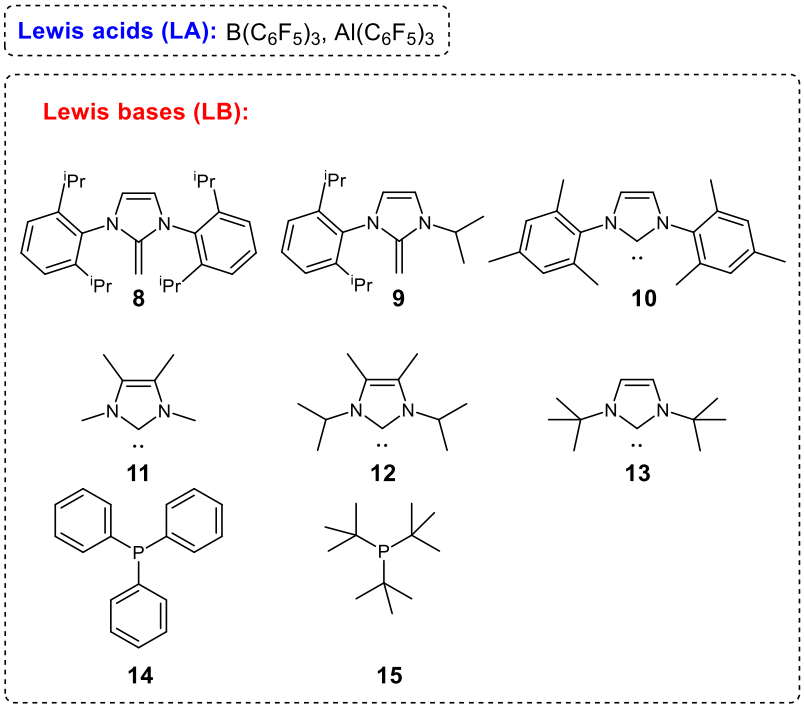

Figure 5.2. Structures of Lewis acids and Lewis bases utilized in organocatalyzed polymerization of polar (di)vinyl monomers.

and represents another example of potential chemoselectivity towards the methacrylic functionality against other non-conjugated olefinic groups.

In this context, Lu and co-workers uncovered the use of CLAs and FLPs for the chemoselective polymerization of divinyl polar monomers with high activities at room temperature (Scheme 5.5).[21] They demonstrated that alane-based Lewis pairs (but not the borane analogue) formed with N-heterocyclic olefins (NHOs) **8** and **9** and NHC **10**, or phosphines **14** and **15**, polymerize VBMA quantitatively with high molecular weight and low to medium $Đ$ values (1.22–1.39), showing a high level of chemoselectivity. The complete retention of the styrenic units was confirmed by ^{1}H NMR and ESI-TOF MS results. Similarly, VMA and AMA were chemoselectively polymerized very rapidly, achieving 100% conversion in only 3 minutes at room temperature. The AMA polymerization was controlled even at high AMA/base ratio of 1600:1, producing syndio-biased atactic PAMA with M_n = 640 kg/mol and $Đ$ = 1.28.

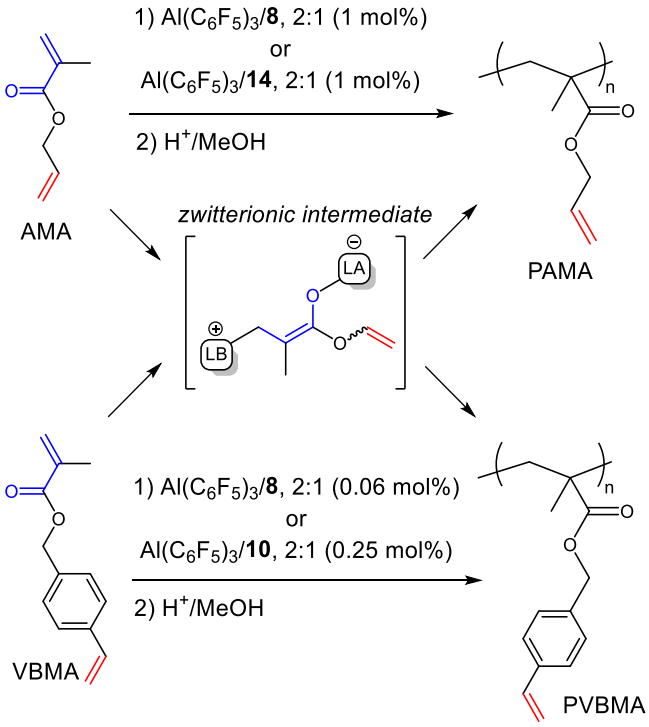

Scheme 5.5. Chemoselective polymerization of AMA (top) and VBMA (bottom) by alane-based FLPs.

The use of borane-based FLPs such as NHC/$B(C_6F_5)_3$ pairs for LPP of methacrylates has shown poorer or even negligible reactivity as compared to the alane analogue $Al(C_6F_5)_3$. It required the use of CLAs formed between non-sterically hindered phosphines and $B(C_6F_5)_3$ to observe unexpectedly high activity for the polymerization of $_\gamma$MMBL (TOF = 24,000 h^{-1}).[39] Variation of the alkyl substituents in selected NHCs paired with $B(C_6F_5)_3$, which required a fine tuning between electric/steric properties of the NHCs, can lead to well controlled methacrylate polymerization.[40] Furthermore, the ability of the NHCs/$B(C_6F_5)_3$ to chemoselectively polymerize AMA monomer was also achieved (Scheme 5.6). Although with relatively low activity in toluene as the solvent, the conversion could be improved by increasing the monomer concentration, or in neat monomer conditions, where the chemoselectivity of the process was preserved. Thus, soluble linear polymers were obtained, with medium molecular weight of M_n = 32.2–50.1 kg/mol and $Đ$ = 1.29–1.62. Analysis of the polymer methyl triads revealed that the polymers were syndiotactic, with [*rr*] = 76–82%. The mechanism for the polymerization reaction, which explains the origin of the chemoselectivity, was proposed to proceed via a bimolecular propagation pathway in which the zwitterionic active species attacks the conjugated C=C bond of the monomer activated by the LA.

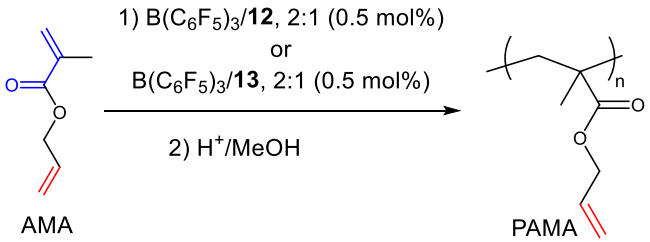

Scheme 5.6. Chemoselective polymerization of AMA by (NHC)/$B(C_6F_5)_3$ pairs.

Certain NHC structures can directly initiate conjugate-addition polymerization of methacrylates and biorenewable MBLs. For example, 1,3-di-*tert*-butylimidazolin-2-ylidene (**13**) mediates rapid polymerization of $_\gamma$MMBL to a bioplastic with extraordinary efficiency, converting

1000−3000 equivalents of monomer in 1 min at room temperature (turn-over frequency, TOF, up to 122 s^{-1}), with up to 1600% catalyst initiation efficiency thanks to facile internal chain transfer.[41] This conjugation-addition polymerization by NHCs proceeds *via* a zwitterionic enolate intermediate.

Subsequently, a series of vinyl-functionalized MBLs were prepared to examine the ability of NHCs to promote chemoselective polymerization of methacrylic bonds as well as improving the brittleness of the obtained polymeric materials.[42] For that purpose, γ-vinyl-α-methylene-γ-butyrolactone (VMBL), γ-vinyl-β-methyl-α-methylene-γ-butyrolactone (VMMBL), and γ-diallyl-α-methylene-γ-butyrolactone (DAMBL) were synthesized from biorenewable itaconic anhydride and their chemoselective polymerization was examined at room temperature (Scheme 5.7). The polymerization of VMBL, even with a remarkably low catalyst loading of NHCs (50 ppm, [M]/[NHC] = 20,000), was still very fast, exhibiting a TOF of 80,000 h^{-1} and producing relatively high molecular weight polymers (M_n = 72.8–73.8 kg/mol) in almost quantitative yields. The relatively high dispersity ($Đ$ = 2.80–2.99) was explained as a consequence of the catalytic production of polymer chains (producing on average 33.6 chains per NHC) due to chain transfer events to monomer. Polymerizations of VMMBL and DAMBL by NHC **13** and 1,3-di-isopropyl-4,5-dimethylimidazolin-2-ylidene (**12**) were less effective overall, including higher catalyst loading (0.5 mol%), longer reaction time (2 or 24h), lower conversions (less than 85%), and less chain transfer (I^* = 220–260%). However, the perfect chemoselectivity of these polymerizations was safeguarded for all monomers investigated, demonstrated by the complete retention of all the pendant vinyl groups and consumption of the conjugated methacrylic bond.

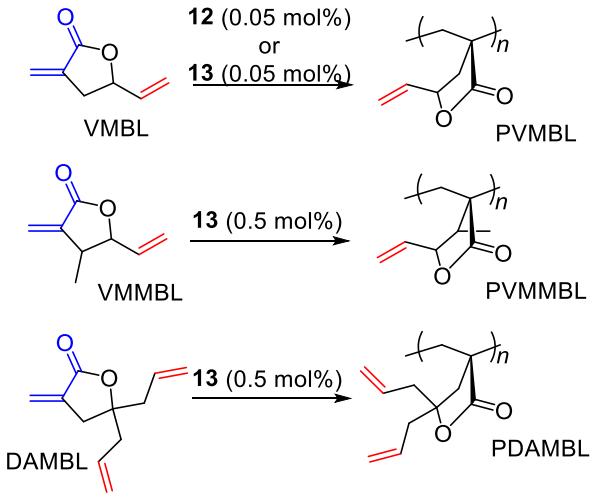

Scheme 5.7. Chemoselective polymerization of multivinyl-functionalized γ-butyrolactones by NHCs.

Alternatively, polymerization of AMA by polyaminophosphazene "superbase" (1-tert-butyl-4,4,4-tris(dimethylamino)-2,2-bs[tris-(dimethylamino)-phosphoranylidenamino)-2Λ^5,4Λ^5-catenadi(phosphazene) (*t*-BuP$_4$, Scheme 5.8) and benzyl alcohol (BA) as the initiator was shown to be chemoselective through the anionic polymerization of the methacrylic C=C double bond.[43] The chemoselectivity was preserved at room temperature (25 °C) up to high monomer conversions (>95.9%). Random copolymers with 2-(*N*,*N*-dimethylamino)ethyl methacrylate (DMAEMA) were also prepared. Changing the polymerization initiator from benzyl alcohol to hydroxyethyl methacrylate (HEMA) produced vinyl-functionalized hyperbranched polymers with high AMA conversions and complete retention of the non-conjugated allyl groups.[12]

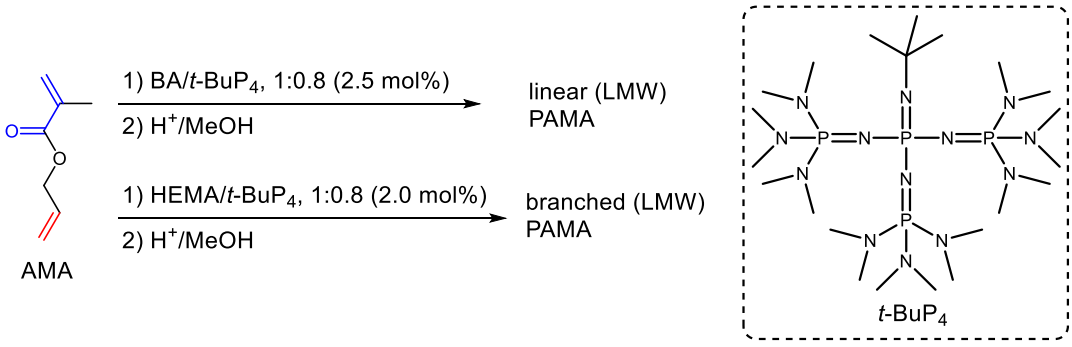

Scheme 5.8. Chemoselective polymerization of AMA by "superbase" *t*-BuP$_4$.

5.5. Post-Functionalization of Vinyl-Containing Stereoregular Polymers

The chemical post-functionalization of polymer chain repeat units and chain-ends has been a fruitfully investigated area in soft materials research, due to numerous opportunities for fine-tuning the functionalities, architectures, topologies, mechanical or thermal properties, as well as the reactivity, polarity and solubility of the targeted functional polymers for specialty applications. A wide variety of post-functionalization methods have been successfully employed over the years, including the well-known and efficient "click" chemistry, such as cycloadditions (e.g., Cu-catalyzed azide/alkyne cycloaddition, CuAAC, and Diels-Alder, DA, reactions) and thiol-ene and thiol-yne coupling reactions; olefin metathesis reactions; Pd-catalyzed (cross)coupling reactions; and oxime/hydrazine functionalization of ketones and aldehydes.[44] Epoxidation of C=C double bonds has also been exploited to functionalized ene-bearing polymers.[45] These strategies also allow obtaining otherwise inaccessible functional materials due to potential incompatibility between the desired chemical functionality and the polymerization method of choice.

We recently reported the first example of highly stereoregular ene-bearing poly(methacrylate)s that are post-functionalized by using thiol-ene "click" reactions.[35] Under photochemical conditions with 2,2-dimethoxy-2-phenylacetophenone (DMPA) as the photoradical initiator, the reaction of highly isotactic PAMA (and highly isotactic PDAA) with two model thiols (4-*tert*-butylbenzylmercaptan and 1-adamantanethiol) was highly efficient, achieving full conversion of the C=C double bonds into the corresponding thio-ethers in short times (2 h) (Scheme 5.9). The disappearance of the olefinic protons and the formation of the new C–SR bonds were confirmed and corroborated by ^{1}H NMR, GPC, DSC, and thermogravimetric analysis (TGA) data of the isolated thiolated polymers. Interestingly, it was showed that the use of a bifunctional

thiol completely cured the vinyl pendant groups in *it*-PAMA, as shown by the FT-IR spectrum of the crosslinked material (Scheme 5.9).

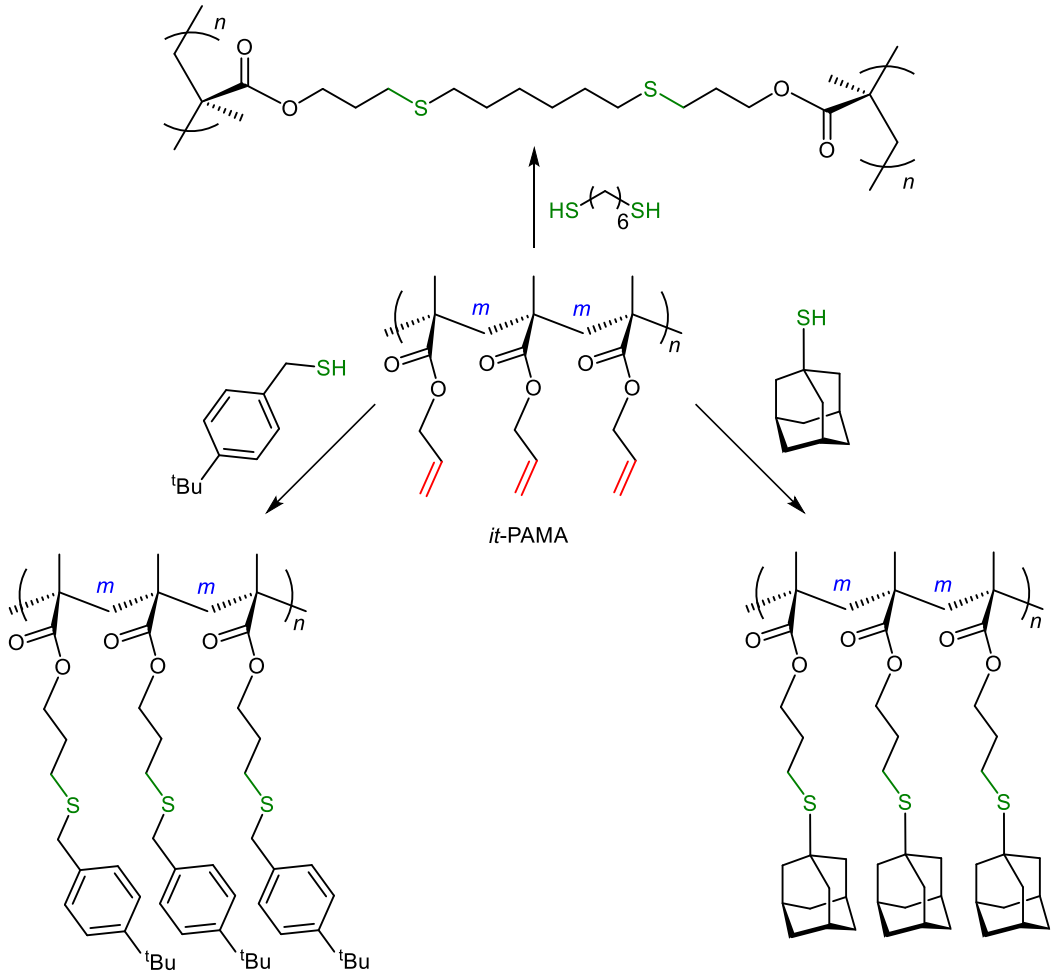

Scheme 5.9. Post-functionalization and photocuring of isotactic PAMA *via* thiol-ene "click" reactions.

Less stereoregular olefin-carrying methacrylic polymers derived from the chemoselective polymerization of VMBA were also post-functionalized via the thiol-ene "click" chemistry.[21] Using benzyl mercaptan as the model thiol and AIBN as the thermal radical initiator, Lu and coworkers showed a complete thiolation of PVBMA to the corresponding thio-ether derivatives.

We later demonstrated that highly syndiotactic methacrylate polymers containing pendant olefin groups in every repeating unit can also be rapidly and completely modified by the thiol-ene "click" reaction to the corresponding thiolated derivatives.[37] To this end, *st*-PVMA (and

acrylamide analogue *st*-PDAA), under photo-induced initiation conditions (DMPA, λ = 350 nm, chloroform, 2 h) was successfully thiolated with 4-*tert*-butylbenzyl and adamantane thio-ethers groups in all repeat units (Scheme 5.10). Again, this quantitative functionalization was corroborated by ^{1}H NMR, GPC, DSC and TGA data of the isolated functionalized polymers. In addition, the mechanical properties of flexible, solvent-casted, photocured thin-films of *st*-PVMA were tuned with increasing amounts of 1,4-benzenedimethanethiol as a bifunctional and rigid crosslinker. This experiment highlighted the opportunities of the thiol-ene "click" chemistry for modifying the loss modulus, storage modulus and glass transition of the photocured materials.

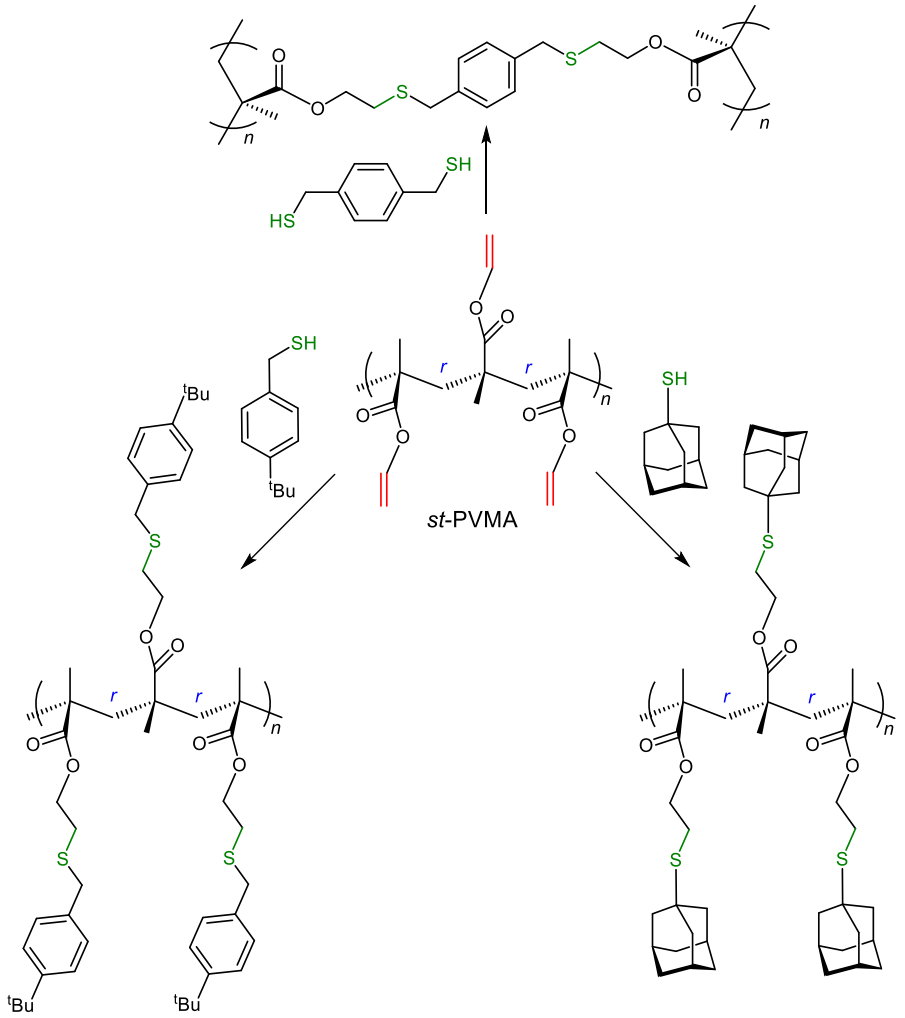

Scheme 5.10. Post-functionalization and photocuring of syndiotactic PVMA *via* thiol-ene "click" reactions.

5.6. Conclusions and Outlook

The chemoselective polymerization of polar divinyl monomers represents an alternative strategy for obtaining densely functionalized materials by direct modification of the reactive pendant group. Application of the metal-mediated coordination polymerization allowed the precision synthesis of precise polymeric structures under ambient conditions, thanks to its livingness as well as quantitative chemoselectivity *and* high stereoselectivity. Thus, choosing the metallocene catalyst of an appropriate symmetry has led to highly isotactic or highly syndiotactic olefin-carrying linear polymers with controlled molecular weight and narrow dispersity. Organocatalysts, in the form of main-group Lewis pairs or NHCs alone and "superbase" *t*-Bu-P_4, were showed to be also highly effective for polymerizing divinyl polar monomers chemoselectively via the conjugate-addition mechanism. Despite its high activity and low catalyst loading, the level of stereochemical control of the organopolymerization, due to its nature of chain-end control, is still considerably lower than the metallocene-mediated chemoselective and stereospecific polymerization by a catalyst site-controlled mechanism. Efficient functionalization of the reactive pendant groups can be readily performed by the thiol-ene "click" reactions, with full conversions of the functional groups and easy purifications of the functionalized polymer products. Thus, the applications of such polymeric materials, which can be also solvent casted and photocured into elastic thin-films, could be expanded to other technological fields, such as biomedicine (drug delivery), membrane separation, sensors, nanoparticles, and so forth, by judicious selection of the materials functionalization and device implementation.

REFERENCES

(1) Hollauf, M.; Trimmel, G.; Knall, A.-C. *Mon. Chem.* **2015**, *146*, 1063-1080.

(2) Carlini, A. S.; Adamiak, L.; Gianneschi, N. C. *Macromolecules* **2016**, *49*, 4379-4394.

(3) (a) Weck, M. *Polym. Int.* **2007**, *56*, 453-460. (b) Yang, S. K.; Ambade, A. V.; Weck, M. *Chem. Soc. Rev.* **2011**, *40*, 129-137. (c) Qu, D.-H.; Wang, Q.-C.; Zhang, Q.-W.; Ma, X.; Tian, H. *Chem. Rev.* **2015**, *115*, 7543-7588. (d) Wei, P.; Yan, X.; Huang, F. *Chem. Soc. Rev.* **2015**, *44*, 815-832. (e) Wojtecki, R. J.; Nelson, A. *J. Polym. Sci. Pol. Chem.* **2016**, *54*, 457-472.

(4) Elacqua, E.; Lye, D. S.; Weck, M. *Accounts Chem. Res.* **2014**, *47*, 2405-2416.

(5) (a) Hentze, H. P.; Antonietti, M. *Reviews in Molecular Biotechnology* **2002**, *90*, 27-53. (b) Schlaad, H.; Antonietti, M. *Eur. Phys. J. E* **2003**, *10*, 17-23. (c) Vilela, F.; Zhang, K.; Antonietti, M. *Energy Environ. Sci.* **2012**, *5*, 7819-7832.

(6) (a) Pollino, J. M.; Weck, M. *Chem. Soc. Rev.* **2005**, *34*, 193-207. (b) South, C. R.; Burd, C.; Weck, M. *Accounts Chem. Res.* **2007**, *40*, 63-74. (c) Durmaz, H.; Sanyal, A.; Hizal, G.; Tunca, U. *Polym. Chem.* **2012**, *3*, 825-835. (d) Romulus, J.; Henssler, J. T.; Weck, M. *Macromolecules* **2014**, *47*, 5437-5449. (e) Liu, S.; Dicker, K. T.; Jia, X. *Chem. Commun.* **2015**, *51*, 5218-5237. (f) Das, A.; Theato, P. *Chem. Rev.* **2016**, *116*, 1434-1495.

(7) (a) Lee, H.-i.; Jakubowski, W.; Matyjaszewski, K.; Yu, S.; Sheiko, S. S. *Macromolecules* **2006**, *39*, 4983-4989. (b) Hwang, J.; Li, R. C.; Maynard, H. D. *J. Control. Release* **2007**, *122*, 279-286. (c) Li, R. C.; Hwang, J.; Maynard, H. D. *Chem. Commun.* **2007**, 3631-3633. (d) Li, Y.; Yang, J.; Benicewicz, B. C. *J. Polym. Sci. Pol. Chem.* **2007**, *45*, 4300-4308. (e) Tsarevsky, N. V.; Bencherif, S. A.; Matyjaszewski, K. *Macromolecules* **2007**, *40*, 4439-

4445. (f) Boyer, C.; Granville, A.; Davis, T. P.; Bulmus, V. *J. Polym. Sci. Pol. Chem.* **2009**, *47*, 3773-3794. (g) Dong, Z.-m.; Liu, X.-h.; Tang, X.-l.; Li, Y.-s. *Macromolecules* **2009**, *42*, 4596-4603. (h) Jia, Z.; Liu, J.; Davis, T. P.; Bulmus, V. *Polymer* **2009**, *50*, 5928-5932. (i) Noy, J.-M.; Koldevitz, M.; Roth, P. J. *Polym. Chem.* **2015**, *6*, 436-447.

(8) Campos, L. M.; Killops, K. L.; Sakai, R.; Paulusse, J. M. J.; Damiron, D.; Drockenmuller, E.; Messmore, B. W.; Hawker, C. J. *Macromolecules* **2008**, *41*, 7063-7070.

(9) Ma, J.; Cheng, C.; Sun, G.; Wooley, K. L. *Macromolecules* **2008**, *41*, 9080-9089.

(10) Ma, J.; Cheng, C.; Wooley, K. L. *Macromolecules* **2009**, *42*, 1565-1573.

(11) ten Brummelhuis, N.; Diehl, C.; Schlaad, H. *Macromolecules* **2008**, *41*, 9946-9947.

(12) Yang, H.; Bai, T.; Xue, X.; Huang, W.; Chen, J.; Qian, X.; Zhang, G.; Jiang, B. *Polymer* **2015**, *72*, 63-68.

(13) (a) Tian, D.; Dubois, P.; Grandfils, C.; Jérôme, R. *Macromolecules* **1997**, *30*, 406-409. (b) Parrish, B.; Breitenkamp, R. B.; Emrick, T. *J. Am. Chem. Soc.* **2005**, *127*, 7404-7410. (c) Riva, R.; Schmeits, S.; Stoffelbach, F.; Jerome, C.; Jerome, R.; Lecomte, P. *Chem. Commun.* **2005**, 5334-5336. (d) Jiang, X.; Vogel, E. B.; Smith, M. R.; Baker, G. L. *Macromolecules* **2008**, *41*, 1937-1944. (e) Duan, Z.; Wang, X.; Gao, Q.; Zhang, L.; Liu, B.; Kim, I. *J. Polym. Sci. Pol. Chem.* **2014**, *52*, 789-795. (f) Baumgartner, R.; Song, Z.; Zhang, Y.; Cheng, J. *Polym. Chem.* **2015**, *6*, 3586-3590. (g) Han, B.; Zhang, L.; Liu, B.; Dong, X.; Kim, I.; Duan, Z.; Theato, P. *Macromolecules* **2015**, *48*, 3431-3437. (h) Si, G.; Zhang, L.; Han, B.; Duan, Z.; Li, B.; Dong, J.; Li, X.; Liu, B. *Polym. Chem.* **2015**, *6*, 6372-6377.

(14) (a) Cheng, C.; Qi, K.; Khoshdel, E.; Wooley, K. L. *J. Am. Chem. Soc.* **2006**, *128*, 6808-6809. (b) Cheng, C.; Khoshdel, E.; Wooley, K. L. *Macromolecules* **2007**, *40*, 2289-2292. (c) Cheng, C.; Qi, K.; Germack, D. S.; Khoshdel, E.; Wooley, K. L. *Adv. Mater.* **2007**, *19*, 2830-

2835. (d) Mangold, S. L.; Carpenter, R. T.; Kiessling, L. L. *Org. Lett.* **2008**, *10*, 2997-3000. (e) Yang, S. K.; Weck, M. *Macromolecules* **2008**, *41*, 346-351. (f) Allen, M. J.; Wangkanont, K.; Raines, R. T.; Kiessling, L. L. *Macromolecules* **2009**, *42*, 4023-4027. (g) Kolonko, E. M.; Pontrello, J. K.; Mangold, S. L.; Kiessling, L. L. *J. Am. Chem. Soc.* **2009**, *131*, 7327-7333. (h) Schaefer, M.; Hanik, N.; Kilbinger, A. F. M. *Macromolecules* **2012**, *45*, 6807-6818. (i) Garcia-Loma, R.; Albeniz, A. C. *RSC Adv.* **2015**, *5*, 70244-70254. (j) Ashok Kothapalli, V.; Shetty, M.; de los Santos, C.; Hobbs, C. E. *J. Polym. Sci. Pol. Chem.* **2016**, *54*, 179-185. (k) Li, Z.-L.; Sun, L.; Ma, J.; Zeng, Z.; Jiang, H. *Polymer* **2016**, *84*, 336-342.

(15) (a) Helms, B.; Mynar, J. L.; Hawker, C. J.; Fréchet, J. M. J. *J. Am. Chem. Soc.* **2004**, *126*, 15020-15021. (b) Malkoch, M.; Thibault, R. J.; Drockenmuller, E.; Messerschmidt, M.; Voit, B.; Russell, T. P.; Hawker, C. J. *J. Am. Chem. Soc.* **2005**, *127*, 14942-14949. (c) Sumerlin, B. S.; Tsarevsky, N. V.; Louche, G.; Lee, R. Y.; Matyjaszewski, K. *Macromolecules* **2005**, *38*, 7540-7545. (d) Quémener, D.; Hellaye, M. L.; Bissett, C.; Davis, T. P.; Barner-Kowollik, C.; Stenzel, M. H. *J. Polym. Sci. Pol. Chem.* **2008**, *46*, 155-173.

(16) Wong, C.-H.; Zimmerman, S. C. *Chem. Commun.* **2013**, *49*, 1679-1695.

(17) Brandrup, J.; Immergut, E. H.; Grulke, E. A. *Polymer handbook*; 4th ed.. ed.; New York : Wiley: New York, 1999.

(18) Odian, G. *Principles of Polymerization*; Wiley, 2004.

(19) (a) Fukuda, W.; Nakao, M.; Okumura, K.; Kakiuchi, H. *J. Polym. Sci. Pol. Chem.* **1972**, *10*, 237-250. (b) Lu, Z.; Lee, S. Y.; Goh, S. H. *Polymer* **1997**, *38*, 5893-5895. (c) Sugiyama, F.; Satoh, K.; Kamigaito, M. *Macromolecules* **2008**, *41*, 3042-3048. (d) Yhaya, F.; Sutinah, A.; Gregory, A. M.; Liang, M.; Stenzel, M. H. *J. Polym. Sci. Pol. Chem.* **2012**, *50*, 4085-4093. (e) Akiyama, M.; Yoshida, K.; Mori, H. *Polymer* **2014**, *55*, 813-823.

(20) (a) Nagelsdiek, R.; Mennicken, M.; Maier, B.; Keul, H.; Hoecker, H. *Macromolecules* **2004**, *37*, 8923-8932. (b) Paris, R.; De La Fuente, J. L. *J. Polym. Sci., Part A: Polym. Chem.* **2005**, *43*, 2395-2406. (c) Paris, R.; De La Fuente, J. L. *J. Polym. Sci., Part A: Polym. Chem.* **2005**, *43*, 6247-6261. (d) Vardarelı, T. K.; Keskıin, S.; Usanmaz, A. *J. Macromol. Sci. Part A-Pure Appl.* **2008**, *45*, 302-311.

(21) Jia, Y.-B.;Ren, W.-M.; Liu, S.-J.; Xu, T.; Wang, Y.-B.; Lu, X.-B. *ACS Macro Lett.* **2014**, 896-899.

(22) Pugh, C.; Percec, V. *Polym. Bull. (Berlin)* **1985**, *14*, 109-116.

(23) Murali Mohan, Y.; Raghunadh, V.; Sivaram, S.; Baskaran, D. *Macromolecules* **2012**, *45*, 3387-3393.

(24) Yasuda, H.; Yamamoto, H.; Yokota, K.; Miyake, S.; Nakamura, A. *J. Am. Chem. Soc.* **1992**, *114*, 4908-4910.

(25) Collins, S.; Ward, D. G. *J. Am. Chem. Soc.* **1992**, *114*, 5460-5462.

(26) Chen, E. Y.-X. *Chem. Rev.* **2009**, *109*, 5157-5214.

(27) Bolig, A. D.; Chen, E. Y.-X. *J. Am. Chem. Soc.* **2004**, *126*, 4897-4906.

(28) Rodriguez-Delgado, A.; Chen, E. Y.-X. *Macromolecules* **2005**, *38*, 2587-2594.

(29) Zhang, Y.; Ning, Y.; Caporaso, L.; Cavallo, L.; Chen, E. Y.-X. *J. Am. Chem. Soc.* **2010**, *132*, 2695-2709.

(30) (a) Miyake, G.; Caporaso, L.; Cavallo, L.; Chen, E. Y.-X. *Macromolecules* **2009**, *42*, 1462-1471. (b) Mariott, W. R.; Chen, E. Y.-X. *Macromolecules* **2004**, *37*, 4741-4743. (c) Miyake, G. M.; Chen, E. Y.-X. *Macromolecules* **2008**, *41*, 3405-3416. (d) Miyake, G. M.; Mariott, W. R.; Chen, E. Y.-X. *J. Am. Chem. Soc.* **2007**, *129*, 6724-6725.

(31) (a) Mariott, W. R.; Chen, E. Y.-X. *Macromolecules* **2005**, *38*, 6822-6832. (b) Mariott, W. R.; Rodriguez-Delgado, A.; Chen, E. Y.-X. *Macromolecules* **2006**, *39*, 1318-1327.

(32) (a) Chen, X.; Caporaso, L.; Cavallo, L.; Chen, E. Y.-X. *J. Am. Chem. Soc.* **2012**, *134*, 7278-7281. (b) Miyake, G. M.; Newton, S. E.; Mariott, W. R.; Chen, E. Y.-X. *Dalton Trans.* **2010**, *39*, 6710-6718.

(33) (a) He, J.; Zhang, Y.; Chen, E. Y.-X. *Macromol. Symp.* **2015**, *349*, 104-114. (b) Zhang, Y.; Caporaso, L.; Cavallo, L.; Chen, E. Y.-X. *J. Am. Chem. Soc.* **2011**, *133*, 1572-1588.

(34) Ning, Y.; Chen, E. Y.-X. *Macromolecules* **2006**, *39*, 7204-7215.

(35) Vidal, F.; Gowda, R. R.; Chen, E. Y.-X. *J. Am. Chem. Soc.* **2015**, *137*, 9469-9480.

(36) Xu, T.; Liu, J.; Lu, X.-B. *Macromolecules* **2015**, *48*, 7428-7434.

(37) Vidal, F.; Falivene, L.; Caporaso, L.; Cavallo, L.; Chen, E. Y.-X. *J. Am. Chem. Soc.* **2016**, *138*, 9533-9547.

(38) (a) Zhang, Y.; Miyake, G. M.; Chen, E. Y.-X. *Angew. Chem.-Int. Edit.* **2010**, *49*, 10158-10162. (b) Zhang, Y.; Miyake, G. M.; John, M. G.; Falivene, L.; Caporaso, L.; Cavallo, L.; Chen, E. Y.-X. *Dalton Trans.* **2012**, *41*, 9119-9134. (c) Chen, E. Y.-X. In *Frustrated Lewis Pairs II: Expanding the Scope*; Erker, G., Stephan, D. W., Eds.; Springer Berlin Heidelberg: Berlin, Heidelberg, 2013, p 239-260.

(39) Xu, T.; Chen, E. Y.-X. *J. Am. Chem. Soc.* **2014**, *136*, 1774-1777.

(40) Chen, J.; Chen, E. Y.-X. *Isr. J. Chem.* **2015**, *55*, 216-225.

(41) Zhang, Y.; Schmitt, M.; Falivene, L.; Caporaso, L.; Cavallo, L.; Chen, E. Y.-X. *J. Am. Chem. Soc.* **2013**, *135*, 17925-17942.

(42) Gowda, R. R.; Chen, E. Y.-X. *ACS Macro Lett.* **2016**, *5*, 772-776.

(43) Yang, H.; Bai, T.; Xue, X.; Huang, W.; Chen, J.; Qian, X.; Jiang, B. *J. Appl. Polym. Sci.* **2015**, *132*, 42758.

(44) (a) Binder, W. H.; Sachsenhofer, R. *Macromol. Rapid Commun.* **2007**, *28*, 15-54. (b) Binder, W. H.; Sachsenhofer, R. *Macromol. Rapid Commun.* **2008**, *29*, 952-981. (c) Gauthier, M. A.; Gibson, M. I.; Klok, H.-A. *Angew. Chem.-Int. Edit.* **2009**, *48*, 48-58. (d) Iha, R. K.; Wooley, K. L.; Nyström, A. M.; Burke, D. J.; Kade, M. J.; Hawker, C. J. *Chem. Rev.* **2009**, *109*, 5620-5686. (e) Mansfeld, U.; Pietsch, C.; Hoogenboom, R.; Becer, C. R.; Schubert, U. S. *Polym. Chem.* **2010**, *1*, 1560-1598. (f) Roth, P. J.; Boyer, C.; Lowe, A. B.; Davis, T. P. *Macromol. Rapid Commun.* **2011**, *32*, 1123-1143. (g) Feng, C.; Li, Y.; Yang, D.; Hu, J.; Zhang, X.; Huang, X. *Chem. Soc. Rev.* **2011**, *40*, 1282-1295. (h) Tasdelen, M. A. *Polym. Chem.* **2011**, *2*, 2133-2145. (i) Tasdelen, M. A.; Kahveci, M. U.; Yagci, Y. *Prog. Polym. Sci.* **2011**, *36*, 455-567. (j) Goldmann, A. S.; Glassner, M.; Inglis, A. J.; Barner-Kowollik, C. *Macromol. Rapid Commun.* **2013**, *34*, 810-849. (k) Tunca, U. *J. Polym. Sci. Pol. Chem.* **2014**, *52*, 3147-3165. (l) Lowe, A. B. *Polym. Chem.* **2014**, *5*, 4820-4870.

(45) He, F.; Wang, Y.-P.; Liu, G.; Jia, H.-L.; Feng, J.; Zhuo, R.-X. *Polymer* **2008**, *49*, 1185-1190

APPENDIX A

Experimental Details and Supporting Information for Chapter 2:

A.1. Materials, Reagents, and Methods

All manipulations with air- and moisture-sensitive chemicals and reagents were performed using standard Schlenk techniques on a dual-manifold line, on a high-vacuum line, or in an inert gas (Ar or N_2)-filled glovebox. NMR-scale reactions were conducted in Teflon-valve-sealed J. Young-type NMR tubes. NMR (^{1}H, ^{13}C, and ^{19}F) spectra were recorded on a Varian Inova 400 MHz or 500 MHz spectrometer. Chemical shifts for ^{1}H and ^{13}C spectra were referenced to internal solvent resonances and are reported as parts per million relative to $SiMe_4$, whereas ^{19}F NMR chemical shifts were referenced and reported relative to $CFCl_3$. Benzene-d_6 and toluene-d_8 were dried over sodium/potassium alloy and vacuum-distilled or filtered, whereas CD_3SOCD_3, CD_2Cl_2, and $CDCl_3$ were dried over activated Davison 4 Å molecular sieves. Chemical shifts were referenced to residual undeuterated solvent resonances and are reported as parts per million relative to $SiMe_4$. HPLC-grade organic solvents were first sparged extensively with nitrogen during filling 20 L solvent reservoirs and then dried by passage through activated alumina (for Et_2O, THF, and CH_2Cl_2) followed by passage through Q-5 supported copper catalyst (for toluene and hexanes) stainless steel columns. HPLC-grade DMF was degassed and dried over CaH_2 overnight, followed by vacuum distillation (CaH_2 was removed before distillation). Elemental analyses were performed by Robertson Microlit Laboratories, Madison, NJ.

Allyl methacrylate (AMA) and methyl methacrylate (MMA) were purchased from Alfa Aesar Chemical Co., while vinyl methacrylate (VMA) was purchased from TCI America. 4-Vinylbenzyl methacrylate (VBMA) was prepared following the known procedures.[1] The

monomers were dried over activated CaH_2 overnight, followed by vacuum distillation (except for VBMA, which was filtered prior to use) and stored in brown bottles at −30 °C inside of a glovebox freezer. MMA was further purified by titration with neat tri(*n*-octyl)aluminum to a yellow end point[2] followed by distillation under reduced pressure. *N*,*N*-diallyl acrylamide (DAA) was prepared using an adapted procedure from that previously reported in literature.[3] Specifically, methacryloyl chloride (15.4 g, 170 mmol) was slowly added to an ice-cooled solution of diallyl amine (16.5 g, 170 mmol) and trimethylamine (17.2 g, 170 mmol) in 400 mL of ethyl acetate, and the resulting mixture was stirred at room temperature for 18 h. The obtained suspension was poured into water and extracted with chloroform (300 mL). The organic layer was washed with water (3 x 200 mL), dried over anhydrous Na_2SO_4, and the solvent was removed via roto-vap. The crude monomer was purified by distillation, drying over CaH_2 overnight, and vacuum distillation (52 °C/250 mTorr), affording 19.4 g (75%) of DAA as a colorless liquid.

^{1}H NMR (C_6D_6, 25 °C) of DAA: δ 6.53 (dd, J = 16.0, 4.0 Hz, 1H, (CO)CH=CH_2), 6.20 (dd, J = 16.0, 12.0 Hz, 1H, (CO)CH=CH_2), 5.68 (m, 1H, NCH_2CH=CH_2), 5.34 (m, 1H, NCH_2CH=CH_2), 5.33 (dd, J = 12.0, 4.0 Hz, 1H, (CO)CH=CH_2), 4.89 (m, 4H, NCH_2CH=CH_2), 3.95 (s, br, 2H, NCH_2CH=CH_2), 3.41 (s, br, 2H, NCH_2CH=CH_2). ^{13}C{^{1}H} NMR (C_6D_6, 25 °C): δ 165.7 (*C*OO), 134.3 (NCH_2CH=CH_2), 134.0 (NCH_2CH=CH_2), 128.5 ((CO)*C*H=CH_2), 128.3 ((CO)CH=*C*H_2), 117.3 (NCH_2CH=*C*H_2), 116.3 (NCH_2CH=*C*H_2), 49.0 (N*C*H_2CH=CH_2), 48.7 (N*C*H_2CH=CH_2). HRMS (APCI): *m/z* calcd for $C_9H_{13}NO$: $[M + H]^+$: 152.1075; found: 152.1072.

Dichlorodimethylsilane, *n*-BuLi (1.6 M in hexanes), tetrakis(dimethylamido)zirconium (IV), trimethylaluminum (2.0 M solution in toluene), potassium hydride, potassium bisulfate, lithium aluminum hydride, 4-tert-butylbenzylmercaptan, and 1-adamantanethiol were purchased from Sigma-Aldrich. Naphthalene, maleic anhydride, aluminum chloride (anhydrous powder),

trimethylsilyl trifluoromethanesulfonate (Me_3SiOTf), and 2,6-di-*tert*-butyl-4-methylphenol (BHT-H) were purchased from Alfa Aesar. Isopropyl isobutyrate was purchased from TCI America and 2,2-dimethoxy-2-phenylacetophenone (DMPA) was purchased from Acros Organics. Diisopropylamine and isopropyl isobutyrate were vacuum-distilled, while BHT-H was recrystallized from hexanes prior to use. All other commercial reagents were used as received.

Tris(pentafluorophenyl)borane, $B(C_6F_5)_3$, was obtained as a research gift from Boulder Scientific Co. and further purified by sublimation. The $B(C_6F_5)_3$·THF adduct was prepared by addition of THF to a toluene solution of the borane at ambient temperature, followed by removal of the volatiles and drying under vacuum. Literature procedures were employed or modified for the preparation of the following ligands or compounds: l-*H*- and 3-*H*-benz[*e*]indene,[4] bis[3,3'-(3-*H*-benz[*e*]indenyl)]dimethylsilane (SBBI),[5] $Me_2C{=}C(O^iPr)OLi$,[6] *rac*-(EBI)ZrMe[$OC(O^iPr){=}CMe_2$] [pre-**1**, EBI = ethylene-bis(η^5-indenyl)],[7] and *rac*-(EBI)Zr^+(THF)[$OC(O^iPr){=}CMe_2$][$MeB(C_6F_5)_3]^-$ (**1**).[7]

Synthesis of *rac*-(SBBI)ZrMe[OC(O^{i}Pr)=CMe$_2$] (pre-2). In an argon-filled glovebox, a 250 mL Schlenk flask was equipped with a stir bar and charged with a solution of $Zr(NMe_2)_4$ (0.35 g, 1.31 mmol) in 15 mL toluene and a solution of SBBI (0.51 g, 1.31 mmol) in 15 mL toluene. The flask was sealed with a rubber septum, removed from the glovebox, and interfaced to a Schlenk line. The reaction mixture was stirred and heated to 108 °C for 24 h, and the co-product NMe_2H was allowed to escape via an oil bubbler under a static N_2 atmosphere. The reaction mixture was evaporated to dryness under reduced pressure, and the residue was recrystallized from 10 mL of toluene at −30 °C for 4 days. Filtration afforded 0.50 g (68%) of the pure *rac*-(SBBI)$Zr(NMe_2)_2$ as orange crystals (recrystallization crop I, 0.35 g; crop II, 0.15 g). ^{1}H NMR (C_6D_6, 25 °C): δ 7.96–7.94 (m, 2H, benz[*e*]ind), 7.57–7.53 (m, 4H, benz[*e*]ind), 7.38–7.37 (m, 2H, benz[*e*]ind), 7.28–

7.25 (m, 4H, benz[*e*]ind), 7.21–7.17 (m, 2H, benz[*e*]ind), 6.25 (d, *J* = 3.1 Hz, 2H, benz[*e*]ind), 1.97 (s, 12H, ZrN*Me*$_2$), 0.83 (s, 6H, Si*Me*$_2$). ^{13}C NMR (C_6D_6, 25 °C): δ 132.0, 131.2, 131.1, 129.3, 128.6, 128.5, 128.4, 128.2, 128.1, 127.9, 127.7, 127.1, 126.4, 125.9, 125.7, 124.8, 124.6, 122.2, 112.6, 110.4, 107.4, 103.2 (benz[*e*]ind), 47.48 (ZrN*Me*$_2$), −1.53 (Si*Me*$_2$).

To a pre-cooled 20 mL toluene solution of *rac*-(SBBI)Zr(NMe$_2$)$_2$ (0.50 g, 0.88 mmol) at −30 °C for 12 h was added a pre-cooled 10 mL toluene solution of AlMe$_3$ (3.00 mL of 2.0 M toluene solution, 5.83 mmol) at −30 °C for 12 h (note that a mixture of *rac*- and *meso*-(SBBI)ZrMe$_2$ was formed when AlMe$_3$ was added directly to the precooled *rac*-(SBBI)Zr(NMe$_2$)$_2$ solution at −30 ºC). Upon stirring, the solution turned from orange to yellow color, and the reaction was allowed to gradually warm to room temperature and stirred for 12 h. The solvent was removed under reduced pressure, and the solid was dried under vacuum. The solid was washed with hexanes and recrystallized from 15 mL of toluene at −30 °C for 3 days. The product was filtered and dried under vacuum to give 0.27 g (60% yield) of the pure *rac*-(SBBI)ZrMe$_2$ as a yellow powder . ^{1}H NMR (C_6D_6, 25 °C): δ 7.88–7.86 (m, 2H, benz[*e*]ind), 7.66–7.64 (m, 2H, benz[*e*]ind), 7.36–7.24 (m, 4H, benz[*e*]ind), 7.23–7.21 (m, 6H, benz[*e*]ind), 5.81 (d, *J* = 3.3 Hz, 2H, benz[*e*]ind), 0.60 (s, 6H, Si*Me*$_2$), −1.16 (s, 6H, Zr*Me*$_2$).

In an argon-filled glovebox, a glass reactor was equipped with a stir bar and charged with 30 mL toluene and *rac*-(SBBI)ZrMe$_2$ (0.27 g, 0.53 mmol). This solution was pre-cooled to −30 °C for 12 h. To this yellow solution was added Me$_3$SiOTf (0.14 g, 0.64 mmol). The color of the reaction mixture gradually changed from yellow to orange. Stirring was maintained for 24 h at ambient temperature, after which more Me$_3$SiOTf (0.14 g, 0.64 mmol) was added. The stirring was continued for an additional 24 h at ambient temperature. The reaction mixture was evaporated to dryness under reduced pressure and the residue was recrystallized using 25 mL toluene at −30

°C for 2 days to afford orange crystals. The resulting crystalline solid collected after filtration was dried in vacuo to give 0.23 g (68% yield) of the pure *rac*-(SBBI)ZrMe(OTf) as a yellowish orange powder. ^{1}H NMR (C_6D_6, 25 °C): δ 8.21 (d, J = 8.2 Hz, 1H, benz[*e*]ind), 7.74–7.65 (m, 3H, benz[*e*]ind), 7.57–7.55 (m, 1H, benz[*e*]ind), 7.38–7.22 (m, 6H, benz[*e*]ind), 7.13–7.12 (m, 1H, benz[*e*]ind), 6.98–6.96 (m, 2H, benz[*e*]ind), 6.08 (d, J = 3.3 Hz, 1H, benz[*e*]ind), 5.38 (d, J = 3.3 Hz, 1H, benz[*e*]ind), 0.57 (s, 3H, Si*Me*$_2$), 0.52 (s, 3H, Si*Me*$_2$), −0.56 (s, 3H, Zr*Me*).

In an argon-filled glovebox, a 60 mL glass reactor was equipped with magnetic stir bar, charged with 20 mL toluene and 0.23 g (0.36 mmol) *rac*-(SBBI)ZrMe(OTf), and then cooled to −30 °C inside a glovebox freezer for 12 h. To this pre-cooled reactor was added $Me_2C{=}C(O^{i}Pr)OLi$ (50.0 mg, 0.36 mmol). The resulting suspension was stirred overnight at ambient temperature, after which it was filtered through a pad of Celite. The solvent of the filtrate was removed in vacuo, yielding pre-**2** as a yellow powder. Recrystallization from toluene layered with hexanes at −30 °C for 4 days gave 0.19 g (86% yield) of the pure pre-**2**. This purification step can be substituted by simple washing of the crude product with 5 mL of hexanes.

^{1}H NMR (C_6D_6, 25 °C) of pre-**2**: δ 7.92–7.90 (m, 1H, benz[*e*]ind), 7.80–7.78 (m, 1H, benz[*e*]ind), 7.63–7.61 (m, 1H, benz[*e*]ind), 7.53–7.49 (m, 2H, benz[*e*]ind), 7.29–7.19 (m, 8H, benz[*e*]ind), 7.02 (d, J = 3.3 Hz, 1H, benz[*e*]ind), 6.44 (d, J = 3.2 Hz, 1H, benz[*e*]ind), 5.79 (d, J = 3.2 Hz, 1H, benz[*e*]ind), 3.23 (sept, J = 6.2 Hz, 1H, OC*H*Me$_2$), 1.63 (s, 3H, =C*Me*$_2$), 1.16 (s, 3H, =C*Me*$_2$), 0.80 (d, J = 6.2 Hz, 3H, OCH*Me*$_2$), 0.78–0.77 (m, 6H, Si*Me*$_2$, OCH*Me*$_2$), 0.65 (s, 3H, Si*Me*$_2$), −0.78 (s, 3H, Zr*Me*). ^{13}C NMR (C_6D_6, 125 MHz, 25 °C): δ 153.8 (=*C*O(OCHMe$_2$)), 132.4, 132.0, 131.2, 129.8, 129.3, 128.8, 128.7, 128.2, 127.4, 127.3, 127.2, 126.8, 126.6, 126.3, 124.6, 124.5, 124.4, 124.0, 123.1, 121.6, 116.2, 114.3, 112.6, 109.5, 96.65, 94.02 (C's of benz[*e*]ind),

84.03 (=*C*Me$_2$), 67.66 (O*C*HMe$_2$), 31.71 (Zr*Me*), 21.90 (OCH*Me$_2$*), 21.76 (OCH*Me$_2$*), 17.48 (=C*Me$_2$*), 17.41 (=C*Me$_2$*), −1.79 (Si*Me$_2$*), −1.90 (Si*Me$_2$*).

Generation and X-ray Structure of *rac*-(SBBI)Zr$^+$(THF)[OC(O^{i}Pr)=CMe$_2$] [MeB(C$_6$F$_5$)$_3$]$^-$ (2). Cationic zirconocene ester enolate **2** was generated from *in situ* mixing of pre-**2** with $(C_6F_5)_3B{\cdot}THF$ in CD_2Cl_2 at room temperature, following the procedure demonstrated for the clean and quantitative generation of the analogous ester enolate **1**.[Error! Bookmark not defined.] In an argon-filled glovebox, a 4 mL glass vial was charged with 12.5 mg (0.02 mmol) pre-**2** and 0.4 mL of CD_2Cl_2, while another vial was charged with 11.7 mg $(C_6F_5)_3B{\cdot}THF$ (0.02 mmol) and 0.4 mL of CD_2Cl_2. The two vials were mixed via pipette at ambient temperature to give instantaneously an orange color solution; subsequent analysis of this orange solution by NMR showed the clean and quantitative formation of ion pair **2**.

^{1}H NMR (CD_2Cl_2, 25 °C) of **2** (isolated crystals): δ 8.05–8.00 (m, 2H), 7.87–7.84 (m, 1H), 7.82–7.79 (m, 1H), 7.72–7.71 (m, 1H), 7.69–7.66 (m, 1H), 7.64–7.61 (m, 2H), 7.60–7.52 (m, 5H), 7.34–7.33 (m, 1H), 7.26–7.14 (C_7H_8), 6.35 (dd, J = 5.7, 3.2 Hz, 2H), 5.33 (CH_2Cl_2), 3.46–3.37 (m, 1H, OC*H*Me$_2$), 3.28–3.20 (m, 4H, α-C*H*$_2$, THF), 2.34 (C_7H_8), 1.35 (s, 3H, =C*Me$_2$*), 1.32 (s, 3H, =C*Me$_2$*), 1.27 (s, 3H, Si*Me$_2$*), 1.25–1.13 (m, 4H, β-C*H*$_2$, THF), 1.10 (d, J = 6.1 Hz, 3H, OCH*Me$_2$*), 0.87 (d, J = 6.1 Hz, 3H, OCH*Me$_2$*), 0.61 (s, 3H, Si*Me$_2$*), 0.48 (s, br, 3H, B*Me*). ^{19}F NMR (CD_2Cl_2, 23°C): δ −133.19 (d, $^3J_{F\text{-}F}$ = 19.7 Hz, 6F, *o*-F), −165.29 (t, $^3J_{F\text{-}F}$ = 20.4 Hz, 3F, *p*-F), −167.88 (m, 6F, *m*-F). ^{13}C NMR (CD_2Cl_2, 125 MHz, 25 °C): δ 154.5 (=*C*O(OCHMe$_2$)), 133.8, 133.5, 132.2, 132.1, 130.8, 129.9, 129.8, 129.5, 129.4, 129.3, 128.9, 128.8, 128.7, 128.4, 127.9, 125.3, 124.8, 124.4, 121.6, 120.9, 118.4, 115.7, 113.9, 112.9, 102.2, 99.36 (C's of benz[*e*]ind; broad and obscured resonances for the *C*$_6$F$_5$ groups due to C–F coupling not included), 91.25 (=*C*Me$_2$), 78.25

(α-*C*H_2, THF), 72.34 (O*C*HMe$_2$), 25.01 (*β*-*C*H_2, THF), 22.31 (OCH*Me$_2$*), 21.42 (OCH*Me$_2$*), 17.79 (=C*Me$_2$*), 17.42 (=C*Me$_2$*), 14.29 (B*Me*, obscured), −1.58 (Si*Me$_2$*), −1.92 (Si*Me$_2$*).

Single crystals of **2** suitable for X-ray diffraction analysis were obtained as follows. A 20 mL glass vial was charged with 12.5 mg (0.02 mmol) of pre-**2**, 11.7 mg of $(C_6F_5)_3B{\cdot}THF$ (0.02 mmol), and 3 mL of toluene. The instantaneously formed orange color solution was carefully layered with 4 mL of hexanes and 0.5 mL of CH_2Cl_2. The vial was cooled to −30 °C and stored inside the glovebox freezer for 7 days to give orange single crystals of **2**. After decanting the solvent, the crystals were quickly coated with a layer of Paratone-N oil (Exxon, dried and degassed at 140 °C/10^{-6} Torr for 16 h) in the glovebox. A crystal was then mounted on a thin glass fiber under a cold stream of dinitrogen gas. Single crystal X-ray diffraction data were acquired on a Bruker Kappa APEX II CCD diffractometer with Mo K_α radiation (λ = 0.71073 Å) and a graphite monochromator. Initial lattice parameters were obtained from a least-squares analysis of more than 100 reflections; these parameters were later refined against all data. The crystal did not show any significant decay during data collection. Data were integrated and corrected for Lorentz and polarization effects using Bruker APEX2 software, and semiempirical absorption corrections were applied using SCALE.[8] Space group assignments were based on systematic absences, *E* statistics, and successful refinement of the structure. The structure was solved by the Patterson method and refined with the aid of successive Fourier difference maps against all data using the SHELXTL 6.14 software package.[9] Thermal parameters for all non-hydrogen atoms were refined anisotropically, while all hydrogen atoms were assigned to ideal positions and refined using a riding model with an isotropic thermal parameter 1.2 times that of the attached carbon atom (1.5 times for methyl hydrogens). In the structure the disordered toluene solvate molecule found in Fourier difference maps was disordered over multiple sites. After numerous attempts to model the

disorder failed to improve agreement factors, SQUEEZE[10] was used to remove the disordered components. Selected crystallographic data for **2**: $C_{58}H_{46}BF_{15}O_3SiZr$, triclinic, space group *P*-1, *a* = 14.6799(11) Å, *b* = 14.8636(11) Å, *c* = 16.1127(11) Å, α = 89.566(4)°, β = 68.846(4)°, γ = 62.936(3)°, *V* = 2867.4(4) Å^3, *Z* = 2, D_{calcd} = 1.495 Mg/m^3, GOF = 1.065, *R*1 = 0.0465 [$I > 2\sigma(I)$], w*R*2 = 0.1156. CCDC-1405015 contains the supplementary crystallographic data. These data can be obtained free of charge from The Cambridge Crystallographic Data Centre via www.ccdc.cam.ac.uk/data_request/cif.

Generation of *rac*-(EBI)Zr[OC(OCH$_2$CH=CH$_2$)=C(Me)CH$_2$C(Me$_2$)C(O^{i}Pr)=O]$^+$ [MeB(C$_6$F$_5$)$_3$]$^-$ (3). In an argon-filled glovebox, B(C$_6$F$_5$)$_3$ (19.0 mg, 0.037 mmol) and AMA (4.1 mg, 0.032 mmol) were premixed in 0.3 mL of CD_2Cl_2 to generate the $(C_6F_5)_3B\cdot$AMA adduct *in situ*. This colorless solution was cooled to −30 °C inside of the glovebox freezer and then added via pipette to a precooled (−30 °C) 4 mL vial containing *rac*-(EBI)ZrMe[OC(O^{i}Pr)=CMe$_2$] (15.7 mg, 0.032 mmol) in 0.3 mL of CD_2Cl_2. The solution turned instantaneously to dark red as a result of formation of cationic complex **3**.

^{1}H NMR (CD_2Cl_2, 25 °C) of **3**: δ 8.05 (t, *J* = 8.4 Hz, 1H, Ar H), 7.95 (d, *J* = 9.2 Hz, 1H, Ar H), 7.40–7.16 (m, 6H, Ar H), 6.31 (d, *J* = 3.2 Hz, 1H, Cp H), 6.29 (d, *J* = 3.2 Hz, 1H, Cp H), 6.25 (d, *J* = 3.2 Hz, 1H, Cp H), 5.96 (d, *J* = 3.2 Hz, 1H, Cp H), 5.87 (m, 1H, OCH$_2$C*H*=CH$_2$), 5.29 (dd, *J* = 20.0, 2.0 Hz, 1H, OCH$_2$CH=C*H*$_2$), 5.23 (dd, *J* = 8.0, 1.6 Hz, 1H, OCH$_2$CH=C*H*$_2$), 4.34 (sept, *J* = 6.2 Hz, 1H, OC*H*Me$_2$), 4.10–3.98 (m, 4H, C*H*$_2$C*H*$_2$), 3.83 (m, 2H, OC*H*$_2$CH=CH$_2$), 2.13 (m, 2H, C*H*$_2$), 1.57 (s, 3H, =C*Me*), 1.40 (d, *J* = 6.2 Hz, 3H, OCH*Me*$_2$), 1.28 (d, *J* = 6.2 Hz, 3H, OCH*Me*$_2$), 1.25 (s, br, 3H, C*Me*$_2$), 1.20 (s, br, 3H, C*Me*$_2$), 0.50 (s, br, 3H, B*Me*). ^{19}F NMR (CD_2Cl_2, 25 °C): δ −133.12 (d, $^3J_{F-F}$ = 19.2 Hz, 6F, *o*–F), −165.32 (t, $^3J_{F-F}$ = 20.3 Hz, 3F, *p*–F), −167.88 (m, 6F, *m*–F).

Isolation of *rac*-(EBI)Zr(THF)[OC(OCH$_2$CH=CH$_2$)=C(Me)CH$_2$C(Me$_2$)C(O^{i}Pr)=O]$^+$ [MeB(C$_6$F$_5$)$_3$]$^-$ (3·THF). In an argon-filled glovebox, a 30 mL glass reactor was charged with 66.0 mg (0.134 mmol) of *rac*-(EBI)ZrMe[OC(O^{i}Pr)=CMe$_2$] dissolved in 8 mL of CH_2Cl_2. Then, 78.3 mg (0.134 mmol) of $(C_6F_5)_3B$·THF in 1 mL of CH_2Cl_2 was added; the mixture was allowed to stir for 10 min at ambient temperature to cleanly generate **1** *in situ*. To this vigorously stirred solution, 16.9 mg (0.134 mmol) of AMA was quickly added from a stock solution in CH_2Cl_2 at room temperature. The solution was allowed to react at room temperature for 24 h, during which the color of the solution changed from dark red to light orange. The solvent was evaporated under vacuum, and the crude product was washed with 3 x 6 mL of hexanes and dried *in vacuo*. The resulting yellow powder was dissolved in CH_2Cl_2 (1 mL), filtered through a small pad of celite and transferred into a 10 mL vial. Pentane (3 mL) was allowed to slowly diffuse at −30 °C for 4 days, after which a bright clear orange oil was obtained. The supernatant was decanted, and the oily product was dried under vacuum to yield 110 mg (68% yield) of **3**·THF as a bright yellow powder.

^{1}H NMR (CD_2Cl_2, 25 °C) of **3**·THF: δ 8.22 (d, J = 8.4 Hz, 1H, Ar H), 7.81 (d, J = 8.8 Hz, 1H, Ar H), 7.43–7.17 (m, 6H, Ar H), 6.23 (d, J = 2.8 Hz, 1H, Cp H), 6.18 (dd, J = 4.0, 4.0 Hz, 1H, Cp H), 6.12 (dd, J = 6.6, 2.6 Hz, 1H, Cp H), 5.98 (dd, J = 8.0, 3.2 Hz, 1H, Cp H), 5.68 (m, 1H, OCH$_2$C*H*=CH$_2$), 5.19 (d, J = 11.2 Hz, 1H, OCH$_2$CH=C*H*$_2$), 5.13 (d, J = 10.8 Hz, 1H, OCH$_2$CH=C*H*$_2$), 4.96 (sept, J = 6.3 Hz, 1H, OC*H*Me$_2$), 4.09 (m, 2H, C*H*$_2$CH$_2$), 3.97–3.80 (m, 2H, CH$_2$C*H*$_2$), 3.66 (s, br, 2H, α-CH$_2$ THF), 3.52 (s, br, 2H, α-CH$_2$ THF), 2.30–2.01 (m, 4H, C*H*$_2$CH=CH$_2$, CH$_2$), 1.87 (m, 4H, β-CH$_2$ THF), 1.25 (d, J = 6.4 Hz, 6H, OCH*Me*$_2$), 1.23–1.16 (9H, =C*Me*, C*Me*$_2$), 0.50 (s, br, 3H, B*Me*). ^{1}H NMR (C_6D_5Br, 25 °C) **3**·THF: δ 7.67 (d, J = 8.4 Hz, 1H, Ar H), 7.36 (d, J = 7.6 Hz, 1H, Ar H), 7.21–6.96 (m, 6H, Ar H), 5.76 (d, J = 2.8 Hz, 2H, Cp H),

5.72 (d, J = 2.4 Hz, 2H, Cp H), 5.64 (m, 1H, OCH_2CH=CH_2), 5.13 (d, J = 10.0 Hz, 1H, OCH_2CH=CH_2), 5.05 (d, J = 14.0 Hz, 1H, OCH_2CH=CH_2), 4.98 (m, 1H, OC$H$$Me_2$), 3.60 (m, 1H, C$H_2CH_2$), 3.48–3.27 (m, 3H, CH_2CH_2), 3.23 (m, 2H, α-CH_2 THF), 3.11 (m, 2H, α-CH_2 THF), 2.23–2.03 (m, 4H, CH_2CH=CH_2, CH_2), 1.42 (m, 4H, β-CH_2), 1.19–1.10 (15H, OCHMe_2, =CMe, CMe_2), 0.93 (s, br, 3H, BMe). ^{19}F NMR (CD_2Cl_2, 25 °C): δ −133.15 (d, $^3J_{F–F}$ = 19.6 Hz, 6F, o–F), −165.26 (t, $^3J_{F–F}$ = 20.5 Hz, 3F, p–F), −167.84 (m, 6F, m–F).

Isolation of *rac*-(EBI)Zr[OC(N(CH_2CH=CH_2)$_2$)=$CHCH_2C(Me_2)C(O^iPr)$=O]$^+$ [$MeB(C_6F_5)_3$]$^-$ (4). In an argon-filled glovebox, a 30 mL glass reactor was charged with 67.5 mg (0.137 mmol) of *rac*-(EBI)ZrMe[OC(O^iPr)=CMe_2] dissolved in 8 mL of CH_2Cl_2. Then, 80.0 mg (0.137 mmol) of $(C_6F_5)_3B$·THF in 1 mL of CH_2Cl_2 was added; the mixture was allowed to stir for 10 min at ambient temperature to cleanly generate **2** *in situ*. To this vigorously stirred solution, 20.7 mg (0.137 mmol) of DAA was quickly added from a stock solution in CH_2Cl_2 at room temperature. The color of the resulting mixture changed instantaneously from dark red to bright yellow. The solution was stirred for an additional 30 min, after which the solvent was evaporated under vacuum to obtain a sticky yellow solid. The crude product was washed with 3 x 6 mL of hexanes and dried in vacuo to give 152 mg (96%) of the pure title complex as a yellow powder. Anal. Calcd for $C_{55}H_{45}BF_{15}NO_3Zr$: C, 57.20; H, 3.93; N, 1.21. Found: C, 57.03; H, 3.79; N, 1.19.

^{1}H NMR (CD_2Cl_2, 0 °C) of **4**: δ 8.07 (d, J = 8.5 Hz, 1H, Ar H), 7.81 (d, J = 9.0 Hz, 1H, Ar H), 7.31–7.10 (m, 6H, Ar H), 5.86 (d, J = 3.0 Hz, 1H, Cp H), 5.79 (m, 1H, NCH_2CH=CH_2), 5.77 (d, J = 3.0 Hz, 1H, Cp H), 5.61 (d, J = 3.0 Hz, 1H, Cp H), 5.55 (m, 1H, NCH_2CH=CH_2), 5.49 (d, J = 3.0 Hz, 1H, Cp H), 5.31 (d, J = 9.5 Hz, 1H, NCH_2CH=CH_2), 5.24 (d, J = 10.0 Hz, 1H, NCH_2CH=CH_2), 5.24 (d, J = 18.0 Hz, 1H, NCH_2CH=CH_2), 5.11 (d, J = 17.5 Hz, 1H, NCH_2CH=CH_2), 4.65 (sept, J = 6.3 Hz, 1H, OC$H$$Me_2$), 4.14 (m, 1H, C$H_2CH_2$), 4.03 (m, 1H,

C*H*$_2$CH$_2$), 3.91 (dd, *J* = 17.0, 2.5 Hz, 1H, NC*H*$_2$CH=CH$_2$), 3.81 (m, 3H, CH$_2$C*H*$_2$, NC*H*$_2$CH=CH$_2$), 3.64 (dd, *J* = 16.7, 6.8 Hz, 1H, NC*H*$_2$CH=CH$_2$), 3.32 (dd, *J* = 14.5, 8.0 Hz, 1H, NC*H*$_2$CH=CH$_2$), 2.11 (d, *J* = 14.0 Hz, 1H, C*H*$_2$), 1.85 (dd, *J* = 14.0, 11.0 Hz, 1H, C*H*$_2$), 1.36 (d, *J* = 6.0 Hz, 3H, OCH*Me*$_2$), 1.23 (d, *J* = 8.5 Hz, 1H, C*H*), 1.22 (s, 3H, C*Me*$_2$), 1.20 (d, *J* = 6.5 Hz, 3H, OCH*Me*$_2$), 1.14 (s, 3H, C*Me*$_2$), 0.46 (s, br, 3H, B*Me*). ^{19}F NMR (CD$_2$Cl$_2$, 25 °C): δ −133.17 (d, $^3J_{F–F}$ = 20.8 Hz, 6F, *o*–F), −165.42 (t, $^3J_{F–F}$ = 21.6 Hz, 3F, *p*–F), −167.97 (m, 6F, *m*–F). ^{13}C NMR (CD$_2$Cl$_2$, 0 °C): δ 184.96 ([*C*(O^{i}Pr)=O]), 171.48 ([O*C*(N(CH$_2$CH=CH$_2$)$_2$)=]), 148.36 (d, $^1J_{C–F}$ = 239.4 Hz, *o*-*C*$_6$F$_5$), 137.62 (d, $^1J_{C–F}$ = 240.0 Hz, *p*-*C*$_6$F$_5$), 136.52 (d, $^1J_{C–F}$ = 245.0 Hz, *m*-*C*$_6$F$_5$), 132.31 (NCH$_2$*C*H=CH$_2$), 131.53 (NCH$_2$*C*H=CH$_2$), 132.38, 130.69, 128.40, 128.20, 127.54, 127.17, 127.14, 125.14, 124.20, 122.41, 122.06, 121.51, 120.70, 119.40, 119.04, 113.50, 99.07, and 96.07 (indenyl carbons), 119.71 (NCH$_2$CH=*C*H$_2$), 118.96 (NCH$_2$CH=*C*H$_2$), 73.59 (O*C*HMe$_2$), 48.85 (N*C*H$_2$CH=CH$_2$), 48.66 (N*C*H$_2$CH=CH$_2$), 42.39 (*C*Me$_2$), 37.69 (*C*H), 36.75 (*C*H$_2$), 31.45 (*C*H$_2$CH$_2$), 30.69 (CH$_2$*C*H$_2$), 27.15 (C*Me*$_2$), 25.83 (C*Me*$_2$), 21.62 (OCH*Me*$_2$), 20.63 (OCH*Me*$_2$), 10.03 (B*Me*).

General Polymerization Procedures. Polymerizations were carried out in 20 mL glass reactors inside an argon-filled glovebox in toluene or methylene chloride at ambient temperature (~23 °C). As an example of a typical procedure for homopolymerization by the pre-activation method, solutions of B(C$_6$F$_5$)$_3$·THF (8.4 mg, 0.014 mmol) and the pre-catalyst *rac*-(EBI)ZrMe[OC(O^{i}Pr)=CMe$_2$] (7.0 mg, 0.014 mmol) were premixed in 5.0 mL of CH$_2$Cl$_2$ or toluene and stirred for 5 min to cleanly generate the corresponding catalyst **1**. Subsequently, 0.5 mL of AMA (4.18 mmol; [AMA]$_0$/[**1**] = 300) was quickly added *via* a syringe to the vigorously stirring solution, and the reaction was allowed to proceed with continuous stirring. The polymerization of the other monomers was performed in an identical fashion, except for VBMA

where 0.3 mL of monomer (1.82 mmol) was employed. Alternatively, the activated monomer method (premixing the monomer with the activator, followed by the addition of the neutral pre-catalyst complex) was also adopted in two runs for catalyst **2** as indicated in Table S1 (entries 2 and 5). In all cases, after the measured time interval, a 0.2 mL aliquot was taken from the reaction mixture *via* syringe and quickly quenched into a 1.5 mL septum cap sealed vial containing 0.6 mL of "wet" $CDCl_3$ stabilized by 250 ppm of BHT-H; the quenched aliquots were later analyzed by ^{1}H NMR to obtain monomer conversion data. The remaining bulk polymerization reaction was quenched after the removal of the last aliquot by addition of 5 mL of 5% HCl-acidified methanol and precipitated into 100 mL of MeOH. The quenched mixture was stirred for 3 h, and the polymer produced was filtered (PVMA, PVBMA, and PDAA were obtained as white powdery solids) or decanted (PAMA was obtained as a colorless thick oil). The isolated polymer was washed with MeOH, pentanes, and dried in a vacuum oven at room temperature overnight to a constant weight.

Block copolymerizations were performed with the *in situ* generated catalyst in the same fashion as described above. Initially, 200 equiv. of the first monomer were quickly added *via* syringe and vigorously stirred for the time interval specified. Then, 200 equiv. of the second monomer were added *via* syringe to the stirring solution and the polymerization was continued for the second specified time interval.

***it*-PAMA.** ^{1}H NMR ($CDCl_3$, 25 °C): δ 5.91 (m, 1H, –$OCH_2C\mathit{H}$=CH_2), 5.31 (d, J = 13.6 Hz, 1H, – OCH_2CH=CH_2), 5.20 (d, J = 8.0 Hz, 1H, –OCH_2CH=CH_2), 4.47 (d, J = 4.4 Hz, 2H, –$OC\mathit{H}_2CH$=CH_2), 2.18 (d, J = 11.6 Hz, 1H, CH_2, *mm*), 1.59 (d, J = 12.0 Hz, 1H, CH_2, *mm*), 1.22 (s, CH_3, *mm*), 1.06 (s, CH_3, *mr*), 0.89 (s, CH_3, *rr*). ^{13}C{^{1}H} NMR ($CDCl_3$, 50 °C): 176.0 (*C*=O, *mmmm*), 132.5 (*C*H=), 118.3 (=*C*H_2), 65.5 (O*C*H_2), 51.6 (quaternary carbon, *mm*), 46.0 (main-chain *C*H_2), 22.2 (CH_3).

***it*-PVMA.** ^{1}H NMR ($CDCl_3$, 25 °C): δ 7.13 (m, 1H, –OC*H*=CH_2), 4.88 (d, J = 13.6 Hz, 1H, – OCH=CH_2), 4.60 (s, br, 1H, –OCH=CH_2), 2.25–1.55 (m, 2H, CH_2), 1.25 (s, CH_3, *mm*), 1.08 (s, CH_3, *mr*), 0.91 (s, CH_3, *rr*). ^{13}C{^{1}H} NMR ($CDCl_3$, 25 °C): 175.1–173.0 (*C*=O), 141.3 (O*C*H=), 98.5 (=*C*H_2), 52.7–50.8 (quaternary carbon), 45.6–44.8 (main-chain *C*H_2), 22.6–17.0 (CH_3).

***it*-PVBMA.** ^{1}H NMR ($CDCl_3$, 25 °C): δ 7.26 (d, J = 8.0 Hz, 2H, C_6H_4), 7.19 (d, J = 8.4 Hz, 2H, C_6H_4), 6.62 (dd, J = 17.4, 11.0 Hz, 1H, –C*H*=CH_2), 5.67 (d, J = 17.6 Hz, 1H, –CH=CH_2), 5.20 (d, J = 10.8 Hz, 1H, –CH=CH_2), 4.88 (s, 2H, –OCH_2), 2.19 (d, J = 12.8 Hz, 1H, CH_2), 1.50 (d, J = 14.0 Hz, 1H, CH_2), 1.14 (s, CH_3, *mm*), 0.96 (s, CH_3, *mr*), 0.74 (s, CH_3, *rr*). ^{13}C{^{1}H} NMR ($CDCl_3$, 25 °C): 176.1 (*C*=O, *mmmm*), 137.4, 135.4, 128.5, 126.4 (*C*$_6$H$_4$), 136.5 (*C*H=CH_2), 114.2 (CH=*C*H_2), 66.4 (O*C*H_2), 51.7 (quaternary carbon, *mm*), 45.8 (main-chain *C*H_2), 22.1 (*C*H_3).

***it*-PDAA.** ^{1}H NMR ($CDCl_3$, 25 °C): δ 5.69 (m, 2H, –NCH_2C*H*=CH_2), 5.09 (m, 4H, –NCH_2CH=CH_2), 4.38–3.72 (m, br, 4H, –NC*H*$_2$CH=CH_2), 2.38 (s, 1H, C*H*, *mm*), 1.71 (s, 1H, CH_2, *mm*), 1.20 (s, 1H, CH_2, *mm*). ^{13}C{^{1}H} NMR ($CDCl_3$, 50 °C): 174.5 (*m*, *C*=O), 134.0 (*C*H=CH_2), 133.4 (*C*H=CH_2), 117.7 (CH=*C*H_2), 117.3 (CH=*C*H_2), 48.9 (N*C*H_2), 48.3 (N*C*H_2), 37.0 (*C*H), 34.3 (*C*H_2).

Polymerization Kinetics. Kinetic experiments were carried out in 20 mL glass reactors inside the glovebox at ambient temperature (~23 °C) using a similar procedure to that already described above. A stock solution of the pre-catalyst **1** was first prepared (72.2 mM in toluene), and predetermined amounts were taken and activated with an equimolar quantity of $B(C_6F_5)_3$·THF in toluene. At appropriate time intervals, 0.2 mL aliquots were withdrawn from the reaction mixture using a syringe and quickly quenched into 1.5 mL septum cap sealed vials containing 0.6 mL of undried "wet" $CDCl_3$ stabilized with 250 ppm of BHT-H. The quenched aliquots were analyzed by ^{1}H NMR to determine monomer conversion values. Specifically, the percent of

unreacted AMA at a given time *t*, was determined by integration of the peaks for AMA (center at 4.97 ppm for the OCH_2 signals) and PAMA (centered at 4.88 ppm for the OCH_2 signals) according to the percent of unreacted AMA = $(\mathbf{A}_{4.97}/\mathbf{A}_{4.88}) \times 100$, where $\mathbf{A}_{4.97}$ is the total integrals for the peaks centered at 4.97 ppm and $\mathbf{A}_{4.88}$ is the total integral for the peaks centered at 4.88 ppm. Apparent rate constants (k_{app}) were extracted by linearly fitting a line to the plot of $\ln([AMA]_0/[AMA]_t)$ vs time *t*.

Post-Functionalization by the Thiol-Ene "Click" Reaction. In a typical reaction by radical photoinitiation, an isolated polymer (100 mg) was dissolved in 1.5 mL of degassed chloroform inside a glovebox. This solution was filtered through a plastic frit (0.45 μm pore size) to eliminate any possible undissolved polymer particles, and charged in a 20 mL glass vial containing a magnetic stirrer, 0.2 equiv of DMPA, and 5-10 equiv of a thiol as specified. The reactor was capped, taken out of the glovebox, and placed inside a photoreactor (Luzchem, LZC-4 photoreactor with a horizontal UVA lamp configuration, radiation centered at 350 nm) where it was stirred at room temperature for 2 h. At this point, 0.1 mL of the solution was withdrawn and quenched into 1.5 mL vials containing 0.6 mL of $CDCl_3$ for conversion quantification by ^{1}H NMR. The remaining mixture was precipitated into 100 mL of methanol; the white sticky product was separated and redissolved in 5 mL of $CHCl_3$. Any insoluble particles were removed by filtration and the filtrate was precipitated in methanol. After stirring overnight, the product was filtered, washed with methanol, and dried in a vacuum oven at 50 °C to a constant weight.

In the reaction by radical thermoinitiation, a polymer (100 mg) was dissolved in 1.5 mL of degassed 1,2-dichlorobenzene inside a glovebox. This solution was filtered through a plastic frit (0.45 μm pore size) to eliminate any undissolved polymer particles, and charged in a 20 mL glass vial containing a magnetic stirrer, 0.5 equiv of AIBN, and 5-10 equiv of a thiol as specified. The

reactor was capped, taken out of the glovebox, and placed in a shaker where it was stirred at 70°C for 24 h. The workup of the reaction was identical to the one mentioned above for the radical photoinitiation.

***it*-PAMA-SR1.** ^{1}H NMR ($CDCl_3$, 25 °C): δ 7.29 (d, J = 8.0 Hz, 2H, Ar H), 7.20 (d, J = 8.0 Hz, 2H, Ar H), 4.00 (s, 2H, OCH_2CH$_2$), 3.64 (s, 2H, SCH_2Ar), 2.46 (t, J = 8.0 Hz, 2H, SCH_2CH$_2$), 2.10 (d, J = 12.0 Hz, 1H, CH$_2$, *mm*), 1.86 (m, 2H, OCH$_2$CH_2), 1.48 (d, J = 12.0 Hz, 1H, CH$_2$, *mm*), 1.28, (s, 9H, ^{t}Bu), 1.16 (s, 3H, CH$_3$, *mm*). ^{13}C{^{1}H} NMR ($CDCl_3$, 25 °C): 176.1, 149.9, 135.3, 128.7, 125.5, 63.6, 51.6, 45.8, 35.8, 34.6, 31.6, 28.1, 22.1.

***it*-PAMA-SR2.** ^{1}H NMR ($CDCl_3$, 25 °C): δ 4.03 (s, 2H, OCH_2CH$_2$), 2.57 (t, J = 8.0 Hz, 2H, SCH_2CH$_2$), 2.12 (d, J = 12.0 Hz, 1H, CH$_2$, *mm*), 2.04 (b, 3H, C*H*-adamantane), 1.90 (m, 2H, OCH$_2$CH_2), 1.86 (s, br, 6H, CH_2-adamantane), 1.69 (s, br, 6H, CH_2-adamantane), 1.53 (d, J = 12.0 Hz, 1H, CH$_2$, *mm*), 1.20 (s, 3H, CH$_3$, *mm*).). ^{13}C{^{1}H} NMR ($CDCl_3$, 25 °C): 176.0 (*C*OO), 63.9 (O*C*H$_2$), 45.8 (S*C*H$_2$CH$_2$), 44.4 (S*C*-adamantane), 43.8 (*C*H-adamantane), 36.54 (*C*H$_2$-adamantane), 29.9 (*C*H$_2$-adamantane), 29.6 (OCH$_2$*C*H$_2$), 22.4 (chain *C*H$_2$), 22.1 (*C*H$_3$).

***it*-PDAA-SR1.** ^{1}H NMR ($CDCl_3$, 25 °C): δ 7.28 s, br, 4H, Ar H), 7.21 (s, br, 4H, Ar H), 3.80 (s, br, 4H, NCH_2CH$_2$), 3.64 (s, br, 4H, SCH_2Ph), 3.24 (s, br, 4H, SCH_2CH$_2$), 2.38 (s, br, 4H, NCH$_2$CH_2), 1.74 (s, br, 1H, chain C*H*, *mm*), 1.29, (s, 18H, ^{t}Bu), 1.16 (s, br, 1H, chain CH_2, *mm*), 0.84 (s, br, 1H, chain CH_2, *mm*).

***it*-PDAA-SR2.** ^{1}H NMR ($CDCl_3$, 25 °C): δ 3.60-2.29 (s, br, 13H, NCH_2CH$_2$, SCH_2CH$_2$, NCH$_2$CH_2, chain C*H*, *mm*), 2.02 (s, br, 3H, C*H*-adamantane), 1.84 (s, br, 6H, CH_2-adamantane), 1.68 (s, br, 6H, CH_2-adamantane), 1.05 (s, br, 1H, chain CH_2, *mm*), 0.91 (s, br, 1H, chain CH_2, *mm*).

Post-Polymerization Photocuring and Film Formation. *it*-PAMA (600 mg) was dissolved in 4.0 mL of degassed chloroform inside of a glovebox, and the subsequent viscous solution was filtered through a plastic frit (0.45 μm pore size) to eliminate any undissolved polymer particle. DMPA (2 wt%) was added and gently stirred until it was totally dissolved. This mixture was transferred outside of the glovebox with a glass pipette to a PTFE mold (2 x 0.5 inches); the mold was located in the photoreactor chamber (Luzchem, LZC-4 photoreactor with top-irradiation configuration, UVA lamps centered at 350 nm) and irradiated for 10 minutes, after which a gel was formed. The gel was allowed to dry slowly under ambient laboratory conditions overnight and then thoroughly dried in a vacuum oven at 50 °C to a constant weight.

Polymer Characterization. Polymer number-average molecular weights (M_n) and molecular weight distributions ($Đ = M_w/M_n$) were measured by gel permeation chromatography (GPC) analyses carried out at 40 °C and a flow rate of 1.0 mL min^{-1}, with DMF as the eluent, on a Waters University 1500 GPC instrument equipped with four PLgel 5 μm mixed-C columns (Polymer Laboratories; linear range of molecular weight = 200–2,000,000) and calibrated using 10 PMMA standards. Chromatograms were processed with Waters Empower software (version 2002).

Glass transition temperatures (T_g) of the polymers were measured by differential scanning calorimetry (DSC) on a Q20 DSC, TA Instruments. Samples were heated until 150–300 °C (depending on the polymer decomposition onset temperature) at 10 °C/min, cooled to −50 °C at 10 °C/min, and then reheated again at 10 °C/min. All T_g values were obtained from the second heating scan, after removing the thermal history, and are reported as half-height midpoints. Maximum rate decomposition temperatures (T_{max}) and decomposition onset temperatures (T_{onset}) of the polymers were measured by thermal gravimetric analysis (TGA) on a Q50 TGA

Termogravimetric Analyzer, TA Instrument. Polymer samples were heated from 20 °C to 800 °C at a rate of 10 °C/min. Values of T_{max} were obtained from derivative (wt %/°C) vs temperature (°C), while T_{onset} values (initial and end temperatures) were obtained from wt % vs temperature (°C) plots.

A.2. Additional Figures and Tables

Table S2.1. Selected results of polar (di)vinyl monomer polymerizations by **2** [a]

run no.	monomer	[M]/[**2**]	Method[b]	Solv.	Yield[c] (%)	M_n[d] (kg/mol)	$Đ$[d] (M_w/M_n)	[*mm*][e] (%)	[*mr*][e] (%)	[*rr*][e] (%)
1	MMA	200	(A)	Toluene	75	26.3	1.16	6.0	37.0	57.0
2	MMA	200	(B)	Toluene	72	24.8	1.35	14.6	30.1	55.3
3	MMA	400	(A)	Toluene	71	40.9	1.23	5.2	38.4	56.4
4	MMA	400	(A)	CH_2Cl_2	76	37.1	1.36	6.8	41.0	52.2
5	MMA	200	(B)	CH_2Cl_2	75	32.0	1.21	8.0	35.3	56.7
6	VMA	200	(A)	CH_2Cl_2	3	31.2	1.58	13.7	31.2	55.1
7	AMA	200	(A)	Toluene	0	–	–	–	–	–
8	DAA	100	(A)	CH_2Cl_2	24	n.d.	n.d.	n.d.	n.d.	n.d.

[a] Conditions: solvent = 5 mL; ambient temperature (~23 °C), time = 24 h; n.d. = not determined. [b] Method (A) = pre-activation (premixing the neutral complex with the activator to generate the corresponding cationic catalyst, followed by addition of monomer to start the polymerization; Method (B) = in-reactor activation (premixing the monomer with the activator, followed by the addition of the neutral complex). [c] Isolated yield measured by gravimetric analysis; runs no 8-9 monomer conversion measured by ^{1}H NMR. [d] Number-average molecular weight (M_n) and polydispersity ($Đ$) determined by GPC relative to PMMA standards. [e] Tacticity measured by ^{1}H with $CDCl_3$ as a solvent at RT.

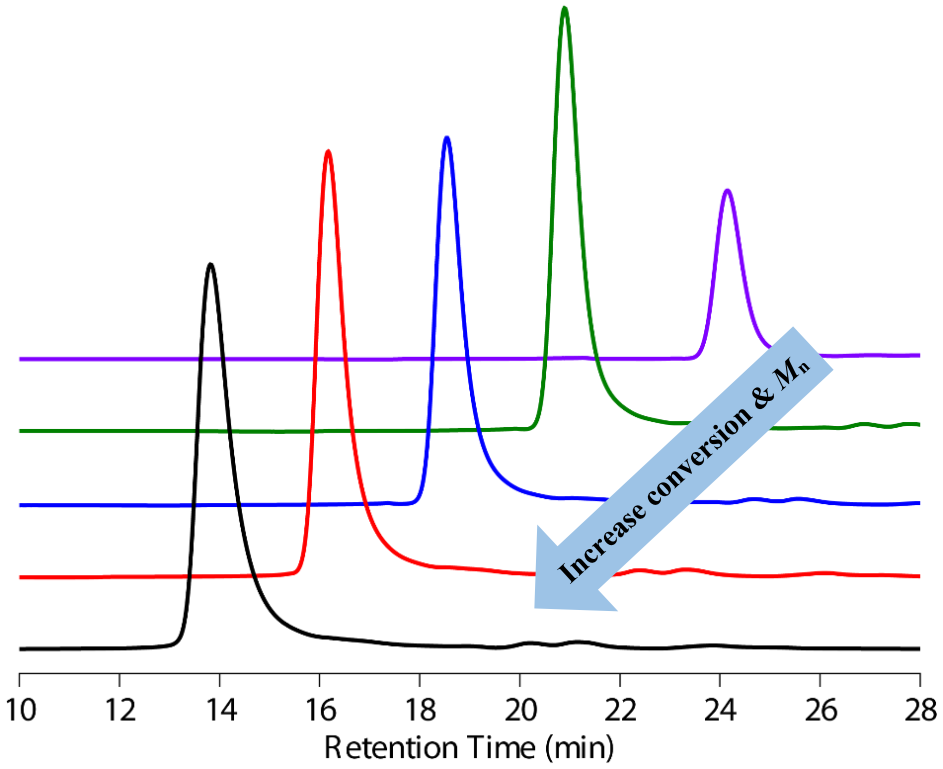

Figure S2.1. Representative GPC traces of *it*-PAMA samples produced by **1** vs. monomer conversion showing an increase in M_n (from top to bottom) as conversion increases. Conditions: $[AMA]_0/[\mathbf{1}]_0 = 300$, toluene, 23 °C

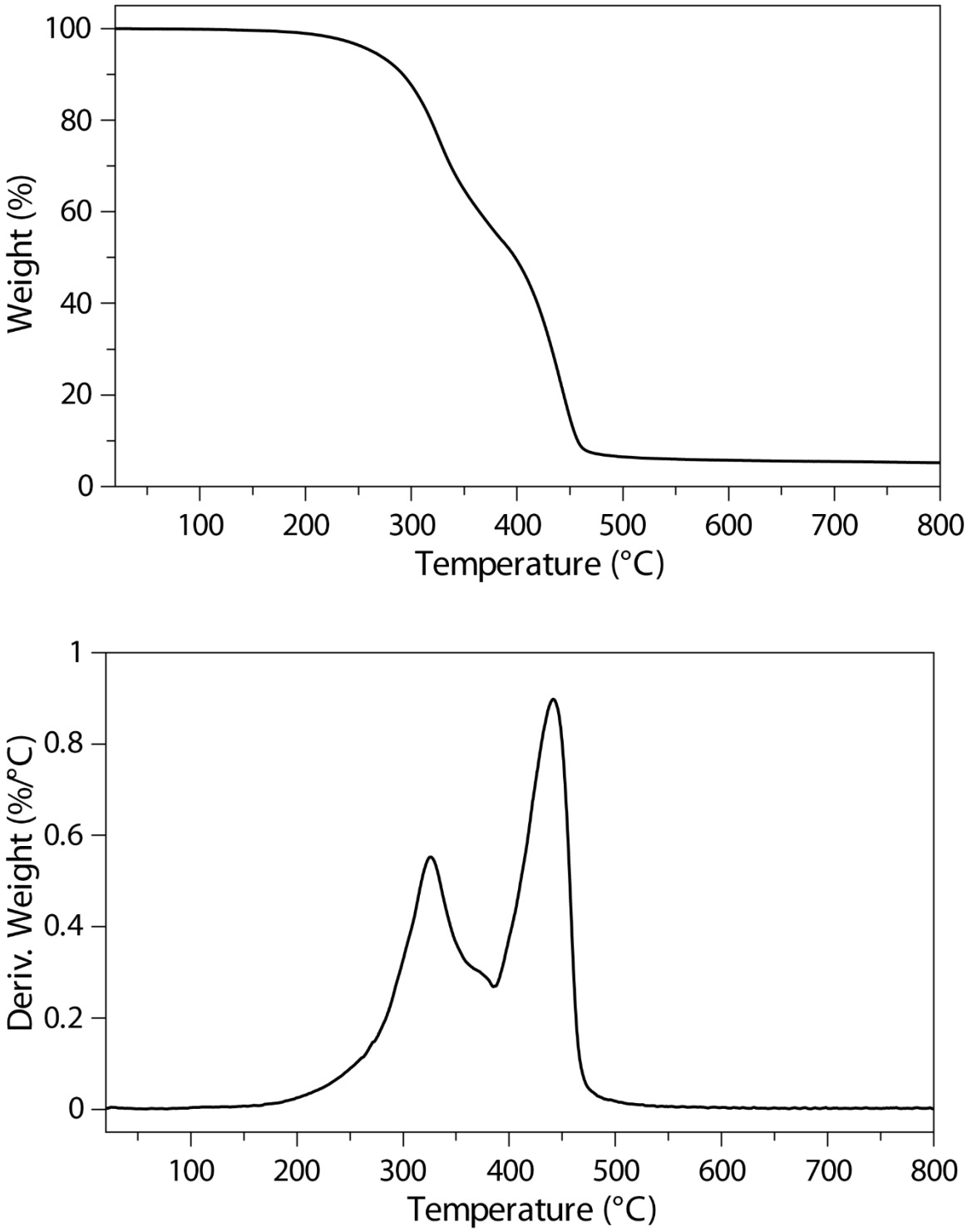

Figure S2.2. TGA traces of *it-rich*-PVMA acquired at a scanning rate of 10 °C/min. Top plot: weight (wt %) vs temperature (°C); bottom plot: derivative (wt %/°C) vs temperature (°C).

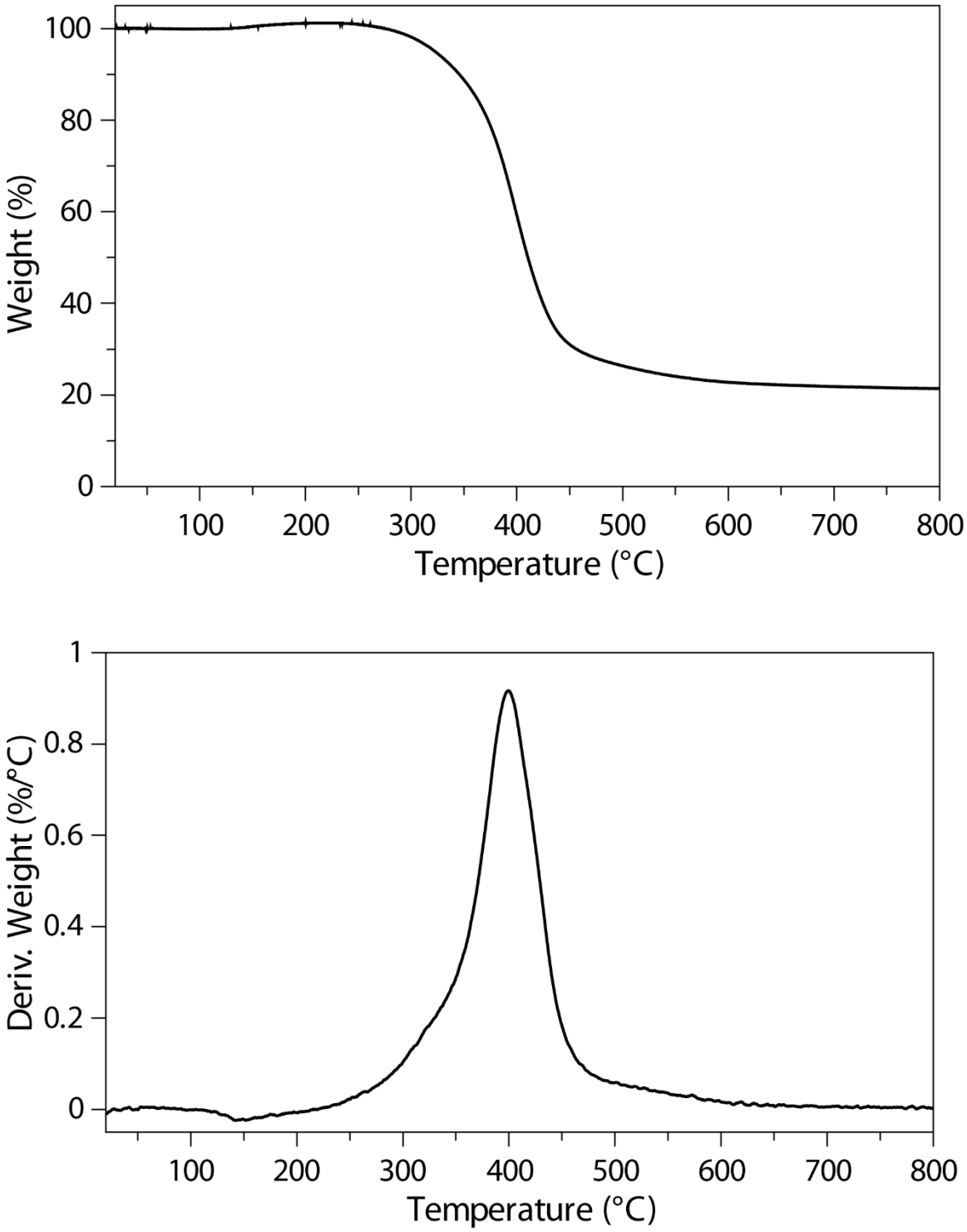

Figure S2.3. TGA traces of *it*-PVBMA acquired at a scanning rate of 10 °C/min. Top plot: weight (wt %) vs temperature (°C); bottom plot: derivative (wt %/°C) vs temperature (°C).

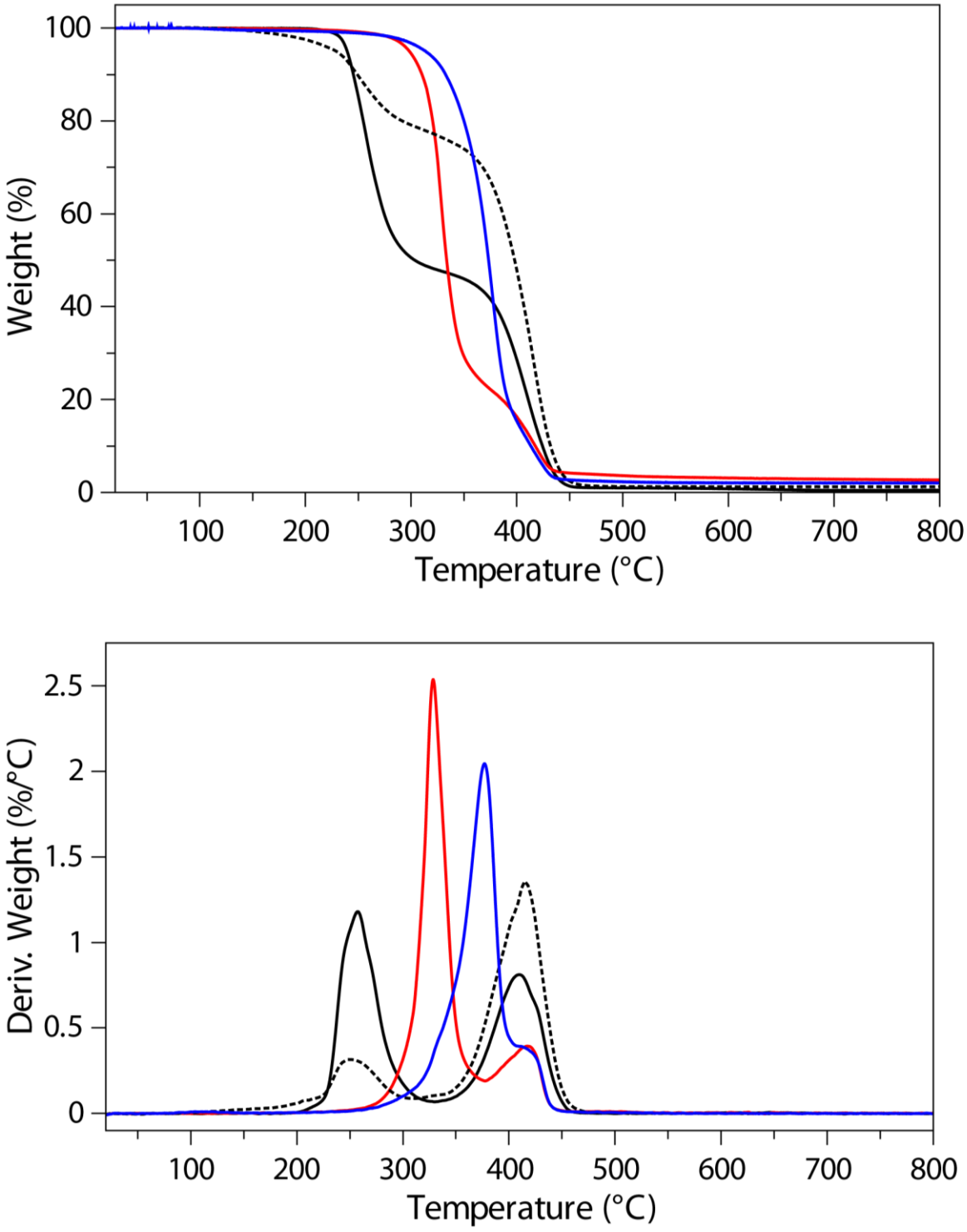

Figure S2.4. TGA traces of *it*-PAMA (solid black), photocured PAMA-*hv* (dashed black), *it*-PAMA-SR1 (red), and *it*-PAMA-SR2 (blue) acquired at a scanning rate of 10 °C/min. Top plot: weight (wt %) vs. temperature (°C); bottom plot: derivative (wt %/°C) vs. temperature (°C).

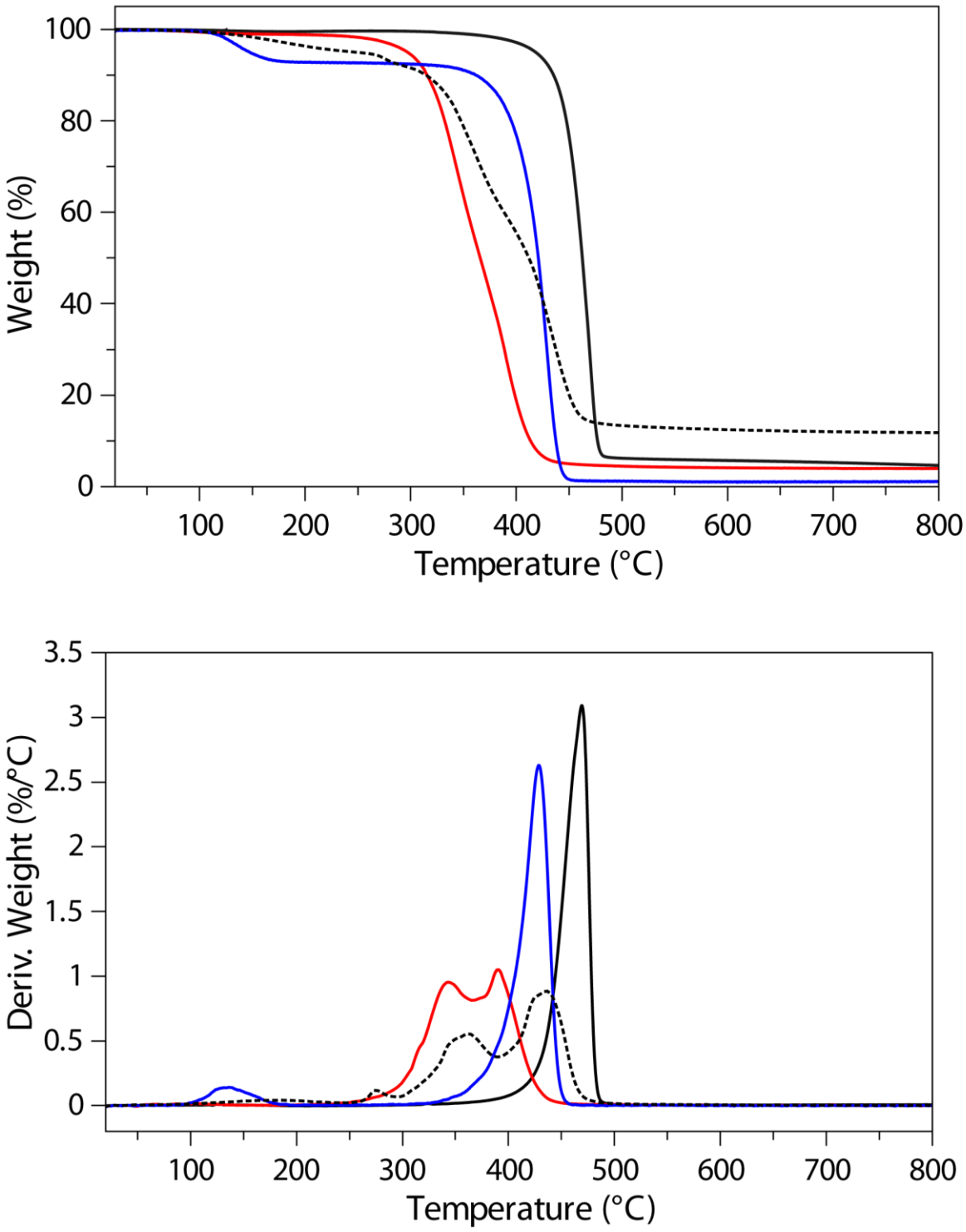

Figure S2.5. TGA traces of *it*-PDAA (solid black), photocured PDAA-*hv* (dashed black), *it*-PDAA-SR1 (red), and *it*-DAA-SR2 (blue) acquired at a scanning rate of 10 °C/min. Top plot: weight (wt %) vs. temperature (°C); bottom plot: derivative (wt %/°C) vs. temperature (°C).

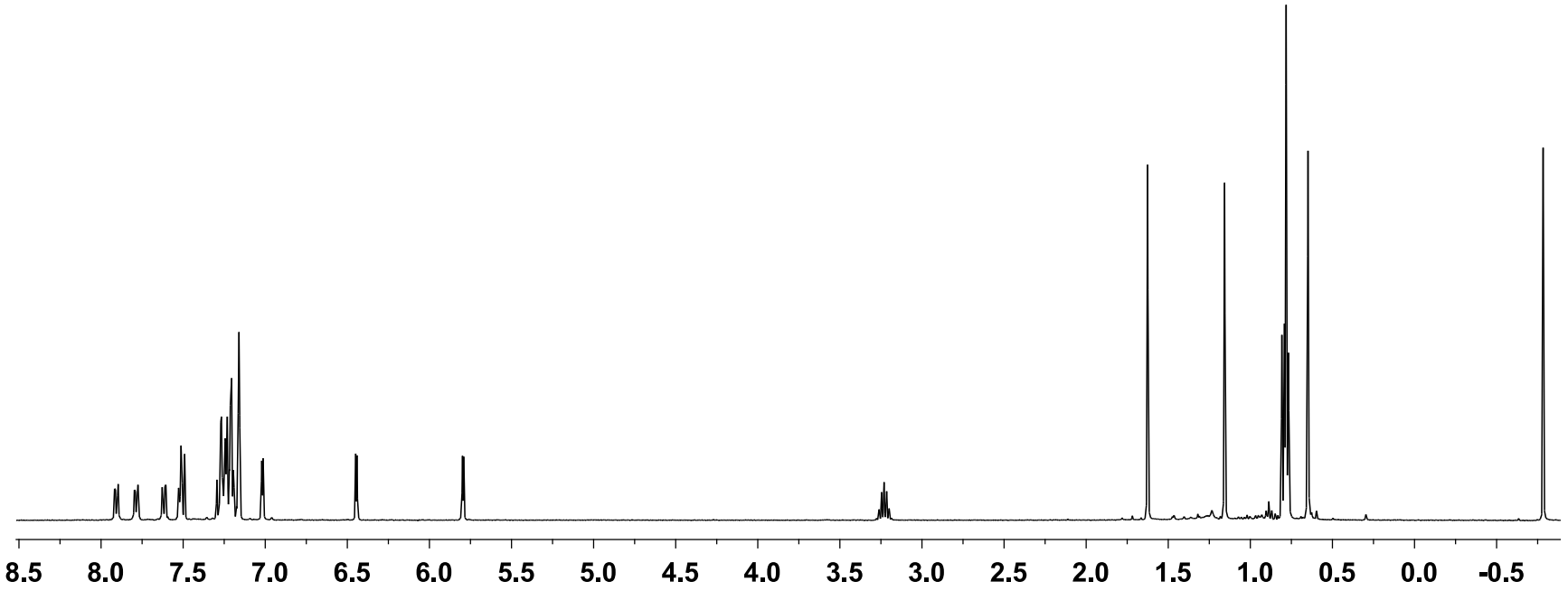

Figure S2.6. ^{1}H NMR (C_6D_6, 25 °C) spectrum of *rac*-(SBBI)ZrMe[OC(O^{i}Pr)=CMe$_2$] (pre-**2**).

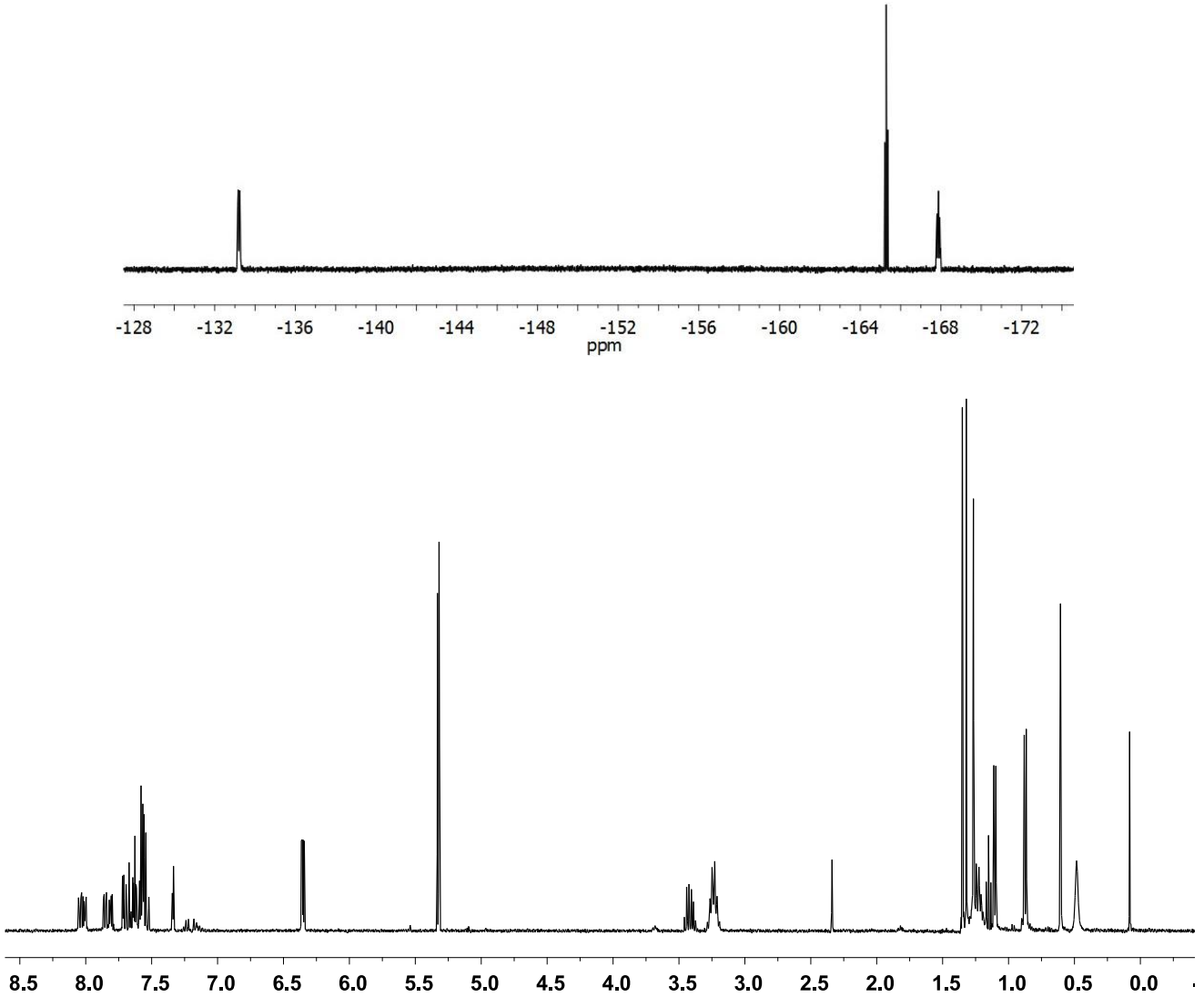

Figure S2.7. ^{19}F and ^{1}H NMR (CD_2Cl_2, 25 °C) spectra of *rac*-(SBBI)Zr^{+}(THF)[OC(O^{i}Pr)=CMe_2][Me$B(C_6F_5)_3$]$^{-}$ (**2**).

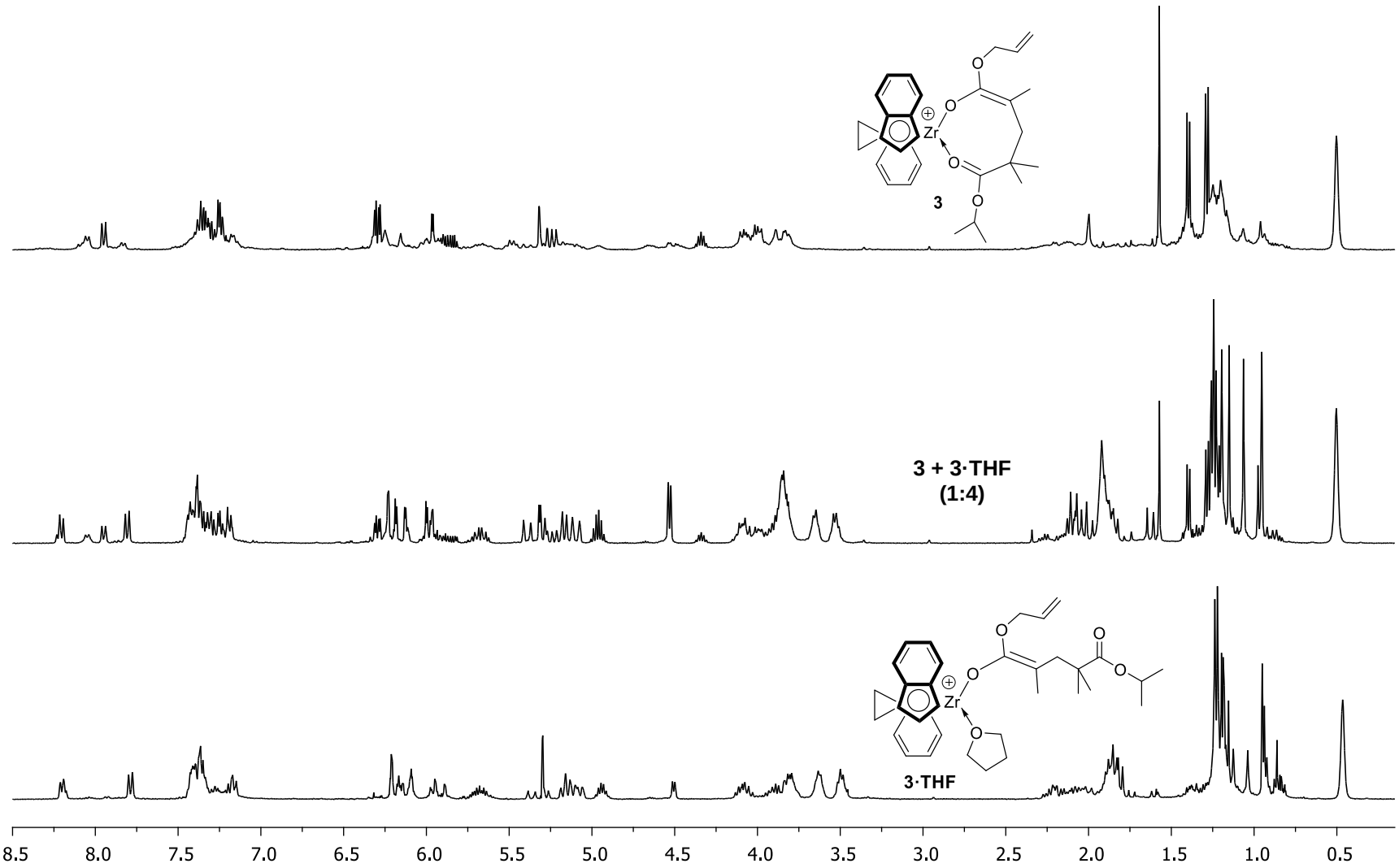

Figure S2.8. ^{1}H NMR spectrum (CD_2Cl_2, 25 °C) of complex **3** (top), complex **3**·THF (bottom), and the initial mixture of **3** + **3**·THF (middle).

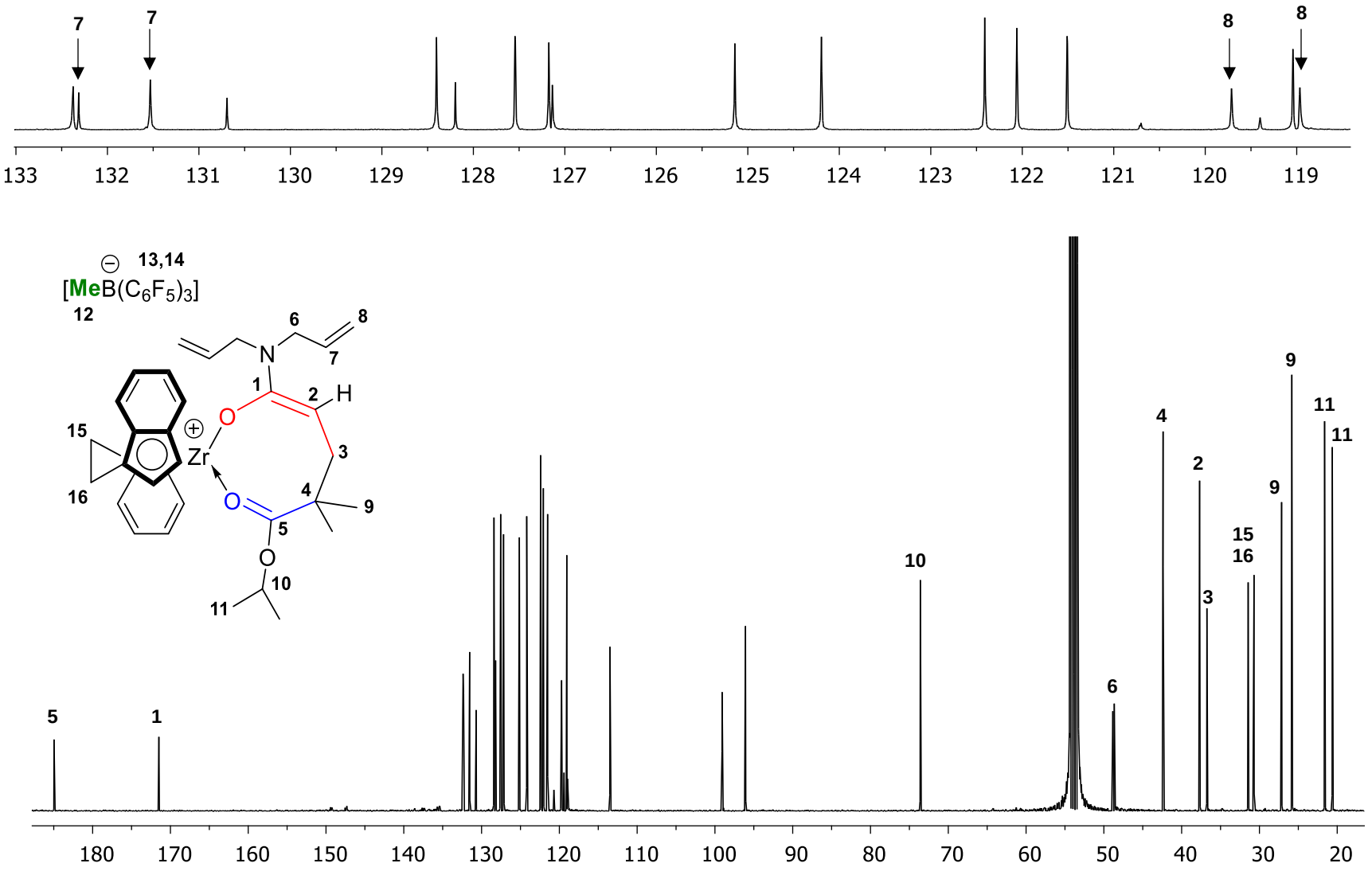

Figure S2.9. ^{13}C (CD_2Cl_2, 0 °C) of complex **4**.

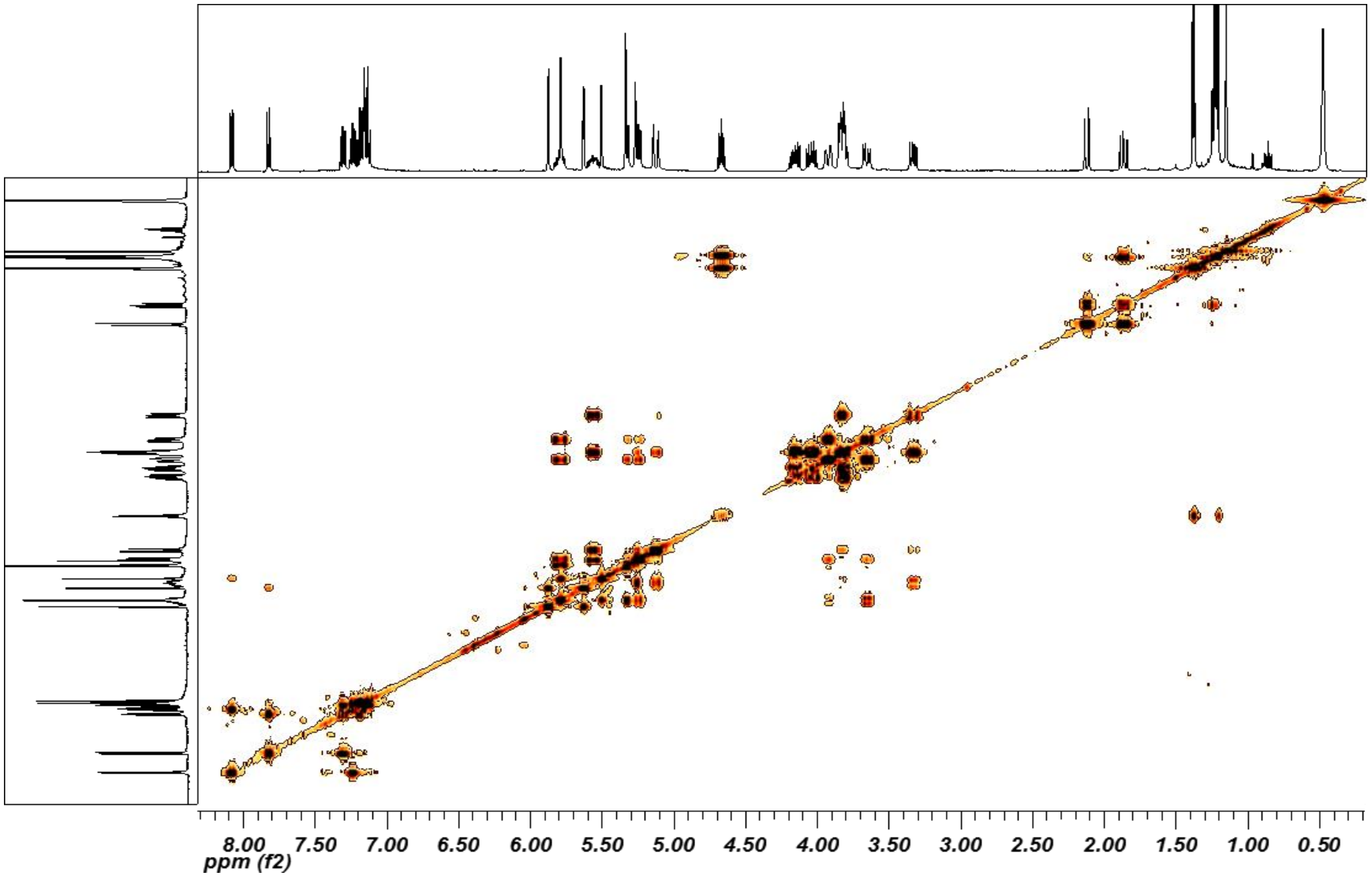

Figure S2.10. 2D COSY NMR spectrum (CD_2Cl_2, 0 °C) of complex **4**.

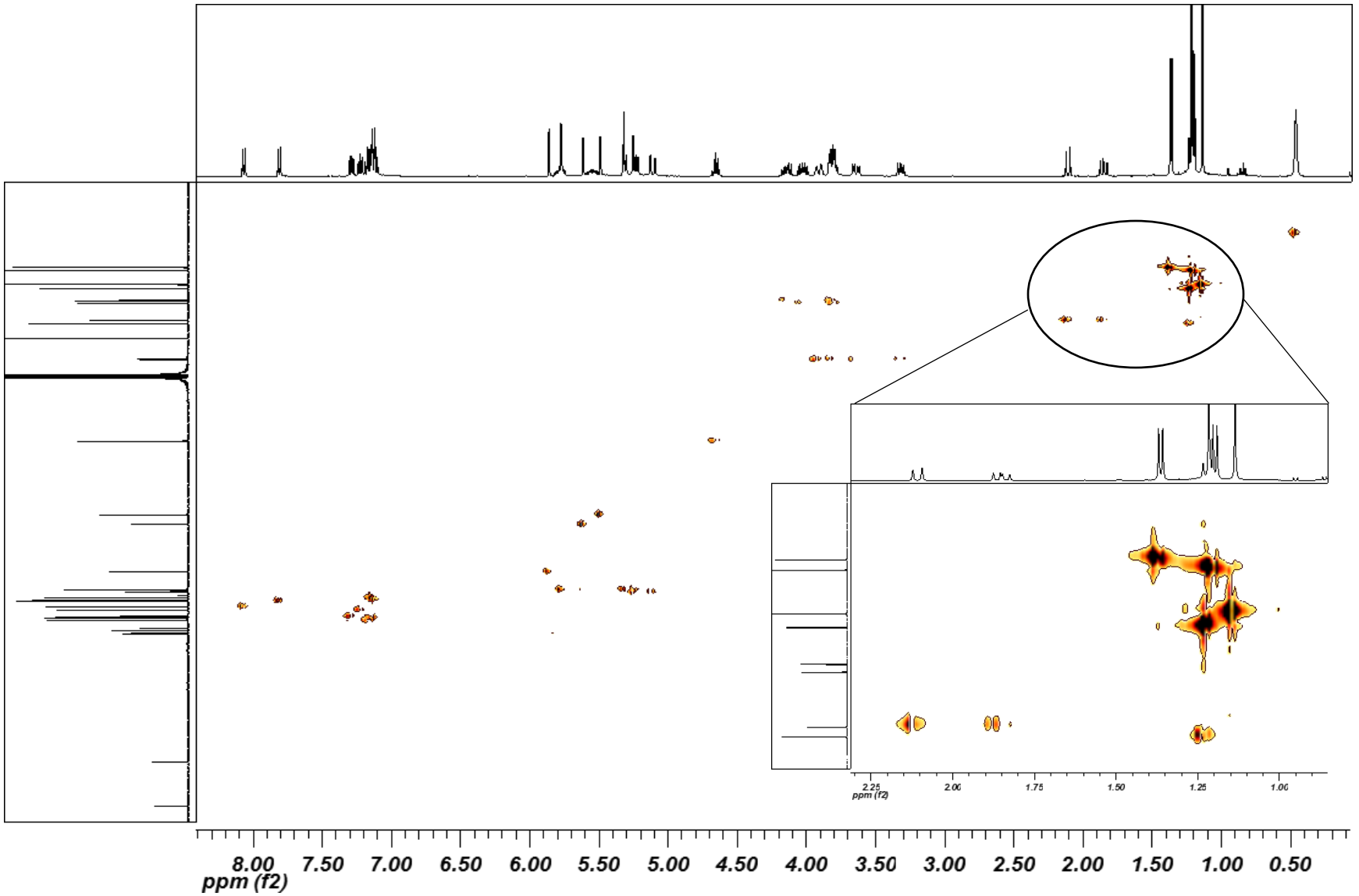

Figure S2.11. 2D HSQC NMR spectrum (CD_2Cl_2, 0 °C) of complex **4**.

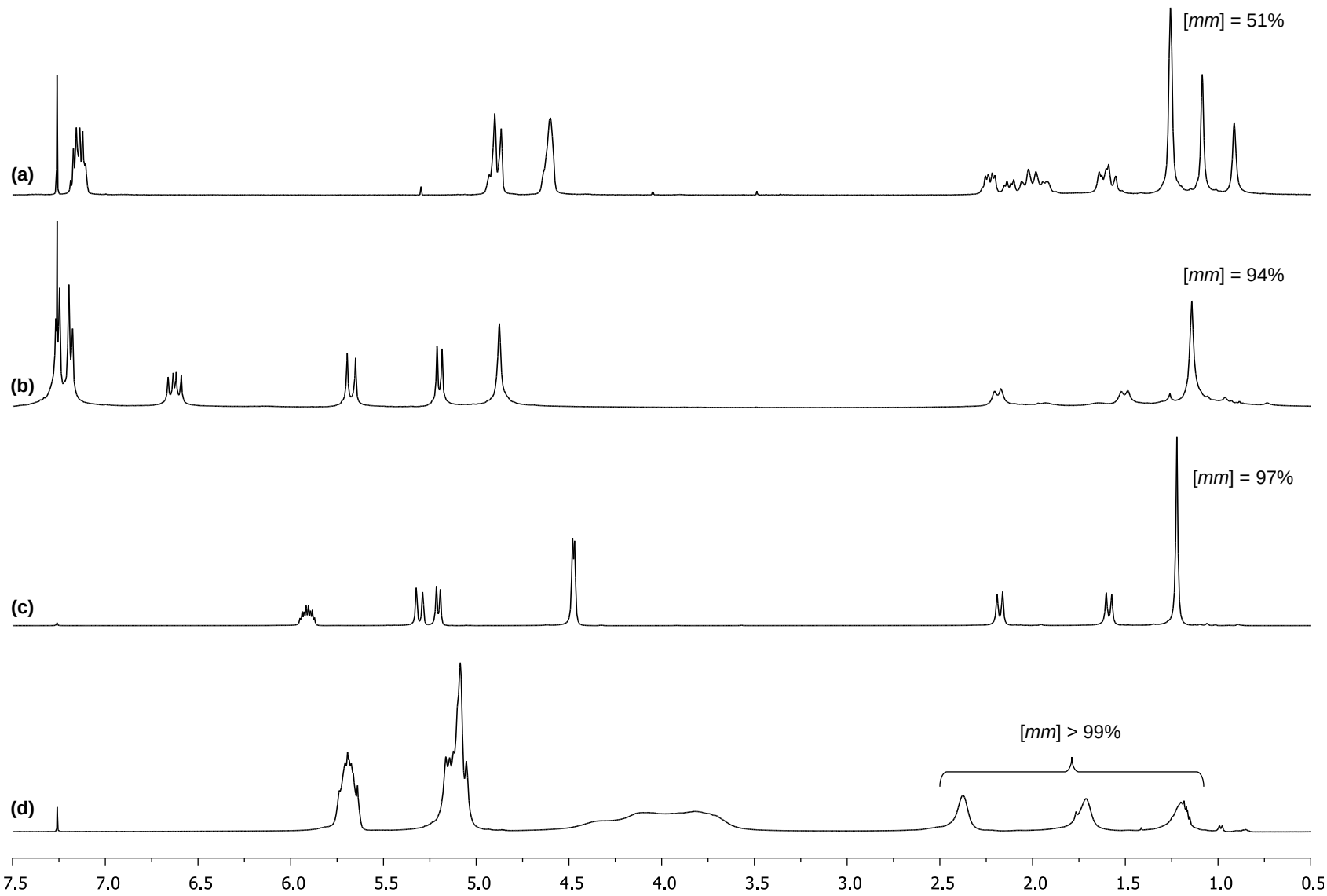

Figure S2.12. Overlay of ^{1}H NMR ($CDCl_3$, 25 °C) spectra of *it-rich*-PVMA (a), *it*-PVBM (b); highly *it*-PAMA (c); and highly *it*-PDAA (d).

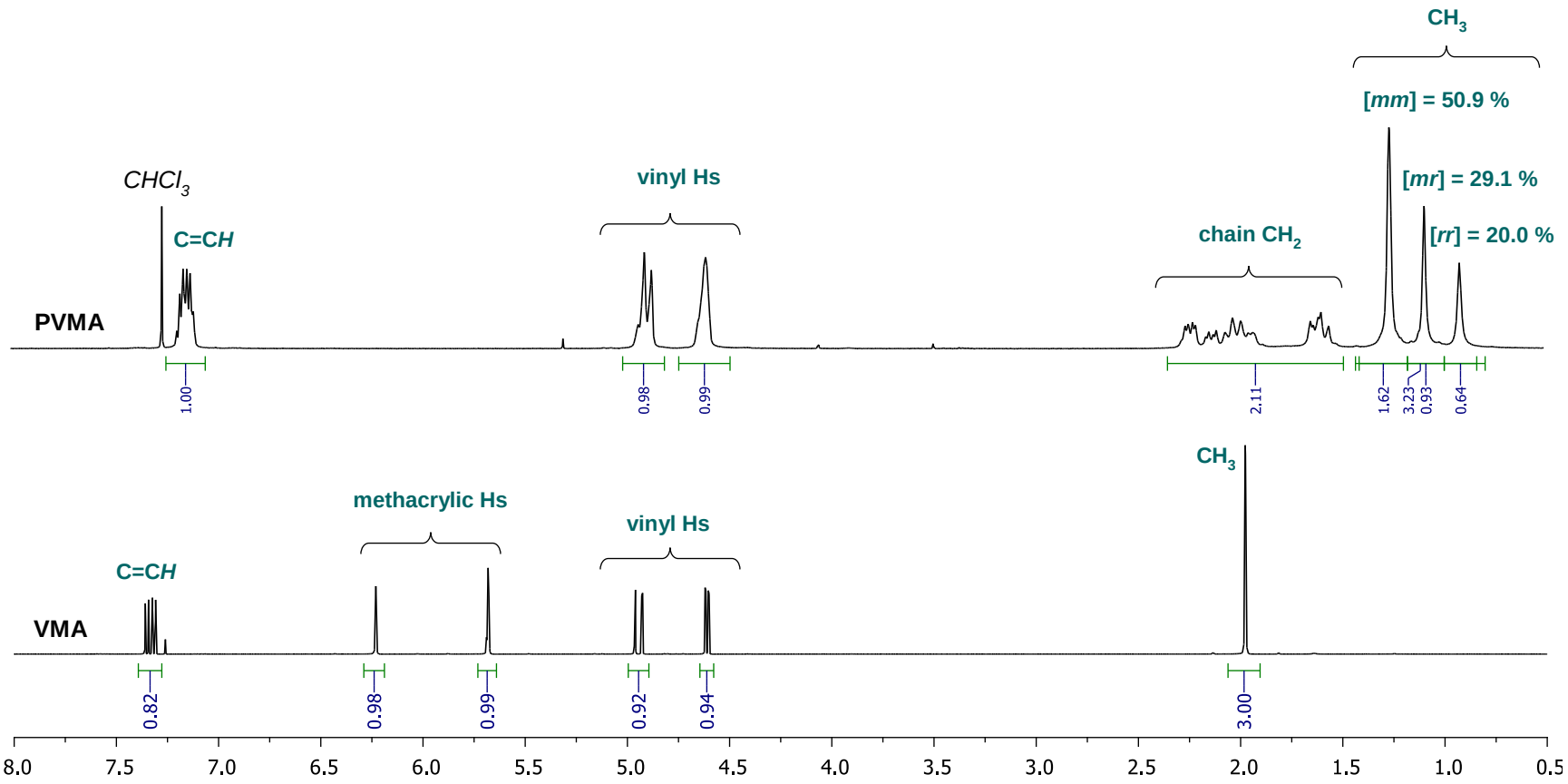

Figure S2.13. Overlay of ^{1}H NMR ($CDCl_3$) spectra of VMA and *it-rich*-PVMA.

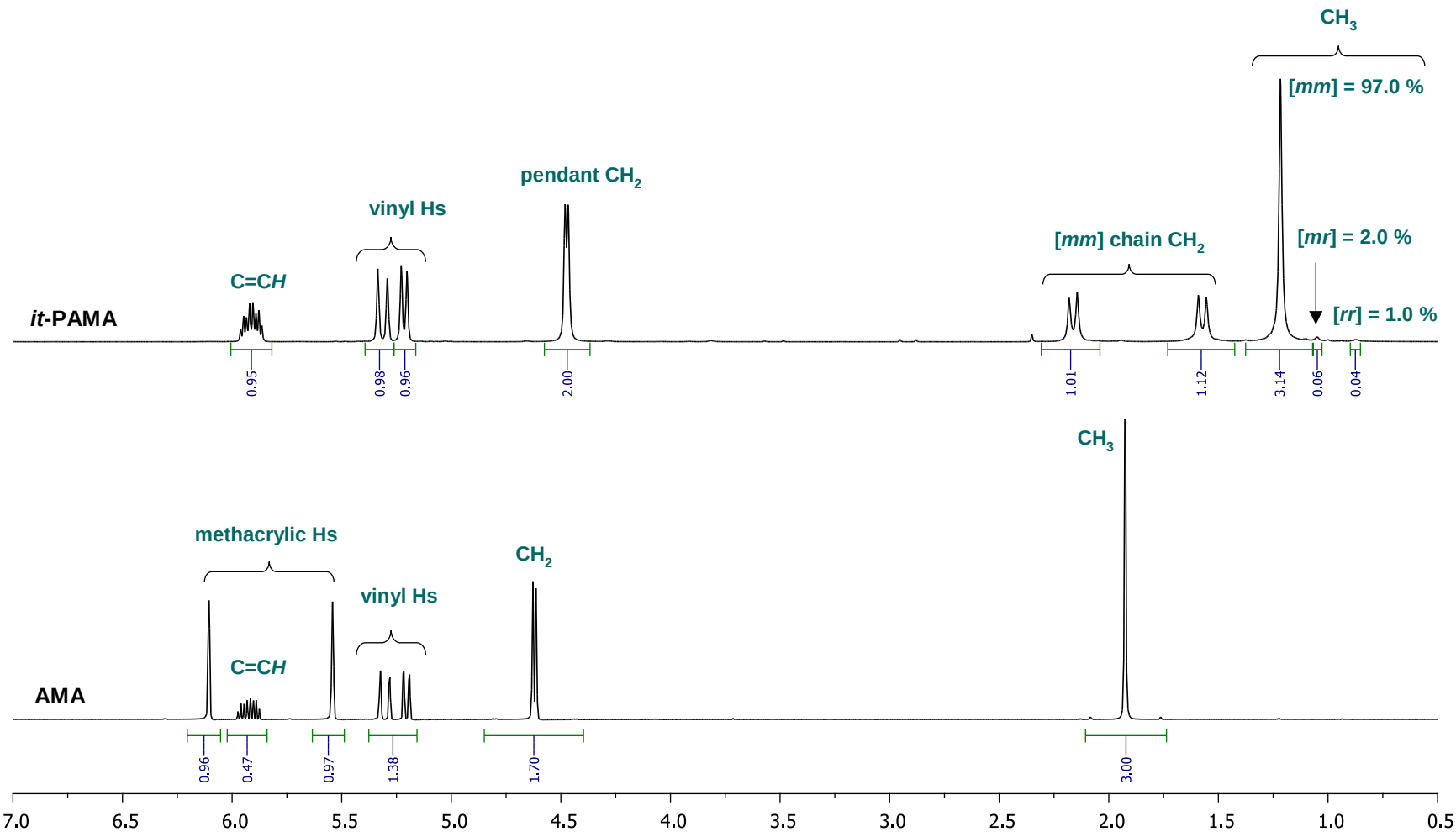

Figure S2.14. Overlay of ^{1}H NMR ($CDCl_3$) spectra of AMA and *it*-PAMA.

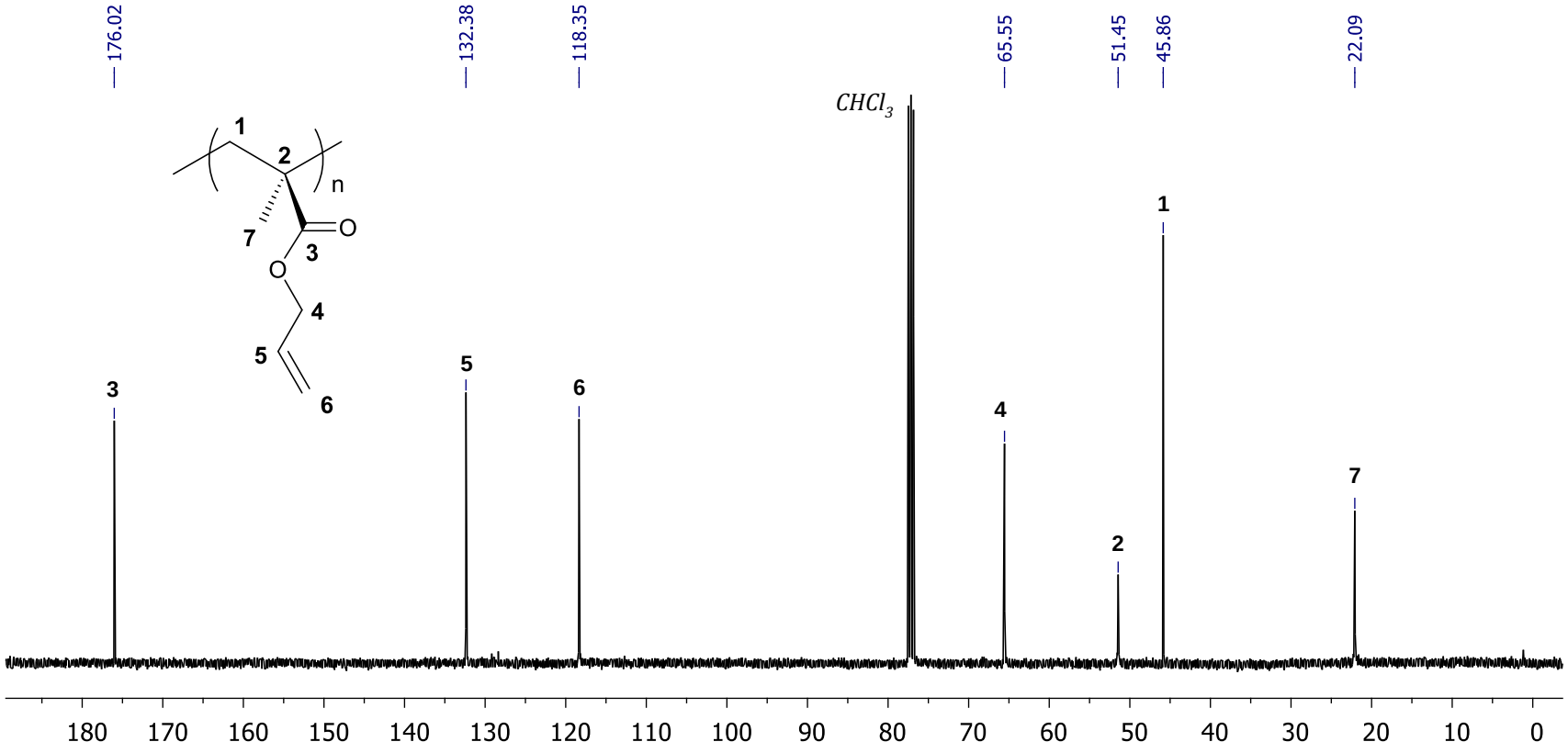

Figure S2.15. ^{13}C NMR ($CDCl_3$) spectrum of *it*-PAMA.

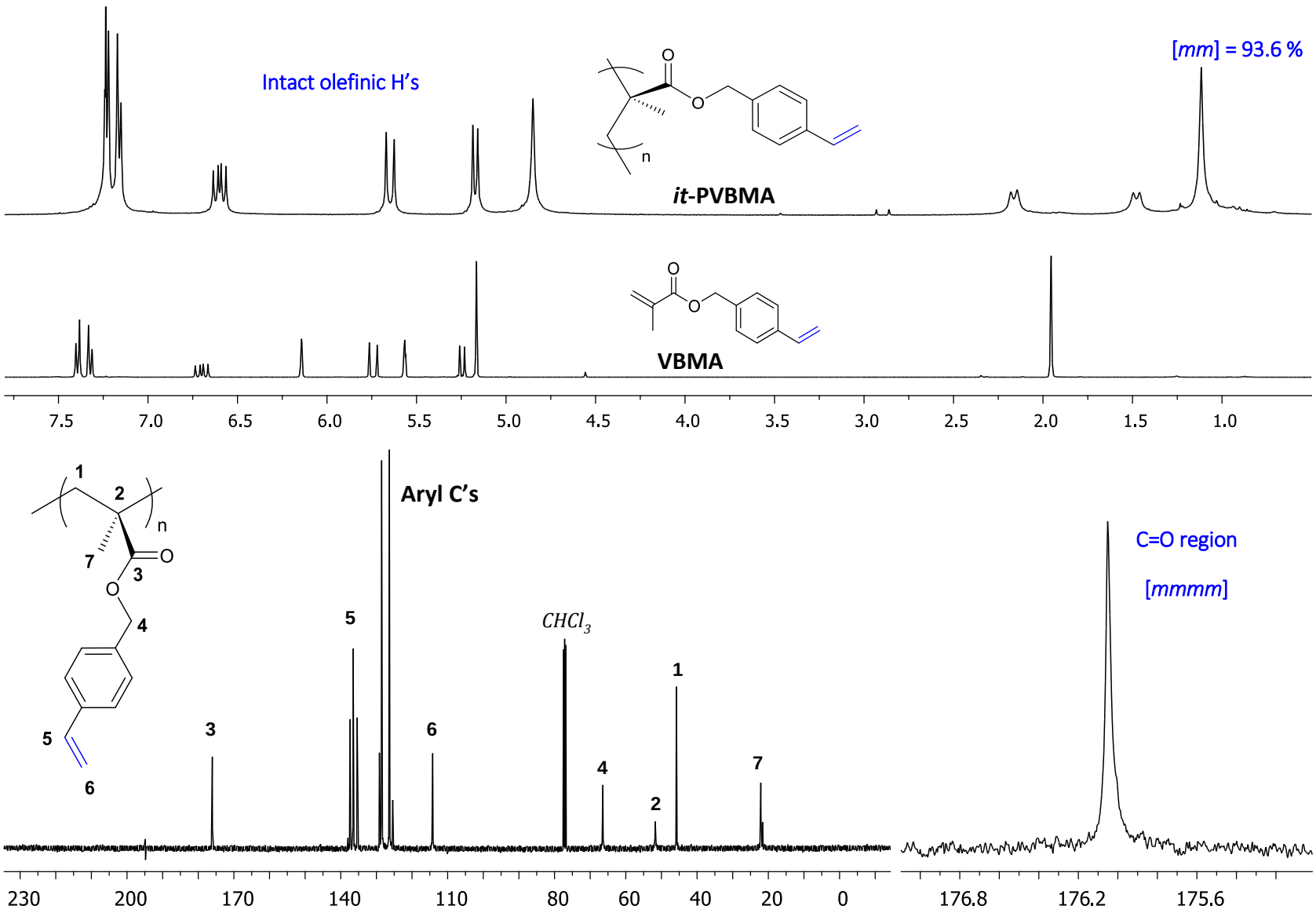

Figure S2.16. Overlay of ^{1}H NMR ($CDCl_3$) spectra of VBMA and *it*-PVBMA and ^{13}C NMR ($CDCl_3$) spectrum of *it*-PVBMA.

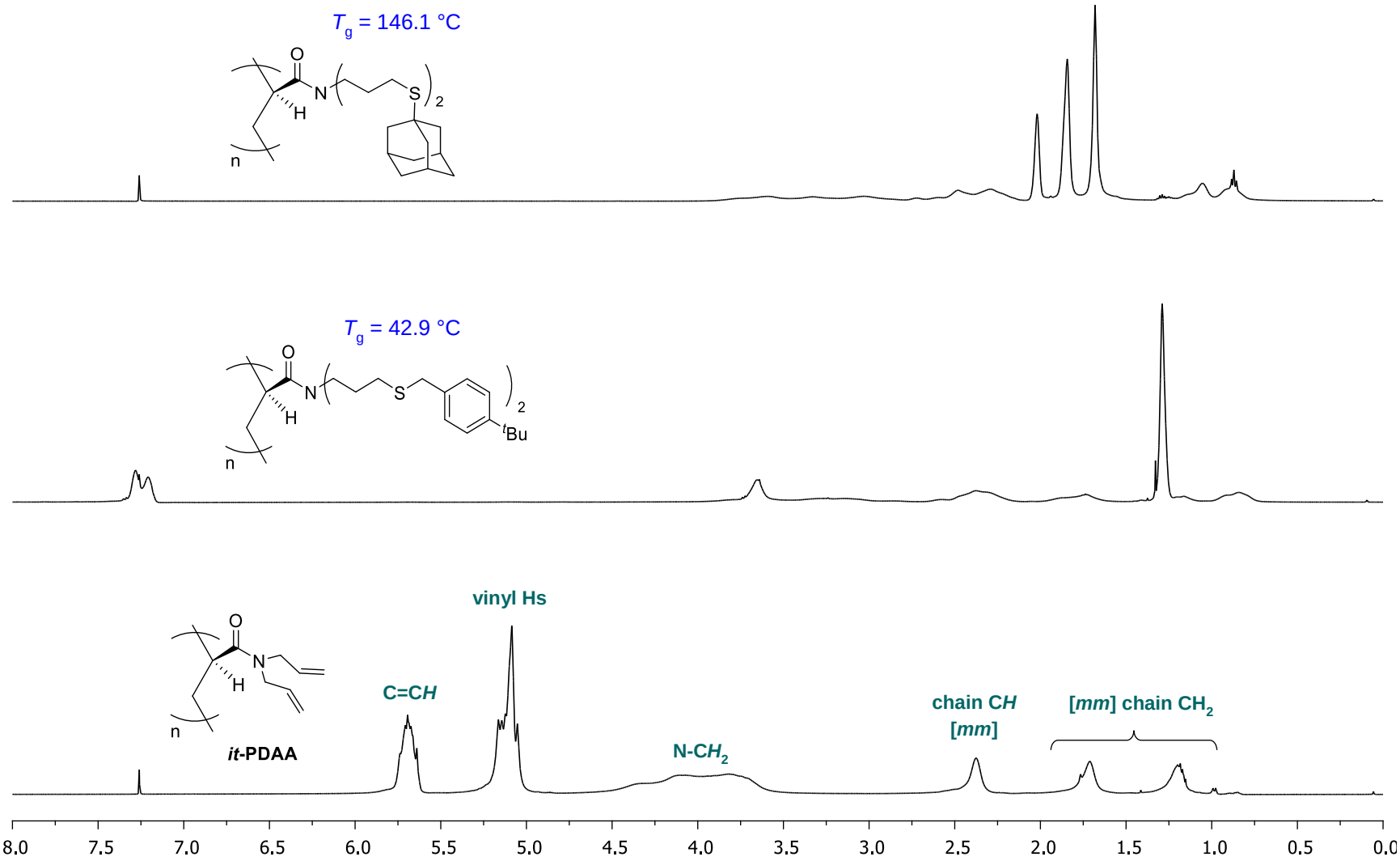

Figure S2.17. Overlay of ^{1}H NMR ($CDCl_3$, 23 °C) spectra of *it*-PDAA (bottom), *it*-PDAA-SR1 (middle), and *it*-PDAA-SR2 (top)

A.3. References

(1) (a) Mohan, Y. M.; Raghunadh, V.; Sivaram, S.; Baskaran, D. *Macromolecules* **2012**, *45*, 3387−3393. (b) Pugh, C.; Percec, V. *Polym. Bull.* **1985**, *14*, 109−116.

(2) Allen, R. D.; Long, T. E.; McGrath, J. E. *Polym. Bull.* **1986**, *15*, 127−134.

(3) Miyake, G.; Caporaso, L.; Cavallo, L.; Chen, E. Y. -X. *Macromolecules* **2009**, *42*, 1462–1471.

(4) Marechal, E.; Chaintron, G. *Bull. Soc. Chim. Fr.* **1967**, *18*, 987–991.

(5) Stehling, U.; Diebold, J.; Kirsten, R.; Röll, W.; Brintzinger, H.-H.; Jüngling, S.; Mülhaupt, R.; Langhauser, F. *Organometallics* **1994**, *13*, 964–970.

(6) (a) Ning, Y.; Caporaso, L.; Correa, A.; Gustafson, L. O.; Cavallo, L.; Chen, E. Y.-X. *Macromolecules* **2008**, *41*, 6910–6919. (b) Rodriguez-Delgado, A.; Chen, E. Y.-X. *J. Am. Chem. Soc.* **2005**, *127*, 961−974.

(7) (a) Mariott, W. R.; Rodriguez-Delgado, A.; Chen, E. Y.-X. *Macromolecules* **2006**, *39*, 1318−1327. (b) Rodriguez-Delgado, A.; Chen, E. Y.-X *Macromolecules* **2005**, *38*, 2587−2594. (c) Bolig, A. D.; Chen, E. Y.-X. *J. Am. Chem. Soc.* **2004**, *126*, 4897–4906.

(8) Sheldrick, G. *SADABS*, Bruker AXS: Madison, WI, 1997.

(9) Sheldrick, G. *SHELXTL*, 6.14; Bruker AXS: Madison, WI, 2004.

(10) Spek, A. L. *J. Appl. Crystallogr.* **2003**, *36*, 7−13.

APPENDIX B

Experimental Details and Supporting Information for Chapter 3:

B.1. Materials, Reagents, and Methods

All synthesis and manipulations with air- and moisture-sensitive chemicals and reagents were performed using standard Schlenk techniques on a dual-manifold Shlenk line or in an inert gas (Ar or N_2)-filled glovebox. NMR-scale reactions were conducted in Teflon-valve-sealed J. Young-type NMR tubes. NMR (^{1}H, ^{13}C, and ^{19}F) spectra were recorded on a Varian Inova 400 MHz or 500 MHz spectrometer. Benzene-d_6 and toluene-d_8 were dried over sodium/potassium alloy and vacuum-distilled or filtered, whereas CD_2Cl_2, and $CDCl_3$ were dried over CaH_2 and vacuum-distilled. Chemical shifts were referenced to residual undeuterated solvent resonances and are reported as parts per million relative to $SiMe_4$. HPLC-grade organic solvents were first saturated with nitrogen during filling of the 20 L solvent reservoirs and then dried by passage through activated alumina (for Et_2O, THF, and CH_2Cl_2) followed by passage through Q-5 supported copper catalyst (for toluene and hexanes) stainless steel columns.

Allyl methacrylate (AMA) and methyl methacrylate (MMA) were purchased from Alfa Aesar Chemical Co., while vinyl methacrylate (VMA) was purchased from TCI America. N,N-diallyl acrylamide (DAA) was prepared following a literature procedure.[1] The monomers were dried over activated CaH_2 overnight, followed by vacuum distillation and stored in brown bottles at −30 °C inside a glovebox freezer. MMA was further purified by titration with tri(*n*-octyl)aluminum to a yellow end point[2] followed by distillation under reduced pressure. Grubbs Catalyst (2^{nd} Gen) (tricyclohexylphosphine) (1,3-dimesityl-4,5-dihydroimidazol-2-ylidene)benzylidene ruthenium dichloride, hexamethylbenzene (HMB), 4-tert-

butylbenzylmercaptan (RSH1), and 1-adamantanethiol (RSH2) were purchased from Sigma-Aldrich. Fullerene C_{60} (powder, 99.5%) was purchased from BeanTown Chemical. 1,4-Benzenedimethanethiol (RSH3) was purchased from TCI America, 2,6-di-*tert*-butyl-4-methylphenol (BHT-H), and benzoyl peroxide (BPO) were purchased from Alfa Aesar, while 2,2-dimethoxy-2-phenylacetophenone (DMPA) was purchased from Acros Organics. BHT-H was recrystallized from hexanes prior to use while HMB was purified by sublimation, and all other commercial reagents were used as received. Tris(pentafluorophenyl)borane, $B(C_6F_5)_3$, and trityl tetrakis(pentafluorophenyl)borate, $[Ph_3C][B(C_6F_5)_4]$, were obtained as research gifts from Boulder Scientific Co.; $B(C_6F_5)_3$ was further purified by sublimation whereas $[Ph_3C][B(C_6F_5)_4]$ was used as received. The $B(C_6F_5)_3$·THF adduct was prepared by addition of THF to a toluene solution of the borane at ambient temperature, followed by removal of the volatiles and drying under vacuum. Literature procedures were employed for the preparation of the following materials or compounds: *it*-PMMA,[3] *st*-PMMA,[4] [*rac*-$C_2H_4(\eta^5$-indenyl$)_2$Zr(THF)]$^+$[OC(O^{i}Pr)=CMe$_2$][MeB$(C_6F_5)_3]^-$ (**1**),[3,5] [Ph_2C(Cp)(2,7-^{t}Bu$_2$-Flu)]Zr[OC(O^{i}Pr)=CMe$_2$]$_2$ (**2**, Cp = η^5-cyclopentadienyl; Flu = η^n-fluorenyl),[4] [Ph_2C(Cp)(Flu)]Zr [OC(O^{i}Pr)=CMe$_2$]$_2$ (**3**),[4] [Ph_2C(Cp)(Flu)]ZrMe[OC(O^{i}Pr)=CMe$_2$] (**4**),[4] and {[Ph_2C(Cp)(Flu)]Zr (THF) [OC(O^{i}Pr)=CMe$_2$]}$^+$[MeB$(C_6F_5)_3]^-$ (**5**).[4]

Isolation of {[Ph_2C(Cp)(Flu)]Zr[OC(OCH=CH$_2$)=CMeCH$_2$C(Me$_2$)C(O^{i}Pr)=O]}$^+$ [MeB$(C_6F_5)_3]^-$ (6). In an argon-filled glovebox, $B(C_6F_5)_3$ (58.0 mg, 0.113 mmol) was charged in a 20 mL vial and dissolved in 1.5 mL of CH_2Cl_2, then VMA (12.7 mg, 0.133 mmol) was added via syringe from a stock solution in CH_2Cl_2. The mixture was gently mixed to generate the $(C_6F_5)_3$B·VMA adduct and then cooled to −30 °C inside the glovebox freezer. A separate 30 mL glass reactor was charged with 71.3 mg (0.113 mmol) of the neutral mono(ester enolate) complex **4** and 8.0 mL of CH_2Cl_2; the solution was also cooled to −30 °C inside the glovebox freezer. The

two solutions were mixed rapidly via pipette to give instantaneously a dark red solution, which was allowed to reach room temperature and then stirred for 30 minutes. The volatiles were removed under vacuum and the dark red solid was washed with hexanes (3 × 6 mL). The hexanes were decanted and 129.5 mg (91.2%) of pure complex **6** was obtained as a dark red solid after drying under vacuum. Cationic complex **6** is stable in cold CH_2Cl_2 solution for up to 24 hours, allowing for in-house NMR characterizations, but its instability in solid state at ambient temperature prevented from its characterization by off-site elemental analysis.

^{1}H NMR (CD_2Cl_2, 25 °C) of **6**: δ 8.38 (d, J = 8.4 Hz, 1H, Flu), 8.26 (d, J = 8.0 Hz, 1H, Flu), 7.94 (m, 3H, Ph), 7.62–7.35 (m, 9H, Flu, Ph), 7.26 (m, 2H, Flu), 6.63 (d, J = 9.2 Hz, 1H, Flu), 6.60 (d, J = 8.8 Hz, 1H, Flu), 6.36 (q, J = 2.9 Hz, 1H, Cp), 5.94 (q, J = 2.8 Hz, 1H, Cp), 5.91 (q, J = 2.9 Hz, 1H, Cp), 5.88 (q, J = 2.6 Hz, 1H, Cp), 5.61 (dd, J_1 = 13.8 Hz, J_2 = 6.2 Hz, 1H, OC*H*=CH_2), 4.38 (d, J = 14.0 Hz, 1H, OCH=C*H*$_2$), 4.07 (d, J = 6.4 Hz, 1H, OCH=C*H*$_2$), 4.06 (sept, J = 6.2 Hz, 1H, OC*H*Me_2), 2.21 (d, J = 14.8 Hz, 1H, C*H*$_2$), 1.58 (d, J = 15.2 Hz, 1H, C*H*$_2$), 1.44 (s, 3H, =C*Me*), 1.28 (s, 3H, C*Me*$_2$), 1.19 (d, J = 6.4 Hz, 3H, OCH*Me*$_2$), 1.18 (s, 3H, C*Me*$_2$), 1.15 (d, J = 6.0 Hz, 3H, OCH*Me*$_2$), 0.48 (s, br, 3H, B*Me*). ^{19}F NMR (CD_2Cl_2, 25 °C): δ −133.14 (d, $^3J_{F–F}$ = 18.8 Hz, 6F, *o*–F), −165.31 (t, $^3J_{F–F}$ = 20.7 Hz, 3F, *p*–F), −167.89 (m, 6F, *m*–F). ^{13}C NMR (CD_2Cl_2, 0 °C): δ 191.14 ([*C*(O^{i}Pr)=O]), 154.10 ([O*C*(OCH=CH_2)=]), 145.44 (O*C*H=CH_2), 144.20, 144.16, 130.26, 130.05, 130.01, 129.99, 129.92, 129.62, 129.31, 129.12, 128.32, 127.69, 126.95, 126.81, 125.29, 124.97, 124.76, 124.48, 124.28, 123.76, 123.32, 121.96, 118.55, 117.87, 113.44, 107.85, 104.01, 84.49 (Flu, Cp and Ph carbons; broad resonances for the C_6F_5 groups due to C–F coupling omitted), 92.78 (OCH=*C*H_2), 80.78 (=*C*Me_2), 76.74 (O*C*HMe_2), 59.64 (*C*Ph_2), 46.20 (*C*Me_2), 40.42 (*C*H_2), 31.65, 24.65 (C*Me*$_2$), 21.81, 21.28 (OCH*Me*$_2$), 16.69 (=C*Me*).

Generation of {[$Ph_2C(Cp)(Flu)$]Zr[$OC(OCH_2CH{=}CH_2){=}CMeCH_2C(Me_2)C(O^iPr){=}O$]}$^+$ [$MeB(C_6F_5)_3$]$^-$ (7). In an argon-filled glovebox, $B(C_6F_5)_3$ (15.5 mg, 0.030 mmol) and AMA (3.8 mg, 0.030 mmol) were premixed in 0.3 mL of CD_2Cl_2 to generate the $(C_6F_5)_3B{\cdot}$AMA adduct *in situ*. This colorless solution was cooled to −30 °C inside the glovebox freezer and then added via pipette to a precooled (−30 °C) 4 mL vial containing **4** (18.8 mg, 0.030 mmol) in 0.3 mL of CD_2Cl_2. The solution turned instantaneously to dark red as a result of the formation of cationic complex **7**. This complex is unstable in either solid state or solution (which decomposes in less than 1 h in CH_2Cl_2), preventing from its characterization by off-site elemental analysis.

^{1}H NMR (CD_2Cl_2, 25 °C) of **7**: δ 8.37 (d, J = 8.4 Hz, 1H, Flu), 8.25 (d, J = 8.4 Hz, 1H, Flu), 7.94 (m, 3H, Ph), 7.61–7.35 (m, 9H, Flu, Ph), 7.23 (m, 2H, Flu), 6.66 (d, J = 2.4 Hz, 1H, Flu), 6.63 (d, J = 2.4 Hz, 1H, Flu), 6.46 (q, J = 3.2 Hz, 1H, Cp), 6.02 (q, J = 2.8 Hz, 1H, Cp), 5.93–5.88 (m, 2H, Cp), 5.46 (m, 1H, Cp), 5.68 (m, 1H, $OCH_2CH{=}CH_2$), 5.17–5.10 (m, 2H, $OCH_2CH{=}CH_2$), 4.10 (sept, J = 6.3 Hz, 1H, $OCHMe_2$), 3.61 (tdd, J_1 = 1.6 Hz, J_2 = 5.6 Hz, J_3 = 13.2 Hz, 1H, $OCH_2CH{=}CH_2$), 3.46 (tdd, J_1 = 1.6 Hz, J_2 = 5.4 Hz, J_3 = 13.0 Hz, 1H, $OCH_2CH{=}CH_2$),), 2.21 (d, J = 15.2 Hz, 1H, CH_2), 1.57 (d, J = 15.2 Hz, 1H, CH_2), 1.46 (s, 3H, =C*Me*), 1.28 (s, 3H, CMe_2), 1.20 (d, J = 6.4 Hz, 3H, $OCHMe_2$), 1.17 (s, 3H, CMe_2), 1.16 (d, J = 6.4 Hz, 3H, $OCHMe_2$), 0.50 (s, br, 3H, B*Me*). ^{19}F NMR (CD_2Cl_2, 25 °C): δ −133.15 (d, $^3J_{F–F}$ = 19.6 Hz, 6F, *o*–F), −165.31 (t, $^3J_{F–F}$ = 20.5 Hz, 3F, *p*–F), −167.89 (m, 6F, *m*–F).

Polymer Characterizations. Polymer number-average molecular weights (M_n) and molecular weight distributions ($Đ = M_w/M_n$) were measured by gel permeation chromatography (GPC) analyses carried out at 40 ºC and a flow rate of 1.0 mL/min, with DMF as the eluent on a Waters University 1500 GPC instrument equipped with one PLgel 5 μm guard and three PLgel 5

μm mixed-C columns (Polymer Laboratories; linear range of MW = 200–2,000,000). The instrument was calibrated with 10 PMMA standards, and chromatograms were processed with Waters Empower software (version 2002).

Glass transition temperatures (T_g) of the polymers were measured by differential scanning calorimetry (DSC) on a Q20 DSC, TA Instruments. Samples were first heated until 150–250 °C (depending on the polymer decomposition onset temperature and/or the thermal crosslinking temperature) at 10 °C min^{-1}, cooled to −50 °C at 10 °C min^{-1}, and then reheated again at 10 °C min^{-1}. All T_g values were obtained from the second heating scan, after removing the thermal history. Maximum rate decomposition temperatures (T_{max}) and decomposition onset temperatures (T_d) of the polymers were measured by thermal gravimetric analysis (TGA) on a Q50 TGA Termogravimetric Analyzer, TA Instruments. Polymer samples were heated from 20 °C to 800 °C under a nitrogen flow of 60 mL min^{-1} at a rate of 10 °C min^{-1}. Values of T_{max} were obtained from derivative (wt% °C^{-1}) vs temperature (°C), while T_d values were obtained from wt% vs temperature (°C) plots.

Storage modulus (E'), loss modulus (E''), and tan δ (E''/E') were measured by dynamic mechanical analysis (DMA) on a Q800 DMA Analyzer, TA Instruments, in a tension film mode at a maximum strain of 0.3% and a frequency of 1 Hz. The samples were heated from −60 to 250 °C at a heating rate of 3 °C min^{-1}. The T_g was calculated as the peak maxima of the tan δ curve. The tacticity of the polymers was analyzed by ^{1}H and ^{13}C NMR based on that of PMMA.[3,4] X-ray powder patterns of the polymers were obtained with a Thermo Scintag X-2 Powder X-Ray Diffractometer with Cu radiation (scan of 2θ = 2–45° with a step size of 0.02° and count time of 2 sec/step). Before analysis, specimens were grinded at room temperature until a fine white powder was obtained.

General Homopolymerization Procedures. All polymerizations were carried out either in 25-mL flame-dried Schlenk flasks interfaced to a dual-manifold Schlenk line for runs using an external temperature bath, or in 20 mL glass reactors inside a glovebox for ambient temperature (~25 °C) runs. In the polymerization by the *pre-activation* method, a predetermined amount of the pre-catalyst and an activator, $B(C_6F_5)_3$·THF or $[Ph_3C][B(C_6F_5)_4]$, in 1:1 molar ratio were premixed to cleanly generate the corresponding cationic catalyst, allowed to equilibrate at the bath temperature (for the runs interfaced to a dual-manifold Schlenk line), and followed by the rapid addition of the monomer to start the polymerization. The amount of monomer (M) was fixed for all the polymerization, whereas the amount of the catalyst (cat) was adjusted according to the [M]/[cat] ratio specified in the polymerization tables. For instance, solutions of $B(C_6F_5)_3$·THF (7.3 mg, 0.0125 mmol) and precatalyst **4** (7.9 mg, 0.0125 mmol) were premixed in 3.0 mL of CH_2Cl_2 and stirred for 5 min to cleanly generate the active specie **5**. Subsequently, 0.3 mL of VMA (2.50 mmol, $[VMA]_0/[\mathbf{5}] = 200$) was quickly added via syringe to the vigorously stirring solution, and the reaction was allowed to proceed with continuous stirring at the equilibrated temperature. Alternatively, $[Ph_3C][B(C_6F_5)_4]$ was the activator of choice for polymerizations using precatalysts **2** and **3**. The polymerization of the other monomers was performed in an identical manner. In the polymerization using the *in-reactor activation* method as indicated in the polymerization table, the monomer and the activator were premixed, followed by addition of the neutral precatalyst complex. In all the cases, after the measured time interval, a 0.1 mL aliquot was taken from the reaction mixture via syringe and quickly quenched into a 1.5 mL vial containing 0.6 mL of undried "wet" $CDCl_3$ stabilized by 250 ppm of BHT-H; the quenched aliquots were later analyzed by ^1H NMR to obtain monomer conversion data. The remaining bulk polymerization reaction was quenched after the removal of the last aliquot by addition of 5 mL of 5% HCl-acidified methanol

and precipitated into 100 mL of MeOH, except for the polymerization of DAA that was precipitated into 100 mL of hexanes (due to the solubility of *st*-PDAA in MeOH). The quenched mixture was stirred for 3 h, and the polymer produced was filtered, washed with MeOH (or hexanes for *st*-PDAA) followed by pentanes, and dried in a vacuum oven at room temperature overnight to a constant weight. The polymer products *st*-PVMA, *st*-PAMA, and *st*-PDAA were obtained as white solids.

***st*-PAMA.** ^{1}H NMR ($CDCl_3$, 25 °C): δ 5.88 (m, 1H, –OCH_2CH=CH_2), 5.32 (d, J = 17.2 Hz, 1H, – OCH_2CH=CH_2), 5.23 (d, J = 10.4 Hz, 1H, –OCH_2CH=CH_2), 4.44 (d, J = 5.2 Hz, 2H, –OCH_2CH=CH_2), 1.82 (s, 2H, CH_2, *rr*), 1.22 (s, CH_3, *mm*), 1.02 (s, CH_3, *mr*), 0.88 (s, CH_3, *rr*). ^{13}C{^{1}H} NMR ($CDCl_3$, 50 °C): 177.0 (*C*=O, *rrrr*), 131.9 (*C*H=), 118.9 (=*C*H_2), 65.7 (O*C*H_2), 54.2 (quaternary carbon, *rr*), 45.3 (main-chain *C*H_2), 17.4 (CH_3).

***st*-PVMA.** ^{1}H NMR ($CDCl_3$, 25 °C): δ 7.14 (dd, J_1 = 6.2 Hz, J_2 = 13.8 Hz, 1H, –O*CH*=CH_2), 4.91 (d, J = 14.0 Hz, 1H, – OCH=CH_2), 4.63 (d, J = 4.8 Hz, 1H, – OCH=CH_2), 1.92 (s, 2H, CH_2, *rr*), 1.27 (s, CH_3, *mm*), 1.08 (s, CH_3, *mr*), 0.94 (s, CH_3, *rr*). ^{13}C{^{1}H} NMR ($CDCl_3$, 50 °C): δ 174.3 (*C*=O, *rrrr*), 141.1 (O*C*H=), 98.9 (=*C*H_2), 53.7 (quaternary carbon, *rr*), 44.8 (main-chain *C*H_2), 17.1 (CH_3).

***st*-PDAA.** ^{1}H NMR ($CDCl_3$, 25 °C): δ 5.64 (s, br, 2H, –NCH_2CH=CH_2), 5.06 (m, br, 4H, –NCH_2CH=CH_2), 3.82 (s, br, 4H, –N*C*H_2CH=CH_2), 2.86 (s, 1H, C*H*, *rr*), 1.79 (s, 2H, CH_2, *rr*). ^{13}C{^{1}H} NMR ($CDCl_3$, 50 °C): δ 174.3 (*r*, *C*=O), 133.9 (*C*H=CH_2), 133.8 (*C*H=CH_2), 118.3 (CH=*C*H_2), 117.6 (CH=*C*H_2), 49.4, 47.3 (N*C*H_2), 36.2 (*C*H), 32.9 (*C*H_2).

General Copolymerization Procedures. For the block copolymerization of MMA with polar divinyl monomers, pre-catalyst **1** (4.6 mg, 0.0093 mmol) was activated with $B(C_6F_5)_3$·THF (5.5 mg, 0.0093 mmol) in 6.0 mL of CH_2Cl_2 in a 20 mL vial inside the glovebox. After stirring for

~ 5 minutes to cleanly generate the corresponding cationic catalyst, 400 equivalents of MMA (0.40 mL, 3.72 mmol) were added under vigorous stirring and the resulting solution was allowed to stir for 30 minutes at which point all MMA was consumed. Subsequently, 178 equivalents of the second monomer AMA (0.20 mL, 1.67 mmol), or alternatively VMA (0.20 mL, 1.66 mmol), were added and the resulting mixture was stirred for an additional 1 h at room temperature. The polymerizations were quenched by addition of 5 mL of 5% HCl-acidified methanol followed by precipitation into 100 mL of methanol, stirred for 3 h, filtered, washed with methanol followed by pentanes, and dried in a vacuum oven at room temperature overnight to a constant weight. The polymer tacticity and the molar composition of the copolymers were determined by ^{1}H NMR of the isolated polymer materials. *it*-PMMA$_{0.83}$-*b*-(*it*-PAMA$_{0.17}$: M_n = 89.6 kg/mol, $Đ$ = 1.37, [*mm*] = 93.1%; (*it*-PMMA$_{0.67}$-*b*-(*at*-PVMA$_{0.33}$: M_n = 76.8 kg/mol, $Đ$ = 1.49, total [*mm*] = 79.8%.

Random copolymerization of 400 equivalents of MMA (0.50 mL, 4.69 mmol) with 43 equivalents of AMA (0.06 mL, 0.502 mmol) was performed in a 20 mL vial inside the glovebox by premixing both monomers in 4.5 mL of CH_2Cl_2 with a predetermined amount of activator $B(C_6F_5)_3$·THF (6.8 mg, 0.0117 mmol). Pre-catalyst **1** (5.8 mg, 0.0117 mmol) was dissolved in 0.5 mL of CH_2Cl_2 and then added to the above vigorously stirred solution mixture. The polymerization reaction was allowed to stir at room temperature for 4 h, after which the polymerization was quenched by addition of 5 mL of 5% HCl-acidified methanol followed by precipitation into 100 mL of methanol, stirred for 3 h, filtered, washed with methanol followed by pentanes, and dried in a vacuum oven at room temperature overnight. The polymer tacticity and the molar composition of the copolymer were determined by ^{1}H NMR of the isolated polymer material. (*it*-PMMA$_{0.88}$-*ran*-(*it*-PAMA$_{0.12}$: M_n = 156 kg/mol, $Đ$ = 1.83, [*mm*] = 95.9%.

Polymerization Kinetics. Experiments on polymerization kinetics were carried out in 20 mL glass reactors inside the glovebox at ambient temperature (~23 °C) using the in-reactor activation method similar to that already described above. First, a predetermined amount of $B(C_6F_5)_3$ (equal molar to the catalyst precursor) was premixed with fixed quantities of VMA (0.4 mL, 3.33 mmol) and hexamethylbenzene (100 mg, 0.62 mmol) as an internal standard (IS) in 3.0 mL of CH_2Cl_2. At this point, a 0.1 mL aliquot was withdrawn from this mixture and injected into a 1.5 mL septum cap sealed vial containing 1.0 mL of undried "wet" MeOH; this sample corresponded to the initial ratio of VMA to IS, $\mathbf{r}_0$, at $t = 0$. Subsequently, the polymerization was started by rapid addition of a solution of pre-catalyst **4** so the total volume of the reaction was 4.0 mL. At appropriate time intervals, 0.1 mL aliquots were withdrawn from the reaction mixture using a syringe and quickly quenched into 1.5 septum cap sealed vials containing 1.0 mL of undried "wet" MeOH; these samples corresponded to the VMA to IS ratio, $\mathbf{r}_t$, at any given time t = n. The quenched aliquots were filtered (0.45 μm pore size nylon filters) to remove the precipitated polymer and then analyzed by an Agilent 1260 Infinity HPLC system equipped with an Agilent Eclipse Plus C18 Column (100 × 4.6 mm; 5:95 water/methanol; 1.0 mL/min, 30 °C) with a UV detector (270 nm) to determine the monomer conversion data. Specifically, the ratio of VMA to IS was determined by the integration of the peaks for VMA ($\mathbf{A}_{VMA}$, retention time = 1.38 min) and IS ($\mathbf{A}_{IS}$, retention time = 3.03 min), so $\mathbf{r}_0 = \mathbf{A}_{VMA(t=0)}/\mathbf{A}_{IS(t=0)}$ and $\mathbf{r}_t = \mathbf{A}_{VMA(t=n)}/\mathbf{A}_{IS(t=n)}$ (Figure S1). The percent of the unreacted VMA can be calculated as $[VMA]_t = (\mathbf{r}_t/\mathbf{r}_0) \times 100$, where $\mathbf{r}_0$ is the initial ratio of VMA to IS and $\mathbf{r}_t$ is the ratio of VMA to IS at any given time. Apparent rate constants (k_{app}) were extracted by linearly fitting a line to the plot of $\ln([VMA]_0/[VMA]_t)$ vs time t.

Post-Functionalization by the Thiol-Ene "Click" Reaction. In a typical reaction, an isolated polymer sample (60 mg) was dissolved in 10 mL of degassed chloroform inside an Ar-filled glovebox. This diluted solution was filtered through a plastic frit (0.45 μm pore size) to eliminate any possible undissolved polymer particles, and charged in a 20 mL glass vial containing a magnetic stirrer, 0.2 equiv of radical photoinitiator (DMPA), and 5 equiv of a thiol (RSH). The reactor was capped, taken out of the glovebox, and placed inside a photoreactor (Luzchem, LZC-4 photoreactor with a horizontal UVA lamp configuration, radiation centered at 350 nm) where it was stirred at room temperature for 2 h. At this point, 0.1 mL of the solution was withdrawn and quenched into a 1.5 mL vial containing 0.6 mL of $CDCl_3$ for conversion quantification by ^1H NMR. The remaining mixture was slowly precipitated into either 100 mL of hexanes (for polymers functionalized with RSH1) or 100 mL of methanol (for polymers functionalized with RSH2) to avoid trapping the excess thiol in the polymer matrix. After stirring overnight, the product was filtered, washed with hexanes (or methanol), and dried in a vacuum oven at 50 °C to a constant weight. The resulting thiolated polymer products were analyzed by GPC and NMR.

***st*-PVMA-SR1:** M_n = 285 kg/mol, $Đ$ = 24.9. ^1H NMR ($CDCl_3$, 25 °C): δ 7.32 (d, J = 6.8 Hz, 2H, Ar H), 7.21 (d, J = 6.8 Hz, 2H, Ar H), 4.06 (s, 2H, OCH_2CH$_2$S), 3.69 (s, 2H, SCH_2Ar), 2.63 (s, 2H, OCH$_2$CH_2S), 1.88 (s, 2H, CH$_2$, *rr*), 1.30 (s, 9H, ^{t}Bu), 0.97 (s, 3H, CH$_3$, *rr*). $^{13}C\{^1H\}$ NMR ($CDCl_3$, 25 °C): δ 177.2 (*C*OO), 150.1, 134.9, 128.9, 125.8 (*C*-aryl), 64.0 (O*C*H$_2$CH$_2$S), 54.1 (quaternary carbon, *rr*), 45.1 (main-chain *C*H$_2$), 36.0 (S*C*H$_2$Ar), 34.6 (*C*(CH$_3$)$_3$), 31.6 (C(*C*H$_3$)$_3$), 29.5 (OCH$_2$*C*H$_2$S), 17.6 (CH$_3$).

***st*-PVMA-SR2:** M_n = 104 kg/mol, $Đ$ = 18.6. ^1H NMR ($CDCl_3$, 25 °C): δ 4.02 (s, 2H, OCH_2CH$_2$S), 2.70 (s, 2H, OCH$_2$CH_2S), 2.06 (b, 3H, C*H*-adamantane), 1.84 (s, br, 8H, CH_2-adamantane, CH$_2$, *rr*), 1.69 (s, br, 6H, CH_2-adamantane), 0.90 (s, 3H, CH$_3$, *rr*). $^{13}C\{^1H\}$ NMR

($CDCl_3$, 25 °C): δ 177.1 (*C*OO), 65.1 (O*C*$H_2$$CH_2$S), 54.2 (quaternary carbon, *rr*), 45.1 (S*C*-adamantane), 44.7 (main-chain *C*H_2), 43.7 (*C*H-adamantane), 36.4 (*C*H_2-adamantane), 29.7 (*C*H_2-adamantane), 24.1 (OCH$_2$*C*H_2S), 17.1 (CH_3).

***st*-PDAA-SR1:** M_n = 1077 kg/mol, $Đ$ = 11.5. ^{1}H NMR ($CDCl_3$, 25 °C): δ 7.27 (s, br, 4H, Ar H), 7.20 (s, br, 4H, Ar H), 3.60 (s, br, 8H, NC*H*$_2$$CH_2$, SC*H*$_2$Ph), 3.20 (s, br, 4H, SC*H*$_2$$CH_2$), 2.63 (s, 1H, main-chain C*H*, *rr*), 2.41 (s, br, 4H, NCH$_2$C*H*$_2$), 1.27, (s, 18H, ^{t}Bu), 0.90 (s, br, 2H, main-chain C*H*$_2$, *rr*). ^{13}C{^{1}H} NMR ($CDCl_3$, 25 °C): δ 173.2 (*C*ON), 149.9, 135.2, 128.6, 125.5 (*C*-aryl), 53.6, 49.6 (N*C*H$_2$$CH_2$), 36.5 (*C*H), 36.1 (S*C*H$_2$Ar), 34.6 (*C*(CH$_3$)$_3$), 31.5 (C(*C*H$_3$)$_3$), 30.3 (S*C*H$_2$). (NCH$_2$*C*H_2 and main-chain *C*H_2 unresolved tetrads are obscured in the spectrum and not included).

***st*-PDAA-SR2:** M_n = 38.0 Kkg/mol, $Đ$ = 4.01. ^{1}H NMR ($CDCl_3$, 25 °C): δ 3.60-2.29 (m, br, 12H, NC*H*$_2$$CH_2$, SC*H*$_2$$CH_2$, NCH$_2$C*H*$_2$), 2.76 (s, main-chain C*H*, *rr*), 2.02 (s, br, 3H, C*H*-adamantane), 1.84 (s, br, 6H, C*H*$_2$-adamantane), 1.68 (s, br, 6H, C*H*$_2$-adamantane), 0.98 (s, br, 1H, chain C*H*$_2$, *rr*). ^{13}C{^{1}H} NMR ($CDCl_3$, 25 °C): δ 173.2 (*C*ON), 53.6, 49.6 (N*C*H$_2$$CH_2$), 44.3 (S*C*-adamantane), 47.7 (main-chain *C*H_2), 43.6 (*C*H-adamantane), 36.5 (*C*H_2-adamantane), 35.9 (*C*H), 30.2 (S*C*H$_2$), 29.8 (*C*H_2-adamantane), 24.4 (NCH$_2$*C*H_2).

Solvent Casting into Thin Films and Photocuring. Thin films made with *st*-PVMA or *st*-PDAA were solvent-casted from concentrated polymer solutions in acetone (50–60 mg mL^{-1}). The polymers solutions were first filtered through a plastic frit (0.45 μm pore size nylon filter) and then transferred into PTFE molds (2 × 0.5 inches) with a syringe. Each solution (~1 mL) was allowed to slowly evaporate for at least 1 hour at room temperature and in the dark, after which a translucent and colorless film was obtained. Alternatively, crosslinked films made by photocuring included 2 wt% of DMPA and different molar % of a crosslinker (1,4-benzenedimethanethiol,

RSH3) into the filtered solution of polymer. The thin films were placed in the photoreactor chamber (Luzchem, LZC-4 photoreactor with top-irradiation configuration, UVA lamps centered at 350 nm) and irradiated for 10 minutes.

PMMA Stereocomplexation and Stereocomplex Photo-crosslinking Procedure. Stereocomplexes of *it*-PMMA with *st*-PAMA or *st*-PVMA were prepared from mixtures of isotactic and syndiotactic polymers in 1:1 and 1:2 molar ratios (approximately 60 mg total). The solid polymer samples were dissolved in acetone or toluene (10 mg mL^{-1}), and the mixtures were stirred at 40 °C until all components dissolved (5-10 min), filtered through a plastic frit (0.45 μm pore size nylon filter), and allowed to evaporate slowly and undisturbed for 3-7 days. The obtained solid was collected and tested for thermomechanical properties. A sample for X-ray powder diffraction analysis was grinded at room temperature until a fine white powder was obtained. Stereocomplex samples for DMA analysis were casted from concentrated solutions in acetone as described above for *st*-PVMA and *st*-PDAA.

The stereocomplex photo-crosslinking procedure was as follows. Samples of *it*-PMMA (fixed to 10 mg) and a syndiotactic polymer (*st*-PVMA or *st*-PAMA, the mass was adjusted according to the molar ratio) were charged in a 20 mL glass vial pre-loaded with 2 wt% of DMPA (radical initiator, 0.4 or 0.6 mg) and 2 mg of hexamethylbenzene as an internal standard (IS). Then, 2.5 mL of acetone was added and the mixture was stirred at 40 °C until all components dissolved (5-10 min). The resulting clear solution was filtrated through a plastic frit (0.45 μm pore size nylon filter) with a syringe to remove any undissolved particle (the mixture of *it*-PMMA and *st*-PAMA quickly gelled when it reached room temperature so filtration was performed quickly with the hot solution). A 0.2 mL aliquot was withdrawn at this point, charged into a 1.5 dram vial, and its solvent was removed with a rotavap. The white residue was redissolved in 0.5 mL of $CDCl_3$ and

analyzed by ^{1}H NMR; this sample corresponded to the initial ratio of polymer to IS, $\boldsymbol{r}_0$. Specifically, the ratio of polymer to IS was determined by the integration of the peak area for *st*-PVMA (7.15 ppm, OC*H*=CH_2, $\boldsymbol{A}_{PVMA}$), *st*-PAMA (4.47 ppm, OCH_2CH=CH_2, $\boldsymbol{A}_{PVMA}$), *it*-PMMA (3.60 ppm, –CH_3, $\boldsymbol{A}_{PVMA}$), and IS (2.23 ppm, –CH_3, $\boldsymbol{A}_{IS}$), for example, $\boldsymbol{r}_0 = \boldsymbol{A}_{PVMA}/\boldsymbol{A}_{IS}$ corresponds to the initial ratio of *st*-PVMA to IS. Subsequently, the rest of the polymer solution was let to evaporate undisturbed and in the dark overnight until a colorless film was obtained (note that the internal standard precipitated separately from the polymer matrix). The vial was placed in the chamber of the UV reactor (Luzchem, top and side irradiation mode) and irradiated (wavelength = 350 nm) for 2 h to obtain a photocrosslinked stereocomplex. Finally, 2 mL of chloroform (non-complexing solvent) was added to the vial containing the photocured material and gently stirred in a mechanical shaker for 24 h at 40 °C. After this time, a 0.2 mL aliquot was withdrawn, treated similarly as described above and the residue analyzed also by ^{1}H NMR; this sample corresponded to the final ratio of polymer to IS, $\boldsymbol{r}_f$, where for instance $\boldsymbol{r}_f = \boldsymbol{A}_{PVMA}/\boldsymbol{A}_{IS}$ corresponds to the final ratio of *st*-PVMA to IS. The percentage of crosslinked *st*-PVMA and *st*-PAMA was calculated as:

$$\text{Crosslinked vinyl polymer (\%)} = \left[1 - \frac{\boldsymbol{r}_f}{\boldsymbol{r}_0}\right] \times 100$$

while the percentage of trapped PMMA in the crosslinked stereocomplex was also calculated as,

$$\text{Trapped PMMA (\%)} = \left[1 - \frac{\boldsymbol{r}_f}{\boldsymbol{r}_0}\right] \times 100$$

The PMMA content expressed as weight percentage (wt%) in the crosslinked stereocomplex was calculated as:

$$\text{PMMA content (wt\%)} = \left\{\frac{(10\text{ mg}) \times (\%\text{ trapped PMMA})}{[(10\text{ mg}) \times (\%\text{ trapped PMMA})] + [(\text{mg}) \times (\%\text{ crosslinked vinyl. polym.})]}\right\} \times 100$$

Finally, the PMMA encapsulation efficiency describes the percentage of the experimental PMMA content (wt%) *vs* the theoretical PMMA content (wt%) in the crosslinked stereocomplex if all the initial PMMA was effectively trapped:

$$\text{PMMA encapsulation efficiency (\%)} = \left\{\frac{\text{experimental PMMA content (wt\%)}}{\text{theoretical PMMA content (wt\%)}}\right\} \times 100$$

Fullerene C_{60} Encapsulation with *st*-PAMA. Samples of *st*-PAMA (M_n = 39.9 kg/mol, $Đ$ = 1.45, [*rr*] = 91.8%), either 10.0, 20.0, or 40.0 mg according to the concentrations described in the table, were dissolved in fullerene C_{60} stock solutions prepared in toluene (1.0 and 2.0 mg.mL^{-1}), or toluene/1,2-dichlorobenzene mixture in 50:50 vol % (10.0 mg.mL^{-1}). The mixtures were gently shaken at room temperature until the polymer material dissolved (no gelation of the solution occurred). The solutions were filtered through a plastic frit (0.45 μm pore size nylon filter) and then transferred into open 20 mL glass vials, which were left to completely evaporate undisturbed inside the fume hood with a dynamic overhead airflow. A dark brown film was obtained and subsequently analyzed by DSC and TGA.

Crosslinking of *ic*-PAMA-C_{60} Inclusion Complex *via* Olefin Metathesis. A 20 mL vial was loaded with a sample of *st*-PAMA (20 mg, M_n = 39.9 kg/mol, $Đ$ = 1.45, [*rr*] = 91.8%), 2 mol% of 2nd Gen. Grubbs catalyst (2.69 mg), and 2 mL of fullerene C_{60} solution (1.0, 2.0 or 10.0 mg mL^{-1}). The mixture was shaken in a shaker at room temperature for 2 h, after which no gelation or precipitation occurred. The vial was removed from the shaker, uncapped and left to slowly evaporate undisturbed inside the fume hood with a dynamic overhead airflow. A dark brown solid was obtained that was no longer soluble in toluene. The solid was washed with toluene (4 × 3 mL), and each washing cycle consisted of stirring for 1 h at room temperature, followed by careful decantation of the supernatant liquid. Finally, the washed crosslinked inclusion complex was dried in a vacuum oven at 50 °C to a constant weight. Control experiments were performed as described

above in 2.0 mL of toluene with no C_{60}. All solid samples were analyzed by TGA to calculate the encapsulated and trapped C_{60} inside the crosslinked network polymer.

B.2. Additional Figures and Tables

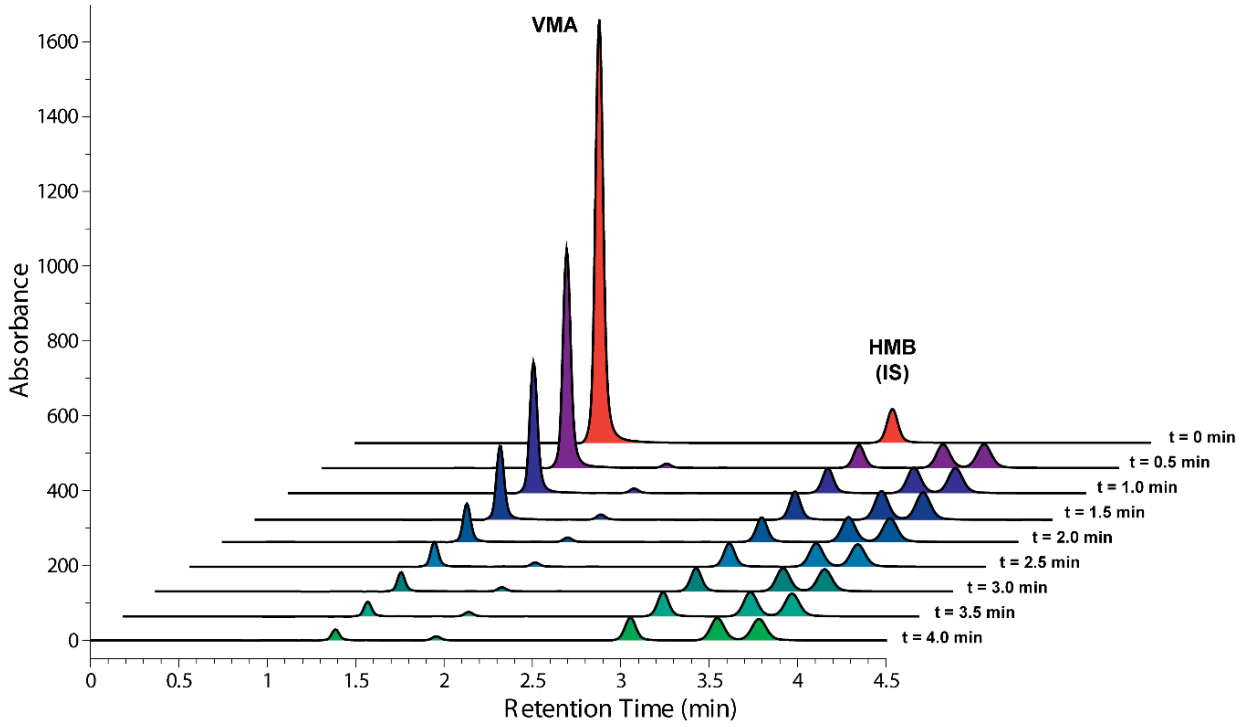

Figure S3.1. Typical set of HPLC chromatograms for the kinetic studies of the VMA polymerization by catalyst **5**.

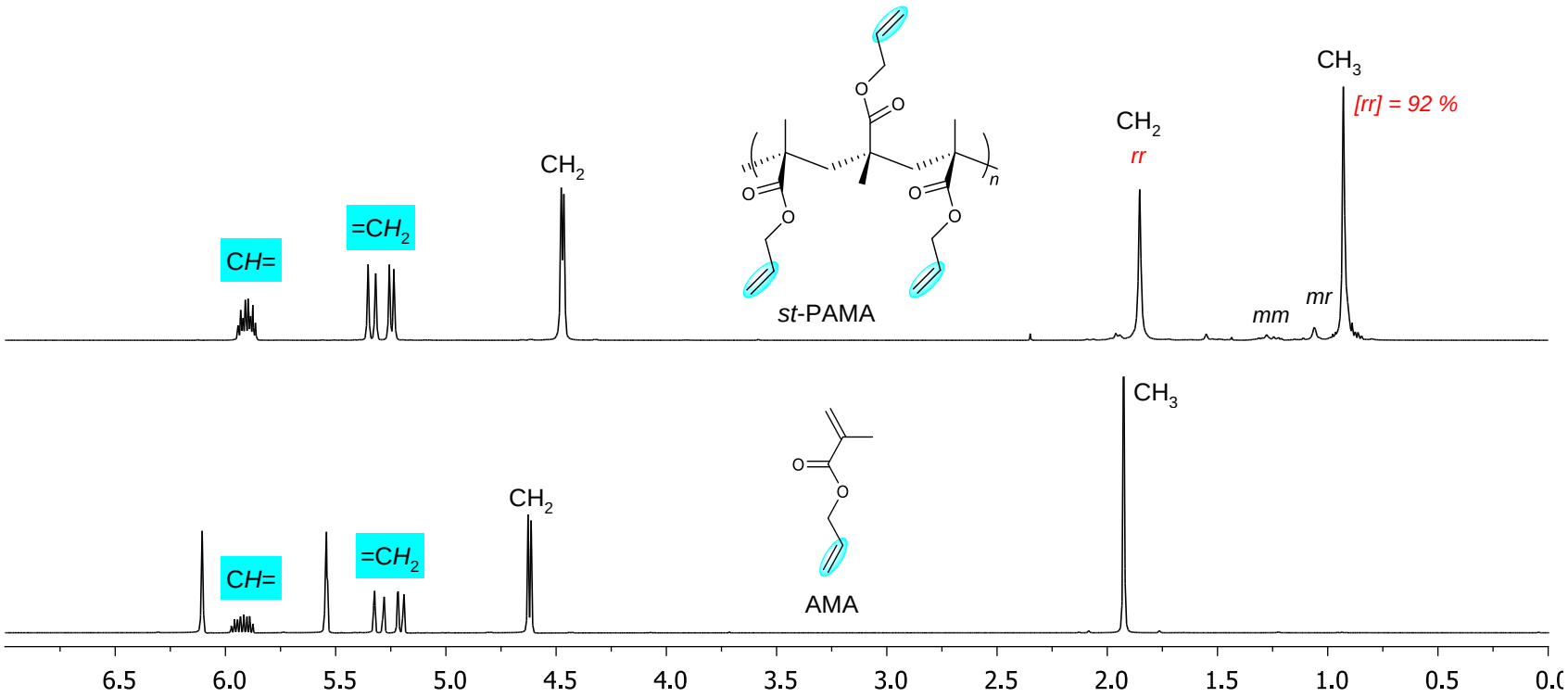

Figure S3.2. Overlay of ^{1}H NMR ($CDCl_3$, 25 °C) spectra of the monomer AMA (bottom) and the polymer *st*-PAMA (top).

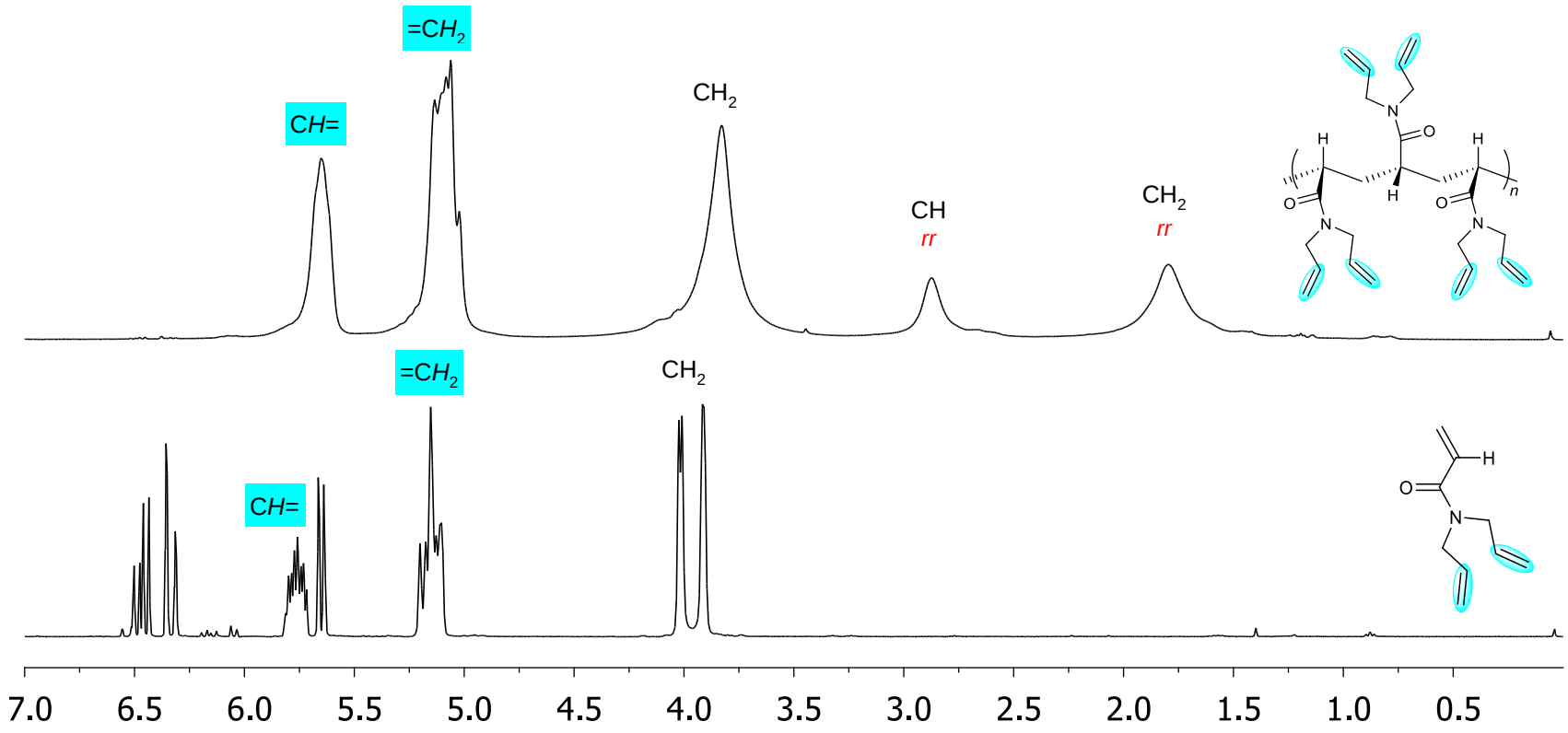

Figure S3.3. Overlay of ^{1}H NMR ($CDCl_3$, 25 °C) spectra of the monomer DAA (bottom) and the polymer *st*-PDAA (top).

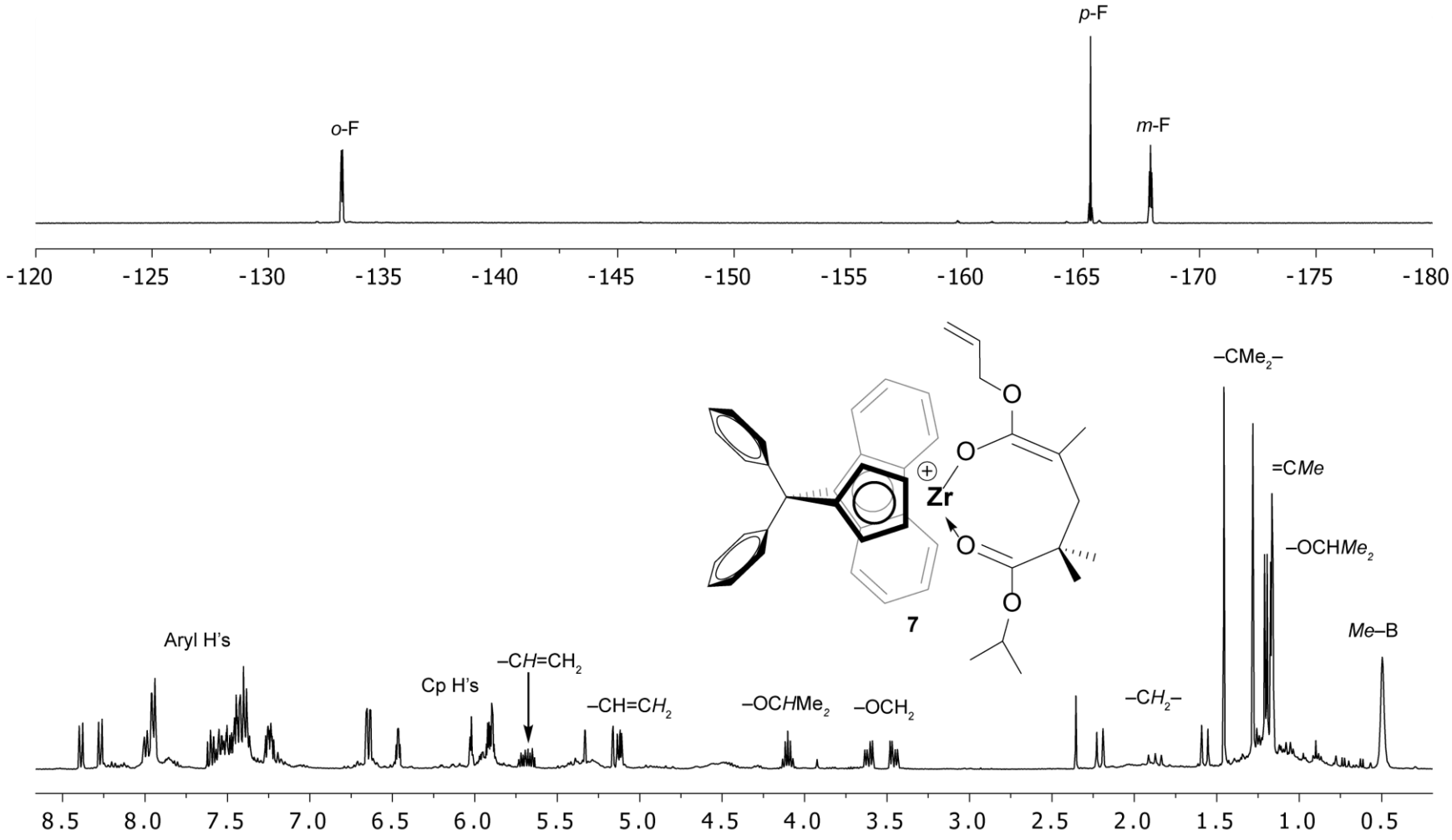

Figure S3.4. ^{1}H (bottom) and ^{19}F NMR (top) spectra (CD_2Cl_2, 25 °C) of *in situ* generated **7** (thermally unstable).

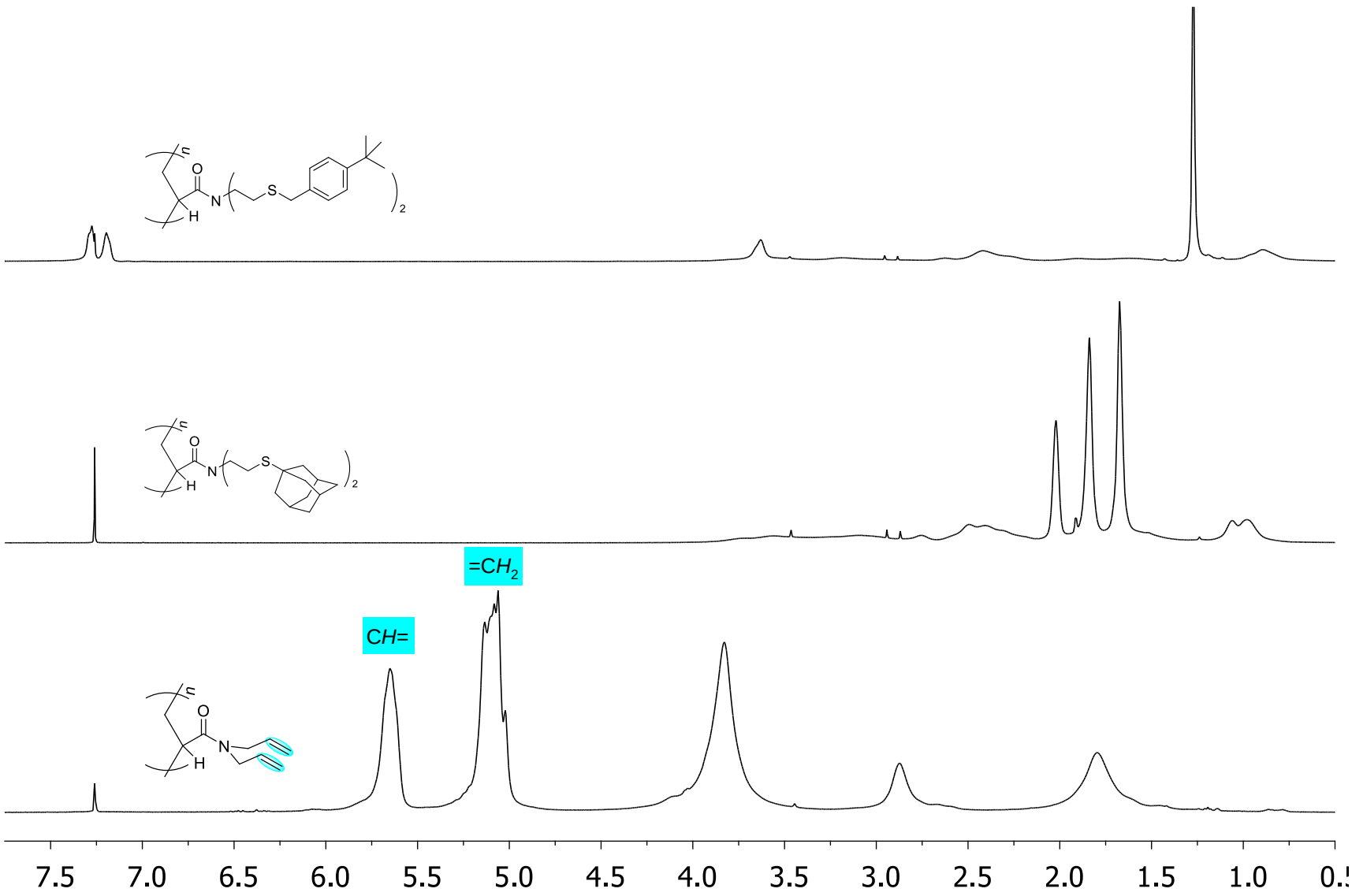

Figure S3.5. Overlay of ^{1}H NMR ($CDCl_3$, 25 °C) spectra of *st*-PDAA (bottom), *st*-PDAA-SR1 (top), and *st*-PDAA-SR2 (middle).

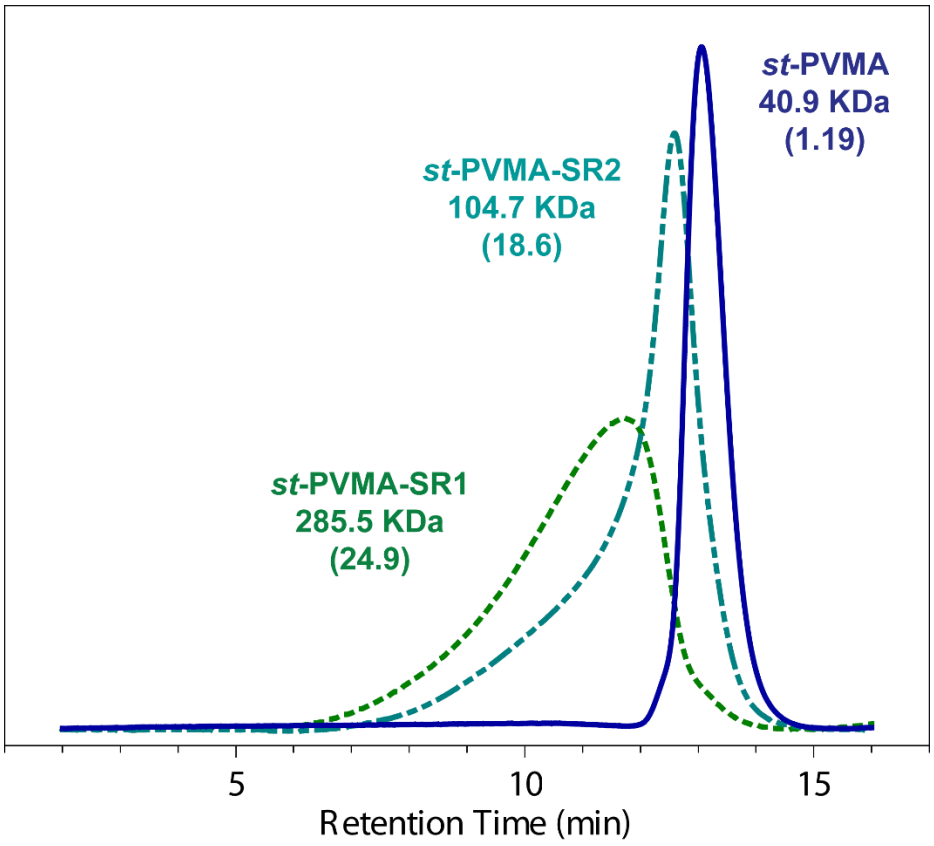

Figure S3.6. GPC traces of *st*-PVMA, *st*-PVMA-SR1, and *st*-PVMA-SR2 and associated M_n and $Đ$ values.

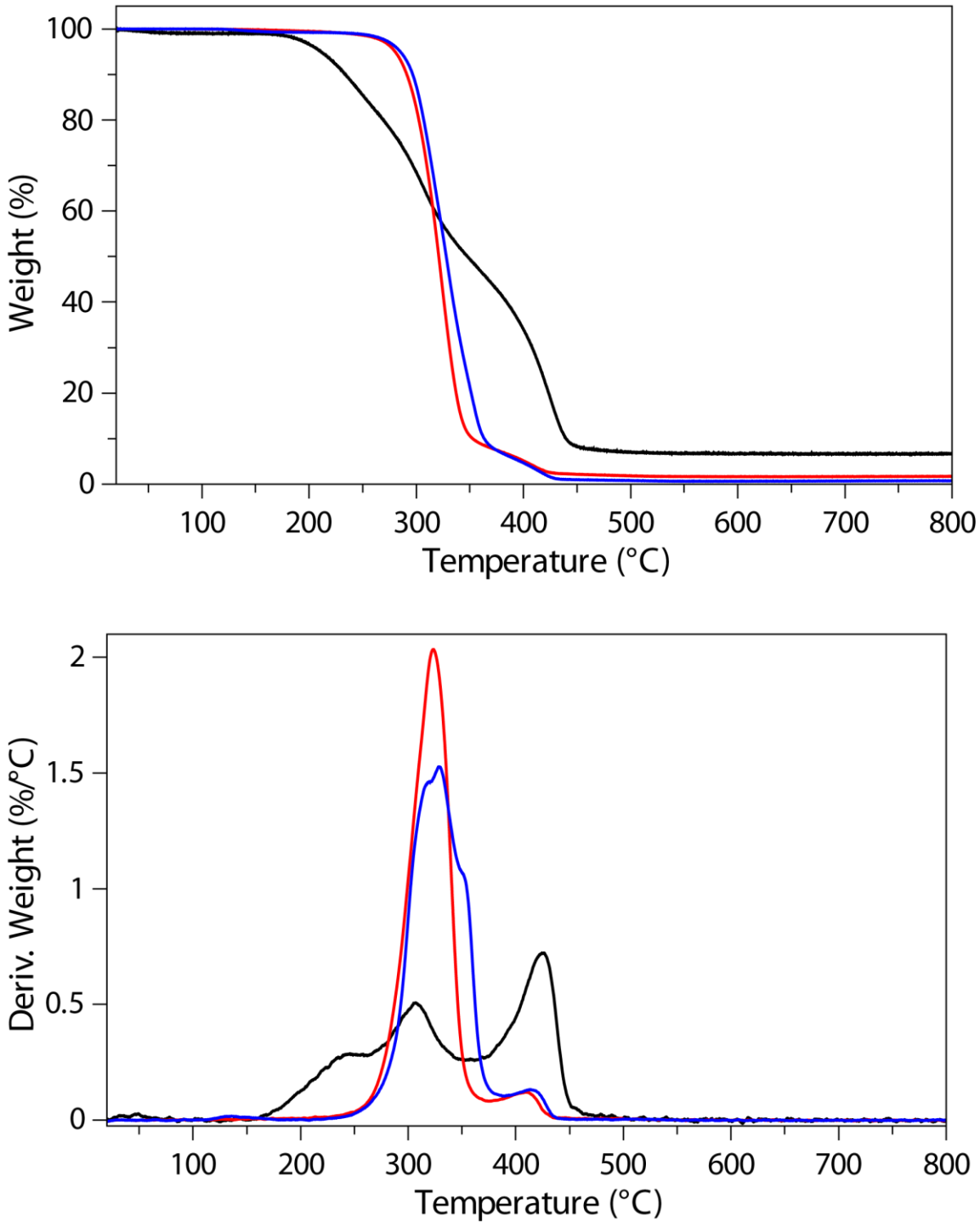

Figure S3.7. TGA (10 °C/min) traces of *st*-PVMA (solid black), *st*-PVMA-SR1 (red), *st*-PVMA-SR2 (blue). Top plot: weight (wt %) vs temperature (°C); bottom plot: derivative (wt % $°C^{-1}$) vs temperature (°C).

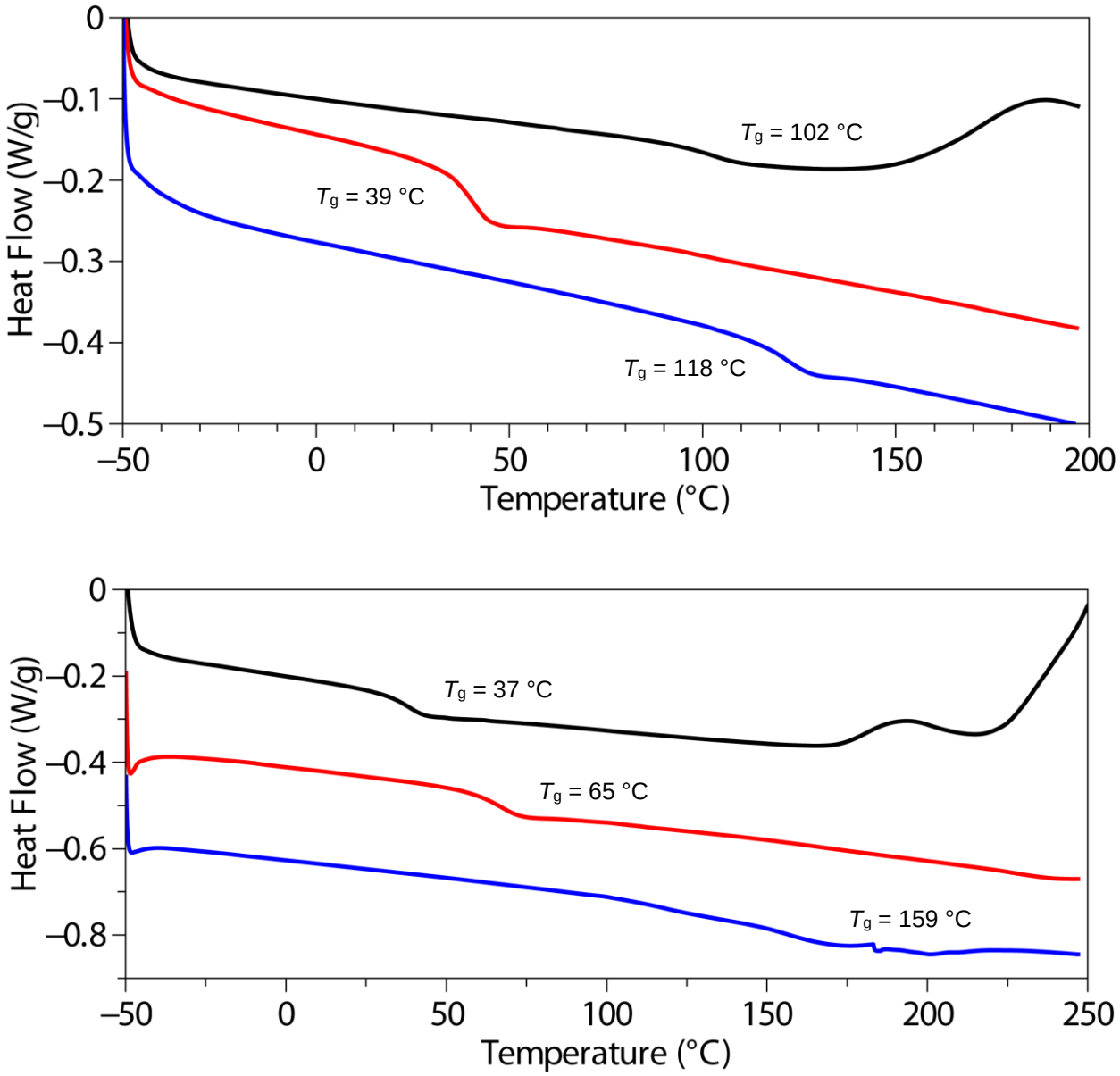

Figure S3.8. DSC (10 °C/min) traces of: (top) *st*-PVMA (black), *st*-PVMA-SR1 (red), and *st*-PVMA-SR2 (blue); (bottom) *st*-PDAA (black), *st*-PDAA-SR1 (red), and *st*-PDAA-SR2 (blue).

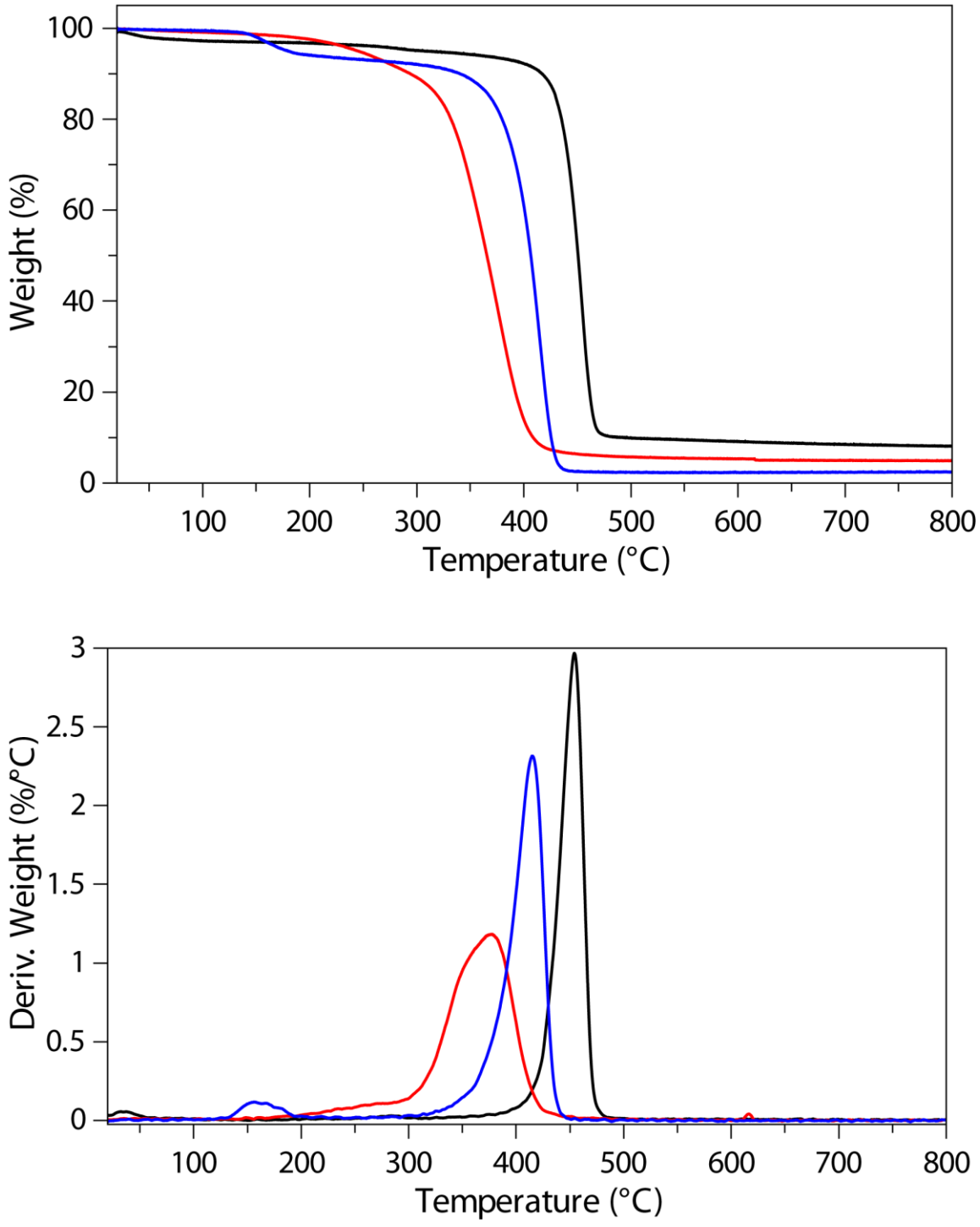

Figure S3.9. TGA (10 °C/min) traces of *st*-PDAA (solid black), *st*-PDAA-SR1 (red), *st*-PDAA-SR2 (blue). Top plot: weight (wt %) vs temperature (°C); bottom plot: derivative (wt % $°C^{-1}$) vs temperature (°C).

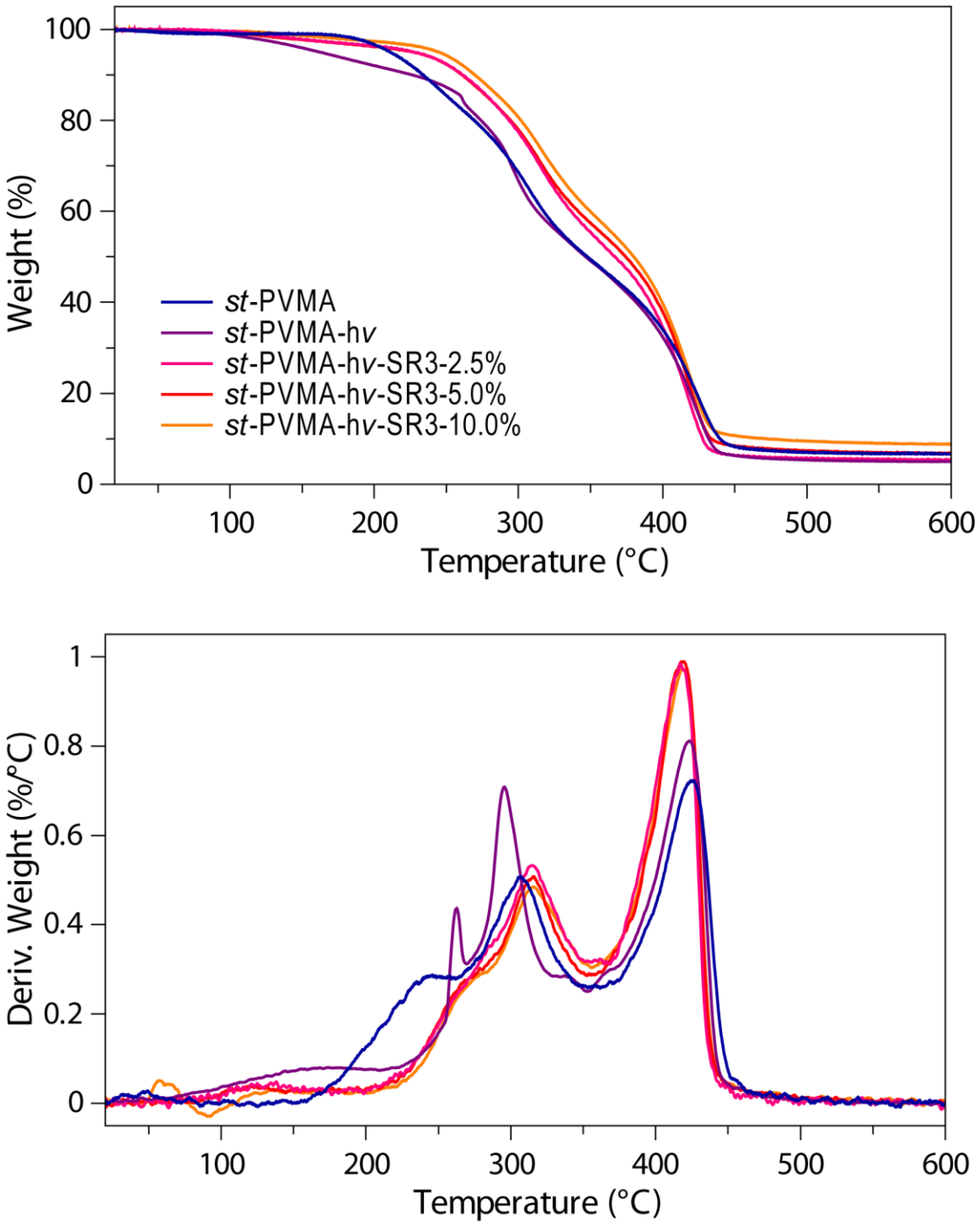

Figure S3.10. TGA traces of *st*-PVMA (blue), *st*-PVMA-hν (purple), *st*-PVMA-hν-SR3-2.5% (pink), *st*-PVMA-hν-SR3-5.0% (red), and *st*-PVMA-hν-SR3-10.0% (orange). Top plot: weight (wt %) vs temperature (°C); bottom plot: derivative (wt % $°C^{-1}$) vs temperature (°C).

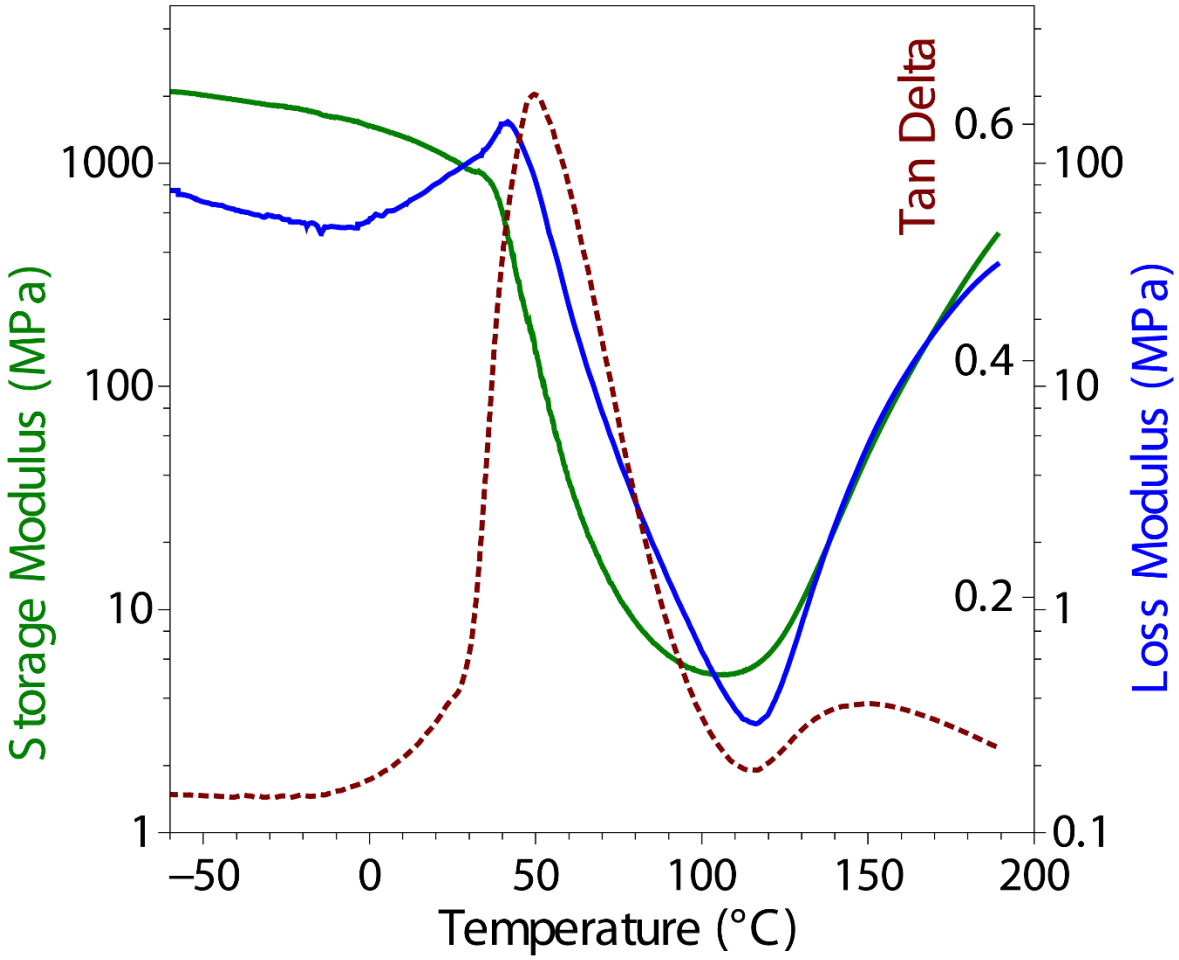

Figure S3.11. Thermal mechanical spectrum of *st*-PDAA-h*v* obtained by DMA analysis.

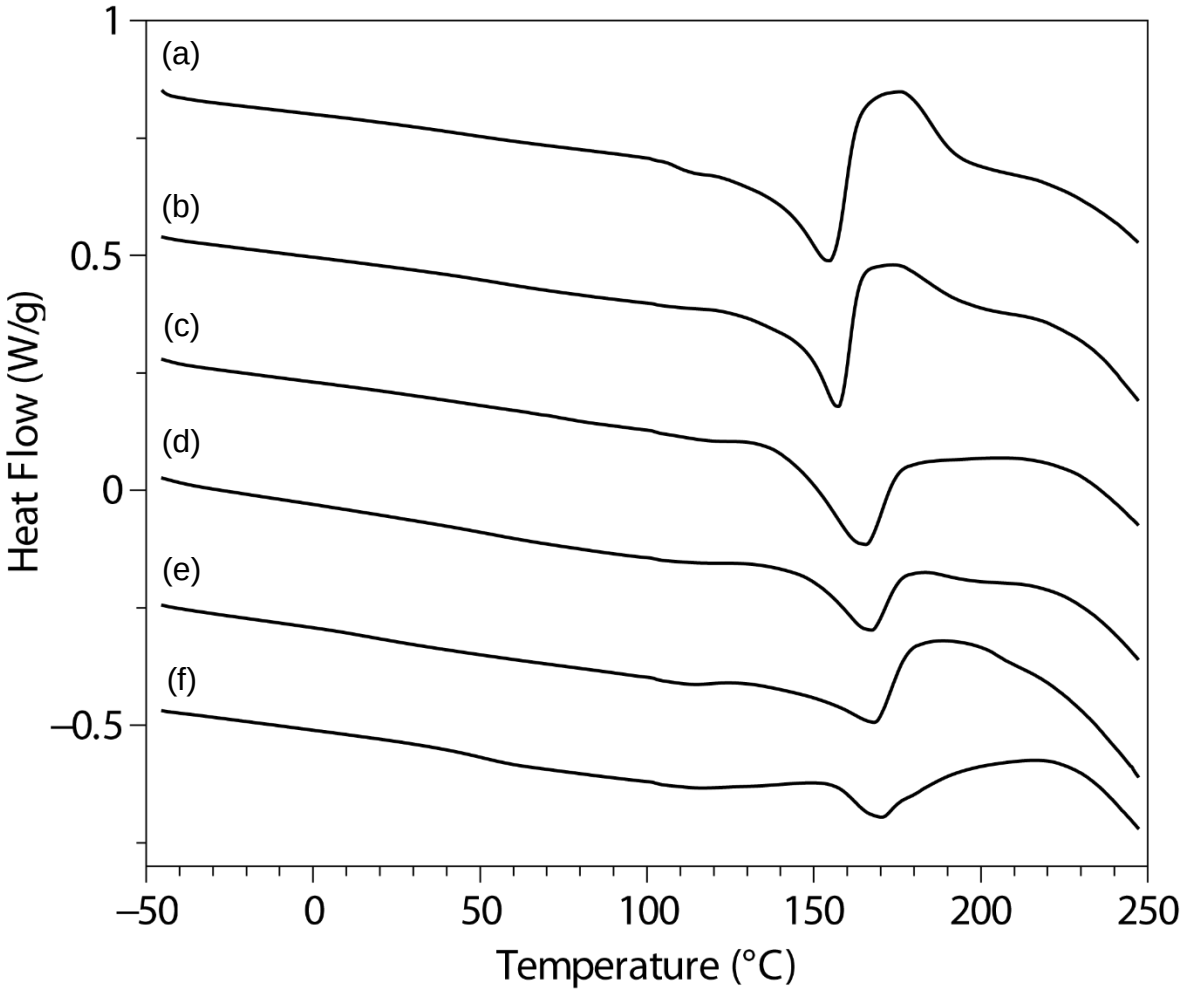

Figure S3.12. DSC (10 °C min^{-1}) thermograms of stereocomplexes with *st*-PAMA as shown in Table 3.3: entry 3 (a), entry 4 (b), entry 5 (c), entry 6 (d), entry 7 (e), and entry 8 (f).

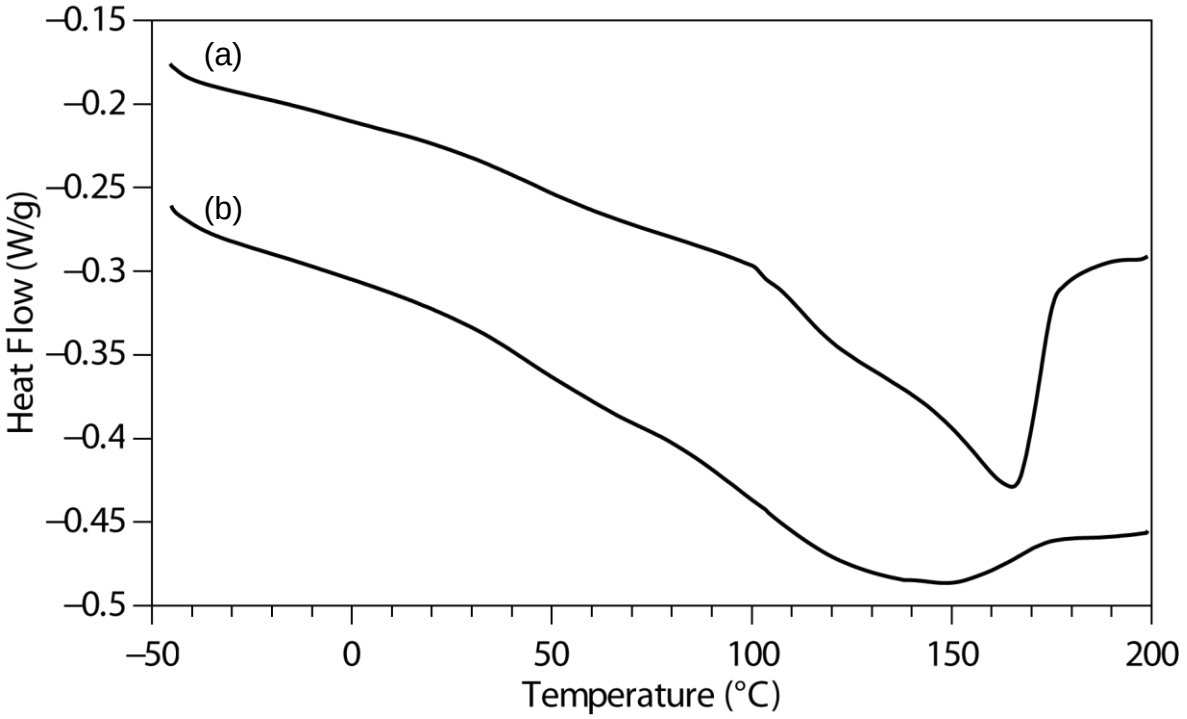

Figure S3.13. DSC (10 °C min^{-1}) thermograms: (a) stereocomplex *sc*-PMMA-PVMA in 1:1 molar ratio and (b) photocured stereocomplex *sc*-PMMA-PVMA-*hv*.

Table S3.1. Photocrosslinking results of control samples obtained from non-complexing solvent (CH_2Cl_2)[a]

entry no.	syndiotactic polymer	isotactic polymer	molar ratio (*st*/*it*)	T_m [b] (°C)	crosslinked vinyl polym.[c] (%)	trapped PMMA[c] (%)	PMMA trapping eff.[c] (%)
1	*st*-PAMA	–	–	–	100	–	–
2	*st*-PAMA	low MW *it*-PMMA	1:1	–	95.8	0.7	0.6
3	*st*-PVMA	–	–	–	82.4	–	–
4	*st*-PVMA	low MW *it*-PMMA	1:1	–	88.7	2.8	2.6

[a] Polymer data: *st*-PAMA, M_n = 39.9 kDa, $Đ$ = 1.45, [*rr*] = 91.8; *st*-PVMA, M_n = 52.1 kDa, $Đ$ = 1.31, [*rr*] = 91.7; low MW *it*-PMMA, M_n = 26.4 kDa, $Đ$ = 1.06, [*mm*] = 92.2. [b] T_m measured by DSC. [c] See the SI for the quantification method.

B.3. Computational Details

All the density functional theory (DFT) calculations were performed using the Gaussian09 package.[6] Geometry optimizations were performed using the BP86 GGA functional of Becke and Perdew[7] with the standard split-valence basis set with a polarization function of Ahlrichs and

coworkers for H, C, and O atoms (SVP keyword in Gaussian),[8] while the quasi relativistic small-core Stuttgart ECP with the associated triple-ζ valence basis set was used for zirconium (SDD keyword in Gaussian09).[9] The reported energies have been obtained via single point energy calculations with the BP86 functional with the triple-ζ basis set of Ahlrichs for H, C, O (TZVP keyword in Gaussian09).[9] Solvent effects were included with the default Gaussian PCM (polarizable continuum solvation model) using toluene and dichloromethane (DCM) as the solvent.[10] Thermal corrections from gas-phase frequency analysis, performed with the SVP basis set on the optimized geometries, were added to this in solvent energy to obtain the free energies. We preferred to use the BP86 functional for stereoselectivity calculations, since it allows an easier comparison with previous work on the polymerization of polar monomers by group 4 metallocene catalysts, which were performed with the BP86 functional. On the other hand, test calculations with the M06 functional, tuned to reproduce a dataset including dispersion stabilized systems, gave overall results strongly consistent with the BP86 calculations, see Table S3.2.

Table S3.2. Comparison of the ΔG_{Stereo} (kcal/mol) of AMA and VMA with C_2-ligated (*S*,*S*)-EBI-Zr system and with C_S-ligated (*S*)-Ph_2C(Cp)Flu-Zr system obtained with different calculation methods

	ΔG_{Stereo} C_2-catalyst BP86/DCM	ΔG_{Stereo} C_S-catalyst BP86/DCM	ΔG_{Stereo} C_2-catalyst BP86/Tol.	ΔG_{Stereo} C_S-catalyst BP86/Tol.	ΔG_{Stereo} C_2-catalyst M06/DCM	ΔG_{Stereo} C_S-catalyst M06/DCM
AMA	5.6	2.2	5.9	1.8	5.0	1.8
VMA	3.1	2.7	3.3	2.6	2.4	1.4

Since the absolute value of ΔG_{Stereo} calculated for AMA polymerization with the C_S-symmetric system was noticeably lower than that calculated with the C_2-symmetric system, despite that fact that the two systems yielded similarly stereoregular syndiotactic and isotactic PAMA materials, we decided to calculate ΔG_{Stereo} for MMA polymerization, as a test case. As both the C_S and C_2-symmetric metallocene catalysts considered here yield similarly highly stereoregular *st*-

PMMA and *it*-PMMA, the ΔG_{Stereo} calculated for MMA should be quite close to that calculated for AMA. Indeed, with the C_2-symmetric system the ΔG_{Stereo} we calculated for MMA, 4.8 kcal/mol, is close to the ΔG_{Stereo} of 5.6 kcal/mol calculated for AMA and clearly larger than the ΔG_{Stereo} of 3.1 kcal/mol calculated for VMA, consistent with the experimental %*mm* values of 95%, 97% and 53%, respectively. Further, with the C_S-symmetric system the ΔG_{Stereo} calculated for MMA, 2.2 kcal/mol, is very close to that calculated for both AMA and VMA, 2.2 and 2.7 kcal/mol, also consistent with the experimental %*rr* values of 92%, 92% and 94%, respectively.

Table S3.3. ΔG_{Stereo} (kcal/mol) of AMA, VMA and MMA additions with C_2-symmetric (*S*,*S*)-EBI-Zr system and with C_S-symmetric (*S*)-Ph_2C(Cp)Flu-Zr system

	C_2-symmetric	C_S-symmetric
AMA	5.6	2.2
VMA	3.1	2.7
MMA	4.8	2.2

The results reported in Table S3.3 indicate a too high ΔG_{Stereo} calculated with the C_2-symmetric catalyst. This is possibly due to: (i) a bad performance of the used functional; (ii) failure to locate the best geometry for the disfavored TS. As for point (i), we tested different functional and solvent model combinations (Table S3.2). While the overall ΔG_{Stereo} values varied with the specific computational protocol, they consistently predict a larger ΔG_{Stereo} for AMA addition at the C_2-catalyst compared to the C_S-catalyst, while for VMA the ΔG_{Stereo} calculated for the C_2 and the C_S-catalyst is much closer. However, the absolute ΔG_{Stereo} for AMA addition at the C_2-catalyst remained too high compared to the experimental results. As for point (ii), we tested a large variety of conformations for both the growing chain and the monomer pendant groups, but we were not able to find any lower energy geometries for the disfavored TS.

Table S3.4. Cartesian coordinates.

88

AMA-EBI-SS-ansa+Si-TS SCF Done: -1821.73876554

A.U.

Zr	-0.483756	-0.918971	-0.156147
O	1.453447	-0.259646	0.148597
C	2.223442	0.469317	0.937651
O	2.943635	-0.173351	1.886133
C	3.186082	-1.605117	1.799066
H	2.484489	-2.130496	2.482340
C	4.609177	-1.877103	2.191552
H	2.981468	-1.937918	0.759029
C	2.300106	1.874511	0.908492
C	3.224818	2.553375	1.898821
H	4.281496	2.564152	1.550140
H	3.224283	2.042177	2.881069
H	2.925619	3.609460	2.053004
C	1.830736	2.618128	-0.324880
H	1.196967	1.928264	-0.921252
H	1.162866	3.456696	-0.023025
C	2.911732	3.221212	-1.298817
C	4.047973	2.214200	-1.571113
C	3.507104	4.540214	-0.753399
C	2.182382	3.543360	-2.624657
C	-2.478141	-2.035041	1.141898
C	-3.848103	-1.787357	0.806490
C	-1.826631	-1.221591	2.163216
C	-2.562230	-0.197527	2.833925
C	-0.475580	-1.697572	2.301562
C	-0.331402	-2.836674	1.451157
C	-1.538675	-3.050887	0.708756
C	-1.811578	-4.171260	-0.267645
H	-2.656659	-4.797250	0.093729
H	-0.928946	-4.842077	-0.291652
C	-2.111908	-3.619556	-1.681603
H	-3.168138	-3.287884	-1.751025
H	-1.995635	-4.420748	-2.444279
C	-1.217577	-2.447289	-2.014037
C	0.229844	-2.468063	-2.131827
C	1.198295	-3.508074	-1.952833
C	0.662857	-1.150836	-2.583522
C	2.039126	-0.916580	-2.873139
C	-0.503518	-0.312726	-2.667220
C	-1.639195	-1.126555	-2.378017
C	0.196558	1.960986	2.163931
H	0.117208	0.867307	2.141044
H	0.756593	2.386643	3.009001
C	-0.738063	2.744329	1.494885
C	-0.919335	4.221795	1.777661
H	-1.915318	4.425376	2.225836
H	-0.856251	4.839758	0.858436
H	-0.149583	4.578013	2.488902
C	-1.583000	2.126592	0.511282
O	-1.473696	0.910470	0.088649
O	-2.549449	2.897176	0.010346
C	-3.461393	2.349908	-0.991367
H	-3.993232	1.477132	-0.556959
H	-2.847102	1.995069	-1.848615
C	-4.405496	3.436422	-1.408622
H	-0.522312	0.736283	-2.988683
H	-2.687289	-0.795394	-2.404213
H	0.567159	-3.465131	1.368896
H	0.269118	-1.328956	3.018093
C	2.948015	-1.951634	-2.703565
C	2.531660	-3.239453	-2.238097
C	-3.892295	0.004130	2.491500
C	-4.531757	-0.783549	1.480413
H	0.888171	-4.518442	-1.645942
H	3.281240	-4.039606	-2.135082
H	4.009471	-1.790032	-2.947972
H	2.363083	0.063094	-3.253801
H	-2.088768	0.397143	3.629623
H	-4.480021	0.769952	3.021451
H	-5.596562	-0.608538	1.260324
H	-4.366703	-2.414735	0.065644
C	-5.743873	3.326189	-1.342760
H	-3.941124	4.351979	-1.816848
H	-6.404213	4.131724	-1.700573
H	-6.233359	2.423486	-0.938239
C	4.964811	-2.680073	3.209988
H	5.380975	-1.386163	1.571849

H	6.022460	-2.881200	3.442308
H	4.211931	-3.174759	3.848182
H	4.752688	2.610813	-2.332038
H	4.635972	1.998321	-0.655292
H	3.652698	1.248058	-1.946839
H	4.171832	5.004827	-1.511797
H	2.709546	5.276216	-0.516252
H	4.113790	4.389952	0.160322
H	2.869282	4.022887	-3.352679
H	1.776878	2.625014	-3.101843
H	1.332861	4.240284	-2.459010

88

AMA-EBI-SS-ansa-Si-TS SCF Done:

-1821.73577108 A.U.

C	0.820309	-2.747410	1.989468
C	1.663059	-1.636394	2.339066
C	0.854338	-0.525813	2.732441
C	-0.517828	-0.954441	2.718084
C	-0.542214	-2.325750	2.221534
Zr	0.559310	-0.969000	0.213737
C	1.888990	-2.992418	-0.598837
C	0.636308	-2.937472	-1.298088
C	0.636900	-1.825958	-2.202175
C	1.931812	-1.203915	-2.127828
C	2.693831	-1.902571	-1.098389
C	2.314422	-4.015241	0.427305
C	1.265006	-4.122222	1.549827
O	1.511128	0.893326	0.019406
C	1.579304	2.104559	-0.425870
O	2.493046	2.927182	0.092474
C	3.404154	2.433593	1.121895
C	0.750819	2.669294	-1.454783
C	0.893771	4.146171	-1.762429
C	-0.120471	1.841121	-2.156630
C	-2.288329	1.702077	-1.092730
C	-1.963798	2.574857	0.104693
C	-3.156429	3.181022	0.936419
C	-2.146083	0.302679	-1.005939
O	-1.377178	-0.336279	-0.140573
C	-3.171627	2.240969	-2.200766
O	-2.789738	-0.442234	-1.935679
C	-3.010839	-1.864585	-1.720133
H	1.221470	0.448272	3.078685
C	-1.733009	-0.328743	3.123524
C	-1.785840	-3.023289	2.105979
H	2.762268	-1.638442	2.314692
H	-0.160731	-1.571988	-2.911872
C	2.543683	-0.139638	-2.859193
C	4.033897	-1.496585	-0.800939
H	3.295115	-3.716304	0.851956
H	2.481660	-5.004017	-0.052894
H	0.383314	-4.692638	1.190123
H	1.666486	-4.699785	2.411462
H	-0.188389	-3.654829	-1.176548
H	3.991387	1.586662	0.708298
C	4.279224	3.569759	1.556926
H	2.786838	2.050390	1.964299
H	1.896852	4.374055	-2.182579
H	0.780823	4.779420	-0.858648
H	0.136130	4.463031	-2.504600
H	-0.634808	2.229509	-3.047386
H	-0.004362	0.752400	-2.106645
H	-3.045356	1.671189	-3.142049
H	-4.252871	2.186485	-1.944669
H	-2.938969	3.305598	-2.402377
H	-1.334326	1.984427	0.802555
H	-1.332831	3.431762	-0.219977
H	-2.225148	-2.441895	-2.253672
C	-4.372365	-2.221358	-2.241370
H	-2.924567	-2.076380	-0.632225
C	-2.555567	3.688390	2.268859
C	-3.802301	4.392458	0.223754
C	-4.233755	2.117824	1.230938
C	3.851021	0.214566	-2.557145
C	4.590966	-0.453927	-1.527131
C	-2.947640	-2.380723	2.510817
C	-2.917956	-1.045432	3.028001
H	1.998588	0.363886	-3.671378
H	4.344006	1.012561	-3.134010
H	5.633419	-0.153063	-1.338366
H	4.628028	-2.034736	-0.045831

H	-1.813982	-4.066624	1.754664
H	-3.910118	-2.914051	2.466246
H	-3.858803	-0.590604	3.374147
H	-1.721784	0.691291	3.536401
C	5.622819	3.526849	1.532659
H	3.757014	4.463886	1.942173
H	6.230512	4.367533	1.902691
H	6.169296	2.646825	1.151811
C	-4.591198	-3.145204	-3.193813
H	-5.220346	-1.687528	-1.776056
H	-5.610326	-3.404043	-3.521553
H	-3.759819	-3.685599	-3.679284
H	-3.332193	4.173806	2.895951
H	-2.116478	2.858009	2.861992
H	-1.753286	4.436434	2.092307
H	-4.547794	4.874571	0.890504
H	-3.042911	5.161126	-0.033983
H	-4.333408	4.111517	-0.705604
H	-5.017511	2.528181	1.902200
H	-4.739680	1.776223	0.303865
H	-3.797160	1.224924	1.722671

88

AMA-EBI-Cis-SS-ansa+Re-TS SCF Done:

-1821.73422923 A.U.

Zr	0.783089	-0.822181	-0.043493
C	2.245797	-0.815175	1.983428
C	0.963061	-0.385515	2.442059
C	0.087073	-1.529272	2.410633
C	0.833945	-2.642786	1.838654
C	2.183943	-2.180392	1.559444
C	3.311616	-2.998245	0.975136
C	2.911133	-3.592396	-0.398221
C	2.102712	-2.614410	-1.223380
C	0.735185	-2.769615	-1.635597
C	0.345497	-1.673425	-2.458350
C	1.498141	-0.830514	-2.638135
C	2.586134	-1.398651	-1.845812
C	3.865836	-0.758977	-1.838278
C	1.726356	0.342370	-3.418997
H	-0.635486	-1.542719	-2.931067
H	3.816388	-3.910062	-0.959837
H	2.308606	-4.512385	-0.257439
H	4.204091	-2.346873	0.869819
H	3.608100	-3.809339	1.676740
C	0.208127	-3.925356	1.714796
C	-1.262054	-1.723673	2.839107
H	0.707458	0.606934	2.829613
O	1.334740	1.156578	-0.370305
C	0.966209	2.403898	-0.267463
C	-0.201014	2.977562	-0.840910
C	-1.052454	2.187548	-1.653248
C	-0.436768	4.463317	-0.647497
O	1.785439	3.259746	0.364371
C	3.097347	2.815302	0.816878
H	0.445831	5.060066	-0.959520
H	-0.627580	4.730038	0.414479
H	-1.304323	4.803210	-1.246265
H	-0.672278	1.224020	-2.025927
H	-1.694683	2.734312	-2.363096
O	-1.262825	-0.345438	-0.112872
C	-1.990271	0.698414	0.173660
O	-1.660440	1.254516	1.357909
C	-2.815145	1.301372	-0.823113
C	-2.582016	2.039922	2.182502
C	-3.666072	2.536781	-0.568451
C	-3.245747	0.413238	-1.987323
H	-4.580704	2.326664	0.022623
H	-4.014143	2.940004	-1.540706
H	-3.111314	3.347443	-0.062081
H	-3.369469	1.062775	-2.883223
H	-2.412831	-0.282888	-2.214066
C	-4.545071	-0.459686	-1.856072
C	-4.587644	-1.369573	-3.107184
C	-4.494633	-1.341268	-0.591220
C	-5.830633	0.398170	-1.840280
H	-5.488720	-2.017336	-3.095013
H	-4.618907	-0.771644	-4.042698
H	-3.698502	-2.033704	-3.157712
H	-6.726838	-0.253673	-1.904971
H	-5.934660	0.995143	-0.912439
H	-5.866830	1.096109	-2.703331

H	-5.395655	-1.986893	-0.530388
H	-3.602383	-2.000709	-0.587444
H	-4.465064	-0.730615	0.336775
H	0.089237	-3.613061	-1.351009
C	2.984816	0.928573	-3.396718
C	4.048090	0.383845	-2.607886
H	0.923685	0.755837	-4.048911
H	3.180856	1.820049	-4.012735
H	5.037113	0.867536	-2.637691
H	4.705175	-1.191036	-1.271731
H	3.147231	-0.189328	1.919389
C	-1.100154	-4.079599	2.153374
C	-1.830100	-2.983336	2.713951
H	0.769054	-4.788244	1.325925
H	-1.581588	-5.067998	2.091648
H	-2.859003	-3.154411	3.066986
H	-1.816865	-0.889784	3.292388
C	3.977138	4.019568	0.971608
H	2.979937	2.277990	1.782906
H	3.503349	2.104653	0.064588
C	4.599672	4.349320	2.116928
H	4.121334	4.630604	0.062435
H	5.272593	5.219223	2.175455
H	4.468825	3.757913	3.039874
C	-2.194129	1.884266	3.623874
H	-2.498606	3.104649	1.881145
H	-3.620386	1.696213	2.010517
C	-3.044839	1.490969	4.589485
H	-1.160564	2.177580	3.883448
H	-2.736388	1.452337	5.646260
H	-4.088442	1.209973	4.364871

88

AMA-EBI-SS-ansa-Re-TS SCF Done:

-1821.73036989 A.U.

Zr	0.177089	-1.038298	-0.235640
O	-1.455222	0.206111	-0.339663
C	-2.188446	1.263896	-0.041455
O	-3.510698	1.071474	0.152752
C	-4.163353	-0.070198	-0.461448
H	-3.629803	-0.995073	-0.154719
C	-5.591024	-0.098701	-0.005198
H	-4.096640	0.028399	-1.567799
C	-1.694858	2.562703	0.195460
C	-2.686888	3.583969	0.717465
H	-3.363362	3.968090	-0.077871
H	-3.343135	3.154687	1.499940
H	-2.154256	4.455671	1.146982
C	-0.431698	3.039707	-0.491958
H	0.187074	2.154201	-0.748478
H	0.181556	3.631774	0.223653
C	-0.587505	3.910177	-1.798232
C	-1.614356	3.293001	-2.770143
C	-1.000282	5.365751	-1.474569
C	0.801537	3.956523	-2.477024
C	0.860487	-3.252599	0.717015
H	1.793762	-3.660621	0.309071
C	0.776826	-2.448367	1.882417
H	1.620386	-2.138326	2.511250
C	-0.617384	-2.200265	2.153721
C	-1.284796	-1.587827	3.254647
H	-0.705115	-1.119972	4.065497
C	-2.673315	-1.649420	3.312023
H	-3.204097	-1.217828	4.174607
C	-3.426386	-2.301787	2.288247
H	-4.520634	-2.369360	2.391961
C	-2.808376	-2.872169	1.178444
H	-3.402239	-3.402970	0.417924
C	-1.385950	-2.831552	1.090879
C	-0.451875	-3.422659	0.147992
C	-0.781324	-4.211734	-1.099666
H	-0.874625	-5.297602	-0.872809
H	-1.776754	-3.897239	-1.480413
C	0.293644	-3.976087	-2.187475
H	1.204666	-4.563432	-1.951864
H	-0.062646	-4.355523	-3.168831
C	0.660261	-2.511727	-2.287681
C	-0.206257	-1.436032	-2.660679
H	-1.261520	-1.541491	-2.951671
C	0.500500	-0.194051	-2.589581
H	0.095194	0.788191	-2.856237
C	1.862889	-0.485567	-2.237853

C	3.034752	0.330043	-2.153802				
H	2.969435	1.413485	-2.336102	88			
C	4.255451	-0.279739	-1.901140	AMA-EBI-Cis-SS-ansa+Re-TS SCF Done:			
H	5.174148	0.327188	-1.880377	-1821.73422923 A.U.			
C	4.356342	-1.694700	-1.690939	Zr	0.783089	-0.822181	-0.043493
H	5.347663	-2.138661	-1.510557	C	2.245797	-0.815175	1.983428
C	3.236474	-2.512823	-1.741763	C	0.963061	-0.385515	2.442059
H	3.338992	-3.603353	-1.624591	C	0.087073	-1.529272	2.410633
C	1.962619	-1.926760	-2.031212	C	0.833945	-2.642786	1.838654
C	-0.648360	1.788984	2.223847	C	2.183943	-2.180392	1.559444
H	-0.929101	0.753752	1.990291	C	3.311616	-2.998245	0.975136
H	-1.374051	2.364885	2.816806	C	2.911133	-3.592396	-0.398221
C	0.694571	2.151005	2.259355	C	2.102712	-2.614410	-1.223380
C	1.185154	3.403721	2.955756	C	0.735185	-2.769615	-1.635597
H	1.834108	3.155273	3.822125	C	0.345497	-1.673425	-2.458350
H	1.789801	4.050945	2.286817	C	1.498141	-0.830514	-2.638135
H	0.329738	3.997506	3.331458	C	2.586134	-1.398651	-1.845812
C	1.665878	1.275594	1.659888	C	3.865836	-0.758977	-1.838278
O	1.395096	0.249008	0.924993	C	1.726356	0.342370	-3.418997
O	2.938189	1.574636	1.934860	H	-0.635486	-1.542719	-2.931067
C	4.012422	0.661549	1.559541	H	3.816388	-3.910062	-0.959837
H	3.955944	-0.235964	2.212509	H	2.308606	-4.512385	-0.257439
H	3.848835	0.343027	0.508100	H	4.204091	-2.346873	0.869819
C	5.317559	1.379335	1.723543	H	3.608100	-3.809339	1.676740
C	6.322303	0.936662	2.499948	C	0.208127	-3.925356	1.714796
H	5.436206	2.307012	1.134899	C	-1.262054	-1.723673	2.839107
H	7.282600	1.472837	2.558215	H	0.707458	0.606934	2.829613
H	6.227659	0.017017	3.103069	O	1.334740	1.156578	-0.370305
C	-6.646043	-0.145879	-0.837685	C	0.966209	2.403898	-0.267463
H	-5.745412	-0.107398	1.088961	C	-0.201014	2.977562	-0.840910
H	-7.677125	-0.211181	-0.455889	C	-1.052454	2.187548	-1.653248
H	-6.521612	-0.126414	-1.934282	C	-0.436768	4.463317	-0.647497
H	0.784775	4.608525	-3.374931	O	1.785439	3.259746	0.364371
H	1.574811	4.357306	-1.787299	C	3.097347	2.815302	0.816878
H	1.130399	2.948081	-2.807230	H	0.445831	5.060066	-0.959520
H	-0.977163	5.984292	-2.396295	H	-0.627580	4.730038	0.414479
H	-2.024085	5.438388	-1.060951	H	-1.304323	4.803210	-1.246265
H	-0.302876	5.831113	-0.746152	H	-0.672278	1.224020	-2.025927
H	-1.670329	3.881250	-3.709918	H	-1.694683	2.734312	-2.363096
H	-1.347868	2.251176	-3.050203	O	-1.262825	-0.345438	-0.112872
H	-2.632953	3.268570	-2.330720	C	-1.990271	0.698414	0.173660

O	-1.660440	1.254516	1.357909	H	4.121334	4.630604	0.062435
C	-2.815145	1.301372	-0.823113	H	5.272593	5.219223	2.175455
C	-2.582016	2.039922	2.182502	H	4.468825	3.757913	3.039874
C	-3.666072	2.536781	-0.568451	C	-2.194129	1.884266	3.623874
C	-3.245747	0.413238	-1.987323	H	-2.498606	3.104649	1.881145
H	-4.580704	2.326664	0.022623	H	-3.620386	1.696213	2.010517
H	-4.014143	2.940004	-1.540706	C	-3.044839	1.490969	4.589485
H	-3.111314	3.347443	-0.062081	H	-1.160564	2.177580	3.883448
H	-3.369469	1.062775	-2.883223	H	-2.736388	1.452337	5.646260
H	-2.412831	-0.282888	-2.214066	H	-4.088442	1.209973	4.364871
C	-4.545071	-0.459686	-1.856072				
C	-4.587644	-1.369573	-3.107184	105			
C	-4.494633	-1.341268	-0.591220	CS-Ph2-AMA-S-Si-TS SCF Done:			
C	-5.830633	0.398170	-1.840280	-2244.20546316 A.U.			
H	-5.488720	-2.017336	-3.095013	C	1.435347	-1.296408	-1.822262
H	-4.618907	-0.771644	-4.042698	C	2.199086	-0.143644	-1.414812
H	-3.698502	-2.033704	-3.157712	C	1.568515	0.996292	-2.024594
H	-6.726838	-0.253673	-1.904971	C	0.477562	0.541908	-2.834008
H	-5.934660	0.995143	-0.912439	C	0.392931	-0.868926	-2.709522
H	-5.866830	1.096109	-2.703331	Zr	-0.032830	0.054948	-0.364899
H	-5.395655	-1.986893	-0.530388	O	-1.517056	-1.372455	-0.109250
H	-3.602383	-2.000709	-0.587444	C	-2.611137	-1.869075	-0.661136
H	-4.465064	-0.730615	0.336775	O	-2.492437	-3.011267	-1.379901
H	0.089237	-3.613061	-1.351009	C	-1.322826	-3.864851	-1.250525
C	2.984816	0.928573	-3.396718	C	3.146734	-0.096382	-0.205288
C	4.048090	0.383845	-2.607886	C	4.037120	-1.353943	-0.070409
H	0.923685	0.755837	-4.048911	C	4.520352	-1.756085	1.194005
H	3.180856	1.820049	-4.012735	C	5.417945	-2.829362	1.312610
H	5.037113	0.867536	-2.637691	C	5.855408	-3.517720	0.166836
H	4.705175	-1.191036	-1.271731	C	5.393651	-3.115909	-1.097527
H	3.147231	-0.189328	1.919389	C	4.495545	-2.039788	-1.215162
C	-1.100154	-4.079599	2.153374	C	1.317000	-1.068328	1.504741
C	-1.830100	-2.983336	2.713951	C	1.423426	-2.491577	1.394594
H	0.769054	-4.788244	1.325925	C	0.558551	-3.300905	2.132896
H	-1.581588	-5.067998	2.091648	C	-0.438156	-2.749956	2.983104
H	-2.859003	-3.154411	3.066986	C	-0.591507	-1.368232	3.090201
H	-1.816865	-0.889784	3.292388	C	0.262302	-0.520083	2.345192
C	3.977138	4.019568	0.971608	C	0.329992	0.926338	2.255470
H	2.979937	2.277990	1.782906	C	1.434573	1.268476	1.367457
H	3.503349	2.104653	0.064588	C	2.059224	0.034040	0.890594
C	4.599672	4.349320	2.116928	C	1.700228	2.654826	1.123763

C	0.965513	3.622036	1.810374	H	1.884676	2.040594	-1.908243
C	-0.074618	3.272730	2.716424	H	-0.177232	1.178804	-3.442860
C	-0.408554	1.935416	2.925097	H	-0.318712	-1.525261	-3.226335
O	-1.332996	1.707199	-0.699313	H	1.643407	-2.334009	-1.535104
C	-2.361723	2.232110	-1.278181	H	-1.603564	3.900056	0.672890
C	-3.330915	1.540689	-2.089703	H	-0.670555	4.311735	-0.802786
C	-3.109071	0.217432	-2.444141	C	-2.218176	5.749689	-0.288663
C	4.152757	1.076339	-0.249004	H	-5.121082	2.733800	-1.663881
C	4.669064	1.543344	-1.476497	H	-5.259390	1.629001	-3.074473
C	5.669785	2.531474	-1.507290	H	-4.309068	3.144061	-3.191524
C	6.179184	3.061046	-0.310177	H	-2.110664	-0.224063	-2.359098
C	5.684973	2.589033	0.919001	H	-3.799968	-0.284551	-3.137027
C	4.684735	1.603969	0.948330	C	-1.768633	-5.272822	-0.979082
O	-2.597883	3.535444	-1.123523	H	-0.687684	-3.475096	-0.427240
C	-1.678460	4.353002	-0.339212	H	-0.748795	-3.813515	-2.201183
C	-4.570608	2.296992	-2.522591	H	-4.716760	-2.473240	-2.239684
C	-3.883244	-1.271847	-0.616901	H	-5.451964	-2.803765	-0.656110
C	-4.166420	-0.187810	0.399966	H	-5.859191	-1.290274	-1.511247
C	-4.993698	-0.563332	1.686061	H	-3.196927	0.229643	0.741579
C	-4.470572	-1.868995	2.317578	H	-4.700874	0.654199	-0.096503
C	-5.030903	-1.993457	-1.292521	H	-4.622732	-2.739223	1.645611
C	-4.810754	0.600017	2.688833	H	-4.999366	-2.087302	3.269394
C	-6.504037	-0.697845	1.383333	H	-3.384946	-1.803475	2.538316
H	2.210050	-2.947679	0.780170	H	-6.732520	-1.561438	0.729694
H	0.666719	-4.395181	2.069921	H	-7.074655	-0.842048	2.324911
H	-1.087001	-3.421502	3.565820	H	-6.900607	0.216144	0.891994
H	-1.357344	-0.938143	3.753401	H	-5.401458	0.427292	3.612570
H	-1.210577	1.660182	3.627257	H	-3.745820	0.715748	2.985160
H	-0.612664	4.065155	3.259358	H	-5.146742	1.565645	2.253713
H	1.208855	4.685392	1.657533	C	-1.522799	6.832843	-0.678144
H	2.516104	2.958402	0.455469	H	-3.235354	5.861465	0.128144
H	4.300804	1.123696	-2.425540	H	-1.939209	7.847924	-0.581703
H	6.058026	2.881565	-2.476682	H	-0.507169	6.749234	-1.102301
H	6.964413	3.832544	-0.333570	C	-1.454173	-6.324001	-1.756888
H	6.082367	2.988911	1.865099	H	-2.374484	-5.416459	-0.066096
H	4.309486	1.245457	1.919489	H	-1.773675	-7.346429	-1.500693
H	4.186531	-1.229327	2.101508	H	-0.858119	-6.204387	-2.678376
H	5.778617	-3.129070	2.309085				
H	6.558982	-4.359565	0.259518	105			
H	5.738638	-3.637616	-2.004074	CS-Ph2-AMA-S-Re-TS SCF Done:			
H	4.162279	-1.725857	-2.216745	-2244.20264497 A.U.			

C	-4.674492	-1.962312	-0.139742	C	1.379187	4.277157	-0.053222
C	-3.948345	-1.309488	0.880850	C	4.660705	2.440733	-1.926509
C	-4.155961	-1.714255	2.216578	C	3.988411	-0.962307	0.198426
C	-5.044554	-2.760906	2.522021	C	3.919998	0.208860	1.152061
C	-5.748924	-3.413775	1.497085	C	4.580848	0.058755	2.574643
C	-5.562699	-3.006617	0.163896	C	4.164917	-1.265657	3.247718
C	-3.073258	-0.077524	0.552194	C	5.337649	-1.529202	-0.196303
C	-4.077148	1.098844	0.525364	C	6.123866	0.147608	2.513334
C	-4.841248	1.363622	-0.632545	C	4.076266	1.244914	3.430149
C	-5.834723	2.356050	-0.627380	H	1.364968	3.971677	1.014939
C	-6.089309	3.098750	0.539549	H	0.413564	3.981595	-0.518149
C	-5.346599	2.832855	1.701783	C	1.639669	5.745564	-0.201715
C	-4.352526	1.837693	1.695613	H	5.084539	2.958739	-1.041184
C	-1.909927	0.133288	1.536515	H	4.404477	3.233624	-2.660986
C	-1.072146	-0.909862	2.069410	H	5.453194	1.809990	-2.373058
C	0.116796	-0.317673	2.605742	H	5.273411	-2.133872	-1.121499
C	0.053809	1.080032	2.376472	H	5.765853	-2.196541	0.584449
C	-1.184937	1.363803	1.709748	H	6.067599	-0.711720	-0.362419
Zr	0.082805	-0.002327	0.065837	C	2.499306	-5.267334	-1.060789
C	-1.703247	0.885867	-1.542898	H	1.109856	-3.711314	-0.487936
C	-2.223483	-0.216925	-0.737526	H	2.132550	-4.333144	0.859178
C	-1.601024	-1.435912	-1.257762	H	4.169686	-0.245065	-2.425916
C	-0.708697	-1.080654	-2.355780	H	2.393895	-0.268434	-1.851143
C	-0.764274	0.357459	-2.525802	H	4.523344	-2.149144	2.679964
C	-0.044746	-2.081628	-3.112483	H	3.060334	-1.350271	3.335468
C	-0.252384	-3.420937	-2.792861	H	4.583240	-1.335517	4.273698
C	-1.073353	-3.778592	-1.685931	H	6.583087	-0.718402	2.000218
C	-1.722234	-2.819400	-0.908025	H	6.546456	0.179622	3.539580
C	-1.927183	2.300947	-1.515622	H	6.454869	1.069924	1.990340
C	-1.289108	3.112618	-2.452510	H	4.543203	1.235572	4.436941
C	-0.393939	2.578950	-3.422808	H	2.975428	1.204900	3.576289
C	-0.125442	1.212413	-3.460601	H	4.323692	2.219278	2.956920
O	1.280308	1.618079	-0.511987	H	4.372117	1.109627	0.675169
C	2.338026	2.233906	-0.923002	H	2.852231	0.464797	1.315908
C	3.447339	1.603205	-1.581335	H	-1.310728	-1.981231	2.079561
C	3.367445	0.241649	-1.851561	H	0.938106	-0.859802	3.089681
O	1.602245	-1.421530	0.188106	H	0.808407	1.819492	2.672465
C	2.857968	-1.785082	0.017766	H	-1.533468	2.358343	1.406296
O	3.089142	-3.026297	-0.464995	H	-2.367976	-3.132083	-0.077951
C	2.123160	-4.080956	-0.224779	H	-1.211483	-4.844108	-1.443863
O	2.444842	3.552100	-0.737303	H	0.222140	-4.211172	-3.393986

H	0.591406	-1.799416	-3.965777
H	0.557687	0.796088	-4.216792
H	0.076207	3.251401	-4.156730
H	-1.502931	4.193293	-2.456401
H	-2.636439	2.739799	-0.802439
H	-4.654745	0.792664	-1.555464
H	-6.415495	2.548726	-1.543068
H	-6.869095	3.876072	0.544048
H	-5.544607	3.397398	2.626510
H	-3.796462	1.628527	2.622772
H	-3.631567	-1.200317	3.036979
H	-5.190195	-3.060950	3.571656
H	-6.446004	-4.231959	1.735747
H	-6.114957	-3.504399	-0.648600
H	-4.541685	-1.655891	-1.189012
C	1.747161	6.594742	0.835312
H	1.711511	6.120519	-1.238539
H	1.894307	7.675069	0.679690
H	1.684249	6.246336	1.880838
C	2.672332	-6.508753	-0.573544
H	2.605542	-5.076554	-2.144245
H	2.904205	-7.358908	-1.234406
H	2.584284	-6.725797	0.505055

105

AMA-CS-Cis-SS-Re-TS SCF Done:

-2244.19738030 A.U.

Zr	0.055930	0.109363	-0.376577
C	1.294040	-0.963190	1.554583
C	0.366180	-0.158963	2.340202
C	0.668329	1.236646	2.087971
C	0.129682	2.423048	2.646999
C	1.773936	1.290376	1.138226
C	2.183158	-0.074304	0.808549
C	3.180841	-0.503747	-0.296043
C	2.182961	-0.545810	-1.465429
C	1.695069	0.599276	-2.188213
C	0.514429	0.221876	-2.907487
C	0.239018	-1.138719	-2.617606
H	-0.581890	-1.740480	-3.026714
C	1.246838	-1.612122	-1.714570
C	1.146471	-2.387243	1.585433
C	-0.602237	-0.768583	3.175355
H	2.157453	1.594400	-2.200503
H	-0.071235	0.878558	-3.563589
O	-1.667160	-1.040607	-0.001929
C	-2.930548	-0.732022	0.112245
C	-3.903139	-1.232050	-0.803751
C	-5.382507	-0.898132	-0.694854
O	-3.141303	0.278438	0.984040
C	-3.540563	-2.500703	-1.571452
C	-3.879084	-3.901586	-0.947378
C	-3.165341	-4.957575	-1.824764
C	-3.352157	-4.003962	0.498524
C	-5.395336	-4.201664	-0.970763
H	-5.892444	-1.203659	-1.630416
H	-5.895484	-1.434873	0.129199
H	-2.447594	-2.487009	-1.759949
H	-4.035158	-2.452848	-2.567917
H	-2.262983	-3.798970	0.551631
H	-3.861749	-3.283179	1.173595
H	-3.531439	-5.020090	0.908154
H	-5.817024	-4.092319	-1.992443
H	-5.972383	-3.543999	-0.290813
H	-5.583419	-5.246362	-0.645435
H	-3.378596	-5.984191	-1.460793
H	-3.503456	-4.901672	-2.881412
H	-2.063191	-4.818342	-1.812844
O	-1.121398	1.774555	-0.856666
C	-2.256865	2.300970	-1.224891
C	-3.358156	1.627508	-1.819494
C	-3.258865	0.259920	-2.179819
C	-4.609813	2.434481	-2.113841
O	-2.421839	3.623812	-1.066748
H	-2.259509	-0.185393	-2.295792
H	-4.000452	-0.103896	-2.910064
H	-5.357973	1.814938	-2.645762
H	-5.088179	2.833423	-1.193311
H	1.314801	-2.631519	-1.316596
C	2.234252	2.577133	0.709079
C	3.872081	-1.860903	-0.027980
C	4.352574	0.481366	-0.513144

C	-1.296890	4.453386	-0.668818	C	6.004999	1.531016	-1.985903
C	-1.812598	5.825598	-0.355445	C	6.650919	2.104176	-0.878133
H	-0.814776	3.988134	0.217018	C	6.155164	1.856055	0.414467
H	-0.551031	4.473821	-1.492946	C	5.020043	1.049475	0.594373
H	-4.385203	3.316895	-2.749135	H	4.390297	0.263822	-2.683615
C	-4.336227	0.397053	1.818301	H	6.390143	1.706115	-3.002782
C	-3.969980	1.128409	3.076769	H	7.541611	2.735863	-1.019567
H	-5.103878	0.972682	1.260951	H	6.657367	2.292051	1.292355
H	-4.735660	-0.612125	2.042131	H	4.645947	0.864320	1.613279
H	-5.565218	0.184470	-0.563566				
C	-4.242225	0.677059	4.314741	82			
H	-3.505449	2.121158	2.934701	VMA-EBI-SS-ansa+Si-TS SCF Done:			
H	-4.019573	1.280227	5.209366	-1743.18242692 A.U.			
H	-4.719888	-0.303724	4.482708	Zr	-0.959080	-0.374109	-0.101261
C	-1.334676	6.953344	-0.910381	O	0.976644	-0.941605	0.436096
H	-2.611441	5.876998	0.406680	C	1.920174	-0.673933	1.309046
H	-1.712395	7.944602	-0.613904	O	1.898584	-1.359823	2.490338
H	-0.543320	6.931351	-1.679564	C	1.232541	-2.569321	2.594016
C	0.175397	-2.956518	2.411018	C	2.916021	0.310927	1.166711
C	-0.687145	-2.159751	3.210831	C	3.923772	0.466956	2.288499
H	1.824280	-3.031690	1.011501	H	4.707599	-0.321088	2.255421
H	0.088781	-4.053469	2.454059	H	3.449972	0.397638	3.287218
H	-1.427232	-2.648708	3.862572	H	4.441586	1.443776	2.212381
H	-1.280357	-0.148961	3.780784	C	3.263098	0.805442	-0.224400
C	1.688544	3.724820	1.285582	H	2.372236	0.667617	-0.872449
C	0.655920	3.655614	2.262346	H	3.452985	1.899717	-0.191173
H	-0.672671	2.362420	3.398021	C	4.496693	0.146664	-0.952031
H	0.271958	4.583820	2.712828	C	4.505189	-1.385617	-0.774882
H	2.079957	4.710015	0.986900	C	5.835136	0.732473	-0.444718
H	3.053709	2.663680	-0.015816	C	4.363227	0.492053	-2.453857
C	4.191623	-2.728727	-1.093838	C	-3.233143	0.293007	1.004160
C	4.922464	-3.908560	-0.866744	C	-4.121078	1.241683	0.402621
C	5.353057	-4.236187	0.429788	C	-2.246404	0.745496	1.980172
C	5.052191	-3.370684	1.496611	C	-2.186985	2.125513	2.343164
C	4.322181	-2.192912	1.268567	C	-1.504643	-0.408866	2.415533
H	3.880526	-2.478478	-2.120144	C	-2.090107	-1.554616	1.796364
H	5.161154	-4.571577	-1.713196	C	-3.134823	-1.150931	0.901413
H	5.926778	-5.158922	0.608015	C	-4.023373	-2.060109	0.083256
H	5.389777	-3.612361	2.516698	H	-5.085176	-1.934187	0.388505
H	4.095028	-1.526463	2.115181	H	-3.764356	-3.111844	0.320543
C	4.868502	0.722246	-1.804188	C	-3.859844	-1.792776	-1.431958

H	-4.465760	-0.915757	-1.739035	C	1.039807	-3.142379	3.793356
H	-4.249835	-2.650947	-2.022295	H	0.932211	-3.015360	1.632241
C	-2.414894	-1.527344	-1.787425	H	0.563112	-4.131028	3.848236
C	-1.301125	-2.447345	-1.635874	H	1.369889	-2.661965	4.726862
C	-1.213870	-3.783678	-1.126320	H	6.681021	0.328992	-1.039964
C	-0.115273	-1.814912	-2.202650	H	5.857202	1.838428	-0.544978
C	1.111659	-2.538349	-2.273422	H	6.036810	0.482163	0.614980
C	-0.486838	-0.492713	-2.631147	H	5.311786	-1.845465	-1.383718
C	-1.892285	-0.356208	-2.429189	H	4.682519	-1.679933	0.280632
C	1.347821	2.010978	1.744283	H	3.542696	-1.838082	-1.090065
H	0.552769	1.286485	1.961710	H	5.230529	0.107488	-3.029836
H	2.007887	2.262798	2.586489	H	3.443645	0.050186	-2.894684
C	1.178301	2.939806	0.714664	H	4.317319	1.590508	-2.613427
C	2.024958	4.192299	0.606344	82			
H	1.413869	5.105339	0.770365	VMA-EBI-SS-ansa-Si-TS SCF Done: -1743.18004043			
H	2.495425	4.301391	-0.392152	A.U.			
H	2.827290	4.183776	1.368651	C	-2.182436	-2.186002	-1.530507
C	0.142884	2.724062	-0.246136	C	-2.278604	-0.920851	-2.208887
O	-0.606895	1.678031	-0.333911	C	-0.990913	-0.531756	-2.687179
O	-0.046683	3.730292	-1.123285	C	-0.071376	-1.595484	-2.386385
C	-1.108605	3.723199	-2.018460	C	-0.806414	-2.613358	-1.642303
H	0.170245	0.241734	-3.113975	Zr	-1.029636	-0.460478	-0.115694
H	-2.492740	0.523507	-2.701906	C	-3.281644	-1.150430	0.835998
H	-1.781152	-2.594408	1.973813	C	-2.251974	-1.577761	1.739224
H	-0.714380	-0.433342	3.175989	C	-1.654736	-0.438637	2.367270
C	1.154616	-3.837852	-1.788066	C	-2.362101	0.729752	1.914504
C	-0.000244	-4.455532	-1.210272	C	-3.342938	0.291614	0.926154
C	-3.070498	3.014002	1.745602	C	-4.167734	-2.034857	-0.009306
C	-4.029614	2.576133	0.776553	C	-3.315643	-2.961026	-0.900265
H	-2.103977	-4.291864	-0.725436	O	-0.717325	1.586662	-0.462263
H	0.071176	-5.495247	-0.854417	C	-0.004257	2.657567	-0.370491
H	2.088635	-4.416407	-1.860920	O	-0.171764	3.623833	-1.297632
H	1.996323	-2.077238	-2.736577	C	-1.167113	3.539817	-2.262091
H	-1.473445	2.469341	3.107312	C	0.967667	2.944734	0.635653
H	-3.053902	4.076087	2.036048	C	1.771288	4.225504	0.527199
H	-4.727303	3.311306	0.345995	C	1.116523	2.061467	1.710467
H	-4.898186	0.913499	-0.304234	C	2.757664	0.426721	1.320526
C	-1.152026	4.629810	-3.006375	C	3.212778	0.899743	-0.048976
H	-1.876433	2.961199	-1.817975	C	4.552733	0.306420	-0.625332
H	-2.010290	4.640866	-3.692658	C	1.796794	-0.602064	1.405198
H	-0.351129	5.371369	-3.146421	O	0.921439	-0.922130	0.480496

C	3.658660	0.642016	2.521601	H	-1.908633	2.744371	-2.095115
O	1.725114	-1.270724	2.595114	H	-1.991283	4.363548	-4.022834
C	1.105729	-2.506297	2.677838	H	-0.414329	5.194491	-3.384311
H	-0.762624	0.379155	-3.255015	C	0.850930	-3.063814	3.873016
C	1.294002	-1.819425	-2.733227	H	0.897811	-2.985345	1.707440
C	-0.143760	-3.811465	-1.226471	H	0.416808	-4.072489	3.916334
H	-3.202523	-0.340489	-2.343708	H	1.090724	-2.550839	4.816756
H	-0.882665	-0.478110	3.145539	H	6.719419	0.612897	-0.493924
C	-2.284699	2.111993	2.268788	H	5.766937	2.070645	-0.085005
C	-4.191378	1.253016	0.288499	H	5.908460	0.721269	1.088850
H	-4.823922	-1.399024	-0.638648	H	5.513233	0.296052	-2.607505
H	-4.852388	-2.628237	0.634833	H	3.727714	0.149883	-2.669683
H	-2.896774	-3.790398	-0.292565	H	4.488035	1.733690	-2.308781
H	-3.942997	-3.445875	-1.680448	H	5.501452	-1.647545	-0.948668
H	-1.970706	-2.621393	1.940031	H	4.693731	-1.503174	0.638104
H	1.120291	5.118846	0.639270	H	3.711331	-1.716734	-0.844864
H	2.279659	4.325493	-0.453422				
H	2.540004	4.269082	1.322394	82			
H	1.707273	2.382146	2.580598	VMA-EBI-SS-ansa+Re-TS SCF Done:			
H	0.334675	1.320551	1.917026	-1743.17520481 A.U.			
H	3.099655	0.583994	3.476136	C	-2.651862	-0.140926	-1.970984
H	4.465445	-0.120768	2.582126	C	-2.403110	-1.523985	-1.603492
H	4.151114	1.632855	2.463802	C	-1.018344	-1.838241	-1.943860
H	2.402999	0.677412	-0.775025	C	-0.421707	-0.646334	-2.480874
H	3.326701	2.004682	-0.040143	C	-1.433500	0.355526	-2.540977
C	4.569145	0.639388	-2.135657	Zr	-1.004424	0.106375	-0.085897
C	5.797340	0.964677	0.014743	C	-3.328519	0.857759	0.562016
C	4.614712	-1.222407	-0.433051	C	-2.545981	2.070418	0.716146
C	-3.133481	3.012642	1.641112	C	-1.622765	1.874649	1.830938
C	-4.075288	2.588074	0.647729	C	-1.814267	0.538329	2.320715
C	1.184244	-3.994821	-1.586260	C	-2.880387	-0.050092	1.574163
C	1.893716	-3.010153	-2.347434	C	-4.468669	0.638436	-0.406153
H	-1.588212	2.448901	3.051186	C	-3.967297	0.596290	-1.869077
H	-3.102372	4.076359	1.924155	O	-0.033041	-1.423323	1.024881
H	-4.739768	3.336392	0.188366	C	0.865276	-1.848731	1.841349
H	-4.955422	0.933365	-0.437345	O	0.844926	-3.136349	2.235451
H	-0.692986	-4.597279	-0.684515	C	-0.192602	-3.999054	1.911278
H	1.699771	-4.928176	-1.310970	C	1.929551	-1.072958	2.417837
H	2.932100	-3.218504	-2.646938	C	3.009976	-1.790282	3.202253
H	1.842406	-1.077071	-3.333032	C	1.915577	0.307798	2.266928
C	-1.184839	4.416022	-3.278101	C	2.983438	0.940814	0.120257

C	3.074069	-0.467245	-0.430944	H	-4.315648	-2.355332	-0.879833
C	3.949123	-0.695096	-1.723488	H	-3.417513	-4.662095	-0.656282
C	1.859904	1.732713	-0.169752	H	-1.045864	-5.193516	-1.249138
O	0.652282	1.297192	-0.453092	C	1.502263	5.278144	-0.778172
C	4.244439	1.648354	0.573631	H	0.321200	3.515672	-1.213235
O	2.039541	3.083849	-0.086512	H	0.838029	5.965499	-1.320046
C	1.204357	3.968359	-0.737381	H	2.401795	5.683293	-0.290916
C	-0.527870	-3.170990	-1.785343	C	-0.175557	-5.254037	2.386152
H	0.605644	-0.544975	-2.848614	H	-0.974877	-3.569727	1.269502
H	-1.299614	1.369209	-2.945881	H	-1.001022	-5.935913	2.138864
C	-3.258301	-2.559318	-1.106313	H	0.643643	-5.621970	3.022086
C	-0.818950	2.965533	2.290720	H	6.043990	-0.968288	-2.308580
H	-1.295210	0.080887	3.172336	H	5.823323	0.332586	-1.110848
H	-3.297879	-1.053038	1.743701	H	5.721006	-1.383242	-0.599048
H	-4.973920	-0.312853	-0.142992	H	4.216930	-2.358496	-3.143143
H	-5.236321	1.432752	-0.280850	H	3.789189	-2.885604	-1.485837
H	-3.826244	1.624896	-2.260778	H	2.535550	-2.176516	-2.558160
H	-4.727757	0.122411	-2.528342	H	4.204927	0.150107	-3.735363
C	-2.638282	3.353763	0.088834	H	2.551372	0.345919	-3.084132
H	2.596519	-2.263533	4.117713	H	3.880022	1.382242	-2.478999
H	3.489982	-2.599942	2.615084				
H	3.795656	-1.076724	3.515915	82			
H	2.649669	0.918313	2.812689	VMA-EBI-SS-ansa-Re-TS SCF Done:			
H	1.005983	0.821890	1.933851	-1743.17406916 A.U.			
H	4.023718	2.474796	1.277071	Zr	-0.972570	0.428395	-0.182421
H	4.806348	2.100701	-0.273095	O	0.980540	1.022651	-0.521971
H	4.928675	0.935469	1.075028	C	2.273410	1.057797	-0.291619
H	2.048444	-0.823878	-0.660326	O	2.878439	2.280339	-0.284635
H	3.465051	-1.153473	0.353839	C	2.343952	3.364879	-0.949459
C	3.601932	-2.105707	-2.254584	C	3.094809	-0.035816	0.039732
C	5.463433	-0.669945	-1.410569	C	4.527342	0.264982	0.435905
C	3.628040	0.353049	-2.808948	H	5.174559	0.480342	-0.442414
C	-0.961967	4.202357	1.680381	H	4.594506	1.150766	1.097288
C	-1.864911	4.394807	0.584700	H	4.971556	-0.601288	0.965095
H	-0.380989	5.061915	2.046736	C	2.737922	-1.425262	-0.448695
H	-1.957295	5.398963	0.142895	H	1.643913	-1.464609	-0.633247
H	-0.147330	2.835566	3.153178	H	2.933422	-2.165873	0.358033
H	-3.355452	3.528752	-0.727938	C	3.463742	-1.952498	-1.746703
C	-1.397664	-4.153839	-1.334965	C	3.466647	-0.889373	-2.864854
C	-2.754702	-3.849101	-0.991722	C	4.916831	-2.395342	-1.453975
H	0.508586	-3.415990	-2.062241	C	2.682141	-3.198953	-2.224687

C	-3.098490	1.255282	0.849127	H	1.859972	-2.767471	4.158503
H	-3.989863	0.648003	0.646088	H	2.442995	-3.476994	2.633420
C	-2.254252	1.095335	1.978984	H	3.358231	-2.139245	3.406742
H	-2.388156	0.361040	2.783163	C	0.228787	-1.832285	1.961949
C	-1.248605	2.126756	1.933052	O	-0.515282	-1.119252	1.191944
C	-0.236138	2.524035	2.856867	O	-0.235518	-3.010964	2.425752
H	-0.081471	1.957860	3.788483	C	-1.549980	-3.413519	2.242920
C	0.500699	3.671557	2.585895	C	3.024663	4.520669	-1.022828
H	1.261023	4.014369	3.304547	H	1.361397	3.188647	-1.411815
C	0.267213	4.440361	1.403910	H	2.596185	5.365265	-1.580012
H	0.853658	5.356932	1.241212	H	4.008574	4.644269	-0.546143
C	-0.690302	4.065076	0.467832	C	-1.969667	-4.565454	2.788927
H	-0.876264	4.684850	-0.423110	H	-2.170441	-2.729474	1.646522
C	-1.470881	2.898663	0.717341	H	-3.014540	-4.877515	2.653609
C	-2.590889	2.307134	0.007143	H	-1.295623	-5.208028	3.375110
C	-3.206487	2.776628	-1.292165	H	3.923039	-1.295273	-3.791730
H	-4.052898	3.474360	-1.103558	H	2.438871	-0.555910	-3.124255
H	-2.455153	3.362049	-1.864167	H	4.045082	0.013269	-2.578263
C	-3.676036	1.564651	-2.130518	H	5.355954	-2.879382	-2.351452
H	-4.624106	1.163034	-1.717657	H	5.578488	-1.549760	-1.186246
H	-3.909898	1.880099	-3.169699	H	4.954734	-3.135991	-0.627233
C	-2.632155	0.469946	-2.131123	H	3.176162	-3.665737	-3.102058
C	-1.298455	0.558812	-2.645112	H	2.621993	-3.969990	-1.427057
H	-0.862622	1.443208	-3.132641	H	1.645087	-2.942001	-2.528936
C	-0.610273	-0.676556	-2.429763				
H	0.412167	-0.902789	-2.751728	82			
C	-1.535439	-1.594565	-1.826227	VMA-EBI-Cis-ansa+Re-TS SCF Done:			
C	-1.446013	-2.984668	-1.499659	-1743.17891290 A.U.			
H	-0.509822	-3.535941	-1.673991	Zr	-0.981010	-0.444800	0.099903
C	-2.574098	-3.630886	-1.017609	C	-2.535555	-0.294531	-1.851577
H	-2.531313	-4.709019	-0.799815	C	-1.225994	-0.343383	-2.418529
C	-3.807375	-2.929101	-0.809889	C	-0.719934	-1.679844	-2.226225
H	-4.684331	-3.485584	-0.443888	C	-1.704852	-2.416607	-1.444092
C	-3.924275	-1.574742	-1.090172	C	-2.833299	-1.531641	-1.195839
H	-4.891500	-1.062156	-0.967759	C	-4.095192	-1.877122	-0.438591
C	-2.790891	-0.877728	-1.620538	C	-3.770357	-2.352401	1.000394
C	2.013715	-0.195798	2.199800	C	-2.633156	-1.564111	1.615813
H	1.316004	0.608028	1.930575	C	-1.336475	-2.068852	1.977753
H	2.950222	0.119650	2.682619	C	-0.562917	-1.037498	2.583918
C	1.542399	-1.487109	2.423337	C	-1.395057	0.132665	2.683676
C	2.342694	-2.521909	3.188870	C	-2.676527	-0.184973	2.059055

C	-3.710357	0.803468	2.021902	H	6.593379	-1.333331	1.797434
C	-1.189231	1.416874	3.271583	H	6.092043	-0.239248	0.484988
H	0.458826	-1.142207	2.968580	H	6.159616	0.360381	2.174732
H	-4.675149	-2.281823	1.642223	H	4.778553	-2.978895	0.987729
H	-3.490564	-3.425184	0.997901	H	3.051500	-2.494484	0.990564
H	-4.748063	-0.980188	-0.412267	H	4.174865	-1.829017	-0.238124
H	-4.672662	-2.657145	-0.982720	H	-0.994436	-3.099409	1.802886
C	-1.473360	-3.795566	-1.132603	C	-2.218307	2.347475	3.224146
C	0.465181	-2.338264	-2.678137	C	-3.470889	2.044103	2.600233
H	-0.739542	0.454618	-2.991098	H	-0.239783	1.650437	3.778006
O	-0.983506	1.647884	0.103512	H	-2.082258	3.334752	3.692450
C	-0.349365	2.620790	-0.488545	H	-4.267796	2.804246	2.607527
C	0.997286	2.996596	-0.265548	H	-4.694140	0.569665	1.586225
C	1.742627	2.321139	0.738450	H	-3.200780	0.580306	-1.873949
C	1.567675	4.180228	-1.020568	C	-0.313989	-4.403762	-1.595636
O	-1.049917	3.409967	-1.340973	C	0.648760	-3.678104	-2.366780
C	-2.437564	3.368564	-1.368833	H	-2.224907	-4.379688	-0.580668
H	0.889748	5.057064	-0.979121	H	-0.140281	-5.471358	-1.389513
H	1.728925	3.954063	-2.096673	H	1.542001	-4.205907	-2.735764
H	2.542251	4.482679	-0.590813	H	1.191335	-1.795281	-3.300700
H	1.185816	1.696972	1.453968	C	-3.108686	3.955081	-2.372330
H	2.588025	2.880312	1.171350	H	-2.901650	2.865866	-0.505766
O	1.132038	-0.534951	0.041450	H	-4.207592	3.957604	-2.358183
C	2.088995	0.133966	-0.517088	H	-2.588240	4.451621	-3.205239
O	1.860952	0.417167	-1.831177	C	2.707345	0.962713	-3.987218
C	3.117467	0.775793	0.232162	H	3.743894	-0.228507	-2.513009
C	2.867545	0.377158	-2.791673	H	3.493520	0.855108	-4.747575
C	4.214368	1.574140	-0.451665	H	1.811416	1.552036	-4.234202
C	3.412367	0.221787	1.622330				
H	5.022201	0.931741	-0.857908	99			
H	4.695147	2.246008	0.288353	CS-Ph2-VMA-S-Si-TS SCF Done:			
H	3.833551	2.198140	-1.281749	-2165.64962194 A.U.			
H	3.773682	1.060887	2.257945	C	1.367727	-1.276688	-1.838379
H	2.452349	-0.117335	2.063270	C	2.138444	-0.132240	-1.422254
C	4.433589	-0.962225	1.779110	C	1.517252	1.015812	-2.028825
C	4.314128	-1.447326	3.243895	C	0.426020	0.572212	-2.845146
C	4.085939	-2.126178	0.829043	C	0.331231	-0.838668	-2.727154
C	5.892888	-0.511404	1.540680	Zr	-0.089464	0.086147	-0.380805
H	5.027874	-2.272393	3.446655	O	-1.607992	-1.334752	-0.152148
H	4.537201	-0.628916	3.960803	C	-2.673244	-1.816247	-0.745148
H	3.293413	-1.825224	3.466829	O	-2.518361	-2.944389	-1.495990

C	-1.371351	-3.713994	-1.402060	H	2.110466	-2.944132	0.762352
C	3.081740	-0.099840	-0.208014	H	0.537220	-4.381328	2.030968
C	3.956872	-1.368192	-0.074240	H	-1.222399	-3.395398	3.509351
C	4.427452	-1.782417	1.191060	H	-1.477306	-0.909913	3.695204
C	5.311161	-2.867204	1.309813	H	-1.331520	1.689960	3.545237
C	5.747077	-3.555221	0.163250	H	-0.717263	4.090502	3.178590
C	5.297991	-3.141503	-1.101862	H	1.167629	4.693441	1.642913
C	4.413958	-2.053834	-1.219672	H	2.486782	2.957620	0.470402
C	1.227894	-1.058912	1.483415	H	4.253365	1.123484	-2.417272
C	1.319964	-2.483277	1.368202	H	6.027434	2.864614	-2.451830
C	0.438742	-3.286087	2.094002	H	6.937489	3.792022	-0.300136
C	-0.562237	-2.727811	2.934983	H	6.041852	2.942254	1.890617
C	-0.706506	-1.345396	3.041290	H	4.252286	1.215403	1.928862
C	0.164173	-0.502699	2.308412	H	4.094656	-1.256334	2.099355
C	0.245242	0.943287	2.221917	H	5.662136	-3.176134	2.306927
C	1.370207	1.276447	1.356106	H	6.439750	-4.406055	0.255948
C	1.989731	0.037198	0.883326	H	5.642054	-3.662904	-2.008929
C	1.652759	2.660132	1.118683	H	4.090685	-1.731200	-2.221713
C	0.907336	3.632791	1.786990	H	1.839370	2.057921	-1.907788
C	-0.161470	3.292995	2.662652	H	-0.219398	1.218865	-3.453872
C	-0.506654	1.958697	2.867601	H	-0.378621	-1.497626	-3.243605
O	-1.378206	1.746455	-0.687063	H	1.562975	-2.318438	-1.558534
C	-2.431043	2.271390	-1.220831	H	-5.191551	2.799411	-1.505624
C	-3.420973	1.603912	-2.008487	H	-5.392176	1.692264	-2.905776
C	-3.206589	0.284379	-2.412379	H	-4.449351	3.205089	-3.071140
C	4.099616	1.062666	-0.241327	H	-2.192656	-0.132459	-2.405500
C	4.623363	1.532785	-1.464390	H	-3.899811	-0.169654	-3.135302
C	5.633613	2.511413	-1.485861	H	-4.722312	-2.381490	-2.442106
C	6.144916	3.027917	-0.283893	H	-5.467481	-2.815169	-0.887760
C	5.643009	2.552561	0.940894	H	-5.914930	-1.275723	-1.675104
C	4.633353	1.576930	0.961024	H	-3.362005	0.227807	0.700439
O	-2.674876	3.584215	-1.028463	H	-4.895030	0.598611	-0.112268
C	-1.774302	4.419278	-0.386205	H	-4.627402	-2.891185	1.417555
C	-4.679210	2.361186	-2.386560	H	-5.010281	-2.354792	3.079681
C	-3.957457	-1.235307	-0.743677	H	-3.421110	-1.951479	2.349957
C	-4.304634	-0.230466	0.336326	H	-6.792796	-1.751341	0.573703
C	-5.099610	-0.738687	1.597498	H	-7.155560	-1.178937	2.221913
C	-4.505234	-2.054978	2.137481	H	-7.052809	-0.002886	0.877154
C	-5.067292	-1.961411	-1.477326	H	-5.539467	0.095056	3.589577
C	-4.967486	0.362017	2.676498	H	-3.907078	0.511915	2.973660
C	-6.602953	-0.930068	1.291612	H	-5.356218	1.336672	2.311800

C	-2.065929	5.722362	-0.249688
H	-0.857703	3.929365	-0.027673
H	-1.348038	6.386700	0.251115
H	-3.006567	6.149103	-0.629148
C	-1.122263	-4.674640	-2.307622
H	-0.738585	-3.495127	-0.527209
H	-0.236060	-5.313160	-2.186761
H	-1.795074	-4.858770	-3.158897

99

CS-Ph2-VMA-S-Re-TS SCF Done:

-2165.64627528 A.U.

C	-4.593197	-1.913668	-0.239413
C	-3.851900	-1.332690	0.813116
C	-4.036555	-1.832116	2.119982
C	-4.916816	-2.901647	2.364305
C	-5.635465	-3.483198	1.306859
C	-5.473143	-2.980646	0.003405
C	-2.980817	-0.081122	0.557518
C	-3.980279	1.096962	0.625619
C	-4.757274	1.443459	-0.501670
C	-5.745899	2.437050	-0.415687
C	-5.981649	3.099397	0.802415
C	-5.225265	2.752079	1.933969
C	-4.236599	1.755312	1.847128
C	-1.801235	0.061006	1.534080
C	-0.956610	-1.014472	1.985762
C	0.243026	-0.457605	2.538064
C	0.178706	0.952069	2.400355
C	-1.069827	1.277367	1.772712
Zr	0.162382	0.010453	0.028610
C	-1.634154	1.020221	-1.485492
C	-2.148597	-0.133256	-0.749759
C	-1.534462	-1.316668	-1.357599
C	-0.658584	-0.890783	-2.443036
C	-0.713484	0.556113	-2.516725
C	0.004702	-1.839891	-3.263724
C	-0.181801	-3.197347	-3.015758
C	-0.990714	-3.624978	-1.926435
C	-1.641105	-2.719291	-1.087993
C	-1.839364	2.432245	-1.349526
C	-1.201657	3.304420	-2.231251
C	-0.329053	2.833628	-3.252367
C	-0.079641	1.470214	-3.396551
O	1.375947	1.654091	-0.472586
C	2.455561	2.295181	-0.752766
C	3.610168	1.735169	-1.388545
C	3.547730	0.409157	-1.806645
O	1.690034	-1.421854	-0.001141
C	2.940464	-1.779023	-0.164622
O	3.176302	-2.980655	-0.766710
C	2.219367	-3.973224	-0.814924
O	2.544976	3.604856	-0.443466
C	1.475399	4.293605	0.111952
C	4.840999	2.597414	-1.575882
C	4.086312	-1.016083	0.131244
C	4.017852	0.051200	1.200013
C	4.612123	-0.281910	2.622722
C	4.139268	-1.664060	3.117523
C	5.434434	-1.566661	-0.288840
C	6.158007	-0.229966	2.631270
C	4.099384	0.811776	3.589277
H	5.203005	3.032430	-0.621465
H	4.634166	3.451549	-2.254960
H	5.663274	2.005080	-2.020878
H	5.391274	-2.049660	-1.284165
H	5.815884	-2.337667	0.416643
H	6.189072	-0.755949	-0.326296
H	4.381740	-0.017114	-2.383329
H	2.575293	-0.091610	-1.910644
H	4.508935	-2.485513	2.470051
H	3.030790	-1.734056	3.141807
H	4.504757	-1.859823	4.147090
H	6.618683	-1.042715	2.038140
H	6.537169	-0.331371	3.669806
H	6.532120	0.737858	2.234981
H	4.526475	0.675311	4.604394
H	2.993341	0.784578	3.689973
H	4.385210	1.827329	3.241094
H	4.527907	0.974104	0.841052
H	2.954260	0.333776	1.346579
H	-1.199122	-2.083810	1.937225

H	1.068682	-1.030359	2.977309
H	0.936528	1.674463	2.729442
H	-1.423902	2.289211	1.542415
H	-2.277073	-3.085946	-0.272304
H	-1.118414	-4.703773	-1.744902
H	0.304100	-3.946489	-3.657988
H	0.630545	-1.503674	-4.104965
H	0.586956	1.103136	-4.192192
H	0.140480	3.554100	-3.939564
H	-1.392569	4.385734	-2.146220
H	-2.536784	2.823594	-0.597970
H	-4.584958	0.936654	-1.464014
H	-6.337446	2.694151	-1.308363
H	-6.757516	3.877713	0.870055
H	-5.408604	3.253169	2.897457
H	-3.669524	1.481816	2.750578
H	-3.500443	-1.375798	2.966472
H	-5.044408	-3.276095	3.392152
H	-6.325440	-4.319713	1.497795
H	-6.037478	-3.421297	-0.833394
H	-4.478591	-1.532913	-1.266225
C	2.513753	-5.169390	-1.351518
H	1.248280	-3.705637	-0.372569
H	1.753064	-5.962242	-1.354665
H	3.503951	-5.383904	-1.780747
C	1.651329	5.546404	0.559379
H	0.524462	3.740881	0.117811
H	0.796531	6.095502	0.978345
H	2.631362	6.044856	0.514360

99

VMA-CS-Cis-SS-Re-TS SCF Done:

-2165.64252321 A.U.

Zr	-0.018388	0.235577	-0.343474
C	1.195615	-0.893995	1.564066
C	0.307557	-0.041317	2.345496
C	0.658532	1.337334	2.066241
C	0.152961	2.553703	2.593233
C	1.761335	1.332718	1.111100
C	2.111639	-0.052798	0.795655
C	3.061370	-0.535296	-0.330111
C	2.033818	-0.538979	-1.476202
C	1.581978	0.622679	-2.197923
C	0.363902	0.297980	-2.881594
C	0.030418	-1.044134	-2.570341
H	-0.836916	-1.604299	-2.941201
C	1.039059	-1.559447	-1.691243
C	0.991702	-2.311051	1.621001
C	-0.672212	-0.598916	3.205182
H	2.093343	1.592884	-2.236754
H	-0.205481	0.978109	-3.527895
O	-1.789185	-0.886195	0.016558
C	-2.986777	-0.478167	0.292353
C	-4.124171	-0.811670	-0.500158
C	-5.514224	-0.324632	-0.127443
O	-3.020487	0.534236	1.212407
C	-4.023408	-2.065551	-1.366173
C	-4.391223	-3.463711	-0.752167
C	-3.950846	-4.523690	-1.790096
C	-3.636564	-3.705609	0.570656
C	-5.911397	-3.618429	-0.520140
H	-6.182380	-0.411096	-1.008265
H	-5.978825	-0.929819	0.677401
H	-2.980205	-2.139924	-1.737438
H	-4.667289	-1.914970	-2.261266
H	-2.538384	-3.621566	0.436727
H	-3.936316	-2.977274	1.354775
H	-3.857972	-4.719498	0.964609
H	-6.489895	-3.401878	-1.442996
H	-6.290381	-2.956449	0.283639
H	-6.148276	-4.660085	-0.218168
H	-4.196938	-5.547227	-1.438907
H	-4.462638	-4.372968	-2.764253
H	-2.855626	-4.484572	-1.972125
O	-1.138808	1.949988	-0.791436
C	-2.256818	2.573352	-1.025784
C	-3.469731	2.012329	-1.489920
C	-3.517316	0.645559	-1.881303
C	-4.682882	2.914329	-1.624009
O	-2.288925	3.916712	-0.841611
H	-2.570494	0.139359	-2.129171
H	-4.357799	0.367168	-2.538451

H	-5.537610	2.356263	-2.052823	C	4.619984	-4.024718	-0.917537
H	-5.006254	3.336251	-0.648792	C	5.070417	-4.362530	0.369583
H	1.063936	-2.576442	-1.281970	C	4.842458	-3.474642	1.436167
C	2.261469	2.594173	0.652018	C	4.164707	-2.264279	1.217681
C	3.694854	-1.921451	-0.069047	H	3.613851	-2.555214	-2.154612
C	4.270380	0.395163	-0.580940	H	4.801788	-4.705344	-1.764094
C	-1.136700	4.655361	-0.643762	H	5.603006	-5.310884	0.540740
H	-4.477481	3.779752	-2.288169	H	5.196635	-3.724505	2.448622
C	-3.953977	0.566898	2.242246	H	3.993905	-1.580786	2.064094
H	-5.519500	0.731557	0.201940				
C	-4.174698	1.688792	2.942926	80			
H	-4.422290	-0.404425	2.466281	MMA-EBI-SS-ansa+-Si-TS SCF Done:			
H	-4.873861	1.664366	3.790421	-1667.06690506 A.U.			
H	-3.682455	2.639080	2.687073	Zr	-0.967000	-0.300038	0.000130
C	-1.214052	5.988368	-0.500853	O	0.806582	-0.905758	0.852104
H	-0.205770	4.069959	-0.622299	C	1.853322	-0.572197	1.592783
H	-0.292981	6.570588	-0.359575	O	1.862044	-0.998056	2.880097
H	-2.177399	6.519437	-0.529093	C	0.973807	-2.047160	3.282766
C	0.010100	-2.827431	2.467612	H	-0.070548	-1.687229	3.382215
C	-0.809617	-1.984509	3.266724	H	1.334434	-2.380993	4.272900
H	1.635300	-2.991231	1.048718	H	1.001255	-2.893348	2.566170
H	-0.119246	-3.919187	2.530190	C	2.925078	0.225873	1.167098
H	-1.554493	-2.434493	3.940813	C	4.005525	0.561587	2.174422
H	-1.309088	0.058212	3.816573	H	4.792065	-0.223856	2.230198
C	1.748829	3.771369	1.200098	H	3.595422	0.670239	3.197007
C	0.711541	3.759135	2.173566	H	4.515184	1.507307	1.900218
H	3.083106	2.638246	-0.074440	C	3.172587	0.424593	-0.312503
H	2.173159	4.735917	0.879287	H	2.274677	0.073073	-0.862752
H	0.345825	4.709802	2.589650	H	3.258774	1.512408	-0.539752
H	-0.653586	2.537555	3.342068	C	4.424259	-0.276033	-0.965059
C	4.769689	0.600825	-1.884480	C	4.559593	-1.737661	-0.490801
C	5.936211	1.357642	-2.097113	C	5.733747	0.490820	-0.666413
C	6.628524	1.912900	-1.008342	C	4.200704	-0.253071	-2.495544
C	6.149039	1.698896	0.296410	C	-3.234086	0.877655	0.625769
C	4.984069	0.944036	0.507286	C	-3.939330	1.722925	-0.290199
H	4.254458	0.154948	-2.749354	C	-2.280225	1.462416	1.563154
H	6.307773	1.506352	-3.123169	C	-2.074162	2.875656	1.577822
H	7.542329	2.504367	-1.174009	C	-1.739150	0.391819	2.358313
H	6.687325	2.121112	1.159506	C	-2.416581	-0.808187	1.979571
H	4.623293	0.784956	1.535398	C	-3.322983	-0.542128	0.901770
C	3.941719	-2.812108	-1.135222	C	-4.252206	-1.532346	0.239810

H	-5.309259	-1.216577	0.379110	H	-4.272238	3.758898	-0.921645
H	-4.157995	-2.506947	0.760360	H	-4.688090	1.301881	-0.978527
C	-3.927722	-1.686357	-1.264888	H	5.376434	-2.254839	-1.036549
H	-4.380193	-0.855852	-1.844523	H	4.790765	-1.802051	0.592281
H	-4.381844	-2.618693	-1.666887	H	3.623518	-2.308188	-0.662340
C	-2.436189	-1.683608	-1.508367	H	6.580372	0.038121	-1.224261
C	-1.474653	-2.653976	-1.014090	H	5.660295	1.553413	-0.981892
C	-1.614743	-3.817285	-0.190091	H	6.004754	0.472261	0.406612
C	-0.172134	-2.326269	-1.581951	H	5.072644	-0.680738	-3.032902
C	0.945400	-3.176097	-1.331887	H	3.305887	-0.844451	-2.787844
C	-0.324649	-1.125202	-2.358929	H	4.056718	0.784071	-2.867777
C	-1.710167	-0.782373	-2.353256				
C	1.409171	2.238744	1.482076	80			
H	0.593971	1.547859	1.727548	MMA-EBI-SS-ansa+Re-TS SCF Done:			
H	2.053260	2.552774	2.316024	-1667.06032075 A.U.			
C	1.382991	2.976993	0.310296	C	-2.666324	-0.768607	-1.759551
C	2.293678	4.162430	0.066088	C	-2.197622	-2.038939	-1.238033
H	1.712153	5.105617	-0.012096	C	-0.804504	-2.205831	-1.644716
H	2.867387	4.066772	-0.878554	C	-0.419793	-1.029319	-2.372371
H	3.012790	4.276026	0.899658	C	-1.566353	-0.190423	-2.476977
C	0.435442	2.616350	-0.714259	Zr	-0.970309	-0.031990	-0.044703
O	-0.330703	1.582532	-0.700368	C	-3.352409	0.546415	0.622673
O	0.374040	3.449279	-1.754975	C	-2.744256	1.855005	0.469805
C	-0.541368	3.167124	-2.830603	C	-1.744286	2.013169	1.522257
H	-1.576813	3.067941	-2.447843	C	-1.714540	0.791584	2.277895
H	-0.243776	2.238450	-3.358338	C	-2.725803	-0.069334	1.750698
H	-0.465399	4.028467	-3.517203	C	-4.493819	-0.010912	-0.194630
H	0.465778	-0.622574	-2.930656	C	-4.072122	-0.221349	-1.667721
H	-2.163868	0.059357	-2.895975	O	0.178617	-1.248069	1.253935
H	-2.274440	-1.798224	2.436906	C	1.101649	-1.396067	2.145187
H	-1.032444	0.499474	3.190921	O	1.234656	-2.575966	2.756276
C	0.769908	-4.303853	-0.542297	C	0.271817	-3.620270	2.527607
C	-0.502639	-4.620392	0.031546	C	2.042144	-0.392535	2.567980
C	-2.785679	3.664362	0.683971	C	3.185892	-0.818478	3.466478
C	-3.709635	3.091973	-0.249582	C	1.864623	0.927263	2.168164
H	-2.596549	-4.102393	0.217247	C	2.873251	1.305752	-0.016618
H	-0.605017	-5.535717	0.635257	C	3.175079	-0.149405	-0.312757
H	1.619087	-4.982239	-0.365553	C	4.073061	-0.478963	-1.564978
H	1.920552	-2.953080	-1.788781	C	1.663902	1.876672	-0.454844
H	-1.387360	3.330163	2.307585	O	0.548801	1.213501	-0.699742
H	-2.659531	4.758216	0.705157	C	4.011586	2.255263	0.302783

O	1.617205	3.225592	-0.559748	H	0.912758	-3.577842	-1.715547
C	0.787524	3.802125	-1.579723	H	-3.925773	-3.017502	-0.274319
C	-0.126226	-3.435740	-1.381044	H	-2.705213	-5.145394	0.128935
H	0.562262	-0.836338	-2.819174	H	-0.332347	-5.437658	-0.605947
H	-1.604890	0.769311	-3.012643	H	4.597073	-2.321204	-2.654569
C	-2.866526	-3.108036	-0.559071	H	4.271832	-2.579223	-0.912177
C	-1.086464	3.272233	1.694523	H	2.911295	-2.294679	-2.048844
H	-1.094669	0.592680	3.161088	H	4.182200	-0.007345	-3.708746
H	-2.986314	-1.062888	2.143022	H	2.521047	0.044170	-3.045306
H	-4.816279	-0.970399	0.258248	H	3.668209	1.375918	-2.695381
H	-5.375271	0.664296	-0.134155	H	6.184495	-0.524880	-2.155605
H	-4.113054	0.738817	-2.221942	H	5.754873	0.933628	-1.225655
H	-4.785301	-0.900672	-2.184541	H	5.934716	-0.642315	-0.388198
C	-3.061542	2.962036	-0.380237				
H	-0.717989	-3.326348	2.932793	80			
H	0.654028	-4.499477	3.075531	MMA-EBI-Cis-SS-ansa+Re-TS SCF Done:			
H	0.176962	-3.842789	1.447750	-1667.06222694 A.U.			
H	2.812631	-1.178940	4.448430	Zr	-1.011572	-0.310781	-0.004466
H	3.777369	-1.649749	3.030165	C	-2.590477	-0.688878	-1.908998
H	3.868244	0.032442	3.654672	C	-1.287991	-0.849731	-2.472892
H	2.502195	1.710967	2.603013	C	-0.745946	-2.083078	-1.964028
H	0.901154	1.260186	1.765598	C	-1.702577	-2.624632	-1.005723
H	3.661675	3.141218	0.868203	C	-2.853149	-1.737420	-0.970632
H	4.510044	2.647007	-0.611326	C	-4.104573	-1.919565	-0.144300
H	4.788430	1.741582	0.903289	C	-3.769041	-1.989675	1.366390
H	2.215375	-0.691134	-0.444946	C	-2.668998	-1.022034	1.746259
H	3.666153	-0.614802	0.570918	C	-1.367840	-1.360412	2.253899
H	-0.262521	3.458296	-1.507774	C	-0.642108	-0.175097	2.566259
H	0.830946	4.895357	-1.426768	C	-1.510862	0.946626	2.324668
H	1.196243	3.556049	-2.583423	C	-2.764169	0.423567	1.786793
C	3.955539	-2.001981	-1.807121	C	-3.823828	1.326734	1.457261
C	5.563713	-0.152874	-1.313658	C	-1.359075	2.349743	2.538077
C	3.583741	0.275787	-2.817712	H	0.370359	-0.134827	2.986046
C	-1.452124	4.333502	0.879710	H	-4.678960	-1.791114	1.973464
C	-2.431179	4.179047	-0.154814	H	-3.444607	-3.013504	1.641903
H	-0.991290	5.321247	1.035141	H	-4.791409	-1.072732	-0.350219
H	-2.702384	5.052667	-0.768116	H	-4.649226	-2.835737	-0.463285
H	-0.352796	3.409689	2.503372	C	-1.427428	-3.871898	-0.357191
H	-3.838125	2.870370	-1.155125	C	0.454687	-2.803310	-2.249101
C	-0.823242	-4.464054	-0.762277	H	-0.822752	-0.205058	-3.227762
C	-2.184365	-4.298598	-0.344840	O	-0.904048	1.693997	-0.538501

C	-0.200566	2.660814	-1.057756	H	-4.457060	3.389800	1.458345
C	1.121920	3.023288	-0.690153	H	-4.788180	0.948136	1.084647
C	1.763800	2.357013	0.385280	H	-3.286193	0.134519	-2.125551
C	1.764866	4.200373	-1.398789	C	-0.253561	-4.545852	-0.666421
O	-0.788861	3.449443	-1.972394	C	0.681130	-4.014284	-1.611376
C	-2.170976	3.240947	-2.302944	H	-2.156309	-4.315673	0.337289
H	1.121887	5.104307	-1.351353	H	-0.044823	-5.519651	-0.196880
H	1.942320	4.004454	-2.478400	H	1.588677	-4.592398	-1.844923
H	2.737823	4.452681	-0.933947	H	1.165107	-2.418889	-2.994969
H	1.142559	1.767068	1.077183	H	-2.465531	4.112447	-2.914703
H	2.594346	2.900079	0.865614	H	-2.295968	2.314609	-2.900835
O	1.084319	-0.515375	-0.000262	H	-2.796829	3.183804	-1.390033
C	2.035037	0.072422	-0.671607	H	2.241672	-0.240698	-3.913466
O	1.741805	0.208592	-1.982742	H	3.003043	1.271574	-3.302837
C	3.098169	0.746356	-0.000428	H	3.626324	-0.345273	-2.762231
C	2.725085	0.233977	-3.037675				
C	4.207935	1.471700	-0.744875	97			
C	3.406991	0.295321	1.424546	MMA-CS-Ph2-S-Si-TS SCF Done:			
H	4.963014	0.787707	-1.183157	-2089.53333943 A.U.			
H	4.755404	2.121273	-0.032536	C	1.351382	-1.056822	-2.029538
H	3.825388	2.123295	-1.551424	C	2.101956	0.036308	-1.465206
H	3.805394	1.172509	1.982340	C	1.480674	1.242756	-1.940459
H	2.448841	0.020148	1.911244	C	0.405971	0.891886	-2.820526
C	4.399374	-0.899617	1.656205	C	0.324773	-0.523524	-2.877548
C	4.319098	-1.249429	3.161567	Zr	-0.153629	0.096232	-0.442732
C	3.985286	-2.133508	0.827847	O	-1.653149	-1.331554	-0.383337
C	5.860304	-0.517901	1.326538	C	-2.771224	-1.746857	-0.957837
H	5.018852	-2.072899	3.414264	O	-2.687092	-2.834891	-1.763989
H	4.587045	-0.377715	3.795602	C	-1.542002	-3.690588	-1.678138
H	3.297442	-1.577451	3.449247	C	3.026028	-0.072737	-0.242960
H	6.548286	-1.334185	1.630863	C	3.912668	-1.339705	-0.250123
H	6.023625	-0.347286	0.243768	C	4.369620	-1.901022	0.962365
H	6.174916	0.398927	1.868583	C	5.272495	-2.976512	0.961624
H	4.652118	-2.992762	1.049962	C	5.741614	-3.507678	-0.253147
H	2.943181	-2.444065	1.048506	C	5.304186	-2.948416	-1.465281
H	4.054977	-1.940191	-0.264342	C	4.400844	-1.870309	-1.463148
H	-0.990652	-2.386550	2.374666	C	1.163930	-1.243865	1.304005
C	-2.412656	3.194618	2.215354	C	1.268873	-2.643370	1.024587
C	-3.637380	2.686875	1.675429	C	0.403784	-3.534045	1.661989
H	-0.431803	2.748299	2.977789	C	-0.593859	-3.087636	2.570009
H	-2.318014	4.276687	2.396448	C	-0.751002	-1.727362	2.835090

C	0.103974	-0.797672	2.196938	H	4.012698	-1.497296	1.922548
C	0.172319	0.649132	2.279749	H	5.612760	-3.401539	1.918936
C	1.285383	1.092552	1.449403	H	6.450211	-4.350415	-0.253871
C	1.915774	-0.076743	0.837168	H	5.672916	-3.346920	-2.423537
C	1.556043	2.496744	1.375266	H	4.088036	-1.430661	-2.423186
C	0.815586	3.377207	2.164626	H	1.792024	2.264075	-1.688322
C	-0.235042	2.925324	3.010915	H	-0.239076	1.599173	-3.357783
C	-0.572810	1.573346	3.055838	H	-0.372120	-1.110613	-3.489492
O	-1.431267	1.804310	-0.597145	H	1.563746	-2.120854	-1.869258
C	-2.437770	2.401525	-1.135871	H	-1.743021	3.916126	1.035113
C	-3.398175	1.823065	-2.045197	H	-0.740527	4.394047	-0.387582
C	-3.185732	0.549866	-2.545820	H	-2.160860	5.416135	0.096370
C	4.034760	1.092149	-0.121832	H	-5.174153	2.993770	-1.515891
C	4.575913	1.700288	-1.274511	H	-5.310785	2.048425	-3.037963
C	5.581287	2.678197	-1.168114	H	-4.336564	3.551730	-2.982338
C	6.069474	3.057042	0.093395	H	-2.203162	0.071250	-2.475686
C	5.549579	2.444192	1.247582	H	-3.876148	0.132279	-3.293059
C	4.545252	1.468554	1.140005	H	-1.768585	-4.557849	-2.324847
O	-2.667221	3.682237	-0.838565	H	-1.377040	-4.030285	-0.635290
C	-1.765474	4.387060	0.033426	H	-0.621119	-3.192860	-2.044052
C	-4.619520	2.642744	-2.410342	H	-4.882377	-2.150186	-2.578036
C	-4.027593	-1.133511	-0.844588	H	-5.640888	-2.607705	-1.037241
C	-4.285300	-0.131637	0.257361	H	-5.995894	-1.009022	-1.748123
C	-5.132170	-0.589996	1.503666	H	-3.307836	0.226503	0.640965
C	-4.636181	-1.948991	2.037048	H	-4.792103	0.764982	-0.168242
C	-5.190161	-1.753932	-1.590950	H	-4.807389	-2.766635	1.306135
C	-4.937770	0.490207	2.593825	H	-5.168050	-2.222843	2.972529
C	-6.641604	-0.673874	1.181044	H	-3.548859	-1.922678	2.258035
H	2.056053	-3.023716	0.361150	H	-6.879956	-1.484942	0.466514
H	0.515472	-4.613709	1.474416	H	-7.222698	-0.873797	2.105891
H	-1.241994	-3.822929	3.070865	H	-7.017190	0.280187	0.753544
H	-1.519332	-1.378864	3.541720	H	-5.531245	0.252336	3.501233
H	-1.382600	1.218505	3.711818	H	-3.872001	0.571883	2.898269
H	-0.777476	3.647949	3.640163	H	-5.263465	1.490180	2.235081
H	1.066318	4.449795	2.144685				
H	2.381090	2.875051	0.758416	97			
H	4.224241	1.399613	-2.273724	MMA-CS-Ph2-S-Re-TS SCF Done:			
H	5.989486	3.139569	-2.081073	-2089.53129405 A.U.			
H	6.858305	3.820604	0.177403	C	-4.571816	-1.765561	-0.539349
H	5.930716	2.724964	2.241964	C	-3.830542	-1.362940	0.593546
H	4.150894	0.997062	2.053655	C	-4.050726	-2.036273	1.813777

C	-4.966331	-3.101176	1.893776	C	4.145084	-0.109007	1.078521
C	-5.685545	-3.503711	0.756495	C	4.793018	-0.624716	2.419309
C	-5.487141	-2.827522	-0.460701	C	4.283849	-2.036232	2.776503
C	-2.925536	-0.110665	0.530141	C	5.438875	-1.551829	-0.678839
C	-3.902392	1.068130	0.751747	C	6.337969	-0.632282	2.354578
C	-4.652042	1.589532	-0.325584	C	4.370170	0.366640	3.528977
C	-5.624200	2.580377	-0.112989	H	1.575206	3.624431	1.804463
C	-5.871029	3.064682	1.184131	H	0.646662	4.137379	0.333902
C	-5.141553	2.542856	2.265273	H	1.936980	5.215437	1.021962
C	-4.168940	1.549541	2.051180	H	5.275061	3.035153	-0.465274
C	-1.762442	-0.138752	1.537017	H	4.588523	3.654716	-1.984838
C	-0.948447	-1.288420	1.838101	H	5.602686	2.178117	-2.009520
C	0.246171	-0.848602	2.494547	H	5.325986	-1.913623	-1.719200
C	0.213580	0.566247	2.566419	H	5.849031	-2.404561	-0.093569
C	-1.014393	1.011063	1.970115	H	6.205204	-0.751163	-0.667542
Zr	0.231837	0.002024	0.073666	H	2.438041	-4.682564	-1.829382
C	-1.520428	1.233032	-1.320507	H	1.140201	-3.628043	-1.137872
C	-2.074246	0.002151	-0.761391	H	2.333658	-4.443160	-0.041141
C	-1.470582	-1.099878	-1.513121	H	4.257161	0.222064	-2.493847
C	-0.552053	-0.550374	-2.504581	H	2.493693	0.115189	-1.899795
C	-0.577388	0.893500	-2.380593	H	4.584069	-2.786920	2.016261
C	0.106007	-1.393239	-3.439476	H	3.175771	-2.062471	2.853794
C	-0.136196	-2.763760	-3.402845	H	4.692211	-2.368564	3.753812
C	-0.990028	-3.317669	-2.406847	H	6.732987	-1.379776	1.640456
C	-1.630742	-2.521889	-1.457213	H	6.761595	-0.878361	3.350966
C	-1.715368	2.618613	-1.009793	H	6.735651	0.362805	2.062568
C	-1.050014	3.587703	-1.758978	H	4.829812	0.095503	4.502173
C	-0.154286	3.241511	-2.810645	H	3.267984	0.372327	3.672127
C	0.088361	1.905370	-3.120277	H	4.688165	1.403587	3.287808
O	1.458345	1.689694	-0.140410	H	4.663459	0.838655	0.806930
C	2.519430	2.356205	-0.449885	H	3.099531	0.178106	1.314843
C	3.599678	1.858371	-1.249926	H	-1.206791	-2.332396	1.618975
C	3.482355	0.586070	-1.802910	H	1.053377	-1.498482	2.853397
O	1.733753	-1.437521	-0.068469	H	0.979324	1.209070	3.018376
C	2.961329	-1.773918	-0.406388	H	-1.339341	2.054602	1.880089
O	3.113594	-2.871779	-1.182098	H	-2.302490	-2.980148	-0.720572
C	2.190167	-3.959474	-1.031376	H	-1.164348	-4.405254	-2.393916
O	2.655587	3.608322	0.000453	H	0.335931	-3.425710	-4.144690
C	1.631740	4.169777	0.840367	H	0.764954	-0.960067	-4.207874
C	4.830242	2.721719	-1.432494	H	0.771485	1.634877	-3.939972
C	4.128343	-1.039607	-0.114332	H	0.336690	4.038070	-3.390477

H	-1.242300	4.651637	-1.547279	H	-3.624424	1.137057	2.914869
H	-2.422990	2.920023	-0.227078	H	-3.515051	-1.721116	2.722514
H	-4.470934	1.222815	-1.347919	H	-5.121611	-3.612831	2.856621
H	-6.194348	2.975257	-0.968500	H	-6.403653	-4.336017	0.818855
H	-6.634210	3.840478	1.351587	H	-6.050892	-3.127200	-1.358073
H	-5.333558	2.903818	3.287964	H	-4.429645	-1.246979	-1.500322

B.4. References

(1) Vidal, F.; Gowda, R. R.; Chen, E. Y.-X. *J. Am. Chem. Soc.* **2015**, *137*, 9469−9480.

(2) Allen, R. D.; Long, T. E.; McGrath, J. E. *Polym. Bull.* **1986**, *15*, 127−134.

(3) (a) Rodriguez-Delgado, A.; Chen, E. Y.-X. *Macromolecules* **2005**, *38*, 2587−2594. (b) Bolig, A. D.; Chen, E. Y.-X. *J. Am. Chem. Soc.* **2004**, *126*, 4897−4906.

(4) (a) Zhang, Y.; Ning, Y.; Caporaso, L.; Cavallo, L.; Chen, E. Y.-X. *J. Am. Chem. Soc.* **2010**, *132*, 2695–2709. (b) Ning, Y.; Chen, E. Y.-X. *J. Am. Chem. Soc.* **2008**, *130*, 2463−2465.

(5) Mariott, W. R.; Rodriguez-Delgado, A.; Chen, E. Y.-X. *Macromolecules* **2006**, *39*, 1318−1327.

(6) Gaussian 09, Revision D.01, Frisch, M. J.; Trucks, G. W.; Schlegel, H. B.; Scuseria, G. E.; Robb, M. A.; Cheeseman, J. R.; Scalmani, G.; Barone, V.; Mennucci, B.; Petersson, G. A.; Nakatsuji, H.; Caricato, M.; Li, X.; Hratchian, H. P.; Izmaylov, A. F.; Bloino, J.; Zheng, G.; Sonnenberg, J. L.; Hada, M.; Ehara, M.; Toyota, K.; Fukuda, R.; Hasegawa, J.; Ishida, M.; Nakajima, T.; Honda, Y.; Kitao, O.; Nakai, H.; Vreven, T.; Montgomery, J. A., Jr.; Peralta, J. E.; Ogliaro, F.; Bearpark, M.; Heyd, J. J.; Brothers, E.; Kudin, K. N.; Staroverov, V. N.; Kobayashi, R.; Normand, J.; Raghavachari, K.; Rendell, A.; Burant, J. C.; Iyengar, S. S.; Tomasi, J.; Cossi, M.; Rega, N.; Millam, J. M.; Klene, M.; Knox, J. E.; Cross, J. B.; Bakken, V.; Adamo, C.; Jaramillo, J.; Gomperts, R.; Stratmann, R. E.; Yazyev, O.; Austin, A. J.;

Cammi, R.; Pomelli, C.; Ochterski, J. W.; Martin, R. L.; Morokuma, K.; Zakrzewski, V. G.; Voth, G. A.; Salvador, P.; Dannenberg, J. J.; Dapprich, S.; Daniels, A. D.; Farkas, Ö.; Foresman, J. B.; Ortiz, J. V.; Cioslowski, J.; Fox, D. J. Gaussian, Inc., Wallingford CT, **2009**.

(7) (a) Becke, A. D. *Phys. Rev. A* **1988**, *38*, 3098–3100. (b) Perdew, J. P. *Phys. Rev. B* **1986**, *33*, 8822–8824. (c) Perdew, J. P. *Phys. Rev. B* **1986**, *34*, 7406–7406.

(8) Weigend, F.; Ahlrichs, R. *Phys. Chem. Chem. Phys.* **2005**, *7*, 3297–3305.

(9) (a) Leininger, T.; Nicklass, A.; Stoll, H.; Dolg, M.; Schwerdtfeger, P. *J. Chem. Phys.* **1996**, *105*, 1052–1059. (b) Kuechle, W.; Dolg, M.; Stoll, H.; Preuss, H. *J. Chem. Phys.* **1994**, *100*, 7535–7542. (c) Haeusermann, U.; Dolg, M.; Stoll, H.; Preuss, H. *Mol. Phys.* **1993**, *78*, 1211–1224.

(10) (a) Tomasi, J.; Mennucci, B.; Cammi, R. *Chem. Rev.* **2005**, *105*, 2999–3094. (b) Barone, V.; Cossi, M. *J. Phys. Chem. A.* **1998**, *102*, 1995–2001.

APPENDIX C

Experimental Details and Supporting Information for Chapter 4:

C.1. Materials, Reagents, and Methods

All synthesis and manipulations with air- and moisture-sensitive chemicals and reagents were performed using standard Schlenk techniques on a dual-manifold Shlenk line or in an inert gas (Ar or N_2)-filled glovebox. NMR-scale reactions were conducted in Teflon-valve-sealed J. Young-type NMR tubes. NMR (^{1}H, ^{13}C, and ^{19}F) spectra were recorded on a Varian Inova 400 MHz or 500 MHz spectrometer. Benzene-d_6 and toluene-d_8 were dried over sodium/potassium alloy and vacuum-distilled or filtered, whereas CD_2Cl_2, C_6D_5Br and $CDCl_3$ were dried over CaH_2 and vacuum-distilled. Chemical shifts were referenced to residual undeuterated solvent resonances and are reported as parts per million relative to $SiMe_4$. HPLC-grade organic solvents were first saturated with nitrogen during filling of the 20 L solvent reservoirs and then dried by passage through activated alumina (for Et_2O, THF, and CH_2Cl_2) followed by passage through Q-5 supported copper catalyst (for toluene and hexanes) stainless steel columns.

Lithium dimethylamide, trimethylsilyl trifluoromethanesulfonate (TMSOTf), methyl magnesium chloride (3.0 M solution in THF), and 2,6-di-*tert*-butyl-4-methylphenol (BHT-H) were purchased from Alfa Aesar Chemical Co., while triflic acid was purchased from Oakwook Chemical. Dimethyl itaconate (DMIA) and itaconic anhydride (IA) were purchased from Alfa Aesar Chemical Co., and they were purified by stirring a CH_2Cl_2 solution with activated CaH_2 overnight, followed by filtration and sublimation of the resulting solid after evaporation (60 °C/200 mTorr and 45 °C/250 mTorr for DMIA and IA, respectively). Diisopropyl itaconate (D^{i}PrIA) was prepared following a literature procedure.[1] Methyl methacrylate (MMA) was purchased from Alfa

Aesar Chemical Co., while dimethyl acrylamide (DMAA) was purchased from TCI America. D^{i}PrIA, MMA, and DMAA were dried over activated CaH_2 overnight, followed by vacuum distillation, degasification by three freeze-pump-thaw cycles, and finally they were stored in brown bottles at −30 °C inside a glovebox freezer. MMA was further purified by titration with tri(*n*-octyl)aluminum to a yellow end point followed by distillation under reduced pressure.[2] Tris(pentafluorophenyl)borane, $B(C_6F_5)_3$, and (η^5-pentamethylcyclopentadienyl)(η^5-*n*-propylcyclopentadienyl)zirconium dichloride [Cp*(^{n}PrCp)$ZrCl_2$], were obtained as research gifts from Boulder Scientific Co.; $B(C_6F_5)_3$ was further purified by sublimation and Cp*(^{n}PrCp)$ZrCl_2$ was used without further purification. The $(C_6F_5)_3B{\cdot}THF$ adduct was prepared by addition of THF to a toluene solution of the borane at ambient temperature, followed by removal of the volatiles and drying under vacuum. Literature procedures were employed for the preparation of the following materials or compounds: *rac*-(EBI)ZrMe[OC(O^{i}Pr)=CMe_2] [**1**, EBI = ethylene-bis(η^5-indenyl)],[3-5] *rac*-(EBI)Zr^{+}(THF)[OC(O^{i}Pr)=CMe_2][$MeB(C_6F_5)_3$]$^{-}$ (**1**$^{+}$),[3-5] Li[OC(O^{i}Pr)=CMe_2],[6,7] and $[H(OEt_2)_2]^{+}B(C_6F_5)_4]^{-}$.[8]

***In Situ* Generation of *rac*-(EBI)Zr[OC(OMe)=C(CH_2COOMe)CH_2C(Me_2)C(O^{i}Pr)=O]$^{+}$ [$MeB(C_6F_5)_3$]$^{-}$ (2a).** In an argon-filled glovebox, complex **1**$^{+}$ was cleanly generated *in situ* by mixing **1** (24.7 mg, 0.050 mmol) and $(C_6F_5)_3B{\cdot}THF$ (29.8 mg, 0.051 mmol) at room temperature in 0.4 mL of CD_2Cl_2 inside a 1.5 dram vial. The resulting dark red solution was chilled to −30 °C inside the glovebox freezer. Then, a stoichiometric amount of DMIA (7.9 mg, 0.050 mmol) was added via syringe at −30 °C from a stock solution in CD_2Cl_2. The subsequent red solution was quickly transferred to a Teflon-valve-sealed J. Young-type NMR tube, and immediately placed on a dry ice/acetone batch until it was analyzed by ^{1}H and ^{13}C NMR at −18 °C.

^{1}H NMR (CD_2Cl_2, −18 °C) of **2a**: δ 8.04 (d, J = 8.5 Hz, 1H, Ar H), 7.96 (d, J = 8.5 Hz, 1H, Ar H), 7.45 (d, J = 8.5 Hz, 1H, Ar H), 7.38–7.21 (m, 5H, Ar H), 6.28 (m, 3H, Cp H), 5.95 (d, J = 3.5 Hz, 1H, Cp H), 4.27 (sept, J = 6.3 Hz, 1H, –OC*H*Me$_2$), 4.31–3.93 (m, 4H, –CH$_2$C*H*$_2$– bridge), 3.66 (bs, 4H, α-THF, free), 3.64 (s, 3H, –OMe), 3.09 (s, 3H, –OMe), 2.89 (d, J = 16.5 Hz, 1H, C*H*$_2$C(O)OMe), 2.81 (d, J = 17.0 Hz, 1H, C*H*$_2$C(O)OMe), 2.29 (d, J = 16.0 Hz, 1H, –C*H*$_2$–), 1.80 (m, 4H, β-THF, free), 1.72 (d, J = 16.0 Hz, 1H, –C*H*$_2$–), 1.38 (d, J = 6.5 Hz, 3H, OCH*Me*$_2$), 1.23 (d, J = 6.5 Hz, 3H, OCH*Me*$_2$), 1.19 (s, 3H, C*Me*$_2$), 1.09 (s, 3H, C*Me*$_2$), 0.47 (s, br, 3H, B*Me*). ^{13}C NMR (CD_2Cl_2, −18 °C): δ 192.45 [*C*(O^{i}Pr)=O], 173.25 [*C*(OMe)=O], 158.62 [O*C*(OMe)=], 148.21 (d, $^1J_{C\text{-}F}$ = 235.5 Hz, Ar*C*–F), 137.45 (d, $^1J_{C\text{-}F}$ = 243.2 Hz, Ar*C*–F), 136.35 (d, $^1J_{C\text{-}F}$ = 246.6 Hz, Ar*C*–F), 133.85, 132.77, 131.77, 129.10, 128.29, 128.11, 127.35, 126.99, 126.64, 126.04, 125.36, 124.45, 123.91, 123.60, 123.39, 118.31, 116.81, 107.79, and 106.47(indenyl carbons), 79.16 (=*C*CH$_2$), 77.28 (O*C*HMe$_2$), 67.94 (α-THF, free), 53.40 (–O*Me*, overlapped with *C*D$_2$Cl$_2$), 51.89 (–O*Me*), 43.98 (*C*Me$_2$), 38.68 (–*C*H$_2$–), 36.00 [*C*H$_2$C(O)OMe], 30.64, 30.45 (–*C*H$_2$CH$_2$– bridge), 28.56 (C*Me*$_2$), 25.71 (β-THF, free), 23.44 (C*Me*$_2$), 21.94 (OCH*Me*$_2$), 20.70 (OCH*Me*$_2$), 10.05 (B-*C*H$_3$). ^{19}F NMR (CD_2Cl_2, 25 °C): δ −133.17 (d, $^3J_{F\text{-}F}$ = 19.2 Hz, 6F, o–Ar*F*), −165.35 (t, $^3J_{F\text{-}F}$ = 20.3 Hz, 3F, p–Ar*F*), −167.92 (m, 6F, m–Ar*F*).

***In Situ* Generation of *rac*-(EBI)Zr[OC(O^{i}Pr)=C(CH$_2$COO^{i}Pr)CH$_2$C(Me$_2$)C(O^{i}Pr)=O]$^+$ [MeB(C$_6$F$_5$)$_3$]$^-$ (2b).** In an argon-filled glovebox, complex **1**$^+$ was cleanly generated *in situ* by mixing **1** (26.4 mg, 0.054 mmol) and $(C_6F_5)_3B\cdot THF$ (31.7 mg, 0.054 mmol) at room temperature in 0.4 mL of CD_2Cl_2 inside a 1.5 dram vial. The resulting dark red solution was chilled to −30 °C inside the glovebox freezer. Then, a stoichiometric amount of D^{i}PrIA (7.9 mg, 0.050 mmol) was added via syringe at −30 °C from a stock solution in CD_2Cl_2. The subsequent red solution was

quickly transferred to a Teflon-valve-sealed J. Young-type NMR tube, and immediately placed on a dry ice/acetone batch until it was analyzed by ^{1}H and ^{13}C NMR at −18 °C.

^{1}H NMR (CD_2Cl_2, −18 °C) of **2b**: δ 8.06 (d, J = 8.5 Hz, 1H, Ar H), 7.92 (d, J = 9.0 Hz, 1H, Ar H), 7.44–7.21 (m, 6H, Ar H), 6.40 (s, br, 1H, Cp H), 6.26 (s, br, 1H, Cp H), 6.23 (s, br, 1H, Cp H), 5.97 (s, br, 1H, Cp H), 4.93 (sept, J = 6.4 Hz, 1H, –OC*H*Me$_2$), 4.19 (bs, 1H, –OC*H*Me$_2$), 4.14–3.94 (m, 4H, –CH$_2$C*H*$_2$– bridge), 3.66 (bs, 4H, α-THF, free), 3.61 (bs, 1H, –OC*H*Me$_2$), 2.89 (d, J = 17.0 Hz, 1H, C*H*$_2$C(O)O^{i}Pr), 2.79 (d, J = 17.0 Hz, 1H, C*H*$_2$C(O)O^{i}Pr), 2.23 (d, J = 16.0 Hz, 1H, –C*H*$_2$–), 1.80 (m, 4H, β-THF, free), 1.71 (d, J = 16.0 Hz, 1H, –C*H*$_2$–), 1.37 (d, J = 6.0 Hz, 3H, OCH*Me*$_2$), 1.23–1.19 (m, 15H, OCH*Me*$_2$), 1.13 (s, br, 3H, C*Me*$_2$), 0.98 (s, 3H, C*Me*$_2$), 0.48 (s, br, 3H, B*Me*). ^{13}C NMR (CD_2Cl_2, −18 °C): δ 192.37 [*C*(O^{i}Pr)=O], 172.30 [*C*(O^{i}Pr)=O], 156.53 [O*C*(O^{i}Pr)=], 148.21 (d, $^{1}J_{C\text{-}F}$ = 235.8 Hz, Ar*C*–F), 137.52 (d, $^{1}J_{C\text{-}F}$ = 253.4 Hz, Ar*C*–F), 136.37 (d, $^{1}J_{C\text{-}F}$ = 249.2 Hz, Ar*C*–F), 132.60, 131.86, 129.11, 128.42, 128.01, 127.27, 126.95, 126.08, 125.84, 124.19, 123.85, 123.43, 122.64, 121.28, 118.47, 116.43, 107.06, and 106.15 (indenyl carbons), 83.50 (=*C*CH$_2$), 76.81 (O*C*HMe$_2$), 68.69 (O*C*HMe$_2$), 67.94 (O*C*HMe$_2$ overlapped with α-THF, free), 43.13 (*C*Me$_2$), 38.43 (–*C*H$_2$–), 36.92 [*C*H$_2$C(O)O^{i}Pr], 30.68, 30.51 (–*C*H$_2$CH$_2$– bridge), 28.99 (C*Me*$_2$), 25.71 (β-THF, free), 23.75 (C*Me*$_2$), 22.05, 21.90, 21.79, 21.73, 21.63, and 20.71 (OCH*Me*$_2$), 9.99 (B-*C*H$_3$). ^{19}F NMR (CD_2Cl_2, 25 °C): δ −133.13 (d, $^{3}J_{F\text{-}F}$ = 18.1 Hz, 6F, o–Ar*F*), −165.27 (t, $^{3}J_{F\text{-}F}$ = 20.3 Hz, 3F, p–Ar*F*), −167.84 (m, 6F, m–Ar*F*).

Isolation of *rac*-(EBI)Zr[OC(OMe)=C(CH$_2$CMe$_2$COO^{i}Pr)CH$_2$C(OMe)=O]$^+$ [MeB(C$_6$F$_5$)$_3$]$^-$ (4a). In an argon-filled glovebox, a 30 mL glass reaction jar was charged with 56.6 mg of complex **1** (0.115 mmol) and dissolved in 3 mL of CH_2Cl_2. Complex **1**$^+$ was cleanly generated *in situ* by adding an equimolar amount of $(C_6F_5)_3B\cdot$THF (67.2 mg, 0.115 mmol) in 1 mL of CH_2Cl_2 at room temperature. After stirring for 5 min, the reaction mixture was cooled to

−30 °C inside the glovebox freezer, and then 18.2 mg of DMIA (0.115 mmol) were added via syringe from a prechilled stock solution in CH_2Cl_2. The reaction mixture was stirred for a total of 24 h at room temperature, after which time the color of the solution slowly changed from the initial red to orange. The solvent was evaporated *in vacuo,* the red residue was thoroughly washed with hexanes (3 × 5 mL), the supernatant decanted, and the volatiles were removed under vacuum. The residue was taken in 0.4 mL of CH_2Cl_2, cooled down to −30 °C inside the glovebox freezer and then hexanes (3 mL) were allowed to slowly diffuse to form a bright red oil after 3 days. The supernatant was decanted, and the oil product was thoroughly dried under vacuum to obtain **4a** as a red foamy powder in quantitative yield. Anal. Calcd for $C_{53}H_{42}BF_{15}O_6Zr$: C, 54.79; H, 3.64. Found: C, 54.51; H, 3.81.

^{1}H NMR (CD_2Cl_2, 25 °C) of **4a**: δ 7.95 (d, J = 8.8 Hz, 1H, Ar H), 7.87 (d, J = 8.8 Hz, 1H, Ar H), 7.46 (d, J = 8.0 Hz, 1H, Ar H), 7.42–7.10 (m, 5H, Ar H), 6.42 (d, J = 3.6 Hz, 1H, Cp H), 6.34 (d, J = 3.6 Hz, 1H, Cp H), 6.31 (d, J = 3.2 Hz, 1H, Cp H), 6.07 (d, J = 3.2 Hz, 1H, Cp H), 4.89 (sept, J = 6.3 Hz, 1H, –OC*H*Me$_2$), 4.06 (m, 4H, –CH$_2$C*H*$_2$– bridge), 3.73 (s, 3H, –OMe), 3.15 (s, 3H, –OMe), 2.73 (d, J = 14.8 Hz, 1H, C*H*$_2$C(O)OMe), 2.67 (d, J = 14.8 Hz, 1H, C*H*$_2$C(O)OMe), 2.34 (d, J = 14.4 Hz, 1H, –C*H*$_2$–), 2.03 (d, J = 14.4 Hz, 1H, –C*H*$_2$–), 1.27 (d, J = 4.8 Hz, 3H, OCH*Me*$_2$), 1.22 (d, J = 6.0 Hz, 3H, OCH*Me*$_2$), 1.12 (s, 3H, C*Me*$_2$), 1.06 (s, 3H, C*Me*$_2$), 0.51 (s, br, 3H, B*Me*). ^{13}C NMR (CD_2Cl_2, 25 °C): δ 189.08 [*C*(OMe)=O], 177.38 [*C*(O^{i}Pr)=O], 157.94 [O*C*(OMe)=], 148.70 (d, $^1J_{C\text{-}F}$ = 234.4 Hz, Ar*C*–F), 137.89 (d, $^1J_{C\text{-}F}$ = 245.3 Hz, Ar*C*–F), 136.88 (d, $^1J_{C\text{-}F}$ = 219.1 Hz, Ar*C*–F), 132.52, 130.83, 128.65, 128.51, 128.03, 127.64, 127.19, 125.77, 125.73, 125.06, 124.95, 124.56, 122.07, 121.61, 117.71, 117.53, 108.26, and 107.60 (indenyl carbons), 79.16 (=*C*CH$_2$), 68.02 (O*C*HMe$_2$), 58.45 (–O*Me*), 53.30 (–O*Me*, overlapped with *C*D$_2$Cl$_2$), 43.43 (*C*Me$_2$), 42.08 (–*C*H$_2$–), 37.77 [*C*H$_2$C(OMe)=O], 30.48, 29.91 (–*C*H$_2$CH$_2$–

bridge), 25.83 (C*Me*$_2$), 25.07 (C*Me*$_2$), 21.81 (OCH*Me*$_2$), 21.76 (OCH*Me*$_2$), 10.35 (B-*C*H$_3$). ^{19}F NMR (CD_2Cl_2, 25 °C): δ −133.11 (d, $^3J_{F\text{-}F}$ = 18.1 Hz, 6F, o–Ar*F*), −165.24 (t, $^3J_{F\text{-}F}$ = 20.3 Hz, 3F, p–Ar*F*), −167.82 (m, 6F, m–Ar*F*).

Isolation of *rac*-(EBI)Zr[OC(O^{i}Pr)=C(CH$_2$CMe$_2$COO^{i}Pr)CH$_2$C(O^{i}Pr)=O]$^+$ [MeB(C$_6$F$_5$)$_3$]$^-$ (4b). In an argon-filled glovebox, a 30 mL glass reaction jar was charged with 54.9 mg of complex **1** (0.112 mmol) and dissolved in 3 mL of CH_2Cl_2. Complex **1**$^+$ was cleanly generated *in situ* by adding an equimolar amount of $(C_6F_5)_3B{\cdot}THF$ (65.2 mg, 0.112 mmol) in 1 mL of CH_2Cl_2 at room temperature. After stirring for 5 min, the reaction mixture was cooled to −30 °C inside the glovebox freezer, and then 24.1 mg of D^{i}PrIA (0.112 mmol) were added via syringe from a prechilled stock solution in CH_2Cl_2. The reaction mixture was stirred for a total of 24 h at room temperature. The solvent was evaporated *in vacuo*, the red residue was thoroughly washed with hexanes (3 × 5 mL), the supernatant decanted, and the volatiles were removed under vacuum. The residue was taken in 0.4 mL of CH_2Cl_2, cooled down to −30 °C inside the glovebox freezer and then hexanes (3 mL) were allowed to slowly diffuse to form a bright red oil after 3 days. The supernatant was decanted, and the oil product was thoroughly dried under vacuum to obtain **4b** as an orange foamy powder in quantitative yield. Anal. Calcd for $C_{57}H_{50}BF_{15}O_6Zr$: C, 56.21; H, 4.14. Found: C, 56.64; H, 4.25.

^{1}H NMR (CD_2Cl_2, 25 °C) of **4b**: δ 8.01 (d, *J* = 8.8 Hz, 1H, Ar H), 7.87 (d, *J* = 8.8 Hz, 1H, Ar H), 7.47 (d, *J* = 8.4 Hz, 1H, Ar H), 7.34–7.23 (m, 5H, Ar H), 6.40 (d, *J* = 3.6 Hz, 1H, Cp H), 6.35 (d, *J* = 3.6 Hz, 1H, Cp H), 6.28 (d, *J* = 3.6 Hz, 1H, Cp H), 6.01 (d, *J* = 3.6 Hz, 1H, Cp H), 4.93 (sept, *J* = 6.2 Hz, 1H, –OC*H*Me$_2$), 4.75 (sept, *J* = 6.3 Hz, 1H, –OC*H*Me$_2$), 4.08–3.98 (m, 4H, –CH$_2$C*H*$_2$– bridge), 3.76 (sept, *J* = 6.2 Hz, 1H, –OC*H*Me$_2$), 2.70 (d, *J* = 14.8 Hz, 1H, C*H*$_2$C(O)O^{i}Pr), 2.65 (d, *J* = 14.8 Hz, 1H, C*H*$_2$C(O)O^{i}Pr), 2.46 (d, *J* = 14.4 Hz, 1H, –C*H*$_2$–), 1.95

(d, J = 14.4 Hz, 1H, –CH_2–), 1.43 (d, J = 6.4 Hz, 3H, OCHMe_2), 1.23 (m, 12H, OCHMe_2), 1.14 (s, 3H, CMe_2), 1.09 (s, 3H, CMe_2), 0.97 (d, J = 6.0 Hz, 3H, OCHMe_2), 0.51 (s, br, 3H, BMe). ^{13}C NMR (CD_2Cl_2, 25 °C): δ 188.12 [C(O^{i}Pr)=O], 177.32 [C(O^{i}Pr)=O], 156.65 [OC(OMe)=], 148.83 (d, $^1J_{C\text{-}F}$ = 235.9 Hz, ArC–F), 137.87 (d, $^1J_{C\text{-}F}$ = 242.8 Hz, ArC–F), 136.77 (d, $^1J_{C\text{-}F}$ = 248.3 Hz, ArC–F), 132.67, 131.18, 128.69, 128.40, 127.95, 127.38, 126.82, 125.58, 125.38, 124.84, 124.75, 124.53, 122.17, 121.68, 117.75, 117.56, 107.27, and 106.67 (indenyl carbons), 81.71 (=CCH$_2$), 79.10 (OCHMe$_2$), 69.11 (OCHMe$_2$), 67.98 (OCHMe$_2$), 43.51 (CMe$_2$), 42.27 (–CH$_2$–), 38.36 [CH$_2$C(O^{i}Pr)=O], 30.62, 30.15 (–CH$_2$CH$_2$– bridge), 25.89 (CMe_2), 25.57 (CMe_2), 22.36, 21.99, 21.88, 21.83, 21.69, and 21.25 (OCHMe_2), 10.04 (B-CH$_3$). ^{19}F NMR (CD_2Cl_2, 25 °C): δ −133.12 (d, $^3J_{F\text{-}F}$ = 18.1 Hz, 6F, o–ArF), −165.27 (t, $^3J_{F\text{-}F}$ = 20.3 Hz, 3F, p–ArF), −167.83 (m, 6F, m–ArF).

Isolation of *rac*-(EBI)ZrMe{OC[OC(O)CH$_2$]=C(CH$_2$CMe$_2$COO^{i}Pr)} (5). In an argon-filled glovebox, a 30 mL glass reaction jar was charged with 116.3 mg of complex **1** (0.236 mmol) and dissolved in 3 mL of CH_2Cl_2. An equimolar amount of itaconic anhydride (26.5 mg, 0.236 mmol) was dissolved in 1 mL of CH_2Cl_2 and quickly added at room temperature *via* pipette. The resulting bright yellow solution was stirred for 30 minutes at ambient temperature, and then the volatiles were removed under vacuum. The yellow residue was washed with 2 mL of hexanes and subsequently dried under vacuum to obtain complex **5** as a bright yellow powder. Yield: 130 mg (91%). Anal. Calcd for $C_{33}H_{36}O_5Zr$: C, 65.64; H, 6.01. Found: C, 65.37; H, 5.81.

^{1}H NMR (CD_2Cl_2, 25 °C) of **5**: δ 7.74 (d, J = 8.8 Hz, 1H, Ar H), 7.47 (d, J = 8.4 Hz, 1H, Ar H), 7.33 (pst, J = 8.8 Hz, 2H, Ar H), 7.24 (pst, J = 7.6 Hz, 1H, Ar H), 7.11 (psq, J = 7.5 Hz, 2H, Ar H), 6.99 (pst, J = 7.6 Hz, 1H, Ar H), 6.58 (d, J = 3.2 Hz, 1H, Cp H), 6.45 (d, J = 3.2 Hz, 1H, Cp H), 5.97 (d, J = 3.2 Hz, 1H, Cp H), 5.95 (d, J = 3.6 Hz, 1H, Cp H), 4.89 (sept, J = 6.3 Hz, 1H, OCHMe$_2$), 3.76–3.56 (m, 4H, –CH_2CH$_2$– bridge), 2.95 (s, 2H, CH_2C(O)O), 1.90 (s, 2H, –

C*H*$_2$–), 1.19 (d, *J* = 6.4 Hz, 6H, OCH*Me*$_2$), 0.99 (s, 3H, C*Me*$_2$), 0.97 (s, 3H, C*Me*$_2$), −0.85 (s, 3H, Zr–C*H*$_3$). ^{13}C NMR (CD_2Cl_2, 25 °C): δ 177.58 [*C*(O^{i}Pr)=O], 174.66 [CH_2*C*(O)=O], 156.01 [O*C*(OC)=], 127.18, 126.76, 125.92, 125.63, 125.24, 125.10, 124.80, 123.61, 123.23, 122.88, 122.45, 121.00, 119.77, 116.58, 113.82, 112.64, 106.75, and 104.35 (indenyl carbons), 76.83 (=*C*CH_2), 67.81 (O*C*HMe_2), 42.86 (*C*Me_2), 38.14 [*C*H_2C(O)=O], 35.37 (–*C*H_2–), 33.02 (Zr–*C*H_3), 28.78, 27.87 (–*C*H_2CH_2– bridge), 25.48, 25.07 (C*Me*$_2$), 21.91 (OCH*Me*$_2$).

***In Situ* Generation of *rac*-(EBI)ZrMe{OC[OC(O)CH$_2$]=C[CH$_2$CMe$_2$C(O^{i}Pr)=O]}$^+$ [MeB(C$_6$F$_5$)$_3$]$^-$ (6).** In an argon-filled glovebox, a 1.5 dram vial was charged with complex **1** (28.5 mg, 0.058 mmol) and 0.15 mL of CD_2Cl_2. Complex **5** was generated *in situ* by adding to **1** an equimolar amount of itaconic anhydride (6.50 mg, 0.058 mmol) from a stock solution in CD_2Cl_2 at room temperature; the subsequent yellow solution was cooled to −30 °C inside the glovebox freezer. In a separate 1.5 dram vial, a B(C_6F_5)$_3$ (29.9 mg, 0.058 mmol) solution in 0.25 mL CD_2Cl_2 was prepared and cooled to −30 °C inside the glovebox freezer. The pre-chilled B(C_6F_5)$_3$ solution was quickly added via pipette to the chilled solution of **5**, thoroughly mixed, and quickly transferred to a Teflon-valve-sealed J. Young-type NMR tube which was immediately placed on a dry ice/acetone batch until it was analyzed by ^{1}H and ^{19}F NMR at room temperature.

^{1}H NMR (CD_2Cl_2, 25 °C) of **6**: δ 8.01 (d, *J* = 8.0 Hz, 2H, Ar H), 7.42–7.31 (m, 6H, Ar H), 6.41 (d, *J* = 3.2 Hz, 2H, Cp H), 6.17 (s, br, 2H, Cp H), 4.94, 4.36 (s, br, 1H, OC*H*Me_2), 4.12 (s, 4H, –C*H*$_2$CH_2– bridge), 3.36 (s, br, 2H, C*H*$_2$C(O)O), 2.00 (s, br, 2H, –C*H*$_2$–), 1.37 (d, *J* = 6.0 Hz, 3H, OCH*Me*$_2$), 1.33 (d, *J* = 6.4 Hz, 3H, OCH*Me*$_2$), 1.30 (s, 3H, C*Me*$_2$), 1.25 (s, 3H, C*Me*$_2$), 0.49 (s, br, 3H, B*Me*). ^{19}F NMR (CD_2Cl_2, 25 °C): δ −133.03 (d, $^3J_{F\text{-}F}$ = 27.1 Hz, 6F, o–Ar*F*), −165.09 (t, $^3J_{F\text{-}F}$ = 20.3 Hz, 3F, p–Ar*F*), −167.71 (m, 6F, m–Ar*F*).

***In Situ* Generation of *rac*-(EBI)Zr{OC(NMe_2)=CCH_2C($CH_2CMe_2COO^iPr$)C[OC(O)]=O}$^+$[$MeB(C_6F_5)_3$]$^-$ (7).** In an argon-filled glovebox, a 1.5 dram vial was charged with complex **1** (27.7 mg, 0.056 mmol) and 0.1 mL of CD_2Cl_2. Complex **5** was generated *in situ* by adding to **1** an equimolar amount of itaconic anhydride (6.31 mg, 0.056 mmol) from a stock solution in CD_2Cl_2 at room temperature. In a separate 1.5 dram vial, $(C_6F_5)_3B$·DMAA adduct was preformed by mixing $B(C_6F_5)_3$ (28.8 mg, 0.056 mmol) in 0.1 mL CD_2Cl_2 with an equimolar amount of DMAA (5.6 mg, 0.056 mmol) from a stock solution in CD_2Cl_2 at room temperature. Upon cooling at −30 °C inside the glovebox freezer, the $(C_6F_5)_3B$·DMAA adduct solution in CD_2Cl_2 was added to the precooled solution of **5**. The resulting orange solution (total volume ~0.6 mL CD_2Cl_2) was quickly transferred to a Teflon-valve-sealed J. Young-type NMR tube, and immediately placed on a dry ice/acetone batch until it was analyzed by ^{1}H, ^{19}F, and ^{13}C NMR at room temperature.

^{1}H NMR (CD_2Cl_2, 25 °C) of **7**: δ 7.89 (d, J = 8.8 Hz, 1H, Ar H), 7.88 (d, J = 9.2 Hz, 1H, Ar H), 7.46 (d, J = 8.4 Hz, 1H, Ar H), 7.33–7.13 (m, 5H, Ar H), 6.57 (d, J = 3.6 Hz, 1H, Cp H), 6.55 (d, J = 3.6 Hz, 1H, Cp H), 6.14 (d, J = 3.2 Hz, 1H, Cp H), 6.02 (d, J = 3.2 Hz, 1H, Cp H), 4.94 (sept, J = 6.3 Hz, 1H, OC*H*Me_2), 4.07–3.95 (m, 6H, –CH_2CH_2– bridge, CH_2C(O)O), 3.26 (s, 3H, N*Me*$_2$), 2.79 (s, 3H, N*Me*$_2$), 2.52 (d, J = 4.0 Hz, 1H, C=C*H*), 2.29 (dd, J_1 = 26.0 Hz, J_2 = 10.8 Hz, 2H, CH_2CH=C), 2.22 (d, J = 14.8 Hz, 1H, –CH_2–), 2.08 (d, J = 14.8 Hz, 1H, –CH_2–), 1.96 (dd, J_1 = 15.2 Hz, J_2 = 5.6 Hz, 2H, CH_2CH=C), 1.24 (d, J = 6.4 Hz, 3H, OCH*Me*$_2$), 1.23 (d, J = 6.4 Hz, 3H, OCH*Me*$_2$), 1.18 (s, 3H, C*Me*$_2$), 1.15 (s, 3H, C*Me*$_2$), 0.51 (s, br, 3H, B*Me*). ^{13}C NMR (CD_2Cl_2, 25 °C): δ 206.45 [*C*(O)=O], 177.75 [*C*(O^{i}Pr)=O], 176.95 [O*C*(NMe_2)=], 175.24 [CH_2*C*(O)=O], 148.70 (d, $^1J_{C\text{-}F}$ = 238.6 Hz, Ar*C*–F), 137.90 (d, $^1J_{C\text{-}F}$ = 244.3 Hz, Ar*C*–F), 136.81 (d, $^1J_{C\text{-}F}$ = 250.3 Hz, Ar*C*–F), 132.89, 130.69, 129.86, 128.17, 127.63, 127.46, 127.26, 126.18, 125.52, 125.41,

124.15, 124.14, 121.82, 121.14, 117.10, 116.33, 108.36, and 106.99 (indenyl carbons), 68.52 (O*C*HMe$_2$), 49.12 (C=*C*H), 47.94 (quaternary C), 47.87 (*C*H$_2$CH=C), 46.97 (*C*Me$_2$), 42.09 (–*C*H$_2$–), 40.58, 39.38 (N*Me*$_2$), 35.06 [*C*H$_2$C(O)=O], 30.63, 29.65 (–*C*H$_2$CH$_2$– bridge), 27.81, 27.06 (C*Me*$_2$), 21.82, 21.79 (OCH*Me*$_2$), 10.34 (B-*C*H$_3$). ^{19}F NMR (CD_2Cl_2, 25 °C): δ −133.12 (d, $^3J_{F\text{-}F}$ = 18.1 Hz, 6F, o–Ar*F*), −165.13 (t, $^3J_{F\text{-}F}$ = 20.3 Hz, 3F, p–Ar*F*), −167.77 (m, 6F, m–Ar*F*).

Isolation of [Cp*(*n*PrCp)Zr(HNMe$_2$)=NMe$_2$]$^+$[B(C$_6$F$_5$)$_4$]$^-$ (9$^+$). In an argon-filled glovebox, a 200 mL glass reaction jar was charged with 1.02 g of Cp*(*n*PrCp)ZrCl$_2$ (2.52 mmol) and dissolved in 50 mL of dry THF. The solution was cooled to −30 °C inside the glovebox freezer, and then a solution of LiNMe$_2$ (490 mg, 9.60 mmol) in 15 mL of THF at −30 °C was added via pipette under vigorous stirring. The solution was allowed to warm to ambient temperature and stirred for another 3 h. Then, the solvent was thoroughly removed under vacuum, and the obtained crude material was extracted with 100 mL of hexanes and filtered through a pad of celite to form an orange oil. The oil was redissolved in 5 mL of hexanes, filtered through a plastic frit (0.45 μm pore size nylon filter); after removing the solvent of the filtrate, the product was left to crystallize in 1 mL of hexanes overnight at −30 °C in the glovebox freezer, after which time bright orange crystals were formed. The mother liquor was decanted and the crystals were dried under vacuum to yield spectroscopically pure product Cp*(*n*PrCp)Zr(NMe$_2$)$_2$ (**9**) as an intense yellow solid. Yield: 400 mg (38%). ^{1}H NMR (C_6D_6, 25 °C) of **9**: δ 5.99 (pst, J = 2.8 Hz, 2H, η^5-C$_5$*H*$_4$*n*Pr), 5.68 (pst, J = 2.6 Hz, 2H, η^5-C$_5$*H*$_4$*n*Pr), 2.90 (s, 12 H, –N(C*H*$_3$)$_2$), 2.48 (t, J = 7.4 Hz, 2H, –C*H*$_2$CH$_2$CH$_3$), 1.89 (s, 15H, η^5-C$_5$*Me*$_5$), 1.61 (sextet, J = 7.4 Hz, 2H, –CH$_2$C*H*$_2$CH$_3$), 0.93 (t, J = 7.4 Hz, 3H, –CH$_2$CH$_2$C*H*$_3$). ^{13}C NMR (C_6D_6, 25 °C): δ 129.36 (η^5-*C*$_5$H$_4$*n*Pr), 118.71 (η^5-*C*$_5$Me$_5$), 111.24, 108.16 (η^5-*C*$_5$H$_4$*n*Pr), 48.64 (–N(*C*H$_3$)$_2$), 31.69 (–*C*H$_2$CH$_2$CH$_3$), 25.12 (–CH$_2$*C*H$_2$CH$_3$), 14.37 (–CH$_2$CH$_2$*C*H$_3$), 12.17 (η^5-C$_5$*Me*$_5$).

In an argon-filled glovebox, **9** (45.2 mg, 0.107 mmol) was charged in a 1.5 dram vial and dissolved in 0.3 mL of CH_2Cl_2, while $[H(OEt_2)_2][B(C_6F_5)_4]$ (88.8, 0.107 mmol) was dissolved in 0.3 mL of CH_2Cl_2 in a different 1.5 dram vial. The two solutions were mixed via glass pipette upon cooling to −30 °C giving a bright yellow solution. The solution was immediately placed back inside the glovebox freezer, and a bright yellow precipitate formed after 2 days. The supernatant was removed, and the residue obtained in quantitative yield was redissolved in 0.4 mL of CH_2Cl_2. Single crystals suitable for X-Ray diffraction were grown from this CH_2Cl_2 solution at −30 °C. Anal. Calcd for $C_{46}H_{39}BF_{20}N_2Zr$: C, 50.14; H, 3.57; N, 2.54. Found: C, 49.74; H, 3.71; N, 2.34.

^{1}H NMR (CD_2Cl_2, 25 °C) of **9**$^+$: δ 6.40 (dd, J_1 = 5.4 Hz, J_2 = 2.6 Hz, 1H, η^5-$C_5H_4{}^n$Pr), 6.08 (dd, J_1 = 5.2 Hz, J_2 = 2.4 Hz, 1H, η^5-$C_5H_4{}^n$Pr), 6.88 (m, 2H, η^5-$C_5H_4{}^n$Pr), 3.04 (s, 6H, –N(CH_3)$_2$), 2.54–2.40 (m, , 9H, *H*N(CH_3)$_2$, –$CH_2CH_2CH_3$), 2.01 (s, 15H, η^5-C_5Me_5), 1.61 (sextet, J = 7.5 Hz, 2H, –$CH_2CH_2CH_3$), 0.90 (t, J = 7.4 Hz, 3H, –$CH_2CH_2CH_3$). ^{13}C NMR (CD_2Cl_2, 25 °C): δ 148.55 (d, $^1J_{C\text{-}F}$ = 239.2 Hz, Ar*C*–F), 138.65 (d, $^1J_{C\text{-}F}$ = 242.6 Hz, Ar*C*–F), 136.67 (d, $^1J_{C\text{-}F}$ = 246.2 Hz, Ar*C*–F), 133.44 (η^5-$C_5H_4{}^n$Pr), 123.55 (η^5-C_5Me_5), 117.48, 114.88, 113.98, 111.98 (η^5-$C_5H_4{}^n$Pr), 66.08 (free O(CH_2CH_3)$_2$), 51.19 (–N(CH_3)$_2$, 43.52, 42.84 (HN(CH_3)$_2$), 31.11 (–$CH_2CH_2CH_3$), 25.34 (–$CH_2CH_2CH_3$), 15.51 (free O(CH_2CH_3)$_2$), 13.70 (–$CH_2CH_2CH_3$), 12.63 (η^5-C_5Me_5). ^{19}F NMR (CD_2Cl_2, 25 °C): δ −133.09 (m, 6F, o–Ar*F*), −163.71 (t, $^3J_{F\text{-}F}$ = 20.3 Hz, 3F, p–Ar*F*), −167.57 (m, 6F, m–Ar*F*).

Synthesis of Cp*(^{n}PrCp)ZrCl[OC(O^{i}Pr)=CMe$_2$] (10). In an argon-filled glovebox, a 200 mL glass reaction jar was charged with 5.00 g of Cp*(^{n}PrCp)$ZrCl_2$ (12.4 mmol) and dissolved in 150 mL of dry Et_2O. The solution was cooled to −30 °C inside the glovebox freezer, and then 3.53 g of freshly made Li(OC(O^{i}Pr)=CMe_2) (25.9 mmol) were added under vigorous stirring. The reaction was left to reach ambient temperature and stirred for another 18 h, after which time the

color of the solution changed from bright red to dark orange. Then, the solvent was throughly removed under vacuum, and the obtained crude material was extracted with 150 mL of hexanes and filtered through a pad of celite to form a red dense oil. This crude material was redissolved in 10 mL of hexanes and kept for crystallization at −30 °C inside the glovebox freezer overnight. Large orange crystals formed, after the mother liquor was decanted, were triturated and dried under vacuum to yield a bright yellow powder of spectroscopically pure product **10**. Yield: 4.51 g (73%).

^{1}H NMR (C_6D_6, 25 °C) of **10**: δ 6.19 (dd, J_1 = 5.2 Hz, J_2 = 2.4 Hz, 1H, η^5-$C_5H_4{}^n$Pr), 5.91 (dd, J_1 = 5.6 Hz, J_2 = 3.2 Hz, 1H, η^5-$C_5H_4{}^n$Pr), 5.72 (dd, J_1 = 5.0 Hz, J_2 = 2.2 Hz, 1H, η^5-$C_5H_4{}^n$Pr), 5.61 (dd, J_1 = 5.4 Hz, J_2 = 3.0 Hz, 1H, η^5-$C_5H_4{}^n$Pr), 4.43 (sept, J = 6.2 Hz, 1H, OC*H*Me$_2$), 2.76 (m, 1H, –C*H*$_2$CH$_2$CH$_3$), 2.63 (m, 1H, –C*H*$_2$CH$_2$CH$_3$), 1.90 (s, 3H, =C*Me*$_2$), 1.85 (s, 15H, η^5-C_5*Me*$_5$), 1.68 (s, 3H, =C*Me*$_2$), 1.55 (m, 2H, –CH$_2$C*H*$_2$CH$_3$), 1.29 (d, J = 6.0 Hz, 3H, OCH*Me*$_2$), 1.22 (d, J = 6.4 Hz, 3H, OCH*Me*$_2$), 0.88 (t, J = 7.4 Hz, 3H, –CH$_2$CH$_2$C*H*$_3$). ^{13}C NMR (C_6D_6, 25 °C): δ 154.86 [O*C*(O^{i}Pr)=], 135.15 (η^5-*C*$_5$H$_4{}^n$Pr), 122.17 (η^5-*C*$_5$Me$_5$), 117.13, 115.15, 113.04, 110.05 (η^5-*C*$_5$H$_4{}^n$Pr), 83.45 (=*C*Me$_2$), 68.29 (O*C*HMe$_2$), 32.19 (–*C*H$_2$CH$_2$CH$_3$), 24.24 (–CH$_2$*C*H$_2$CH$_3$), 22.39, 21.86 (OCH*Me*$_2$), 18.16, 17.64 (=C*Me*$_2$), 14.21 (–CH$_2$CH$_2$*C*H$_3$), 11.91 (η^5-C_5*Me*$_5$).

***In Situ* Generation of [Cp*(^{n}PrCp)Zr(THF)Me]$^+$[MeB(C$_6$F$_5$)$_3$]$^-$ (11$^+$).** In an argon-filled glovebox, a 200 mL glass reaction jar was charged with 5.00 g of Cp*(^{n}PrCp)ZrCl$_2$ (12.4 mmol), dissolved in 150 mL of dry Et$_2$O, and the solution was cooled to −30 °C inside the glovebox freezer. Subsequently, 8.5 mL of MeMgCl solution (3.0 M in THF, 25.5 mmol) were added under vigorous stirring and the mixture turned immediately into a milky slurry. The reaction mixture was allowed to warm to ambient temperature and stirred for an additional hour. An aliquot of the reaction mixture revealed quantitative and clean conversion to the title product. The reaction

mixture was filtered through a medium porosity frit with a small pad of celite, and then the celite was washed with 3 × 50 mL of Et_2O. The volatiles were removed under vacuum, the resulting light tan residue was extracted with 150 mL of hexanes, and then filtered through a fine porosity frit with a small pad of celite. The volatiles of the final filtrate were evaporated, and the remaining residue was redissolved in 10 mL of hexanes. The concentrated solution was cooled at −30 °C, and crystals formed after 2 h. The solvent was decanted, and the crystals were dried under vacuum for 5 h, affording an off-white powder as the spectroscopically pure product Cp*(^{n}PrCp)$ZrMe_2$ (**11**). Yield: 3.87 g (86%). ^{1}H NMR (C_6D_6, 25 °C) of **11**: δ 5.71 (pst, J = 2.6 Hz, 2H, η^5-$C_5H_4{}^n$Pr), 5.35 (pst, J = 2.6 Hz, 2H, η^5-$C_5H_4{}^n$Pr), 2.46 (t, J = 7.6 Hz, 2H, –$CH_2$$CH_2CH_3$), 1.73 (s, 15H, η^5-C_5Me_5), 1.60 (sextet, J = 7.4 Hz, 2H, –$CH_2CH_2$$CH_3$), 0.93 (t, J = 7.2 Hz, 3H, –$CH_2CH_2CH_3$), −0.34 (s, 6H, Zr–CH_3). ^{13}C NMR (C_6D_6, 25 °C): δ 129.20 (η^5-$C_5H_4{}^n$Pr), 117.13 (η^5-C_5Me_5), 111.94, 108.88 (η^5-$C_5H_4{}^n$Pr), 32.70 (Zr–CH_3), 32.54 (–$CH_2CH_2CH_3$), 25.34 (–$CH_2CH_2CH_3$), 14.21 (–$CH_2CH_2CH_3$), 11.68 (η^5-C_5Me_5).

In an argon-filled glovebox, **11** (44.0 mg, 0.121 mmol) was charged in a 1.5 dram vial and dissolved in 0.8 mL of CH_2Cl_2, while $(C_6F_5)_3B$·THF (70.7 mg, 0.121 mmol) was dissolved in 0.8 mL of CH_2Cl_2 in a different 1.5 dram vial. The two solutions were mixed via glass pipette upon cooling to −30 °C giving a bright yellow solution instantaneously. The solvent was evaporated and the residue was washed with hexanes (4 × 5 mL). The final product **11**$^+$ was thoroughly dried under vacuum to form a yellow oil in quantitative yield. Anal. Calcd for $C_{42}H_{40}BF_{15}OZr$: C, 53.23; H, 4.25. Found: C, 53.06; H, 4.25.

^{1}H NMR (CD_2Cl_2, 25 °C) of **11**$^+$: δ 6.25 (dd, J_1 = 5.4 Hz, J_2 = 2.6 Hz, 1H, η^5-$C_5H_4{}^n$Pr), 6.03 (dd, J_1 = 5.8 Hz, J_2 = 3.0 Hz, 1H, η^5-$C_5H_4{}^n$Pr), 5.90 (dd, J_1 = 5.8 Hz, J_2 = 3.0 Hz, 1H, η^5-$C_5H_4{}^n$Pr), 5.79 (dd, J_1 = 5.2 Hz, J_2 = 2.8 Hz, 1H, η^5-$C_5H_4{}^n$Pr), 3.66 (m, 4H, α–CH_2, THF), 2.45 (m, 1H, –

C*H*$_2$CH$_2$CH$_3$), 2.33 (m, 1H, –C*H*$_2$CH$_2$CH$_3$), 2.07 (m, 4H, β–C*H*$_2$, THF), 1.98 (s, 15H, η^5-C$_5$*Me*$_5$), 1.59 (m, 2H, –CH$_2$C*H*$_2$CH$_3$), 0.92 (t, *J* = 7.4 Hz, 3H, –CH$_2$CH$_2$C*H*$_3$), 0.48 (s, br, 6H, Zr–C*H*$_3$, B–C*H*$_3$). ^{13}C NMR (CD_2Cl_2, 25 °C): δ 148.65 (d, $^1J_{C\text{-}F}$ = 240.1 Hz, Ar*C*–F), 137.88 (d, $^1J_{C\text{-}F}$ = 240.9 Hz, Ar*C*–F), 136.69 (η^5-*C*$_5$H$_4$*^{n}*Pr), 136.75 (d, $^1J_{C\text{-}F}$ = 244.2 Hz, Ar*C*–F), 124.60 (η^5-*C*$_5$Me$_5$), 116.67, 116.59, 114.11, 112.30 (η^5-*C*$_5$H$_4$*^{n}*Pr), 75.63 (α–*C*H$_2$, THF), 47.75 (Zr–*C*H$_3$), 32.09 (–*C*H$_2$CH$_2$CH$_3$), 25.67 (β–*C*H$_2$, THF), 25.19 (–CH$_2$*C*H$_2$CH$_3$), 13.78 (–CH$_2$CH$_2$*C*H$_3$), 12.01 (η^5-C$_5$*Me*$_5$), 10.57 (B–*C*H$_3$). ^{19}F NMR (CD_2Cl_2, 25 °C): δ −133.20 (d, $^3J_{F\text{-}F}$ = 18.1 Hz, 6F, o–Ar*F*), −165.21 (t, $^3J_{F\text{-}F}$ = 20.3 Hz, 3F, p–Ar*F*), −167.85 (m, 6F, m–Ar*F*).

Synthesis of Cp*(*^{n}*PrCp)Zr(OTf)$_2$ (12). A similar procedure described for the preparation of *rac*-(EBI)Zr(OTf)$_2$ [3] was modified for the synthesis of Cp*(*^{n}*PrCp)Zr(OTf)$_2$. In an argon-filled glovebox, a 200 mL glass reaction jar was charged with 1.30 g of Cp*(*^{n}*PrCp)ZrMe$_2$ (3.57 mmol) and 100 mL of toluene. The clear solution was cooled to −30 °C inside the glovebox freezer, and then 0.66 mL of triflic acid (7.46 mmol) were slowly added. The reaction turned yellow immediately and a precipitate formed. The reaction was allowed to warm up to ambient temperature and stirred overnight, after which time the solution darkened and the precipitate dissolved. The solution mixture was filtered through a pad of celite and slow evaporation of the solvent produced golden color cylindrical crystals. Crystals of **12** were collected, washed with 3 × 5 mL of cold toluene followed by 3 × 10 mL of hexanes, and finally dried under vacuum for 4 h to obtain **12** as spectroscopically pure golden crystalline solid. Yield: 2.13 g (94%). Anal. Calcd for $C_{20}H_{26}F_6O_6S_2Zr$: C, 38.02; H, 4.15. Found: C, 38.31; H, 4.15.

^{1}H NMR (C_6D_6, 25 °C) of **12**: δ 6.36 (pst, *J* = 2.6 Hz, 2H, η^5-C$_5$*H*$_4$*^{n}*Pr), 6.07 (pst, *J* = 2.6 Hz, 2H, η^5-C$_5$*H*$_4$*^{n}*Pr), 2.41 (t, *J* = 7.6 Hz, 2H, –C*H*$_2$CH$_2$CH$_3$), 1.67 (s, 15H, η^5-C$_5$*Me*$_5$), 1.34 (sextet, *J* = 7.4 Hz, 2H, –CH$_2$C*H*$_2$CH$_3$), 0.75 (t, *J* = 7.2 Hz, 3H, –CH$_2$CH$_2$C*H*$_3$). ^{13}C NMR (C_6D_6, 25 °C): δ

139.04 (η^5-*C*$_5$H$_4$*^{n}*Pr), 128.52 (η^5-*C*$_5$Me$_5$), 119.88 (q, $^1J_{C\text{-}F}$ = 318.2 Hz, *C*F$_3$SO$_3$–), 119.13, 117.74 (η^5-*C*$_5$H$_4$*^{n}*Pr), 30.82 (–*C*H$_2$CH$_2$CH$_3$), 24.58 (–CH$_2$*C*H$_2$CH$_3$), 13.54 (–CH$_2$CH$_2$*C*H$_3$), 11.50 (η^5-C$_5$*Me*$_5$). ^{19}F NMR (C$_6$D$_6$, 25 °C): δ −76.62 (C*F*$_3$SO$_3$–).

Isolation of Cp*(*^{n}*PrCp)Zr(THF)[OC(O*^{i}*Pr)=CMe$_2$]$^+$[MeB(C$_6$F$_5$)$_3$]$^-$ (14$^+$). This synthesis involves three steps. In the first step, a 200 mL glass reaction jar was charged with 2.12 g of **11** (5.83 mmol), dissolved in 100 mL of toluene, and the clear solution was cooled to −30 °C inside the glovebox freezer. Separately, 1.32 g of TMSOTf (5.94 mmol) were charged in a 20 mL vial, dissolved in 10 mL of toluene and cooled to −30 °C inside the glovebox freezer. The cooled solution of TMSOTf was added to the vigorously stirring solution of **11** with a glass pipette, the mixture was allowed to reach room temperature and then stirred overnight. An aliquot of the reaction mixture revealed 80% conversion to Cp*(*^{n}*PrCp)Zr(OTf)Me (**13**). Thus, the reaction mixture was cooled again to −30 °C, added 0.25 extra equivalents of TMSOTf and stirred for other 24 h. The clear reaction mixture was concentrated to 2 mL of toluene and layered with 3 mL of hexanes. Pale green crystals formed after cooling at −30 °C overnight, and the mother liquor was decanted and the crystals were rinsed with 3 × 1 mL of hexanes and dried under vacuum to afford 1.23 g of **13**. Concentrating the mother liquor and cooling it overnight produced a second crop of crystals (550 mg), in a total yield of 87%. ^{1}H NMR (C$_6$D$_6$, 25 °C) of **13**: δ 6.20 (dd, J_1 = 5.2 Hz, J_2 = 2.4 Hz, 1H, η^5-C$_5$*H*$_4$*^{n}*Pr), 5.78 (dd, J_1 = 5.6 Hz, J_2 = 3.2 Hz, 1H, η^5-C$_5$*H*$_4$*^{n}*Pr), 5.54 (dd, J_1 = 5.6 Hz, J_2 = 3.2 Hz, 1H, η^5-C$_5$*H*$_4$*^{n}*Pr), 5.37 (dd, J_1 = 5.2 Hz, J_2 = 2.4 Hz, 1H, η^5-C$_5$*H*$_4$*^{n}*Pr), 2.46 (m, 1H, –C*H*$_2$CH$_2$CH$_3$), 2.22 (m, 1H, –C*H*$_2$CH$_2$CH$_3$), 1.61 (s, 15H, η^5-C$_5$*Me*$_5$), 1.43 (m, 2H, –CH$_2$C*H*$_2$CH$_3$), 0.83 (t, J = 7.2 Hz, 3H, –CH$_2$CH$_2$C*H*$_3$), 0.33 (s, 3H, Zr–C*H*$_3$). ^{13}C NMR (C$_6$D$_6$, 25 °C): δ 133.92 (η^5-*C*$_5$H$_4$*^{n}*Pr), 121.69 (η^5-*C*$_5$Me$_5$), 120.11 (q, $^1J_{C\text{-}F}$ = 318.3 Hz, *C*F$_3$SO$_3$–), 115.47, 113.13, 112.89, 112.54 (η^5-*C*$_5$H$_4$*^{n}*Pr), 40.29 (Zr–*C*H$_3$), 31.71 (–*C*H$_2$CH$_2$CH$_3$), 25.03 (–

$CH_2CH_2CH_3$), 13.90 ($-CH_2CH_2CH_3$), 11.33 (η^5-C_5Me_5). ^{19}F NMR (C_6D_6, 25 °C): δ −77.15 (CF_3SO_3-).

In the second step, a 200 mL glass reaction jar was charged with 1.23 g of **13** (2.47 mmol) and dissolved in 100 mL of dry toluene. The solution was cooled to −30 °C inside the glovebox freezer, and then 0.36 g of freshly prepared Li(OC(O^{i}Pr)=CMe$_2$) (2.64 mmol) were added under vigorous stirring while the solution turned bright yellow. The reaction was left to reach ambient temperature and then stirred for a total of 3 h, after which time an aliquot of the reaction mixture revealed full conversion to Cp*(^{n}PrCp)ZrMe[OC(O^{i}Pr)=CMe$_2$] (**14**). The volatiles were removed *in vacuo* and the remaining orange oily residue was extracted in 100 mL of hexanes and then filtered through a fine porosity frit with a small pad of celite. The solvent was evaporated and the extraction and filtration was repeated. Product **14** was obtained as a thick orange oil after thorough drying under vacuum. Yield: 810 mg (68%). ^{1}H NMR (C_6D_6, 25 °C) of **14**: δ 5.98 (dd, J_1 = 5.4 Hz, J_2 = 2.2 Hz, 1H, η^5-$C_5H_4{}^n$Pr), 5.78 (dd, J_1 = 5.4 Hz, J_2 = 3.0 Hz, 1H, η^5-$C_5H_4{}^n$Pr), 5.63 (dd, J_1 = 5.2 Hz, J_2 = 2.4 Hz, 1H, η^5-$C_5H_4{}^n$Pr), 5.28 (dd, J_1 = 5.4 Hz, J_2 = 3.0 Hz, 1H, η^5-$C_5H_4{}^n$Pr), 4.07 (sept, J = 6.1 Hz, 1H, OC*H*Me$_2$), 2.57 (m, 1H, $-CH_2CH_2CH_3$), 2.41 (m, 1H, $-CH_2CH_2CH_3$), 1.88 (s, 3H, =C*Me*$_2$), 1.79 (s, 15H, η^5-C_5Me_5), 1.66 (s, 3H, =C*Me*$_2$), 1.55 (m, 2H, $-CH_2CH_2CH_3$), 1.20 (d, J = 6.4 Hz, 3H, OCH*Me*$_2$), 1.18 (d, J = 6.4 Hz, 3H, OCH*Me*$_2$), 0.90 (t, J = 7.4 Hz, 3H, $-CH_2CH_2CH_3$), 0.15 (s, 3H, Zr–CH_3). ^{13}C NMR (C_6D_6, 25 °C): δ 154.00 [O*C*(O^{i}Pr)=], 130.36 (η^5-$C_5H_4{}^n$Pr), 118.35 (η^5-C_5Me_5), 114.21, 113.76, 109.57, 107.71 (η^5-$C_5H_4{}^n$Pr), 82.53 (=*C*Me$_2$), 67.40 (O*C*HMe$_2$), 31.69 ($-CH_2CH_2CH_3$), 27.48 (Zr–CH_3), 24.86 ($-CH_2CH_2CH_3$), 22.23, 22.06 (OCH*Me*$_2$), 18.24, 17.60 (=C*Me*$_2$), 14.22 ($-CH_2CH_2CH_3$), 11.47 (η^5-C_5Me_5).

In the third step, a similar procedure described for the preparation of *rac*-(EBI)Zr$^+$(THF)[OC(O^{i}Pr)=CMe$_2$][MeB(C_6F_5)$_3$]$^-$ [5] was modified for the synthesis of **14**$^+$. In an

argon-filled glovebox, a 30 mL glass reaction jar was charged with 43.2 mg of Cp*(^{n}PrCp)ZrMe[OC(O^{i}Pr)=CMe$_2$] (0.090 mmol) and 3 mL of CH_2Cl_2; the light yellow solution was cooled to −30 °C inside the glovebox freezer. Separately, a 1.5 dram vial was charged with 52.6 mg (0.090 mmol) of $(C_6F_5)_3B{\cdot}THF$, dissolved in 1 mL of CH_2Cl_2, and cooled to −30 °C inside the glovebox freezer. Both solutions were mixed via glass pipette, and the resulting mixture changed instantaneously to orange. The solution was stirred for 10 minutes, after which the volatiles were removed under vacuum to afford a viscous orange oil. The crude material was thoroughly washed with hexanes (3 × 5 mL) and subsequently dried under vacuum to form a sticky orange oil in quantitative yield. Anal. Calcd for $C_{48}H_{50}BF_{15}O_3Zr$: C, 54.29; H, 4.75. Found: C, 54.14; H, 4.66.

^{1}H NMR (CD_2Cl_2, 25 °C) of **14**$^+$: δ 6.28 (dd, J_1 = 5.2 Hz, J_2 = 2.8 Hz, 1H, η^5-C$_5H_4$^{n}Pr), 6.21 (dd, J_1 = 5.0 Hz, J_2 = 2.6 Hz, 1H, η^5-C$_5H_4$^{n}Pr), 6.18 (dd, J_1 = 5.4 Hz, J_2 = 3.0 Hz, 1H, η^5-C$_5H_4$^{n}Pr), 6.04 (dd, J_1 = 5.0 Hz, J_2 = 2.2 Hz, 1H, η^5-C$_5H_4$^{n}Pr), 4.16 (m, 2H, α–CH_2, THF), 4.02 (m, 3H, OC*H*Me$_2$, overlapping with α–CH_2, THF), 2.52 (m, 1H, –CH_2CH$_2$CH$_3$), 2.28 (m, 1H, –CH_2CH$_2$CH$_3$), 2.17 (m, 4H, β–CH_2, THF), 2.05 (s, 15H, η^5-C$_5$*Me*$_5$), 1.64 (s, 3H, =C*Me*$_2$), 1.53 (s, 3H, =C*Me*$_2$), 1.51 (m, 2H, –CH$_2$CH_2CH$_3$), 1.22 (d, J = 6.0 Hz, 3H, OCH*Me*$_2$), 1.20 (d, J = 5.2 Hz, 3H, OCH*Me*$_2$), 0.85 (t, J = 7.4 Hz, 3H, –CH$_2$CH$_2$CH_3), 0.49 (s, br, 3H, B–CH_3). ^{13}C NMR (CD_2Cl_2, 25 °C): δ 154.87 [O*C*(O^{i}Pr)=], 148.69 (d, $^1J_{C\text{-}F}$ = 235.3 Hz, Ar*C*–F), 137.88 (d, $^1J_{C\text{-}F}$ = 243.6 Hz, Ar*C*–F), 136.97 (η^5-*C*$_5$H$_4$^{n}Pr), 136.78 (d, $^1J_{C\text{-}F}$ = 246.8 Hz, Ar*C*–F), 126.79 (η^5-*C*$_5$Me$_5$), 120.09, 119.15, 114.48, 113.24 (η^5-*C*$_5$H$_4$^{n}Pr), 89.89 (=*C*Me$_2$), 77.77 (α–*C*H$_2$, THF), 72.60 (O*C*HMe$_2$), 30.76 (–*C*H$_2$CH$_2$CH$_3$), 25.98 (β–*C*H$_2$, THF), 24.60 (–CH$_2$*C*H$_2$CH$_3$), 22.26, 21.95 (OCH*Me*$_2$), 19.08, 17.73 (=C*Me*$_2$), 13.71 (–CH$_2$CH$_2$*C*H$_3$), 12.12 (η^5-C$_5$*Me*$_5$), 10.42 (B–*C*H$_3$). ^{19}F NMR

(CD_2Cl_2, 25 °C): δ −133.12 ($^3J_{F\text{-}F}$ = 18.4 Hz, 6F, o–Ar*F*), −165.27 (t, $^3J_{F\text{-}F}$ = 21.6 Hz, 3F, p–Ar*F*), −167.86 (m, 6F, m–Ar*F*).

***In Situ* Generation of Cp*(^{n}PrCp)ZrMe[O=C(OMe)C(=CH$_2$)CH$_2$COOMe]$^+$ [MeB(C$_6$F$_5$)$_3$]$^-$ (15a).** In an argon-filled glovebox, complex **11**$^+$ was cleanly generated *in situ* by mixing at room temperature complex **11** (25.2 mg, 0.069 mmol) and $(C_6F_5)_3B\cdot THF$ (41.3 mg, 0.071 mmol) in a total of 0.5 mL of CD_2Cl_2 inside a 1.5 dram vial. The bright yellow solution was chilled to −30 °C inside the glovebox freezer. Then, a stoichiometric amount of DMIA (11.0 mg, 0.069 mmol) was added via syringe at −30 °C from a stock solution in CD_2Cl_2. The subsequent red solution was quickly transferred to a Teflon-valve-sealed J. Young-type NMR tube, and immediately placed on a dry ice/acetone batch until it was analyzed by ^{1}H and ^{13}C NMR at −18 °C.

^{1}H NMR (CD_2Cl_2, −18 °C) of **15a**: δ 6.30 (s, 1H, C=C*H*$_2$), 6.20 (d, *J* = 2.0 Hz, 1H, η^5-C$_5$*H*$_4^n$Pr), 6.00 (d, *J* = 2.5 Hz, 1H, η^5-C$_5$*H*$_4^n$Pr), 5.95 (s, 1H, C=C*H*$_2$), 5.91 (d, *J* = 2.5 Hz, 1H, η^5-C$_5$*H*$_4^n$Pr), 5.82 (d, *J* = 2.0 Hz, 1H, η^5-C$_5$*H*$_4^n$Pr), 3.78 (s, 3H, –OMe), 3.72 (s, 3H, –OMe), 3.66 (m, 4H, α–C*H*$_2$, THF, free), 3.33 (d, *J* = 16.5 Hz, 1H, –C*H*$_2$–), 3.28 (d, *J* = 17.5 Hz, 1H, –C*H*$_2$–), 2.38 (m, 1H, –C*H*$_2$CH$_2$CH$_3$), 2.28 (m, 1H, –C*H*$_2$CH$_2$CH$_3$), 1.93 (s, 15H, η^5-C$_5$*Me*$_5$), 1.80 (m, 4H, β–C*H*$_2$, THF, free), 1.54 (m, 2H, –CH$_2$C*H*$_2$CH$_3$), 0.89 (t, *J* = 7.3 Hz, 3H, –CH$_2$CH$_2$C*H*$_3$), 0.43 (s, br, 3H, B–C*H*$_3$), 0.27 (s, 3H, Zr–C*H*$_3$). ^{13}C NMR (CD_2Cl_2, −18 °C): δ 183.10 [CH$_2$*C*(OMe)=O], 169.64 [*C*(OMe)=O], 148.21 (d, $^1J_{C\text{-}F}$ = 236.2 Hz, Ar*C*–F), 137.48 (d, $^1J_{C\text{-}F}$ = 243.0 Hz, Ar*C*–F), 136.33 (d, $^1J_{C\text{-}F}$ = 245.8 Hz, Ar*C*–F), 134.84 (η^5-*C*$_5$H$_4^n$Pr), 132.66 (C=*C*H$_2$), 131.08 (*C*=CH$_2$), 122.79 (η^5-*C*$_5$Me$_5$), 116.19, 115.21, 113.63, 111.66 (η^5-*C*$_5$H$_4^n$Pr), 67.99 (α–*C*H$_2$, THF, free), 56.69 (–OMe), 54.24 (–OMe, overlapped with CD_2Cl_2), 40.73 (Zr–*C*H$_3$), 39.22 (–*C*H$_2$–), 31.63 (–*C*H$_2$CH$_2$CH$_3$), 25.70 (β–*C*H$_2$, THF, free), 25.25 (–CH$_2$*C*H$_2$CH$_3$), 13.66 (–CH$_2$CH$_2$*C*H$_3$), 11.69 (η^5-

C_5Me_5), 9.90 (B–CH_3). ^{19}F NMR (CD_2Cl_2, 25 °C): δ −133.18 (d, $^3J_{F\text{-}F}$ = 17.7 Hz, 6F, o–Ar*F*), −165.30 (t, $^3J_{F\text{-}F}$ = 20.3 Hz, 3F, p–Ar*F*), −167.91 (m, 6F, m–Ar*F*).

***In Situ* Generation of Cp*(*n*PrCp)ZrMe[O=C(O*i*Pr)C(=CH$_2$)CH$_2$COO*i*Pr]$^+$ [MeB(C$_6$F$_5$)$_3$]$^-$ (15b).** In an argon-filled glovebox, complex **11**$^+$ was cleanly generated *in situ* by mixing at room temperature complex **11** (29.5 mg, 0.081 mmol) and $(C_6F_5)_3B\cdot THF$ (48.3 mg, 0.083 mmol) in a total of 0.5 mL of CD_2Cl_2 inside a 1.5 dram vial. The bright yellow solution was chilled to −30 °C inside the glovebox freezer. Then, a stoichiometric amount of D*i*PrIA (17.4 mg, 0.081 mmol) was added via syringe at −30 °C from a stock solution in CD_2Cl_2. The subsequent red solution was quickly transferred to a Teflon-valve-sealed J. Young-type NMR tube, and immediately placed on a dry ice/acetone batch until it was analyzed by ^{1}H and ^{13}C NMR at −18 °C.

^{1}H NMR (CD_2Cl_2, −18 °C) of **15b**: δ 6.26 (s, 1H, C=CH_2), 6.23 (d, *J* = 2.5 Hz, 1H, η^5-C_5H_4*n*Pr), 6.04 (d, *J* = 2.5 Hz, 1H, η^5-C_5H_4*n*Pr), 5.90 (s, 1H, C=CH_2), 5.88 (dd, J_1 = 5.5 Hz, J_2 = 3.0 Hz, 1H, η^5-C_5H_4*n*Pr), 5.79 (dd, J_1 = 4.8 Hz, J_2 = 2.3 Hz, 1H, η^5-C_5H_4*n*Pr), 4.96 (sept, *J* = 6.3 Hz, 1H, OC*H*Me$_2$), 4.79 (sept, *J* = 6.3 Hz, 1H, OC*H*Me$_2$), 3.66 (m, 4H, α–CH_2, THF, free), 3.31 (d, *J* = 17.0 Hz, 1H, –CH_2–), 3.22 (d, *J* = 17.0 Hz, 1H, –CH_2–), 2.41 (m, 1H, –CH_2CH$_2$CH$_3$), 2.28 (m, 1H, –CH_2CH$_2$CH$_3$), 1.92 (s, 15H, η^5-C_5Me_5), 1.80 (m, 4H, β–CH_2, THF, free), 1.54 (m, 2H, –CH$_2$CH_2CH$_3$), 1.28 (d, *J* = 6.0 Hz, 3H, OCH*Me*$_2$), 1.27 (d, *J* = 6.5 Hz, 3H, OCH*Me*$_2$), 1.24 (d, *J* = 6.5 Hz, 3H, OCH*Me*$_2$), 1.22 (d, *J* = 6.0 Hz, 3H, OCH*Me*$_2$), 0.89 (t, *J* = 7.5 Hz, 3H, –CH$_2$CH$_2$CH_3), 0.44 (s, br, 3H, B–CH_3), 0.24 (s, 3H, Zr–CH_3). ^{13}C NMR (CD_2Cl_2, −18 °C): δ 181.95 [CH$_2$*C*(O*i*Pr)=O], 168.42 [*C*(O*i*Pr)=O], 148.20 (d, $^1J_{C\text{-}F}$ = 235.4 Hz, Ar*C*–F), 137.48 (d, $^1J_{C\text{-}F}$ = 243.5 Hz, Ar*C*–F), 136.39 (d, $^1J_{C\text{-}F}$ = 245.0 Hz, Ar*C*–F), 134.87 (η^5-*C*$_5$H$_4$*n*Pr), 132.05 (C=*C*H$_2$), 131.62 (*C*=CH$_2$), 122.63 (η^5-*C*$_5$Me$_5$), 116.16, 115.06, 113.40, 111.34 (η^5-*C*$_5$H$_4$*n*Pr), 76.04

(O*C*HMe$_2$), 71.91 (O*C*HMe$_2$), 67.98 (α–*C*H$_2$, THF, free), 40.08 (–*C*H$_2$–), 39.65 (Zr–*C*H$_3$), 31.69 (–*C*H$_2$CH$_2$CH$_3$), 25.72 (β–*C*H$_2$, THF, free), 25.30 (–CH$_2$*C*H$_2$CH$_3$), 21.52, 21.47, 21.24, 21.15 (OCH*Me*$_2$), 13.71 (–CH$_2$CH$_2$*C*H$_3$), 11.69 (η^5-C$_5$*Me*$_5$), 9.60 (B–*C*H$_3$). ^{19}F NMR (CD_2Cl_2, 25 °C): δ −133.15 (d, $^3J_{F\text{-}F}$ = 18.4 Hz, 6F, o–Ar*F*), −165.35 (t, $^3J_{F\text{-}F}$ = 20.3 Hz, 3F, p–Ar*F*), −167.93 (m, 6F, m–Ar*F*).

Isolation of Cp*(*n*PrCp)Zr[OC(Ome)=C(CH$_2$COOMe)CH$_2$C(Me$_2$)C(O*i*Pr)=O]$^+$ [MeB(C$_6$F$_5$)$_3$]$^-$ (16a). Inside an argon-filled glovebox, a 30 mL glass reaction jar was charged with 42.4 mg of complex **14** (0.089 mmol) and dissolved in 3 mL of CH_2Cl_2. Complex **14**$^+$ was cleanly generated *in situ* by adding 52.0 mg of $(C_6F_5)_3B\cdot THF$ (0.089 mmol) in 1 mL of CH_2Cl_2 at room temperature, accompanied by a rapid color change from light yellow to orange. After stirring for 5 min, the reaction mixture was cooled to −30 °C inside the glovebox freezer, and then 14.1 mg of DMIA (0.089 mmol) were added via syringe from a prechilled stock solution in CH_2Cl_2. The reaction mixture was stirred for a total of 15 min, during which time the color of the solution slowly turned bright yellow as it reached room temperature. The volatiles were removed under vacuum, and the oily yellow residue was thoroughly washed with hexanes (3 × 5 mL). Each washing cycle consisted in vigorous stirring for 5 minutes and then removal of the supernatant liquid with a glass pipette. A bright yellow foamy solid was obtained after drying the oily residue under vacuum for several h in quantitative yield. Anal. Calcd for $C_{51}H_{52}BF_{15}O_6Zr$: C, 53.36; H, 4.57. Found: C, 53.71; H, 4.40.

^{1}H NMR (CD_2Cl_2, 25 °C) of **16a**: δ 6.56 (s, br, 1H, η^5-C$_5$*H*$_4$*n*Pr), 6.35 (s, br, 1H, η^5-C$_5$*H*$_4$*n*Pr), 6.00 (s, br, 1H, η^5-C$_5$*H*$_4$*n*Pr), 5.94 (s, br, 1H, η^5-C$_5$*H*$_4$*n*Pr), 4.96 (sept, *J* = 6.4 Hz, 1H, OC*H*Me$_2$), 3.66 (s, 3H, OC*H*$_3$), 3.43 (s, 3H, OC*H*$_3$), 3.10 (d, *J* = 16.8 Hz, 1H, C*H*$_2$C(O)OMe), 2.93 (d, *J* = 16.8 Hz, 1H, C*H*$_2$C(O)OMe), 2.64 (d, *J* = 16.0 Hz, 1H, –C*H*$_2$–), 2.37 (m, 1H, –C*H*$_2$CH$_2$CH$_3$), 2.06

(s, 15H, η^5-C$_5$*Me*$_5$), 2.01 (m, 1H, –C*H*$_2$CH$_2$CH$_3$), 1.84 (d, *J* = 15.6 Hz, 1H, –C*H*$_2$–), 1.51 (m, 2H, –CH$_2$C*H*$_2$CH$_3$), 1.49 (d, *J* = 6.4 Hz, 3H, OCH*Me*$_2$), 1.42 (d, *J* = 6.4 Hz, 3H, OCH*Me*$_2$), 1.40 (s, 6H, C*Me*$_2$), 0.85 (t, *J* = 7.4 Hz, 3H, –CH$_2$CH$_2$C*H*$_3$), 0.48 (s, br, 3H, B–C*H*$_3$). ^{13}C NMR (CD$_2$Cl$_2$, 25 °C): *δ* 193.78 [*C*(O^{i}Pr)=O], 173.50 [*C*(OMe)=O], 160.38 [O*C*(OMe)=], 148.71 (d, $^1J_{C\text{-}F}$ = 239.9 Hz, Ar*C*–F), 137.89 (d, $^1J_{C\text{-}F}$ = 243.1 Hz, Ar*C*–F), 136.78 (d, $^1J_{C\text{-}F}$ = 246.0 Hz, Ar*C*–F), 134.75 (η^5-*C*$_5$H$_4$^{n}Pr), 126.58 (η^5-*C*$_5$Me$_5$), 120.77, 118.85, 118.21, 111.49 (η^5-*C*$_5$H$_4$^{n}Pr), 83.12 (=*C*CH$_2$), 76.47 (O*C*HMe$_2$), 54.96 (–O*Me*), 51.95 (–O*Me*), 45.00 (*C*Me$_2$), 38.51 (–*C*H$_2$–), 36.75 [*C*H$_2$C(O)OMe], 31.45 (C*Me*$_2$), 31.38 (–*C*H$_2$CH$_2$CH$_3$), 25.21 (–CH$_2$*C*H$_2$CH$_3$), 24.51 (C*Me*$_2$), 21.96, 21.78 (OCH*Me*$_2$), 13.71 (–CH$_2$CH$_2$*C*H$_3$), 12.00 (η^5-C$_5$*Me*$_5$), 10.46 (B–*C*H$_3$). ^{19}F NMR (CD$_2$Cl$_2$, 25 °C): *δ* −133.08 (d, $^3J_{F\text{-}F}$ = 19.20 Hz, 6F, o–Ar*F*), −165.30 (t, $^3J_{F\text{-}F}$ = 20.3 Hz, 3F, p–Ar*F*), −167.88 (m, 6F, m–Ar*F*).

Isolation of Cp*(^{n}PrCp)Zr[OC(O^{i}Pr)=C(CH$_2$COO^{i}Pr)CH$_2$C(Me$_2$)C(O^{i}Pr)=O]$^+$ [MeB(C$_6$F$_5$)$_3$]$^-$ (16b). Inside an argon-filled glovebox, a 30 mL glass reaction jar was charged with 46.8 mg of complex **14** (0.098 mmol) and dissolved in 3 mL of CH$_2$Cl$_2$. Complex **14**$^+$ was cleanly generated *in situ* by adding 57.2 mg of (C$_6$F$_5$)$_3$B·THF (0.098 mmol) in 1 mL of CH$_2$Cl$_2$ at room temperature, accompanied by a rapid color change from light yellow to orange. After stirring for 5 min, the reaction mixture was cooled to −30 °C inside the glovebox freezer, and then 21.0 mg of D^{i}PrIA (0.098 mmol) were added via syringe from a prechilled stock solution in CH$_2$Cl$_2$. The reaction mixture was stirred for a total of 15 minutes, during which time the color of the solution slowly turned bright yellow as it reached room temperature. The volatiles were removed under vacuum, and the oily yellow residue was thoroughly washed with hexanes (3 × 5 mL). Each washing cycle consisted in vigorous stirring for 5 minutes and then removal of the supernatant liquid with a glass pipette. A bright yellow foamy solid was obtained after drying the oily residue

under vacuum for several h in quantitative yield. The elemental analyses gave unsatisfying results, presumably due to its limited thermal stability at ambient temperature.

^{1}H NMR (CD_2Cl_2, 25 °C) of **16b**: δ 6.60 (s, br, 1H, η^5-$C_5H_4{}^n$Pr), 6.37 (s, br, 1H, η^5-$C_5H_4{}^n$Pr), 6.00 (s, br, 1H, η^5-$C_5H_4{}^n$Pr), 5.94 (s, br, 1H, η^5-$C_5H_4{}^n$Pr), 4.98 (m, 2H, two OC*H*Me$_2$ overlapped), 4.08 (sept, J = 6.3 Hz, 1H, OC*H*Me$_2$), 3.14 (d, J = 16.4 Hz, 1H, C*H*$_2$C(O)O^{i}Pr), 2.95 (d, J = 16.8 Hz, 1H, C*H*$_2$C(O)O^{i}Pr), 2.64 (d, J = 15.6 Hz, 1H, –C*H*$_2$–), 2.40 (m, 1H, –C*H*$_2$CH$_2$CH$_3$), 2.04 (s, 16H, η^5-C_5Me_5 overlapped with C*H*$_2$CH$_2$CH$_3$), 1.90 (d, J = 15.6 Hz, 1H, –C*H*$_2$–), 1.51 (m, 2H, –CH$_2$C*H*$_2$CH$_3$), 1.49 (d, J = 6.0 Hz, 3H, OCH*Me*$_2$), 1.45 (s, 3H, C*Me*$_2$), 1.42 (d, J = 6.4 Hz, 3H, OCH*Me*$_2$), 1.40 (s, 3H, C*Me*$_2$), 1.29 (d, J = 6.0 Hz, 3H, OCH*Me*$_2$), 1.23 (m, 6H, OCH*Me*$_2$), 1.16 (d, J = 6.0 Hz, 3H, OCH*Me*$_2$), 0.86 (t, J = 7.2 Hz, 3H, –CH$_2$CH$_2$C*H*$_3$), 0.50 (s, br, 3H, B–C*H*$_3$). ^{13}C NMR (CD_2Cl_2, 25 °C): δ 193.71 [*C*(O^{i}Pr)=O], 172.51 [*C*(O^{i}Pr)=O], 158.51 [O*C*(O^{i}Pr)=], 148.69 (d, $^1J_{C\text{-}F}$ = 235.8 Hz, Ar*C*–F), 137.88 (d, $^1J_{C\text{-}F}$ = 243.4 Hz, Ar*C*–F), 136.77 (d, $^1J_{C\text{-}F}$ = 244.7 Hz, Ar*C*–F), 134.33 (η^5-*C*$_5$H$_4{}^n$Pr), 126.37 (η^5-*C*$_5$Me$_5$), 120.86, 118.37, 118.16, 111.57 (η^5-*C*$_5$H$_4{}^n$Pr), 85.01 (=*C*CH$_2$), 76.34 (O*C*HMe$_2$), 69.75 (O*C*HMe$_2$), 68.08 (O*C*HMe$_2$), 44.98 (*C*Me$_2$), 37.79 (–*C*H$_2$–), 37.07 [*C*H$_2$C(O)O^{i}Pr], 32.02 (C*Me*$_2$), 31.34 (–*C*H$_2$CH$_2$CH$_3$), 25.37 (–CH$_2$*C*H$_2$CH$_3$), 24.62 (C*Me*$_2$), 22.68, 22.04, 21.99, 21.93, 21.77, and 21.47 (OCH*Me*$_2$), 13.69 (–CH$_2$CH$_2$*C*H$_3$), 11.97 (η^5-C$_5$*Me*$_5$), 10.44 (B–*C*H$_3$). ^{19}F NMR (CD_2Cl_2, 25 °C): δ −133.06 (d, $^3J_{F\text{-}F}$ = 19.20 Hz, 6F, o–Ar*F*), −165.27 (t, $^3J_{F\text{-}F}$ = 20.5 Hz, 3F, p–Ar*F*), −167.84 (m, 6F, m–Ar*F*).

***In Situ* Generation of Cp*(^{n}PrCp)ZrMe{OC[OC(O)CH$_2$]=C(CH$_2$CMe$_2$COO^{i}Pr)} (18).** Inside an argon-filled glovebox, complex **18** was cleanly and instantaneously generated by mixing 31.6 mg of complex **14** (0.066 mmol) and 7.4 mg of IA (0.066 mmol) in 0.5 mL of CD_2Cl_2 at ambient temperature.

^{1}H NMR (CD_2Cl_2, 25 °C) of **18**: δ 5.90 (dd, J_1 = 5.4 Hz, J_2 = 2.6 Hz, 1H, η^5-$C_5H_4{}^n$Pr), 5.73 (pst, J = 2.8 Hz, 2H, η^5-$C_5H_4{}^n$Pr), 5.70 (dd, J_1 = 5.4 Hz, J_2 = 2.6 Hz, 1H, η^5-$C_5H_4{}^n$Pr), 4.92 (sept, J = 6.3 Hz, 1H, OC*H*Me$_2$), 3.04 (s, 2H, C*H*$_2$C(O)–O), 2.33 (m, 2H, –C*H*$_2$CH$_2$CH$_3$), 2.11 (s, 2H, –C*H*$_2$–), 1.91 (s, 15H, η^5-C_5Me_5), 1.51 (sextet, J = 7.4 Hz, 2H, –CH$_2$C*H*$_2$CH$_3$), 1.21 (d, J = 6.4 Hz, 6H, OCH*Me*$_2$), 1.07 (s, 3H, C*Me*$_2$), 1.05 (s, 3H, C*Me*$_2$), 0.89 (t, J = 7.4 Hz, 3H, –CH$_2$CH$_2$C*H*$_3$), −0.06 (s, 3H, Zr–C*H*$_3$). ^{13}C NMR (CD_2Cl_2, 25 °C): δ 177.67 [CH$_2$*C*(O)–O], 174.94 [*C*(O^{i}Pr)=O], 158.51 [O*C*(OC)=], 132.18 (η^5-*C*$_5$H$_4{}^n$Pr), 119.85 (η^5-*C*$_5$Me$_5$), 113.85, 112.84, 110.78, 110.43 (η^5-*C*$_5$H$_4{}^n$Pr), 76.08 (=*C*CH$_2$), 67.82 (O*C*HMe$_2$), 42.84 (*C*Me$_2$), 38.22 (–*C*H$_2$–), 35.42 [*C*H$_2$C(O)–O], 31.61 (–*C*H$_2$CH$_2$CH$_3$), 30.32 (Zr–*C*H$_3$), 25.59, 25.15 (C*Me*$_2$), 24.86 (–CH$_2$*C*H$_2$CH$_3$), 21.91 (OCH*Me*$_2$), 14.09 (–CH$_2$CH$_2$*C*H$_3$), 11.57 (η^5-C_5Me_5).

General Polymerization Procedures. Polymerizations were carried out in 20 mL glass reactors inside of a glovebox for ambient temperature (~25 °C) runs. In control polymerizations of MMA and DMAA with cationic complexes **9**$^+$, **11**$^+$, and **14**$^+$, a predetermined amount of pre-catalyst (**9**, **11** or **14**) and activator — $[H(OEt_2)_2]^+B(C_6F_5)_4]^-$ for **9**, or $(C_6F_5)_3B{\cdot}THF$ for **11** and **14** — were premixed at room temperature in 1:1 molar ratio to cleanly generate the corresponding cationic catalyst, and followed by rapid addition of the monomer (100 or 150 equivalents) to start the polymerization. For example, solutions of $(C_6F_5)_3B{\cdot}THF$ (20.5 mg, 0.035 mmol) and precatalyst **14** (16.7 mg, 0.035 mmol) were premixed in 3.0 mL of CH_2Cl_2 and stirred for 2 minutes to cleanly generate the active species **14**$^+$. Subsequently, the monomer DMAA (0.54 mL, $[DMAA]_0/[\mathbf{14}^+]$ = 150) was quickly added via syringe to the vigorously stirring solution, and the reaction was allowed to proceed with continuous stirring at ambient temperature.

Alternatively, polymerizations that required the pre-formation of itaconate-based complexes **2a**(**b**), **15a**(**b**), and **16a**(**b**) started with the pre-activation of the neutral zirconocenes **1**, **11**, and **14**

with $(C_6F_5)_3B{\cdot}THF$ as described above. The solutions of $\mathbf{1}^+$, $\mathbf{11}^+$, and $\mathbf{14}^+$ were stirred for 2 min at room temperature, and then cooled to −30 °C inside the glovebox freezer. The itaconate adducts and complexes were generated *in-situ* by adding one equivalent of the dialkyl itaconate from a prechilled stock solution, and then stirred for 2 min. To prevent any decomposition or complex evolution, the monomer was quickly added (100 or 150 equivalents) via syringe to start the polymerization. Polymerizations carried out by **4a**(**b**) were started similarly, but solutions of **1+** with stoichiometric amounts of dialkyl itaconates were stirred at room temperature for 48 h before the addition of the monomer, ensuring full conversion of **2a**(**b**) into the thermodynamic products **4a**(**b**). For instance, in a typical polymerization $(C_6F_5)_3B{\cdot}THF$ (18.8 mg, 0.032 mmol) and precatalyst **1** (15.7 mg, 0.032 mmol) were premixed in 3.0 mL of CH_2Cl_2, stirred for 2 min to cleanly generate the active species $\mathbf{1}^+$, and then cooled to −30 °C inside the glovebox freezer. Complex **2a** was *in-situ* generated by addition of an equimolar amount of DMIA (5.05 mg, 0.032 mmol) from a precooled stock solution in CH_2Cl_2. After stirring the mixture for 2 min, the polymerization was quickly started by adding DMAA (0.5 mL, $[DMAA]_0/[\mathbf{2a}] = 150$) via syringe to the vigorously stirring solution, and the reaction was allowed to proceed with continuous stirring at ambient temperature.

For those polymerization runs with preformation of complex **5**, precatalyst **1** (14.1 mg, 0.029 mmol) was dissolved in 3 mL of CH_2Cl_2 and then, an equimolar amount of itaconic anhydride (3.21 mg, 0.029 mmol) was added from a stock solution in CH_2Cl_2 at ambient temperature. The bright yellow solution was cooled down to −30 °C, and the polymerization was immediately started by adding a solution of DMAA (or MMA) and $B(C_6F_5)_3$ (14.7 mg, 0.029 mmol), in [**5**]/[act]/[M] ratios of 1:1:150, via a glass pipette. The reaction was allowed to proceed with continuous stirring at ambient temperature for 24 h.

In all the cases, after the measured time interval, a 0.1 mL aliquot was taken from the reaction mixture via syringe and quickly quenched into a 1.5 mL vial containing 0.6 mL of undried "wet" $CDCl_3$ stabilized by 250 ppm of BHT-H; the quenched aliquots were later analyzed by ^1H NMR to obtain monomer conversion data. The remaining bulk polymerization reaction was quenched after the removal of the last aliquot by addition of 5 mL of 5% HCl-acidified methanol and precipitated into 100 mL of MeOH (for MMA runs) or Et_2O (for DMAA runs). The quenched mixture was stirred for 3 h, and the polymer obtained was filtered, washed with MeOH (or Et_2O), and dried in a vacuum oven at 50 °C overnight to a constant weight.

Polymer Characterizations. Polymer number-average molecular weights (M_n) and molecular weight distributions ($Đ = M_w/M_n$) were measured by gel permeation chromatography (GPC) analyses carried out at 40 ºC and a flow rate of 1.0 mL/min, with DMF as the eluent on a Waters University 1500 GPC instrument equipped with one PLgel 5 μm guard and three PLgel 5 μm mixed-C columns (Polymer Laboratories; linear range of MW = 200–2,000,000). The instrument was calibrated with 10 PMMA standards, and chromatograms were processed with Waters Empower software (version 2002).

The tacticity of the polymers was analyzed by ^1H and ^{13}C NMR based on that of PMMA.[3,5,9] The isolated low molecular weight samples were analyzed by matrix-assisted laser desorption/ionization time-of-flight mass spectrometry (MALDI-TOF MS). The experiment was performed on a Microflex-LRF mass spectrometer (Bruker Daltonics, Billerica, MA) in positive ion, reflector mode using a 25 kV accelerating voltage. A thin layer of a 1% NaI solution was first deposited on the target plate, followed by 0.6 µl of both sample and matrix (dithranol, 10 mg/mL in MeOH). The mixture was then spotted on top of the NaI layer and allowed to air dry. External calibration was done using a peptide calibration mixture (4 to 6 peptides) on a spot adjacent to the

sample. The raw data was processed in the FlexAnalysis software (version 3.4.7, Bruker Daltonics).

Table S4.1. Results of acrylates control polymerization by metallocene catalysts.[a]

run no.	Catalyst	Monomer	Time (h)	conv.[b] (%)	M_n[c] (kg/mol)	$Đ$[c]	I*[d] (%)	[*mm*][e] (%)	[*mr*][e] (%)	[*rr*][e] (%)
1	**11**$^+$	MMA	24	100	13.8	1.21	109	2.6	22.8	74.6
2	**11**$^+$	DMAA	3	100	464 (70%)	1.23	3.2	n.d.	n.d.	n.d.
					43.7 (30%)	1.25	34			
3	**14**$^+$	MMA	24	100	17.5	1.20	86	3.3	23.5	73.2
4	**14**$^+$	DMAA	1	100	21.0	1.16	71	n.d.	n.d.	n.d.
5	**15a**	MMA	24	85	10.0	1.62	87	4.3	24.2	71.5
6	**15a**	DMAA	24	100	365(47%)	1.28	3	n.d.	n.d.	n.d.
					40.7(53%)	1.24	25			
7	**15b**	MMA	24	91	10.4	1.71	90	3.7	23.3	73.0
8	**15b**	DMAA	24	100	274(86%)	1.26		n.d.	n.d.	n.d.
					23.1(14%)	1.19				

[a]Conditions: solvent (DCM) = 3 mL; ambient temperature (~23 °C); $[M]_0/[catalyst]_0$ = 150, except for runs 5 to 8, where $[M]_0/[catalyst]_0$ = 100; n.d. = not determined. [b]Monomer (M) conversion measured by ^{1}H NMR. [c]Number-average molecular weight (M_n) and polydispersity ($Đ$) determined by gel-permeation chromatography (GPC) relative to PMMA standards. [d]Initiator efficiency (I*) = M_n(calcd)/M_n(exptl), where M_n(calcd) = MW(M) × $[M]_0/[catalyst]_0$ × conversion% + MW of chain-end groups. [e]Tacticity measured by ^{1}H NMR in $CDCl_3$.

X-Ray crystallography. The molecular structure of **9**$^+$ was determined by single crystal X-ray crystallography (Table S4.2). Single crystals were coated with Paratone-N oil and mounted under a cold stream of dinitrogen gas. Single crystal X-ray diffraction data were acquired on a Bruker Kappa APEX II CCD diffractometer with Mo Kα radiation (λ = 0.71073 Å) and a graphite monochromator. Initial lattice parameters were obtained from a least-squares analysis of more than 100 reflections; these parameters were later refined against all data. None of the crystals showed significant decay during data collection. Data were integrated and corrected for Lorentz and polarization effects using Bruker APEX3 software, and semi-empirical absorption corrections were applied using SCALE.[10] Space group assignments were based on systematic absences, E statistics, and successful refinement of the structures. Structures were solved using Direct Methods

and were refined with the aid of successive Fourier difference maps against all data using the SHELXTL 6.14 software package.[11] Thermal parameters for all non-hydrogen atoms were refined anisotropically. All hydrogen atoms were assigned to ideal positions and refined using a riding model with an isotropic thermal parameter 1.2 times that of the attached carbon atom (1.5 times for methyl hydrogens).

C.2. Crystal Structure Report for $[Cp^*(^n PrCp)Zr(HNMe_2)=NMe_2]^+[B(C_6F_5)_4]^-$ (9^+)

A clear light yellow rod-like specimen of $C_{184}H_{156}B_4F_{80}N_8Zr_4$, approximate dimensions 0.160 mm x 0.236 mm x 0.385 mm, was used for the X-ray crystallographic analysis. The X-ray intensity data were measured. A total of 2022 frames were collected. The total exposure time was 14.04 h. The frames were integrated with the Bruker SAINT software package using a narrow-frame algorithm. The integration of the data using a monoclinic unit cell yielded a total of 9019 reflections to a maximum θ angle of 26.37° (0.80 Å resolution), of which 9019 were independent (average redundancy 1.000, completeness = 100.0%, R_{int} = 0.00%, R_{sig} = 6.87%) and 6336 (70.25%) were greater than $2\sigma(F^2)$. The final cell constants of a = 13.8112(9) Å, b = 20.5825(13) Å, c = 15.5423(10) Å, β = 92.875(3)°, volume = 4412.6(5) $Å^3$, are based upon the refinement of the XYZ-centroids of 9700 reflections above 20 σ(I) with 4.749° < 2θ < 62.06°. Data were corrected for absorption effects using the Multi-Scan method (SADABS). The ratio of minimum to maximum apparent transmission was 0.846. The calculated minimum and maximum transmission coefficients (based on crystal size) are 0.8700 and 0.9430.

The structure was solved and refined using the Bruker SHELXTL Software Package, using the space group $P2_1/n$, with Z = 1 for the formula unit, $C_{184}H_{156}B_4F_{80}N_8Zr_4$. The final anisotropic full-matrix least-squares refinement on F^2 with 645 variables converged at R1 = 5.58%, for the

observed data and wR2 = 15.39% for all data. The goodness-of-fit was 1.081. The largest peak in the final difference electron density synthesis was 1.122 $e^-/Å^3$ and the largest hole was -0.582 $e^-/Å^3$ with an RMS deviation of 0.125 $e^-/Å^3$. On the basis of the final model, the calculated density was 1.659 g/cm^3 and F(000), 2216 e^-. Twin fraction for domain one and two are 66.19% and 33.81%, respectively.

Table S4.2. Sample and crystal data for $\mathbf{9}^+$.

Identification code	ec116	
Chemical formula	$C_{184}H_{156}B_4F_{80}N_8Zr_4$	
Formula weight	4407.28 g/mol	
Temperature	100(2) K	
Wavelength	0.71073 Å	
Crystal size	0.160 x 0.236 x 0.385 mm	
Crystal habit	clear light yellow rod	
Crystal system	monoclinic	
Space group	$P2_1/n$	
Unit cell dimensions	a = 13.8112(9) Å	α = 90°
	b = 20.5825(13) Å	β = 92.875(3)°
	c = 15.5423(10) Å	γ = 90°
Volume	4412.6(5) $Å^3$	
Z	1	
Density (calculated)	1.659 g/cm^3	
Absorption coefficient	0.372 mm^{-1}	
F(000)	2216	

Table S4.3. Data collection and structure refinement for $\mathbf{9}^+$.

Theta range for data collection	1.64 to 26.37°
Reflections collected	9019
Independent reflections	9019 [R(int) = 0.0000]
Coverage of independent reflections	100.0%
Absorption correction	Multi-Scan

Max. and min. transmission	0.9430 and 0.8700	
Structure solution technique	direct methods	
Structure solution program	XT, VERSION 2014/5	
Refinement method	Full-matrix least-squares on F^2	
Refinement program	SHELXL-2014/7 (Sheldrick, 2014)	
Function minimized	$\Sigma\, w(F_o^2 - F_c^2)^2$	
Data / restraints / parameters	9019 / 0 / 645	
Goodness-of-fit on F^2	1.081	
Δ/σ_{max}	0.001	
Final R indices	6336 data; $I>2\sigma(I)$	R1 = 0.0558, wR2 = 0.1288
	all data	R1 = 0.0985, wR2 = 0.1539
Weighting scheme	$w = 1/[\sigma^2(F_o^2)+(0.0698P)^2+8.5769P]$ where $P = (F_o^2+2F_c^2)/3$	
Largest diff. peak and hole	1.122 and -0.582 eÅ^{-3}	
R.M.S. deviation from mean	0.125 eÅ^{-3}	

Table S4. Bond lengths (Å) for **9**$^+$.

Zr1-N1	2.076(4)	Zr1-N2	2.386(4)
Zr1-C13	2.496(4)	Zr1-C12	2.502(4)
Zr1-C3	2.522(4)	Zr1-C14	2.529(4)
Zr1-C11	2.535(4)	Zr1-C15	2.538(4)
Zr1-C4	2.550(4)	Zr1-C5	2.579(4)
Zr1-C2	2.590(4)	Zr1-C1	2.592(4)
C1-C2	1.412(6)	C1-C5	1.435(5)
C1-C6	1.505(6)	C2-C3	1.438(6)
C2-C7	1.512(6)	C3-C4	1.421(6)
C3-C8	1.509(6)	C4-C5	1.425(6)
C4-C9	1.508(5)	C5-C10	1.511(6)
C6-H6A	0.98	C6-H6B	0.98
C6-H6C	0.98	C7-H7A	0.98
C7-H7B	0.98	C7-H7C	0.98
C8-H8A	0.98	C8-H8B	0.98
C8-H8C	0.98	C9-H9A	0.98

C9-H9B	0.98	C9-H9C	0.98
C10-H10A	0.98	C10-H10B	0.98
C10-H10C	0.98	C11-C12	1.426(6)
C11-C15	1.426(6)	C11-C16	1.512(6)
C12-C13	1.412(6)	C12-H12	1.0
C13-C14	1.406(7)	C13-H13	1.0
C14-C15	1.399(6)	C14-H14	1.0
C15-H15	1.0	C16-C17	1.524(7)
C16-H16A	0.99	C16-H16B	0.99
C17-C18	1.509(7)	C17-H17A	0.99
C17-H17B	0.99	C18-H18A	0.98
C18-H18B	0.98	C18-H18C	0.98
C19-N1	1.479(6)	C19-H19A	0.98
C19-H19B	0.98	C19-H19C	0.98
C20-N1	1.482(6)	C20-H20A	0.98
C20-H20B	0.98	C20-H20C	0.98
C21-N2	1.497(7)	C21-H21A	0.98
C21-H21B	0.98	C21-H21C	0.98
C22-N2	1.490(6)	C22-H22A	0.98
C22-H22B	0.98	C22-H22C	0.98
N2-H1	0.96(5)	B1-C29	1.656(6)
B1-C35	1.656(7)	B1-C23	1.657(6)
B1-C41	1.665(6)	C23-C24	1.393(6)
C23-C28	1.395(6)	C24-F1	1.355(5)
C24-C25	1.388(6)	C25-F2	1.347(5)
C25-C26	1.370(6)	C26-F3	1.346(5)
C26-C27	1.381(6)	C27-F4	1.354(5)
C27-C28	1.373(6)	C28-F5	1.365(5)
C29-C34	1.385(6)	C29-C30	1.389(6)
C30-F6	1.366(5)	C30-C31	1.390(6)
C31-F7	1.346(5)	C31-C32	1.372(7)
C32-F8	1.345(5)	C32-C33	1.374(7)
C33-F9	1.347(5)	C33-C34	1.387(6)

C34-F10	1.374(5)	C35-C36	1.397(6)
C35-C40	1.397(6)	C36-F11	1.359(5)
C36-C37	1.383(6)	C37-F12	1.342(5)
C37-C38	1.376(6)	C38-F13	1.342(5)
C38-C39	1.378(6)	C39-F14	1.353(5)
C39-C40	1.373(7)	C40-F15	1.361(5)
C41-C46	1.388(6)	C41-C42	1.401(6)
C42-F16	1.361(5)	C42-C43	1.382(6)
C43-F17	1.354(5)	C43-C44	1.370(7)
C44-F18	1.346(5)	C44-C45	1.377(7)
C45-F19	1.349(5)	C45-C46	1.380(6)
C46-F20	1.353(5)		

Table S5. Bond angles (°) for $\mathbf{9}^{+}$.

N1-Zr1-N2	93.84(14)	N1-Zr1-C13	133.45(15)
N2-Zr1-C13	91.15(15)	N1-Zr1-C12	121.39(14)
N2-Zr1-C12	123.96(14)	C13-Zr1-C12	32.83(14)
N1-Zr1-C3	108.12(14)	N2-Zr1-C3	132.98(14)
C13-Zr1-C3	101.59(15)	C12-Zr1-C3	79.05(14)
N1-Zr1-C14	104.45(15)	N2-Zr1-C14	77.55(15)
C13-Zr1-C14	32.49(15)	C12-Zr1-C14	53.72(15)
C3-Zr1-C14	131.88(15)	N1-Zr1-C11	88.73(14)
N2-Zr1-C11	130.16(14)	C13-Zr1-C11	54.56(15)
C12-Zr1-C11	32.88(14)	C3-Zr1-C11	92.32(14)
C14-Zr1-C11	53.85(14)	N1-Zr1-C15	79.65(15)
N2-Zr1-C15	99.13(14)	C13-Zr1-C15	53.89(15)
C12-Zr1-C15	53.88(15)	C3-Zr1-C15	124.97(14)
C14-Zr1-C15	32.05(14)	C11-Zr1-C15	32.66(14)
N1-Zr1-C4	84.87(14)	N2-Zr1-C4	114.96(15)
C13-Zr1-C4	133.45(15)	C12-Zr1-C4	110.64(15)
C3-Zr1-C4	32.53(14)	C14-Zr1-C4	164.27(15)
C11-Zr1-C4	114.84(14)	C15-Zr1-C4	143.36(14)

N1-Zr1-C5	95.66(14)	N2-Zr1-C5	83.96(14)
C13-Zr1-C5	130.89(14)	C12-Zr1-C5	127.87(14)
C3-Zr1-C5	53.62(14)	C14-Zr1-C5	153.39(14)
C11-Zr1-C5	145.33(14)	C15-Zr1-C5	174.50(14)
C4-Zr1-C5	32.26(14)	N1-Zr1-C2	138.07(14)
N2-Zr1-C2	107.59(14)	C13-Zr1-C2	82.84(15)
C12-Zr1-C2	75.54(15)	C3-Zr1-C2	32.65(13)
C14-Zr1-C2	115.00(15)	C11-Zr1-C2	102.86(14)
C15-Zr1-C2	129.33(14)	C4-Zr1-C2	53.57(13)
C5-Zr1-C2	53.10(13)	N1-Zr1-C1	127.70(14)
N2-Zr1-C1	80.11(14)	C13-Zr1-C1	98.76(15)
C12-Zr1-C1	103.73(14)	C3-Zr1-C1	53.42(13)
C14-Zr1-C1	124.11(14)	C11-Zr1-C1	133.96(14)
C15-Zr1-C1	152.64(14)	C4-Zr1-C1	53.38(13)
C5-Zr1-C1	32.23(12)	C2-Zr1-C1	31.62(14)
C2-C1-C5	108.5(4)	C2-C1-C6	125.1(4)
C5-C1-C6	125.0(4)	C2-C1-Zr1	74.1(3)
C5-C1-Zr1	73.4(2)	C6-C1-Zr1	129.3(3)
C1-C2-C3	107.6(4)	C1-C2-C7	124.7(4)
C3-C2-C7	127.0(4)	C1-C2-Zr1	74.3(2)
C3-C2-Zr1	71.1(2)	C7-C2-Zr1	127.7(3)
C4-C3-C2	108.2(4)	C4-C3-C8	124.4(4)
C2-C3-C8	126.2(4)	C4-C3-Zr1	74.8(2)
C2-C3-Zr1	76.3(2)	C8-C3-Zr1	125.0(3)
C3-C4-C5	107.9(4)	C3-C4-C9	123.8(4)
C5-C4-C9	127.8(4)	C3-C4-Zr1	72.7(2)
C5-C4-Zr1	75.0(2)	C9-C4-Zr1	124.1(3)
C4-C5-C1	107.7(4)	C4-C5-C10	127.3(4)
C1-C5-C10	123.6(4)	C4-C5-Zr1	72.7(2)
C1-C5-Zr1	74.4(2)	C10-C5-Zr1	128.9(3)
C1-C6-H6A	109.5	C1-C6-H6B	109.5
H6A-C6-H6B	109.5	C1-C6-H6C	109.5
H6A-C6-H6C	109.5	H6B-C6-H6C	109.5

C2-C7-H7A	109.5	C2-C7-H7B	109.5
H7A-C7-H7B	109.5	C2-C7-H7C	109.5
H7A-C7-H7C	109.5	H7B-C7-H7C	109.5
C3-C8-H8A	109.5	C3-C8-H8B	109.5
H8A-C8-H8B	109.5	C3-C8-H8C	109.5
H8A-C8-H8C	109.5	H8B-C8-H8C	109.5
C4-C9-H9A	109.5	C4-C9-H9B	109.5
H9A-C9-H9B	109.5	C4-C9-H9C	109.5
H9A-C9-H9C	109.5	H9B-C9-H9C	109.5
C5-C10-H10A	109.5	C5-C10-H10B	109.5
H10A-C10-H10B	109.5	C5-C10-H10C	109.5
H10A-C10-H10C	109.5	H10B-C10-H10C	109.5
C12-C11-C15	106.4(4)	C12-C11-C16	125.7(4)
C15-C11-C16	127.6(4)	C12-C11-Zr1	72.3(3)
C15-C11-Zr1	73.8(2)	C16-C11-Zr1	124.6(3)
C13-C12-C11	108.7(4)	C13-C12-Zr1	73.3(2)
C11-C12-Zr1	74.8(3)	C13-C12-H12	125.3
C11-C12-H12	125.3	Zr1-C12-H12	125.3
C14-C13-C12	107.5(4)	C14-C13-Zr1	75.1(2)
C12-C13-Zr1	73.8(2)	C14-C13-H13	125.7
C12-C13-H13	125.7	Zr1-C13-H13	125.7
C15-C14-C13	108.8(4)	C15-C14-Zr1	74.3(2)
C13-C14-Zr1	72.4(2)	C15-C14-H14	125.4
C13-C14-H14	125.4	Zr1-C14-H14	125.4
C14-C15-C11	108.5(4)	C14-C15-Zr1	73.6(3)
C11-C15-Zr1	73.6(3)	C14-C15-H15	125.5
C11-C15-H15	125.5	Zr1-C15-H15	125.5
C11-C16-C17	112.0(4)	C11-C16-H16A	109.2
C17-C16-H16A	109.2	C11-C16-H16B	109.2
C17-C16-H16B	109.2	H16A-C16-H16B	107.9
C18-C17-C16	113.7(4)	C18-C17-H17A	108.8
C16-C17-H17A	108.8	C18-C17-H17B	108.8
C16-C17-H17B	108.8	H17A-C17-H17B	107.7

C17-C18-H18A	109.5	C17-C18-H18B	109.5
H18A-C18-H18B	109.5	C17-C18-H18C	109.5
H18A-C18-H18C	109.5	H18B-C18-H18C	109.5
N1-C19-H19A	109.5	N1-C19-H19B	109.5
H19A-C19-H19B	109.5	N1-C19-H19C	109.5
H19A-C19-H19C	109.5	H19B-C19-H19C	109.5
N1-C20-H20A	109.5	N1-C20-H20B	109.5
H20A-C20-H20B	109.5	N1-C20-H20C	109.5
H20A-C20-H20C	109.5	H20B-C20-H20C	109.5
N2-C21-H21A	109.5	N2-C21-H21B	109.5
H21A-C21-H21B	109.5	N2-C21-H21C	109.5
H21A-C21-H21C	109.5	H21B-C21-H21C	109.5
N2-C22-H22A	109.5	N2-C22-H22B	109.5
H22A-C22-H22B	109.5	N2-C22-H22C	109.5
H22A-C22-H22C	109.5	H22B-C22-H22C	109.5
C19-N1-C20	106.2(3)	C19-N1-Zr1	136.1(3)
C20-N1-Zr1	117.6(3)	C22-N2-C21	108.4(4)
C22-N2-Zr1	119.5(3)	C21-N2-Zr1	114.4(3)
C22-N2-H1	100.(3)	C21-N2-H1	98.(3)
Zr1-N2-H1	113.(3)	C29-B1-C35	114.1(3)
C29-B1-C23	112.1(3)	C35-B1-C23	101.8(3)
C29-B1-C41	102.2(3)	C35-B1-C41	114.1(3)
C23-B1-C41	113.1(3)	C24-C23-C28	112.8(4)
C24-C23-B1	126.5(4)	C28-C23-B1	120.5(4)
F1-C24-C25	114.2(4)	F1-C24-C23	121.3(4)
C25-C24-C23	124.5(4)	F2-C25-C26	120.5(4)
F2-C25-C24	120.2(4)	C26-C25-C24	119.3(4)
F3-C26-C25	120.8(4)	F3-C26-C27	119.9(4)
C25-C26-C27	119.3(4)	F4-C27-C28	120.5(4)
F4-C27-C26	120.1(4)	C28-C27-C26	119.3(4)
F5-C28-C27	116.4(4)	F5-C28-C23	118.8(4)
C27-C28-C23	124.8(4)	C34-C29-C30	112.3(4)
C34-C29-B1	120.6(4)	C30-C29-B1	126.9(4)

F6-C30-C29	121.3(4)	F6-C30-C31	114.1(4)
C29-C30-C31	124.6(4)	F7-C31-C32	119.9(4)
F7-C31-C30	120.5(4)	C32-C31-C30	119.6(4)
F8-C32-C31	120.3(4)	F8-C32-C33	120.6(4)
C31-C32-C33	119.1(4)	F9-C33-C32	120.4(4)
F9-C33-C34	120.9(4)	C32-C33-C34	118.7(4)
F10-C34-C29	119.3(4)	F10-C34-C33	115.0(4)
C29-C34-C33	125.7(4)	C36-C35-C40	112.5(4)
C36-C35-B1	127.0(4)	C40-C35-B1	120.3(4)
F11-C36-C37	114.7(4)	F11-C36-C35	120.7(4)
C37-C36-C35	124.5(4)	F12-C37-C38	120.1(4)
F12-C37-C36	120.2(4)	C38-C37-C36	119.6(4)
F13-C38-C37	120.0(4)	F13-C38-C39	121.4(4)
C37-C38-C39	118.6(4)	F14-C39-C40	120.5(4)
F14-C39-C38	119.6(4)	C40-C39-C38	119.9(4)
F15-C40-C39	116.0(4)	F15-C40-C35	119.4(4)
C39-C40-C35	124.7(4)	C46-C41-C42	112.6(4)
C46-C41-B1	120.0(4)	C42-C41-B1	127.3(4)
F16-C42-C43	115.4(4)	F16-C42-C41	120.5(4)
C43-C42-C41	124.1(4)	F17-C43-C44	119.6(4)
F17-C43-C42	120.3(4)	C44-C43-C42	120.1(4)
F18-C44-C43	120.5(4)	F18-C44-C45	120.9(4)
C43-C44-C45	118.5(4)	F19-C45-C44	119.6(4)
F19-C45-C46	120.9(4)	C44-C45-C46	119.6(4)
F20-C46-C45	116.0(4)	F20-C46-C41	119.0(4)
C45-C46-C41	124.9(4)		

C.3. Additional Figures

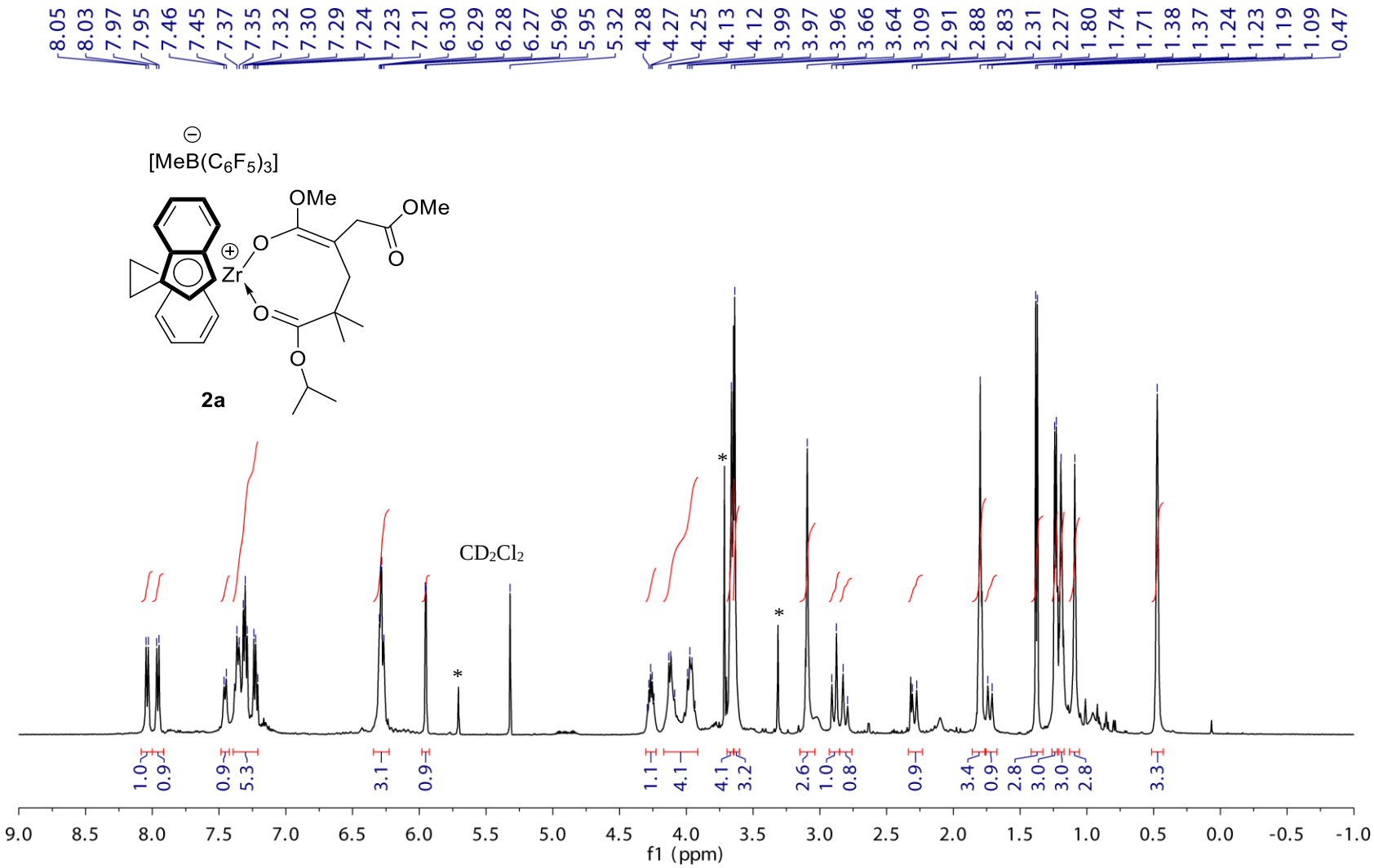

Figure S4.1. ^{1}H NMR spectrum (CD_2Cl_2, −18 °C, 500 MHz) of *rac*-(EBI)Zr[OC(OMe)=C(CH_2COOMe)CH_2C(Me_2)C(O^{i}Pr)=O]$^{+}$ [$MeB(C_6F_5)_3$]$^{-}$ (**2a**). (* = excess dimethyl itaconate for comparison)

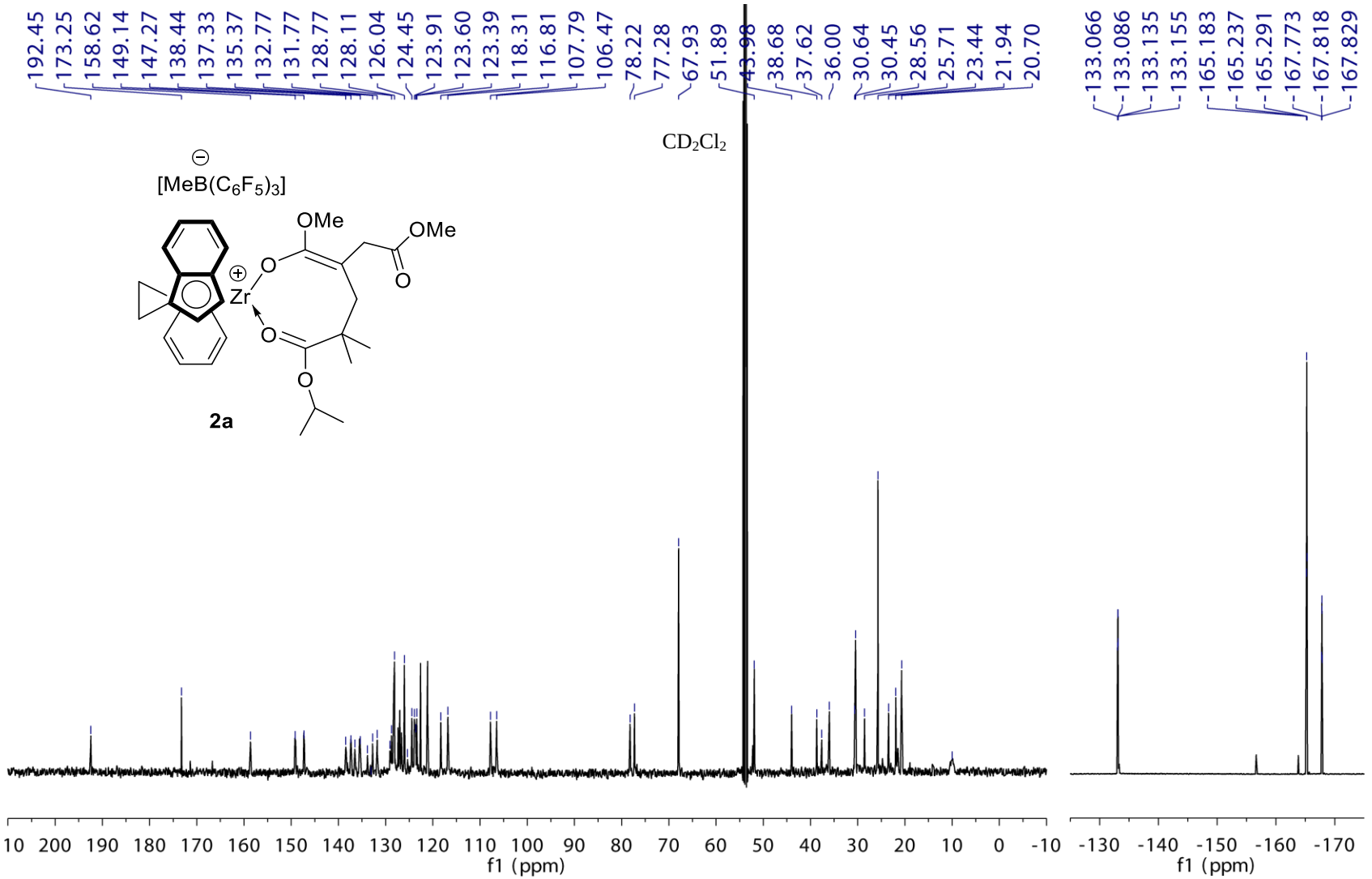

Figure S4.2. ^{13}C (left) and ^{19}F (right) NMR spectra (CD_2Cl_2, −18 °C, 500 MHz) of *rac*-(EBI)Zr[OC(OMe)= C(CH_2COOMe)$CH_2C(Me_2)C(O^iPr)$=O]$^+$ $[MeB(C_6F_5)_3]^-$ (**2a**). Minor peaks due to excess $(C_6F_5)_3B{\cdot}THF$ used in the NMR scale reaction were also present in ^{19}F NMR.

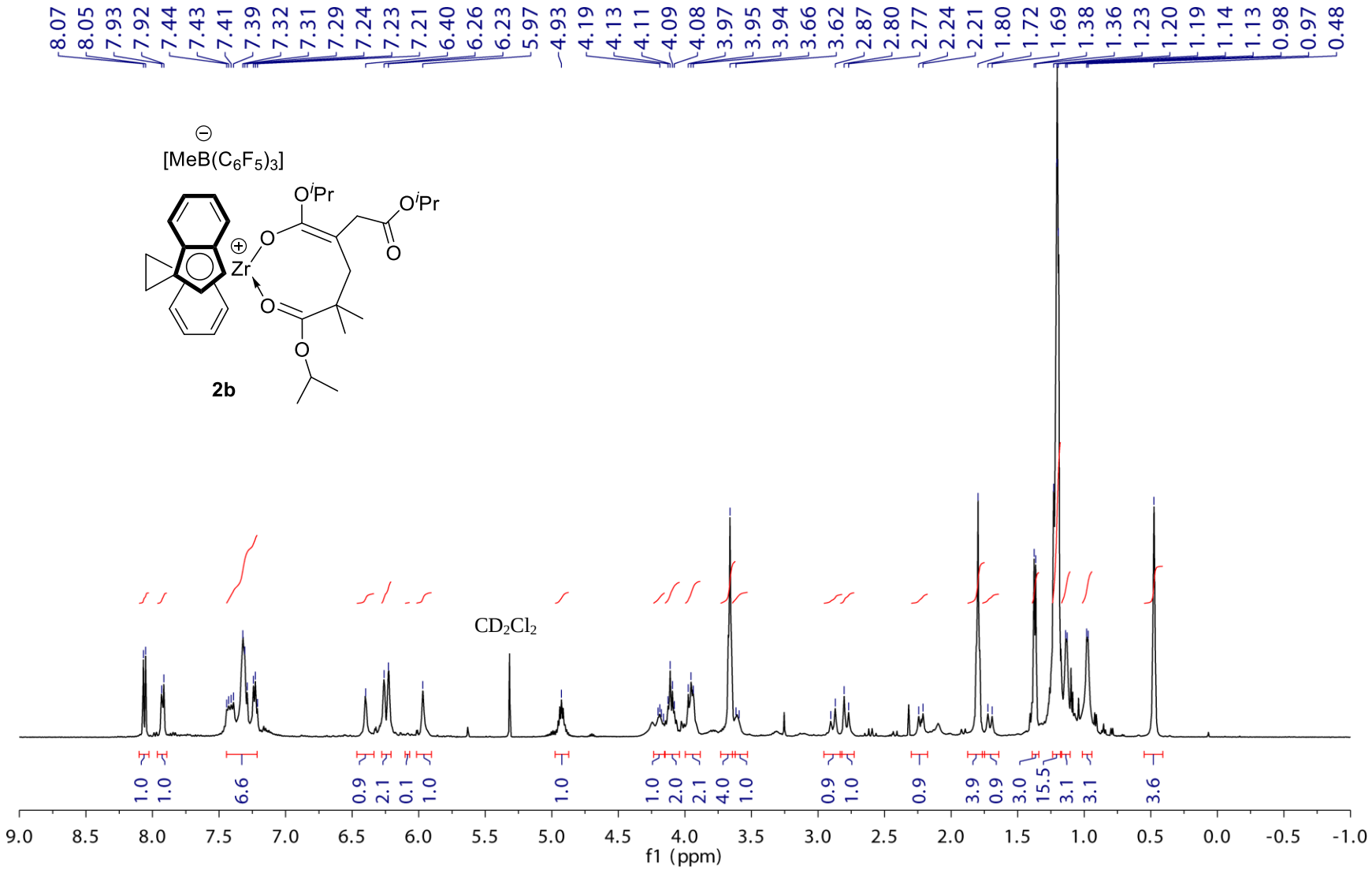

Figure S4.3. ^{1}H NMR spectrum (CD_2Cl_2, −18 °C, 500 MHz) of *rac*-(EBI)Zr[OC(O^{i}Pr)=C(CH_2COO^{i}Pr)CH_2C(Me_2)C(O^{i}Pr)=O]$^{+}$ [$MeB(C_6F_5)_3$]$^{-}$ (**2b**).

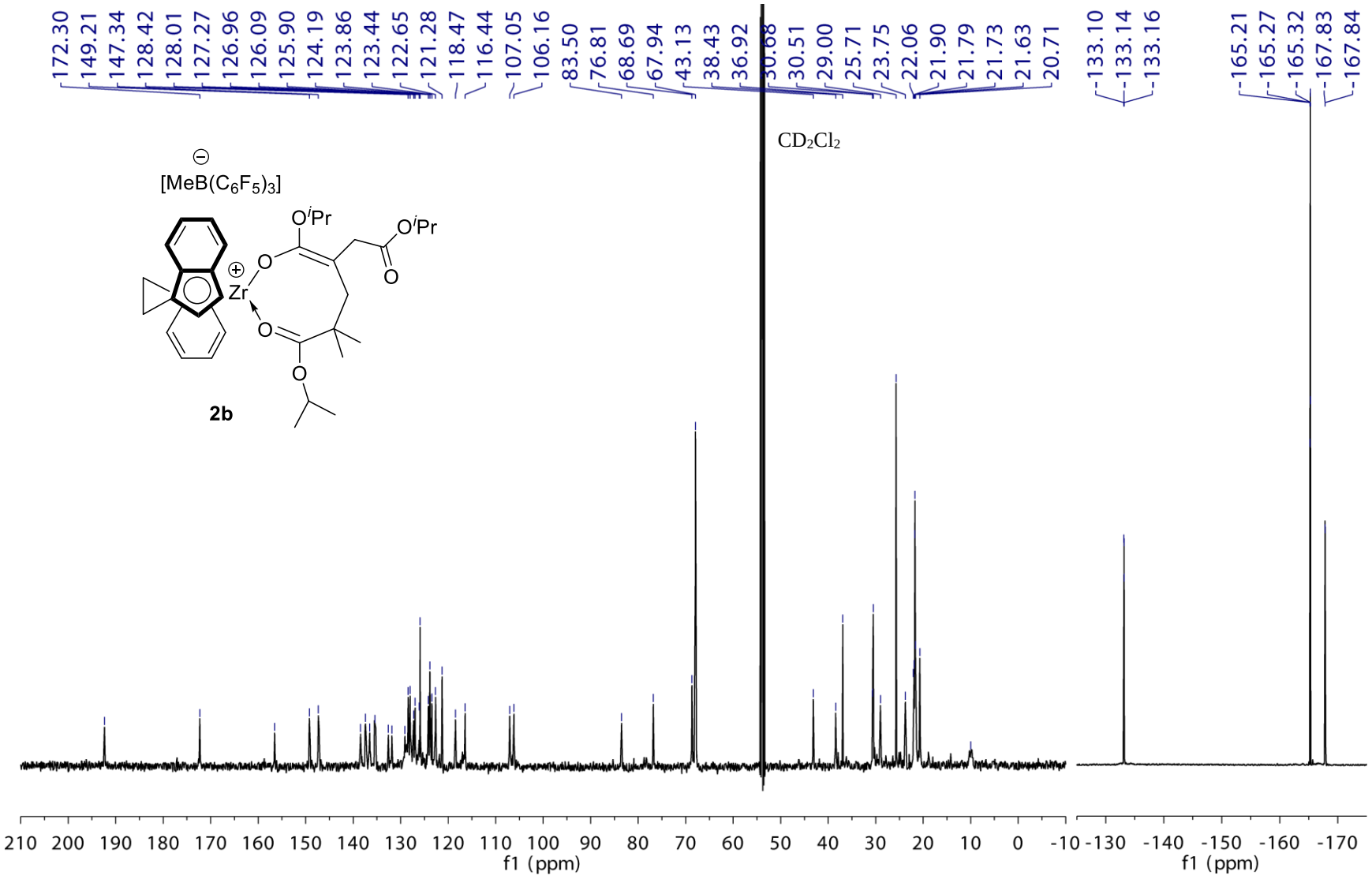

Figure S4.4. ^{13}C (left) and ^{19}F (right) NMR spectra (CD_2Cl_2, −18 °C, 500 MHz) of *rac*-(EBI)Zr[OC(O^{i}Pr)= C(CH_2COO^{i}Pr)CH_2C(Me_2)C(O^{i}Pr)=O]$^+$ [$MeB(C_6F_5)_3$]$^-$ (**2b**).

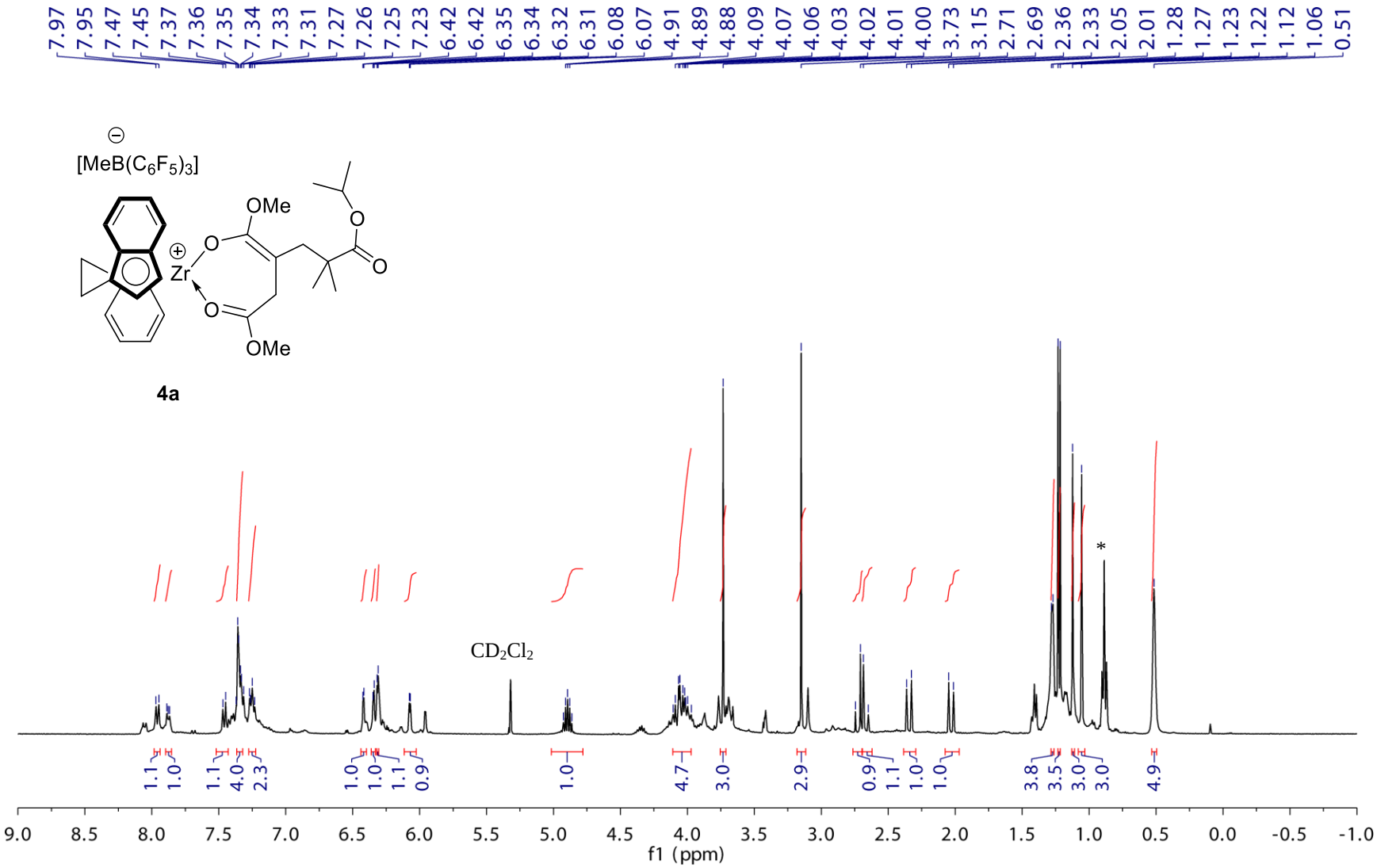

Figure S4.5. ^{1}H NMR spectrum (CD_2Cl_2, 25 °C, 400 MHz) of *rac*-(EBI)Zr[OC(OMe)=C($CH_2CMe_2COO^iPr$)CH_2C(OMe)=O]$^+$ $[MeB(C_6F_5)_3]^-$ (**4a**). (* = hexanes)

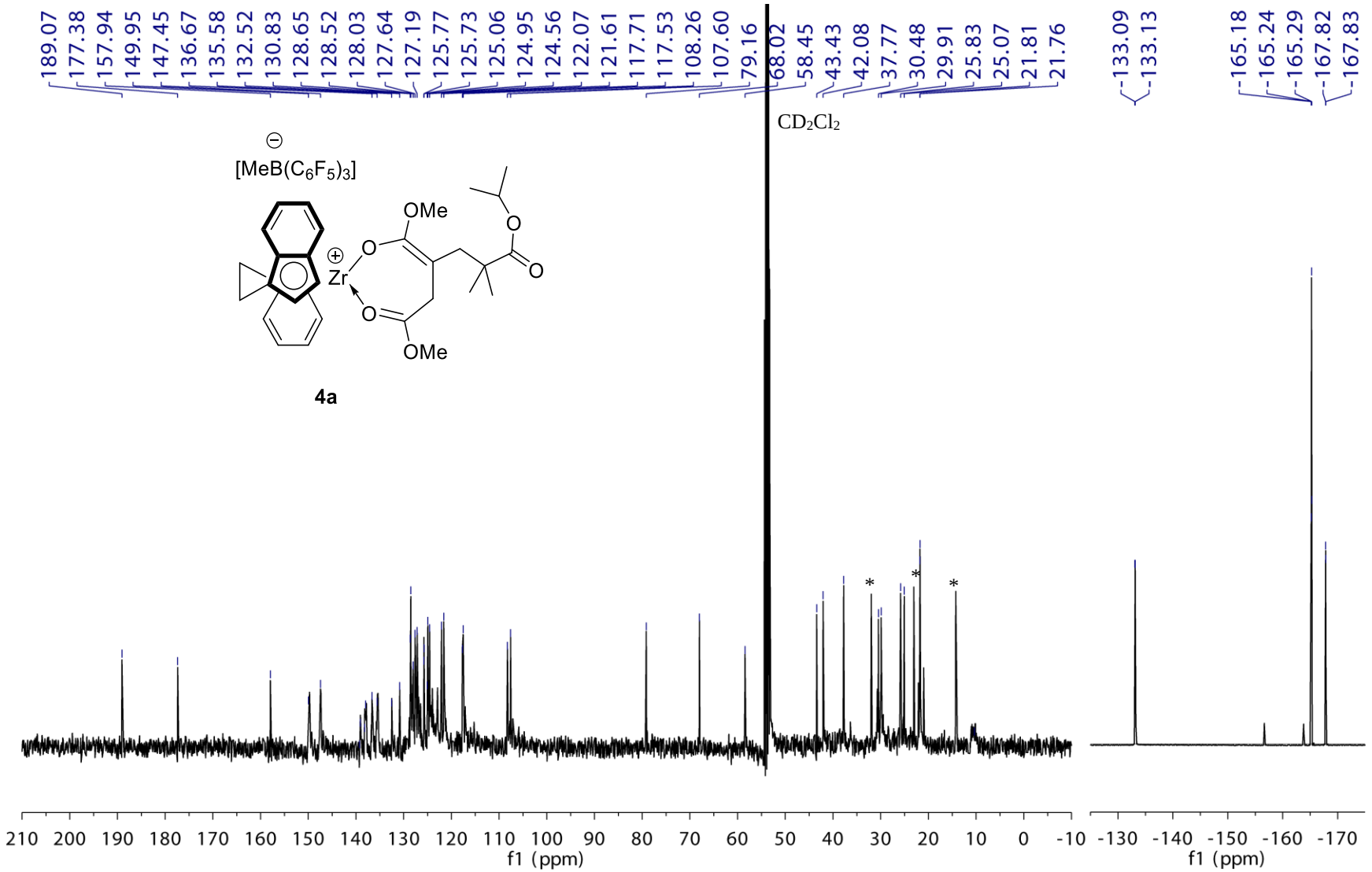

Figure S4.6. ^{13}C (left) and ^{19}F (right) NMR spectra (CD_2Cl_2, 25 °C, 400 MHz) of *rac*-(EBI)Zr[OC(OMe)= C($CH_2CMe_2COO^iPr$)CH_2C(OMe)=O]$^+$ $[MeB(C_6F_5)_3]^-$ (**4a**). * = hexanes; minor peaks due to excess $(C_6F_5)_3B{\cdot}THF$ used in the NMR scale reaction were also present in ^{19}F NMR.

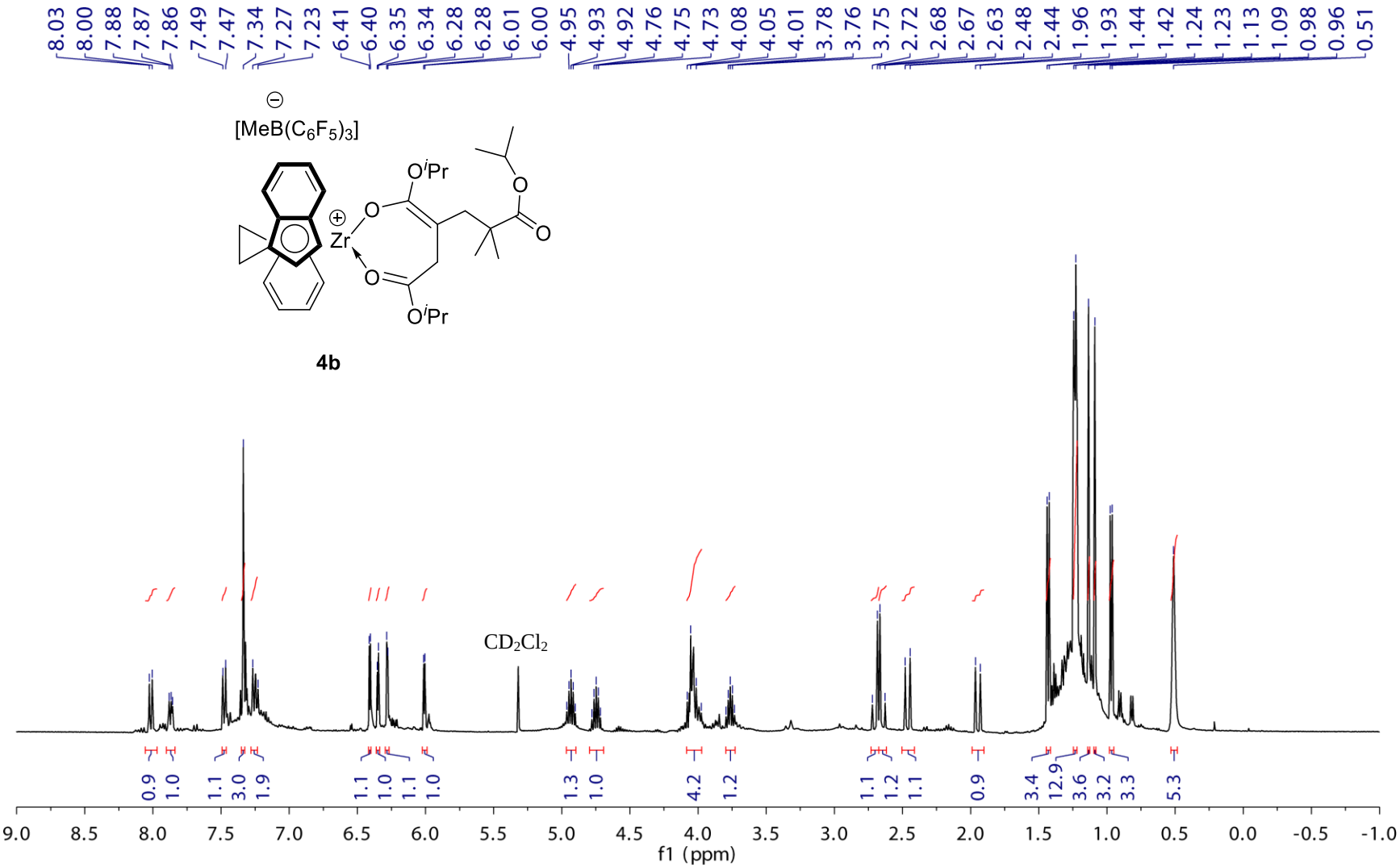

Figure S4.7. ^{1}H NMR spectrum (CD_2Cl_2, 25 °C, 400 MHz) of *rac*-(EBI)Zr[OC(O^{i}Pr)=C($CH_2CMe_2COO^{i}Pr$)CH_2C(O^{i}Pr)=O]$^{+}$ [$MeB(C_6F_5)_3$]$^{-}$ (**4b**).

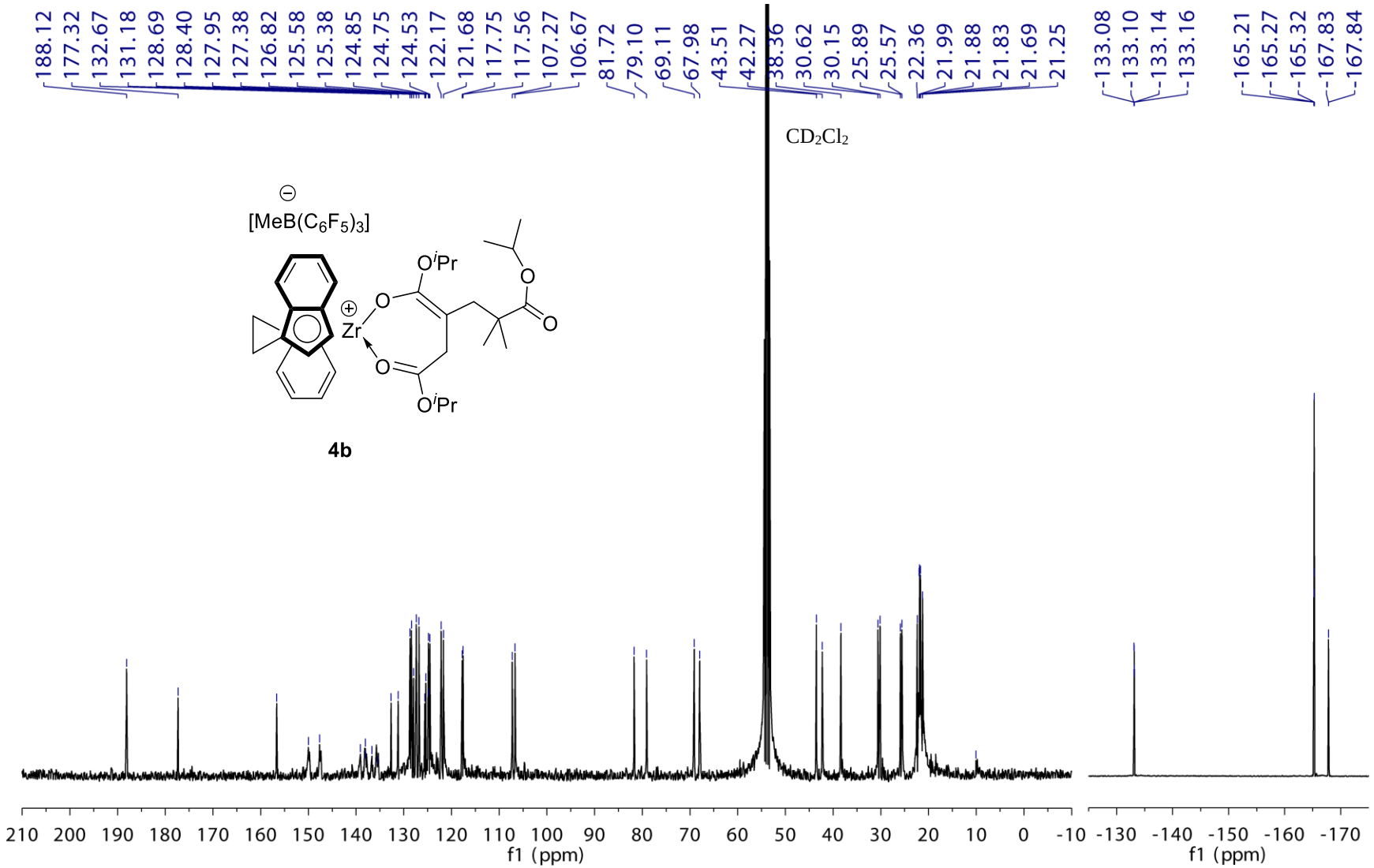

Figure S4.8. ^{13}C (left) and ^{19}F (right) NMR spectra (CD_2Cl_2, 25 °C, 400 MHz) of *rac*-(EBI)Zr[OC(O^{i}Pr)= C($CH_2CMe_2COO^iPr$)CH_2C(O^{i}Pr)=O]$^+$ $[MeB(C_6F_5)_3]^-$ (**4b**).

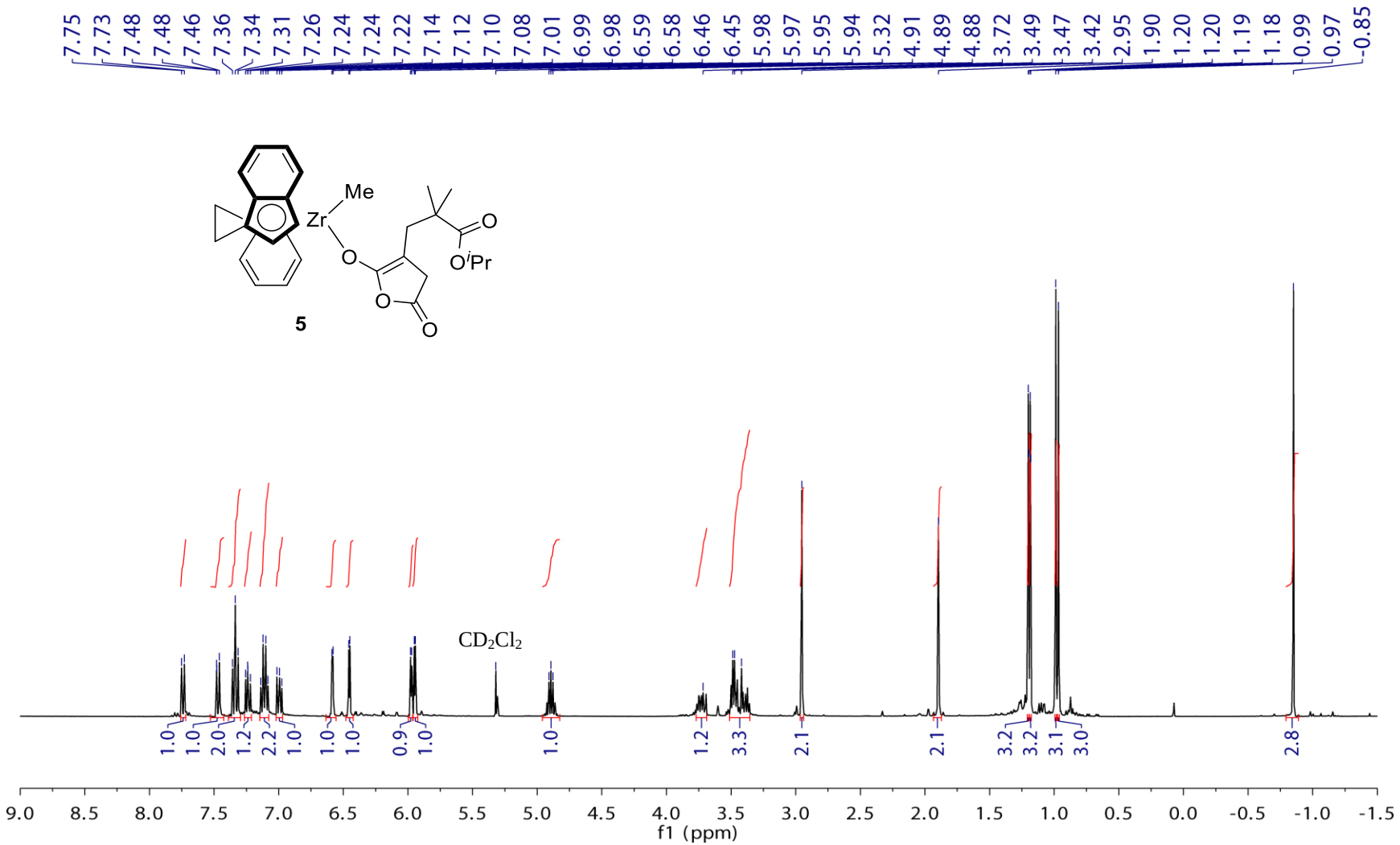

Figure S4.9. ^{1}H NMR spectrum (CD_2Cl_2, 25 °C, 400 MHz) of *rac*-(EBI)ZrMe{OC[OC(O)CH_2]=C($CH_2CMe_2COO^iPr$)} (**5**).

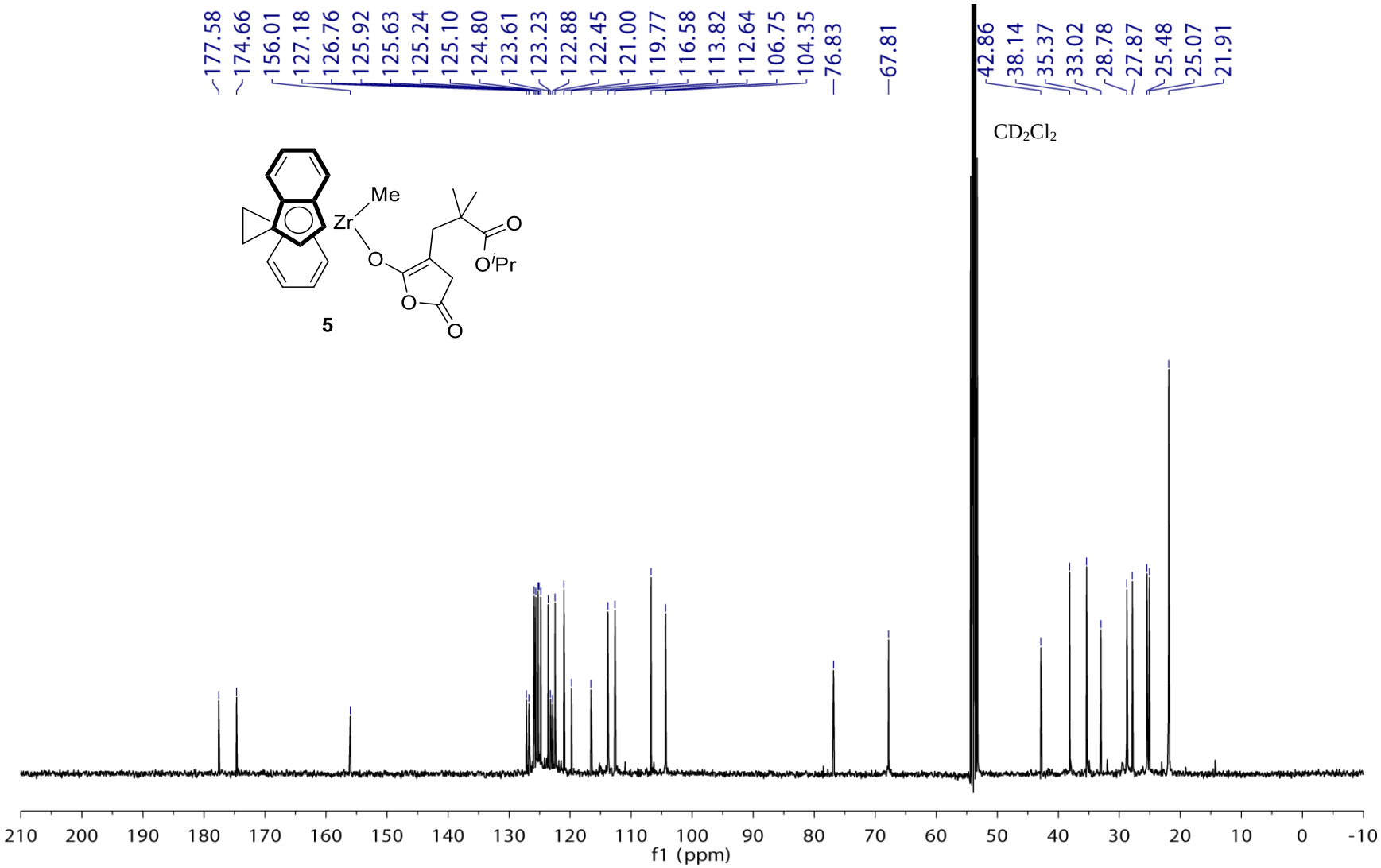

Figure S4.10. ^{13}C NMR spectrum (CD_2Cl_2, 25 °C, 400 MHz) of *rac*-(EBI)ZrMe{OC[OC(O)CH_2]=C($CH_2CMe_2COO^iPr$)} (**5**).

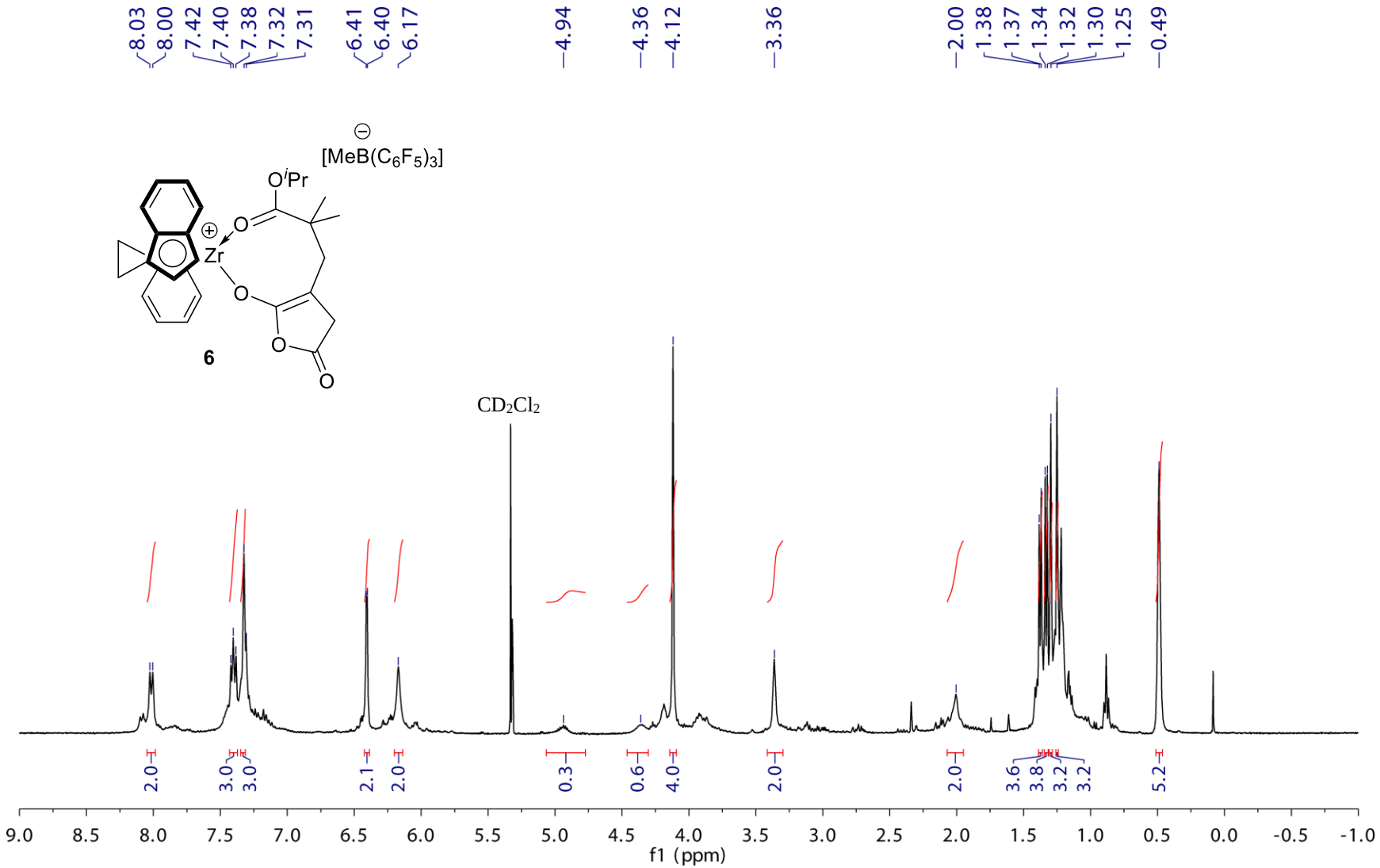

Figure S4.11. ^{1}H NMR spectrum (CD_2Cl_2, 25 °C, 400 MHz) of *rac*-(EBI)ZrMe{OC[OC(O)CH_2]=C[$CH_2CMe_2C(O^iPr)$=O]}$^+$ $[MeB(C_6F_5)_3]^-$ (**6**).

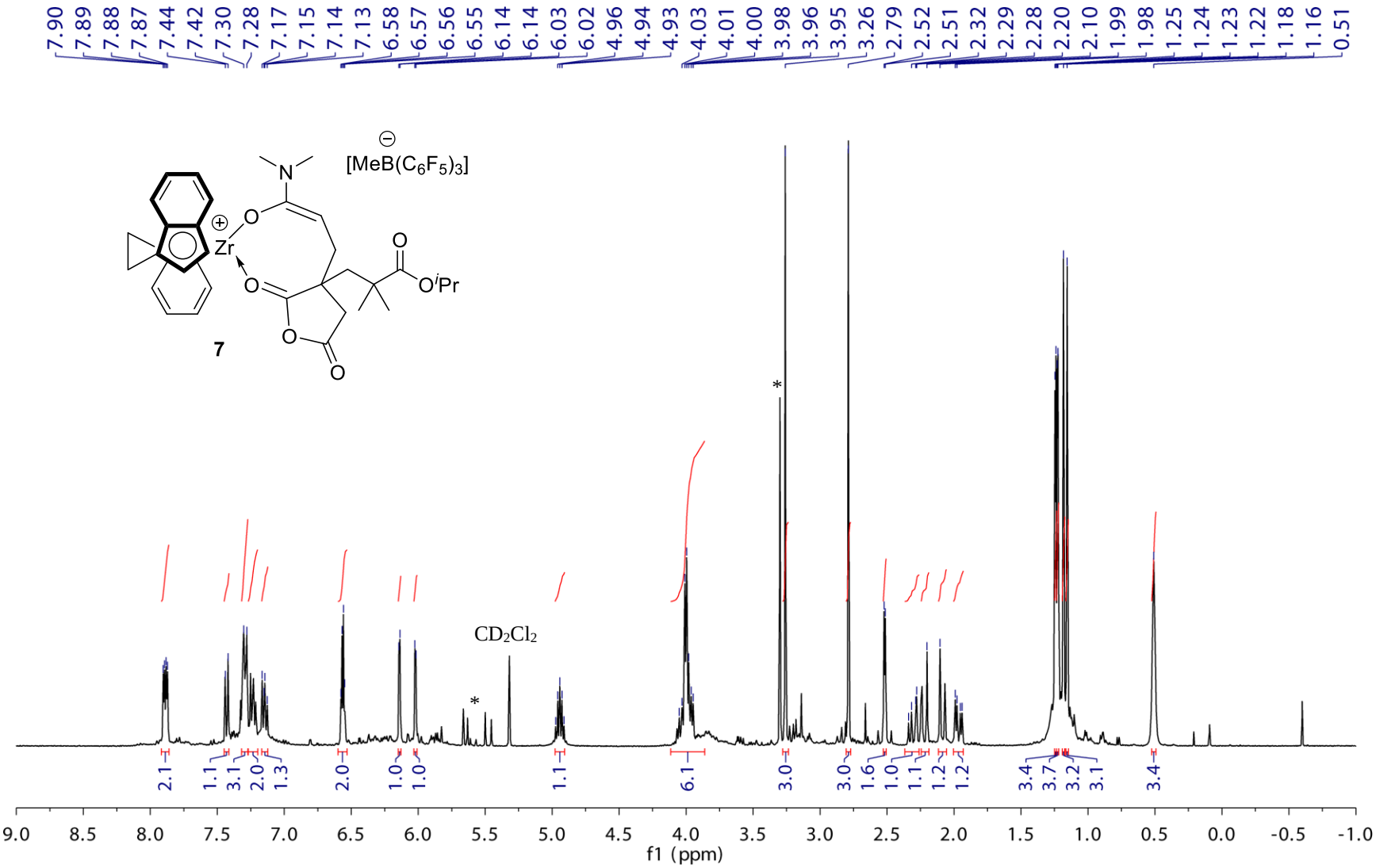

Figure S4.12. ^{1}H NMR spectrum (CD_2Cl_2, 25 °C, 400 MHz) of *rac*-(EBI)Zr{OC(NMe$_2$)=CCH$_2$C(CH$_2$CMe$_2$COO^{i}Pr)C[OC(O)]=O}$^+$ [MeB(C$_6$F$_5$)$_3$]$^-$ (**7**). (* = excess (C$_6$F$_5$)$_3$B·DMAA)

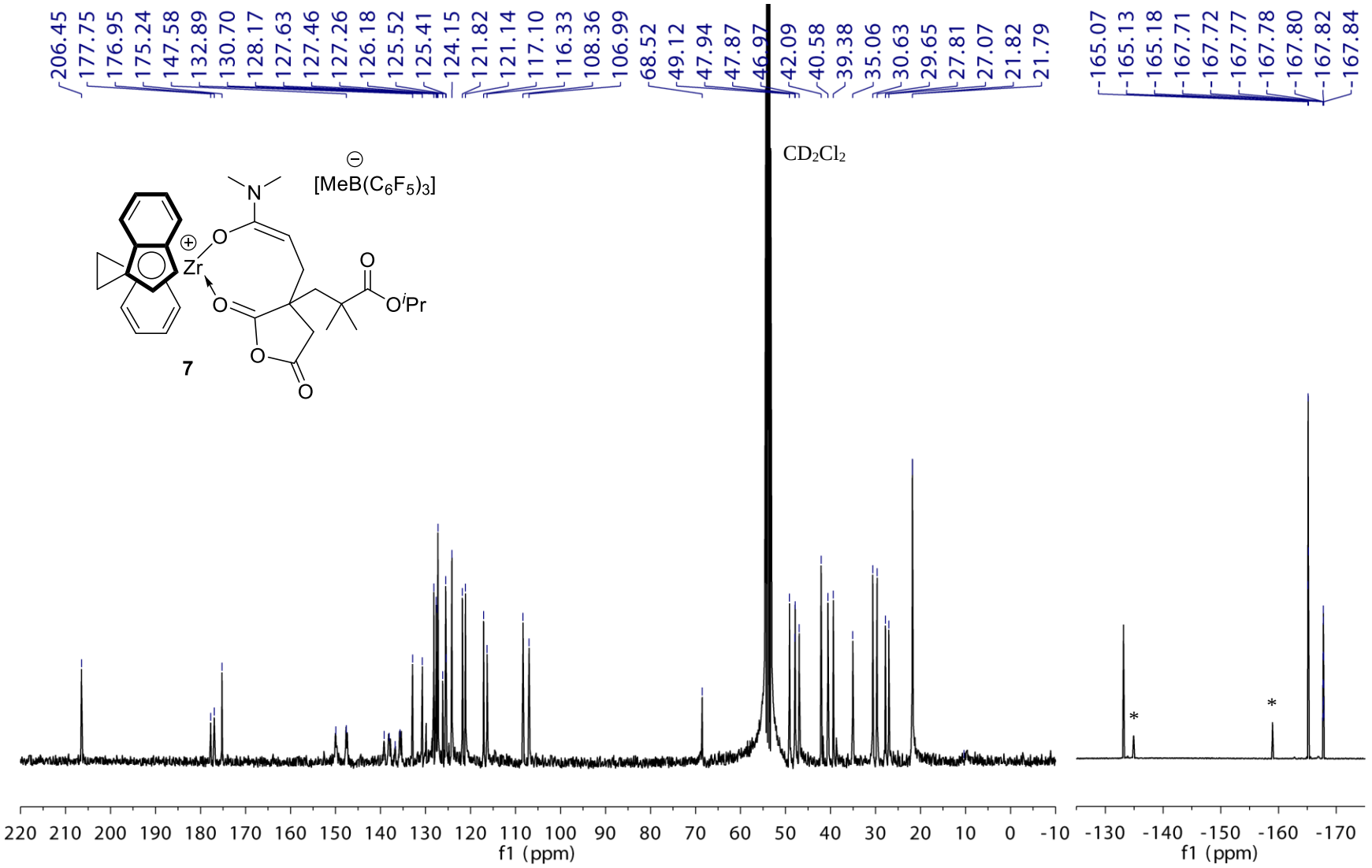

Figure S4.13. ^{13}C (left) and ^{19}F (right) NMR spectra (CD_2Cl_2, 25 °C, 400 MHz) of *rac*-(EBI)Zr{OC(NMe_2)=CCH_2C($CH_2CMe_2COO^iPr$)C[OC(O)]=O]}$^+$ $[MeB(C_6F_5)_3]^-$ (**7**). (* = excess $(C_6F_5)_3B$·DMAA)

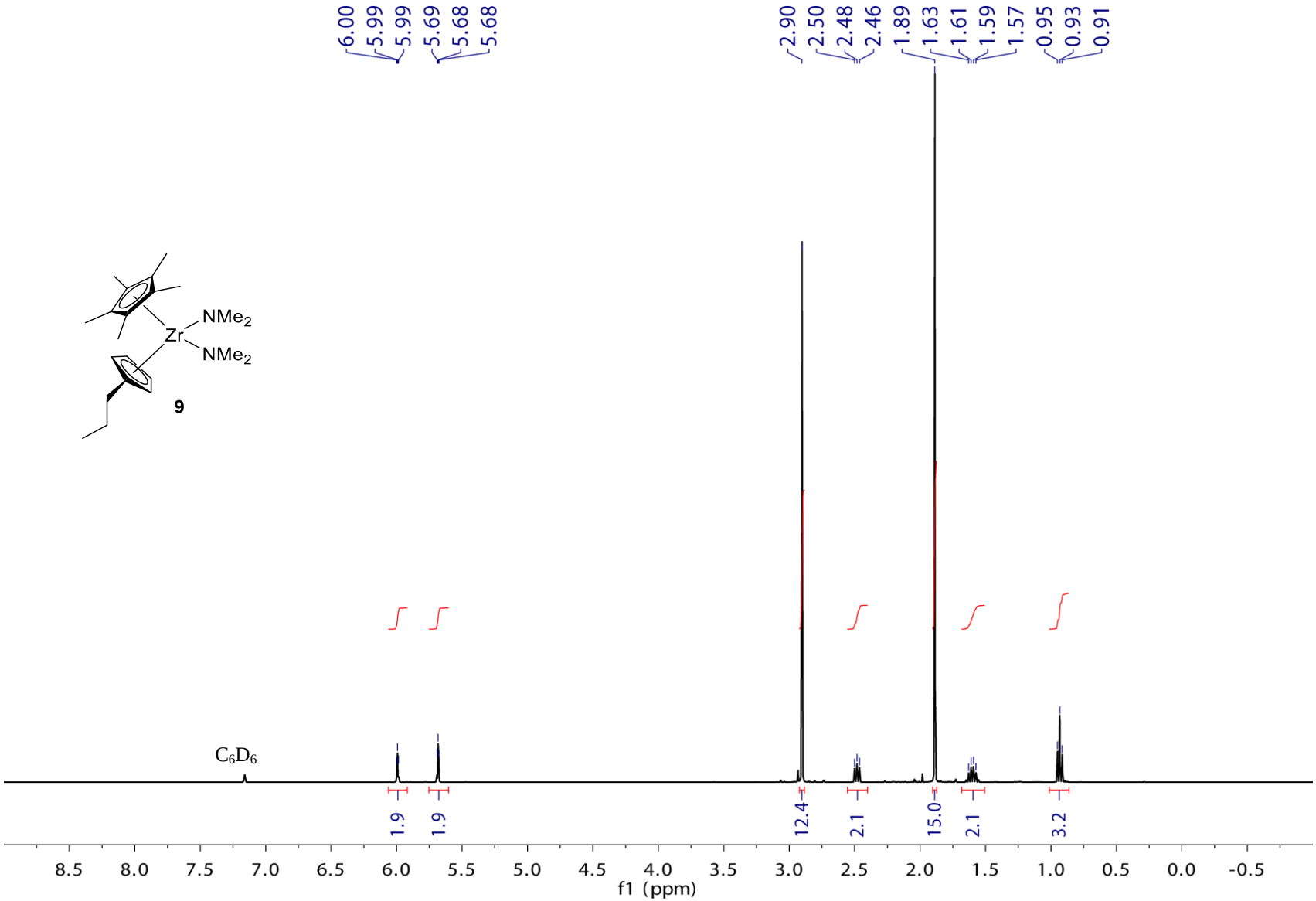

Figure S4.14. ^{1}H NMR spectrum (C_6D_6, 400 MHz, 25 °C) of Cp*(^{n}PrCp)Zr(NMe_2)$_2$ (**9**).

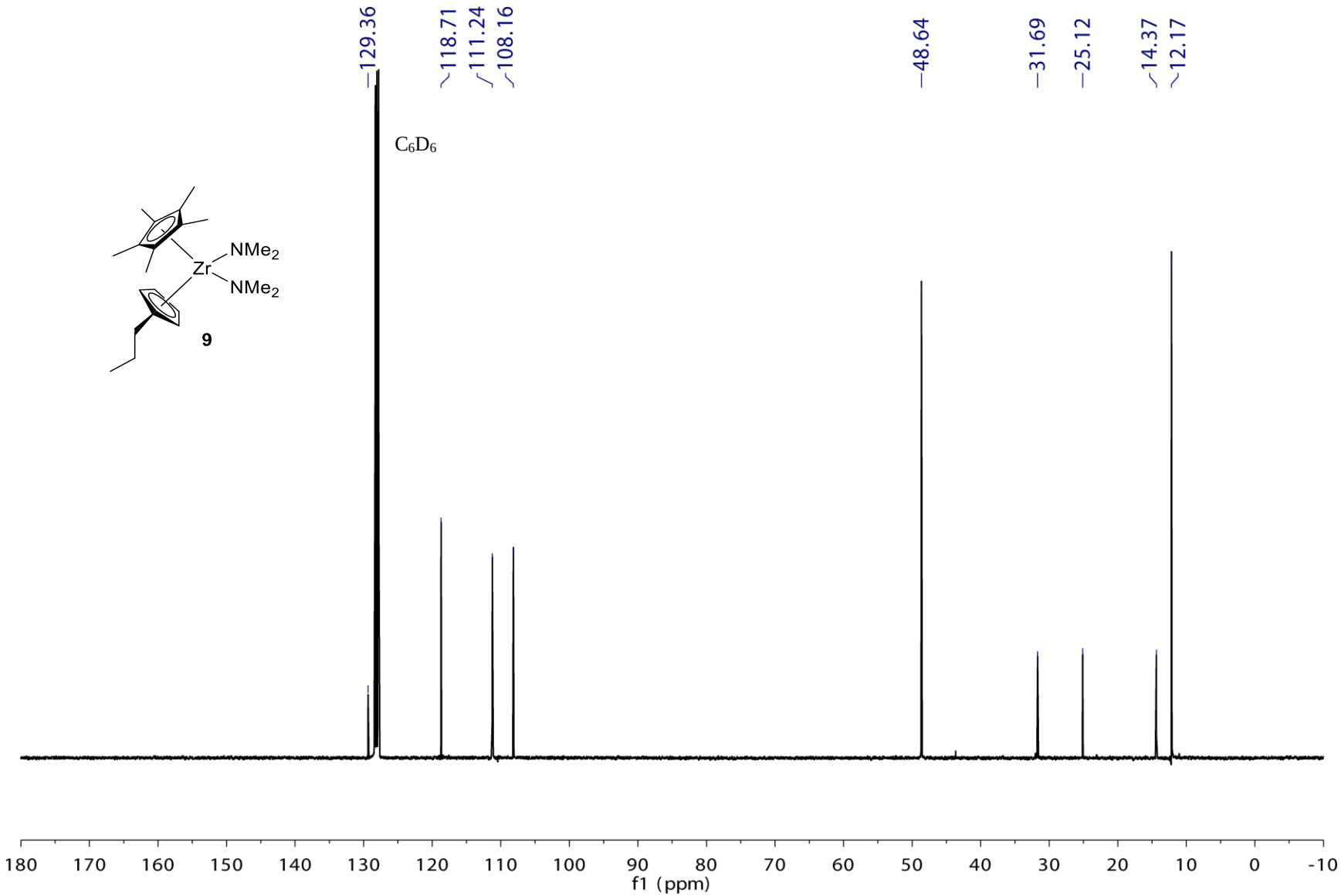

Figure S4.15. ^{13}C NMR spectrum (C_6D_6, 400 MHz, 25 °C) of Cp*(^{n}PrCp)Zr(NMe_2)$_2$ (**9**).

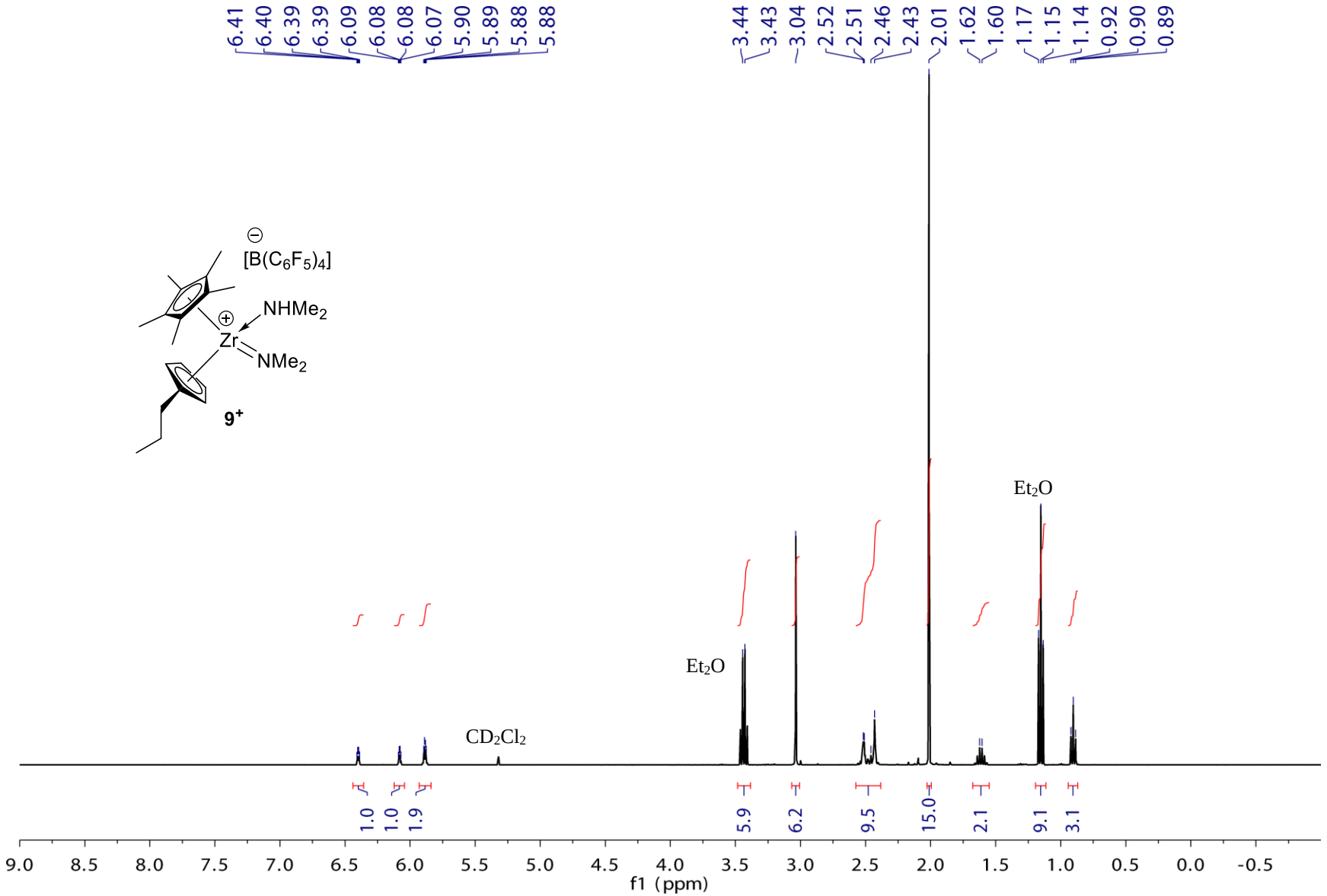

Figure S4.16. ^{1}H NMR spectrum (CD_2Cl_2, 25 °C, 400 MHz) of $[Cp^*(^{n}PrCp)Zr(HNMe_2)=NMe_2]^+ [B(C_6F_5)_4]^-$ (**9**$^+$).

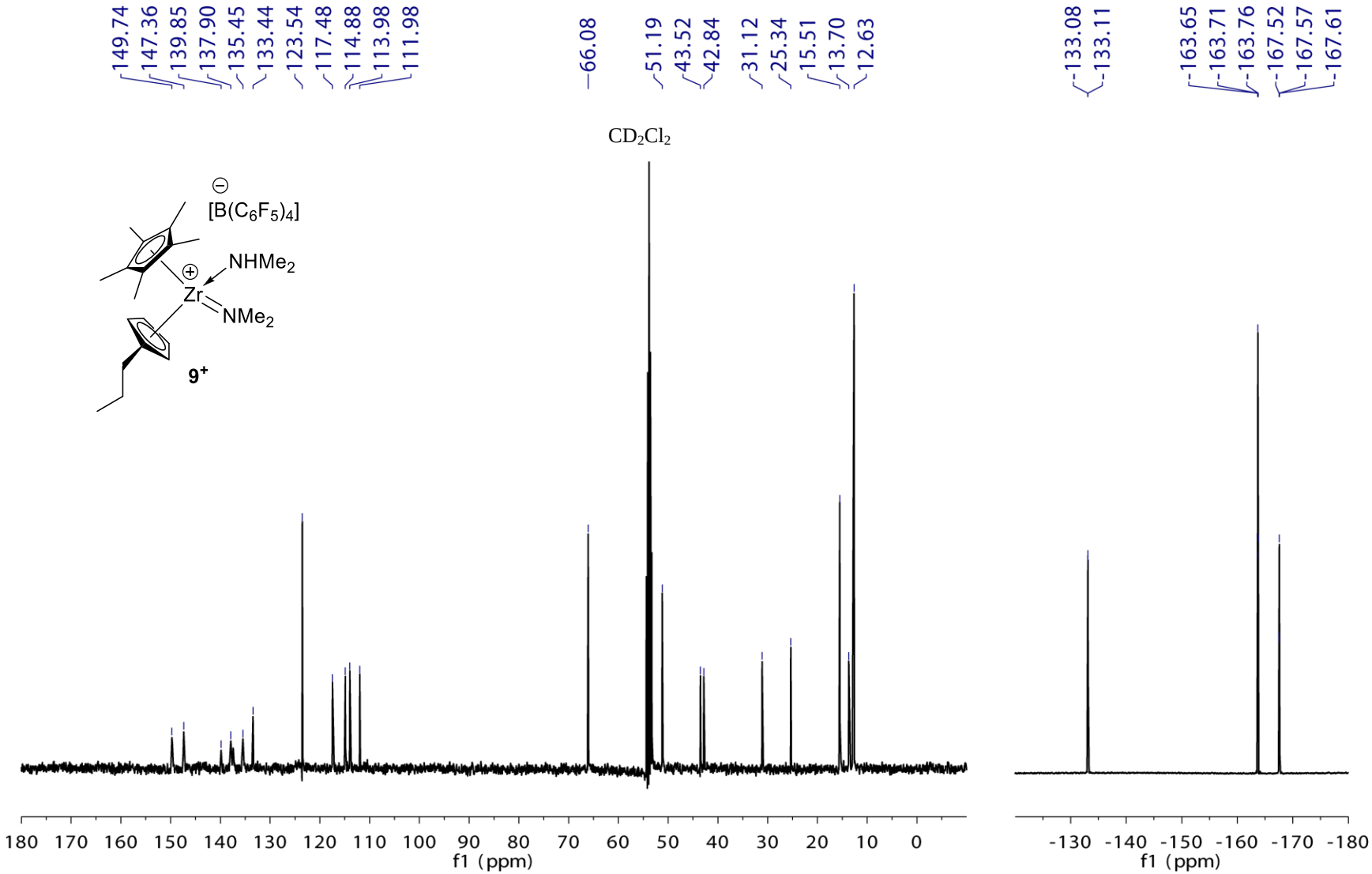

Figure S4.17. ^{13}C (left) and ^{19}F (right) NMR spectra (CD_2Cl_2, 25 °C, 400 MHz) of $[Cp^*(^nPrCp)Zr(HNMe_2)=NMe_2]^+ [B(C_6F_5)_4]^-$ (**9**$^+$).

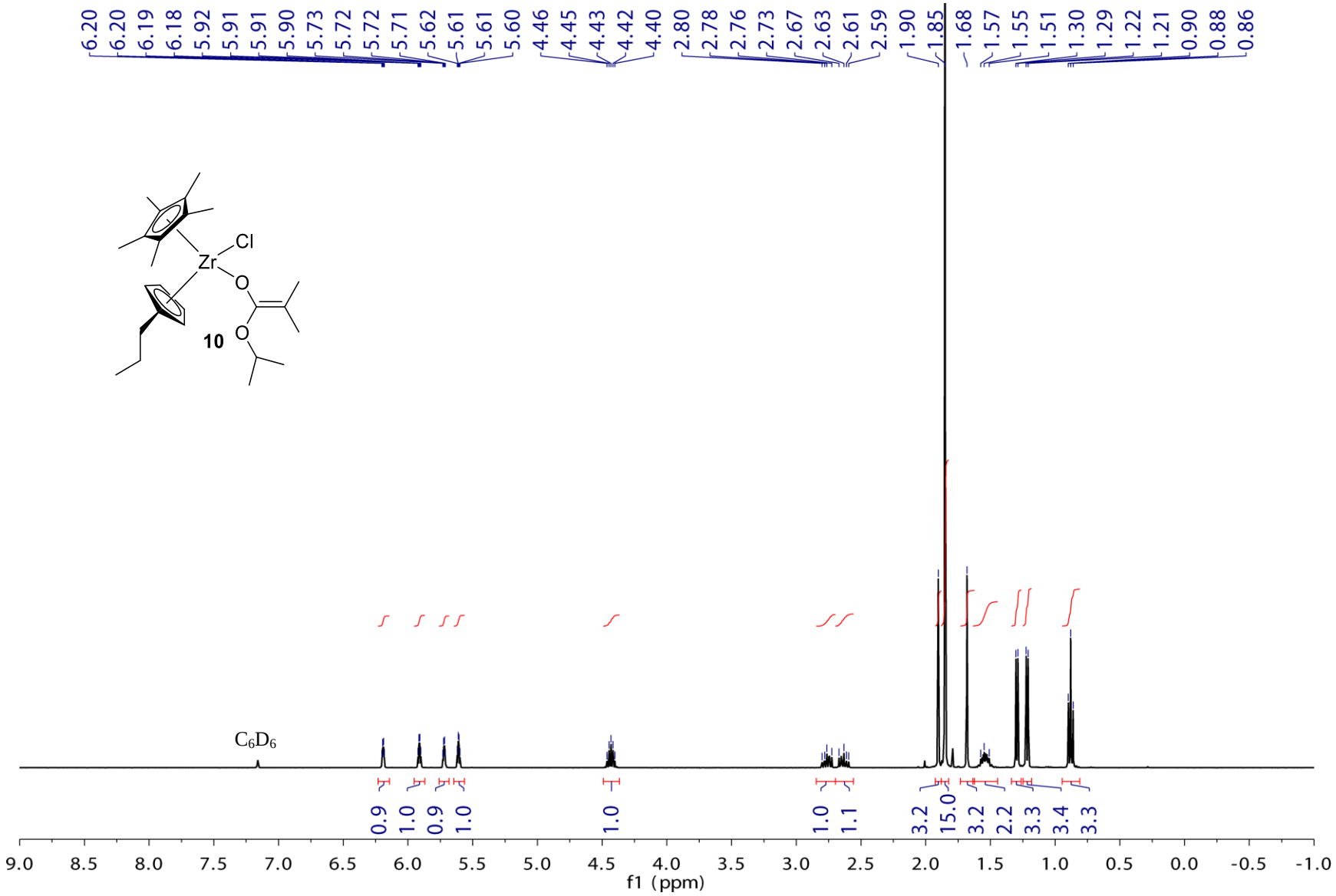

Figure S4.18. ^{1}H NMR spectrum (C_6D_6, 25 °C, 400 MHz) of Cp*(^{n}PrCp)ZrCl[OC(O^{i}Pr)=CMe$_2$] (**10**).

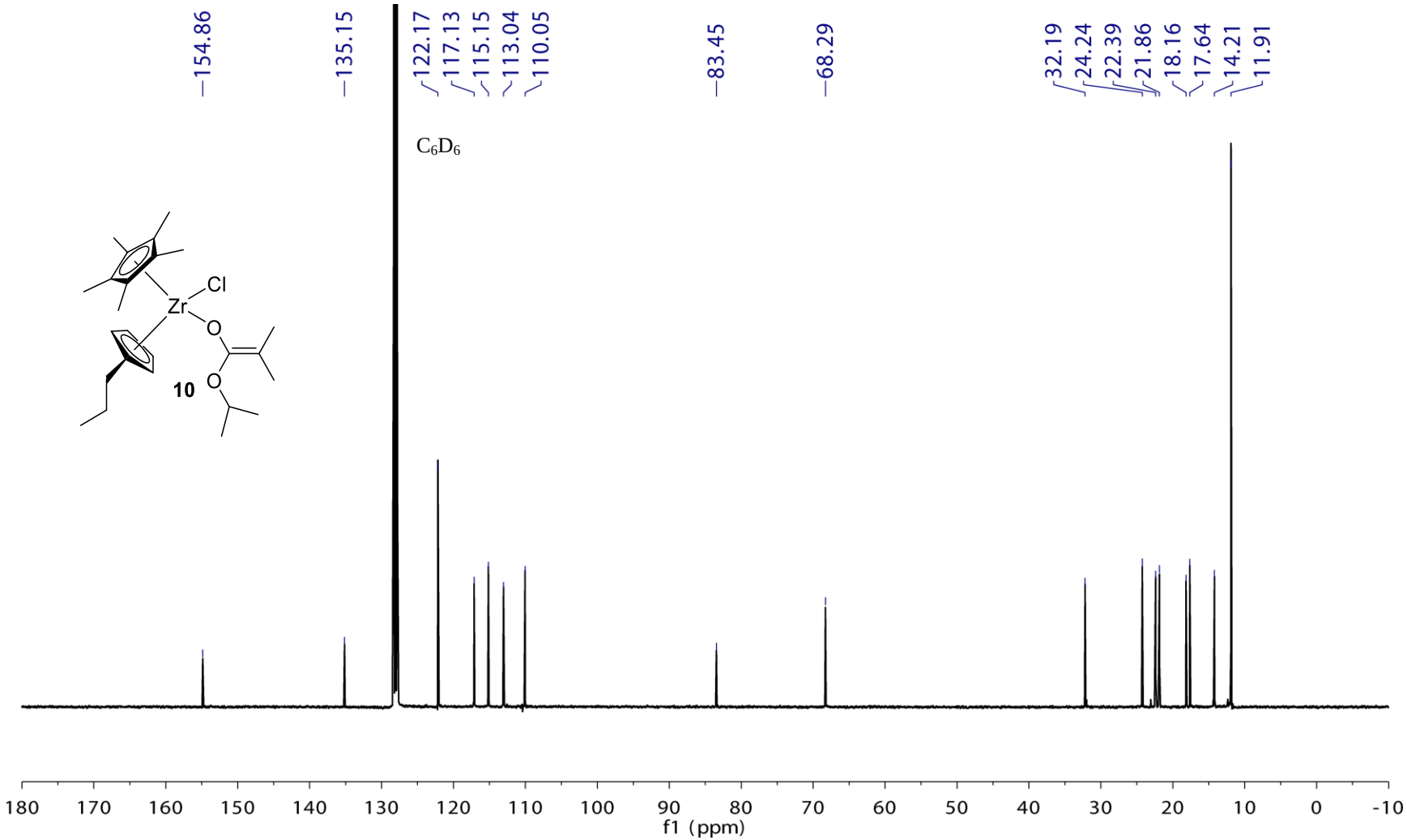

Figure S4.19. ^{13}C NMR spectrum (C_6D_6, 25 °C, 400 MHz) of Cp* (^{n}PrCp)ZrCl[OC(O^{i}Pr)=CMe$_2$] (**10**).

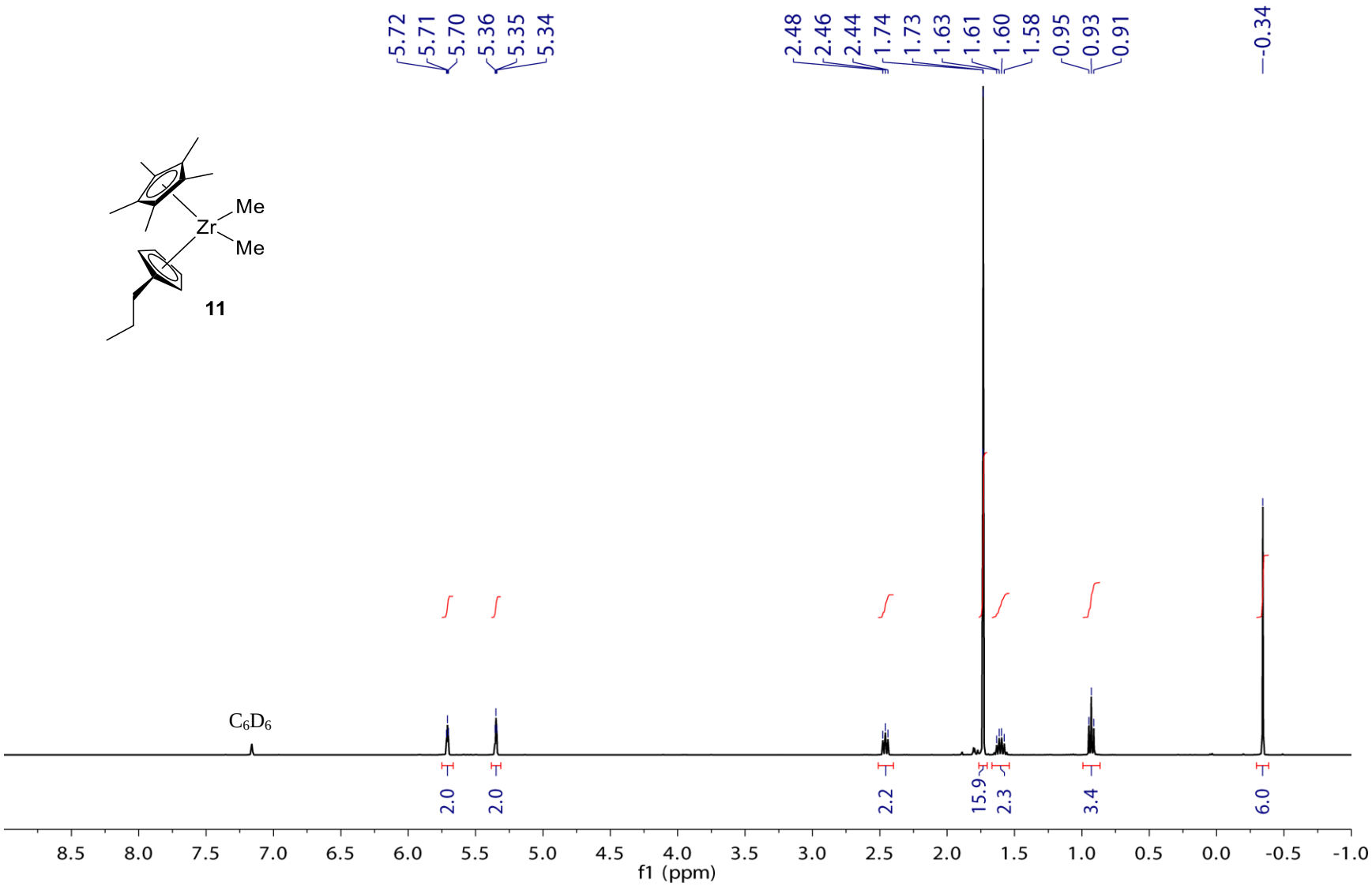

Figure S4.20. ^{1}H NMR spectrum (C_6D_6, 25 °C, 400 MHz) of Cp*(^{n}PrCp)ZrMe$_2$ (**11**).

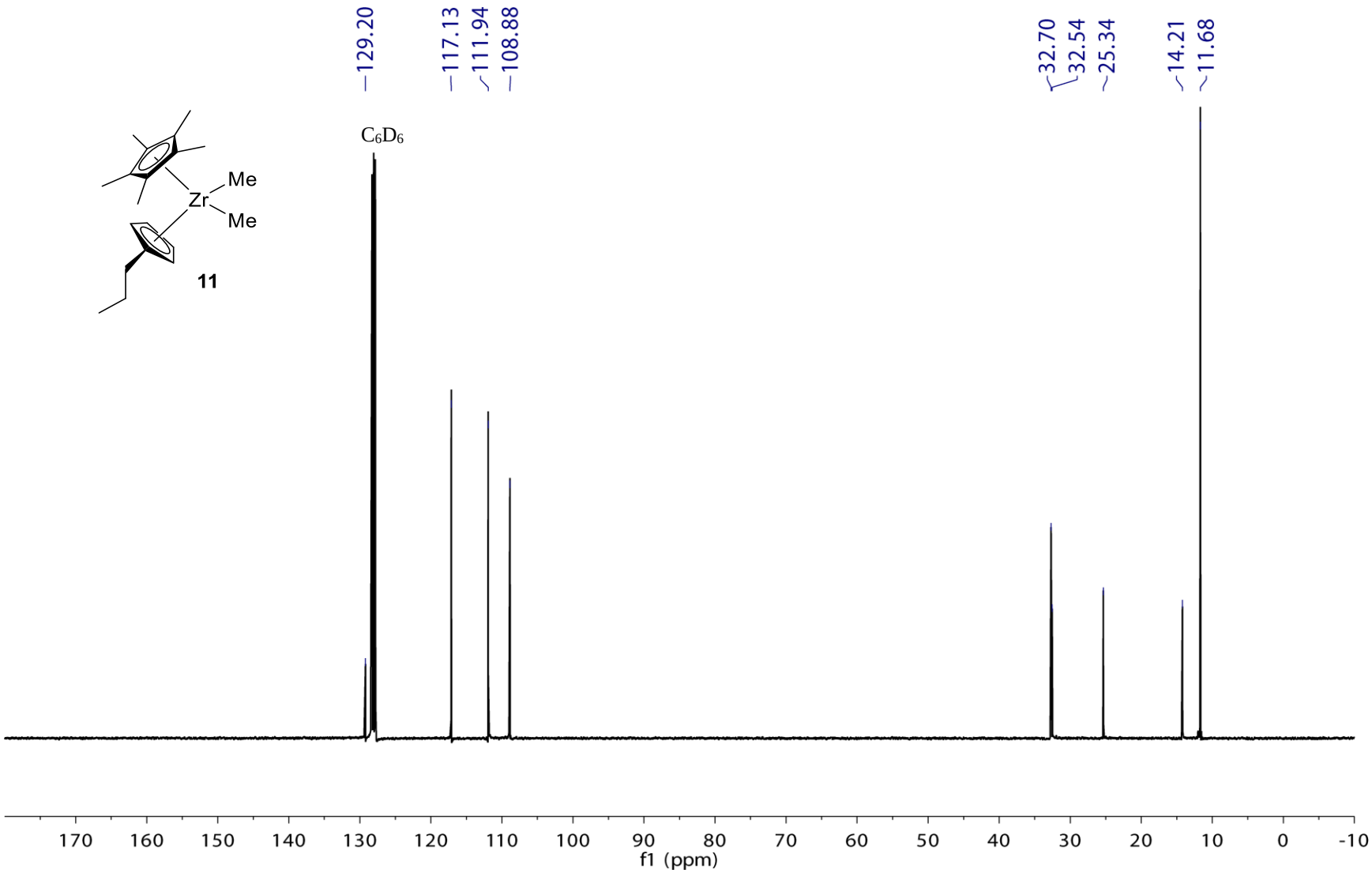

Figure S4.21. ^{13}C NMR spectrum (C_6D_6, 25 °C, 400 MHz) of Cp*(^{n}PrCp)$ZrMe_2$ (**11**).

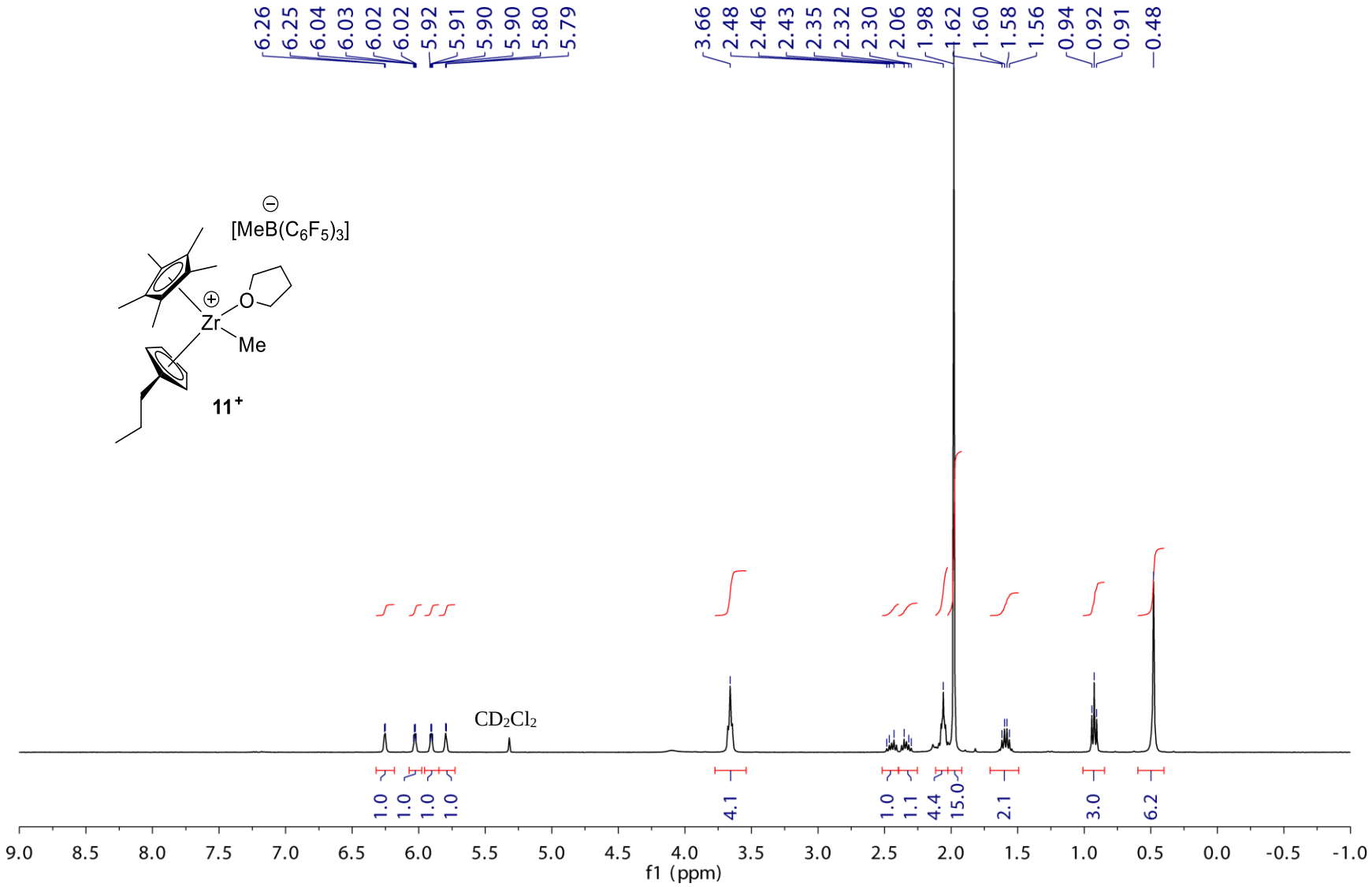

Figure S4.22. ^{1}H NMR spectrum (CD_2Cl_2, 25 °C, 400 MHz) of [Cp*(^{n}PrCp)Zr(THF)Me] $^{+}$[$MeB(C_6F_5)_3$]$^{-}$ (**11**$^{+}$).

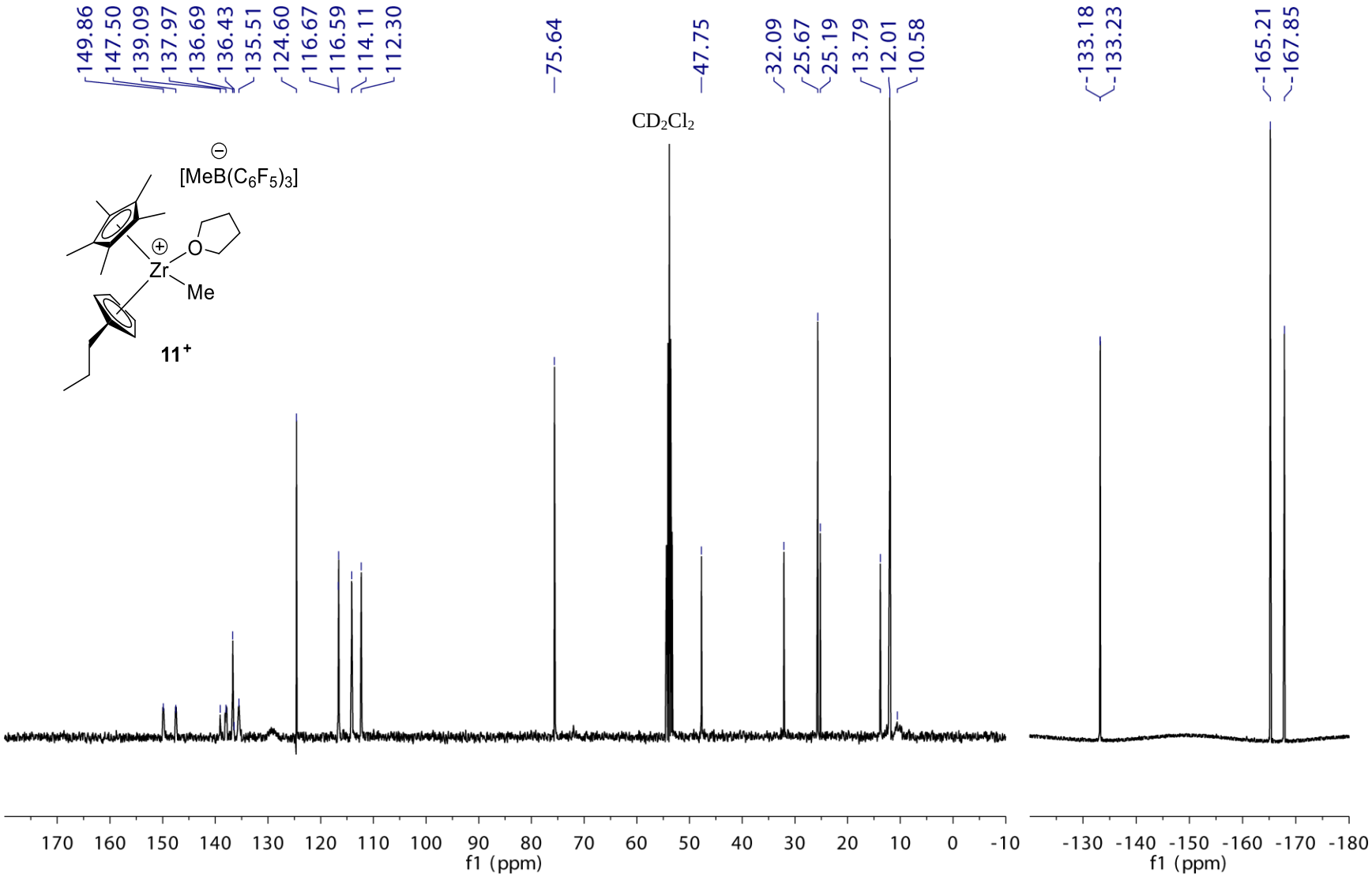

Figure S4.23. ^{13}C (left) and ^{19}F (right) NMR spectra (CD_2Cl_2, 25 °C, 400 MHz) of $[Cp^*(^nPrCp)Zr(THF)Me]^+[MeB(C_6F_5)_3]^-$ (**11**$^+$).

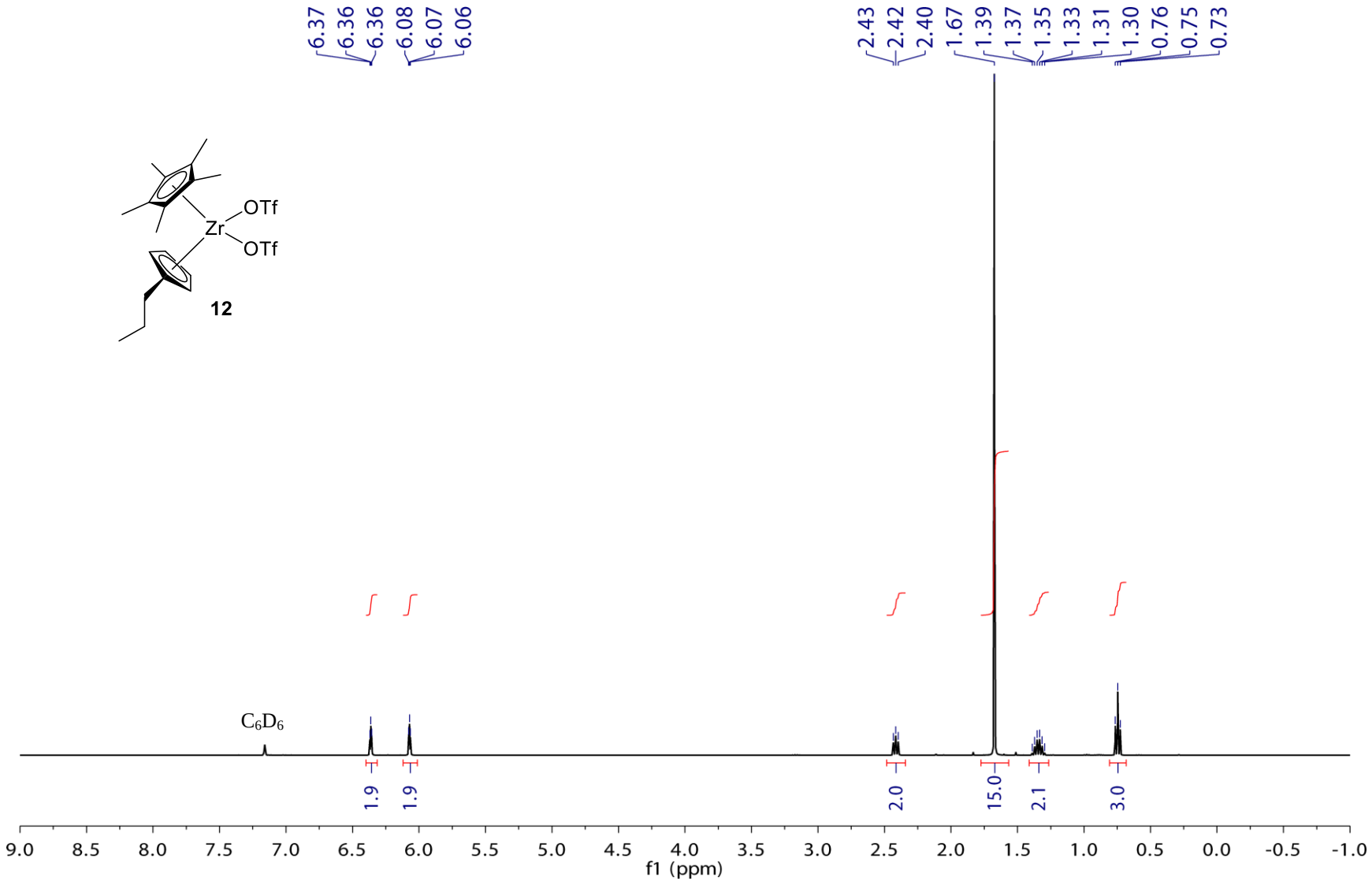

Figure S4.24. ^{1}H NMR spectrum (C_6D_6, 25 °C, 400 MHz) of Cp*(^{n}PrCp)Zr(OTf)$_2$ (**12**).

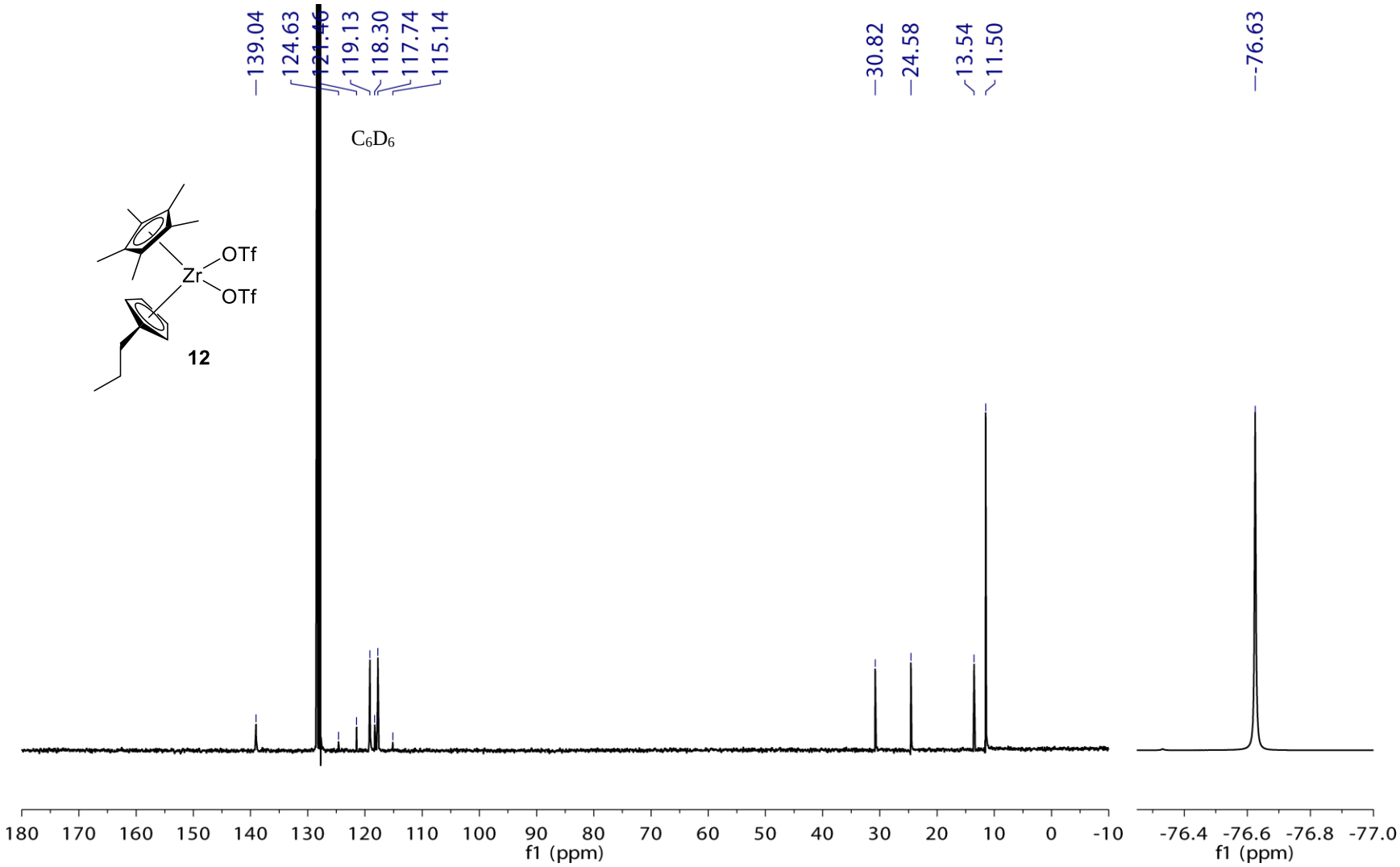

Figure S4.25. ^{13}C (left) and ^{19}F (right) NMR spectra (C_6D_6, 25 °C, 400 MHz) of Cp*(^{n}PrCp)Zr(OTf)$_2$ (**12**).

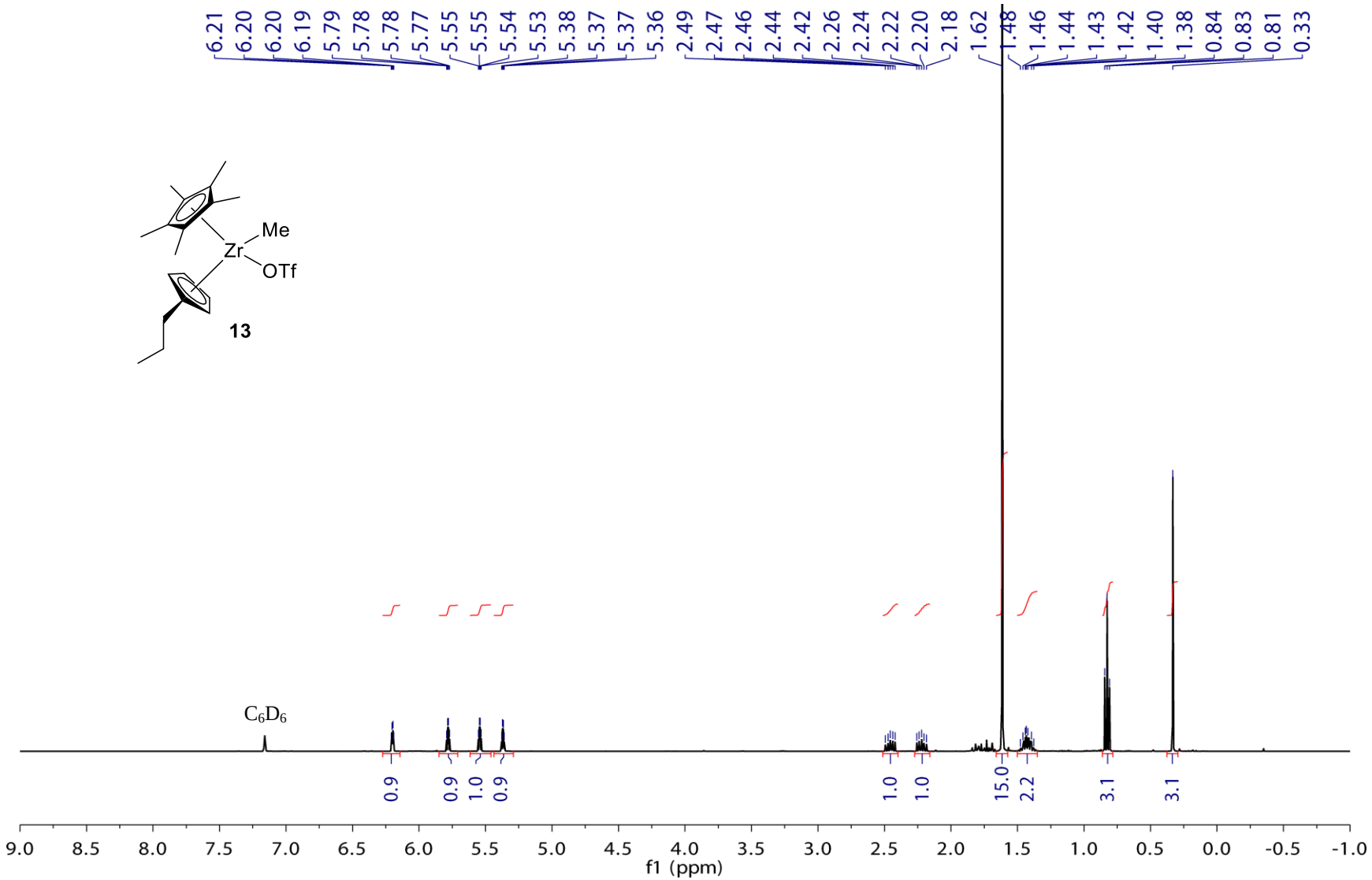

Figure S4.26. ^{1}H NMR spectrum (C_6D_6, 25 °C, 400 MHz) of Cp*(^{n}PrCp)Zr(OTf)Me (**13**).

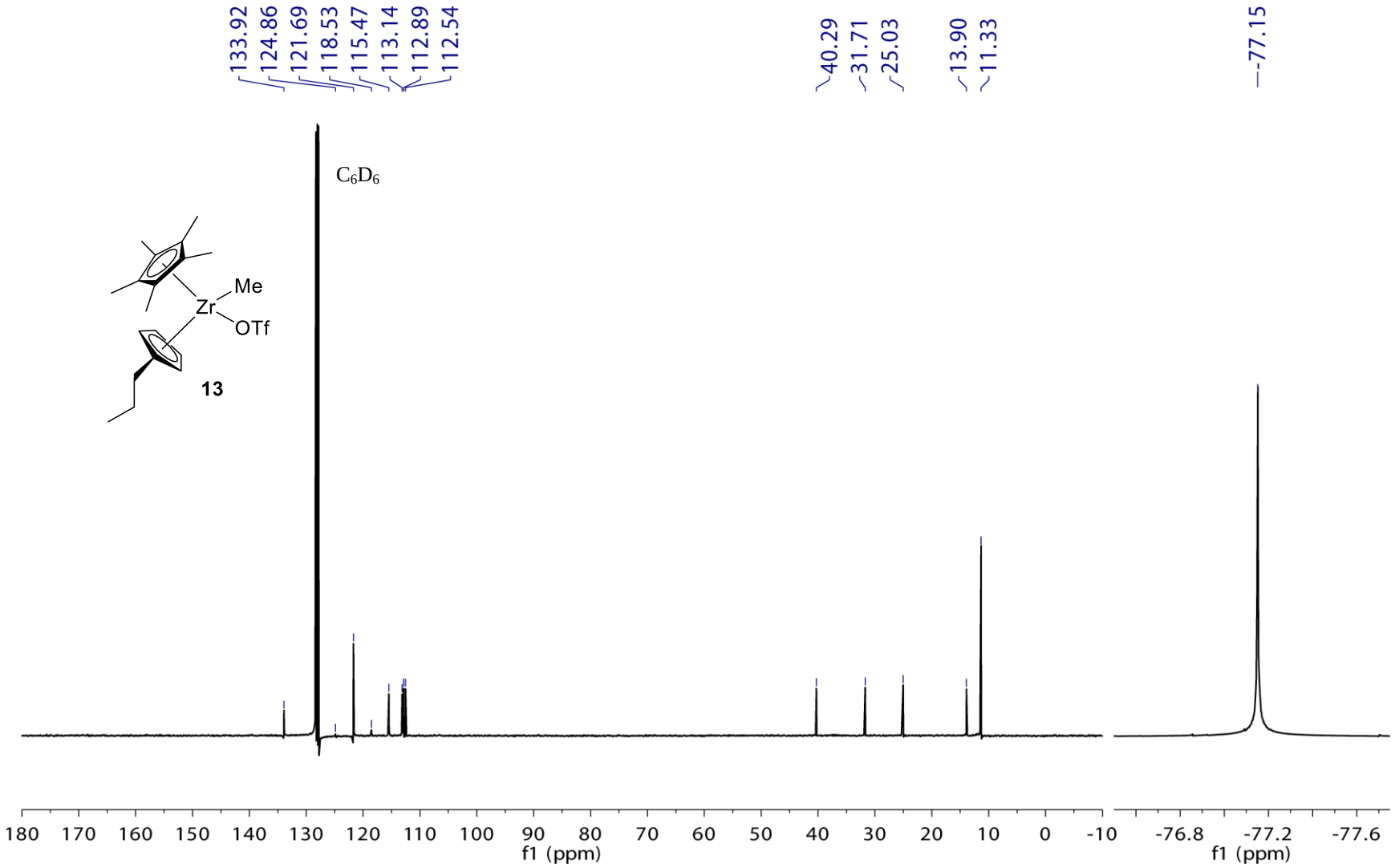

Figure S4.27. ^{13}C (left) and ^{19}F (right) NMR spectra (C_6D_6, 25 °C, 400 MHz) of Cp*(^{n}PrCp)Zr(OTf)Me (**13**).

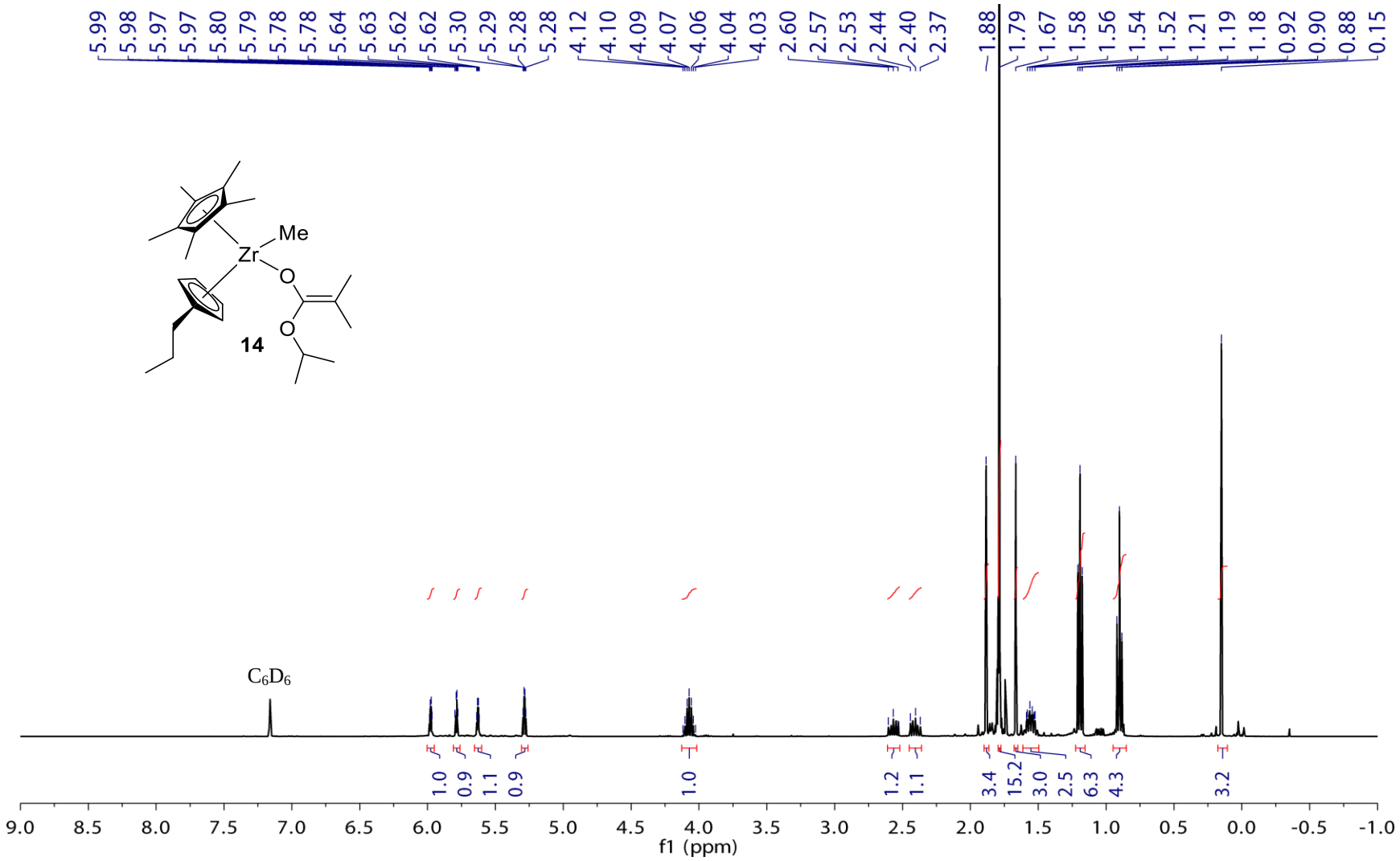

Figure S4.28. ^{1}H NMR spectrum (C_6D_6, 25 °C, 400 MHz) of Cp*(^{n}PrCp)ZrMe[OC(O^{i}Pr)=CMe$_2$] (**14**).

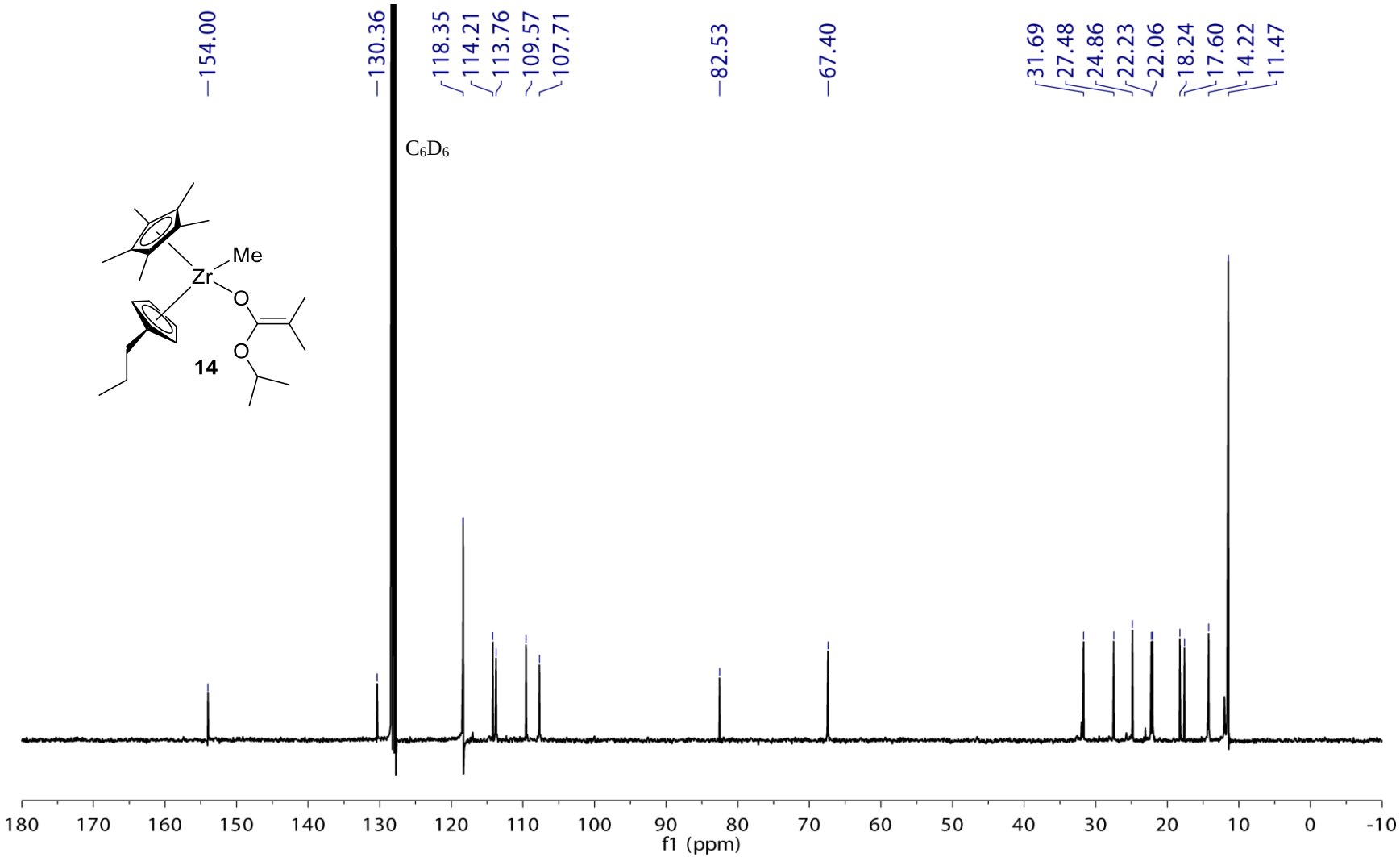

Figure S4.29. ^{13}C NMR spectrum (C_6D_6, 25 °C, 400 MHz) of Cp*(^{n}PrCp)ZrMe[OC(O^{i}Pr)=CMe_2] (**14**).

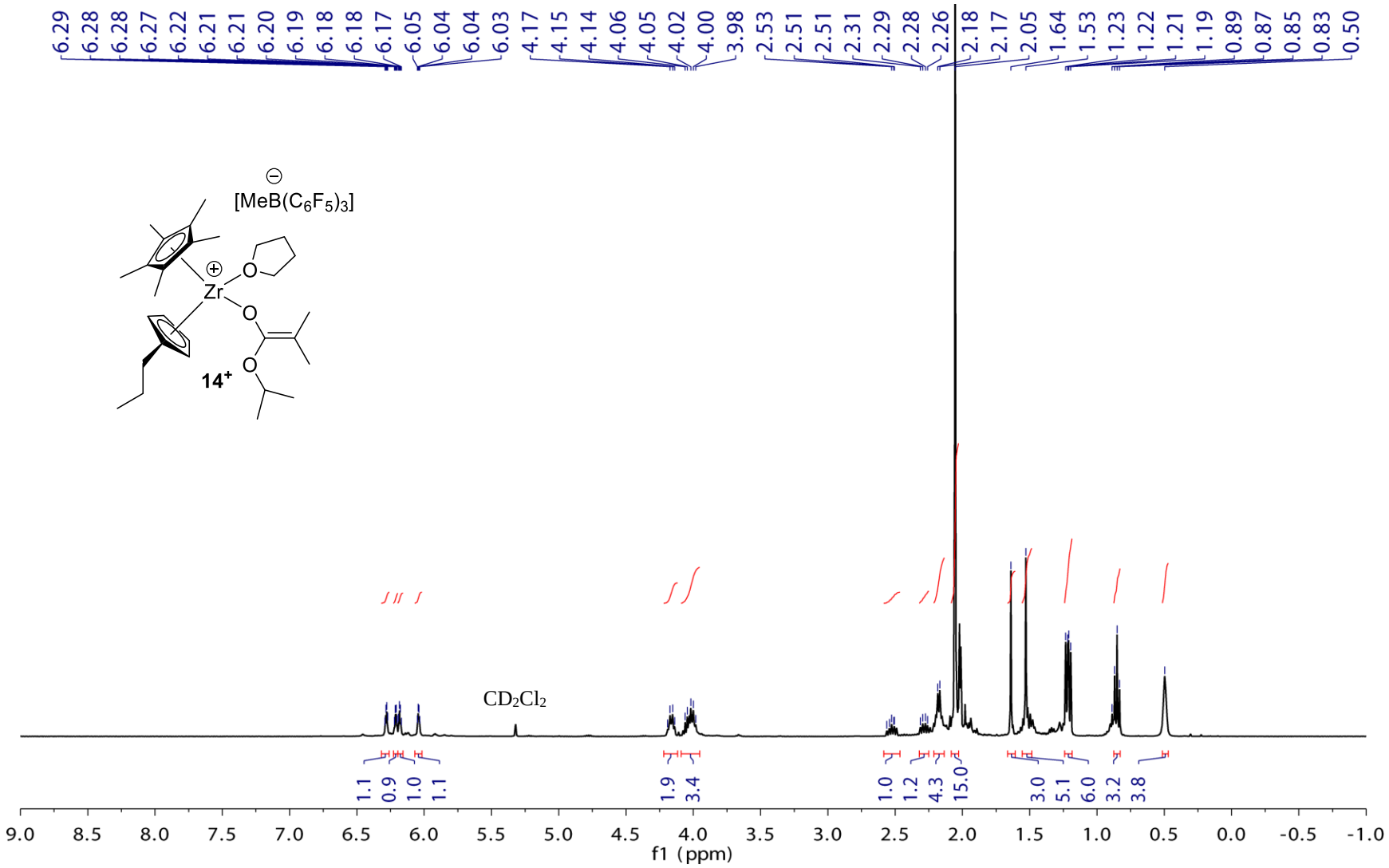

Figure S4.30. ^{1}H NMR spectrum (CD_2Cl_2, 25 °C, 400 MHz) of Cp*(^{n}PrCp)Zr(THF)[OC(O^{i}Pr)=CMe_2]$^{+}$ [$MeB(C_6F_5)_3$]$^{-}$ (**14**$^{+}$).

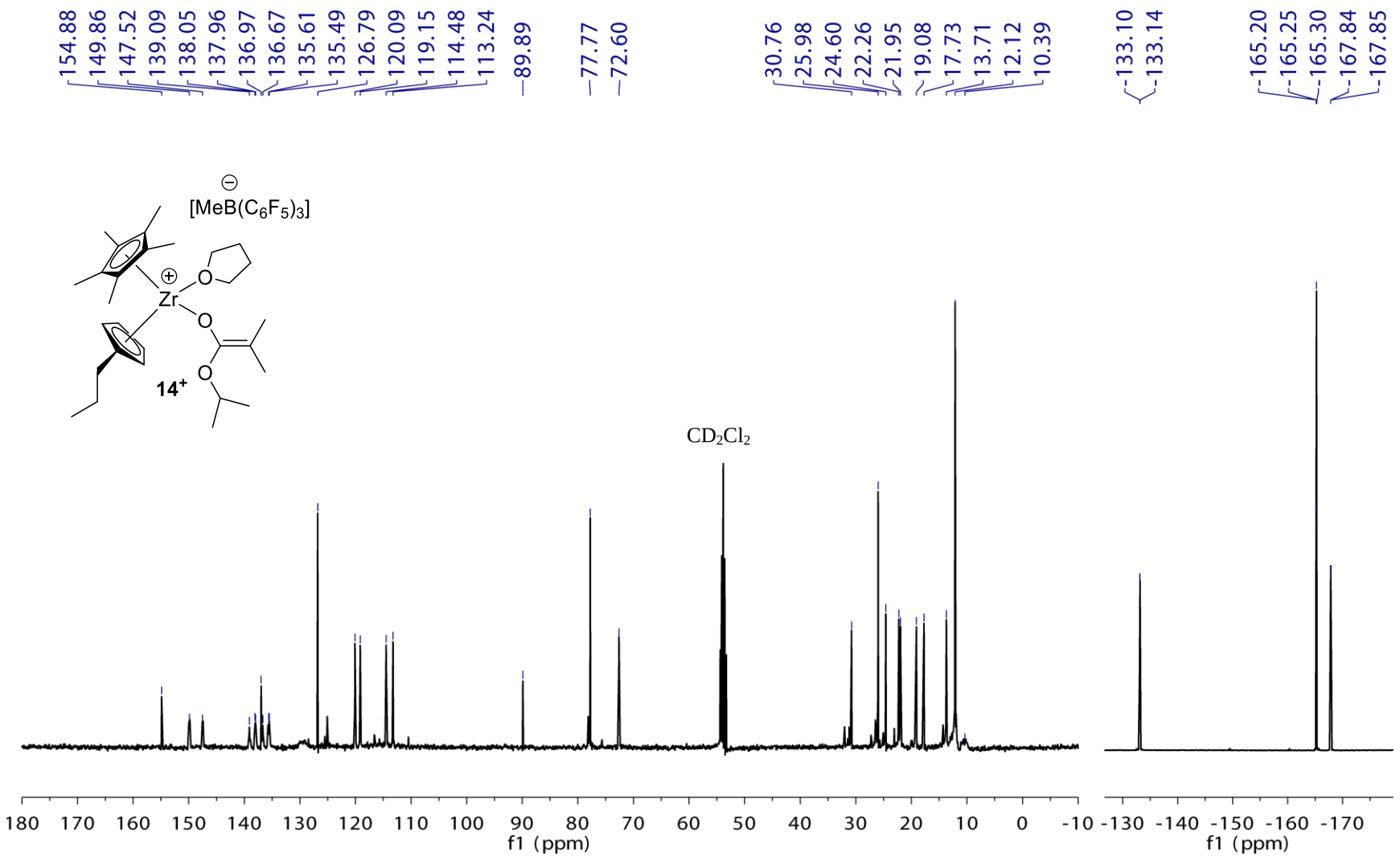

Figure S4.31. ^{13}C (left) and ^{19}F (right) NMR spectra (CD_2Cl_2, 25 °C, 400 MHz) of Cp*(^{n}PrCp)Zr(THF)[OC(O^{i}Pr)=CMe$_2$]$^+$[MeB(C_6F_5)$_3$]$^-$ (**14**$^+$).

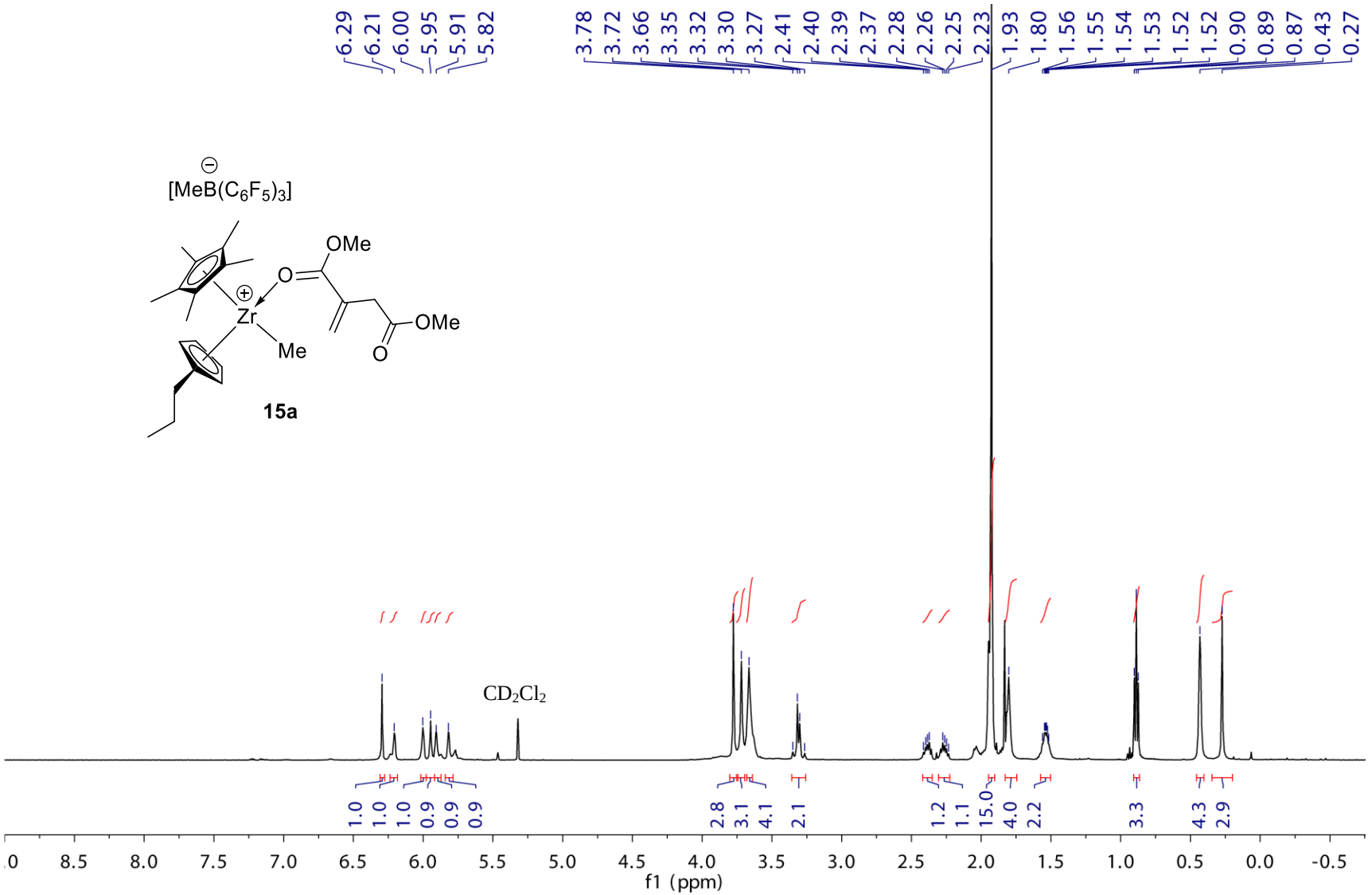

Figure S4.32. ^{1}H NMR spectrum (CD_2Cl_2, −18 °C, 500 MHz) of Cp*(^{n}PrCp)ZrMe[O=C(OMe)C(=CH_2)CH_2COOMe]$^{+}$ [$MeB(C_6F_5)_3$]$^{-}$ (**15a**).

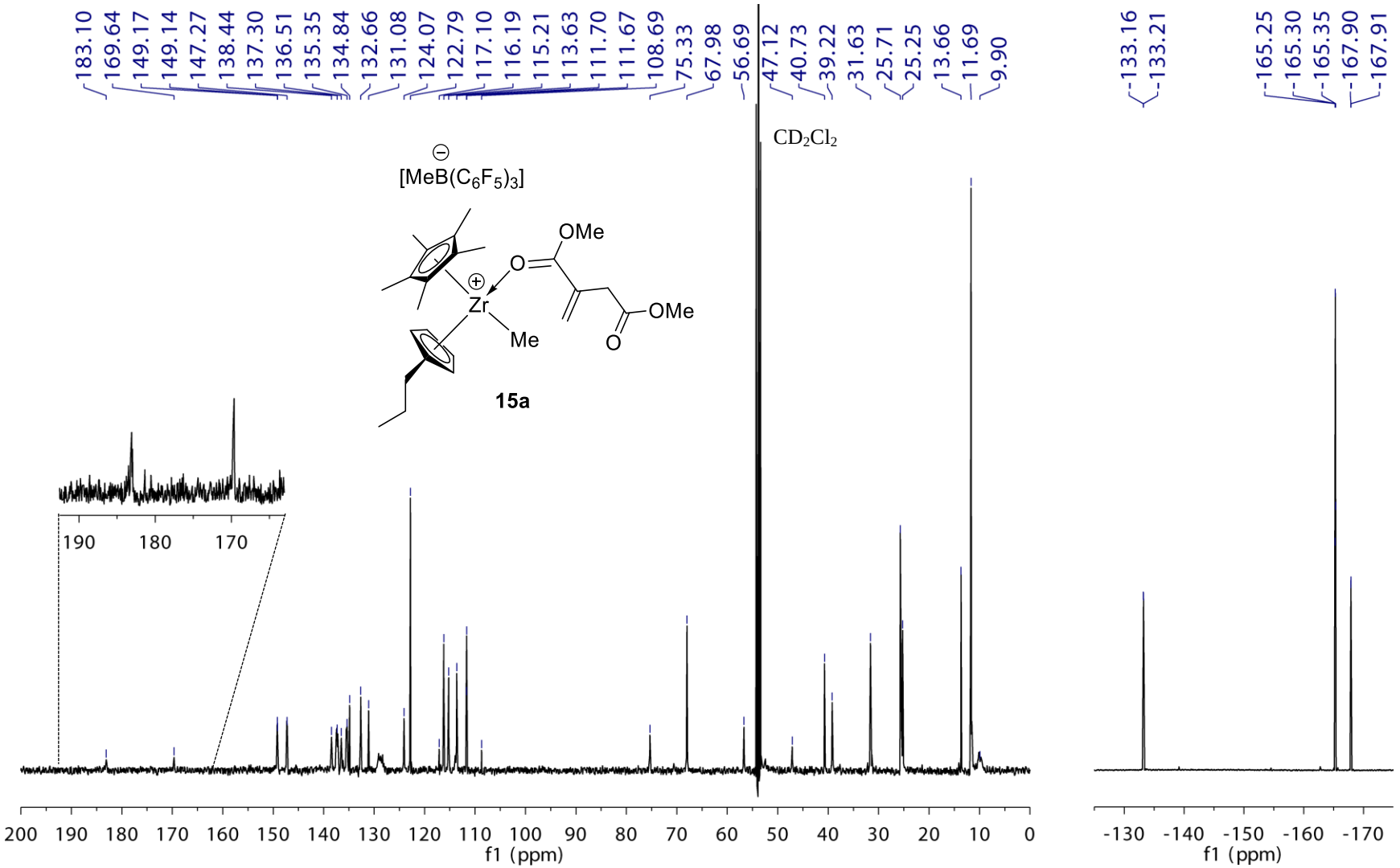

Figure S4.33. ^{13}C (left) and ^{19}F (right) NMR spectra (CD_2Cl_2, −18 °C, 500 MHz) of Cp*(^{n}PrCp)ZrMe[O=C(OMe)C(=CH_2)CH_2COOMe]$^+$ $[MeB(C_6F_5)_3]^-$ (**15a**).

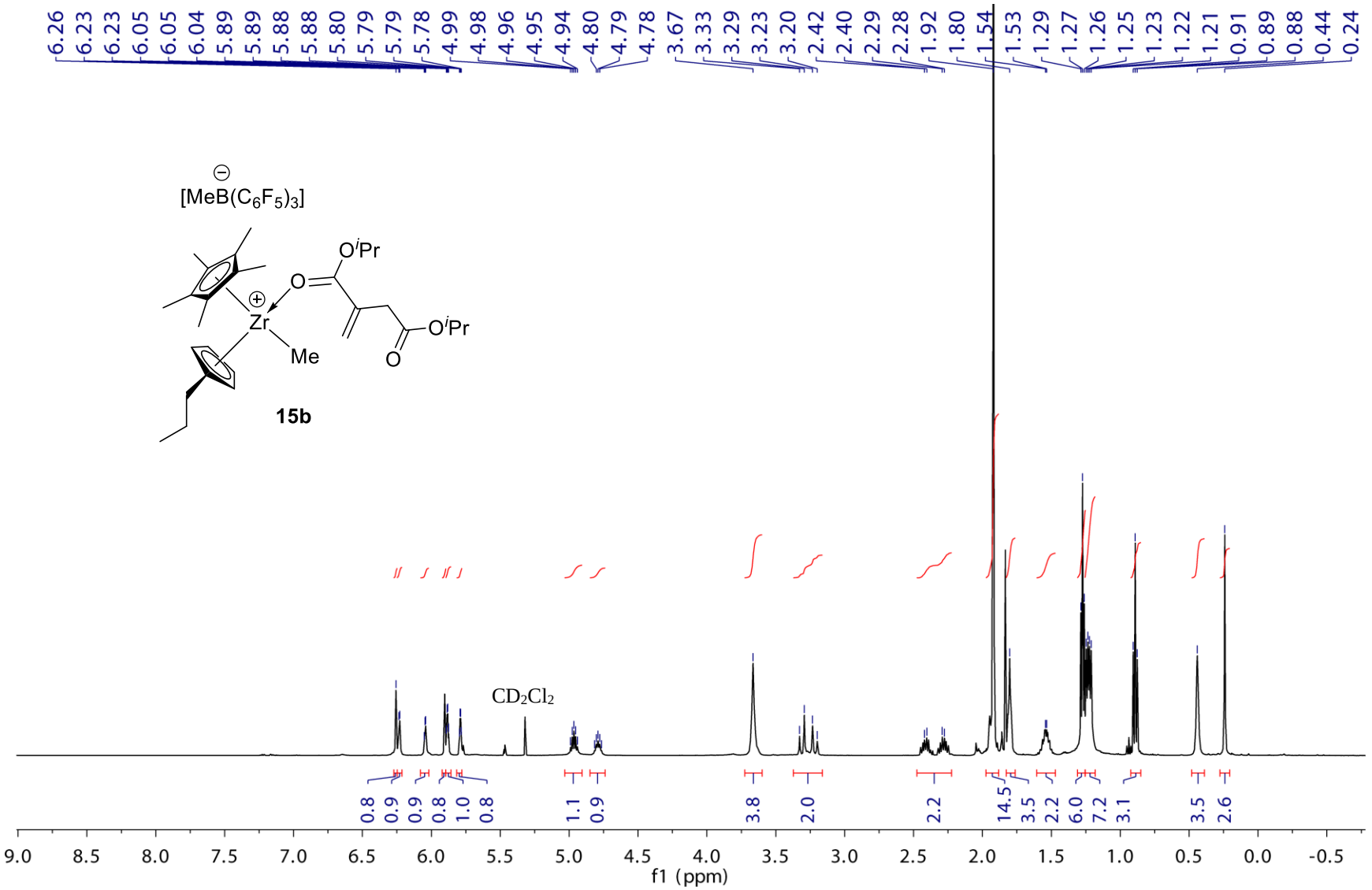

Figure S4.34. ^{1}H NMR spectrum (CD_2Cl_2, −18 °C, 500 MHz) of Cp*(^{n}PrCp)ZrMe[O=C(O^{i}Pr)C(=CH_2)CH_2COO^{i}Pr]$^{+}$ [$MeB(C_6F_5)_3$]$^{-}$ (**15b**).

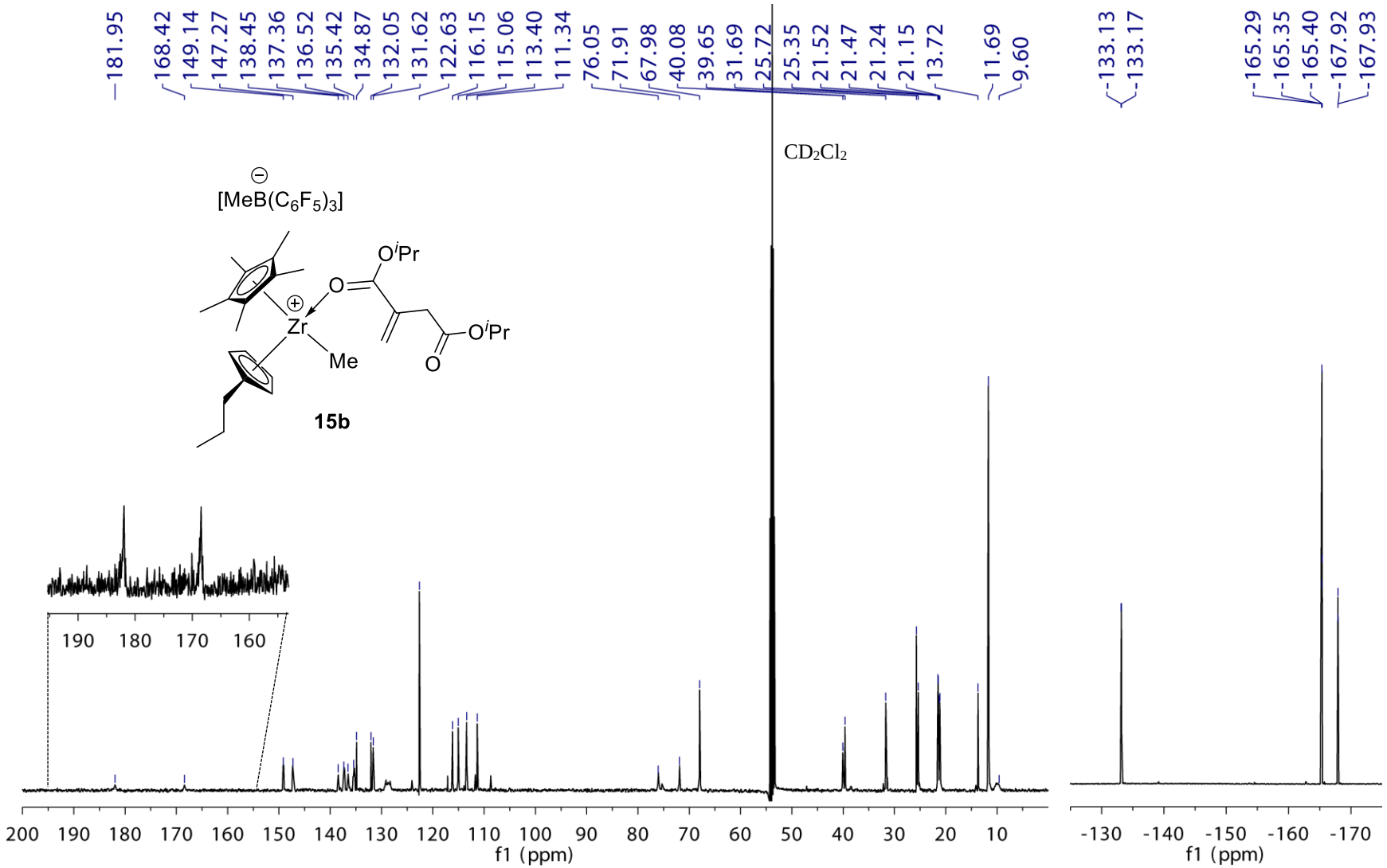

Figure S4.35. ^{13}C (left) and ^{19}F (right) NMR spectra (CD_2Cl_2, −18 °C, 500 MHz) of Cp*(^{n}PrCp)ZrMe[O=C(O^{i}Pr)C(=CH_2)CH_2COO^{i}Pr]$^{+}$ [$MeB(C_6F_5)_3$]$^{-}$ (**15b**).

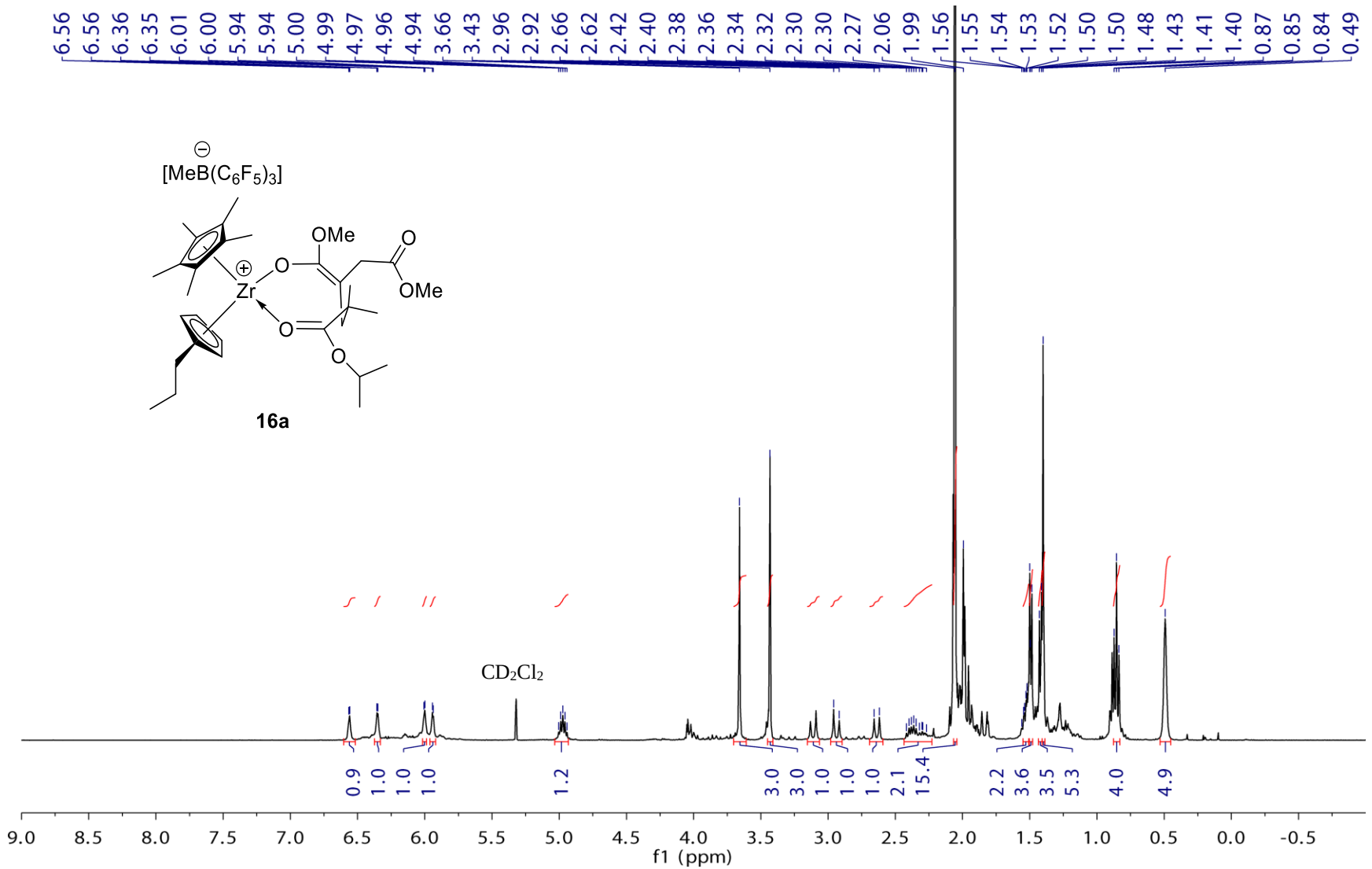

Figure S4.36. ^{1}H NMR spectrum (CD_2Cl_2, 25 °C, 400 MHz) of Cp*(^{n}PrCp)Zr[OC(OMe)=C(CH_2COOMe)CH_2C(Me_2)C(O^{i}Pr)=O]$^{+}$ [MeB(C_6F_5)$_3$]$^{-}$ (**16a**).

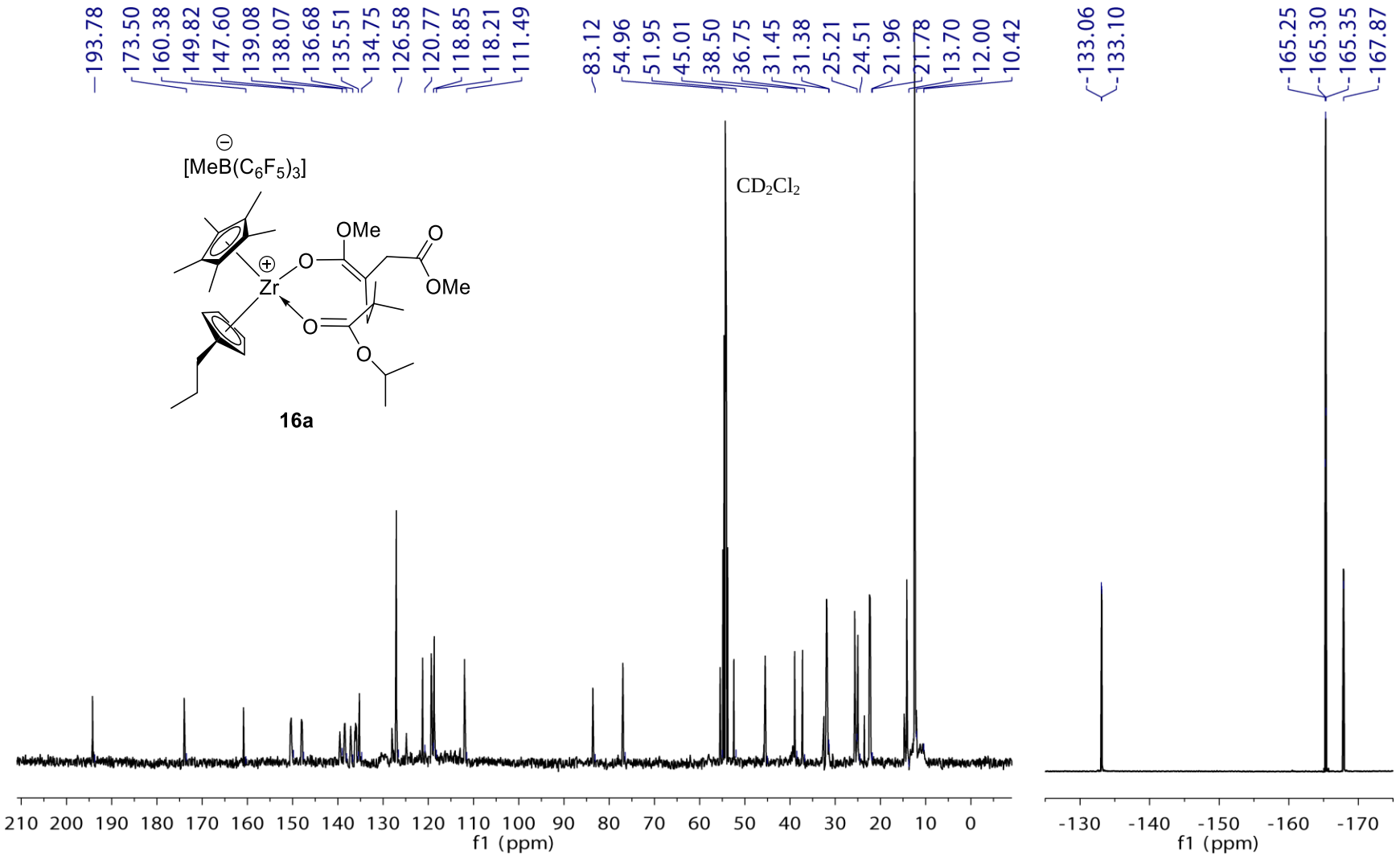

Figure S4.37. ^{13}C (left) and ^{19}F (right) NMR spectra (CD_2Cl_2, 25 °C, 400 MHz) of Cp*(^{n}PrCp)Zr[OC(OMe)=C(CH_2COOMe)CH_2C(Me_2)C(O^{i}Pr)=O]$^{+}$ [MeB(C_6F_5)$_3$]$^{-}$ (**16a**).

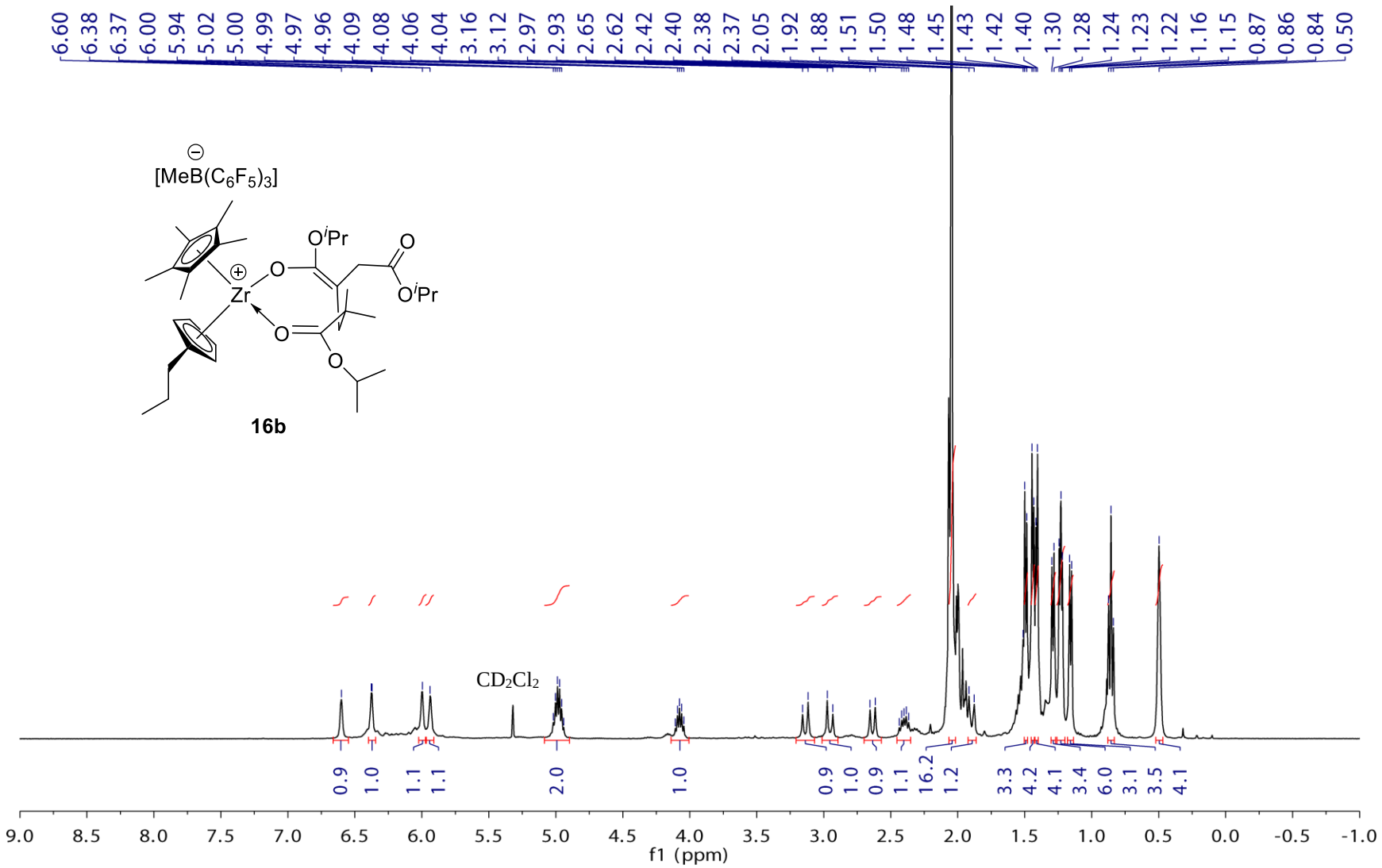

Figure S4.38. ^{1}H NMR spectrum (CD_2Cl_2, 25 °C, 400 MHz) of Cp*(^{n}PrCp)Zr[OC(O^{i}Pr)=C(CH_2COO^{i}Pr)CH_2C(Me_2)C(O^{i}Pr)=O]$^{+}$ [$MeB(C_6F_5)_3$]$^{-}$ (**16b**).

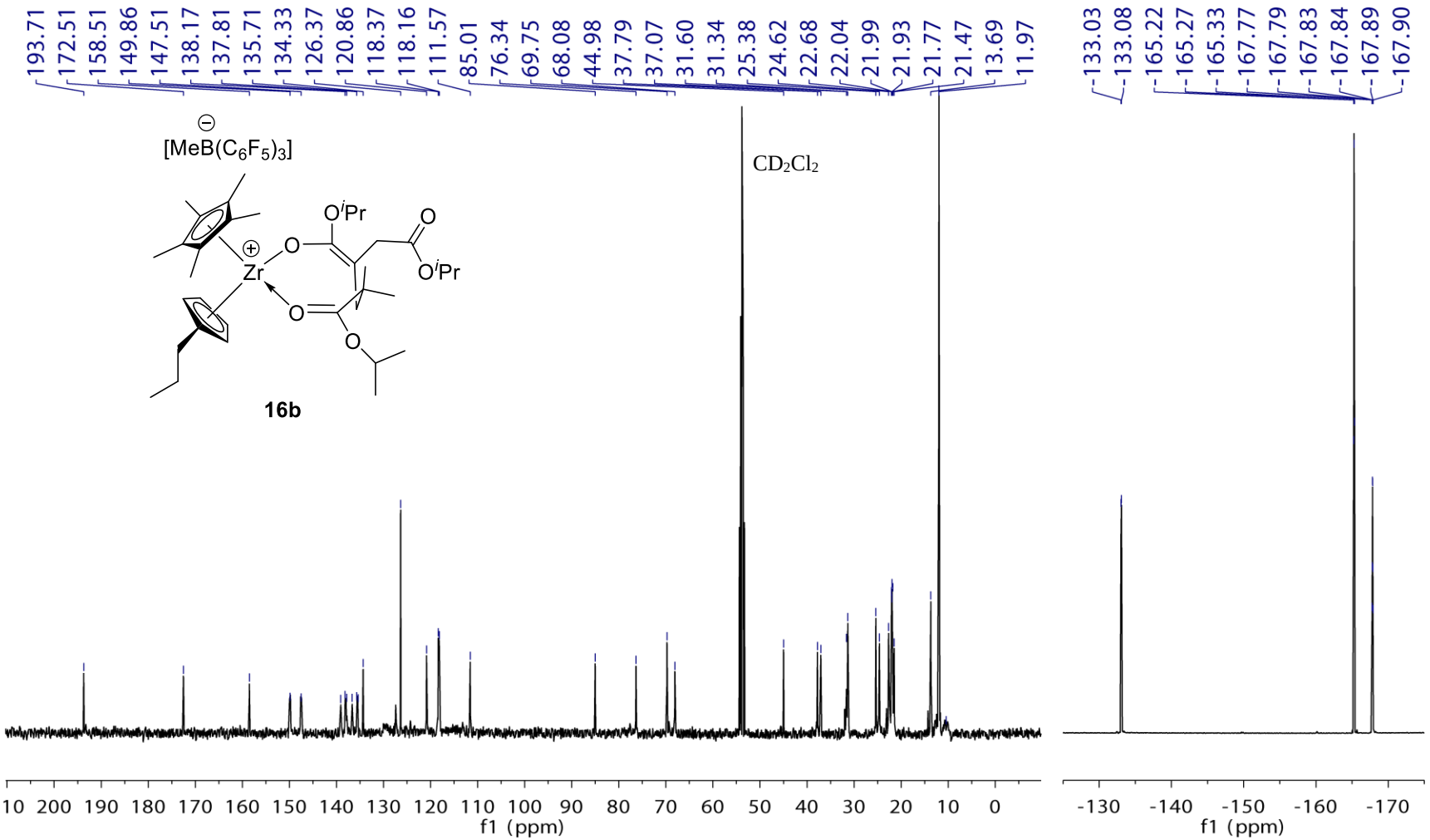

Figure S4.39. ^{13}C (left) and ^{19}F (right) NMR spectra (CD_2Cl_2, 25 °C, 400 MHz) of Cp*(^{n}PrCp)Zr[OC(O^{i}Pr)=C(CH_2COO^{i}Pr)CH_2C(Me_2)C(O^{i}Pr)=O]$^{+}$ $[MeB(C_6F_5)_3]^{-}$ (**16b**).

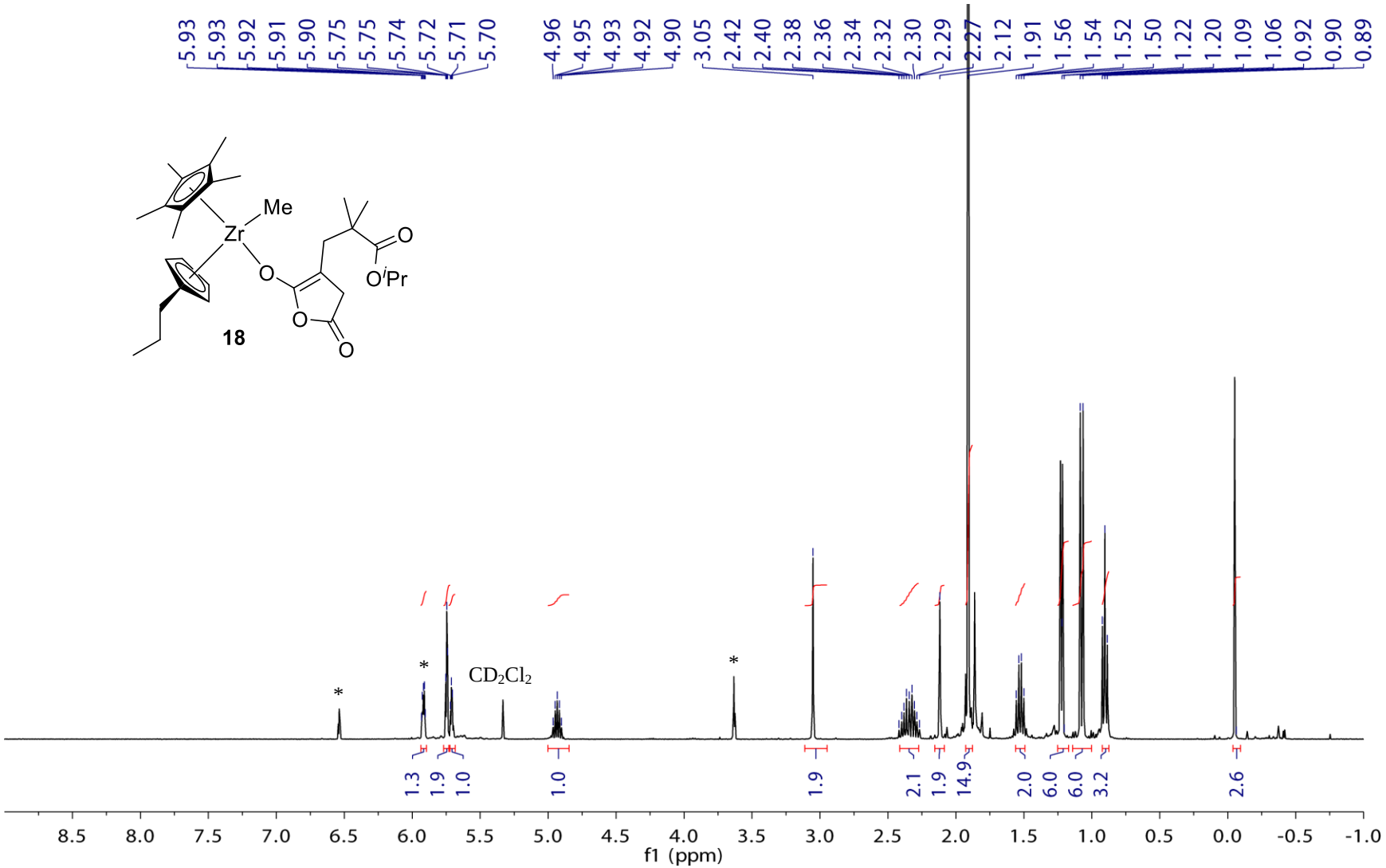

Figure S4.40. ^{1}H NMR spectrum (CD_2Cl_2, 25 °C, 400 MHz) of Cp*(^{n}PrCp)ZrMe{OC[OC(O)CH_2]=C($CH_2CMe_2COO^{i}Pr$)} (**18**). (* = excess itaconic anhydride for comparison).

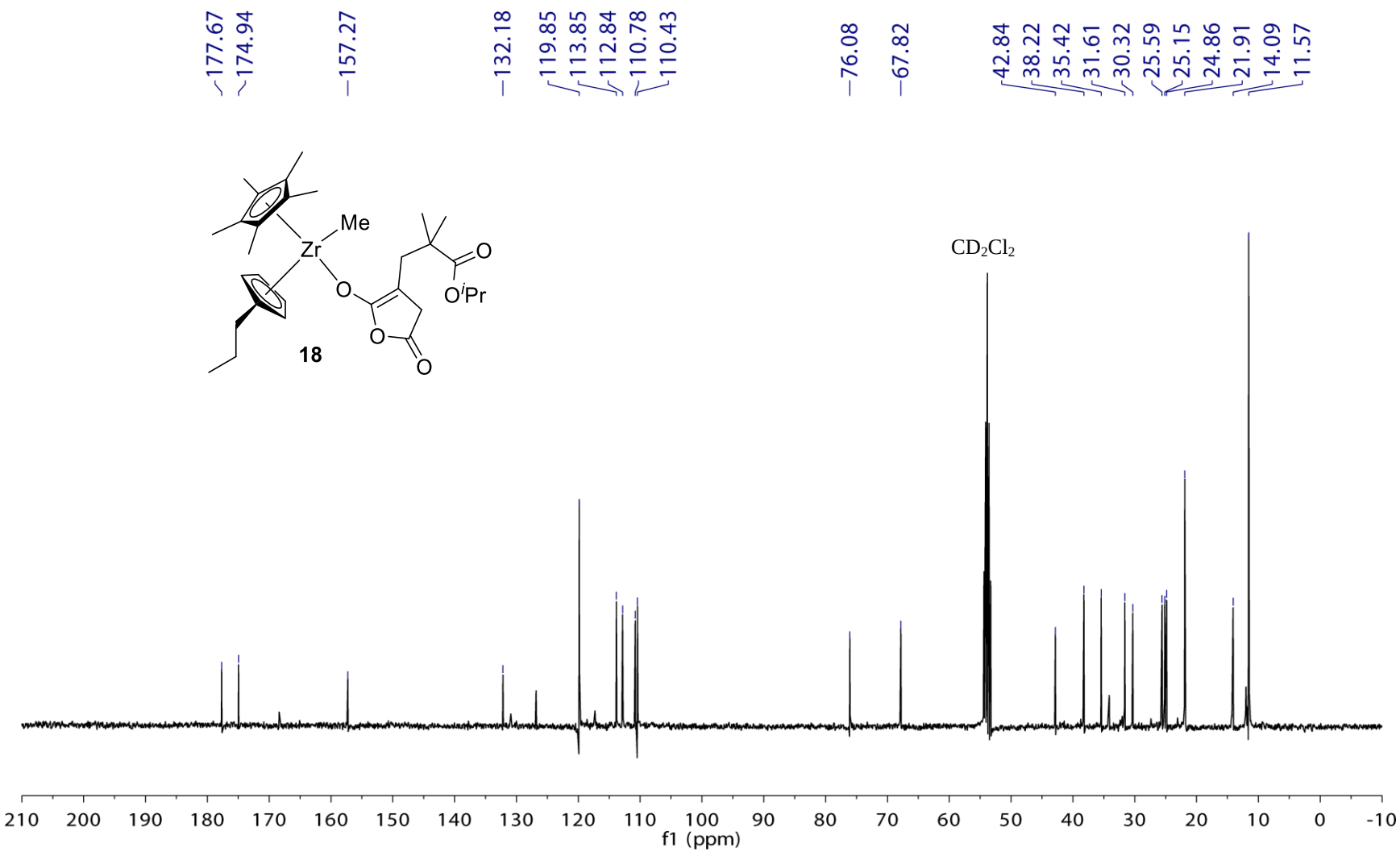

Figure S4.41. ^{13}C NMR spectrum (CD_2Cl_2, 25 °C, 400 MHz) of Cp*(^{n}PrCp)ZrMe{OC[OC(O)CH_2]=C($CH_2CMe_2COO^{i}Pr$)} (**18**).

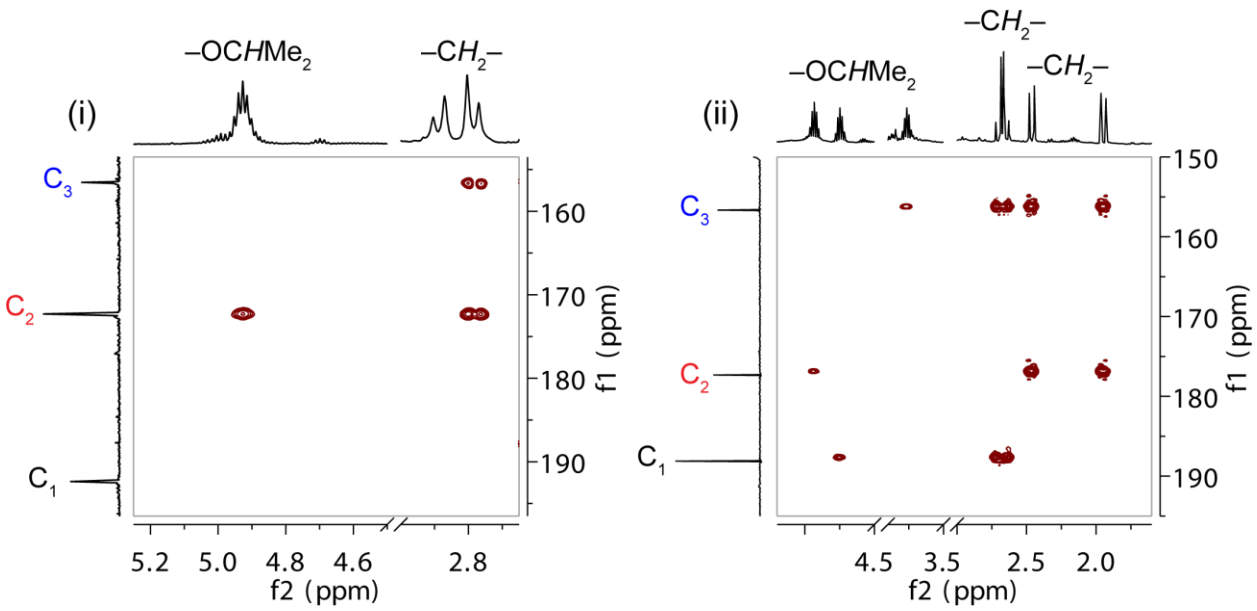

Figure S4.42. Selected portions of ^{13}C–^{1}H HMBC (CD_2Cl_2, −5 °C) 2D NMR spectra of complexes **2b** (i) and **4b** (ii) are shown for comparison.

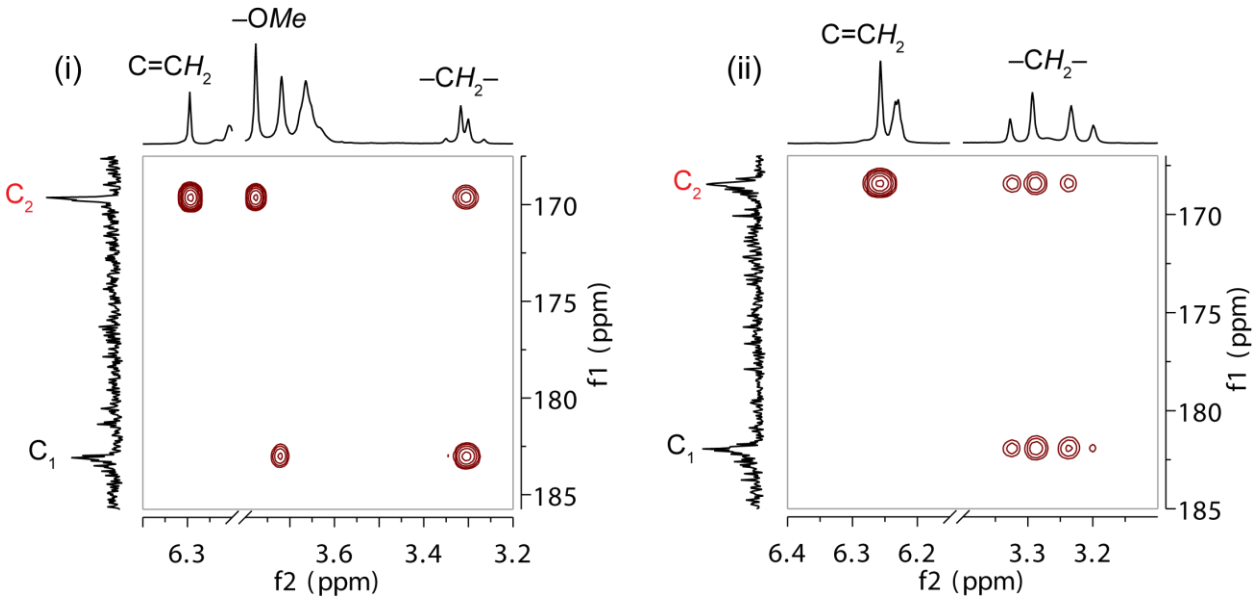

Figure S4.43. Selected portions of ^{13}C–^{1}H HMBC (CD_2Cl_2, −5 °C) 2D NMR spectra of complexes **15a** (i) and **15b** (ii) are shown for comparison.

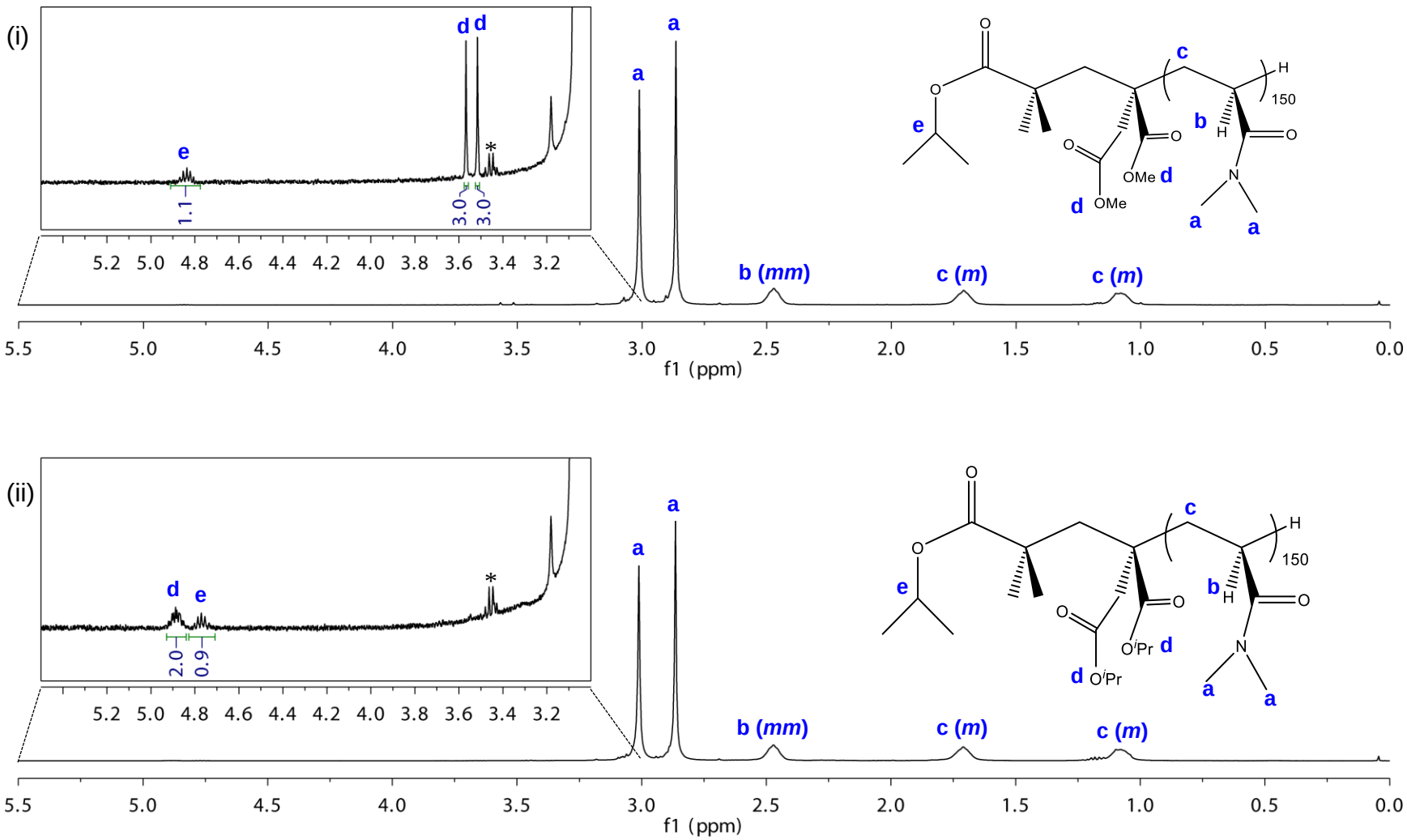

Figure S4.44. ^{1}H NMR spectra ($CDCl_3$, 25 °C) of highly *it*-PDMAA obtained by catalysts **2a** (i) and **2b** (ii), highlighting the characteristic signals of the polymer end-groups (* = residual Et_2O).

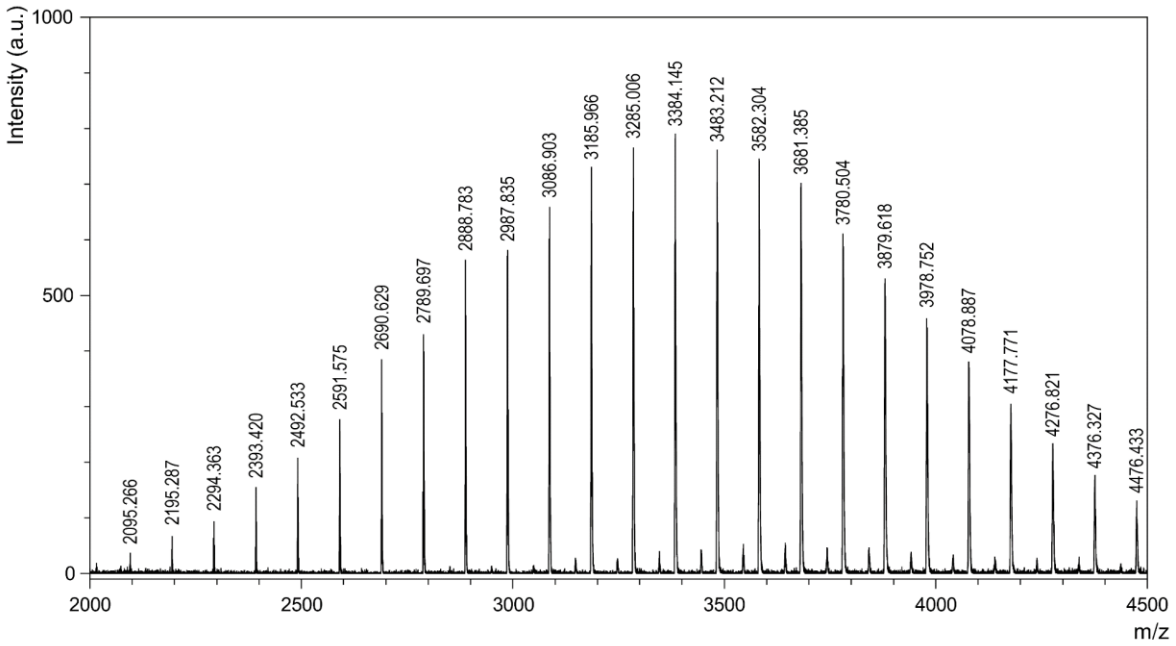

Figure S4.45. Portion of the MALDI-TOF mass spectrum of the low-molecular-weight PDMAA produced by **16a** at ambient temperature in CH_2Cl_2.

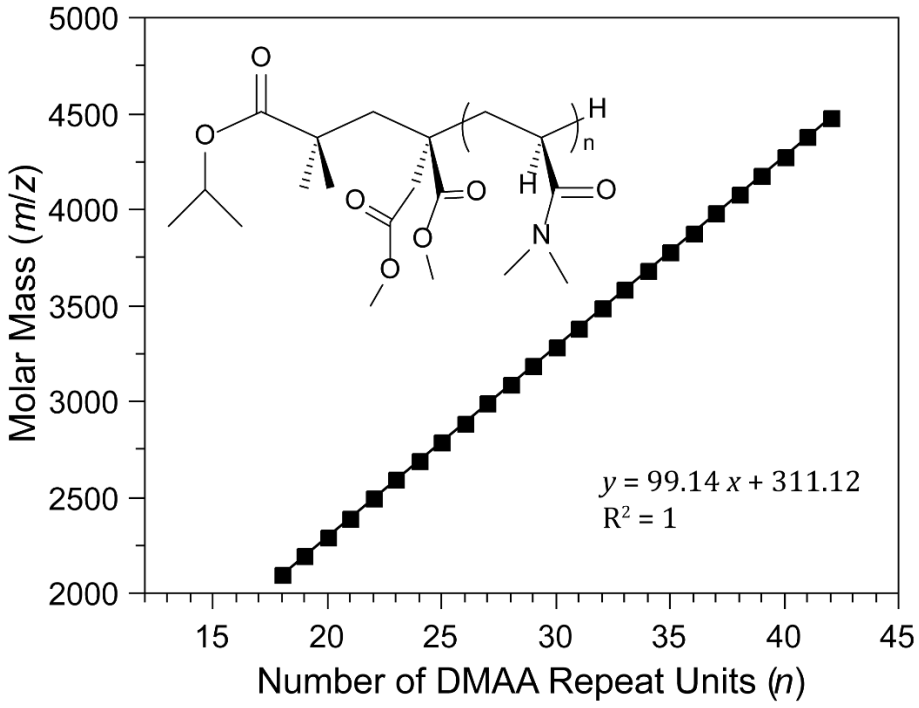

Figure S4.46. Plot of *m*/*z* values from the MALDI-TOF spectrum in Figure S4.45 vs the number of DMAA repeat units (*n*).

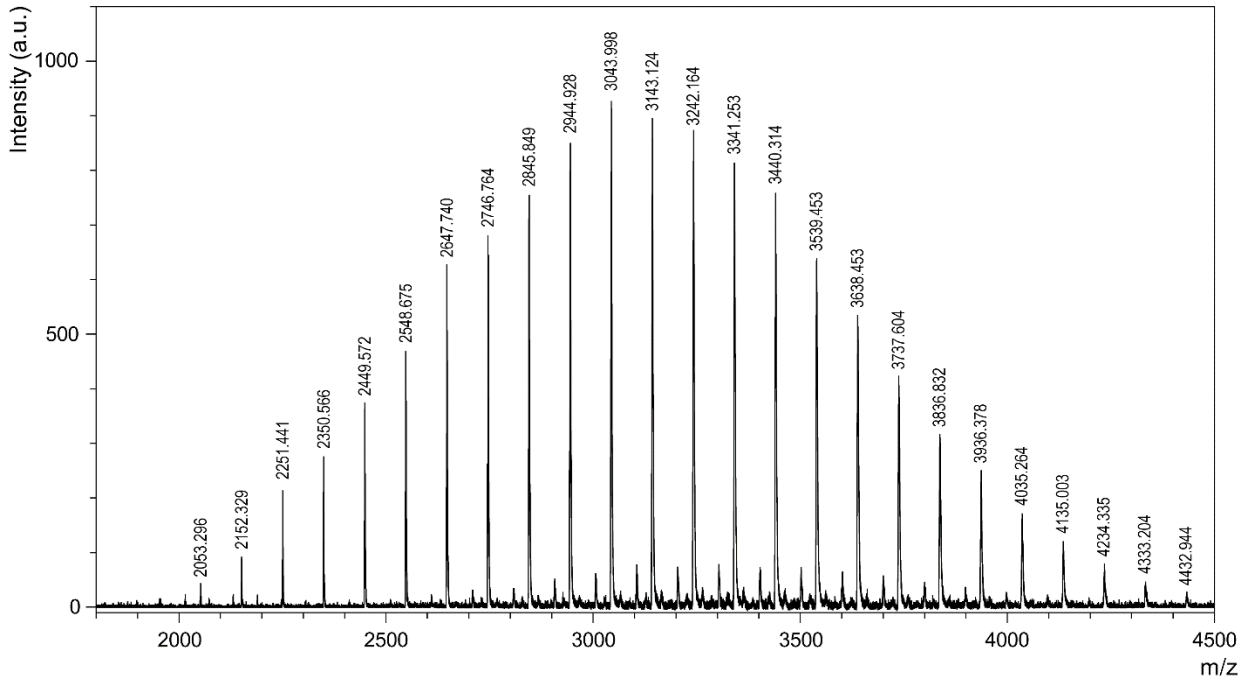

Figure S4.47. Portion of the MALDI-TOF mass spectrum of the low-molecular-weight PDMAA produced by **16b** at ambient temperature in CH_2Cl_2.

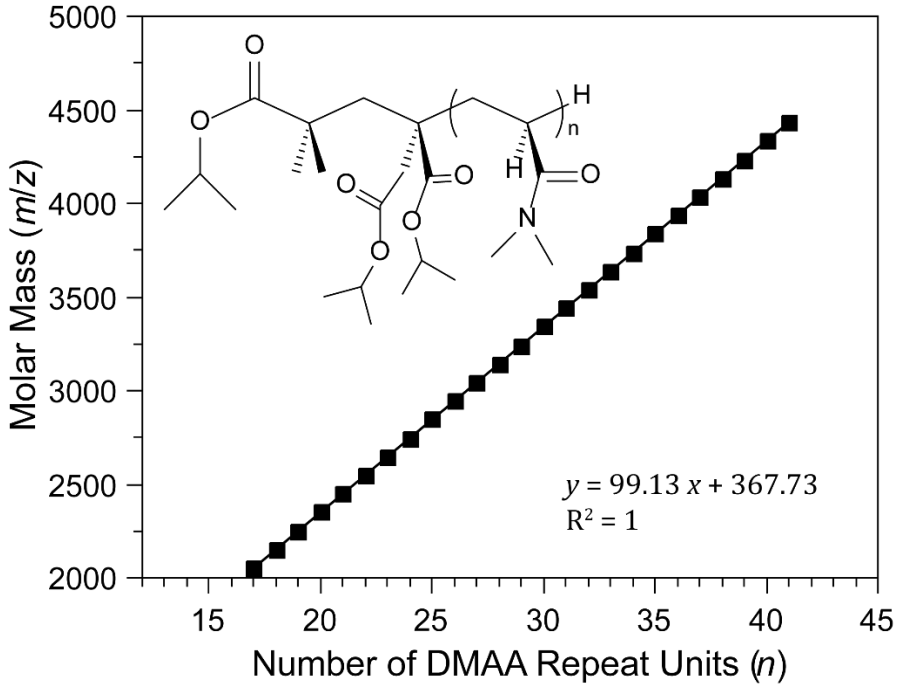

Figure S4.48. Plot of *m*/*z* values from the MALDI-TOF spectrum in Figure S4.47 vs the number of DMAA repeat units (*n*).

C.4. References

(1) Otsu, T.; Yamagishi, K.; Yoshioka, M. *Macromolecules* **1992**, *25*, 2713-2716.

(2) Allen, R. D.; Long, T. E.; McGrath, J. E. *Polym. Bull. (Berlin)* **1986**, *15*, 127-134.

(3) Bolig, A. D.; Chen, E. Y. X. *J. Am. Chem. Soc.* **2004**, *126*, 4897-4906.

(4) Mariott, W. R.; Rodriguez-Delgado, A.; Chen, E. Y. X. *Macromolecules* **2006**, *39*, 1318-1327.

(5) Rodriguez-Delgado, A.; Chen, E. Y. X. *Macromolecules* **2005**, *38*, 2587-2594.

(6) Ning, Y.; Caporaso, L.; Correa, A.; Gustafson, L. O.; Cavallo, L.; Chen, E. Y. X. *Macromolecules* **2008**, *41*, 6910-6919.

(7) Rodriguez-Delgado, A.; Chen, E. Y. X. *J. Am. Chem. Soc.* **2005**, *127*, 961-974.

(8) Jutzi, P.; Müller, C.; Stammler, A.; Stammler, H.-G. *Organometallics* **2000**, *19*, 1442-1444.

(9) (a) Zhang, Y.; Ning, Y.; Caporaso, L.; Cavallo, L.; Chen, E. Y.-X. *J. Am. Chem. Soc.* **2010**, *132*, 2695–2709. (b) Ning, Y.; Chen, E. Y.-X. *J. Am. Chem. Soc.* **2008**, *130*, 2463−2465.

(10) Sheldrick, G. M. *SADABS*

(11) Sheldrick, G, M. *SHELXTL*, v. 6.12; Bruker AXS: Madison, WI, 1999.